The Hydrogenation of Nitrobenzene Over Metal Catalysts

Elaine A. Gelder

PhD Thesis

Department of Chemistry

The University of Glasgow

April 2005

ABSTRACT

The catalytic hydrogenation of nitrobenzene is an industrially important reaction used in the commercial production of aniline for use in the polyurethane industry. A mechanism for the reaction was first proposed by Haber in 1898 and has been widely accepted despite never being fully delineated. During this study the nitrobenzene hydrogenation reaction was investigated, over a range of metal catalysts, to probe the mechanism of hydrogenation and catalyst deactivation.

Initial investigations over Pd/C catalysts revealed the reaction to be sensitive to the solvent and the nature of the carbon support. However more importantly it was shown that the first intermediate in Haber's scheme, nitrosobenzene, could not act as an intermediate to nitrobenzene hydrogenation. As a result, a new reaction mechanism was proposed where the hydrogenation of nitrobenzene and nitrosobenzene proceed *via* separate mechanistic routes, linked by a common adsorbed intermediate; the surface concentration of this adsorbed species controls the hydrogenation pathway followed. Further investigation over Raney nickel suggests this mechanism to be valid over other metals and not specific to palladium.

A series of novel bimetallic catalysts were also prepared for use in this study. Characterisation of these catalysts was carried out to determine the nature of the metal-metal interaction on the surface. The evidence suggests mixed metal particles may have been formed on some catalysts.

The activity of these catalysts was found to be greatly enhanced following pre-treatment with water vapour in a hydrogen atmosphere. It was postulated that partial oxidation of the metal active sites was occurring and that these systems were more active due to the enhanced adsorption of nitrobenzene. The copper nickel/systems were found to show enhanced catalytic activity, whereas all systems containing cobalt displayed irreversible deactivation following water treatment, which was attributed to the formation of irreducible cobalt aluminum spinel from the CoO formed on the surface.

ACKNOWLEDGEMENTS

First and foremost thanks must go to my supervisor David Jackson for all his help and advice throughout the past few years; for being available at all times for consultation and to answer questions no matter how small or stupid, and for being ready with the white board pen to clear up my misconceptions. Thanks must also go to my supervisors at Johnson Matthey Catalysts in Billingham, Martin Lok and Mike Watson, for their input and continuing interest in this thesis.

I am also very grateful to various other people who have helped me to make this project successful. These include Ron Spence for technical support in Glasgow; Jill Turner at Johnson Matthey for her guidance in synthesizing the catalysts and for facilitating the submission and collection of samples for a number of characterization techniques; Malcolm Kett, also at Johnson Matthey, for his help in collecting the Raman spectra and for carrying out the XPS analysis and aiding in the interpretation of the results; and also to the fourth year project students who have contributed with related research which has helped to fill in the bigger picture, namely David Williams and Graham Ormsby.

A big thank-you must also go to Andy Monaghan for his flexibility in sharing equipment and for all the entertainment during the slow times. The endless cups of tea, chocolate doughnuts and heated debates were very much appreciated. Thanks also to the remaining members of the research group in Glasgow: Elaine Vass, Elaine Opara, Arran Canning, Sreekala Rugmini, Kenneth Hindle and Sharon Burns for making the three years an interesting and memorable experience.

The Hydrogenation of Nitrobenzene over Metal Catalysts

The work contained in this thesis, submitted for the degree of Doctor of Philosophy, is my own original work, except where due reference is made to other authors. No material within has been previously submitted for a degree at this or any other university.

Elaine Gelder, April 2005

CONTENTS

E. A. Gelder, S. D. Jackson and C. M. Lok, A study of nitrobenzene hydrogenation over palladium/carbon catalysts, *Catal. Letts.*, **84** (2002) 205-208

E. A. Gelder, S. D. Jackson and C. M. Lok, The hydrogenation of nitrobenzene to aniline: a new mechanism, *Chem. Commun.*, **4** (2005) 522-524

Content of Figures

Content of Tables

Content of Equations

1.0 INTRODUCTION

1.1 Heterogeneous Catalysis

The definition of a catalyst has evolved since Berzelius first invented the term in 1836 [1]. Generally, a catalyst is considered to be substance that will increase a chemical reaction without becoming used up during the process. A catalyst can increase the rate of a chemical reaction and speed its attainment of equilibrium, however, the reaction thermodynamics must be obeyed. Unfeasible reactions cannot be forced by use of a catalyst and neither can the thermodynamic equilibrium position be altered. Catalysts can take any physical form and are known as homogenous catalysts if they are in the same state as the reagents in the reaction it is promoting. During heterogeneous catalysis, a solid catalyst is used to accelerate a gas phase or liquid phase reaction. The catalysts usually consist of small metal particles dispersed across an inert support material such as alumina or silica [2]. The use of a support helps to increase the metal surface area and also leads to increased thermal stability. The use of catalysts in industry is widespread with approximately 90 % of industrial products encountering a catalyst at some point in their synthesis [3]. Therefore, the area of catalysis is of vital importance to the modern economy and for future industrial developments where existing processes need to be improved for economic or environmental reasons.

1.1.1 The Catalytic Process

The catalytic process can be split into five separate stages, known collectively as the catalytic cycle [3]. A summary of these processes is shown in Figure 1.1 and each stage is described in more detail below.

Figure 1.1: The catalytic cycle

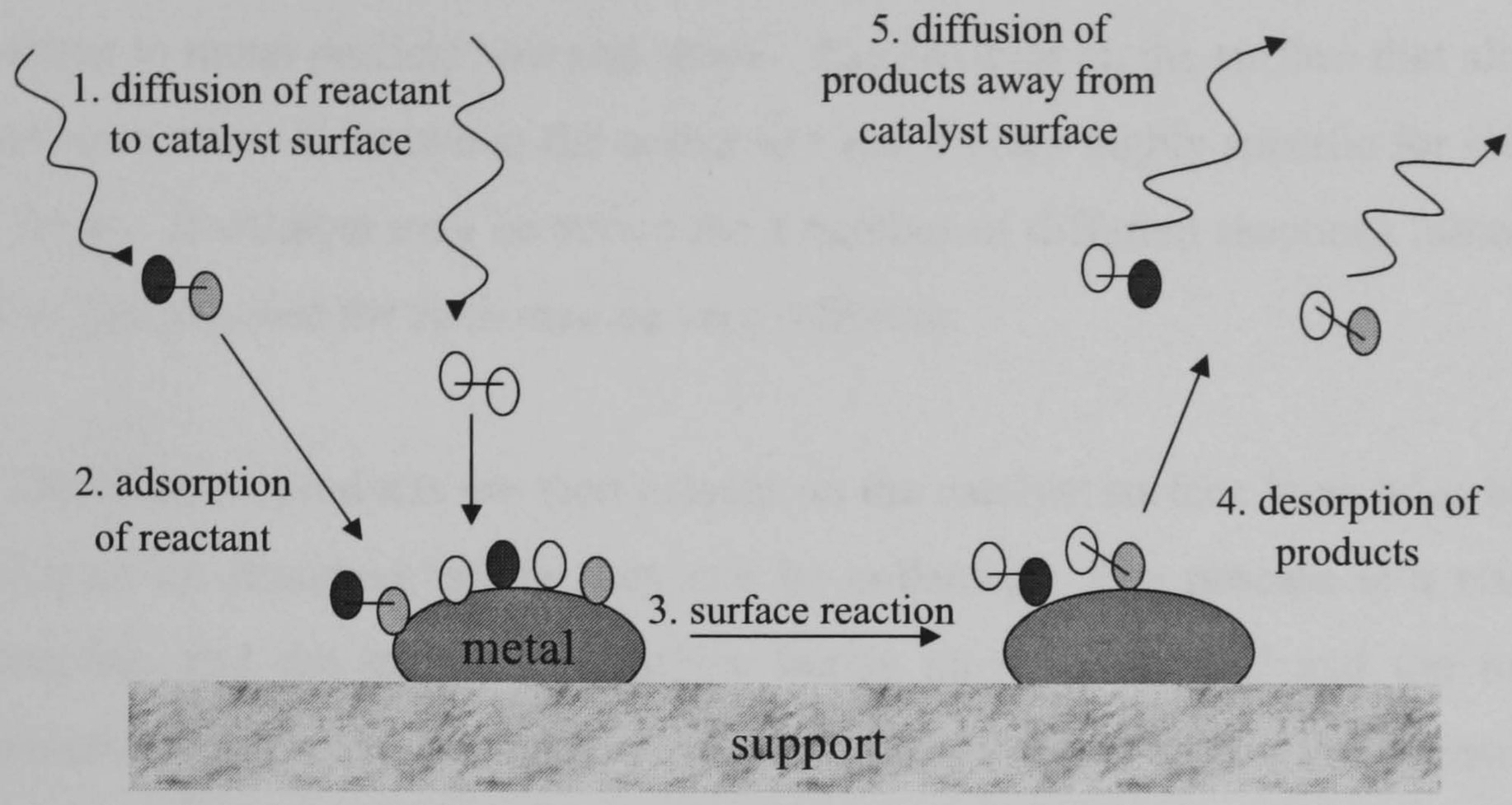

1. The initial stage is the transport of the reactant to the catalyst surface. This may be a gas phase diffusion, or liquid phase diffusion. In some reactions, such as liquid phase hydrogenation reactions, where a solvent is commonly employed, the hydrogen gas must diffuse through the reactant and solvent to reach the submerged catalyst [4].

2. The reactants must then adsorb to the catalyst surface before any chemical reaction can occur. When molecules are associated with the metal surface through weak interactions, where the internal bonds in the molecule are unaffected, it is known as physisorption. Once adsorbed, molecules may diffuse or migrate across the surface until a catalytically active site is located. Physisorption often acts as a precursor state for stronger adsorption or chemisorption to occur [4, 5]. This involves the formation of actual bonds with the metal surface and a weakening or breaking of bonds within the molecule. The adsorption of a molecule that remains intact is known as associative adsorption whereas the chemisorption of a molecule that breaks into separate entities is known as dissociative chemisorption.

3. When both reactants are adsorbed and in the correct locations and orientations, the chemical reaction can occur facilitated by the catalyst. Transformations are carried out upon the catalyst surface and many reactions are sensitive to metal particle size and shape. The position on the surface that allows the reaction to occur is known as the active site and is often highly specific for individual reactions. A catalyst may be active for a number of different reactions although the active site required for each may be very different.

4. The reaction products are then present on the catalyst surface in an adsorbed state and must be desorbed before they can be collected. The process is a reverse of adsorption and the product to surface bonds must be severed and the molecule released into the reaction media. Any products that do not desorb and remain on the catalyst surface can have a detrimental effect on the catalytic activity.

5. The final stage in the catalytic cycle involves the diffusion of the products away from the catalyst surface and through the reaction media.

1.1.2 Catalyst Lifetime

All catalysts lose activity over time. Although the catalyst is not consumed during the catalytic reaction, a number of processes can occur which renders the catalyst less active as time goes on. The life of a catalyst is defined as being the period of time for which the catalysts keeps a sufficient level of activity or selectivity for the desired product [6]. In industrial processes maximising the active life of the catalyst is a major concern. When the catalyst no longer exhibits a level of activity that is economically attractive, the chemical plant is shut down and the catalyst replaced or regenerated. This is an expensive process and leads to a loss of productivity and income. Therefore, optimising the length of time the catalyst is left in steam is a fine balance. Efforts are concentrated on improving industrial catalysts to make them more resistant to deactivation processes and to extend their active lives. The main causes of loss of catalytic activity are described below.

1.1.3 Catalyst Deactivation

The causes of catalyst deactivation can be divided into three main categories; those with mechanical causes, those with thermal causes and those with chemical causes [6, 7]. All contribute to a loss of catalytic activity and have to be considered during the design of industrial reactors and processes.

1.1.3.1 Mechanical Causes

Mechanical failure of the catalysts can occur as a result of physical damage caused to the catalyst bed during operation of the reactor system. This can lead to a loss of catalytic material or active surface area and ultimately to a reduction in the activity of the catalyst. Industrial catalysts are prone to mechanical failure as they are frequently used in pellet, sphere or extrudate forms [7] which can become crushed due to the weight of the catalyst bed or to the load in the reactor. A decrease in the internal surface area of the catalysts particles can then occur as the catalyst pore system becomes blocked and inaccessible to the reactant molecules. Decay of the catalyst pellets by the mechanical workings of the reactor during operation is known as attrition and can lead to a reduction in size of the catalyst particles or more seriously a total break up of catalyst pellets and a generation of powdered catalyst debris known as "fines" [8]. This is a particular problem in liquid phase and slurry reactors where mechanical stirrers are used. Other mechanisms include the leaching of metal particles from the catalyst support into the reaction media and erosion of catalyst particles or coatings under high gas velocity conditions. To a certain extent a degree of mechanical failure is unavoidable but can be reduced by considering the catalyst preparation method, the catalyst support properties and the thermal and chemical pre-treatment of catalysts before use in a commercial reaction [7, 9-11].

1.1.3.2 Thermal Causes

Degradation of catalyst particles can occur as a result of the thermal treatment experienced during a catalytic reaction. The most common and significant thermal deactivation process is known as sintering and involves a loss of the catalytically

active metal surface area through a merging of metal particles into large crystallites [12-15]. At elevated reaction temperatures small, well-dispersed metal crystallites show a tendency to migrate across the support surface to form larger metal particles (Figure 1.2). There are several mechanisms of crystallite growth involving the migration of entire metal particles, the migration of individual metal atoms from one particle to another and the vapour transport of metal to join another crystallite [7]. The latter mechanism can only occur at very high temperatures and is relatively rare. The implication of a sintered metal supported catalyst is that the catalytic potential is reduced as the active metal surface area has significantly decreased. Sintering is an irreversible deactivation process and badly affected catalysts have to be replaced. However, at moderate reaction temperatures, the process is kinetically slow and can be prevented or minimised by carefully controlling the reaction conditions.

Figure 1.2: Sintering

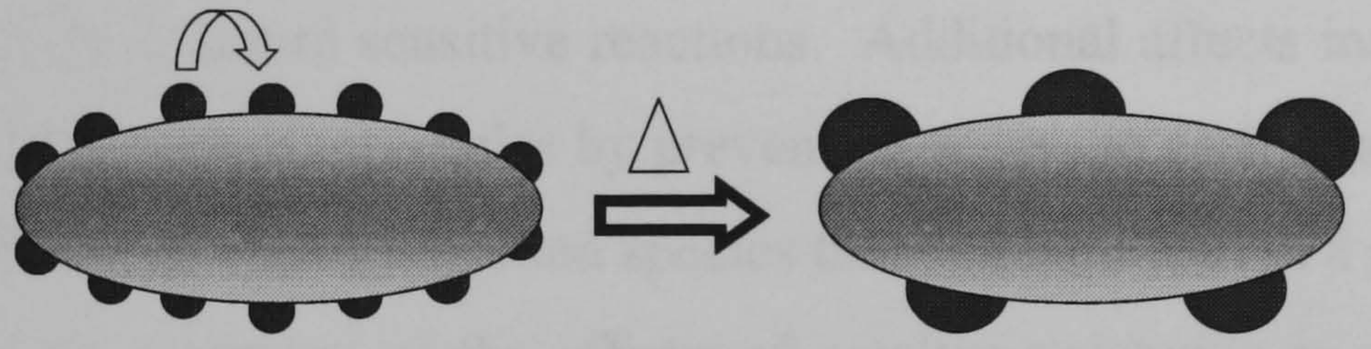

1.1.3.3 Chemical Causes

Catalyst deactivation can also be caused as a result of unfavourable chemical reactions in the reaction mixture. The two most important chemical causes of activity loss are poisoning of the catalyst and carbon lay down.

1.1.3.3.1 Poisoning

Catalyst poisoning is caused by the strong adsorption of a species to the catalyst surface leading to a decrease in catalytic activity [7, 13, 16]. Poisoning can be caused by chemisorption of the reactants, products, reaction intermediates or by impurities in feed gases and solvents. The ability of a species to act as a poison is dependent on the strength of its adsorption on the catalyst relative to the reactants. A more strongly adsorbing species will successfully compete for sites on the catalyst surface and decrease the active sites available for the catalytic process, leading to an overall loss in activity. The adsorbed poison can hinder the catalyst in several ways. The simplest way is by physically blocking the catalytically active sites on the catalysts and preventing adsorption of the reactants. However, additional changes to the catalyst surface structure and properties can also occur [16]. For example, chemisorption of a species may lead to the electronic modification of neighbouring metal atoms as a result of the strong interaction and diminishing the ability of these sites to adsorb the reactant species. The surface structure may also be changed significantly leading to an alteration in the catalytic properties of the catalyst, especially in structure sensitive reactions. Additional affects include, hampering the reaction of adsorbed molecules by preventing access to each other and the slowing of surface diffusion of the adsorbed species that can both lead to a reduction in catalytic function. A summary of the effects of catalyst poisoning is shown in Figure 1.3. Common catalyst poisons include species that possess a high degree of functionality and/or electronegativity. Sulfur containing [17-20] and nitrogen containing molecules [21-24] are an example of this although halides [25], heavy metals [26] and molecules with adsorb through multiple bonds [27] are also well known to act as catalyst poisons.

Figure 1.3: Effects of catalyst poisoning

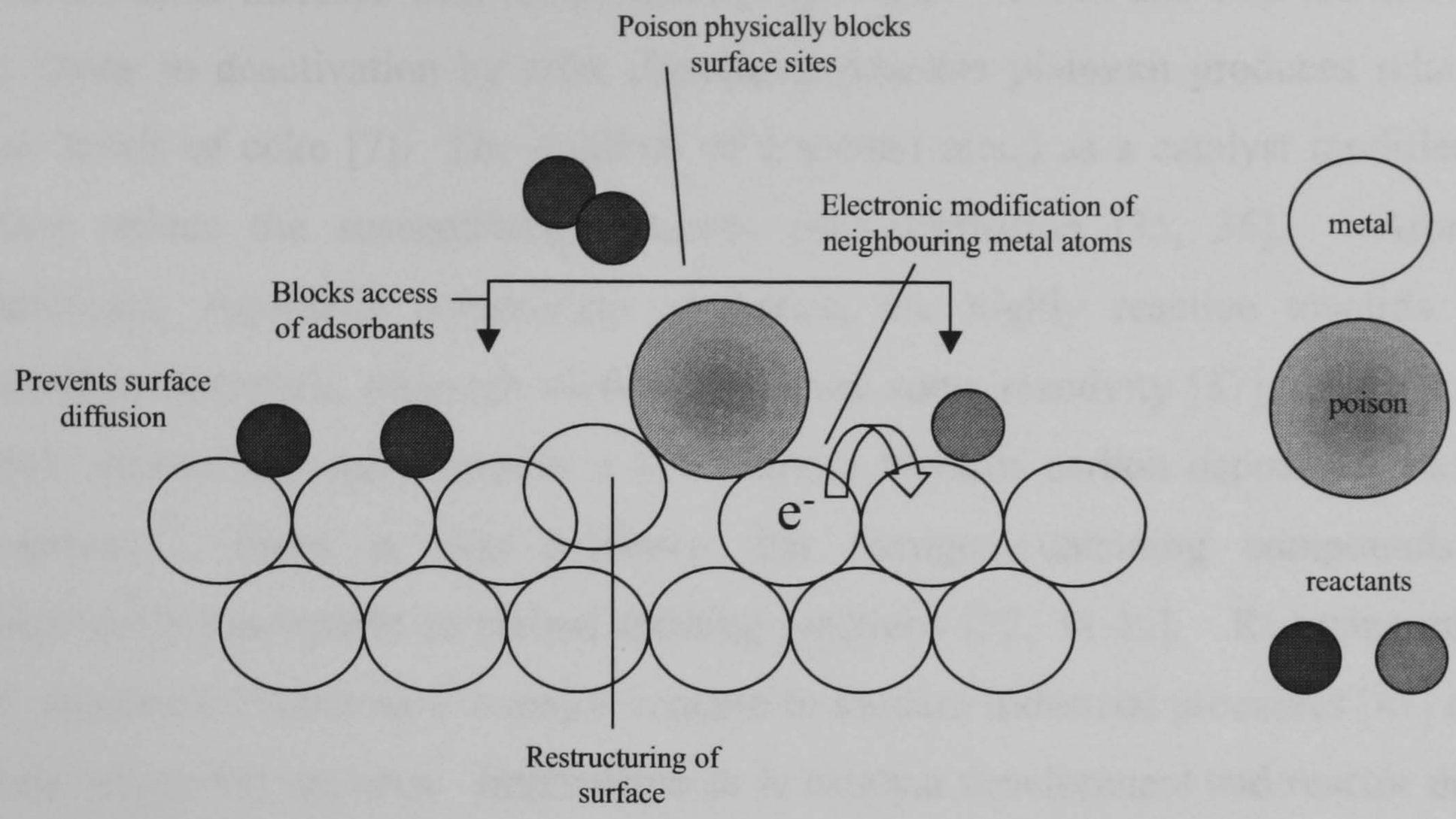

1.1.3.3.1 Carbon Lay down

The reaction of surface species to generate a deposit of carbonaceous material on the catalyst surface is known as carbon lay down or coking [28, 29]. The generation of high molecular weight hydrocarbon deposits can occur through the decomposition, condensation and polymerisation of starting materials, products or intermediate species during the catalytic reaction. Coked catalysts can become deactivated if the carbon overlayer interferes with the catalytic process. For instance if a layer of strongly chemisorbed material, or a multilayer of weakly bonded coke, forms across the active surface, the metal sites become inaccessible to the other species and reaction is prevented. Entire metal particles can become encased in coke and are rendered completely inactive as a result. Coke deposits can also penetrate into the pore systems of the catalyst support and block these channels, resulting in a dramatic loss of available surface area and a loss in activity. Under severe conditions, plugging the pores with carbonaceous material can lead to catastrophic failure and a rupturing of the catalyst particles if the internal structure is fatally strained. The rate and extent of carbon formation is a complex area that is highly dependent on the reaction conditions, the type of supported metal and the nature of the coke precursors

[28]. Numerous intricate coking mechanisms describing a wide range of deposit types have been proposed in the literature [13, 30-33] and they are generally considered to increase with temperature [34]. Nickel, cobalt and iron are known to be prone to deactivation by coke deposition whereas platinum produces relatively low levels of coke [7]. The addition of a second metal as a catalyst modifier can often reduce the susceptibility towards coke formation [35, 36]. Aromatic molecules, especially polynuclear aromatics, are highly reactive towards coke formation reactions, although olefins also show some reactivity [37], while straight chain alkane molecules display a low activity towards carbon deposition forming reactions. There is also evidence that nitrogen-containing compounds are particularly susceptible to carbon forming reactions [22, 38-40]. Reducing coking of commercial catalysts is a major concern to modern industrial processes [41] and a focus of current research. Improvements in catalyst development and reactor design are sought to minimise the coking problem as much as possible.

1.2 The Aniline Industry

Aniline is a vitally important chemical that is used extensively in laboratory organic synthesis and larger scale industrial applications [42-44]. A reliable method of aniline production is required to provide a constant feed to many wide ranging industries including the pharmaceutical, automotive and construction industries.

1.2.1 The Synthesis of Aniline

There are several methods of synthesising aniline using a variety of starting materials but nitrobenzene is the classical and the most frequently used feedstock. On the small scale, aniline can be produced by the chemical reduction of nitrobenzene in a process known as the Bechamp reaction [45-47] (Figure 1.4). This traditional method involves the use of iron and water in the presence of hydrochloric acid to reduce the nitro-group to the amine. This was also the first method used in the industrial production of aromatic amines back in 1854 and had the advantage that

valuable iron oxide pigments could be salvaged from the iron oxide residues produced as a side product during the reaction [47]. The Bechamp reaction is still currently utilised by Bayer to produce a range of iron oxide pigments using a batch process but not for the commercial production of aniline.

Figure 1.4: The Bechamp Reaction.

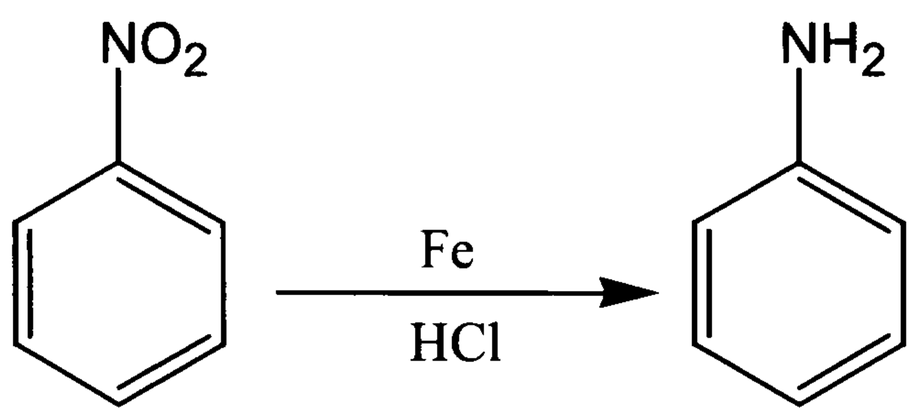

More recently, the Bechamp reaction was surpassed by a more economically viable route, the catalytic hydrogenation of nitrobenzene. In this process the aromatic nitro-group is reacted with three mole equivalents of hydrogen gas, in the presence of a suitable catalyst, to produce the amine and water. This hydrogenation is very easily carried out under relatively mild conditions and produces only a very low level of by-products and impurities. As it does proceed so easily, it occurs rapidly over most metals and is often employed as a reference reaction to compare the activity of other hydrogenation catalysts [48-54] and of new reactor systems [55-59]. Currently, using the heterogeneously catalysed hydrogenation of nitrobenzene, aniline can be produced with greater than 99 % selectivity. Details of the commercial reactions in operation and industrial catalysts are given in a following section (Section 1.2.2).

Although utilised to a lesser extent, three additional catalytic routes have been used in the production of aniline. The first route involves the amination of chlorobenzene [45]. For instance, the Kanto Electrochemical Co. Process involves the ammonolysis of chlorobenzene using aqueous ammonia over a Niewland catalyst: a mixture of copper (I) chloride and ammonium chloride, to produce aniline and hydrochloric acid as reaction products. This process is 91 % selective for the amine and was previously employed by Bayer until 1986 when it was discontinued for economic reasons [45].

A second route towards aniline, uses phenol as the starting material and again involves ammonia in the amination process [45, 47]. The hydroxyl group on phenol is reacted with gaseous ammonia over an $Al_2O_3.SiO_2$ catalyst to produce aniline and water as products. This method has become of greater importance over recent years as phenol technology has progressed. The development of a novel single-stage transformation of benzene to phenol has increased the availability of phenol as a feedstock [60].

In addition, Du Pont have investigated a third route to aniline using benzene as the starting material to produce aniline directly without the need for a nitrobenzene intermediate [45]. Benzene is reacted with concentrated ammonia over a NiO/Ni catalyst promoted with zinc oxide. An aniline selectivity of 97 % was observed with this route although a maximum benzene conversion of only 13 % was achieved and proved to be a barrier to industrial scale production.

Despite the investigations into these alternative route the method of choice for the production of aniline continues to be the hydrogenation of nitrobenzene using a heterogeneous catalyst.

A summary of all four methods is shown in Figure 1.5.

Figure 1.5: Industrial routes to aniline

(i) The catalytic hydrogenation of nitrobenzene

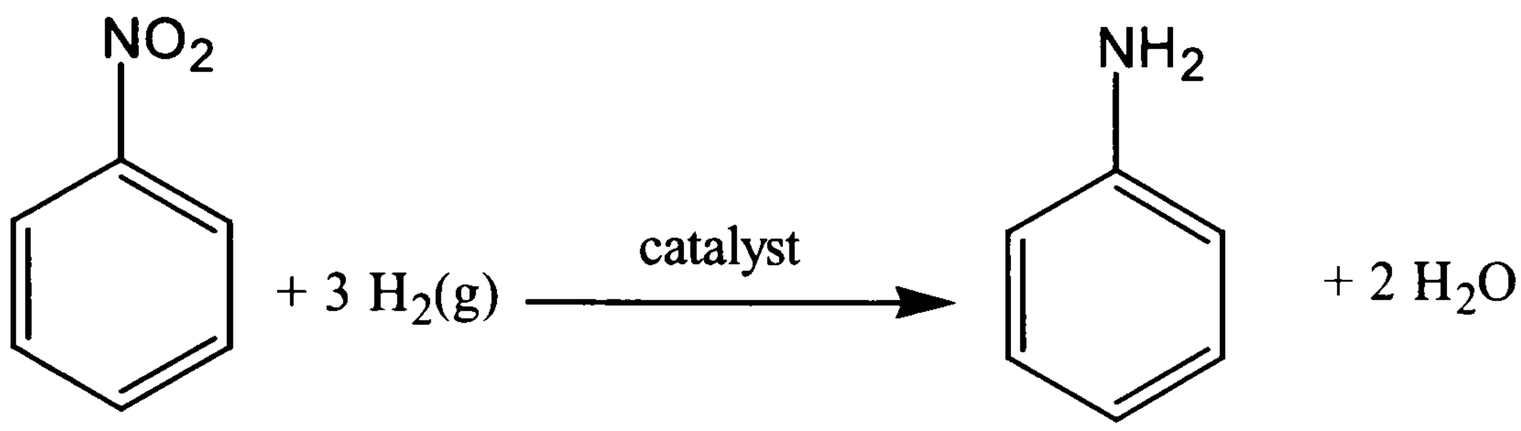

(ii) The amination of chlorobenzene

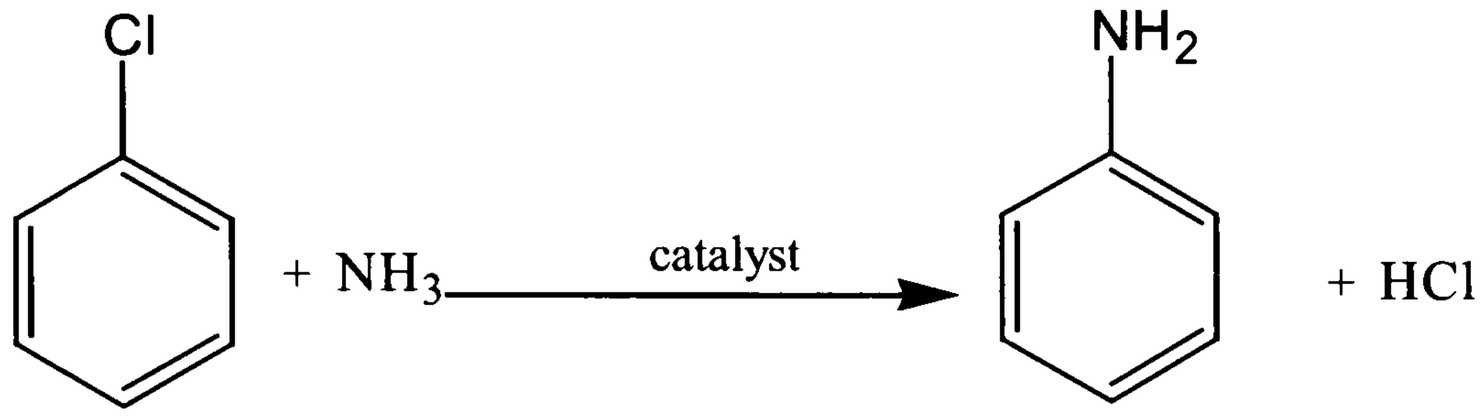

(iii) The amination of phenol

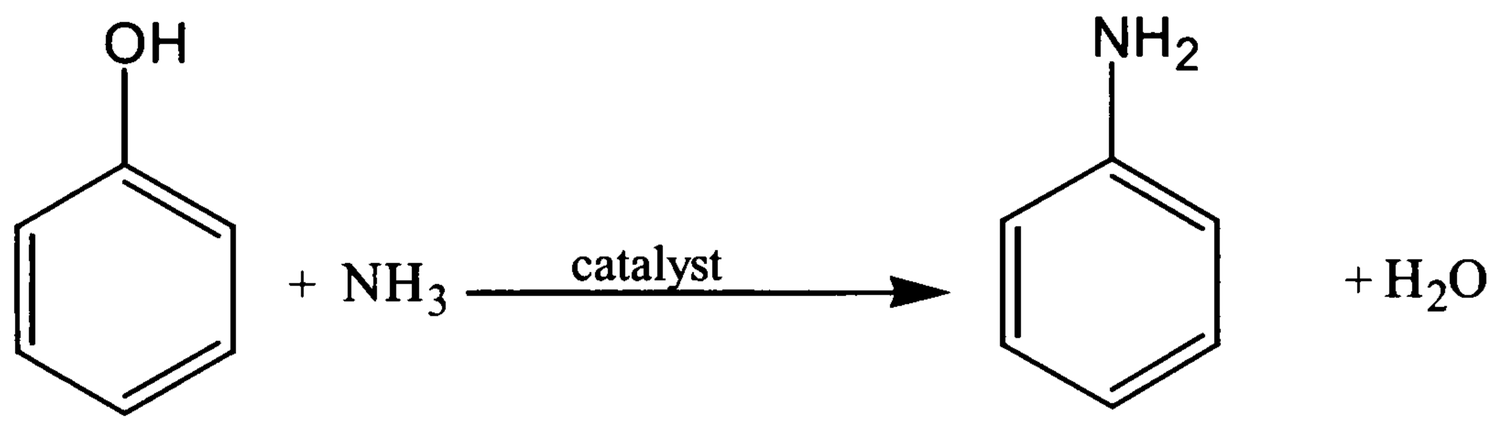

(iv) The amination of benzene

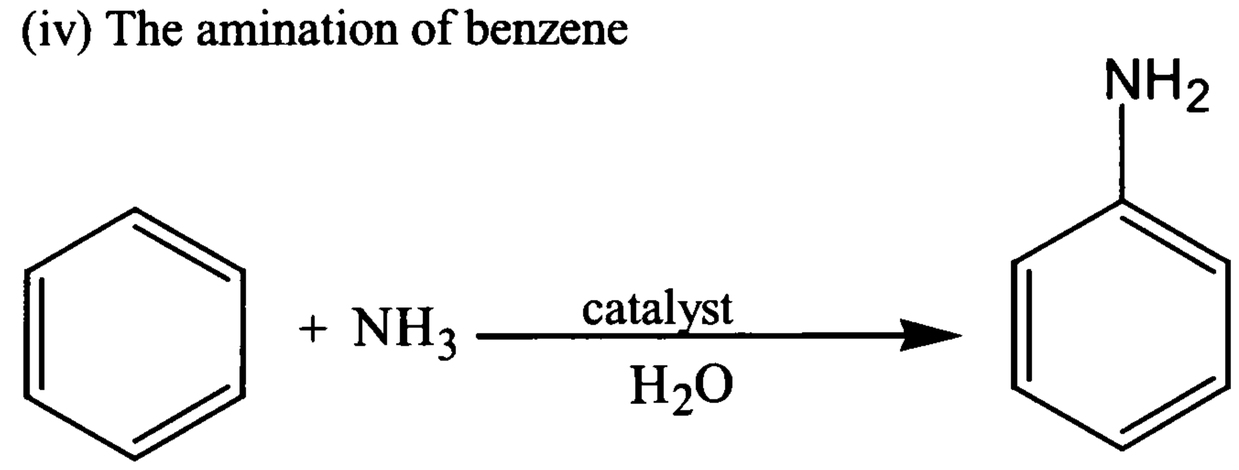

1.2.2 The Commercial Production of Aniline

As already stated, the commercial production of aniline is carried out almost exclusively using a heterogeneous catalyst to effect the hydrogenation of nitrobenzene. The basic reaction is illustrated in Figure 1.5 however; the reaction conditions and industrial catalysts vary widely depending on the specific aniline producer.

During 2001, the global capacity for aniline stood at 3.0 million tonne/year and total production reached 2.6 million tonne/year [47]. The majority of global aniline production is centred in the U.S, Western Europe and Asia with Western Europe alone contributing 42.2 % to the world's aniline stocks [61-63]. In 2003, five companies dominated the European market and between them produced the entire Western European aniline output. These organisations were Bayer, Huntsman, BASF, Dow and Quimigal and the percentage contribution made by each company is shown in Figure 1.6 [47].

Figure 1.6: Aniline Capacity Share by Company in Western Europe, 2003

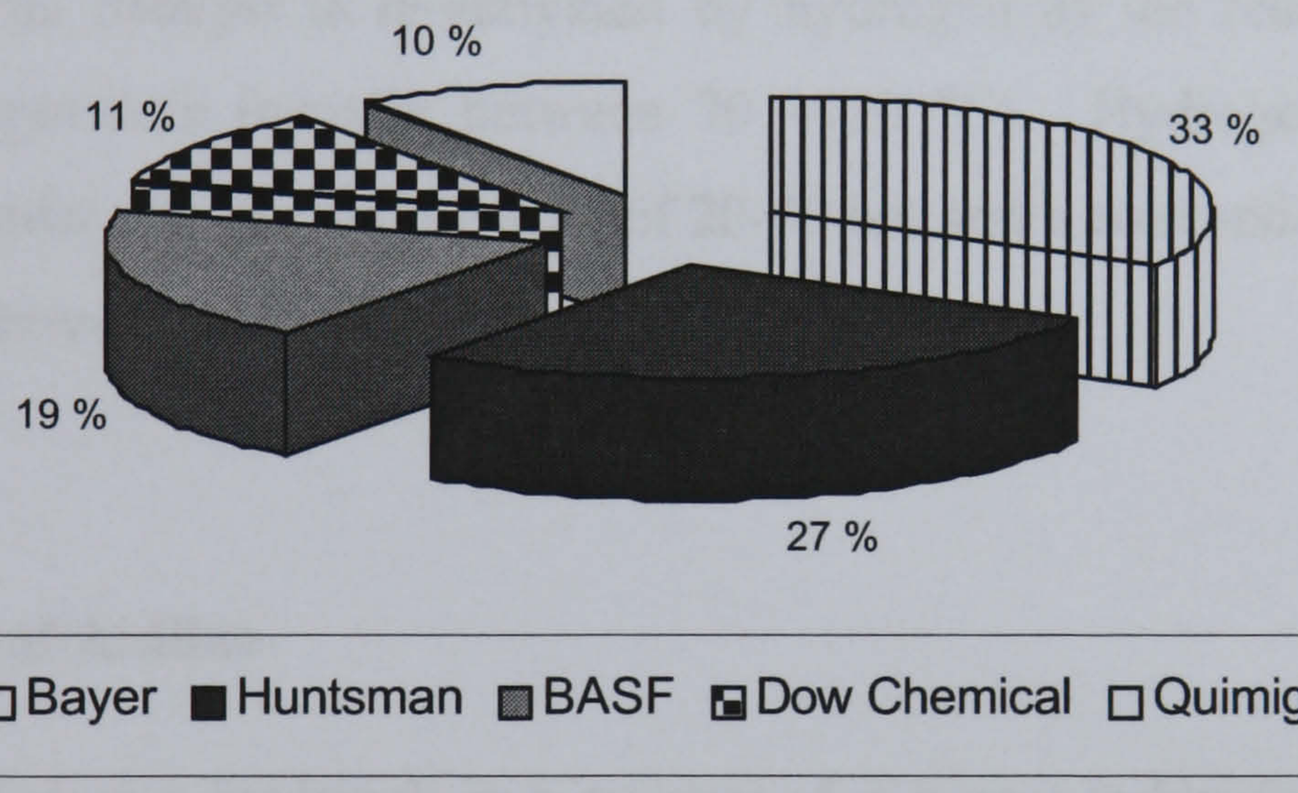

The nitrobenzene hydrogenation process may be carried out in either the gas phase or liquid phase and both are used in commercial production.

Of the aniline producers using a gas phase process, Bayer utilises a fixed-bed of NiS catalyst that has been activated using copper or chromium [46]. Reactions are performed at temperatures ranging from 573-748 K and aniline selectivities greater than 99 % are achieved. The catalyst bed is prone to catalyst deactivation due to carbon deposition but can be regenerated in air at 523-623 K followed by H_2 (g) passivation.

On the other hand, a fluidised bed is utilised for the hydrogenation process operated by BASF using catalysts based on copper with chromium, barium and zinc oxides on a SiO_2 support [46]. Reaction conditions range between 543-563 K in temperature and 1-5 bar in pressure and a large excess of hydrogen is used. This method exhibits a high selectivity for aniline at 99.5 % but is also subject to deactivation of the catalyst bed that must be regenerated in air at regular intervals throughout production.

The liquid phase hydrogenation of nitrobenzene is also performed industrially with Huntsman employing a semi-continuous batch process using a stirred tank reactor to produce aniline [64]. A typical catalyst consists of 55 % by weight of nickel supported on Kieselguhr extrudates that has been pre-reduced and stabilised before use [65]. The catalyst is re-activated by hydrogen as the reactor vessel reaches reaction temperature (usually between 70 –150 ^{o}C). Hydrogenation is generally performed under a hydrogen pressure of 20-40 bar and a conversion in excess of 99.7 % can be achieved.

1.2.3 Uses of Aniline

Aniline is used as a feedstock in a number of different industries leading to a wide range of industrial and everyday applications. A representation of the relative end use of aniline is shown in Figure 1.7.

Figure 1.7: Uses of Aniline in the Global Market, 2003

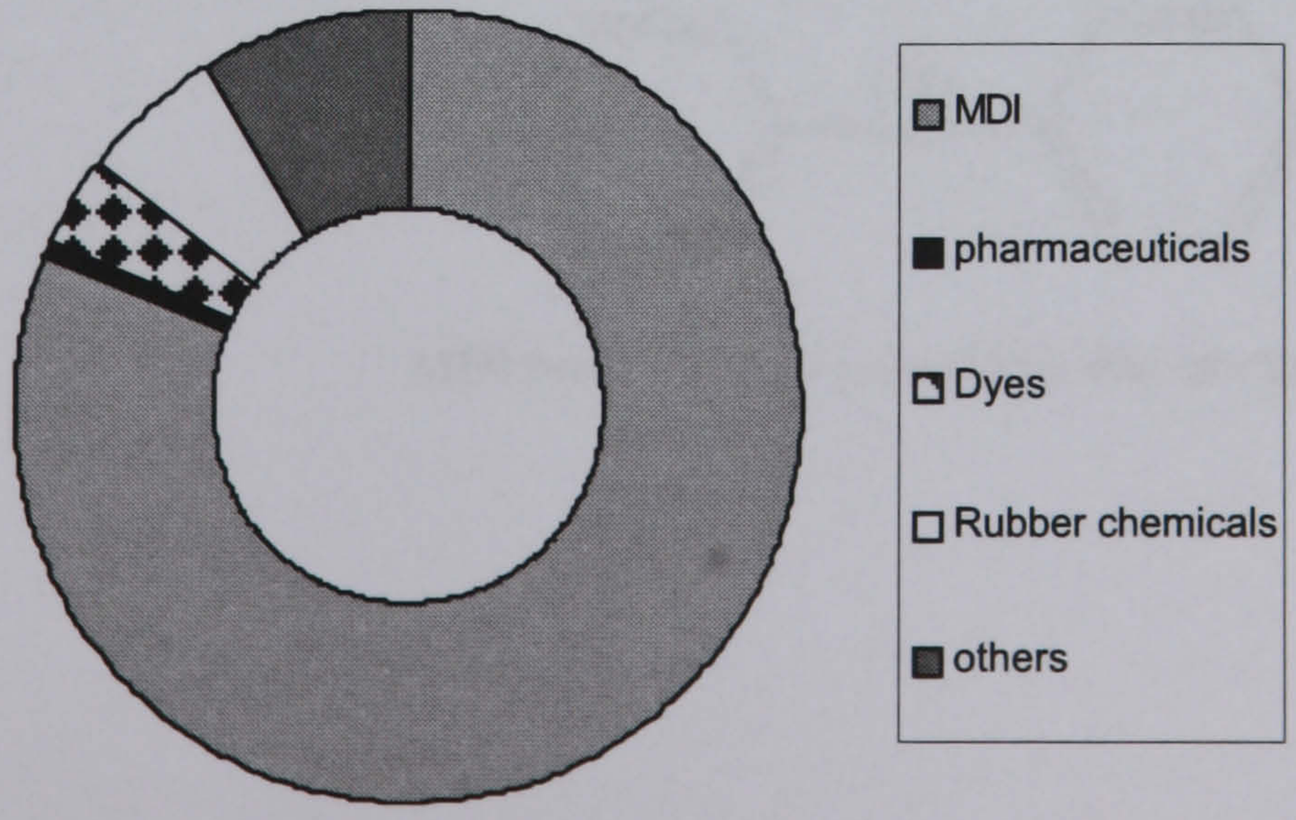

The vast majority of global aniline, between 80%-85%, is consumed in the production of MDI (methylene di-para-phenylene isocyanate) [46, 47, 62]. MDI is synthesised in a two-phase process, shown in Figure 1.8 [66, 67], including condensation with formaldehyde to produce a dimeric species then phospenation to transorm the amine functionality to isocyanate groups. This is also a growing industry, as presently, the demand for MDI is increasing steadily at 6%-8% per year [47]. MDI is then polymerised and used to synthesise extremely versatile materials known as polyurethanes.

The majority of the remainder of the aniline supply is used in the production of a number of other products namely aniline dyes, rubber additives and pharmaceuticals. In addition, it is also utilised by the agricultural industry to synthesis pesticides and herbicides and to make photographic developers, explosives and speciality fibres [68].

Figure 1.8 The Synthesis of MDI from Aniline.

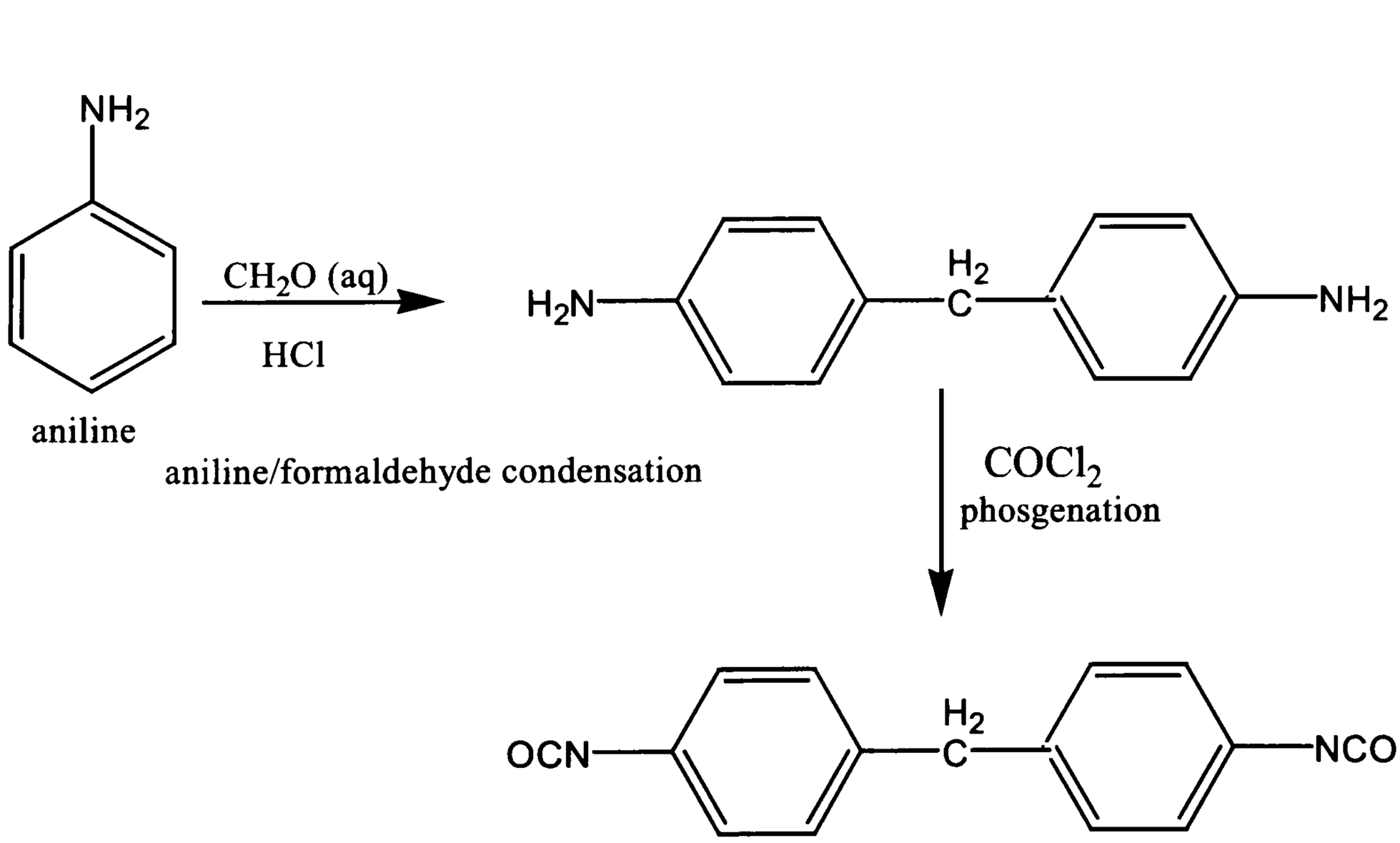

MDI (methylene di-para-phenylene isocyanate)

1.2.3.1 Polyurethanes

Polyurethanes are synthesised by diisocyanate addition polymerisation, a method discovered by Bayer in 1937 [66]. This involves the reaction of a diisocyanate with a polyhydroxyl compound in the presence of a suitable catalyst and additives [44, 66, 69, 70]. A variety of diisocyanates and hydroxylated compounds can be used in the reaction leading to a range of polymeric products with different physical properties. The most common commercial methods utilise a diisocyanate and hydroxyl terminated polyester or polyether. The formation of polyurethane is shown in Figure 1.9.

Figure 1.9: The formation of a polyurethane.

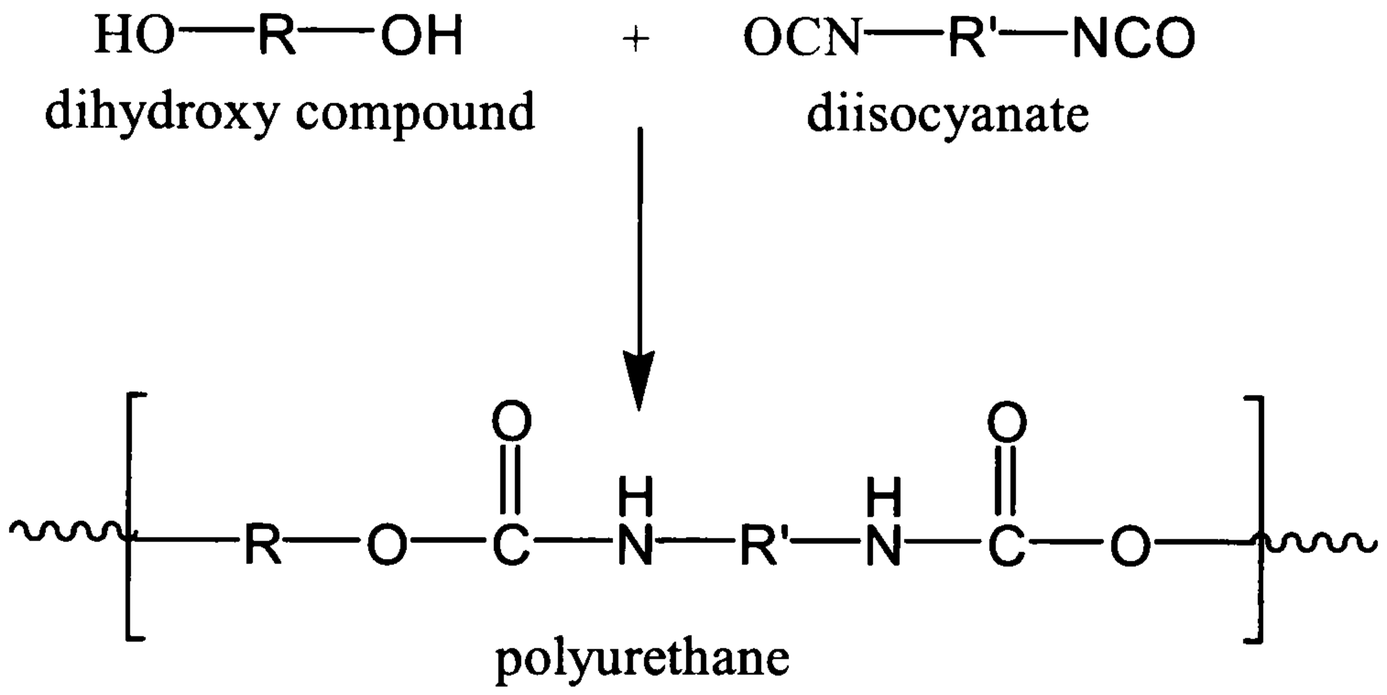

MDI polyurethanes are versatile polymers used in the manufacture of rigid and semi-rigid foams, elastomers and coating resins. These materials are typically used in the construction industry for building insulation, white goods industry for insulation, in the automotive industry for car interiors and in the sportswear industry for flexible trainer soles [67, 71, 72].

1.3 The Heterogeneously Catalysed Hydrogenation of Nitrobenzene

As previously stated the nitrobenzene hydrogenation reaction is widely used as a test reaction to rate the activity of novel hydrogenation catalysts or reactor systems. As a result there is a huge amount of literature available in the scientific press citing the use of this reaction. Despite this, relatively little information exists regarding the actual reaction and its mechanism. The following sections aim to summarise the literature relevant to this thesis, those focusing on the reaction kinetics, reaction mechanism or some other aspect of the reaction, and it is not intended to review every study using the nitrobenzene hydrogenation reaction.

1.3.1 Adsorption of Nitrobenzene and Aniline to the Catalyst

The initial step in any heterogeneously catalysised reaction involves the adsorption of the reactant species on to the active metal surface. The nitrobenzene molecule has two main functionalities available for bonding to a metal surface: the nitro group, via the lone pairs on oxygen, and the aromatic ring. Both can interact with the metal surface and the dominant interaction will effect the orientation of the molecule with respect to the surface plane. The same is true of aniline and the possible interactions and molecule orientations are displayed in Figure 1.10.

Figure 1.10: The adsorption of nitrobenzene and aniline to a catalyst surface

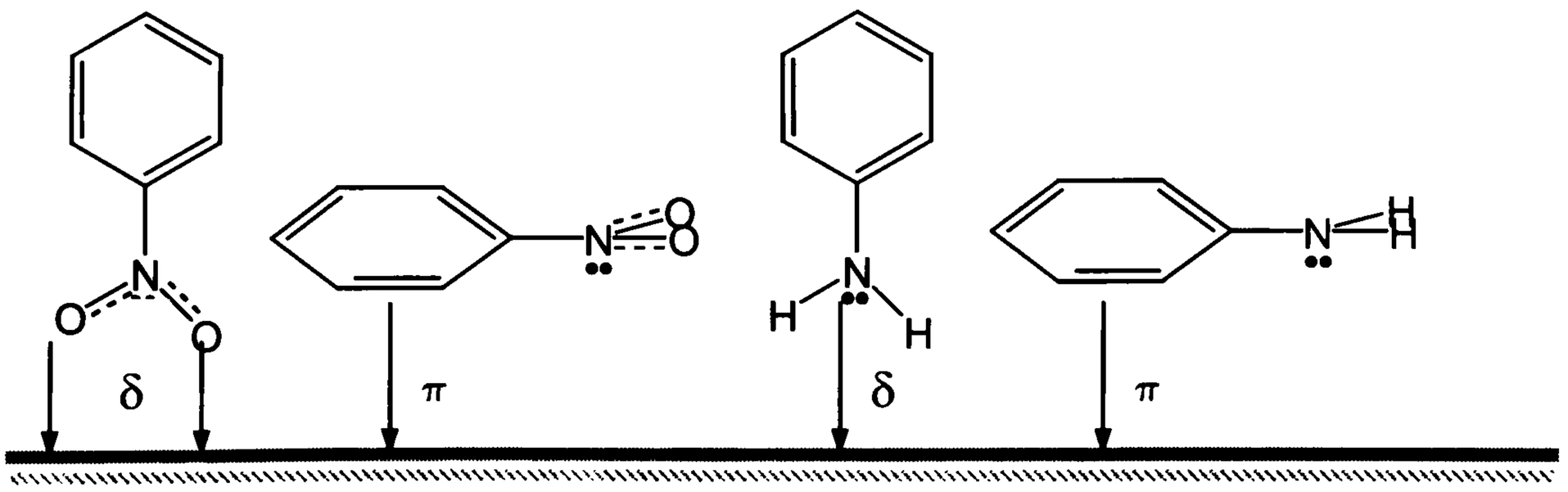

The nitrogen atom in the nitrobenzene molecule is part of the nitro motiety, a strongly electronegative group, whereas the nitrogen atom in the aniline molecule is bonded to hydrogen atoms. Therefore, the adsorption behaviour of both molecules would be expected to be very different.

The adsorption of the reactant, nitrobenzene, and the product, aniline, onto the surface of a range of metals has been investigated using a variety of surface science techniques. Chen and co workers [73] used Fourier transform IR spectroscopy to study the adsorption of nitrobenzene onto a Cu (110) surface. They reported that the adsorbed molecule was orientated at an angle of 43 +/- 5 ^{o} away from the metal plane indicating that the nitro group was directly involved in bonding to the copper surface and although a degree of π-bonding was possibly occuring, the dominant interaction was the sigma bond. Chen also reported that the adsorbed nitrobenzene could be decomposed through dissociation of the nitro group to form adsorbed benzene. This again suggests that a strong surface interaction had occurred via the nitrogen atom allowing the internal nitrobenzene C-N bond to be broken before the ring aromaticity was lost. A similar tilted orientation was also observed in a variety of other nitro containing aromatics, at low temperature and multilayer coverage. Adsorption through the nitro group, was also observed in a number of other studies including two by Leonid Gorb's group, investigating the adsorption of nitrobenzene onto alumino-silicate minerals using experimental techniques and computer simulation [74, 75]. Their investigations could find no stable structure involving the adsorption of nitrobenzene via π-interactions with the aromatic ring. Further analysis using density functional theory by the same authors [76] found both nitrobenzene and nitrosobenzene to adsorb to an iron oxide surface via the nitrogen functionality. In addition, infra red studies by Meijers and Ponec also reveal the nitrobenzene molecule to be adsorbed via the nitro-group [77]. However, early electron spin resonance measurements regarding the adsorption of nitrobenzene to metal oxides does not completely rule out some level of π-interaction through the aromatic ring [78].

The adsorption of aniline onto a variety of metal surfaces has also been thoroughly discussed in the chemical literature. Huang, Fischer and Gland, in their study of the

Pt (111) surface [79], established a tilted orientation, similar to that seen with nitrobenzene, with adsorption occurring via the nitrogen lone pair. However, in the presence of coadsorbed hydrogen the orientation altered to a parallel position and π-bonding of the aromatic ring to the surface became the dominant interaction. This situation was also confirmed by these authors in later publications using the Ni (111) and Ni (110) surfaces [80, 81]. Whereas, Meijers and Ponec [77] found little perturbation of the aromatic infra-red signals on adsorption of aniline to metal oxides suggesting the aromatic ring was not involved in bonding to the surface.

1.3.2 The Reaction Kinetics and Thermodynamics

Once the reactants have become adsorbed to the catalyst, the catalytic reaction can occur. A catalyst can allow kinetically inert reactions to proceed at ambient pressures and temperatures, or dramatically increase the rate of an already viable reaction. However, a catalyst cannot initiate reactions that are thermodynamically impossible.

1.3.2.1 The Thermodymanics of Nitrobenzene Hydrogenation

The nitro group is one of the most easily performed of all functional group hydrogenations [82] with only the hydrogenation of the acetylene group occurring almost as fast. As a result only very mild reaction conditions are required [83]. The apparent activation energy for nitrobenzene hydrogenation has been determined over a number of supported metal catalysts including nickel [84-87], copper [84], palladium and platinum [86-88] and palladium/silver alloys [89]. All activation energies were calculated between the range of 12-104 kJ mol^{-1} showing that hydrogenation is extremely facile. An estimated value of the equilibrium constant for the nitrobenzene hydrogenation reaction of 1.53×10^{84} at standard temperature and pressure appears in the literature [86] and indicates that reaction may be considered totally irreversible for all practical purposes. In addition, the transformation is extremely exothermic with quoted ΔH values of 545 kJ mol^{-1} [58] and 443 kJ mol^{-1} which is equivalent to an adiabatic temperature increase of 2400 K

mol^{-1} [90]. Therefore, controlling the temperature during the reaction is a major consideration and for this reason solvents are commonly employed during liquid phase reactions to help dissipate the heat.

1.3.2.2 The Kinetics of the Nitrobenzene Reaction

There have been many studies on the kinetics of the hydrogenation of nitrobenzene, the majority of which were in the liquid phase and a variety of kinetic proposals have been put forward.

1.3.2.2.1 Kinetics of Liquid Phase Hydrogenation

As expected for a hydrogenation reaction, a first order dependence on hydrogen concentration was widely reported [91-93]. Hatziantoniou, Andersson and Schöön [59] also reported a first order dependence on hydrogen at pressures below 0.3 bar, and that the order began to approach zero as the pressure was raised further. However, some variations from this were also described. For instance, Aramendia and coworkers, using pressures of 4-7 bar, found a partial reaction order with respect to hydrogen that increased towards first order as the reaction temperature was increased [88]. However, Metcalfe and Rowden reported a higher order in the range of 1.23-1.28 with respect to the hydrogen concentration [89], when working at hydrogen pressures below 1 bar, and Collins and coworkers a reaction order exceeding 2 at 1 bar [94]. The order of reaction with respect to hydrogen appears to be a complicated area that can be affected by a number of factors including temperature, reactor pressure and mass of catalyst. However, at sufficently high pressures the rate dependence on hydrogen was generally found to be first order.

Similarly, wide variations in the reaction order with respect to the nitrobenzene concentration have been reported in the scientific literature. Like the hydrogen order, the value for nitrobenzene appears to influenced by a high number of factors. Zero order reactions with respect to nitrobenzene, at concentrations around 0.3 mol L^{-1}, have been reported by Li et al. in their hydrogenation study over a supported

platinum catalyst [93]. A reaction order equal to zero was also determined by Collins, Smith and Davis using 1 mol L^{-1} concentrations of nitrobenzene [94]. In addition, a study of nitrophenol hydrogenation by Yao and Emmett displayed a zero order dependence on the nitroarene at concentrations ranging between 0.3-0.7 mol L^{-1} [92]. However, the situation is possibly more complex than this, as a variety of other observations have also been discussed. A zero order dependence on the nitro-compound has been reported by Kalantri and Chandalla [95] over supported palladium at a variety of temperatures and pressures. Partial order reaction orders have also been reported for the substrate. For example a recent study by Holler et al. [91] states a zero order reaction dependence at high nitrobenzene concentrations (greater than 0.1 mol L^{-1}), whereas, a first order reaction dependence when the nitrobenzene concentration was low. This was similar to work published by Hatziantoniou's group [59], where a first order dependence on nitrobenzene concentration was experienced under 0.02 mol L^{-1}, tending towards zero order as the concentration was increased above this point. Conversly, Metcalfe and Rowden found that at concentrations below 0.15 mol L^{-1} the reaction proceeded with a zero oder dependence on the nitrobenzene concentration, however, as the concentration was increased above 0.15 mol L^{-1}, the reaction rate began to decrease indicating the nitrobenzene reaction order had become negative [89]. Other studies reporting a negative reaction order with respect to the nitrobenzene concentration were published by Acres and Bond in 1966 [96] and Acres and Cooper in 1972 [97]. Fractional reaction orders with respect to nitrobenzene have also been reported. For example, an additional study by Yao and Emmett on the hydrogenation of aromatic nitrocompounds has shown a partial reaction order with respect to the nitrocompound [87]. As with hydrogen, the order of reaction with respect to nitrobenzene is variable and appears to be sensitive to the specfic reaction conditions.

1.3.3 The Reaction Mechanism

1.3.3.1 Haber's mechanism

Despite, or possibly as a result of, the large number of often-conflicting studies on the reaction kinetics, the only proposed mechanistic scheme for the hydrogenation of nitrobenzene was published by Haber back in 1889 [98] (Figure 1.11). A three-step process was described for the electrochemical reduction of nitrobenzene to aniline. First, one of the nitrogen-oxygen bonds is hydrogenolysed, and an oxygen atom lost, to produce the first intermediate, nitrosobenzene. This is followed by addition of two hydrogen atoms across the remaining nitrogen–oxygen double bond to give the compound, phenylhydroxylamine. The third step involves loss of the second oxygen to form the final product, aniline. Haber also described the formation of dimeric by-products, azoxybenzene, azobenzene and hydrazobenzene, explaining their formation as a result of the reaction of the two intermediate products, nitrosobenzene and phenylhydroxylamine. One of these dimeric compounds, hydrazobenzene, could also undergo a rearrangement reaction to produce a species coupled via the aromatic rings. In addition, hydrogenation of the aromatic ring in the product aniline to produce cyclohexylamine was also proposed.

Figure 1.11: Haber's nitrobenzene hydrogenation mechanism

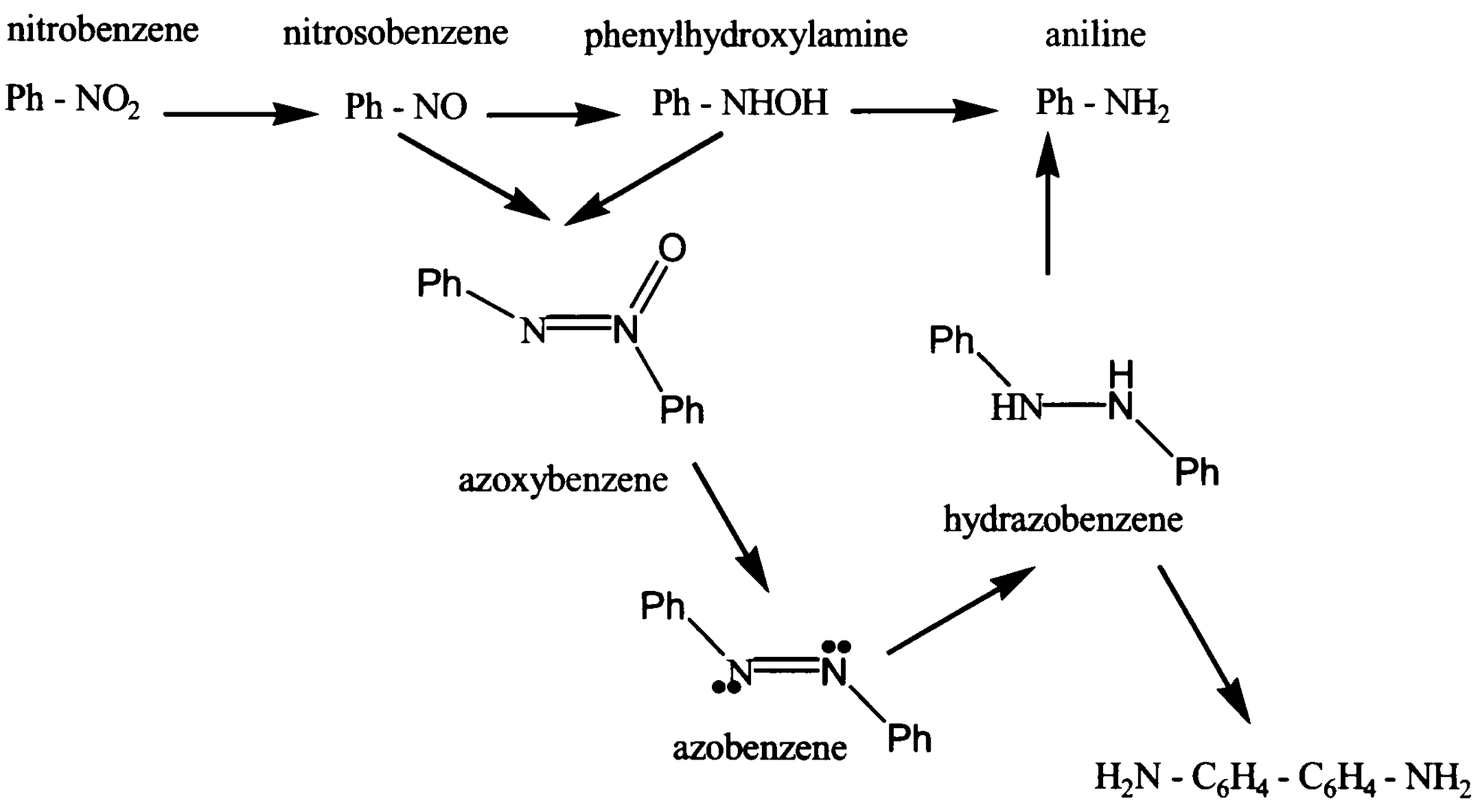

1.3.3.2 Other Mechanistic Studies

Of the few published studies probing the reaction mechanism few were carried out in the gaseous phase. Brown and Henke back in 1922 [99] investigated the reaction over copper and nickel and Gharda and Sliepevich (1960) over copper [100]. Aniline was produced as the sole product over copper and over-hydrogenation products, such as cyclohexyamine, benzene and ammonia were observed over nickel. Due to the lack of by-products little mechanistic information could be deduced.

Studies by Debus and Jungers in 1958 [85] examined the hydrogenation of nitrobenzene, nitrosobenzene, phenylhydroxylamine, azoxybenzene, azobenzene and hydrazobenzene over Raney nickel. It was reported that all six compounds hydrogenated through to aniline with different by-products observed in each reaction. During hydrogenation of nitrobenzene, low levels of phenylhydroxylamine were identified as the only other product. However, during the hydrogenation of nitrosobenzene, hydrazobenzene was detected and explained as a result of the reaction of nitrosobenzene and phenylhydroxylamine to form azoxybenzene and further hydrogenated to hydrazobenzene. No intermediate species were observed during the hydrogenation of phenylhydroxylamine. Hydrogenation of the three dimeric species followed the predicted pattern: azoxybenzene to azobenzene to hydrazobenzene before finally producing aniline. As a result of their research Debus and Jungers concluded that the mechanism for the hydrogenation of nitrobenzene was complex and involved a number of concurring reactions and added a level of complexity to Haber's scheme. However, they did not propose any adaptation to the basic mechanistic framework. Nitrosobenzene was thought to react with aniline to form azobenzene, in addition to the reaction with pheylhydroxylamine to form azoxybenzene. It was also suggested that phenylhydroxylamine was able to undergo a rearrangement to form para-hydroxy-aniline, which did not react further but remained in solution as a by-product. Since this publication, no further reports of the identification of this species in nitrobenzene hydrogenation mixtures appear to have been made.

Burge, Collins and Davis examined the liquid phase reaction over Raney nickel [101]. The immediate appearance of azoxybenzene from nitrobenzene was observed

and the production of aniline commenced after a considerable hydrogenation time. Two additional reaction intermediates were visible; one identified as azobenzene and one thought to be hydroxyazobenzene. No nitrosobenzene or phenylhydroxylamine were detected throughout the reaction. The authors concluded that their results could be adequately explained using the Haber mechanism on the basis of two important assumptions. Firstly, it was proposed that the hydrogenation of nitrosobenzene and phenylhydroxylamine occurred rapidly, as did a coupling reaction between the two to form azoxybenzene and hence neither compound was visible in solution. It was also assumed that nitrobenzene was more strongly adsorbed than azoxybenzene throughout the reaction to explain the high levels of the dimeric species present throughout hydrogenation. However, throughout the paper no explanation was offered as to why the production of aniline was apparently delayed until after the azoxybenzene concentration had reached a maximum.

Wisniak and Klein [86] investigated the liquid phase reaction over Raney nickel in 1984 and reported that the Haber mechanism was not valid for their experimental results. Furthermore, they proposed that the hydrogenation mechanism was more complex than first thought and most likely involved a surface phenomonen unaccounted for in previous mechanistic studies. During experimental work only azoxybenzene and azobenzene were observed as intermediate products, so the involvement of other species could only be arrived at through speculation. However, a number of reaction schemes were tested, all based on Haber's original proposal, but with varying degrees of complexity. The reaction of phenylhydroxylamine and nitrosobenzene to form azoxybenzene, the reaction of aniline with both intermediate species and with nitrobenzene, and a route avoiding nitrosobenzene and phenylhydroxylamine completely, were all considered but rejected due to poor data fitting.

Maestro, Aracil and Martínez [102] studied the nitrobenzene hydrogenation mixture using GC-MS and identified the presence of nitrosobenzene, phenylhydroxylamine, azoxybenzene and azobenzene in addition to nitrobenzene and aniline. Reactions were done over Raney nickel at atmospheric pressure under a flow of hydrogen, so would be expected to proceed much more slowly than pressurised reactions, which

may explain the ability to detect the intermediate species more easily. On the basis of the identification of the intermediates specified in Haber's mechanism in their reaction mixtures, Maestro concluded that this mechanism was followed over Raney nickel in the liquid phase. However, no other supporting evidence was supplied.

In 2000, Holler and coworkers [91] published a study of the nitrobenzene hydrogenation reaction over supported platinum and palladium catalysts. Over the palladium catalysts only nitrobenzene and aniline were observed; no intermediate species were detected. However, over platinum a range of additional species was identified (nitrosobenzene, phenylhydroxylamine, azoxybenzene and azobenzene). The mechanism suggested for the transformation over both catalysts was identical to Haber's initial publication. Justification for this mechanism was provided by an in-depth kinetic analysis of the experimental reaction rates and invoked an Eley-Rideal type mechanism, where gaseous molecular hydrogen was reacted with adsorbed nitrobenzene. The validity of this assumption, especially over platinum and palladium metals, is questionable as hydrogen would be expected to dissociate into a chemisorbed state at the catalytic surface [103].

1.3.3.3 Hydrogenation of Haber's Proposed Intermediates

The hydrogenation of nitrosobenzene and the other intermediate species in Haber's scheme has not been studied extensively and to date few studies into these reactions have been published in the scientific press. However, all have been shown to hydrogenate through to aniline and are detailed in a review by Figueras and Coq in 2001 [104].

Scholnik and co-workers performed a number of hydrogenations using Raney nickel back in 1941 [105], including that of nitrobenzene, nitrosobenzene and phenylhydroxylamine. Under identical experimental conditions, it was found that nitrosobenzene would not react, with no up-take of hydrogen observed, whereas nitrobenzene hydrogenation proceeded through to aniline with a smooth rate. They concluded that nitrosobenzene was not acting as an intermediate to nitrobenzene hydrogenation. However, no alternative mechanism was suggested.

In 1994, Smith, Song, Gasior and Malz [106] investigated the nitrosobenzene reaction over a selection of Pd/SiO_2 catalysts at low pressure and room temperature. They also performed the hydrogenation of nitrobenzene and phenylhydroxylamine, azoxybenzene and azobenzene. It was reported that nitrobenzene and phenylhydroxylamine hydrogenated through to aniline in a smooth reaction with very low levels of by-product/intermediate formation. In contrast, the reaction profile for nitrosobenzene hydrogenation was markedly different. Nitrosobenzene was immediately hydrogenated to azoxybenzene, which was then reacted to form aniline and hydrazobenzene. Phenylhydroxylamine and azobenzene were also detected in the reaction mixture. Further experiments hydrogenated azoxybenzene and azobenzene to form hydrazobenzene, which could not be hydrogenated further under these reaction conditions. Significantly, Smith et al also reported a higher rate of reaction during the hydrogenation of nitrosobenzene than with nitrobenzene but, despite this, concluded that Haber's mechanism had been followed.

The reactivity of phenylhydroxylamine over a variety of clay catalysts was examined by Grošková and co-workers in 2000 [107]. Phenylhydroxylamine was found to produce aniline and nitrosobenzene via a disproportionation reaction in a variety of solvents at neutral and alkaline pHs. Azoxybenzene was also detected in some reactions and thought to be the product of nitrosobenzene and phenylhydroxylamine coupling. Azoxybenzene was also identified in some reaction mixtures when no nitrosobenzene was detected. Studies in the reactivity of nitrosobenzene [108, 109] have also shown that phenylhydroxylamine will react readily with nitrosobenzene to form azoxybenzene under alkaline conditions. It should be noted though that these studied were performed in the absence of hydrogen and the reactivies may change dramatically under hydrogenation conditions.

The hydrogenation of azobenzene has also been studied by Prasad and coworkers [110, 111] and was found to smoothly proceed to aniline over a Raney nickel catalyst. Hydrazobenzene was identified as the only visible intermediate and could be isolated if reaction conditions were favourable.

1.3.3.4 Selective Hydrogenation of Nitrobenzene to an Intermediate

Since Haber's publication in the 1890s many attempts have been made to attain the intermediate species in the nitrobenzene to aniline hydrogenation pathway. For example, subsequent studies have focused on the selective hydrogenation of nitrobenzene to one of the intermediate products. Karwa and Rajadhyaksha investigated the catalytic hydrogenation of nitrobenzene to phenylhydroxylamine [112] and to hydrazobenzene [113]. It was reported that the hydrogenation process can be ceased before aniline production by manipulating the reaction conditions. For example, poisoning the catalyst with Me_2SO and the use of a polar solvent both led to an increased production of phenylhdroxylamine and a reduction in the amount of aniline formed, while highly basic conditions favoured the formation of hydrazobenzene from nitrobenzene (a point also noted in an earlier study by Samuelson et al [49]). Azobenzene, azoxybenzene and aniline were also observed during the formation of hydrazobenzene although nitrosobenzene and phenylhydroxylamine were undetected throughout hydrogenation.

Furst and co-workers investigated the selective reduction of nitrobenzene to the reaction intermediates using Raney nickel and hydrazine hydrate [114, 115] and found the reaction to proceed to azoxybenzene and hydrazobenzene and also found that nitrosobenzene could be reduced to aniline using the same methodology.

1.3.3.4 Hydrogenation of Aniline

Haber's mechanism also suggested that cyclohexylamine could be formed through further hydrogenation of the aromatic ring after aniline had been produced. Early investigations by Devereux, Payne and Peeling in 1957 [116] and Greenfield in 1964 [117] found aniline to hydrogenate through to cyclohexylamine as expected and platinum metal to be the most effective catalyst, although rhodium, ruthenium and palladium were also active. More recent studies by Pitara's group in 1996 [118] examined the hydrogenation of nitrobenzene using a Pt/C catalyst and observed the production of cyclohexylamine but only at an acidic pH. In neutral solution, the nitrobenzene hydrogenation reaction proceeded to completion with 100 % selectivity

to aniline, however, in an acidified solution, only 30 % selctivity to aniline was achieved due to the over hydrogenation of the product to cyclohexylamine.

Narayanan and co-workers investigated the gas phase aniline hydrogenation reaction over a range of supported catalysts [119-121]. Nickel, cobalt and rhodium metals all effectively catalysed the reaction predominately producing cyclohexylamine, although several other by-products, such as N-phenylcyclohexylamine and dicyclohexylamine, were observable over nickel, particularly at high metal loadings.

Further studies by Mink and Horváth [122] investigated the hydrogenation of aniline vapour over alkali promoted nickel catalysts and found the reaction to proceed to cyclohexylamine with the formation of a number of by-products including dicyclohexylamine and ammonia. In addition, in the presence of water additional hydrolysis products such as cyclohexanone and cyclohexanol could be detected.

1.3.3.5 Theoretical Studies

The nitrobenzene hydrogenation reaction has also been the subject of theoretic quantum-chemical studies by Kochetova and Klyuyev [123]. The characteristics of the reactant, product and intermediates and their possible interactions were all examined. Haber's mechanism was used as a basis and it was proposed that this mechanism was consistent with both their calculations and the available experimental data. Furthermore, the same general mechanism is also proposed for the hydrogenation of another aromatic nitro-compound, 1-(4-nitrobenzyl)-1,2,4-triazole, with many of the intermediates observed experimentally [104]. A similar reaction scheme is also suggested for the reaction of nitro-aliphatic compounds.

1.3.3.6 The Effect of Reaction Solvent

Highly exothermic reactions, such as the nitrobenzene hydrogenation reaction often employ a solvent to help dissipate the excess heat generated during reaction and to prevent the occurence of an explosion. Industrial liquid phase reactions use

aniline/nitrobenzene mixtures [65] however, due to the toxicity of aniline, a more common organic solvent is preferred for smaller scale applications. Hydrogenation reactions require a solvent which contains no easily hydrogenated functional groups and which will not strongly adsorb on to the catalyst surface and compete for the metal active sites. The solubility of gaseous hydrogen is also a consideration, which limits the use of water as a reaction solvent. As a result, the preferred reaction solvents are lower alcohols, ethers or esters, although polyalcohols and acidic solutions are also occasionally employed [82, 124].

The choice of solvent can have a marked effect on the rate of hydrogenation. For example, the choice of a primary or secondary alcohol can have a significant influence on the rate of the reaction. The hydrogenation of nitrobenzene proceeds much more rapidly in methanol than in isopropanol [125]. The use of alcohols as hydrogenation solvents are by far the most popular solvents despite evidence in the literature that this can lead to the N-alkylation of the products [126, 127]. The formation of these compounds has been noted during previous research [128] at very low levels and perhaps for this reason these by-products often go un-reported.

Furthermore, the reaction solvent has also been reported to have an influence on the reaction kinetics. Yao and Emmett have described a variation in the reaction order with respect to the aromatic nitrocompound with the nature of the solvent [87]. In this study two mixed solvent systems were employed: a water-ethanol and a water-dioxane solution. Increasing the water concentration of both solvents was found to reduce the nitroarene reaction order from one to zero.

Kochetova et al [129] have calculated that the total charge on the nitrogen atom in the nitro group is of a positive nature and can be reduced by coordination of alcoholic solvent molecules to a nitro group oxygen via hydrogen bonding. The total charge on the nitrogen in the reaction intermediates is lowered more in an ethanol solvent than in isopropanol. This is postulated to account for the more rapid hydrogenation in ethanol than in isopropanol. The same study also suggests a variation in the rate determining step of the hydrogenation depending on the solvent employed. In ethanol, the rate determining stage is reported to be the initial

hydrogenation of nitrobenzene, whereas, in isopropanol it is reported as the hydrogenation of the nitrosobenzene intermediate. Studies on the interaction of both methanol and isopropanol with the surface of carbon catalysts have been published and show complex interactions involving the decomposition of both molecules [130, 131]. Methanol has been shown to dissociate to adsorbed CH_3O- and –H, whereas isopropanol can associately adsorb to the surface aswell as dissociating and providing adsorbed hydrogen in a similar manner to methanol. However, the effect of the extent of hydrogen dissociation on the rate of catalysis was not investiagted.

1.3.3.7 Deactivation of Nitrobenzene Hydrogenation Catalysts

Like all catalysts, those used for the hydrogenation of nitrobenzene have a limited active life and slowly lose activity over time. Compared with other industrial processes, catalysts used for aniline production deactivate relatively quickly and extending the active life of commercial catalysts is a major industrial concern. Presently, the causes and mechanisms of the deactivation process are not completely understood and require more research.

The deactivation behaviour of commercial supported copper catalysts has been the subject of investigation in several published studies. Dvorak and coworkers [132] extensively examined the deactivation of an industrial catalyst supplied by BASF and Petrov et al [133] studied the deactivation of a series of commercial Kieselghur supported copper catalysts. Three concurrent deactivation processes were found to be occurring throughout the reaction. Firstly, a layer of carbonaceous material was formed across the catalyst surface. The coked layer, possibly generated by the interaction of the nitrobenzene hydrogenation intermediates at the surface, was found to contain high levels of nitrogen. None of the components of the coke were detected in the gas steam but appeared to be only forming on the catalyst surface. Increasing the nitrobenzene flow rate lead to an increase in the rate of carbon deposition and was attributed to an increase in surface concentration of adsorbed intermediates. As a result of the carbon deposition process, the catalyst pellets were weakened and displayed increased evidence of attrition and mechanical crushing. Secondly, the copper particles were found to undergo rapid sintering at 350 °C

leading to a loss in catalytic activity although aniline selectivity appeared unaffected. Thirdly, the catalysts proved to be sensitive to poisoning by sulfur or chlorine containing contaminants in the gaseous feed stream. In particular, very low levels of thiophene, a common trace impurity in some nitrobenzene sources, was found to cause a dramatic decrease in catalytic activity (typically a 70 % decline). Poisoning of the catalysts in this way lead to an increase in the rate of carbon deposition and a substantial amount of carbon lay down was observed. It has been well reported that commercial copper catalysts for hydrogenation applications readily undergo deactivation through sintering and poisoning with sulfided or chlorinated species, but deactivation via a coking mechanism is rare as reaction temperatures are generally kept low to minimise the sintering contribution [134]. However, the high exotherm generated during the nitrobenzene hydrogenation reaction may lead to a number of carbon forming reactions at the catalyst surface becoming more favourable.

Babkova examined the catalyst regeneration procedures of commercial nitrobenzene hydrogenation catalysts in 1990 [135]. The operational industrial process uses a steam/air mixture, followed by air, followed by nitrogen to reduce the catalyst back to a more active form. However, repeated high temperature treatment can increase the sintering rate of the catalyst and lead to further loss of active metal surface area. Currently, the catalyst bed is replaced after a small number of regenerations causing great expense and research is ongoing to try to improve the efficiency of the regeneration process.

In addition to investigations into the deactivation of commercial nitrobenzene catalysts, several studies have also appeared in the literature describing the deactivation of supported palladium catalysts used for smaller scale aniline production [58, 90, 136]. Like the industrial catalysts, the main source of deactivation involved the deposition of heavyweight carbonaceous material across the catalyst surface. Unlike the copper catalyst, sintering of the palladium did not contribute to the overall catalyst deactivation with good metal dispersion maintained post-reaction. The coke precursors were not conclusively identified although the addition of aniline to the reaction appeared to have little or no effect on either the rate of carbon deposition or the rate of hydrogenation. It was suggested that

nitrobenzene itself might enhance coke formation. The contribution of the hydrogenation by-products, azoxybenzene, azobenzene and hydrazobenzene, to coke formation was also considered but no definitive conclusions could be drawn. Coke formation on the palladium nitrobenzene hydrogenation catalysts was considered to be a complex process where many simultaneous mechanisms are possible.

1.4 HDC Catalysts

For use in this research a set of catalysts were synthesised using a technique known as the HDC (Highly Dispersed Catalyst) preparation. The method of synthesis is described below in Section 1.4.1 and is outlined in several patents [137-139]. The aim in developing the method was to produce highly dispersed supported metal catalysts with small metal particle sizes that could be maintained at high loadings. Traditional catalyst preparation techniques such as incipient wetness and impregnation can lead to large metal crystallites with poor dispersion, particularly with metals such as cobalt and nickel. Although these methods can produce very efficient catalysts, the metal surface area and hence catalytic potential is not fully exploited. For example, cobalt on silica catalysts can be synthesised using standard methods to attain a cobalt surface area per gram between 6 $m^2 g^{-1}$ to 65 $m^2 g^{-1}$ but with an alumina support the cobalt surface area can only reach between 15 –26 $m^2 g^{-1}$ [140]. For some industrial applications the use of an alumina support is preferred and, using the HDC method, an alumina supported catalyst with a surface area between 30 –80 $m^2 g^{-1}$ can be achieved with metal loadings between 3-40 % by weight of cobalt. Likewise, nickel/alumina catalysts can be synthesised using precipitation of nickel hydroxide to give catalysts with a metal surface area between 50-55 $m^2 g^{-1}$ with relatively large nickel particles ranging between 5-60 nm [141]. Whereas, HDC synthesis can produce nickel/alumina catalysts between 5-40 % loading by weight of metal with a nickel surface areas from 80-300 $m^2 g^{-1}$ and small metal crystallites (1-5 nm) [142, 143].

1.4.1 Synthesis of HDC Catalysts [137-139, 144]

In the HDC method the metals are precipitated from solution onto the alumina support in a similar way to previous deposition-precipitation methods [145-147]. However, the HDC technique uses higher pHs to increase the interaction between the alumina support surface and the solubilised metal cations. At normal pH, the hydroxylated alumina and the metal cations both carry a postive charge and as a result, large clusters of metal crystallites are deposited. HDC preparation uses a high pH, to induce a negative charge on the surface of the alumina by deprotonation of the hydroxyl groups and to increase the attraction between the metal cations and the alumina. This is represented in Figure 1.12.

Figure 1.12: Interaction between metal cations and alumina at low and high pH

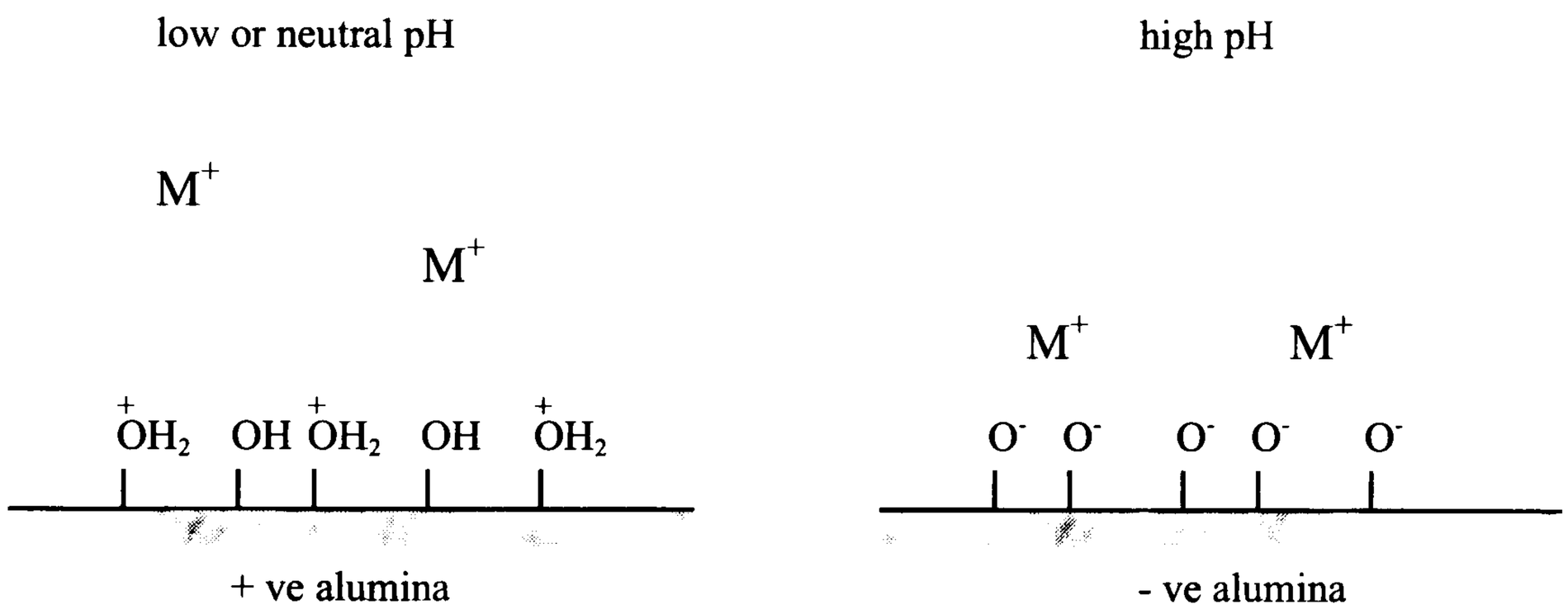

Metal hydroxycarbonate salts are used as the metal precursor in these preparations but due to the low water solubility of these compounds they are dissolved in concentrated ammonia solution and subsequently converted to metal ammonia complexes which are highly soluble and useful for catalyst preparation. The alumina support is then added to the metal ammine solution and stirred to form a suspension. The solution is then heated to 80 °C to distil off the ammonia ligands and cause de-stabilisation of the metal ammine complexes. As the deposition proceeds, the metal cations react with the de-protonated hydroxyls on the alumina surface, which effectively act as an anchor to stabilise the metal-support interaction. As further ammonia ligands are lost, the metal cations will also bind to the carbonate anions

also present in the solution. The precipitation process can be followed by measuring the pH, which decreases steadly throughout deposition and stabilises out to a constant value when all ammonia has been removed from the preparative solution. The resulting catalyst, consisting of small crystallites of metal carbonate salts dispersed across the alumina support can be collected by filtration and the raw catalyst processed in the desired way. A summary of HDC catalyst preparation is shown in Figure 1.13.

Figure 1.13: The HDC Method.

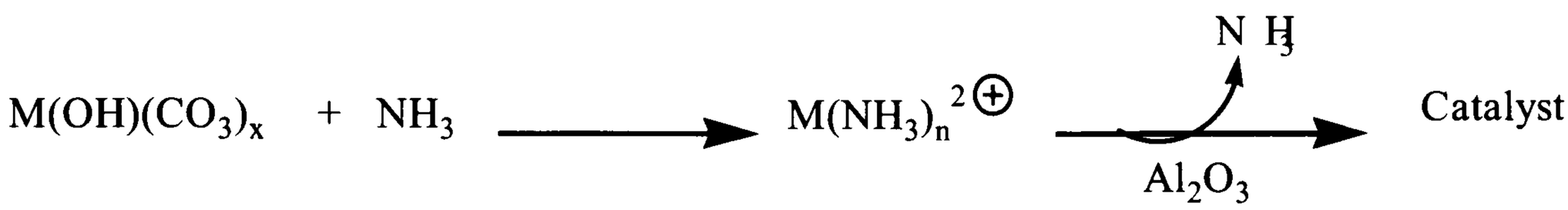

The HDC preparative technique is known to be a highly effective route for the synthesis of highly dispersed and homogeneous single metal catalysts and has been used commercially to prepare a range of catalysts using cobalt, nickel and palladium, alumina supported catalysts. However, it is with the preparation of cobalt containing catalysts that the majority of benefits are observed.

It has been well documented in the academic press that cobalt reacts strongly with the alumina support during catalyst preparation leading to the formation of cobalt aluminate. This species is extremely difficult to reduce and can be considered catalytically inactive under most reaction conditions. Although cobalt aluminate formation may play a role in helping to bond the active cobalt to the support material, it is desirable to minimise its formation. For this reason, cobalt catalysts are often prepared using high metal loadings to increase the proportion of reducible cobalt present on the catalyst surface and weight loadings of at least 20 % are generally preferred. With expensive metals, such as cobalt, the HDC method of catalyst preparation allows high loaded catalysts to be synthesised whilst maintaining high dispersion and small metal particles.

In addition, the HDC method also allows less reactive aluminas, such as delta-alumina, to be utilised during catalyst preparation as the high pH increases the interaction with the metal precursor. Aluminas of this type are often desirable because of their low water content [148]. The choice of alumina for use in traditional preparative techniques is normally limited to reactive gamma types to obtain a suitably strong interaction with the support. However, gamma aluminas have proved too reactive for use in HDC catalyst synthesis, particularly with cobalt, where most of the deposited cobalt produced non-catalytically active cobalt aluminate.

1.4.2 Uses of HDC Catalysts

The HDC method of catalyst preparation is used to produce a number of catalysts for a wide range of industrial applications. Nickel, cobalt and palladium alumina supported catalysts prepared in this way are all commercially available.

Ni/Al_2O_3 HDC catalysts are sold for selective hydrogenation applications in the gasoline sector, where it is required to hydrogenate a range of C5+ fractions to prevent gumming of the gasoline product whilst maintaining a high aromatics content of the fuel [149]. They are also utilised in a number of other hydrogenations including the production of fatty alcohols from methyl esters, sugar to polyols, aldehydes and ketones to alcohols and the dearomatisation of white oils. Other applications include amination reactions with alcohols or aldehydes and ketones with ammonia [150-152].

Co/Al_2O_3 HDC catalysts are sold commercially for use in the hydrogenation of aromatics and aldehydes and as amination catalysts [151, 152].

2.0 PROJECT AIMS

The general objectives of this thesis were to investigate the nitrobenzene hydrogenation reaction over a range of mixed metal catalysts to gain a greater understanding of the hydrogenation reaction mechanism and of the industrial catalyst deactivation problem.

More specifically, the intention was to collect data from a variety of mechanistically probing reactions, including the use of isotopic labeling, NMR and doping of intermediates, to either completely delineate Haber's mechanism, or to provide a viable alternative mechanism in the event of disproving Haber's proposal. The ultimate aim was to provide some clarification to the largely conflicting situation concerning Haber's schematic appearing in the chemical literature over the legitimacy of the mechanistic route of the transformation from nitrobenzene to aniline. In addition to resolving this complex discussion which has existed for the past century, these reactions were also performed with the intent of gathering information to deepen our understanding of the possible causes of deactivation through the hydrogenation process and lead to further investigations of the loss of activity occurring during the laboratory scale reactions. It was planned to carry out this work in the liquid phase using a laboratory autoclave and a selection of supported palladium catalysts as this was known to be a reliable, accurate and repeatable way of collecting large quantities of comparable reaction data.

In addition, the project was also intended to investigate the use of a new type of bimetallic catalyst based on cobalt, copper and nickel. These catalysts were to be prepared on site at Johnson Matthey Catalysts in Billingham using a commercial preparation method. This method has been widely employed in the production of single metal catalysts for supply to the chemical industries, however limited research has been carried out on the simultaneous precipitation to two metals. It was aimed to study the HDC method throughout catalyst preparation to ascertain the effect of adding a second metal during the deposition process. The final catalysts were to be studied using a range of surface characterization techniques, including UV-Vis, XPS and SEM to gather information on the nature to the metal-to-metal interaction of the

surface of the catalyst particles. Ultimately, it was desired to establish if this preparation route had the potential to produce suitable industrial bimetallic hydrogenation catalysts. To investigate this further the novel catalysts were to be utilized as solid catalysts in the vapour phase hydrogenation of nitrobenzene to investigate their effectiveness in comparison with standard precious metal catalysts to determine if these novel catalysts possessed any advantageous properties worth investigating further with a view to improving the existing commercially available catalysts in the future.

Furthermore, the process was to be examined from an industrial perspective to gain an insight into the deactivation of the commercial nitrobenzene hydrogenation catalysts. It was of particular interest to evaluate the rate of catalyst deactivation with these new catalysts with the aim of extending the active life of the current industrial catalysts and reducing the frequency of catalyst bed replacements and increasing the cost efficiency during commercial aniline production. These experiments were preformed in the gas phase using a specifically designed micro-reactor similar to those used in industrial research.

3.0 EXPERIMENTAL SECTION

3.1 Catalyst Preparation

3.1.1 Preparation of Pd/C Catalysts

Three palladium/carbon catalysts were supplied from Johnson Matthey Catalysts. These catalysts were prepared by impregnation using a solution of $Pd(NO_3)$. Three different powdered activated carbon supports were used: Norit CN1 (surface area 1400 $m^2 g^{-1}$), Norit CA1 (surface area 1400 $m^2 g^{-1}$) and Norit SX Ultra (surface area 1200 $m^2 g^{-1}$). Sufficient palladium nitrate solution, to produce a palladium loading of 3 %, was added to each support. The resulting suspensions were dried and calcined at 423 K for 3 hours.

3.1.2 Preparation of 1 % Pd/alumina Catalyst

The 1 % Pd/ alumina catalyst used in this research was a commercial catalyst also supplied from Johnson Matthey Catalysts and consisted of palladium supported on 1.2 mm θ-alumina trilobes (surface area 110 $m^2 g^{-1}$) with a pore volume of 0.55 $cm^3 g^{-1}$. This catalyst was prepared by contact with an aqueous solution of Na_2PdCl_4 and was chemically reduced with N_2H_4 and finally dried in air at 105 °C.

3.1.3 Preparation of 10 % Cu/silica Catalyst

This catalyst was prepared by Elaine Vass, in the University of Glasgow Catalysis Department using a wet impregnation technique. Copper (II) nitrate trihydrate (42.248 g) dissolved in 150 ml of deionised water was added to Grace C10 silica

beads, 100 g (surface area 300 $m^2 g^{-1}$). Excess water was rotary evaporated off at 353 K for 30 minutes then the catalyst dried in an oven (333 K) for 1 week.

3.1.4 Preparation of Cu, Co and Ni/Alumina Catalysts

Twelve metal catalysts containing Cu, Co, Ni or mixtures of these metals were prepared using a technique known as the HDC (Highly Dispersed Catalyst) method developed at Johnson Matthey Catalysts [137-139, 144]. Three metal ammine solutions were prepared for the synthesis, using copper, nickel and cobalt hydroxy carbonates.

All materials, the ammonium carbonate chip, copper (II) carbonate, nickel (II) hydrogencarbonate and cobalt (II) carbonate were purchased from Aldrich. The demineralised water was obtained from the internal supply in the Johnson Matthey complex at Billingham.

3.1.4.1 Preparation of Copper Tetraammine Solution (~2.36 w/w % Cu)

Ammonia solution (0.688 L), and demineralised water (2.977 L) were added to a round-bottomed flask and mixed thoroughly. The mixture was then agitated using mechanical stirrer (215 rpm) as ammonium carbonate chip (233 g) was added to the flask. The solution was left mixing until all of the chips had dissolved completely. Blue copper (II) carbonate (177 g) was then added in ~25 g portions with constant stirring over a period of several hours and reacted to form the bright blue ammine complex according to Equation 3.1. Following this the solution was stirred overnight and then filtered using a Bűchner apparatus to remove any undissolved material.

$$\underset{\text{blue}}{CuCO_3} + 4NH_3(aq) \longrightarrow \underset{\text{bright blue}}{[Cu(NH_3)_4]^{2+}(aq)} + CO_3^{2-} \qquad \text{Equ. 3.1}$$

3.1.4.2 Preparation of Nickel Hexammine Solution (~ 2.5 w/w % Ni)

Ammonia solution (0.563 L), water (1.877 L), ammonium carbonate chip (152 g) and nickel (II) hydrogencarbonate (205.2 g) were used to prepare the solution in the same way as outlined above in Section 2.1.4.1 and the nickel ammine complex was formed according to Equation 3.2. A colour change from green to blue was observed during the preparation.

$$\underset{\text{green}}{NiCO_3} + 6NH_3(aq) \longrightarrow \underset{\text{blue}}{[Ni(NH_3)_6]^{2+}(aq)} + CO_3^{2-} \qquad \text{Equ. 3.2}$$

3.1.4.3 Preparation of Cobalt Hexammine solution (~ 2.9 w/w % Co)

Ammonia solution (1.918 L), water (1.877 L), ammonium carbonate chip (198 g) and cobalt (II) carbonate (218 g) were used to prepare the solution in the same way as described in Section 3.1.4.1. Equation 3.3 shows the transformation involved in the production of the crimson cobalt hexammine complex from the purple carbonate starting material.

$$\underset{\text{purple}}{CoCO_3} + 6NH_3(aq) \longrightarrow \underset{\text{crimson}}{[Co(NH_3)_6]^{2+}(aq)} + CO_3^{2-} \qquad \text{Equ. 3.3}$$

3.1.4.4 Preparation of HDC Catalysts

All catalysts were prepared using a powdered δ-alumina support: Puralox HP-14/150 by Sasol (surface area 151 $m^2 g^{-1}$). Three single metal and nine mixed metal catalysts were prepared and are listed in Table 3.1. The bimetallic catalysts were prepared so that the metal loading was fixed at 20 % by weight throughout.

Table 3.1: Catalysts made using highly dispersed catalyst (HDC) preparation method

	Mixed Metal		
Single Metal	**copper- nickel**	**copper- cobalt**	**nickel- cobalt**
20 % Cu	15 % Cu/ 5 % Ni	15 % Cu/ 5 % Co	15 % Ni/ 5 % Co
20 % Ni	10% Cu/ 10 % Ni	10 % Cu/ 10 % Co	10 % Ni/ 10 % Co
20 % Co	5 % Cu/ 15 % Ni	5 % Cu/ 15 % Co	5 % Ni/ 15 % Co

The calculated volumes of metal ammine solutions were added to a 5 litre round-bottomed flask, fitted with a reflux condenser, pH probe and mechanical stirrer. The stirrer was set at 260 rpm and the alumina support (80 g) slowly added to the stirred solution. The reaction mixture was then refluxed until all ammonia had been distilled off and metal deposition was complete. This was visible by a change in the colour of the solution. The pH of the reaction mixture was monitored throughout the course of the reaction and following full deposition, reflux was continued for 15 minutes to age the reaction mixture. After this, the hot reaction mixtures were filtered via a Bűchner flask to collect the coloured alumina supported catalysts. A clear water filtrate was also obtained. Following washing with demineralised water, the catalysts were left to air dry on the Bűchner for 30 minutes and then dried overnight (12 hours) in an oven (478 K).

3.1.5 Raney Nickel Catalyst

Raney 2800 nickel (nickel content <89 %) was purchased from Sigma Aldrich for use as nitrobenzene hydrogenation catalyst. The activated catalyst was received as an aqueous slurry and only required washing with the reaction solvent to remove the water before use in a reaction.

3.2 Catalyst Characterisation

3.2.1 Characterisation of Pd/C Catalysts

3.2.1.1 CO Chemisorptions on Pd/C Catalysts

The dispersion of each of the three palladium/carbon catalysts was measured using CO chemisorption carried out in a glass pulse-flow micro-reactor. A sample of catalyst (0.250 g) was placed in the reactor and purged in a flow of He (30 $cm^3 min^{-1}$) for 30 minutes. Reduction was then carried out for 30 minutes at 313 K in flowing hydrogen (30 $cm^3 min^{-1}$). After cooling to room temperature in a flow of helium (30 $cm^3 min^{-1}$), pulses of carbon monoxide were passed over the catalyst via a sample loop, which allowed delivery of the gas with a specific volume and pressure. Adsorptions were analysed using an online Pye series 104 gas chromatograph with a Porapak Q column. Integration of the chromatograph peaks allowed calculation of the number of moles of adsorbed CO, and therefore, the average dispersion using the relationship described in Equation 3.4. The CO:Pd ratio was taken as 1:2 to determine the number of surface metal atoms. The total number of metal atoms present was calculated from the metal loading.

$$\% \text{ dispersion} = \frac{\text{no of surface metal atoms}}{\text{total no of metal atoms}} \times 100 \qquad \text{Equation 3.4}$$

The dispersion can also be correlated to the average metal particle size, according to the relationship shown below in Equation 3.5. This methodology makes the assumption that the metal particles exist on the catalyst surface as hemispherical entities with uniform diameters.

$$\% \text{ dispersion} = \frac{A \times 6}{\delta \times Sa \times Na \times d} \qquad \text{Equation 3.5 [3]}$$

where, A = atomic weight

δ = density of metal

Sa = average surface area occupied by 1 active atom

Na = Avogadro's number

d = average particle diameter

This expression can be simplified to the following for palladium (Equation 3.6):

$$\% \text{ dispersion} = \frac{109}{d} \qquad \text{Equation 3.6 [153]}$$

3.2.2 Characterisation of HDC Catalysts

3.2.2.1 Elemental Analysis

Elemental analysis of the 12 HDC catalysts was carried out at the Clitheroe site of Johnson Matthey Catalysts using an XRF fusion technique. A sample of catalyst (0.5 g) previously ignited at 1173 K was weighed out into a 95 % Pt/5 % Au crucible. Sodium tetraborate (8.5 g) was then added and the sample fused to produce a glass disk that was then analysed for nickel, copper, cobalt, and aluminium using a PANanalytical MagiX PRO XRF spectrometer.

3.2.2.2 Catalyst Particle Size Analysis

The size of the catalyst particles was determined using a laser diffraction particle sizing technique using a long-bed Malvern Mastersizer X particle size analyser. A fixed wavelength (λ=633 nm) 2mW He-Ne gas laser with 18 mm beam expansion and a 31 element solid state detector with angular array optimised for light scattering measurement were employed to collect diffraction data between scattering angles of 0.1 and 50 °. The catalyst samples were examined as a de-ionised water suspension that was stirred at 1200 rpm, pumped at 50 % power of a 0-3100 rpm pump and exposed to 80 % power of a 40 kHz ultrasonic bath.

The laser diffraction measurements evaluate the size of the catalyst particles using the equivalent sphere model. This theory assumes that in the analysis each particle exists as a spherical entity so that when the diameter is measured experimentally, the volume of the sphere can be derived and used as a description of the particle. Therefore, the technique gives no information about the shape of the catalyst particles but can be used to compare the sizes of similar catalysts as the particles can be shown to be equivalent to a larger or smaller equivalent sphere. As the sizing measurement evaluates all particles in the sample, a large range of particle volumes is obtained. In this analysis three values are quoted. The volume median diameter, or D(v, 0.5), is the median diameter at which 50 % of the particle volume can be found above this value and 50 % below. The D(v, 0.1) and D(v, 0.9) are also quoted and these refer to the diameter when 10 % of the particles sampled lie below this value and 90 % above it and the opposite end of the scale when 90 % of the particles lie below this value and only 10 % are larger respectively. These are also known as the 10^{th} and 90^{th} percentiles and give an indication of the overall particle size distribution.

3.2.2.3 Temperature Programmed Reduction

Temperature programmed reduction (TPR) of the newly synthesised HDC catalysts was performed to give an indication of the number and reducibility of the precursor states present in each sample. This was measured using 0.1 g of catalyst in a

Quantachrome Corporation TPR/TPD with 5 % H_2 in N_2 and a linear heating rate of 5 $degmin^{-1}$ over a temperature range of 293 to 1373 K.

3.2.2.4 BET Isotherms of HDC Catalysts

The BET nitrogen isotherms of the twelve HDC catalysts were measured on a Micromeritics ASAP 2400 gas adsorption analyser using a static barometric method. Measurements were taken using both "as received" and reduced catalyst samples (0.5 g). The "as received" catalysts were outgassed at 413 K in flowing nitrogen for one hour prior to the nitrogen absorption experiment at 77 K. The reduced samples were run without the outgassing step. Nitrogen adsorption and desorption isotherms were collected and used to derive the BET surface area, which quantifies the entire surface area of the catalyst, including the metal and the porous support material. The pore volume of each catalyst was also measured using a relative pressure of 0.98 on the desorption branch. The average pore diameter was also calculated using this method.

3.2.2.5 Chemisorption Studies on HDC Catalysts

Chemisorption techniques were used to determine the metal surface area (the area of the catalytically active species) of all twelve novel HDC catalysts. The analysis was performed at Johnson Matthey Catalysts in Billingham. The surface area of the nickel and cobalt present in the catalysts was determined using hydrogen chemisorption whereas the copper surface area was measured using reactive N_2O chemisorption.

3.2.2.5.1 Cobalt and Nickel Surface Areas

The metal surface areas of the cobalt and nickel containing HDC catalysts were obtained using a Micromeritics ASAP 2010 in chemisorption mode. Analysis was performed using 0.5 g of sample and a hydrogen adsorption isotherm obtained using a static volumetric method. An isotherm was generated at a temperature of 308 K for nickel and 423 K for cobalt. From the plot of hydrogen adsorbed versus pressure, data points were selected along the near horizontal plateau region and extrapolated back to give the value of hydrogen uptake at zero pressure. This corresponds to the volume of hydrogen on the chemisorbed monolayer (V_m). For both nickel and cobalt one molecule of hydrogen is assumed to adsorb to two atoms of metal according to Equation 3.7.

$$2\,Ni\,(surface) + H_2\,(g) \rightarrow 2Ni\text{-}H\,(ads) \qquad \text{Equation 3.7}$$

Therefore in the surface area calculation (Equation 3.8) it is necessary to multiply by two (the stoichiometry factor), to take this into account.

$$S_m = \frac{V_m.S_F.N_A}{22414.\sigma_A} \qquad \text{Equation 3.8}$$

Where,

V_m = volume of hydrogen in chemisorbed monolayer

S_F = stoichiometry factor

N_A = Avogardo's number

σ_A = the surface density of the metal atoms.

An assumption of the surface density is required in this calculation, as values for particular metals are not known with any certainty, however there are generally accepted values for each metal. These are shown in Table 3.2.

Table 3.2: Accepted values of the surface density for cobalt and nickel [154]

Metal	Surface density (x 10^{19} atoms m^{-2})
cobalt	1.51
nickel	1.54

3.2.2.5.2 Copper surface areas

The metal surface area of the copper containing catalysts was calculated using reactive N_2O chemisorption. The catalyst samples (1-2 g) were loaded into separate reactors and place in a modified GC oven, before being purged with He (g) for 2 minutes. The catalysts were the reduced in 5 % H_2/He at 503 K, using a temperature ramp of 8 deg min^{-1} and holding for 3 hours. After cooling to 341 K in He, the analysis gas, 2.5 % N_2O/He, was then passed over each catalyst and allowed to react according to Equation 3.9. The evolved N_2 (g) was measured using a katharometer to compare the relative rates of heat loss into the exit gas using a Wheatstone bridge circuit to measure changes in the resistance of internal heating coils as they cool.

$$N_2O(g) + Cu \rightarrow N_2(g) + CuO \qquad \text{Equation 3.9.}$$

Using the resistance measurements and the thermal conductivity of each gas, the composition of the exit gas, and hence the quantity of evolved N_2 present can be determined. The copper surface area is then calculated by using Equation 3.8 as described in Section 3.2.2.5.1.

3.2.2.6 UV-Vis Spectroscopy

The UV-Vis Spectra of the twelve alumina-supported catalysts were collected using a Varian Cary 500 scan UV-Vis-NIR spectrophotometer. Samples were run in a preying mantis over a 1900-190 nm range with a scan rate of 200 nm min^{-1} and a resolution of 2 nm. Catalyst samples were diluted with the alumina support to reduce adsorption in the visible range.

3.2.2.7 Raman Spectroscopy

Raman spectra were collected on a Labram Infinity Raman spectrophotometer using a green laser (532 nm, solid state, 10 mW) through an 800 μm confocal hole with a grating of 1800 gr mm^{-2}. Three 120 second long acquisitions over a 0-1500 cm^{-1} range were taken for each sample.

3.2.2.8 X-Ray Photoelectron Spectroscopy

The XPS spectra were obtained using a M-probe spectrometer and an Al Kα, 1486 eV monochromatic x-ray source. Spectra were collected under broad scan conditions. (binding energy scan range 0-1100 eV, spot size 1000 μ, max resolution 1.4 eV, charge neutraliser 1 eV, scans 50 at 0.5 eV/point and a power setting of 180 W.

3.2.2.9 Scanning Electron Microscopy (SEM)

Three of the catalyst samples, 10 % Ni/10 % Cu/Al_2O_3, 10 % Cu/10 % Co/Al_2O_3 and 10 % Ni/10 % Co/Al_2O_3, were examined using SEM with EDX. Polished sectional mounts of the catalyst samples were prepared and the polished faces were vacuum carbon coated. The SEM images were collected under the following operating

conditions; a beam current of 100 nA, an accelerating voltage of 20 kV, a resolution of 256 x 192 pts, a frame time of 1 x 50 s, a dwell time of 50 ms and a 1000x magnification.

3.3 Catalyst Testing

3.3.1 Reagents

All reagents and solvents (nitrosobenzene, azobenzene, cyclohexylamine, aniline, methanol and isopropanol) were obtained from Sigma Aldrich with the exception of nitrobenzene that was obtained from Fluka.

Reactions performed with nitrobenzene supplied by Sigma Aldrich displayed evidence of catastrophic catalyst deactivation most likely caused by a trace impurity, possibly sulfur based, present in the the reagent. Distillation or Raney nickel purification could not remove the poison, therefore the Sigma Aldrich sourced nitrobenzene could not be used during catalyst testing. This problem was not encountered when using Fluka sources nitrobenzene. Previous work by Anderson [126], on nitrobenzene hydrogenation has shown the reaction to be greatly affected by trace impurities and hence the choice of a suitable nitrobenzene supply is crucial.

All reaction gases were sourced from BOC Gases and are listed as follows: hydrogen (99.995 % purity), nitrogen (purity 99.998 %), argon (purity 99.998 %) and deuterium (purity 99.995 %).

3.3.2 Stirred Tank Reactions

A series of reactions was performed in a stirred autoclave reactor to investigate liquid phase nitrobenzene hydrogenation. The three carbon supported palladium catalysts (Pd/CA1, Pd/CN1 and Pd/CSXU) were utilised most frequently, however additional

reactions were carried out using the 1 % Pd/alumina catalyst. Reactions were attempted using 20 % Cu/alumina and 10 % Cu/silica catalyst but neither catalyst could be reduced successfully in the stirred tank reactor.

3.3.2.1 Stirred Tank Reactor

A Bűchi laboratory autoclave (model bep 9801 e) was used for all liquid phase hydrogenation reactions and is shown in Figure 3.1. The reactor consisted of a 0.5 L jacketed glass vessel capable of holding pressures up to 6 bar. The reactor was heated using a Julabo heating circulator to pass heated oil around the vessel jacket. The reactor was fitted with a Bűchi 300 mechanical stirrer with a rate that could be varied between 0-2400 rpm, a gas inlet via a Bűchi gas flow controller, an injection/sampling tube, a thermocouple connected to the external Julabo heating system, a Bűchi pressure gauge, and pressure release valve. The pressure release valve was also fitted with a bursting disc to prevent damage to the glass vessel in the event of serious over pressure. The gas control system allowed variation of both the inlet gas pressure and the rate of gas flow into the reactor and could be used to supply either hydrogen or argon gas. A drainage tap on the base of the reactor allowed the vessel to be emptied easily post reaction.

Figure 3.1: Stirred tank reactor

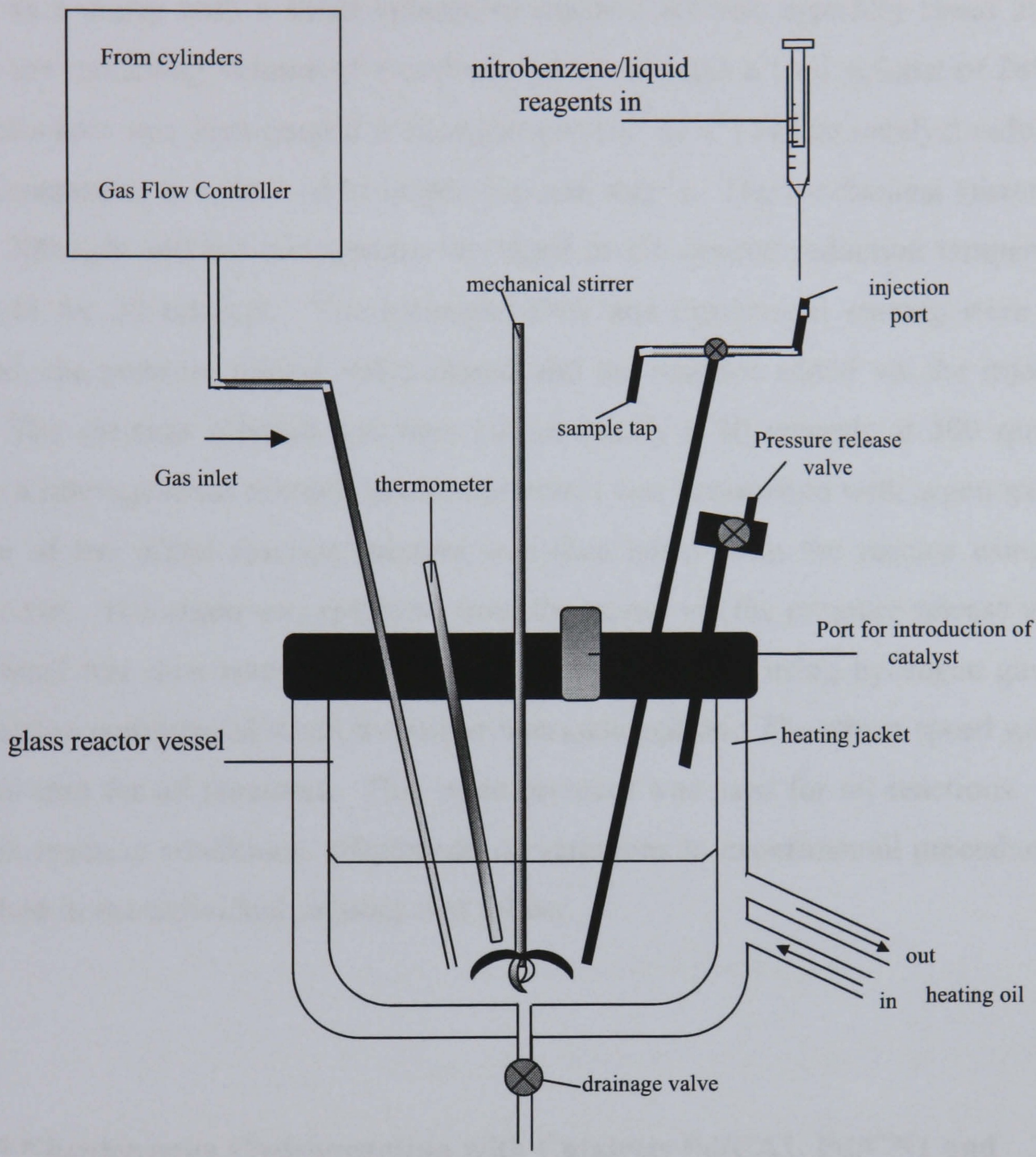

3.3.2.2 Reaction Procedure

Before any experimental procedure was commenced, the vessel was purged with argon gas using the gas flow control system. The catalyst was added to the reaction vessel as a slurry with a small volume of reaction solvent, typically about 20 ml, before the remaining volume of liquid was added to make a total volume of 280 ml. The autoclave was then purged with argon (30 cm^3 min^{-1}) before catalyst reduction was commenced in a flow of hydrogen (30 cm^3 min^{-1}). The mechanical stirrer was set to 300 rpm and the temperature increased to the desired reduction temperature and held for 30 minutes. The hydrogen flow and mechanical stirring were then stopped, the pressure release valve closed and the reactant added via the injection port. The reaction solution was then stirred briefly (~30 seconds at 500 rpm) to ensure a homogeneous mixture before the vessel was pressurised with argon gas. A sample of the initial reaction mixture was then taken from the reactor using the sample tap. The argon was removed from the vessel via the pressure release valve. The vessel was then taken to the desired reaction pressure using hydrogen gas and the reaction commenced when the stirrer was switched on. The stirrer speed was set at 1000 rpm for all reactions. This basic protocol was used for all reactions. Any specific reaction conditions, adaptations or variations to experimental procedure are described in the individual sections that follow.

3.3.2.3 Nitrobenzene Hydrogenation with Catalysts Pd/CA1, Pd/CN1 and Pd/CSXU

Nitrobenzene hydrogenation experiments were carried out using the three carbon-supported palladium catalysts (Pd/CA1, Pd/CN1 and Pd/CSXU) in two different reaction solvents: methanol and isopropanol (IPA). The catalyst (0.05 g) was reduced at 313 K following the procedure outlined above in Section 2.3.2.2 before nitrobenzene (18 ml, 0.17 mol) was injected and the reaction commenced at 0.5 bar g pressure and 313 K. The reactions were performed for 90 minutes and monitored using the gas flow controller to quantify the number of moles of hydrogen gas consumed during the reaction. Samples of the hydrogenation mixture post-reaction

were also removed and analysed using a Chrompack CP 9000 GC, with an FID detector fitted with a 30 m FFAP column.

3.3.2.4 Deactivation Experiments Using Recovered Pd/C Catalysts

Deactivation experiments using Pd/CA1, Pd/CN1 and Pd/CSXU were carried out in both methanol and IPA. To ensure reactions reached completion within a convenient time scale, the gas pressure and temperature were increased to 5 bar g and 323 K and the mass of catalyst to 0.1 g. Each run was left until complete hydrogenation of nitrobenzene (18 ml, 0.17 mol) had taken place, then the catalyst was recovered from the reactor, washed in methanol and replaced back into the reactor with fresh reaction solvent and used to perform another hydrogenation. Each catalyst was used for three successive runs. The reaction was monitored using hydrogen uptake and samples were also removed at regular time intervals and analysed using a Varian 3400 GC fitted with a FID detector and a DB 5 30 m column.

3.3.2.5 Deactivation Experiments using Repeated Injections.

Catalyst Pd/CSXU was used to perform deactivation experiments in both methanol and IPA. The catalyst (0.1 g) was reduced and used at a temperature of 323 K and at a pressure of 5 bar g. Post-reaction, the catalyst was left *in situ* and re-reduced in hydrogen for 30 minutes before another injection of nitrobenzene (18 ml, 0.17 mol) was added to the reactor and was hydrogenated under identical conditions. This procedure was repeated three times until four successive additions of nitrobenzene had been added and reacted to completion. Throughout all runs samples were removed at time intervals and analysed by GC using a Varian 3400 with a FID detector and a DB 5 30 m column.

3.3.2.6 Doping with Aniline and Water

Hydrogenations were also carried out were the reaction mixture was doped with the products aniline and water. These reactions were carried out with 0.1 g of Pd/CSXU, in methanol at 323 K and 5 bar g. Five separate doping experiments were carried out, two using aniline, two using water and one involving the addition of both products. One mole equivalent of aniline and two mole equivalents of water were added to the reaction mixture. These amounts were calculated to give the number of moles that would be produced during complete reaction of nitrobenzene to its products, as described in Equation 3.10. In two of the experiments, the dopant, aniline (15 ml, 0.7 mol) or water (2.1 ml, 0.34 mol) was added to the reaction solution, using the injection port, directly after catalyst reduction and mixed thoroughly under an argon atmosphere before the nitrobenzene reagent (18 ml, 0.17 mol) was added to the reactor. In another two experiments the dopant was added after nitrobenzene had been injected and mixed with the reaction solution under an argon atmosphere. In the last experiment, the nitrobenzene, aniline and water were added simultaneously as a mixture through the injection port and the standard reaction protocol followed.

$$PhNO_2 + 3H_2 \rightarrow PhNH_2 + 2H_2O \qquad \text{Equation 3.10}$$

Samples were removed for analysis using a Finnigan Thermoquest TraceGC-MS fitted with a 25 m DB-5 column. The gas consumption was also recorded using the gas flow controller system.

3.3.2.7 Hydrogenation of d_5- Nitrobenzene

In this experiment, d_5-nitrobenzene (18 ml, 0.17 mol) was used in place of nitrobenzene. Catalyst Pd/CSXU (0.1 g) was used to perform hydrogenation at 323 K and 5 bar g in a methanol solvent. Samples were analysed using a Varian CP-3800

GC fitted with a 25 m DB-5 column and coupled to a Saturn 2000 trace MS detector. Vials were also prepared for NMR analysis by addition of d_4-methanol to the reaction samples (100 µl d^4-methanol to 0.6 ml of reaction solution). They were then analysed by ^1H NMR, using a Bruker-spectrospin 400 Ultrashield NMR spectrometer. The hydrogen consumption throughout the experiment was also monitored. An analogous reaction using fully hydrogenated nitrobenzene was also carried out and analysed in an identical way that so that a comparison of the NMR [^1H] spectra of both reactions could be made.

3.3.2.8 Reaction using Deuterium Gas

An experiment was carried out using deuterium gas in place of hydrogen. Catalyst Pd/CSXU (0.1 g) was utilised to perform the hydrogenation of nitrobenzene (18 ml, 0.17 mol) under 2 bar g pressure, at 323 K and using methanol as the reaction solvent. Samples were removed for analysis by GC-MS and ^1H NMR using the same instrumentation as described above with the use of d^5-nitrobenzene in Section 3.3.2.7.

3.3.2.9 Hydrogenation of Nitrosobenzene and Azobenzene

The hydrogenation of nitrosobenzene and azobenzene was carried out with catalyst Pd/CSXU (0.1 g). The experimental procedure described in Section 3.3.2.2 was followed exactly with the exception of addition of nitrosobenzene or azobenzene instead of nitrobenzene. Due to the high expense of both compounds quantities equivalent to half those used for previous nitrobenzene hydrogenation were used. For nitrosobenzene an amount equal to half the moles of nitrobenzene was added (9.01 g, 0.085 mol), however for azobenzene (7.735 g, 0.0425 mol) an amount equal to one quarter the number of moles used for nitrobenzene hydrogenation was used as two molecules of nitrosobenzene would be required to form one molecule of azobenzene. As both compounds were solid and did not adequately dissolve in a

small volume of solvent, they were added to the reaction chamber in their solid form. After catalyst reduction at 323 K, the hydrogen flow was maintained (30 cm^3 min^{-1}) while the pressure release valve was closed and the port in the roof of the reactor opened. Against this counter current of hydrogen the entire mass of starting material was added to the vessel via a filter funnel. The plug was then replaced and the hydrogen flow ceased. After purging with argon gas and thorough mixing (800 rpm for 1 minute) the standard reaction procedure was commenced using a temperature of 323 K and a pressure of 2 bar g. The mixture was sampled at regular time intervals for analysis using a Varian CP-3800 GC fitted with a 25 m DB-5 column and coupled to a Saturn 2000 trace MS detector and the gas consumption monitored using the gas flow controller.

3.3.2.10 Reaction of Nitrosobenzene with Deuterium Gas

Nitrosobenzene (9.01 g, 0.085 mol) was reacted with deuterium gas following the procedure exactly as outlined in the hydrogenation of nitrosobenzene and azobenzene Section 2.3.2.9. In addition, samples were removed for GC-MS and ^1H MNR analysis using the instrumentation described in Section 3.3.2.7.

3.3.2.11 Azobenzene Hydrogenation with Water as a Dopant

These experiments were performed using catalyst Pd/CSXU (0.1 g) in methanol. The catalyst was reduced following normal procedure then the water dopant (2.1 ml, 0.34 mol) was added to the reactor and mixed with the catalyst and solvent before azobenzene (7.735 g, 0.0425 mol) was added to the solution as a solid following the procedure described in Section 3.3.2.9 (The hydrogenation of nitrosobenzene and azobenzene). Hydrogenation was then commenced at 2 bar g and 323 K. Samples were removed for analysis using a Varian CP-3800 GC fitted with a 25 m DB-5 column and coupled to a Saturn 2000 trace MS detector and the gas consumption monitored using the mass flow controller.

3.3.2.12 Reactions Doped with Nitrosobenzene, Azobenzene and Cyclohexylamine

Hydrogenations of nitrobenzene doped with nitrosobenzene, azobenzene and cyclohexylamine were carried out using catalyst Pd/CSXU. The quantity of dopant was calculated so that an equimolar amount of nitrobenzene and the second reagent were present. A reaction pressure of 2 bar g, a temperature of 323 K and a catalyst mass of 0.1 g were used throughout. In each case the dopant was added prior to nitrobenzene either through the injection port (cyclohexylamine (16.7 ml, 0.17 mol)) or as a solid via the port in the roof of the vessel (nitrosobenzene (9.01 g, 0.085 mol) and azobenzene (7.74 g, 0.0425 mol)) following the procedure in Section 3.3.2.9. After mixing, the nitrobenzene (9.0 ml, 0.085 mol) or in the cyclohexylamine reaction (18 ml, 0.17 mol) was added and reaction commenced. Samples were removed for analysis on a Varian CP-3800 GC fitted with a 25 m DB-5 column and coupled to a Saturn 2000 trace MS detector. The gas consumption was also monitored using the gas flow controller.

3.3.2.13 Aniline Hydrogenation

The hydrogenation of aniline (15.8 ml, 0.17 mol) was attempted with Pd/CSXU (0.1 g), which had been reduced following standard procedure. Methanol and IPA were used as reaction solvents and a pressure and temperature of 5 bar g and 323 K used for both reactions. The experiment was carried out following standard procedure and monitored using a Varian CP-3800 GC fitted with a 25 m DB-5 column and coupled to a Saturn 2000 trace MS detector. The gas consumption was also measured.

3.3.2.1.4 Hydrogenation using the Carbon Supports as Catalysts

The hydrogenation of nitrobenzene (18 ml, 0.17 mol) was attempted using the three carbon supports in place of metal loaded catalysts. The support material (0.1 g), Norit CA1, Norit CN1 or Norit SX Ultra were each added to the reactor with the solvent and the standard reduction procedure followed. A temperature of 232 K, a pressure of 5 bar g and a catalyst mass of 0.1 g were used throughout and methanol was used as the reaction solvent. The reaction was monitored using the hydrogen uptake from the gas flow controller.

3.3.2.15 Hydrogenation using 1 % Pd/alumina Catalyst

The commercial 1 % palladium/alumina catalyst (0.1 g) was used to perform the hydrogenation of nitrobenzene (18 ml, 0.17 mol) under a range of conditions, including in the presence of water (2.1 ml, 0.34 mol), aniline (15.8 ml, 0.17 mol) and cyclohexylamine (16.7 ml, 0.17 mol). Reactions were preformed exactly as described in Section 2.3.2.12 for use of Pd/C catalyst. The reaction solvent was methanol; the reaction temperature was 323 K and the reaction pressure 2 bar g. Reactions were analysed using the gas consumption and using a Varian CP-3800 GC fitted with a 25 m DB-5 column and coupled to a Saturn 2000 trace MS detector.

3.3.3 Raney Catalysis

The Raney nickel was used to perform the hydrogenation of nitrobenzene, nitrosobenzene and azobenzene. As the catalyst was purchased as an active slurry, no alkali activation process was necessary.

3.3.3.1 Experimental Set-up

The hydrogenation experiments were carried out in a 250 ml three-necked round-bottomed flask, fitted with two reflux condensers and a submerged gas inlet tube connected to an external hydrogen source. The apparatus used in shown in Figure 3.2. Gas flow was channelled through a 2 bar pressure gauge and further controlled using a needle valve before entering the reaction vessel via the gas inlet tube. The gas flow rate was measured as it exited the vessel through a bubble flow meter. A magnetic stirrer/heating mantle and silicone oil bath was used to provide stirring and to heat the reaction mixture to the desired temperature.

3.3.3.2 The Hydrogenation of Nitrobenzene, Nitrosobenzene and Azobenzene.

The round-bottomed flask, containing a small volume of methanol (~25 ml) was placed on the balance and zeroed. The Raney catalyst was then added to the solvent using a plastic spoon to scoop a portion of slurry from the container and add it directly to the methanol. Any residue on the spoon was washed into the flask using a Pasteur pipette and methanol from inside the flask. The weight of slurry was then noted. Due to the wet form of the catalyst, the actual mass used in each experiment was variable however all ranged between 4.8 – 6.0 g of wet slurry. Another aliquot of methanol (~ 25 ml) was then added to the flask and swirled gently. After the catalyst had settled to the bottom, the now cloudy methanol was decanted off through a side arm. The washing procedure was repeated with three further times with methanol. Throughout the catalyst washing care was taken to ensure that the Raney catalyst remained under a layer of solvent at all times and did not become exposed to air. This not only prevented catalyst deactivation but also reduced the risk from the dry pyrophoric material. In the last decantation of methanol, as much solvent as possible was removed while still ensuring the catalyst was entirely covered. Then 165 ml of methanol was added to the flask making the volume up to about 190 ml. A magnetic stirrer bar was then added, the reflux condensers attached and the flask placed in the oil bath set at a temperature of 313 K and allowed to equilibrate to the

reaction temperature. The reagent was then added to the flask. Nitrobenzene (10 ml, 0.097 mol) was added via syringe whereas nitrosobenzene (10.38 g, 0.097 mol) or azobenzene (8.83 g, 0.0485 mol) were added as solids directly to the reaction vessel. The solution was stirred for 60 seconds to ensure complete mixing of the nitrobenzene reagent, or for nitrosobenzene and azobenzene to dissolve, before a 0.25 ml portion was removed by syringe for analysis. The hydrogen flow was then started and the gas inlet tube placed into the reaction vessel. At this point the timer was started. All reactions were run for a total time of 8 hours and 0.25 ml samples were removed at 30 minute intervals for analysis by GC-MS on a Varian CP-3800 GC fitted with a 25 m DB-5 column and coupled to a Saturn 2000 trace MS detector.

Figure 3.2: Raney nickel experimental set-up

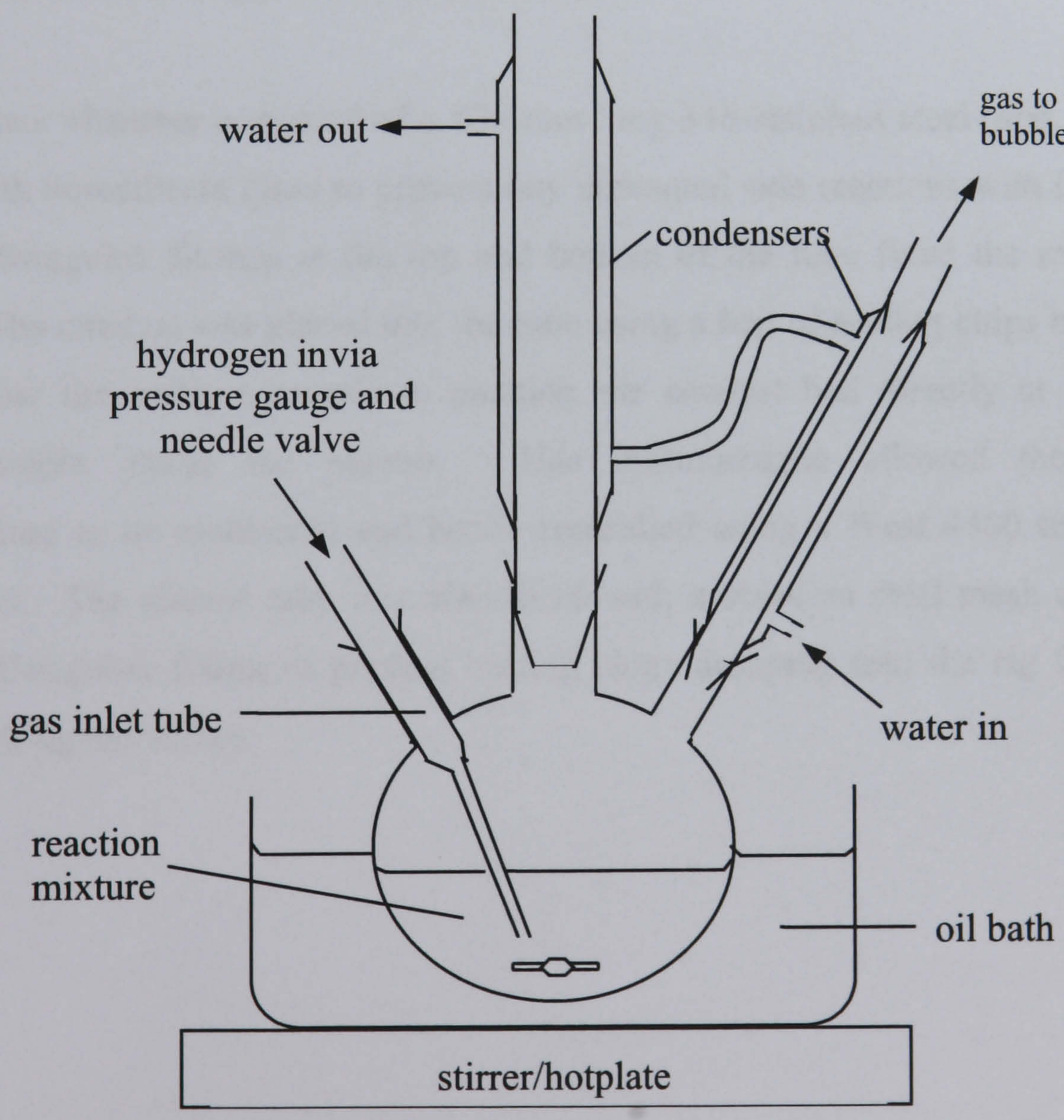

3.3.4 Micro-reactor studies

The hydrogenation of nitrobenzene was also studied using a four-tube micro-reactor where the nitrobenzene reagent was introduced as a vapour and flowed over a fixed bed of catalyst.

3.3.4.1 Micro-reactor

The catalysts were tested for nitrobenzene hydrogenation activity using a specially designed micro-reactor, illustrated in Figure 3.3. The rig was constructed using 316-stainless steel tubing and the appropriate Swagelok valves and fittings. The rig was constructed prior to the experimental work commencing but a reaction protocol for operation of the micro-reactor and a full commissioning of the rig had to be completed before the apparatus was put into use.

The reactor chamber consisted of a 600 mm long 316-stainless steel tube, internally lined with borosilicate glass to prevent any unwanted side reactions with the reactor walls. Swagelok fittings at the top and bottom of the tube fixed the reactor into place. The catalyst was placed into the tube using a bed of boiling chips both above and below the catalyst sample to position the catalyst bed directly at the tip of thermocouple inside the reactor. This thermocouple allowed the reaction temperature to be monitored and hence controlled using a West 4400 temperature controller. The reactor tube was also fitted with a stainless steel mesh disc at the bottom Swagelok fitting to prevent boiling chips dropping into the rig framework and blocking the valves.

Figure 3.3: Micro-reactor set-up

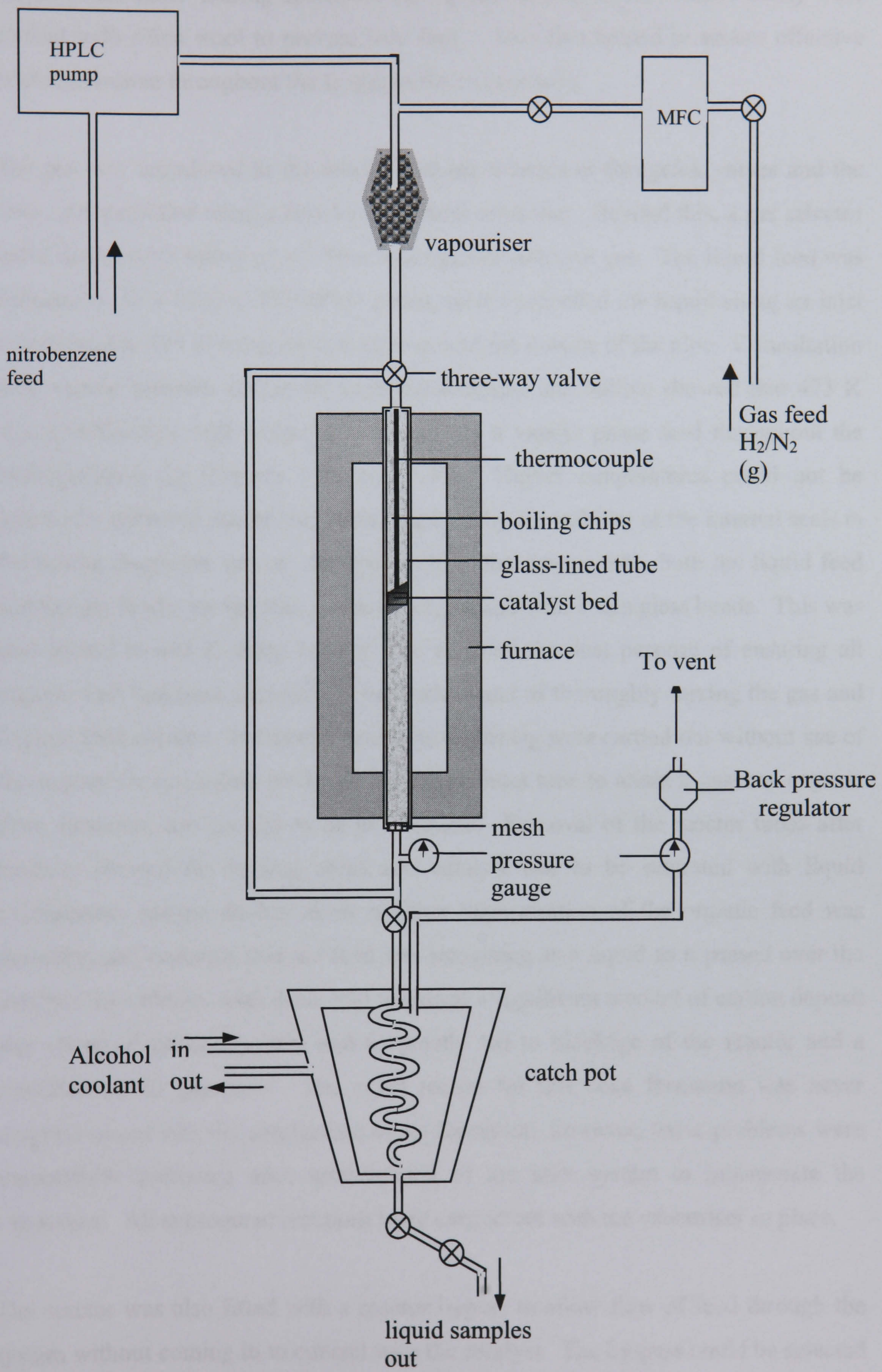

The reactor was heated using a single zone LCP furnace that encased the entire length of the tube. During operation, the top and bottom of the furnace cavity were packed with silica wool to prevent heat loss. This also helped to ensure effective heat distribution throughout the length of the reactor tube.

The gas was introduced to the reactor through a series of Swagelok valves and the flow rate controlled using a Brooks mass flow controller. Beyond this, a gas selector valve enabled the selection of either hydrogen or nitrogen gas. The liquid feed was introduced via a Gilston 307 HPLC pump, which propelled the liquid along an inlet tube heated to 473 K using heating tape around the outside of the pipe. Consultation with vapour pressure curves for both nitrobenzene and aniline showed that 473 K was a sufficiently high temperature to achieve a vapour phase feed throughout the hydrogenation rig (Figures 3.4a and 3.4b). Higher temperatures could not be practically achieved due to limitations imposed by the stability of the internal seals in the heated Swagelok valves. Before reaching the reactor tube, both the liquid feed and the gas feed were fed into a vapouriser, packed with 3 mm glass beads. This was also heated to 473 K using heating tape and had the dual purpose of ensuring all organic feed had been successfully vapourised and of thoroughly mixing the gas and organic feed streams. Initial trial reactions on the rig were carried out without use of the vapouriser and relied solely on the heated inlet tube to attain a gaseous organic flow, however, this proved to be problematic. Removal of the reactor tubes after reaction showed the boiling chips and catalyst bed to be saturated with liquid nitrobenzene raising doubts about whether vapourisation of the organic feed was occurring and concerns that the feed was remaining as a liquid as it passed over the catalyst. In addition, with these trial reactions a significant amount of carbon deposit was observed inside the tube and frequently led to blockage of the reactor and a cessation of the gas flow. The exact reason for this coke formation was never understood nor was the mechanism of its formation, however, these problems were successfully overcome after modification of the inlet system to incorporate the vapouriser. All subsequent reactions were carried out with the vapouriser in place.

The reactor was also fitted with a reactor bypass to allow flow of feed through the system without coming in to contact with the catalyst. The by-pass could be selected

using the three-way valve directly above the reactor tube and the two-way valve located on the exit piping below the reactor. The by-pass was also heated to 473 K using heating tape.

Figure 3.4a: Vapour pressure vs temperature curve for nitrobenzene

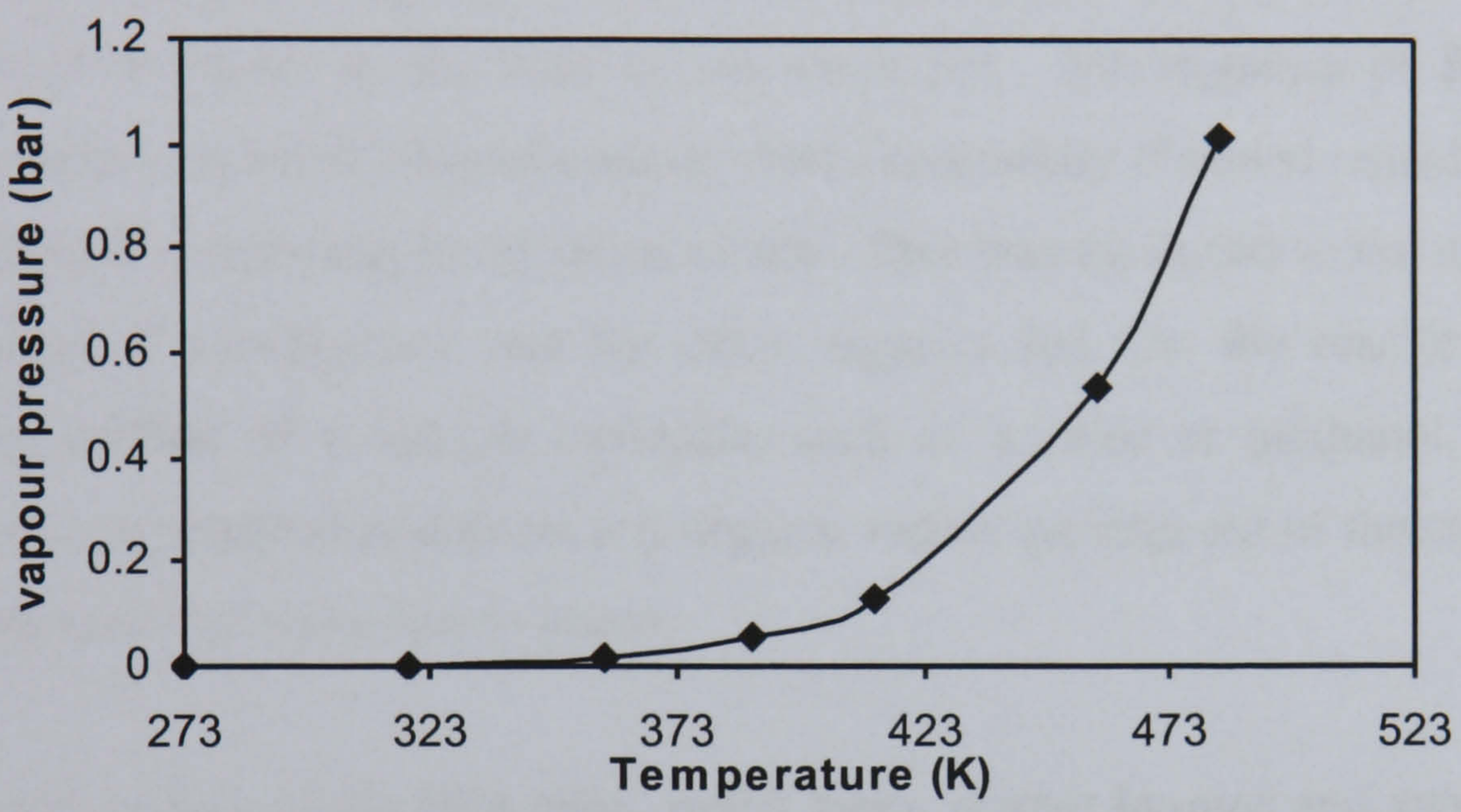

Figure 3.4b: Vapour pressure vs temperature curve for aniline

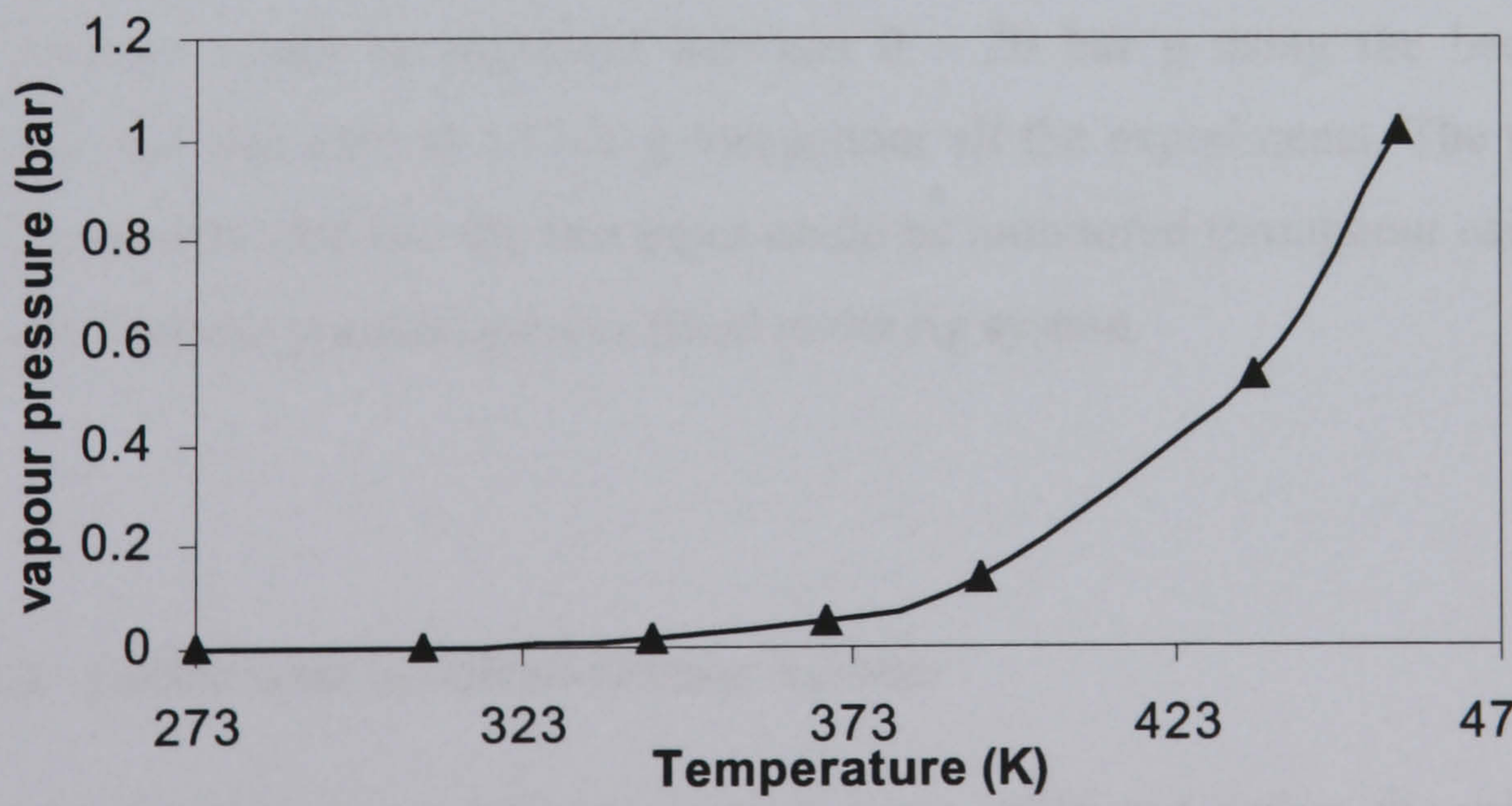

After the feed stream had passed over the catalyst bed it was carried from the reactor tube through the exit pipes, heated to 473 K using heating tape, before passing into the catch pot at the bottom. This chamber could be cooled to 273 K with an external alcohol coolant system using a Betta-Tech coolant circulator. The organic exit feed was then condensed and held in the catch pot. The gas feed steam exited the pot via the pipe leaving the roof of the catch pot chamber, through a Kenmac back-pressure regulator valve, used to control the pressure inside the reaction tube, and into the gas extraction. Liquid samples were removed from the catch pot by manipulation of two consecutive valves at the base of the catch pot. Investigation of the sampling procedure revealed that liquid samples were successfully obtained regardless whether the coolant system was in operation or not. This was attributed to the relatively low volatility of nitrobenzene and the other organics fed into the reactor. However, during feeding of a volatile molecule, such as acetone or methanol, the coolant system was required to prevent any organic vapour passing out of the catch pot with the gas feed and being lost to waste.

The temperature of the inlet pipes, outlet pipes, reactor by-pass and vapouriser were held constant at 473 K throughout all the experimental work. All heated tubes were insulated using glass wool and aluminium tape. The temperature of the reactor tube was varied between 373 – 773 K during initial rig optimisation experiments but was held constant at 473 K throughout the majority of reactions described in this thesis. The pressure could be regulated between 0 – 20 bar g using the back-pressure regulator but was kept at 10 bar g throughout all the experiments. The pressure in both the reactor tube and the exit pipes could be monitored throughout using the two Bourdon Sedeme pressure gauges fitted to the rig system.

3.3.4.2 Calibration of Micro-reactor System

Both the liquid and gas delivery systems were calibrated before the micro-reactor was put into use. The mass flow controller was calibrated with hydrogen gas using a bubble flow meter and a soapy solution. The calibration curve is shown in Figure 3.5. The mass flow controller was not calibrated for nitrogen as this gas was only

used for leak testing and was not required to flow with a controlled rate or used during the hydrogenation reaction.

Calibration of the HPLC pump controlling the liquid feed was also carried by measuring the volume of feed removed from a measuring cylinder and comparing it with the set pump rate. This graph is shown in Figure 3.6 and shows that liquid is pumped through the system at a value exactly double the set rate. Therefore, throughout operation of the HPLC pumps the set values were adjusted so as to be half of that required for the reaction.

Figure 3.5: Calibration of hydrogen through the mass flow controller.

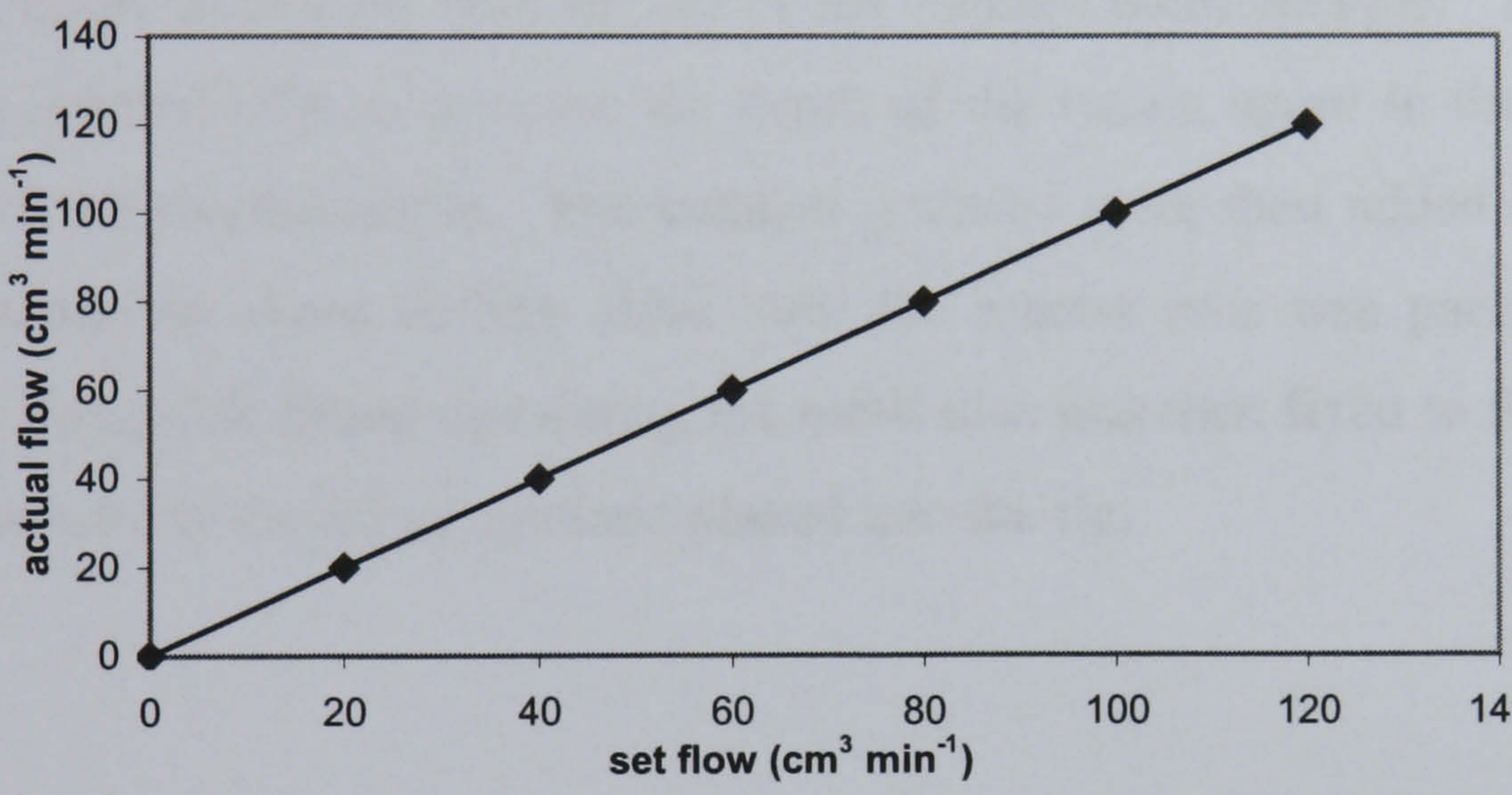

Figure 3.6: Calibration of HPLC pump

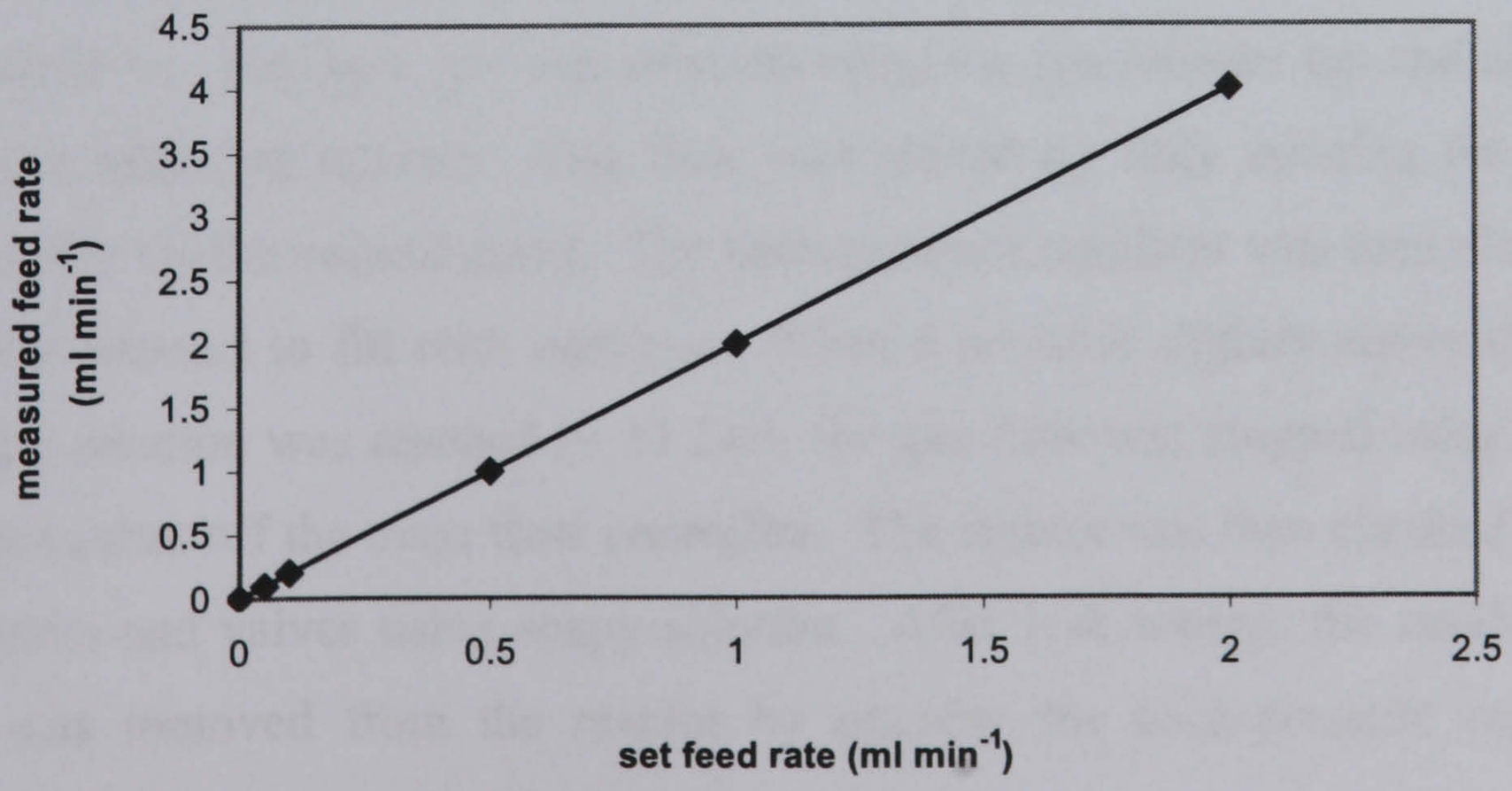

3.3.4.3 Preparation of Reactor Tubes

All catalysts tested for gas phase nitrobenzene hydrogenation activity existed in a powder form. Before introduction to the reactor, each catalyst was pressed into a disc using a hydraulic press, under no vacuum at 5 bar for 5 minutes, then re-ground into granules using a mortar and pestle. After sieving, granules with a particle diameter between 200-450 μm were retained for use in the reactor. The only exception was catalyst Pd/CSXU that did not press easily into discs. Instead this catalyst was added in the original powder form but two plugs of glass wool were packed into the tube, both above and below the catalyst bed, to prevent the fine granules dropping through the boiling chip packing. In each experiment 0.5 g of catalyst was used for the reaction. The reactor tube was inverted and filled with boiling chips until level with the tip of the internal thermocouple. This was tested using a marked tube to measure the depth of the vacant space in the reactor to the depth of the thermocouple. The catalyst granules were then added directly on top and covered by more boiling chips until the reactor tube was packed fully. The bottom Swagelok fitting containing the mesh disc was then fixed to the tube and the whole assembly turned upright and placed into the rig.

3.3.4.4 Micro-reactor Preparation

After fitting the reactor tube to the rest of the rig, the micro-reactor control unit was switched on. Nitrogen gas was selected using the gas selector tap and all valves on the gas inlet line opened. Gas flow was started by fully opening the mass flow controller via the control panel. The back-pressure regulator was then closed and the reactor allowed to fill with nitrogen. When a pressure slightly above that required for the reaction was reached (~ 11 bar), the gas flow was stopped using the control panel to shut off the mass flow controller. The reactor was then checked for leaks at all joints and valves using soapy solution. After leak testing, the residual nitrogen gas was removed from the reactor by opening the back-pressure regulator and allowing the gas to vent.

3.3.4.5 Catalyst Reduction

The catalyst was then reduced according to the pre-determined conditions determined by the TPR data. These are listed in Table 3.3. The appropriate heating program was selected and allowed to run. Hydrogen gas was selected using the gas selector tap and the gas flow started using the control panel to open the mass flow controller valve to controlled flow. All catalysts were reduced in a flow of 15 cm^3 min^{-1} H_2 gas.

3.3.4.6 Reaction Procedure using Nitrobenzene Feed

Each catalyst in Table 3.3 was reduced according to the described procedure. The temperature was adjusted to that required for reaction and reaction tube pressurised to 10 bar using hydrogen. The hydrogen flow was then set to 25 cm^3 min^{-1} and the organic flow commenced at 0.1 ml min^{-1} using the HPLC pump controls. Throughout the reactions samples were removed at 1 hour time intervals and analysed.

Table 3.3: Catalyst reduction procedures

CATALYST	TEMPERATURE (K)	RAMP RATE (K min^{-1})	HOLD TIME (Hour)
Pd/CSXU	473	1	1
1 % Pd	473	1	1
20 % Cu	473	2	8
20 % Ni	723	2	8
20 % Co	873	2	8
15% Cu/ 5 % Ni	723	2	8
10% Cu/ 10 % Ni	723	2	8
5 % Cu/ 15 % Ni	723	2	8
15 % Cu/ 5 % Co	873	2	8
10 % Cu/ 10 % Co	873	2	8
5 % Cu/ 15 % Co	873	2	8
15 % Ni/ 5 % Co	873	2	8
10 % Ni/ 10 % Co	873	2	8
Puralox alumina support	873	2	8
5 % Ni/ 15 % Co	873	2	8
10 % Cu/silica	373	1	1
	423	1	1
	473	1	1
	523	1	1

3.3.4.7 Reactions where Catalyst was Pre-Treated with Water

Nitrobenzene hydrogenation with a pre-treated catalyst was carried out using catalysts Pd/CSXU, 1 % Pd/alumina, 20 % copper, 20 % nickel, 20 % cobalt, 10 % Cu/10 % Ni, 10 % Cu/10 % Co, 10 % Ni/10 % Co and the alumina support. After reduction following the procedure outlined in Table 3.3, the reaction temperature was adjusted to 473 K. Distilled water vapour was then passed over the catalyst bed for 1

hour under a hydrogen flow of 25 cm^3 min^{-1} and using the same liquid flow rate of 0.1 ml min^{-1}. After this period, the feed was switched to nitrobenzene and the reaction continued as usual, maintaining a hydrogen flow of 25 cm^3 min^{-1}.

3.3.4.8 Reactions using Deuterium Gas

Experiments with catalyst Pd/CSXU following the procedure described in Section 2.3.4.6 were also performed using deuterium in place of hydrogen.

3.3.5 Sample Analysis

Throughout all liquid phase and gas phase hydrogenation experiments, samples were removed from the reaction vessel at regular timed intervals and analysed using GC or GC-MS. The majority of analysis was performed using a Varian GC-MS (CP 3800 CG and Saturn 2000 MS) fitted with a 25 m DB5 capillary column. Samples consisting of a neat product (e.g. samples exiting the micro-reactor when a neat feed was used) were diluted in methanol before running through the GC. Samples resulting from a reaction with a mixed feed, such as with water or solvent, or from the stirred tank reactor were run without further dilution.

2.3.4.1 Varian GC-MS Operating Conditions

Throughout all sample analysis the GC-MS operating conditions were held constant. The injector temperature was set at 513 K. The column carrier gas was helium and was maintained at a constant pressure of 6.0 psi (equivalent to a continuous helium flow of 5 ml min^{-1}). The column oven was initially kept at 353 K and was ramped to 493 K at a rate of 15 deg min^{-1} and then held at 493 K for 10 minutes. The MS detector was operated in "RIC mode" that used the area under the peaks as a measure of concentration in a similar way to an integrator. This was used instead of the "quan

ion" mode that used the relative strength of the principal ion in the mass spectrum to give a measure of concentration as it gave more reliable and repeatable calibration results.

3.3.5.2 Calibration of Varian GC-MS

All GC and GC-MS equipment was calibrated fully before being put into use. As an example, the calibration of the Varian GC-MS is shown here. Calibrations were carried out for nitrobenzene, aniline, nitrosobenzene, azobenzene, azoxybenzene and cyclohexylamine. Standard solutions for each of the components were made up and a series of dilutions performed to obtain a series of solutions of known concentration. These were then analysed on the GC-MS to determine the area of the peak generated in the resulting chromatogram. Three injections were taken for each standard and an average of the peak areas taken. A graph of the concentration of the standards verus the peak areas then gave the calibration graph for each component that could be used to quantitatively analyse reaction samples using the generated peak areas to determine the concentration of the reagents present.

3.3.5.2.1 Nitrobenzene Calibration

The concentration of the calibration standards analysed and the corresponding peak areas determined from the GC chromatogram for the nitrobenzene calibration are shown below in Table 3.4. The calibration graph is shown in Figure 3.7.

Table 3.4: Calibration data for nitrobenzene

concentration (mol L^{-1})	peak area (counts)			
	1	2	3	average
0	0	0	0	0
0.116	219042	218511	239162	225572
0.232	508958	488785	495510	497751
0.348	668305	751846	712220	710790
0.464	883016	1003294	912218	932843
0.580	1115588	1011355	983820	1036921

Figure 3.7: Calibration graph for nitrobenzene.

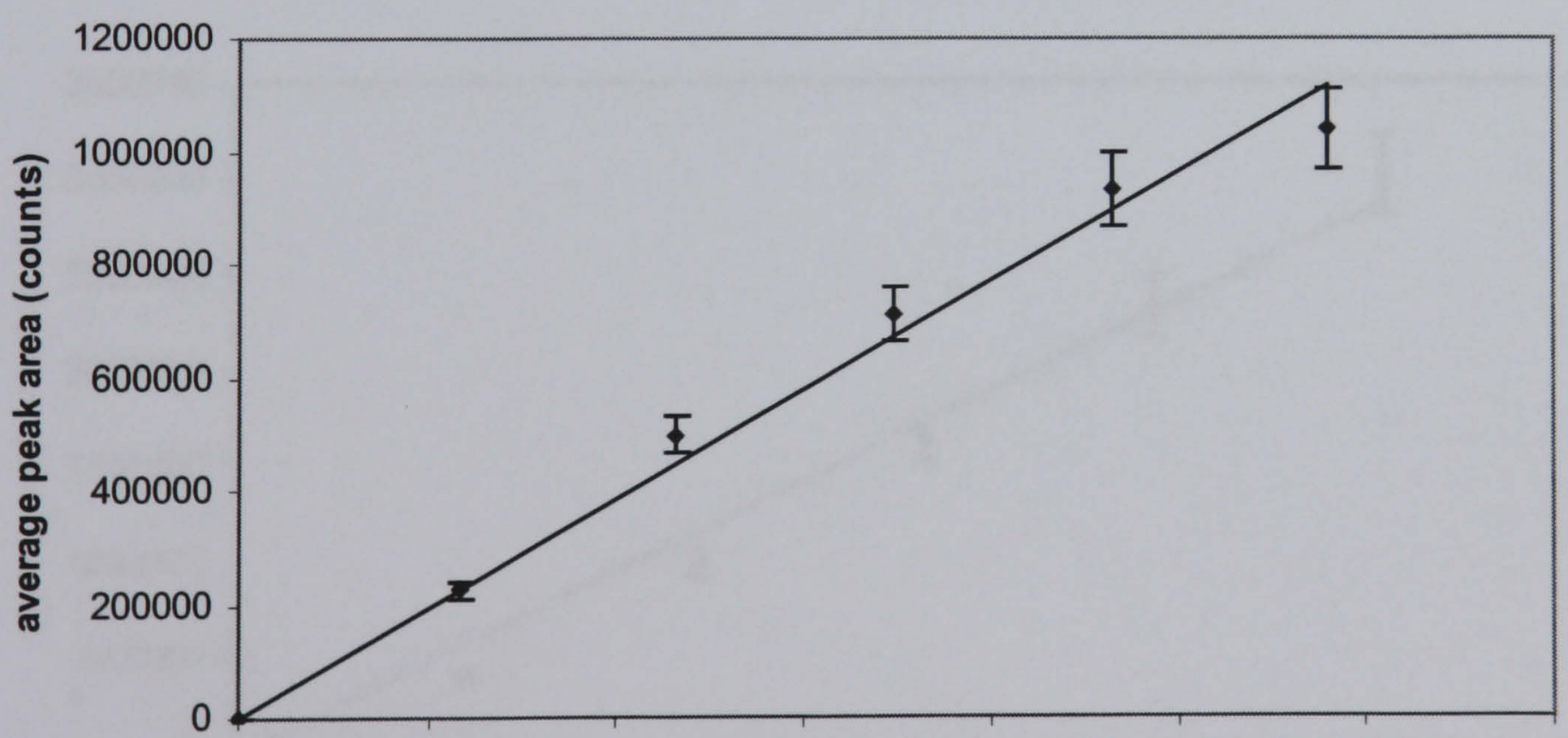

3.3.5.2.2 Aniline Calibration

The concentration of the calibration standards analysed and the corresponding peak areas determined from the GC chromatogram are displayed in Table 3.5 and the calibration graph in Figure 3.8.

Table 3.5: Calibration data for aniline

concentration (mol L^{-1})	peak area (counts)			
	1	2	3	average
0	0	0	0	0
0.116	384993	398025	403882	395633
0.232	985561	994646	987515	989241
0.348	1501238	1681683	1652640	1611854
0.464	2450331	2131056	2358991	2313459
0.580	3100235	2818886	3100235	3006452

Figure 3.8: Calibration Graph for aniline

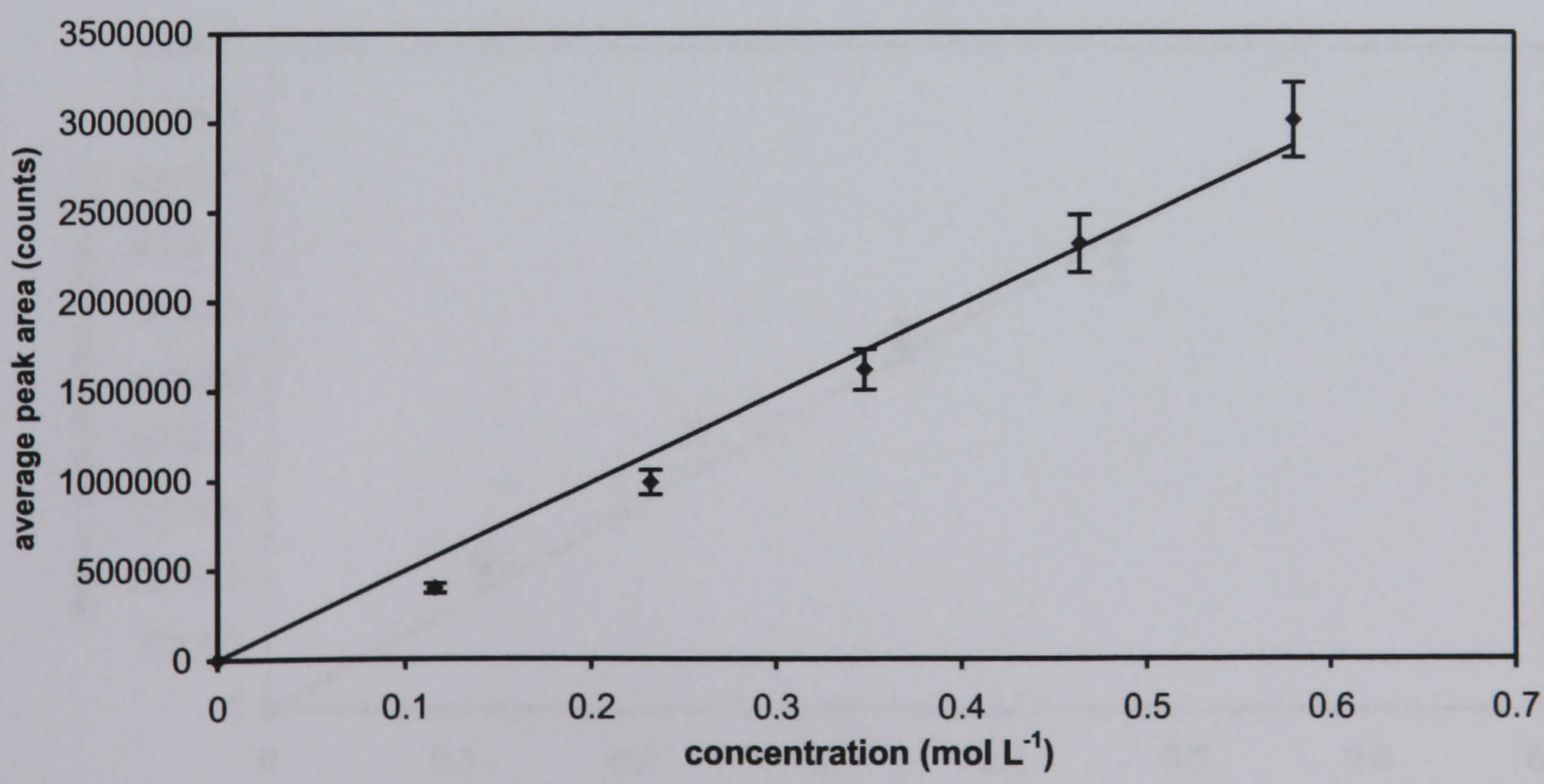

3.3.5.2.3 Nitrosobenzene Calibration

The concentration of the calibration standards standards analysed and the corresponding peak areas determined from the GC chromatogram are displayed in Table 3.6 and the calibration graph in Figure 3.9.

Table 3.6: Calibration data for nitrosobenzene

concentration (mol L^{-1})	peak area (counts)			
	1	2	3	average
0	0	0	0	0
0.116	108462	114257	110181	110967
0.232	215170	205660	216894	212575
0.348	272878	280716	280983	278192
0.464	319946	356070	333589	336535
0.580	362453	331039	333639	342377

Figure 3.9: Calibration graph for nitrosobenzene

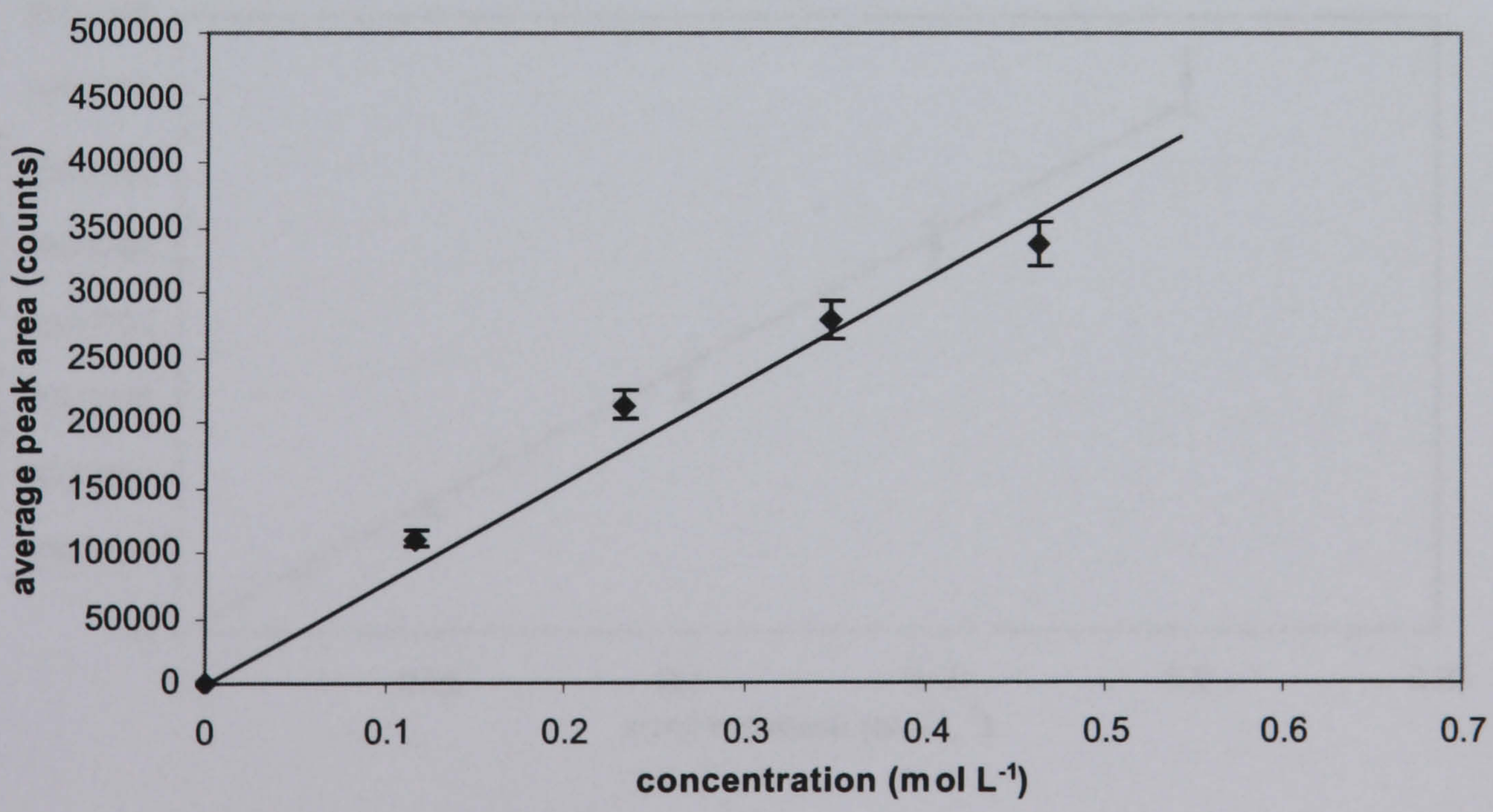

3.3.5.2.4 Azobenzene Calibration

The concentration of the calibration standards standards analysed and the corresponding peak areas determined from the GC chromatogram are displayed in Table 3.7 and the calibration graph in Figure 3.10.

Table 3.7: Calibration data for azobenzene

concentration (mol L^{-1})	peak area (counts)			
	1	2	3	average
0.000	0	0	0	0
0.025	774687	802855	791668	789737
0.050	1622539	1591314	1646482	1620112
0.100	3173862	3259928	3116504	3183431
0.150	4935610	5296590	4752137	4994779
0.200	6659886	7312697	7447702	7140095

Figure 3.10: Calibration graph for azobenzene

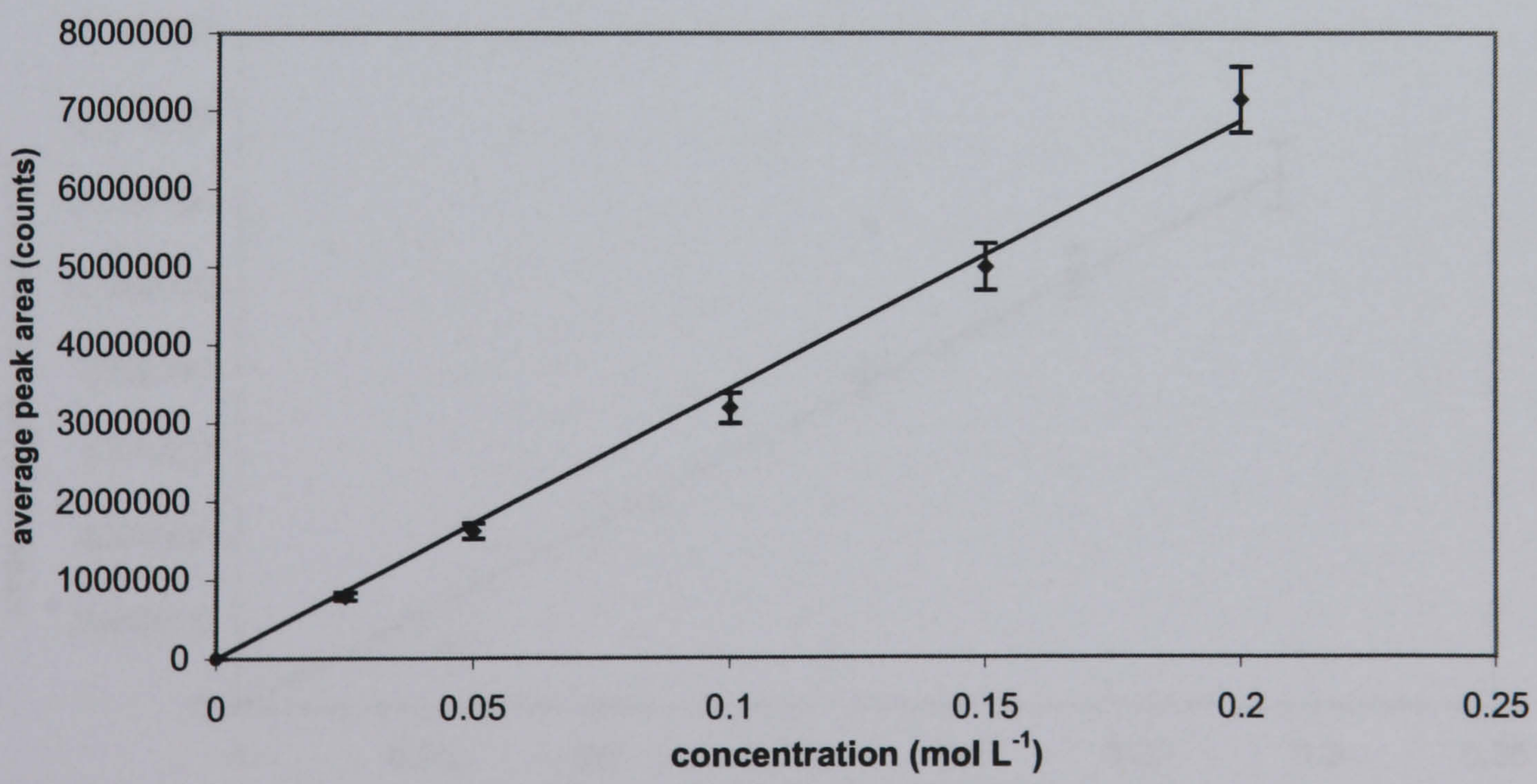

3.3.5.2.5 Azoxybenzene Calibration

The concentration of the calibration standards standards analysed and the corresponding peak areas determined from the GC chromatogram are displayed in Table 3.8 and the calibration graph in Figure 3.11.

Table 3.8: Calibration data for azoxybenzene

concentration (mol L^{-1})	peak area (counts)			
	1	2	3	average
0.000	0	0	0	0
0.058	1370842	1400054	1412907	1394601
0.174	8068050	7796383	7498791	7787741
0.232	9965112	10694540	10119874	10329826
0.290	13089852	11774767	13046990	12637203

Figure 3.11: Calibration graph for azoxybenzene

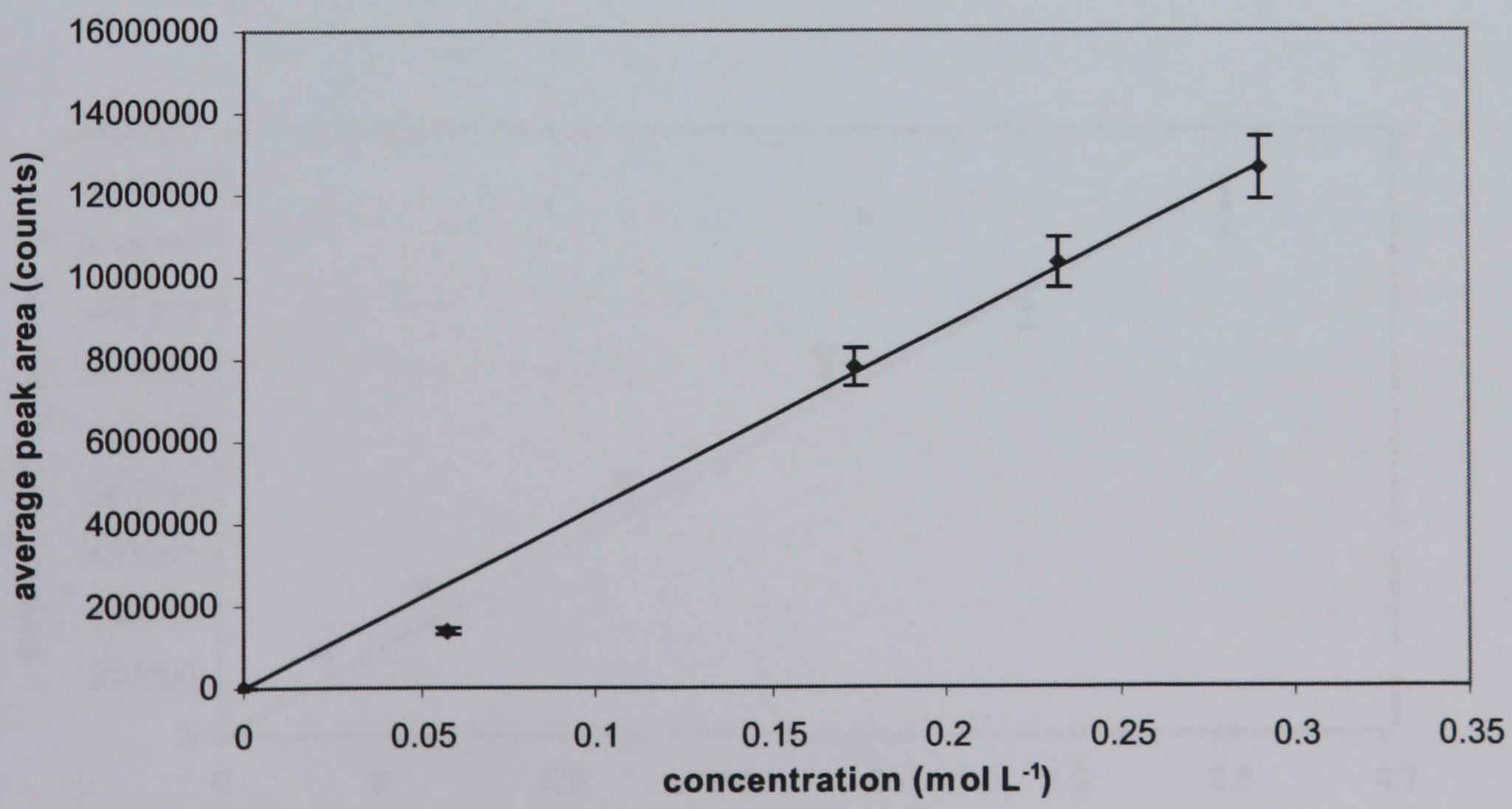

3.3.5.2.6 Cyclohexylamine Calibration

The concentration of the calibration standards standards analysed and the corresponding peak areas determined from the GC chromatogram are displayed in Table 3.9 and the calibration graph in Figure 3.12.

Table 3.9: Calibration data for cyclohexylamine

concentration (mol L^{-1})	peak area (counts)			
	1	2	3	average
0.000	0	0	0	0
0.060	274018	278467	282818	278434
0.120	530662	484215	447742	487540
0.240	790389	851281	818189	819953
0.360	1227196	1226570	1124455	1192740
0.480	1469371	1397421	1382470	1416421
0.600	1768352	1738111	1728408	1744957

Figure 3.12: Calibration Graph for Cyclohexylamine

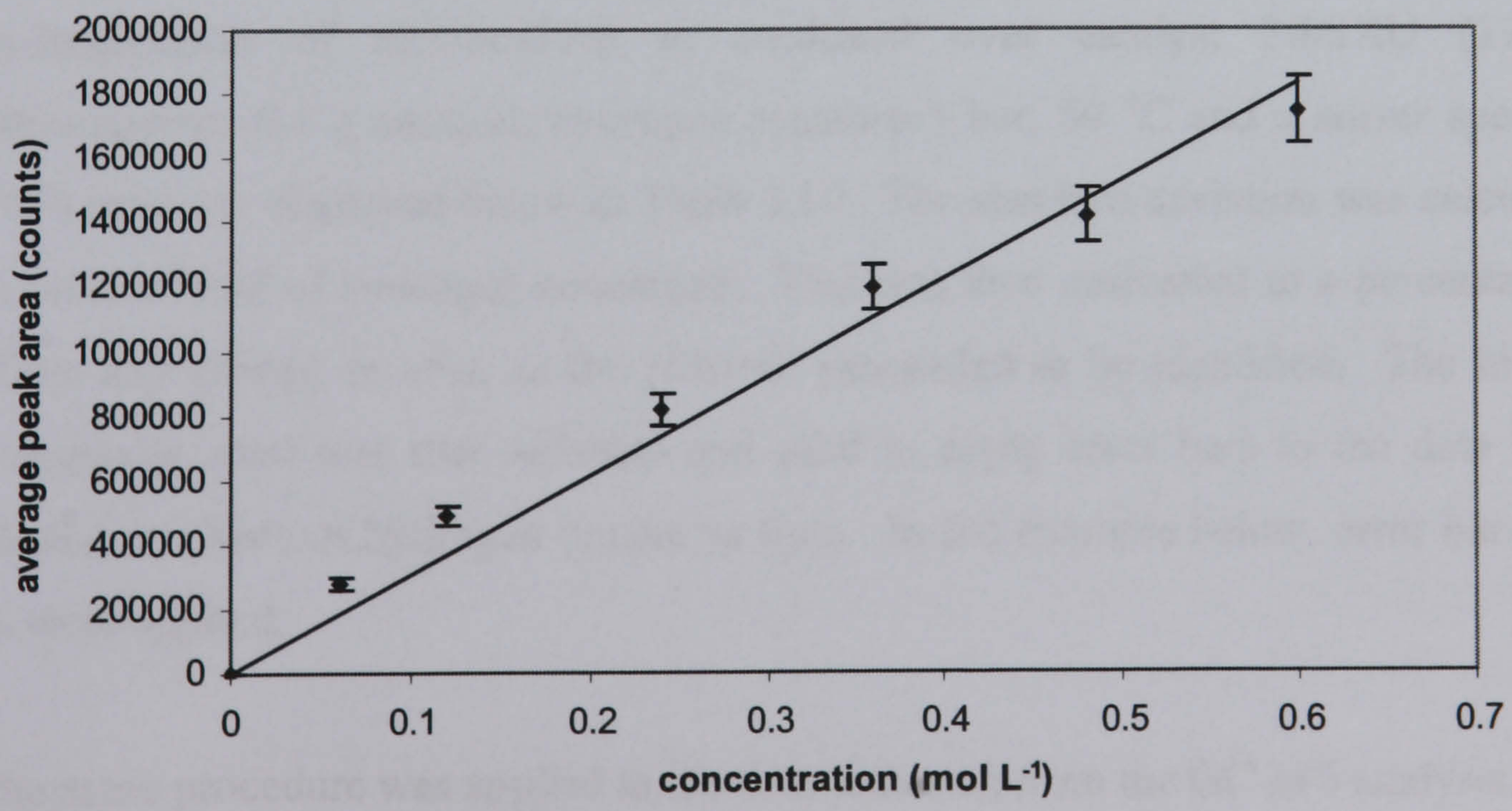

3.3.6 Calculation of Experimental Error

The experimental error associated with the measurements taken during catalyst testing was determined using standard analytical methods. Data collected from duplicate hydrogenation reactions (experiments performed under identical reaction conditions) were complied and used to determine the standard deviation of the results throughout the measurement. The standard deviation was calculated using Equation 3.11.

$$S = \sqrt{\frac{\Sigma (x_i - x^-)^2}{N - 1}} \qquad \text{Equation 3.11}$$

where,

s = standard deviation

x_i = experimental value

x' = average value

N = number of measurements

For reactions performed in the Büchi autoclave, errors were calculated on the hydrogen uptake data and on the the GC analysis. For reactions performed in the microreactor, errors were calculated on the GC analysis. As an example, the values used to calculate the standard deviation in the hydrogen uptake results for the hydrogenation of nitrobenzene in methanol over catalyst Pd/SXU (17 ml nitrobenzene, 0.1 g catalyst, hydrogen pressure 5 bar, 50 °C and a stirrer speed of 1000 rpm) are displayed below in Table 3.10. The standard deviation was calculated in units of mol of hydrogen consumed. This was then converted to a percentage to allow any change in error as the reaction proceeded to be identified. The highest percentage error was then selected and used to apply error bars to the data when plotted as charts of hydrogen uptake vs time. In the example below, error bars of 6 % were applied.

The same procedure was applied to the data collected from the GC-MS analysis. The nitrobenzene concentrations obtained during the GC-MS analysis of the reactions described above, and the calculated standard deviations are displayed in Table 3.11.

In this example errors of 6 % were applied to the data when plotting the results as charts of concentration versus time. The same calculations were perfomed on the measured aniline concentrations and those of any intermediate species as the reaction progressed.

Table 3.10: Calculation of standard deviation on hydrogen uptake data

	hydrogen uptake (mol)				standard deviation	
Time (min)	Exp 1	Exp 2	Exp 3	average	mol	%
0	0	0	0	0	0.0000	0.00
10	0.0780	0.0768	0.0765	0.0771	0.0008	1.03
20	0.1524	0.1426	0.1404	0.1451	0.0064	4.40
30	0.2067	0.1945	0.1938	0.1983	0.0073	3.66
40	0.3000	0.2778	0.2879	0.2886	0.0111	3.85
50	0.3230	0.2934	0.3121	0.3095	0.0150	4.84
60	0.3879	0.3609	0.3769	0.3752	0.0136	3.62
70	0.4297	0.3832	0.3998	0.4042	0.0236	5.83
80	0.4354	0.4178	0.4237	0.4256	0.0090	2.10
90	0.4458	0.4338	0.4367	0.4388	0.0063	1.43

Table 3.11: Calculation of standard deviation on GC-MS data

	nitrobenzene concentration (mol L^{-1})				standard deviation	
Time (min)	Exp 1	Exp 2	Exp 3	average	mol L^{-1}	%
0	0.610	0.593	0.589	0.597	0.011	1.87
10	0.512	0.509	0.511	0.511	0.002	0.30
20	0.433	0.427	0.423	0.428	0.005	1.18
30	0.336	0.328	0.331	0.332	0.004	1.22
40	0.284	0.273	0.265	0.274	0.010	3.48
50	0.236	0.229	0.230	0.232	0.004	1.63
60	0.153	0.144	0.147	0.148	0.005	3.10
70	0.066	0.061	0.059	0.062	0.004	5.82
80	0.011	0.010	0.010	0.010	0.001	5.59
90	0.002	0.001	0.001	0.001	0.000	0.00

When the hydrogen uptake or GC-MS data were used to calculate an initial reaction rate in either the liquid phase or microreactor hydrogenations, the error associated with this calculation was also determined. The hydrogen uptake data from duplicate experiments were used to calculate an initial rate of reaction from plots of hydrogen uptake vs time. A gradient was determined from the initial part of the plot, where a linear relationship between the hydrogen uptake and reaction time was observed. In the example used above, the hydrogen uptake data displayed in Table 3.10, the

gradient was calculated over the first 30 minutes of hydrogenation. The plots used to calculate the gradient in this example are displayed in Figure 3.13.

Figure 3.13: Calculation of initial rate

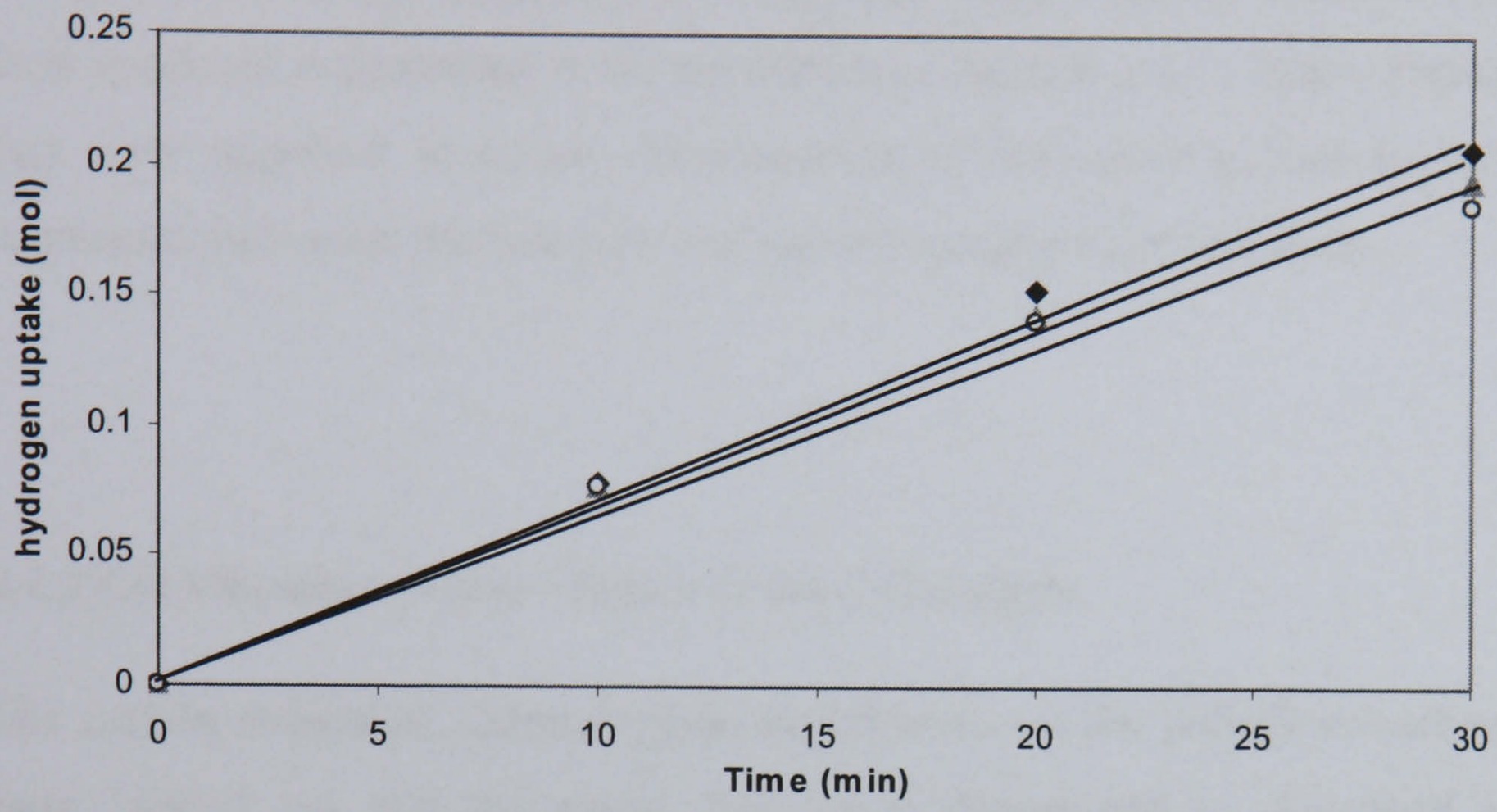

The initial rates from the above plot and the mean rate were then used to calculate the standard deviation of the rate value. The rates and the calculated standard deviations are displayed in Table 3. 12. If the standard deviation calculated for the intial rates was less than those calculated on the individual measurements, as in this example, the error determined to each associated with each individual measurement, in this case 6 %, was applied to the rate data.

Table 3.12: Standard deviation in reaction rates

		standard deviation	
reaction	initial rate (mol min^{-1})	(mol min-1)	%
Exp 1	6.89	0.08	1.2
Exp 2	6.48	0.09	1.4
Exp 3	6.61	0.11	1.7

The same methodology was applied when calculating errors on all the rate data presented in this thesis.

4.0 RESULTS

4.1 Characterisation of Pd/C Catalysts

The palladium/carbon catalysts were supplied ready-made by Johnson Matthey and their synthesis is described in the experimental Section 3.1.1. Some characterisation data were supplied, however, determination of the active palladium surface area, dispersion and metal particle size was carried out as part of this study.

4.1.1 CO Chemisorptions Studies of Pd/C Catalysts

The carbon monoxide chemisorption experiments on the palladium/carbon catalysts were carried out and the metal dispersions determined as described in Section 3.2.1.1. The three catalysts showed significantly different average dispersions with catalyst, Pd/CN1 showing the lowest average dispersion (8.9 %), whereas catalyst Pd/CSXU gave the highest average dispersion with a value of 42.0 % (Table 4.1). Calculation of the average metal particle size showed, as expected, that catalyst Pd/CN1 had the largest metal particles and that catalyst Pd/CSXU had the smallest.

Table 4.1: Carbon monoxide chemisorption results

catalyst	carbon support	% loading	dispersion (%)	average particle size (nm)
Pd/CN1	Norit CN1	3	8.9	12.2
Pd/CA1	Norit CA1	3	12.6	8.7
Pd/CSXU	Norit SX Ultra	3	42.0	2.6

4.2 Preparation and Characterisation of Co, Cu, Ni HDC Catalysts

Twelve catalysts were synthesised using the HDC method and were characterised using a variety of techniques. Observations during the preparation of these catalysts and the results of catalyst characterisation are described below.

4.2.1 pH Changes During HDC Catalyst Synthesis

The pH of the metal solutions was monitored throughout preparation of the HDC catalysts. The depositions were carried out under high pH conditions to facilitate a strong interaction between the positive metal ions and the negatively charged alumina support material. Figures 4.1-4.4 show how the pH altered during preparation of the various catalysts. The pH changes during the synthesis of the three single metal catalysts are shown in Figure 4.1, the copper-nickel catalysts in Figure 4.2, the nickel-cobalt catalysts in Figure 4.3 and the cobalt-copper catalysts in Figure 4.4. In all cases, the pH decreased fairly rapidly over the first 0-30 minutes of the deposition process as the ammonia was distilled off and then levelled off during the rest of the procedure after complete removal of the ammonia had occurred.

Figure 4.1: Change in pH during synthesis of the single metal HDC catalysts

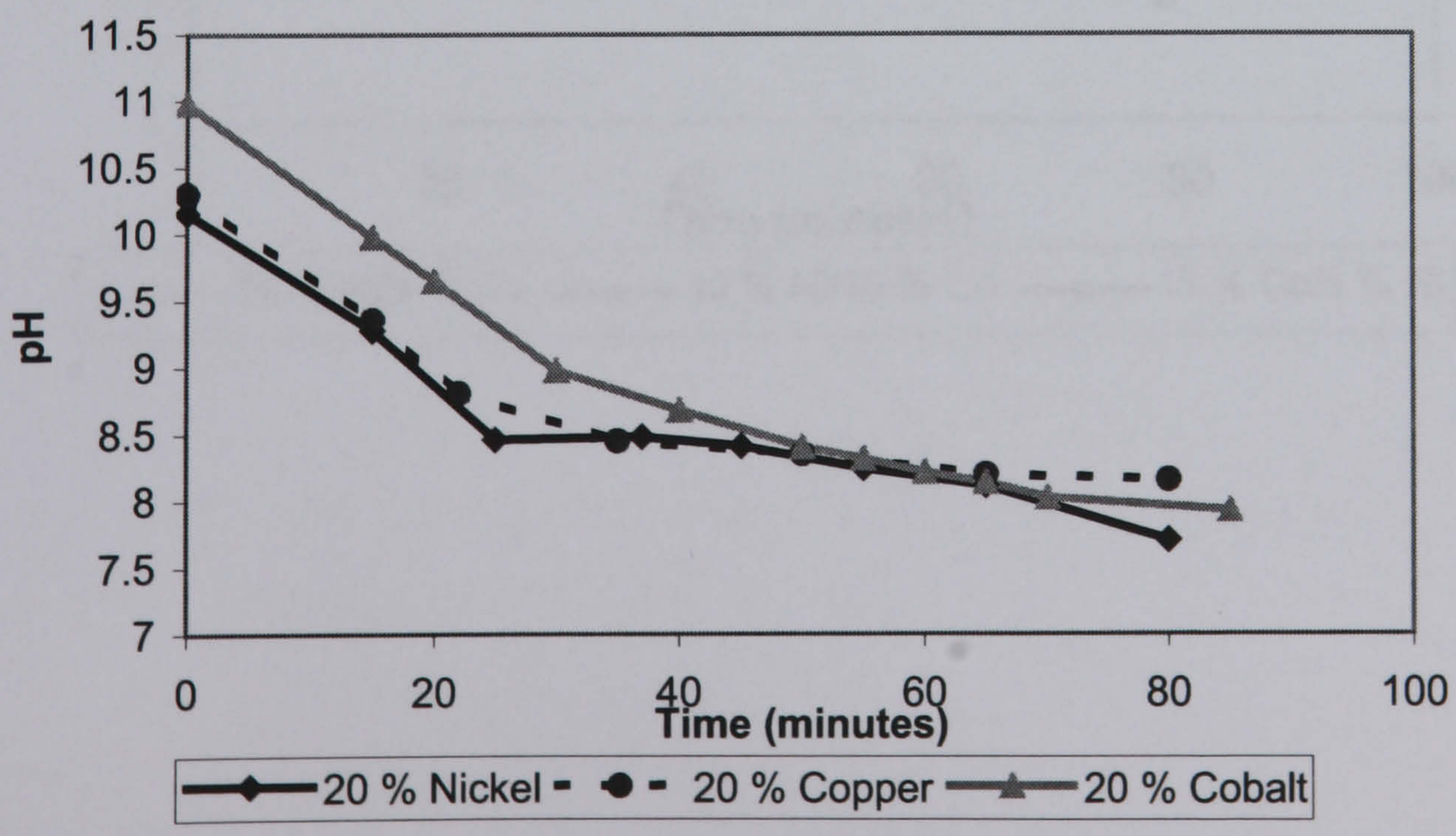

Figure 4.2: Change in pH during synthesis of copper-nickel HDC catalysts

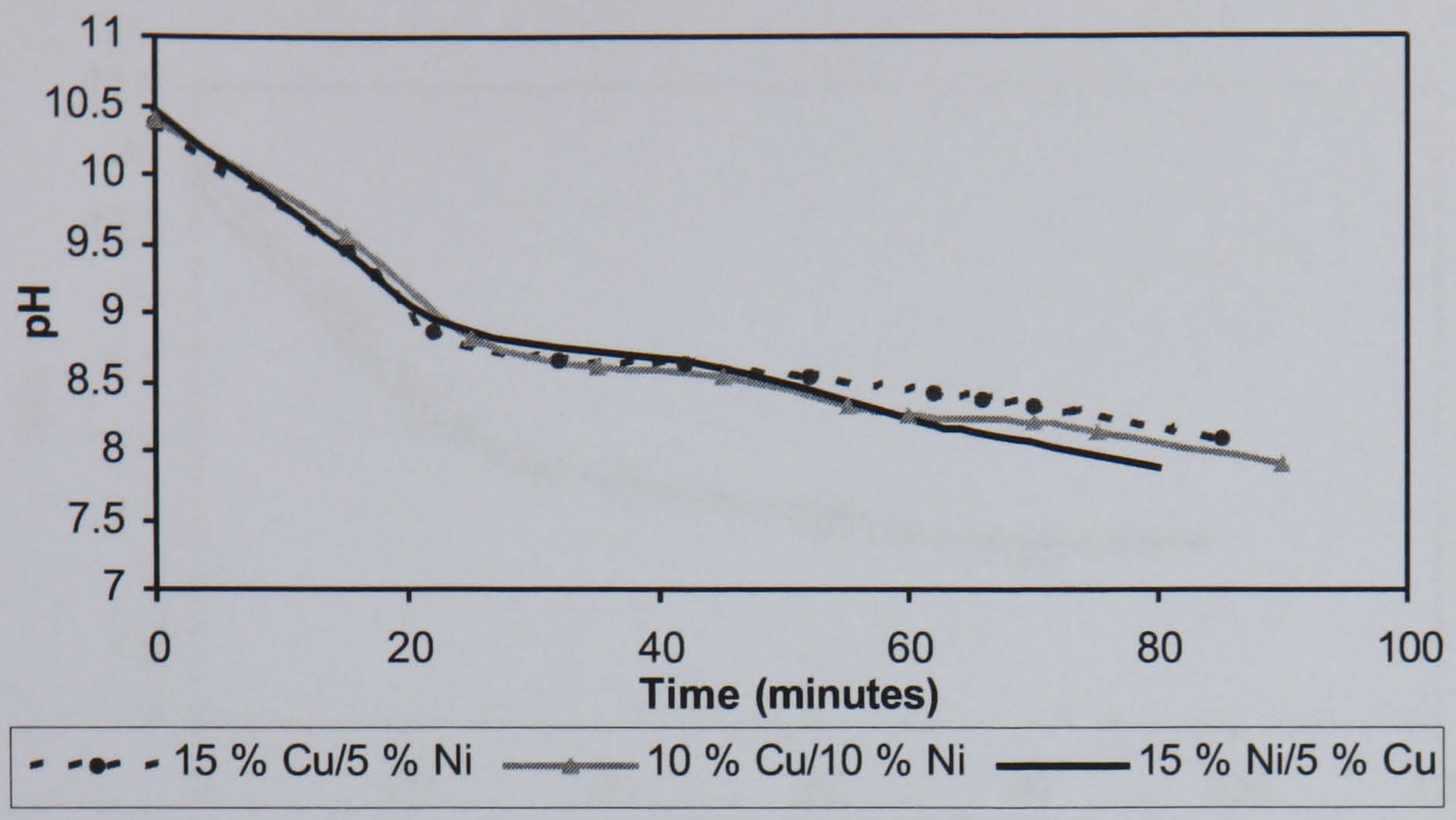

Figure 4.3: Change in pH during synthesis of nickel-cobalt HDC catalysts

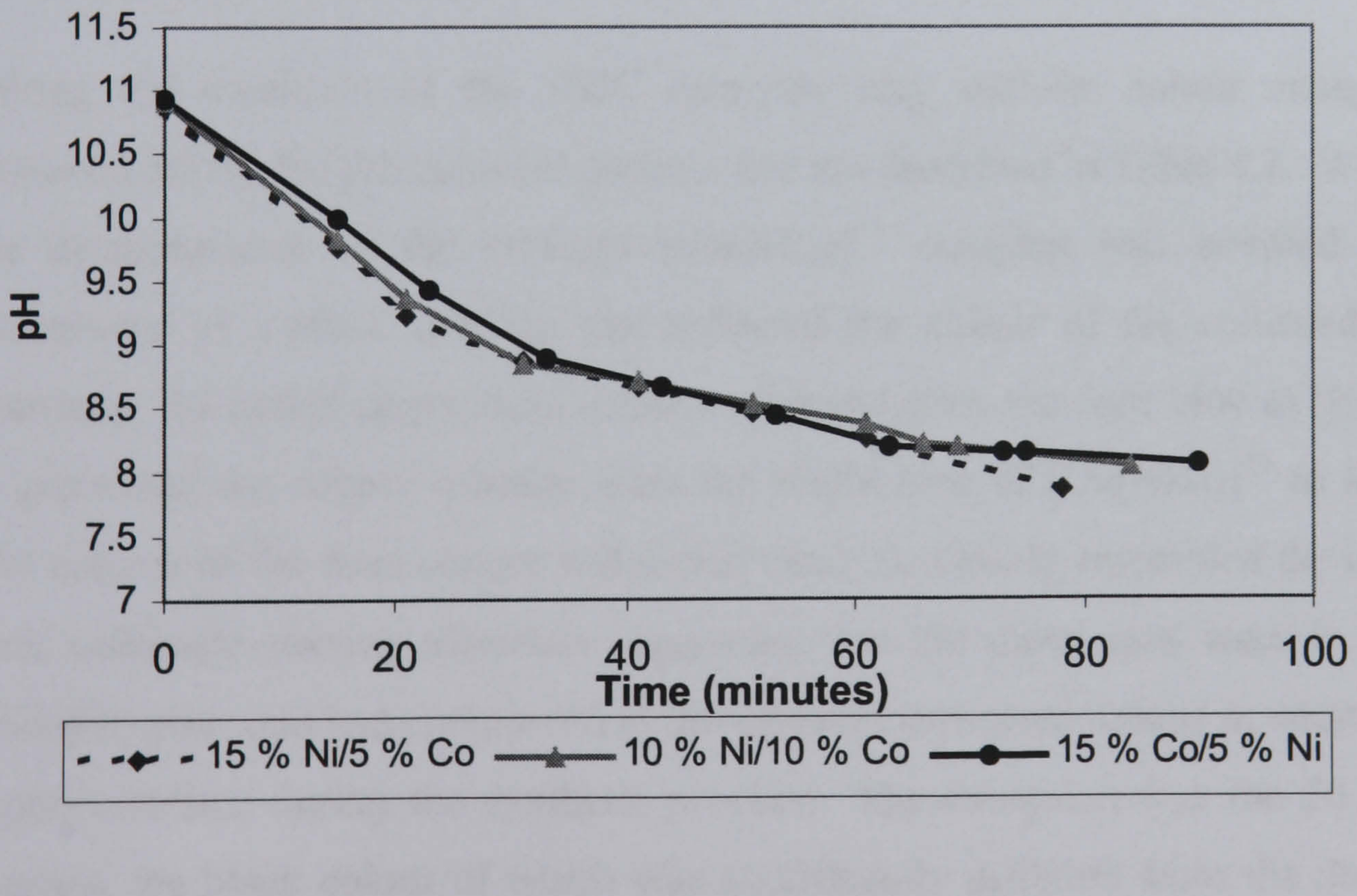

Figure 4.4: Change in pH during the synthesis of the cobalt-copper HDC catalysts

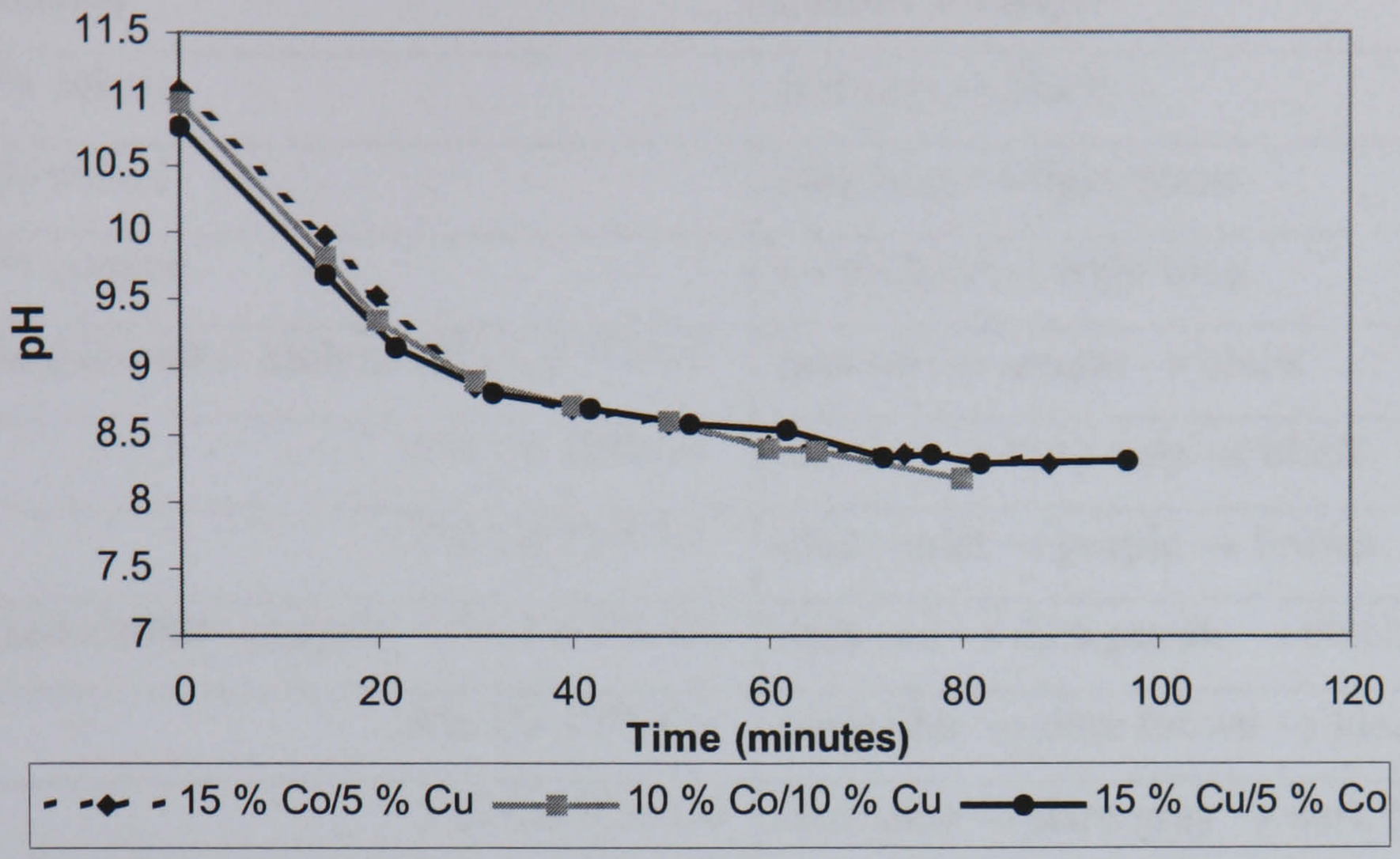

4.2.2 Colour Changes During Preparation of HDC Catalysts

During the synthesis of the HDC catalysts very definite colour changes were observed during the precipitation process and are described in Table 4.2. With cobalt the disappearance of the crimson $[Co(NH_3)]^{2+}$ complex was coupled with the appearance of a black solution that reflected the colour of the collected catalyst. Similarly, the nickel preparation solution changed from the dark blue of $[Ni(NH_3)]^{2+}$ to green and the copper solution from the bright blue of $[Cu(NH_3)]^{2+}$ to light blue. The colours of the final copper and nickel catalysts closely resembled the colours of their carbonate starting materials suggesting that the metal ions were in the same oxidation state and had complexed to the solvated carbonate anions in addition to the support surface during the synthetic process. The exception was the 20 % cobalt catalyst, the black colour of which was significantly different from the deep purple colour of the carbonate salt suggesting that an additional change to the cobalt ions had occurred during catalyst preparation.

Table 4.2: Colour changes during the preparation of HDC catalysts

Catalysts	**Colour Changes**
20 % cobalt	crimson → black
20 % nickel	dark blue → light green
20 % copper	bright blue → light blue
Mixed cobalt – nickel: 15% Co 5% Ni	crimson → purple → black
10% Co 10% Ni	crimson → burgundy → black
5% Co 15% Ni	dark violet → purple → brown
Mixed cobalt- copper: 15% Co 5% Cu	dark red → dark purple → black
10% Co 10% Cu	navy blue → dark brown → black
5 % Co 15% Cu	dark blue → dark grey → dark brown
Mixed copper- nickel: 15% Cu 5% Ni	bright blue → dark blue → khaki green
10% Cu 10% Ni	bright blue → dark blue → khaki green
5% Cu 15% Ni	bright blue → turquoise → green

During the synthesis of the bimetallic catalysts two distinct colour changes were observed for each preparation, suggesting that two distinct metal depositions were occurring; one metal was precipitating first with the second metal following after the initial lay down was complete. However, the situation appeared more complex when the series of colour changes were considered. For example, in the preparations involving cobalt and nickel, the vibrant red colour of $[Co(NH_3)]^{2+}$ was clearly visible and could be traced easily. With the 15 % Co/5 % Ni and 5 % Co/15 % Ni catalysts the crimson colour disappeared completely from solution leaving the blue $[Ni(NH_3)_6]^{2+}$ complex in solution. The nickel was then deposited as the rest of the ammonia was distilled off leaving a solution very close in colour to that of the final catalysts. However, the reverse situation was observed during the synthesis of the 10 % Co/10 % Ni catalyst where the red colour persisted in solution after the blue nickel complex had disappeared and the cobalt was deposited second. An identical scenario was observed in the preparation of the copper-cobalt catalysts where the vibrant red

of the cobalt hexammine complex was easily observable. In the 15 % Co/ 5 % Cu and 5 % Co/15 % Cu catalysts preparations, the cobalt colour appeared to disappear first, leaving predominantly the $[Cu(NH_3)_4]^{2+}$ complex in solution. However, with the 10 % Co/10 % Cu catalyst this situation was reversed and the bright blue copper complex appeared to disintegrate first followed by the cobalt complex. The catalyst preparations involving copper and nickel showed a different pattern. During preparation of the 15 % Cu/5 % Ni and 10 % Cu/10 % Ni catalyst the bright blue copper complex disappeared leaving the dark blue $[Ni(NH_3)_6]^{2+}$ complex in solution. Whereas the colour changes involved in the synthesis of the 5 % Cu/15 % nickel catalyst suggested that the nickel complex deposited first to form the green surface complex, followed by the $[Cu(NH_3)_4]^{2+}$.

As a result it was difficult to draw definite conclusions about the nature of the deposition process. Initial observations suggested that a two-step process with two distinct precipitations was occurring, however, the order that the metal ions were laid down on the catalyst surface was not straightforward. Considering the relative reactivities of the three metals towards alumina (Co>Ni>Cu), cobalt would be expected to precipitate preferentially, followed by the nickel and then the copper. However, the experimental results show that this is not always the case. The order of deposition can change and may be affected by the relative loading of each metal.

4.2.3 Elemental Analysis of HDC Catalysts

Elemental analysis of all twelve HDC catalysts was preformed as described in Section 3.2.2.1 and confirmed that their preparations had been performed successfully and that the precipitated metals were present in the intended quantities. Samples were initially analysed by XRF against the corresponding metal oxide standards and the percentage metal content calculated from this value. The results are displayed in Table 4.3.

Table 4.3: Metal contents of HDC catalysts

catalyst	% CuO	% Cu	% NiO	% Ni	% CoO	% Co
20% Ni			23.9	18.8		
20% Cu	27.1	21.7				
20% Co					23.5	18.5
15% Co/ 5% Ni			6.2	4.9	17.5	13.8
10% Co/ 10% Ni			13.2	10.4	10.6	8.3
5% Co/ 15% Ni			18.5	14.4	6.1	4.8
15% Cu/ 5% Ni	20.7	16.5	6	4.7		
10% Cu/ 10% Ni	13.9	11.1	12.6	9.9		
5% Cu/ 15% Ni	6.4	5.1	18.8	14.8		
15% Co/ 5% Cu	6.7	5.4			19.3	15.2
10% Co/ 10% Cu	14.2	11.3			11.5	9
5% Co/ 15% Cu	21.3	17			6.2	4.9

4.2.4 Catalyst Particle Size Analysis

The size of the catalyst particles in the twelve HDC samples was determined using the technique described in Section 3.2.2.2. The data displayed in Table 4.4 clearly showed that all catalysts had very similar particle size distributions, lying between 9.5 and 91.9 μm, with little variation in the D(v, 0.5) value. The average volume median diameter for the twelve samples had a value of 41.3 μm and this does not vary beyond +/- 10 % of this value between catalysts.

Table 4.4: Catalyst particle size data

catalyst	particle size (μm)		
	D (v, 0.1)	D (v, 0.5)	D (v, 0.9)
20 % Ni	10.0	40.9	85.9
20 % Co	12.6	45.5	90.2
20 % Cu	15.8	39.6	80.0
15 % Ni/5 % Cu	9.5	41.1	90.6
10 % Ni/10 % Cu	11.7	43.7	91.4
5 % Ni/15 % Cu	12.0	42.9	91.2
15 % Cu/5 % Co	15.7	41.8	86.6
10 % Cu/10 % Co	12.4	37.9	82.8
5 % Cu/15 % Co	13.3	42.5	91.9
15 % Co/ 5 % Ni	11.4	42.6	88.0
10 % Co/10 % Ni	10.4	37.5	76.3
5 % Co/15 % Ni	10.2	40.1	88.6

4.2.5 Temperature Programmed Reduction

The Temperature Programmed Reduction profiles of all twelve HDC catalysts were collected as described in Section 3.2.2.3. The results for the three single metal catalysts are displayed in Table 4.5. The profile of both the 20 % copper catalyst and the 20 % nickel catalyst displayed one main reduction peak, appearing at 225 °C and 529 °C respectively. In both cases this has been attributed to the reduction of the metal +2 ion down to the zero valent state, which is consistent with previous assignments on similar catalyst systems published in the chemical literature [143, 155, 156].

However, the cobalt reduction profile revealed the presence of three separate forms of reducible cobalt ion: a main peak centred around 586 °C which corresponded to the majority of cobalt ions present in the sample, a smaller lower temperature peak at 299 °C and another small peak at the relatively high temperature of 846 °C. The main middle temperature peak has been assigned to the reduction of Co^{2+} to cobalt metal. However, in addition the low temperature peak is thought to arise from the reduction of cobalt(III) to cobalt(II) or the reduction of the precursor carbonate ligands still present in the catalyst sample. The high temperature peak is due to the presence of catalytically inactive cobalt alumina spinel, $CoAlO_4$ resulting from a strong reaction of cobalt with the alumina during synthesis of the catalysts. These transformations also are in agreement with the available literature [157].

Table 4.5: TPR analysis of single metal HDC catalysts

Catalyst	T_{min} (°C)	T_{max} (°C)	T_{final} (°C)
20 % Cu	130	225	268
20 % Ni	364	529	884
20 % Co	143	299	325
	422	586	726
	726	846	974

The TPR profiles of the bimetallic HDC catalysts were examined using the peak positions from the single metal reduction profiles as a reference. Comparisons of the profiles obtained for each series of mixed metal catalysts are displayed in Figures 4.5-4.7.

Figure 4.5: TPR profiles – copper and nickel catalysts

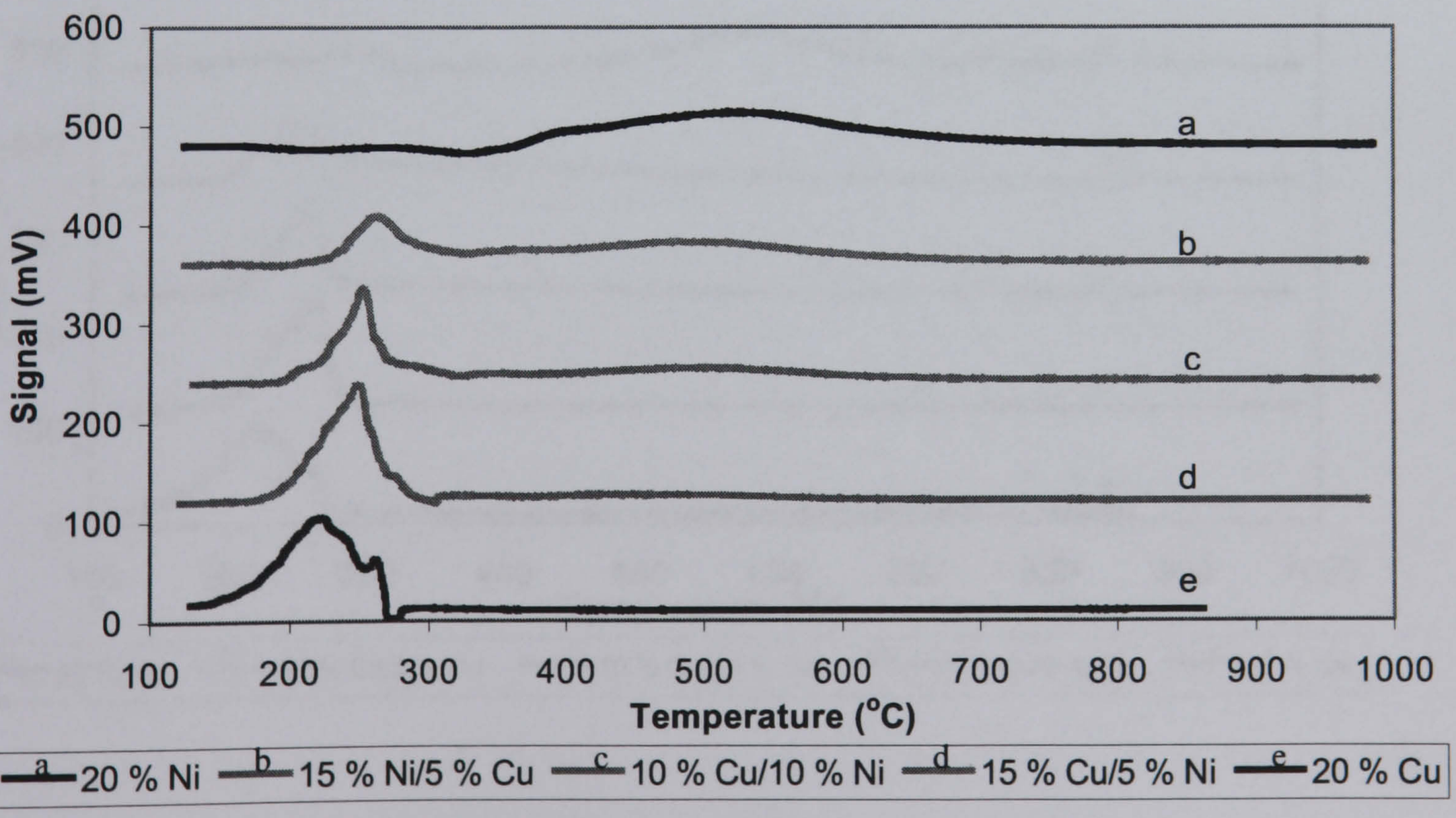

Figure 4.6: TPR profiles – nickel and cobalt catalysts

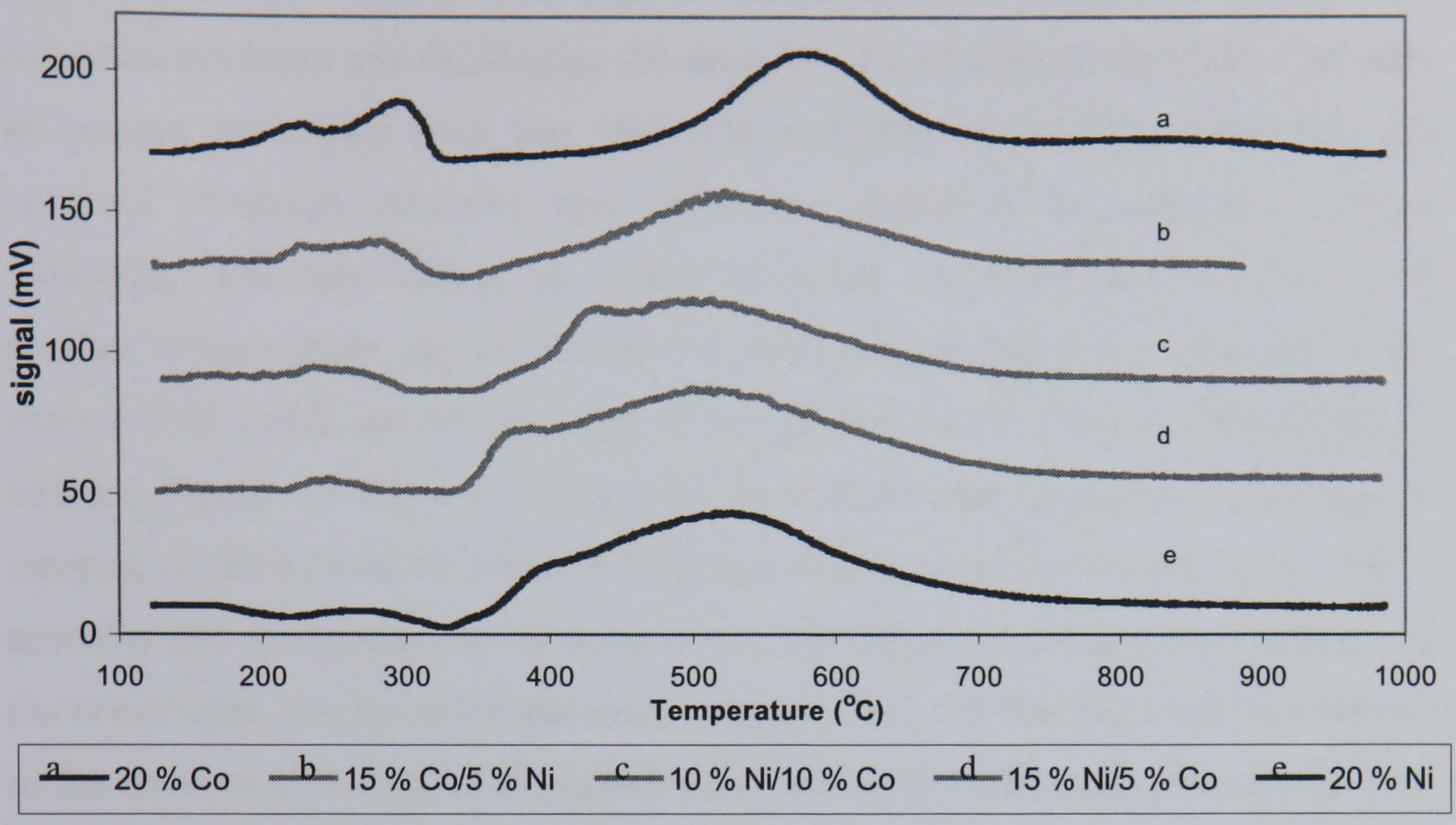

Figure 4.7: TPR profiles – cobalt and copper catalysts

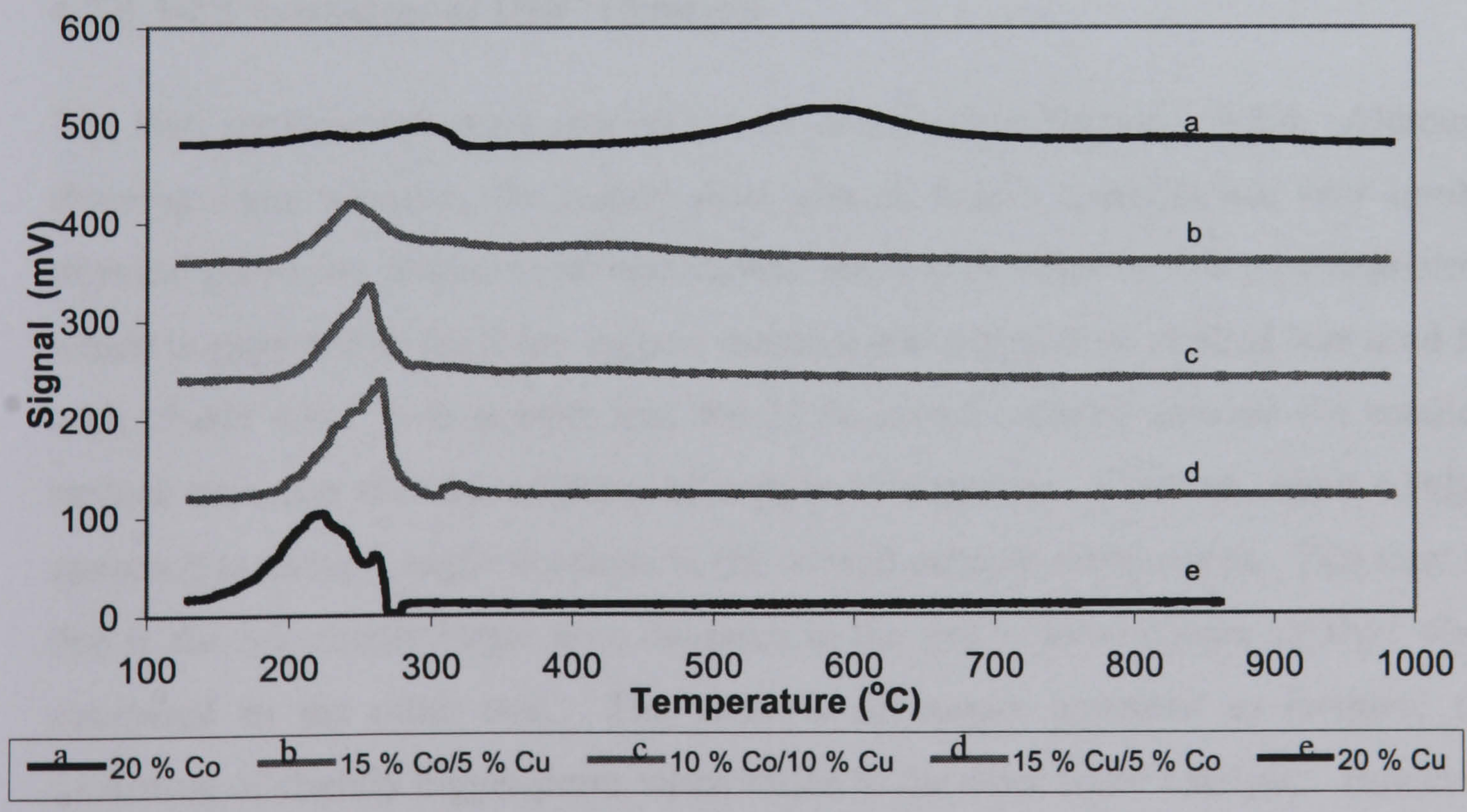

In all three figures, the effect of adding another, more easily reducible, metal can be clearly observed. In Figure 4.5, the nickel reduction peak was shifted to lower temperature when copper was present indicating that copper was acting as a reduction promoter and facilitating the delivery of hydrogen to the nickel particles. In contrast the copper peak was shifted to a slightly higher temperature with the presence of nickel indicating that nickel was acting as an inhibitor to copper reduction. The same effects are visible in Figure 4.6 which shows the reduction profiles of the copper and cobalt catalysts with copper acting as a promoter to the reduction of cobalt and cobalt acting as an inhibitor to the reduction of copper. In addition Figure 4.7 displays the data for the nickel/cobalt catalysts. In this case, a merging of the two metal peaks to form one reduction peak was observed. This is probably due to simultaneous shifting of the nickel peak to a higher temperature and the cobalt peak to a lower temperature, although from the data there is only evidence of the downward shifting of the cobalt peak due to the undefined nature of the large peak in the reduction profile.

4.2.6 BET Isotherms of HDC Catalysts

The BET experiments were carried out as described in Section 3.2.2.4. Although showing some variation, the results show that all twelve catalysts had very similar physical properties with comparable surface areas, pore volumes and pore diameters, which is expected as the same support material and preparation method was used for each (Table 4.6). It is notable that the 20 % copper catalyst showed the smallest surface area and that the addition of copper to either the nickel or cobalt catalyst appeared to cause a slight decrease in the overall catalyst surface area. This may be due to the marginally larger pore diameter in the single metal copper catalyst when compared to the other two. The addition of copper appeared to facilitate the formation of slightly bigger pores when added to the other metal catalysts. However, although the pore diameters showed some variation, the average pore volumes did not appear to change greatly or follow any significant pattern.

Table 4.6: BET surface area, pore volume and pore diameter results for the HDC catalysts.

	surface area ($m^2 g^{-1}$)		average pore diameter (μm)		pore volume [0.98 des] $m^2 g^{-1}$	
	as prepared	reduced	as prepared	reduced	as prepared	reduced
20 % Ni	178	184	93	126	0.41	0.58
20 % Cu	105	122	190	175	0.50	0.53
20 % Co	182	159	116	162	0.52	0.64
15 % Ni/5 % Cu	177	172	97	126	0.43	0.58
10 % Ni/10 % Cu	156	166	115	142	0.45	0.59
5 % Ni/15 % Cu	133	155	141	153	0.47	0.59
15 % Cu/5 % Co	127	135	158	165	0.50	0.56
10 % Cu/10 % Co	139	165	135	162	0.47	0.66
5 % Cu/15 % Co	156	163	118	143	0.46	0.58
15 % Co/ 5 % Ni	170	147	115	155	0.49	0.57
10 % Co/10 % Ni	165	175	111	140	0.46	0.61
5 % Co/15 % Ni	131	174	122	133	0.40	0.42

4.2.7 Chemisorption Studies of HDC Catalysts

Metal surface area measurements were made for all twelve HDC catalysts. These were obtained as explained in Section 3.2.2.5. Hydrogen chemisorption was used to determine the nickel and cobalt surface areas and N_2O reactive chemisorption used to determine the total surface area of the copper containing catalysts. Previous studies have found that the decomposition of N_2O will also occur over both nickel [158, 159] and cobalt [160, 161], so these experiments are in effect a measure of the total metal surface area across the catalyst. The results are shown in Table 4.7.

Of the three single metal catalysts 20 % nickel is shown to have the largest surface area with a value of 29.6 m^2g^{-1} on the reduced catalyst sample. The 20 % cobalt catalyst had a surface area value of 20.2 m^2g^{-1}, which is comparable with the nickel catalyst, however the 20 % copper catalyst displayed a very much lower metal surface area of 6.43 m^2g^{-1}. This indicates that the copper catalyst consists of a more poorly dispersed metal phase with relatively large metal particles, when compared with the cobalt and nickel catalysts.

Table 4.7: Metal surface areas of HDC catalysts

catalyst	metal surface area (m^2 g^{-1})			
	nickel and cobalt		nickel, cobalt and copper	
	oxidic weight	reduced weight	oxidic weight	reduced weight
20 % Ni	23.6	29.6		
20 % Co	17.5	20.2		
20 % Cu			5.2	6.4
15 % Ni/5 % Cu	15.2	18.5	20.9	24.7
10 % Ni/10 % Cu	10.0	11.9	12.9	15.3
5 % Ni/15 % Cu	5.1	6.1	10.0	12.0
15 % Co/5 % Cu	2.3	2.8	10.1	12.2
10 % Co/10 % Cu	3.4	4.0	15.7	18.6
5 % Co/15 % Cu	6.5	7.5	20.0	22.9
15 % Ni/ 5 % Co	15.1	17.8		
10 % Ni/10 % Co	25.0	30.2		
5 % Ni/15 % Co	27.2	34.1		

With the nickel-copper systems, the addition of 5 % copper caused an initial decrease in the total metal surface area, to 24.7 m^2 g^{-1}, when compared to the single nickel catalyst (29.6 m^2 g^{-1}). As the amount of nickel was decreased and the copper content increased the total metal surface area also decreased. A metal surface area of 12.0 m^2 g^{-1} was obtained for the 15 % Cu/5 % Ni catalyst, a value that was lower than the other nickel-copper systems, but substantially larger than that determined for the 20 % copper catalyst of 6.4 m^2 g^{-1}. The addition of 5 % nickel in this case had doubled the active metal area.

A similar trend is also observed with the cobalt-copper systems where the 15 % Co/5 % Cu catalyst gave a total metal surface area of 12.2 m^2 g^{-1}, a much smaller active area than the 20 % cobalt catalyst at 20.2 m^2 g^{-1}. However, in these systems, the total surface area increased as the cobalt:copper ratio changed in favour of copper with the 15 % Cu/5 % Co catalyst giving a metal surface area of 22.8 m^2 g^{-1}.

Furthermore, the addition of cobalt to nickel also induced an increase in the total metal surface area of the catalyst. The 15 % Ni/5 % Co catalyst had a total metal surface area of 17.8 m^2 g^{-1}, which was lower than either of the nickel or cobalt single metal systems. Metal surface areas of 30.2 m^2 g^{-1} and 34.1 m^2 g^{-1} were obtained for

the nickel-cobalt catalysts containing 10 % cobalt and 15 % cobalt respectively, values which were both an improvement on the metal surface areas of the 20 % Ni and 20 % Co catalysts.

The trends in total metal surface area with metal content are shown in Figure 4.8.

Figure 4.8: Total metal surface areas of the HDC catalysts

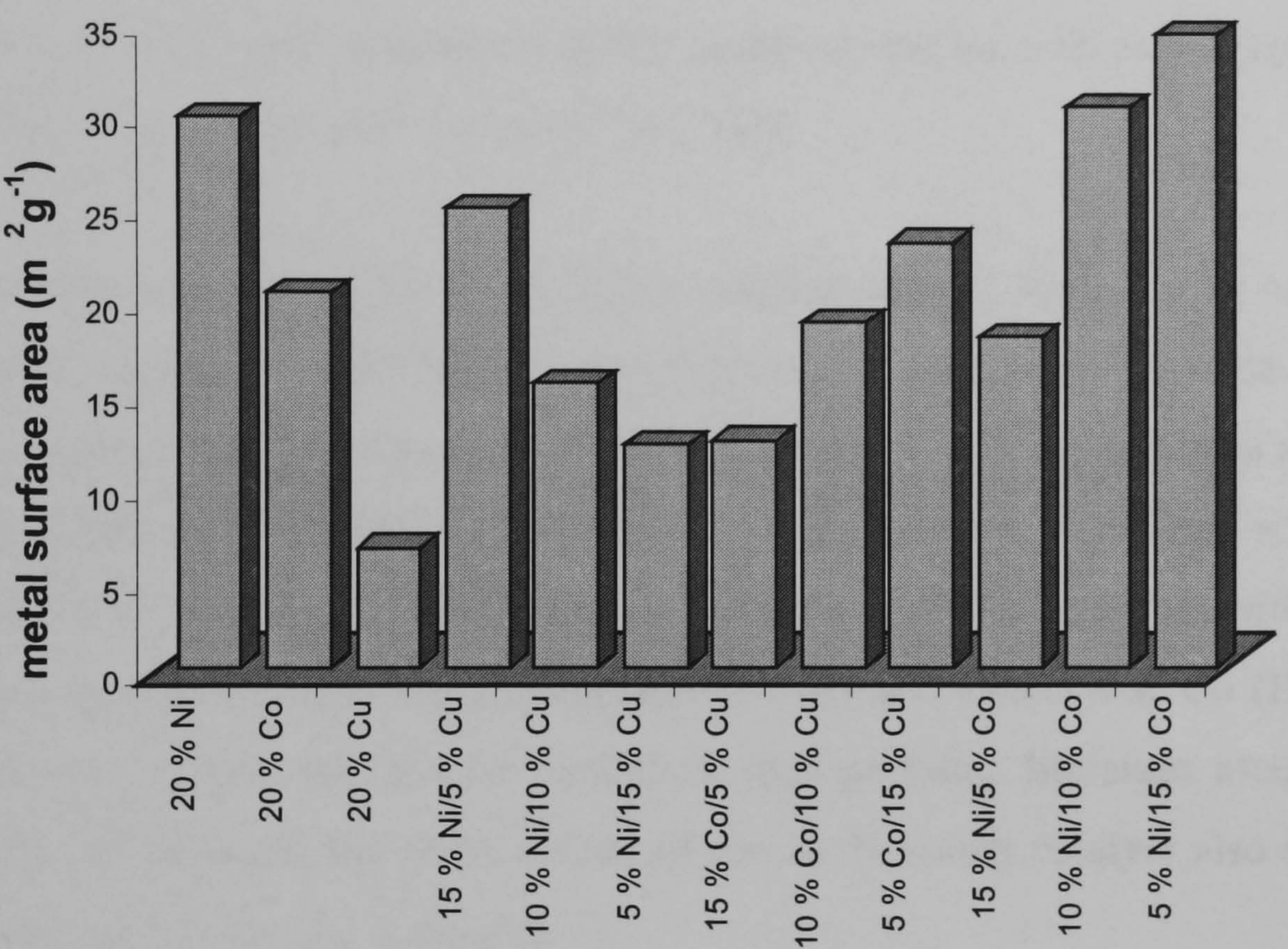

4.2.8 Electronic Spectroscopy

The electronic spectra of the three single metal catalysts displayed some clearly definable bands that are listed in Table 4.8. A single band was observed in the spectrum of the 20 % copper catalyst, which is indicative of an six ligand coordinated d^9 metal ion where only one electronic transition is possible [162]. The absence of any band in the 1600 nm region confirmed that no tetrahedral copper ions were present. In addition, the observed band was broad and spread over a relatively

long range, down to around 650 nm, which explained the light blue colour of the catalyst. The observed spectra was also comparable with other published spectra of alumina supported CuO where the shape of the band displayed asymmetry towards the shorter wavelength [163, 164]. This shape along with the colour of the catalyst suggested that the copper ions were present as Cu (II) and the colour suggested they were most likely complexed with the carbonate precursor ligands.

The electronic spectrum of the 20 % Ni catalyst displayed three bands at 380, 654 and 1122 nm, which is expected for octahedrally coordinated Ni (II) where three electronic transitions are allowed [162]. The catalyst is coloured green, which is suggestive of Ni (II) and comparison of the observed spectra with published spectra of bulk NiO suggests that this is correct [165, 166].

The electronic spectrum of the 20 % cobalt catalyst showed three bands; two large broad bands around 455 and 699 nm containing poorly defined fine structure and one much less intense band at 1466 nm. The band centred at 455 nm has been assigned to the transitions of octahedral Co (III) ions, whereas the band at 699 nm is thought to originate from tetrahedral Co (II) [162]. Comparison of this spectrum with that of cobalt spinel, that contains both tetrahedral Co (II) and octahedral Co (III) ions, shows identical bands and is also consistent with previous literature assignments [167, 168]. In addition, the black colour of the 20 % cobalt catalyst also suggests that a cobalt spinel (Co_3O_4) is present.

As an additional aid to interpretation of the electronic spectra results, the spectra of the three aqueous metal preparative solutions were also collected and compared to those from the solid catalysts. In each case the spectra obtained from the solutions was extremely similar to those of the appropriate metal catalyst indicating that the metal ions were present in the same oxidation states as in the ammine solutions.

Table 4.8: Analysis of electronic spectra of single metal HDC catalysts

Catalyst	**Colour**	**Bands (nm)**	**Assignment**
20 % Cu	Light green	811	Cu (II) d→d Six coordinate Cu (II)
20 % Ni	Light green	380	Ni(II) d→d, octahedral $^3A_{2g} \rightarrow {}^3T_{1g}$ (P)
		654	Ni(II) d→d, octahedral $^3A_{2g} \rightarrow {}^3T_{1g}$ (F)
		1122	Ni (II) d → d octahedral $^3A_{2g} \rightarrow {}^3T_{2g}$
20 % Co	Black	455	Co (III) d→d octahedral $^4T_{1g}$ (F) → $^4T_{1g}$ (P)
		699	Co (II) d→d tetrahedral $^4A_2 \rightarrow {}^4T_1$ (P)
		1466	Co

The electronic spectra of the nine bimetallic HDC catalysts also displayed evidence of these bands although the influence of the second metal on the coordination environment of each metal can be clearly observed. The data from these spectra are displayed in Tables 4.9-4.11.

Table 4.9: Analysis of electronic spectra of copper/nickel HDC catalysts

Catalyst	**Colour**	**Bands (nm)**	**Assignment**
15% Cu/ 5% Ni	Khaki green	268	LMCT (ammonia)
		352	Ni(II) d→d $^2A_{2g} \rightarrow {}^3T_{2g}$
		611	Ni (II) d→d $^3A_{2g} \rightarrow {}^3T_{1g}$ (F)
		657	Ni (II) d→d $^3A_{2g} \rightarrow {}^3T_{1g}$ (F)
		802	Cu (II) d→d
10% Cu/ 10% Ni	Light khaki green	423	Ni(II) d→d $^2A_{2g} \rightarrow {}^3T_{2g}$
		611	Ni (II) d→d $^3A_{2g} \rightarrow {}^3T_{1g}$ (F)
		659	Ni (II) d→d $^3A_{2g} \rightarrow {}^3T_{1g}$ (F)
		803	Cu (II) d→d
15% Ni/ 5% Cu	Green	267	LMCT (ammonia)
		420	Ni(II) d→d $^2A_{2g} \rightarrow {}^3T_{2g}$
		734	Ni (II) d→d $^3A_{2g} \rightarrow {}^3T_{1g}$ (F)
		802	Cu (II) d→d

With the mixed copper/nickel catalysts all three bands originating from the nickel ions were clearly visible in the spectra of all three catalysts. The shortest wavelength band was visible at 380 nm in the 15% copper 5% nickel catalyst, a position that is comparable with the pure nickel catalyst. However, in spectra of the other two catalysts this band becomes shifted to around 400 nm indicating the immediate chemical environment of the complex sphere has been altered. Furthermore, the middle wavelength nickel band (the $^3A_{2g} \rightarrow {}^3T_{1g}$ (F) transition) had been split into two bands in the spectra of the 10 % copper/ 10 % nickel catalyst and the 15 % copper / 5 % nickel catalysts. This splitting may have been caused by spin orbit coupling and mixing of the $^3T_{1g}$ (F) and ^1E_g states that can occur when the field strength of the ligands is weak and the two states close in energy [166]. Interestingly, this was only observed in the two catalysts with the higher copper loadings and not with the lowest copper loading suggesting that the amount of copper on the surface is important. However, this splitting does show that the immediate coordination environment of the nickel ions was directly affected by the presence of copper. Moreover, the third nickel band, around 1120 nm, appeared to be missing from the spectra of all three bimetallic catalysts. This band had possibly been moved to around the same wavelength as the copper band and was obscured by the copper signal or became relatively weak compared with the other bands and was not observable.

Table 4.10: Analysis of electronic spectra of cobalt/copper HDC catalysts.

Catalyst	**Colour**	**Bands (nm)**	**Assignment**
15% Co/ 5% Cu	Black	264	LMCT (ammonia)
		403	Co (III) d→d, octahedral, $^4T_{1g}(F) \rightarrow {}^4T_{1g}(P)$
		609	Co(II) d→d, tetrahedral $^4A_2 \rightarrow {}^4T_1$ (P)
		633	Co(II) d→d, tetrahedral $^4A_2 \rightarrow {}^4T_1$ (P)
10% Co/ 10% Cu	Black	265	LMCT (ammonia)
		609	Co(II) d→d, tetrahedral $^4A_2 \rightarrow {}^4T_1$ (P)
		656	Co(II) d→d, tetrahedral $^4A_2 \rightarrow {}^4T_1$ (P)
		801	Cu (II) d→d
15% Cu/ 5% Co	Dark khaki green	260	LMCT (ammonia)
		603	Co(II) d→d, tetrahedral $^4A_2 \rightarrow {}^4T_1$ (P)
		655	Co(II) d→d, tetrahedral $^4A_2 \rightarrow {}^4T_1$ (P)
		803	Cu (II) d→d

Examination of the electronic spectra of all three cobalt/copper catalysts revealed the presence of an additional band around 260 nm. Due to the relatively high energy, this band could not arise from a metal d → d transition but must involve a charge transfer from a ligand. Therefore, this band was assigned to originate from the presence of residual ammonia ligands from the preparation procedure. Evidence of band splitting was again observed with these catalysts. The band arising from tetrahedrally coordinated Co (II), or the $^4A_2 \rightarrow {}^4T_1$ (P) transition, was shown to split

in the presence of copper, allowing transitions to neighbouring doublet states to gain intensity and give more defined fine structure or, in this case, cause a split in the band [162]. The band arising from the $^4T_{1g}(F) \rightarrow {}^4T_{1g}(P)$ transition, corresponding to octahedral Co (III), was only visible in the spectrum of the 15 % Co/5 % Cu catalyst and was absent from the spectra of the other two catalysts. This could indicate the absence of surface Co (III) species in these catalysts and is again sensitive to the copper loading. Furthermore, the copper band is not visible in the spectrum of the 15 % Co/ 5 % Cu catalyst suggesting there was a lack of surface copper. However, as the copper loading increases this band becomes noticeable.

Interpretation of the electronic spectra of the nickel-cobalt catalysts was considerably more complicated as the d $\rightarrow$ d transitions arising from both metals were relatively close in energy and therefore appeared in close proximity to each other in the spectrum. The spectra collected from the single metal catalysts, described in Table 4.8, show that a total of six electonic transition bands could be expected in the spectra of the mixed nickel-cobalt catalysts although Table 4.11 shows the fewer band were actually observed. The spectra of the 15 % Co/ 5 % Ni catalyst displayed four bands in total, two of which appeared to originate from the nickel and two from the cobalt. Although these bands were expected to have been shifted away from their original positions in the spectra of the isolated metals, the relative order of the energies of these bands has been used to assign the particular transition causing the absorbance. Like the previous mixed metal systems the lower energy transitions around 1122 and 1466 nm were not visible in the spectra suggesting they were very weak when compared to the other transitions. However, the spectra of the 10 % Co/10 % Ni catalyst showed only two absorption bands: one at 458 nm and one at 686 nm. The broad and asymmetric shape of the bands suggested that this was due to the signals originating from the two metals coincidently appearing at the same place on the spectrum and obscuring each other. The spectra of the 5 % Co/15 % Ni catalyst contained three bands, one at relatively high energy similar to those observed in the spectra of the cobalt/copper catalysts that have already been ascribed to arise from ligand to metal charge transfer from ammonia ligands left behind from the preparation method. The spectra also showed only two bands arising from the metals present on the catalyst surface. In this case, it is probable that they arise from nickel

as this was the predominant ion in the sample and the wavelength of the bands appeared closest to those assigned as nickel transitions in the 15 % Co/5 % Ni catalyst. The cobalt bands would be much less intense and most likely to be covered by the more dominant nickel bands.

Table 4.11 Analysis of electronic spectra of nickel-cobalt HDC catalysts

Catalyst	**Colour**	**Bands(nm)**	**Assignment**
15% Co/ 5% Ni	Black	453	Ni(II) d→d, octahedral $^3A_{2g} \rightarrow {}^3T_{1g}$ (P)
		584	Co(III) d→d, octahedral $^4T_{1g}$ (F) → $^4T_{1g}$ (P)
		630	Ni(II) d→d, octahedral $^3A_{2g} \rightarrow {}^3T_{1g}$ (F)
		691	Co (II) d→d tetrahedral $^4A_2 \rightarrow {}^4T_1$ (P)
10% Co/ 10% Ni	Very dark green	458	Ni(II) d→d, octahedral $^3A_{2g} \rightarrow {}^3T_{1g}$ (P) and Co(III) d→d octahedral $^4T_{1g}$ (F) → $^4T_{1g}$ (P)
		686	Ni(II) d→d, octahedral $^3A_{2g} \rightarrow {}^3T_{1g}$ (F) and Co (II) d→d tetrahedral $^4A_2 \rightarrow {}^4T_1$ (P)
15% Ni/ 5% Co	Dark khaki green	231	LMCT (ammonia)
		357	Ni(II) d→d, octahedral $^3A_{2g} \rightarrow {}^3T_{1g}$ (P)
		634	Ni(II) d→d, octahedral $^3A_{2g} \rightarrow {}^3T_{1g}$ (F)

4.2.9 Raman Spectroscopy

Raman spectra were collected for all twelve catalysts and for the alumina support. These were then compared with reference spectra. The spectra of the alumina support displayed a strong, sharp signal at around 480 cm^{-1} that was also clearly visible in the Raman spectra of all the prepared catalysts.

The Raman spectra of the 20 % Co catalyst showed a series of bands at 200, 488, 532 and 691 cm^{-1} respectively. These bands are characteristic of Co_3O_4 spinel [169-171]. A comparison of the Raman spectra of this catalyst and spinel is shown in Figure 4.9.

The Raman spectra of the 20 % Ni catalyst was compared to the spectra of its metal oxides. Figure 4.10 shows a comparison of the Raman spectra of NiO with the 20 % Ni catalyst. The two most intense bands at 558 cm^{-1} and 1065 cm^{-1} in the Raman spectra of the metal oxide were clearly visible in the spectra of the catalyst.

The spectra obtained for the 20 % Cu catalyst was unfortunately noisy and ill defined and did not allow a good comparison with copper reference spectra.[7]

Figure 4.9: Comparison of Raman spectra of 20 % cobalt with Co_3O_4

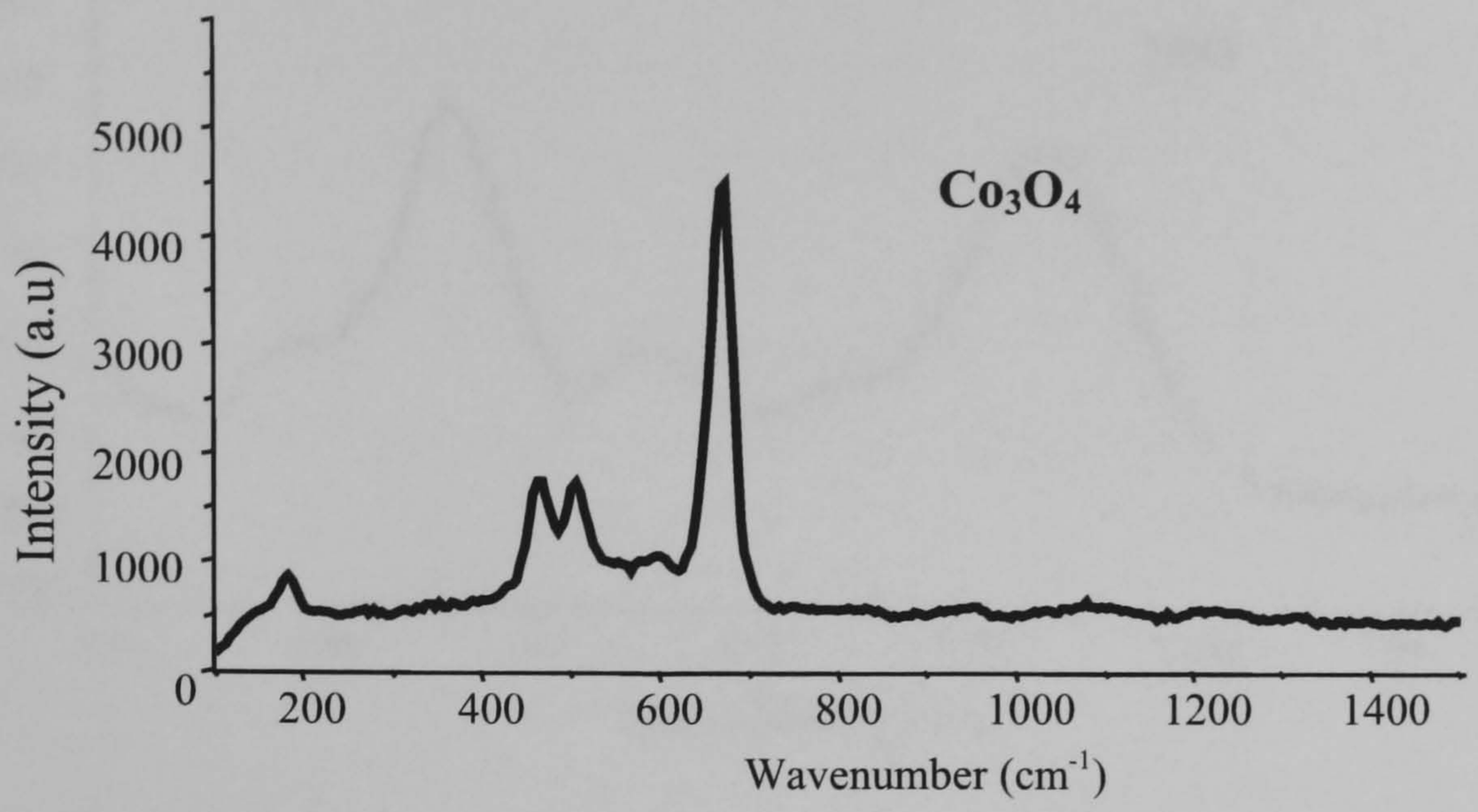

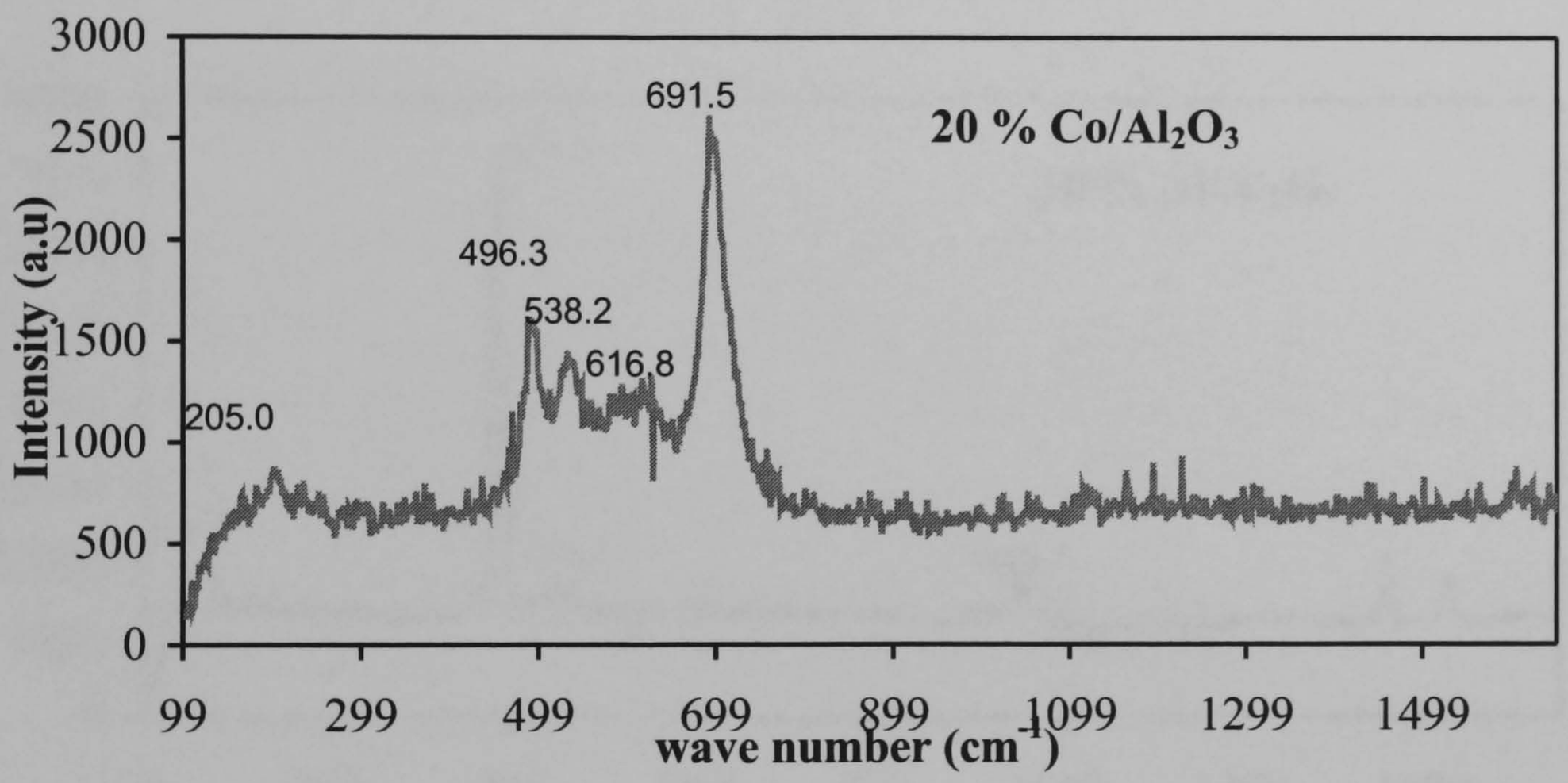

Figure 4.10: Comparison of Raman spectra of 20 % nickel with NiO

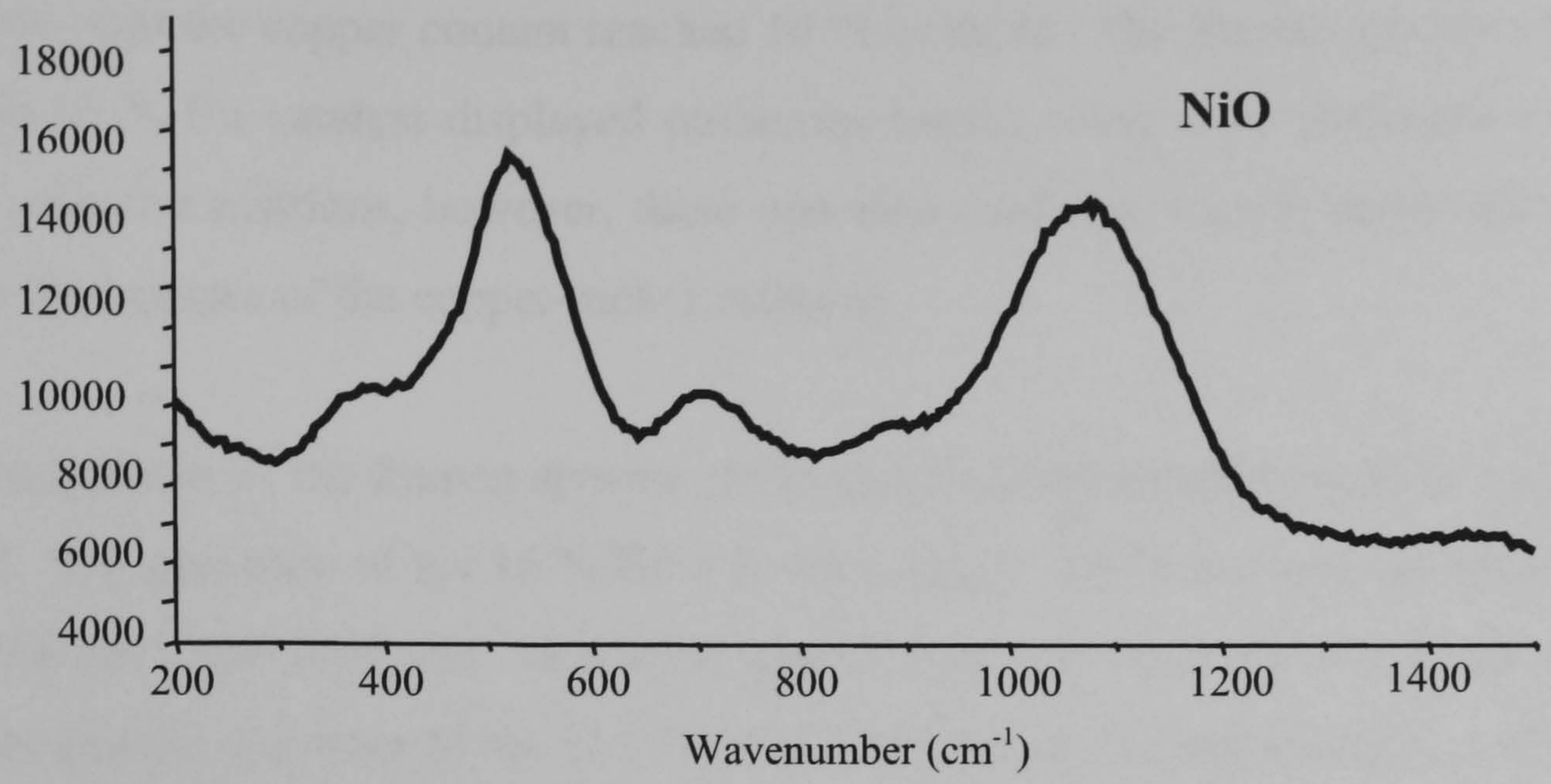

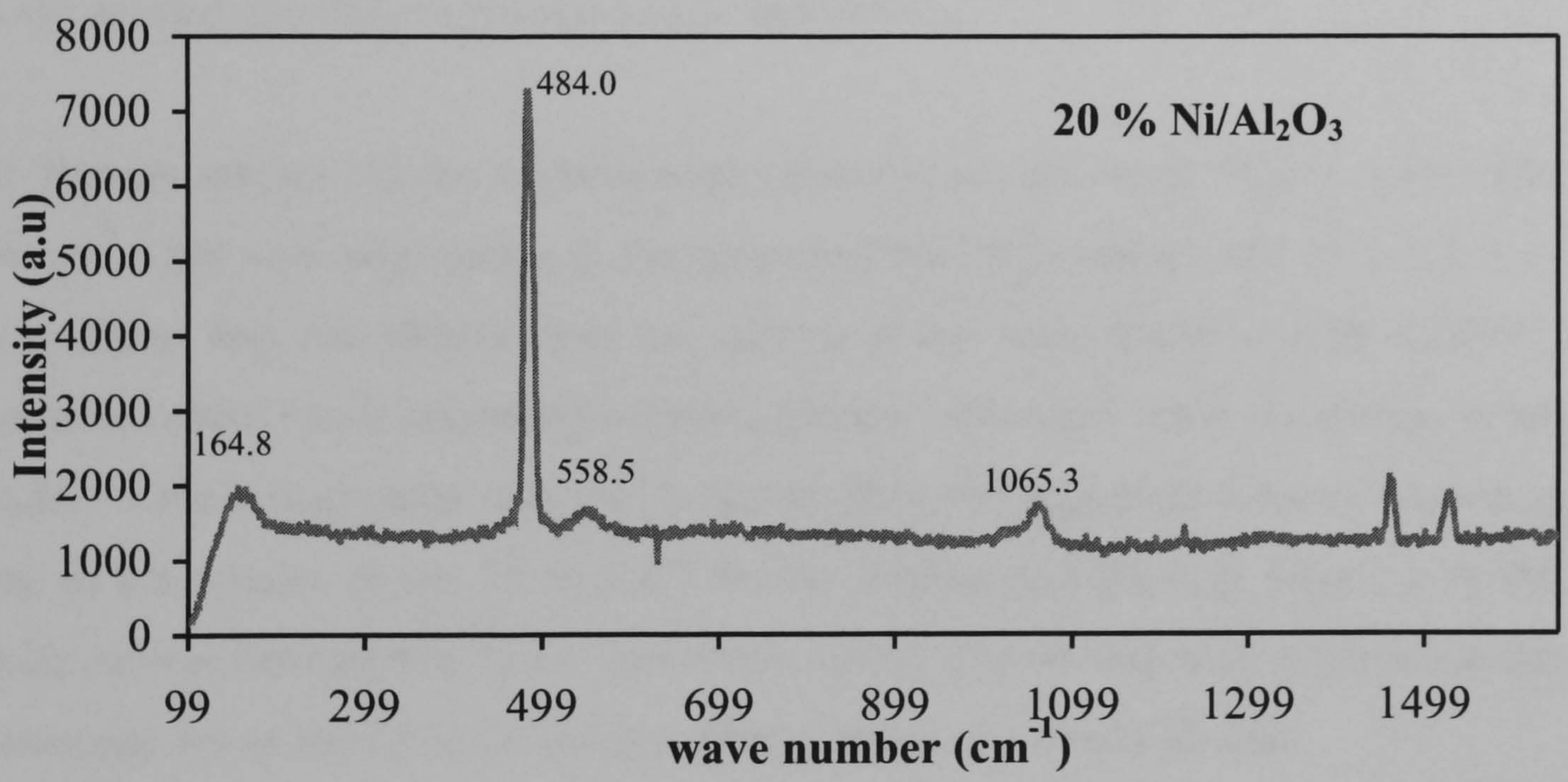

The Raman spectra of the mixed metal catalysts proved to be complex and difficult to interpret. However, some valuable information could be drawn. For instance, comparison of a series of catalysts across the range from one single metal to the other (eg. 20 % Cu, 15 % Cu/5 % Ni, 10 % Cu/10 % Ni, 15 % Ni/5% Cu and 20 % Ni) showed a gradual change in the spectra. The spectrum of the 15 % Cu/5 % Ni catalysts closely resembled the 20 % Cu, whereas, the 15 % Ni/5 % Cu spectra resembled that of 20 % Ni. A comparison of the Raman spectra for the copper-nickel catalysts is displayed in Figure 4.11. The most prominent bands from the

nickel spectrum at 1065 cm^{-1} and 558 cm^{-1} were absent from the spectra of the 15 % Ni/5 % Cu and 15 % Cu/5 % Ni catalysts and the copper band at 306 cm^{-1} was not visible until the copper content reached 10 % or more. The Raman spectra of the 10 % Ni/10 % Cu catalyst displayed numerous bands; some were attributed to nickel and copper transitions, however, there was also evidence of new bands not seen in the other spectra of the copper-nickel catalysts.

A comparison of the Raman spectra of the nickel-cobalt catalysts is shown in Figure 4.12. The spectrum of the 15 % Ni/ 5 % Co catalyst clearly showed the nickel bands at 558 cm^{-1} and 1065 cm^{-1} that were absent from the other spectra in the catalyst series and the spectrum of the 15 % Co/5 % Ni catalyst displayed cobalt bands at 691 cm^{-1} and 496 cm^{-1}. The Raman spectrum of the 10 % Ni/10 % Co catalyst was poorly defined and did not provide much information.

The Raman spectra for the copper-cobalt catalysts are shown in Figure 4.13. The 306 cm^{-1} band was only visible in the spectra of the 20 % copper and 15 % Cu/5 % Co catalysts and was absent from the spectra of the other copper-cobalt catalysts. The three cobalt bands appearing between 496 cm^{-1}-616 cm^{-1} were not visible in the spectra of the mixed metal catalysts however, they did appear as a broad undefined peak in the spectra of the 15 % Cu/5 % Co catalyst and grew in intensity as the cobalt content increased to 15 %. Definition of these peaks was only achieved in the Raman spectra of the 20 % Co catalyst when copper was totally absent.

Figure 4.11: Raman spectra of the copper-nickel catalysts.

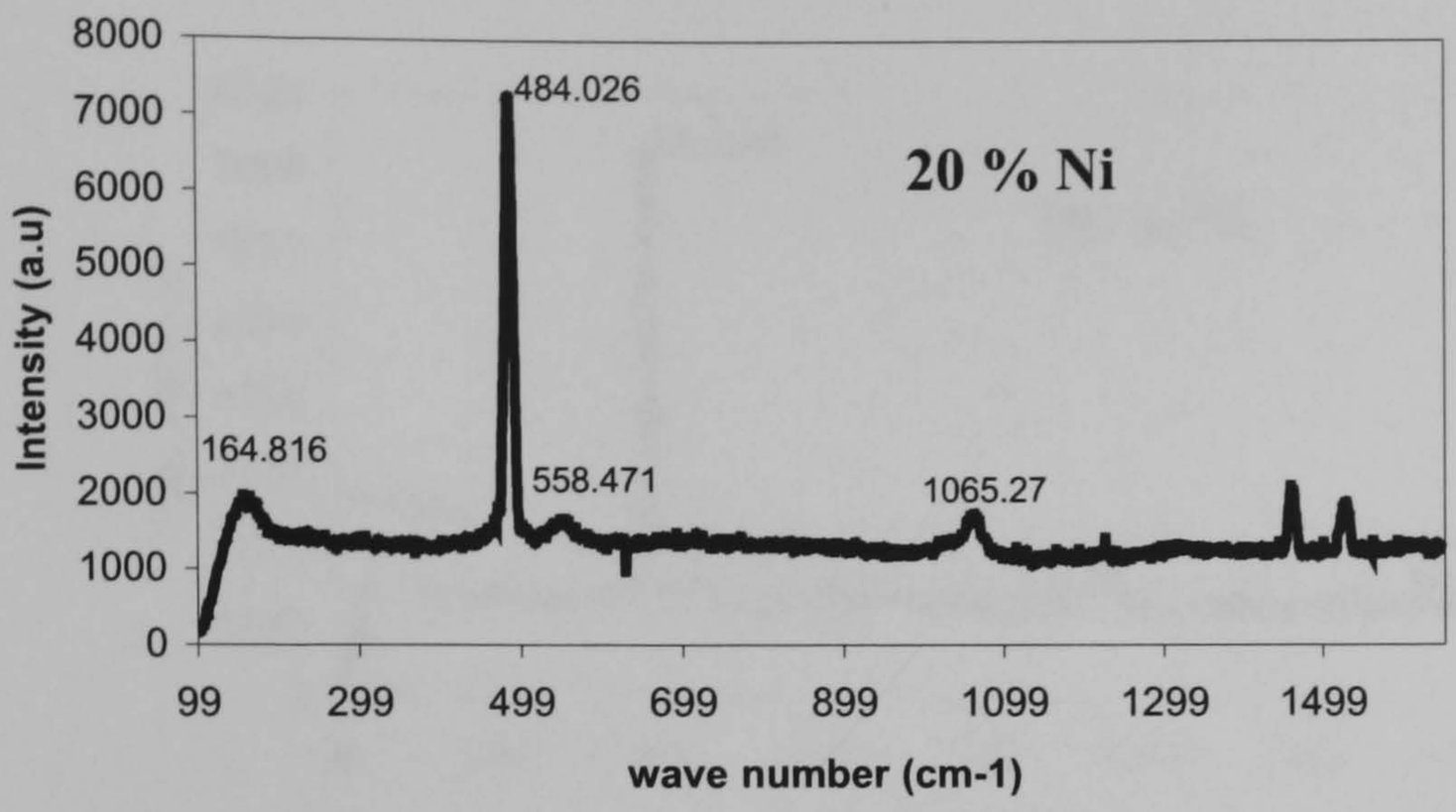

Figure 4.12: Raman spectra of the nickel-cobalt catalysts

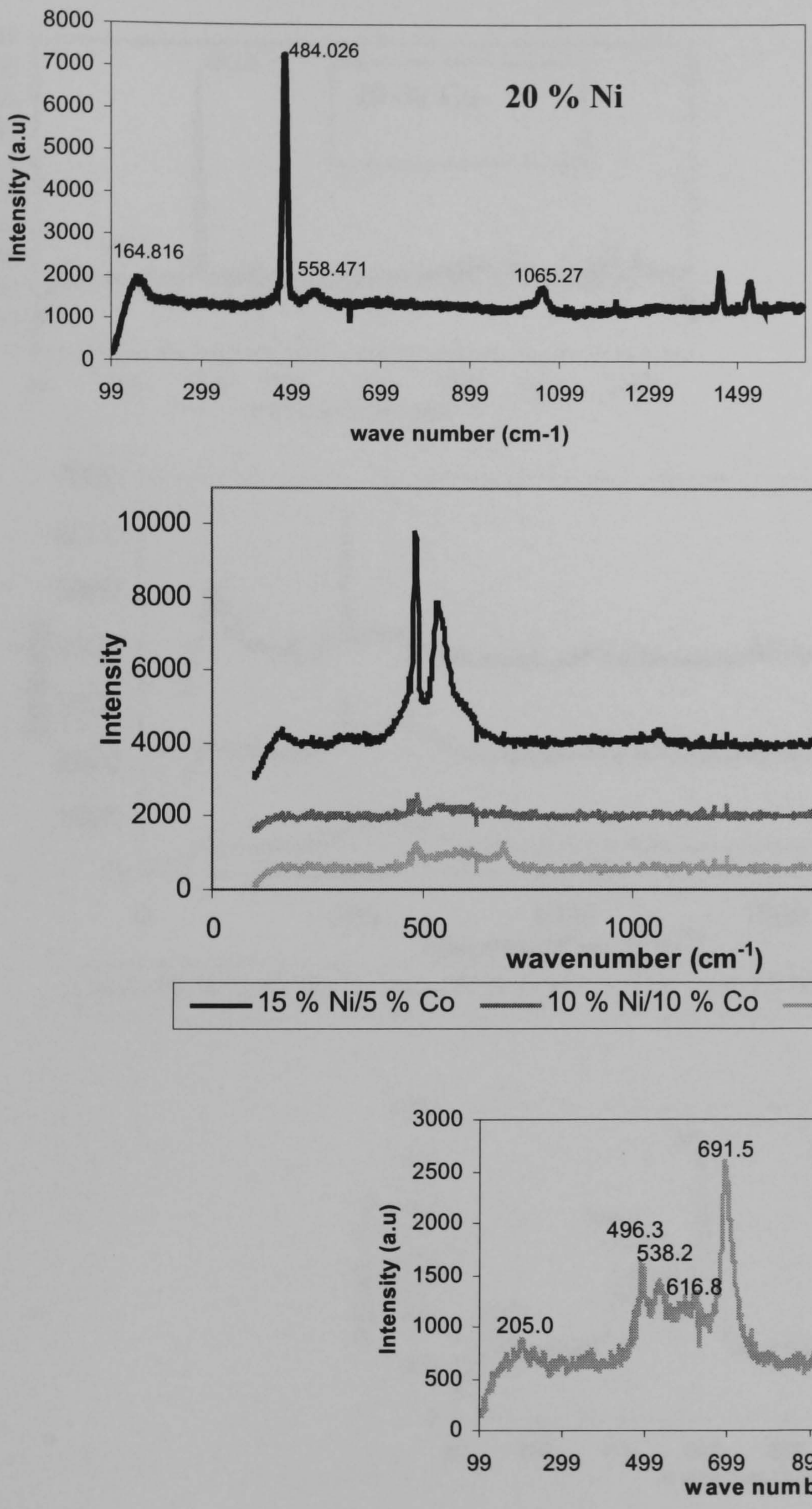

Figure 4.13: Raman spectra of copper-cobalt catalysts.

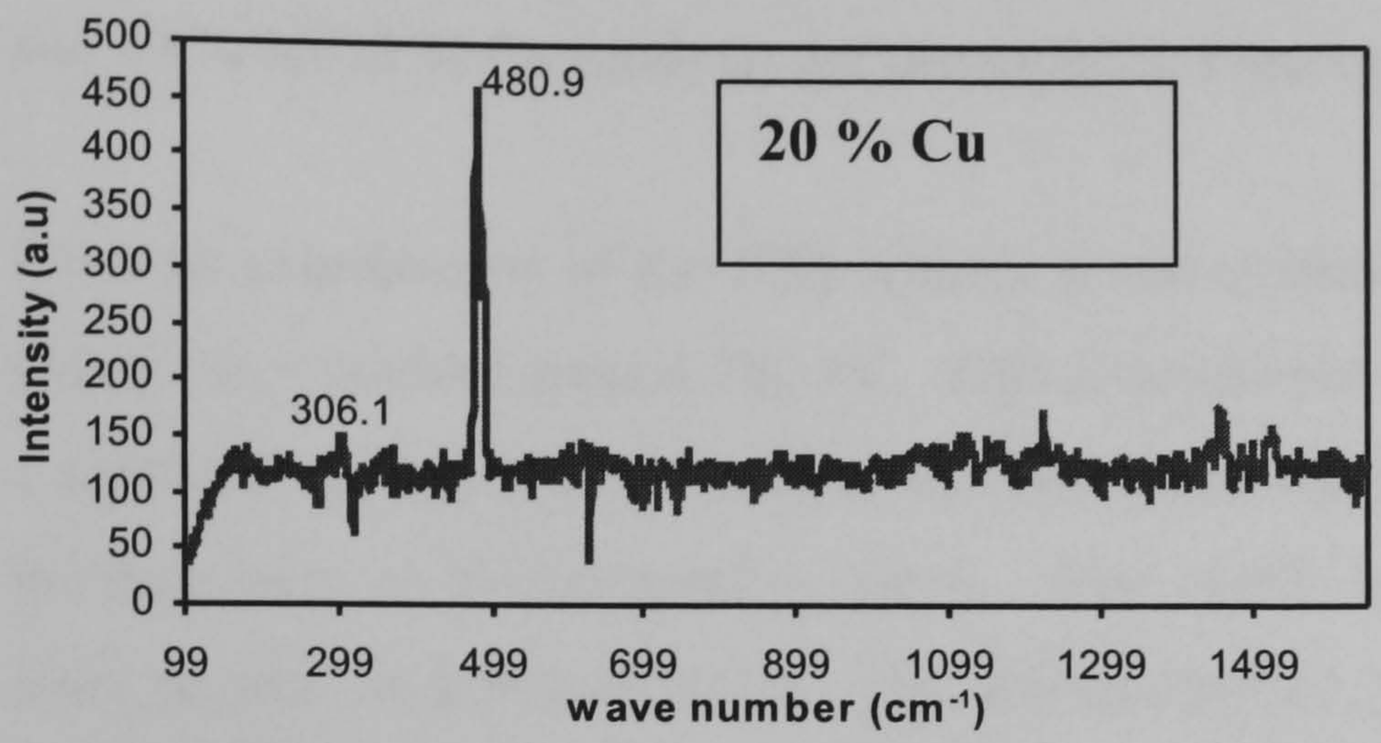

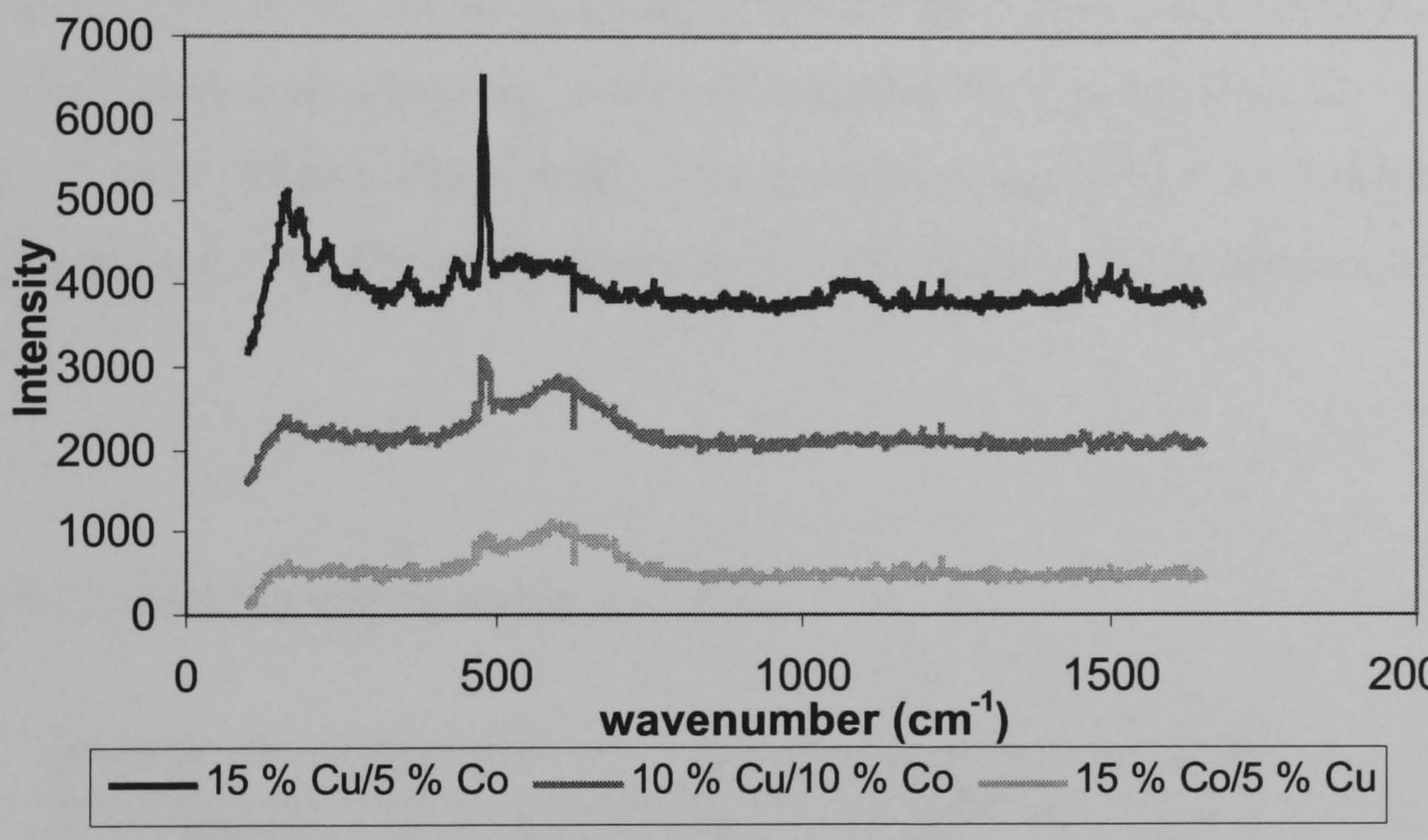

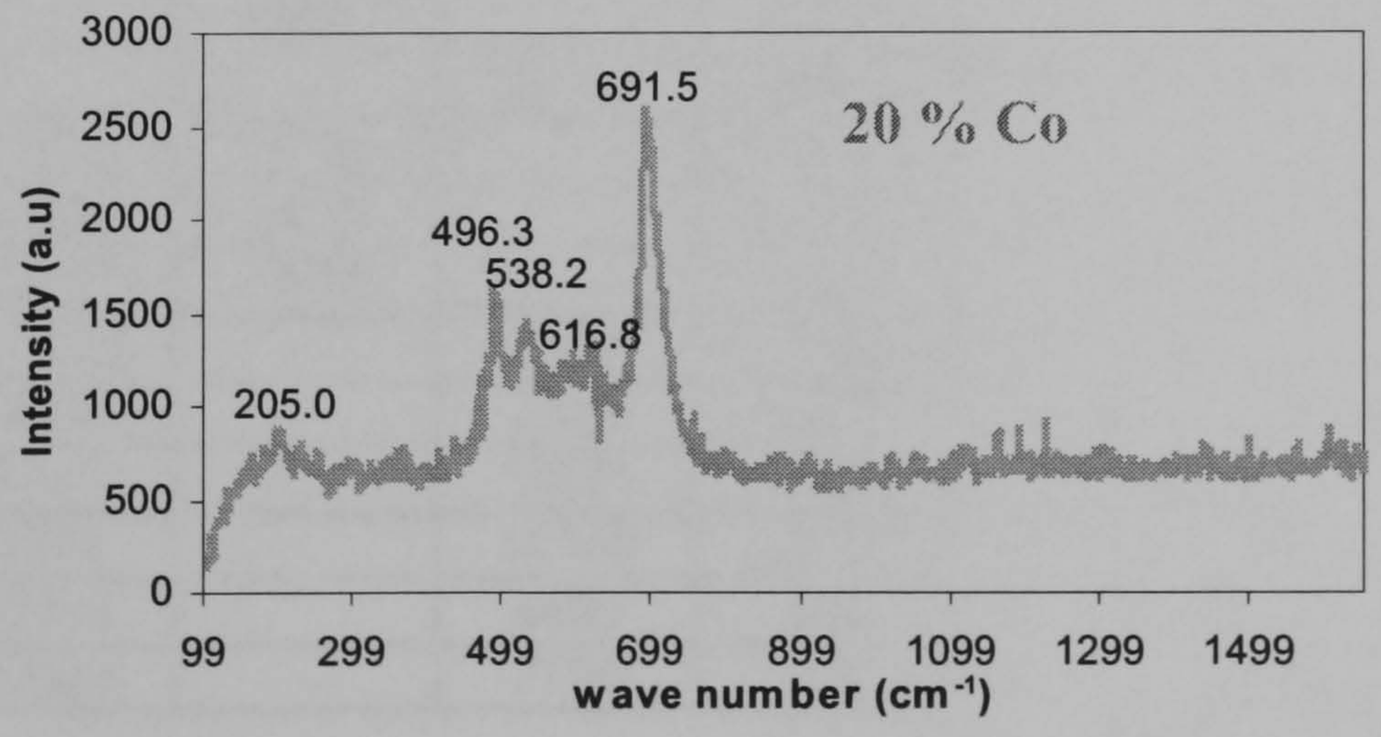

4.2.10 XPS Spectroscopy

The XPS spectra of all twelve HDC catalysts were collected according to the method outlined in Section 3.2.2.8. As an example the XPS spectra of the 10 % Cu/10 % Ni and 10 % Ni/10 % Co catalysts are displayed in Figures 4.14 and 4.15 respectively.

From an examination of the XPS spectra it was evident that the carbon 1s peak was present as a doublet around 285 eV. This is consistent with the signal obtained from a carbonate group, [172] as a final state mulitplet splitting effect is expected due to the lone pairs on the carbonate oxygen. Also visible were the core metal transitions from copper, nickel and cobalt. For further analysis the most prominent of these peaks were considered. More specifically, the Cu $2p^{3/2}$ peak visible around 930 eV, the Ni $2p^{3/2}$ peak with a binding energy of around 850 eV and the cobalt $2p^{3/2}$ signal at 775 eV were utilised. These peaks were referenced against the Al 2s peak arising from the support. A table of the intensity of these signals is displayed in Table 4.12 [173].

Table 4.12: Measured XPS intensities [173].

	Intensity (cps)			
sample	Cu $2p^{3/2}$	Ni $2p^{3/2}$	Co $2p^{3/2}$	Al 2s
20 % Cu	12958			798
20 % Ni		55941		4720
20 % Co			26831	6608
15% Ni/5% Cu	11865	33135		748
10% Ni/10% Cu	8233	13791		604
5% Ni/15% Cu	19912	10106		1475
15% Ni/5% Co	23495		5397	846
10% Ni/10% Co	16339		7898	1201
5% Ni/15% Co	9645		19531	3641
15% Co/5% Cu	2872		10786	2611
10% Co/10 % Cu	12731		4499	698
5% Co/15% Cu	20824		2799	435

Figure 4.14: XPS spectrum of 10 % Ni/10 % Cu catalyst

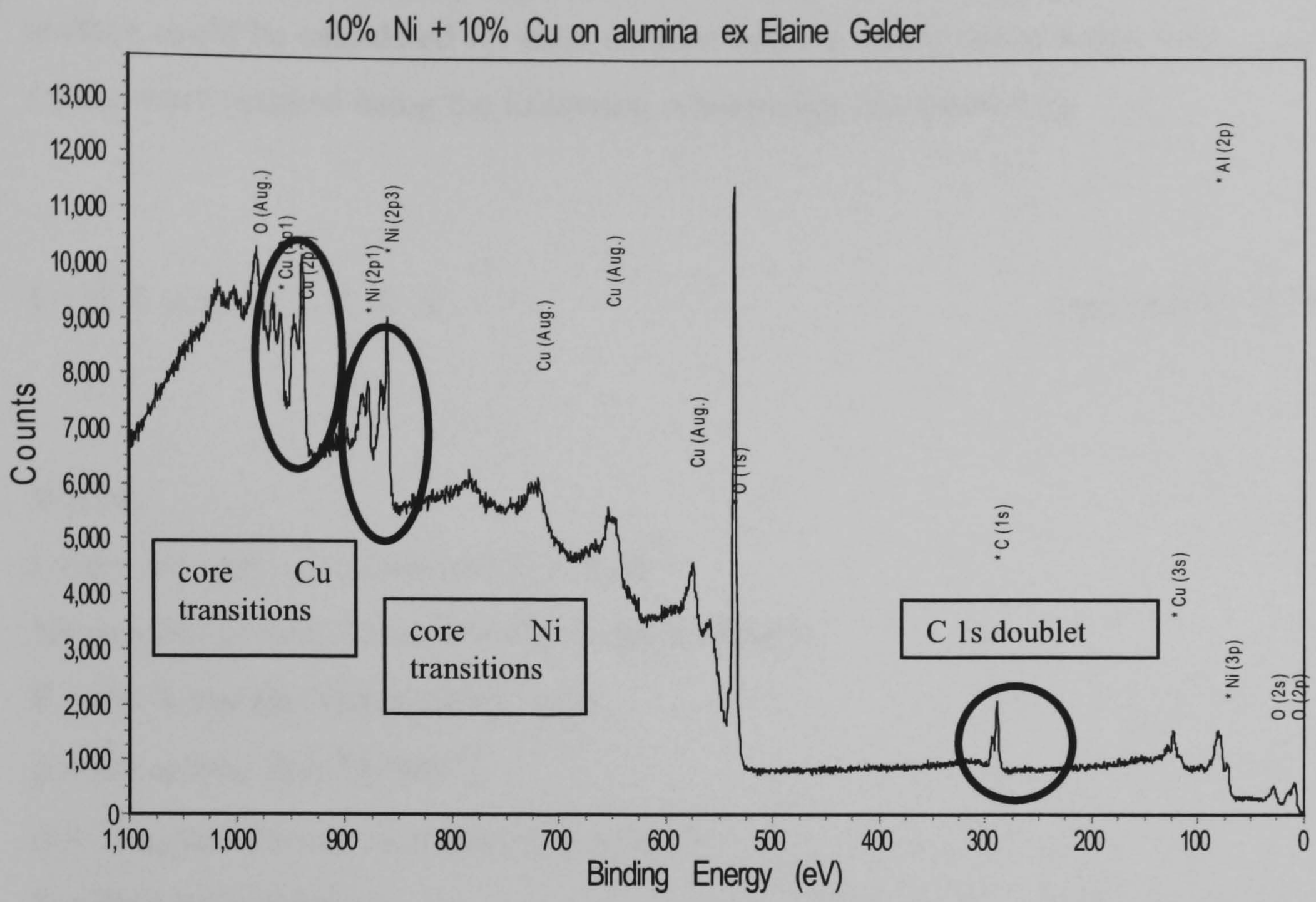

Figure 4.15: XPS spectrum of 10 % Ni/10 % Co catalyst

From the intensity signals, the surface atomic percentages of the metals on the surface could be calculated for each catalyst and are displayed in Table 4.13. These values were reached using the following relationship (Equation 4.1).

$I = N.\ f.\ \rho.\ \sigma.\ T.\ \lambda.\ A.\ \theta.\ Y$ Equation 4.1 [172]

Where,

I = the intensity of a photoemission peak

N= number of atoms associated with the XPS peak

F = the X-ray flux (photons/cm^2.sec)

ρ = the atomic density (cm^{-3})

σ = the photoionisation cross section (cm^2)

T = detector efficiency

λ = inelastic mean free path of the photoelectron (cm)

A = analysed area (cm^2)

θ = angular efficiency factor

Y = photoelectric efficiency factor

The atomic percentages are then calculated using the relationship below (Equation 4.2).

$\text{Atomic \% i} = (N_i / \Sigma N_{atom}) \times 100$ Equation 4.2. [172]

Table 4.13: Atomic percentages

sample	atomic percentages					
	Cu	Ni	Co	O	C	Al
20 % Cu	5.8			52.6	35.6	6.0
20 % Ni		13.8		59.6	11.8	14.8
20 % Co			6.3	60.0	9.7	24.0
15 % Ni/5 % Cu	4.6	12.2		74.0	1.9	7.3
10 % Ni/10 % Cu	4.7	6.1		57.2	23.7	8.3
5 % Ni/15 % Cu	6.7	2.0		50.6	29.3	11.4
15 % Ni/ 5 % Co		10.9	3.5	58.3	14.3	7.2
10 % Ni/10 % Co		7.6	3.2	52.6	23.1	9.2
5 % Ni/15 % Co		4.1	4.7	51.2	20.7	17.3
15 % Co/5 % Cu	1.6		5.5	52.3	17.4	23.3
10 % Co/10 % Cu	5.2		1.9	54.7	34.3	3.9
5 % Co/15 % Cu	6.8		0.9	58.7	31.0	2.7

The atomic percentages shown in Table 4.13 allow the exact quantities of ions of each metal to be compared in addition to the metal present by weight loading. However, examination of the results show an unexpectedly high level of carbon in the catalysts containing predominantly copper. The cause of the additional carbon present in these catalysts has not been identified but may be due to additional retained carbonate ligands from the catalyst synthesis process. In addition low levels of chlorine were identified in the XPS spectra of the mixed nickel and cobalt catalysts. The origin of this chlorine cannot be explained as the same metal solutions were used to prepare all catalyst listed above and all catalysts samples treated in an identical manner. However, as the levels of chlorine are so low, less than 5 % of the atoms present on the surface, these catalysts were used in the same way as the other HDC catalysts when catalyst testing was commenced.

In addition to the determination of the atomic percentages, the intensity values can also be used to ascertain the metal:support ratios. These data were extremely useful as they gave an indication of how the metal is dispersed over the support. For instance, a well-dispersed catalyst with well spread out particles will cover the support much more efficiently and give a much higher metal: support surface ratio than a poorly dispersed catalyst [173]. These ratios are shown in Table 4.14.

Table 4.14: Measured intensity ratios for metal $2p^{3/2}$ and Al 2s peaks

sample	intensity ratios		
	Cu $2p^{3/2}$: Al 2s	Ni $2p^{3/2}$: Al 2s	Co $2p^{3/2}$: Al 2s
20 % Cu	16.2		
20 % Ni		11.9	
20 % Co			4.1
15 % Ni/5 % Cu	15.9	44.3	
10 % Ni/10 % Cu	13.6	22.9	
5 % Ni/15 % Cu	13.5	6.9	
15 % Ni/ 5 % Co		27.8	6.4
10 % Ni/10 % Co		13.6	6.6
5 % Ni/15 % Co		2.7	5.4
15 % Co/5 % Cu	1.1		4.1
10 % Co/10 % Cu	18.2		6.5
5 % Co/15 % Cu	47.9		6.4

The data listed in Table 4.14 revealed some interesting observations. Considering only the monometallic cases showed that the 20 % cobalt catalyst had a substantially smaller intensity ratio than the 20 % copper and nickel samples suggesting that the cobalt particles were much larger and more poorly dispersed than the copper and nickel crystallites. There are also a number points to make concerning the intensity ratios of the bimetallic catalysts.

Examination of the Cu $2p^{3/2}$:Al 2s ratios in the mixed copper-nickel catalysts showed a slightly lower value to that observed for the 20 % copper catalyst with little variation down the series despite the increasing levels of copper present on the surface. As a result it can be inferred that while the size of the individual copper particles may have been increasing, the number of crystallites was not increasing and the copper dispersion was not improved by the presence of nickel. However, the Cu $2p^{3/2}$: Al 2s ratios for the cobalt-copper catalyst showed a dramatic effect upon the addition of increasing levels of cobalt. The intensity ratio for the 5 % Co/15 % Cu catalyst had a value of 47.87 which was much larger than that observed for the 20 % copper catalyst despite a lower weight loading. The 10 % Co/10 % Cu catalyst also gave an intensity ratio that was higher than the monometallic copper sample that strongly suggests the presence of cobalt greatly improved the dispersion of the copper metal across the surface and than a large number of smaller copper

crystallites were forming. However, this trend was not carried through to the 15 % Co/5 % Cu catalyst, where an intensity ration of 1.1 was observed indicating very poor metal dispersion.

The Ni $2p^{3/2}$:Al 2s ratios also showed some significant trends. An initial improvement of the nickel dispersion was indicated upon the addition of a second metal: either copper or nickel. With all but the lowest nickel loadings, an intensity ratio greater than that observed with the 20 % nickel catalyst is produced, which again leads to the presumption that the presence of the additional metal is facilitating the dispersion of nickel across the catalyst surface. The low intensity ratios resulting from the 5 % Ni/15 % Cu and the 5 % Ni/15 % Co catalyst may be due to the much lower quantities of nickel on the surface or the amalgamation of the available nickel in to large ill-dispersed particles.

An entirely different pattern is seen in the Co $2p^{3/2}$: Al 2s intensity ratios. Although the intensity ratios are higher, and hence the cobalt better dispersed than in the 20 % cobalt catalyst a much less dramatic increase is observed as with the copper and nickel cases. Furthermore, the intensity ratio appears to be mostly unaffected by both the loading of the cobalt and the second metal. This suggests that the presence of copper or nickel has no affect on the cobalt deposition process or on the dispersion of cobalt ions across the alumina support.

4.2.11 Scanning Electron Microscopy

SEM images of the three 10 %/10 % mixed metal catalysts; 10 % Cu/10 % Ni/Al_2O_3, 10 % Ni/10 % Co/Al_2O_3 and 10 % Cu/10 % Co/Al_2O_3 were collected using the method described in Experimental Section 3.2.2.9. Elemental distribution maps were also produced using an EDX facility to determine how the cobalt, copper and nickel were situated across the catalyst particles.

The SE image and the elemental distribution maps for the 10 % Cu/10 % Ni catalyst are shown in Figure 4.16. The greyscale SE image shown in part (a) depicts catalysts particles around 50 μm across in diameter, which is in agreement with the catalyst particle size analysis detailed in Section 4.2.4, where a D (ν, 50) value of 43.71 μm was determined. Although in grey-scale, two distinct types of catalyst particles are observable. In addition to the larger grey particles, smaller almost white particles indicating a different chemical composition are visible around the edges of the larger particles. Examination of the elemental distribution maps revealed that nickel was present on the alumina particles as an evenly distributed layer. The almost uniform yellow colour indicates that the nickel surface concentration is mainly constant. In contrast, the copper distribution map shows very low levels of copper are spread across the larger catalyst particle surface. It is not absent completely, but the blue colour in the map indicates only a very low surface concentration of copper is present. The majority of the copper is present in localised crystallites, showing as pink or white to indicate very high copper intensity, about 2 μm or less in diameter. These crystallites appear to decorate the edges of the larger support granules. Therefore, in this catalyst precursor state, with the metals present as the carbonate salts, they appear to remain discrete and have not formed homogeneously mixed metal particles.

Figure 4.17 shows the SE image and elemental distribution maps for the 10 % Ni/10 % Co catalyst. A range of particle sizes is visible, however most are approximately 40 μm in diameter which is similar to the D(ν, 50) value of 37.6 μm determined during particle size analysis. Examination of the elemental distribution maps show that both metals, both nickel and cobalt, are evenly distributed across the catalyst particles. The surface concentration of each metal across each particle is generally uniform with only very small areas with an increased cobalt or nickel intensity. In this catalyst, both metal carbonate salts have intermixed successfully and certainly, in the unreduced catalyst precursor state, mixed metal catalyst particles have been formed.

The images collected from the finally tested catalyst, the 10 % Cu/10 % Co catalyst are displayed in Figure 4.18. With this catalyst the grey-scale SE micrograph

confirms the previous catalyst particle size analysis results of 37.5 μm for the D(ν, 50), with catalyst particles ranging from around 10 – 80 μm. From this image, the situation described for the 10 % Cu/10 % Ni catalyst is again in evidence. The larger catalyst particles appear to be decorated around the periphery with much smaller particles, less than 2 μm in diameter, with an entirely different chemical composition. The elemental distribution map revealed that these smaller particles are composed of copper, which is mostly localised on these particles, similar to as in the 10 % Cu/10 % Ni catalyst. Cobalt, in contrast is practically homogenously distributed across the larger catalyst particles. These images imply that the cobalt carbonate ions are well dispersed across the support surface, however the copper carbonate has formed discrete crystallites and has not mixed with the cobalt to form mixed metal particles in the precursor state.

Figure 4.16: SEM and EDX mapping images of 10 % Cu/10 % Ni catalyst

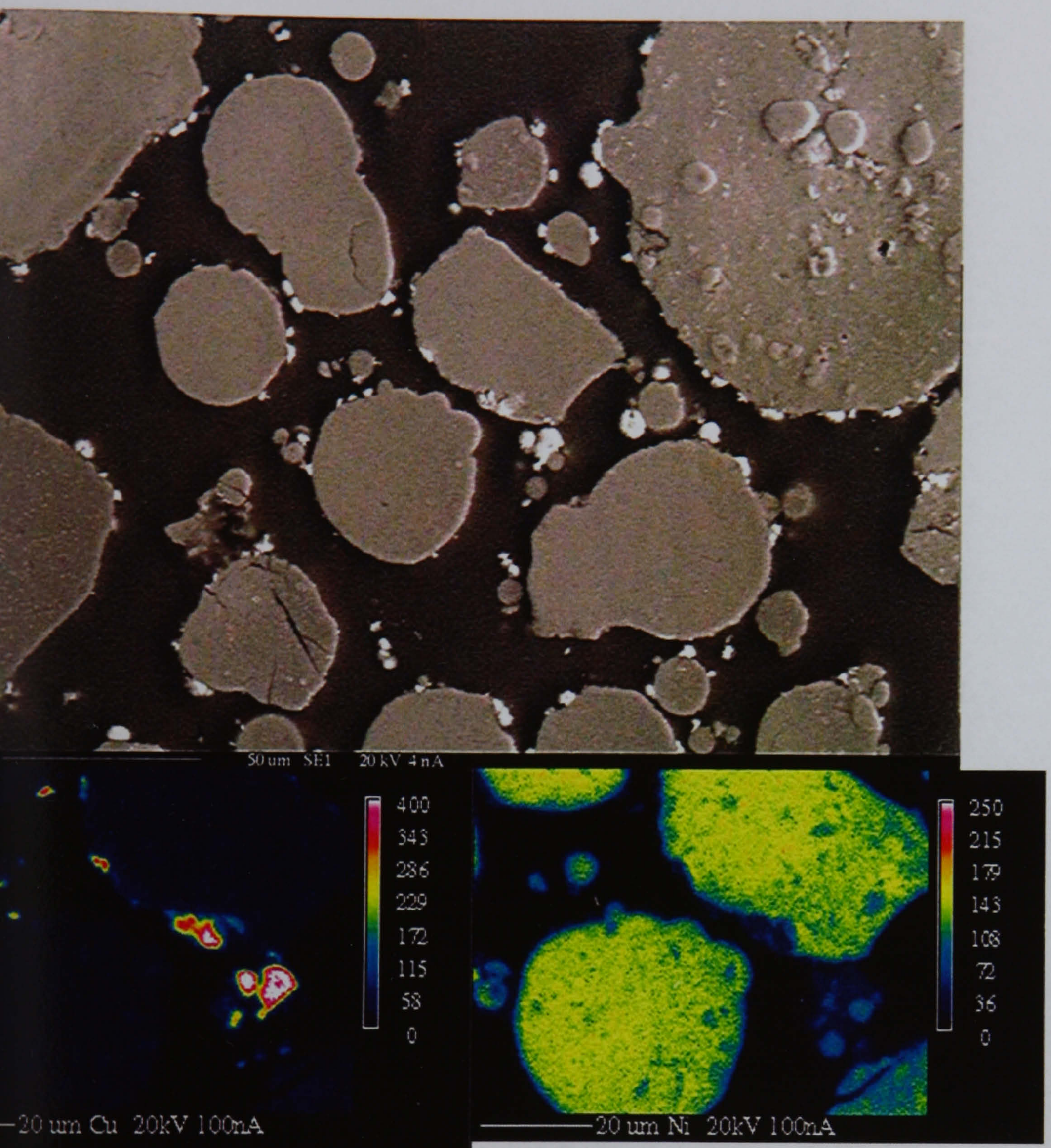

Figure 4.17: SEM and EDX mapping images of 10 % Co/10 % Ni catalyst

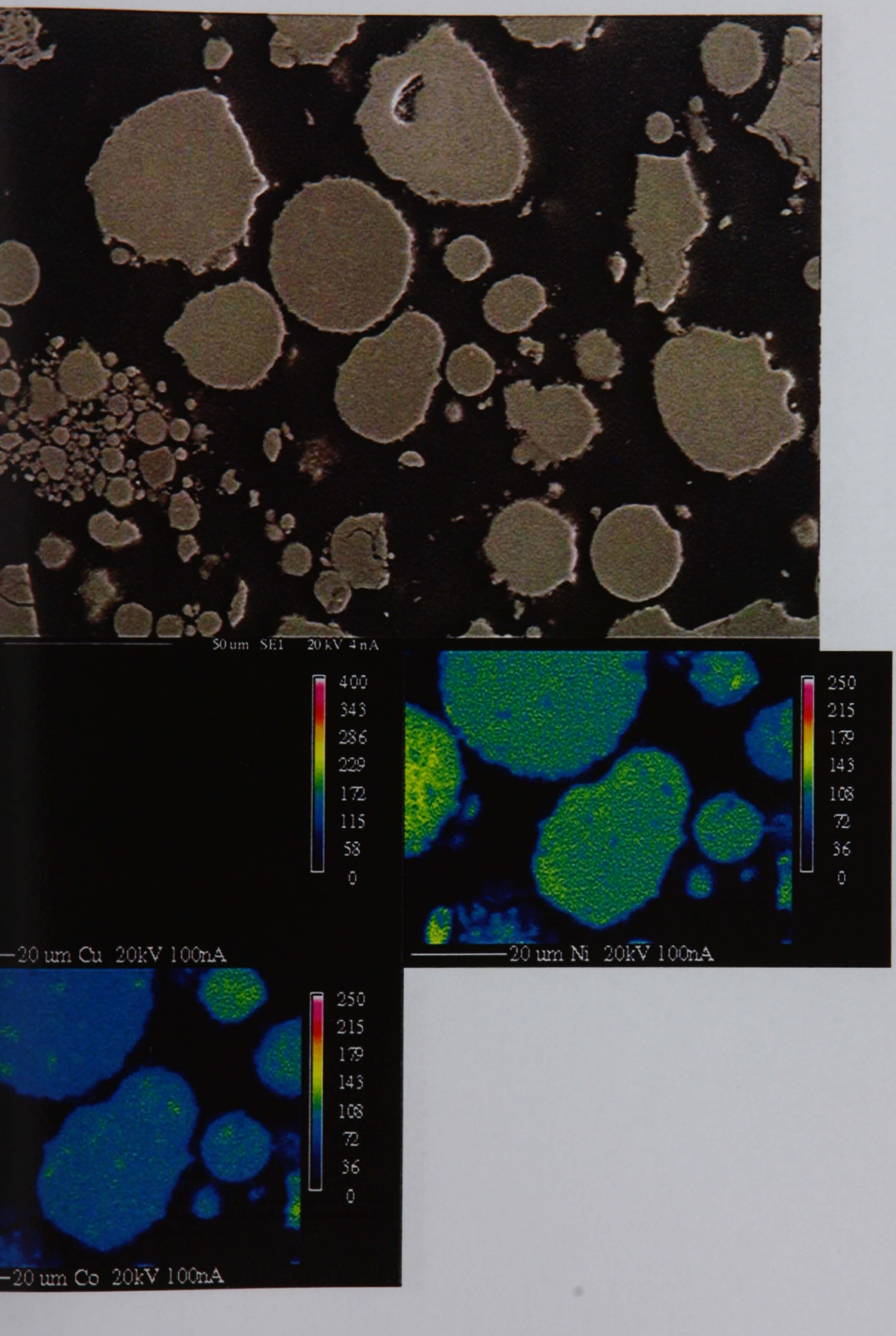

Figure 4.18: SEM and EDX mapping images of 10 % Co/10 % Cu catalyst

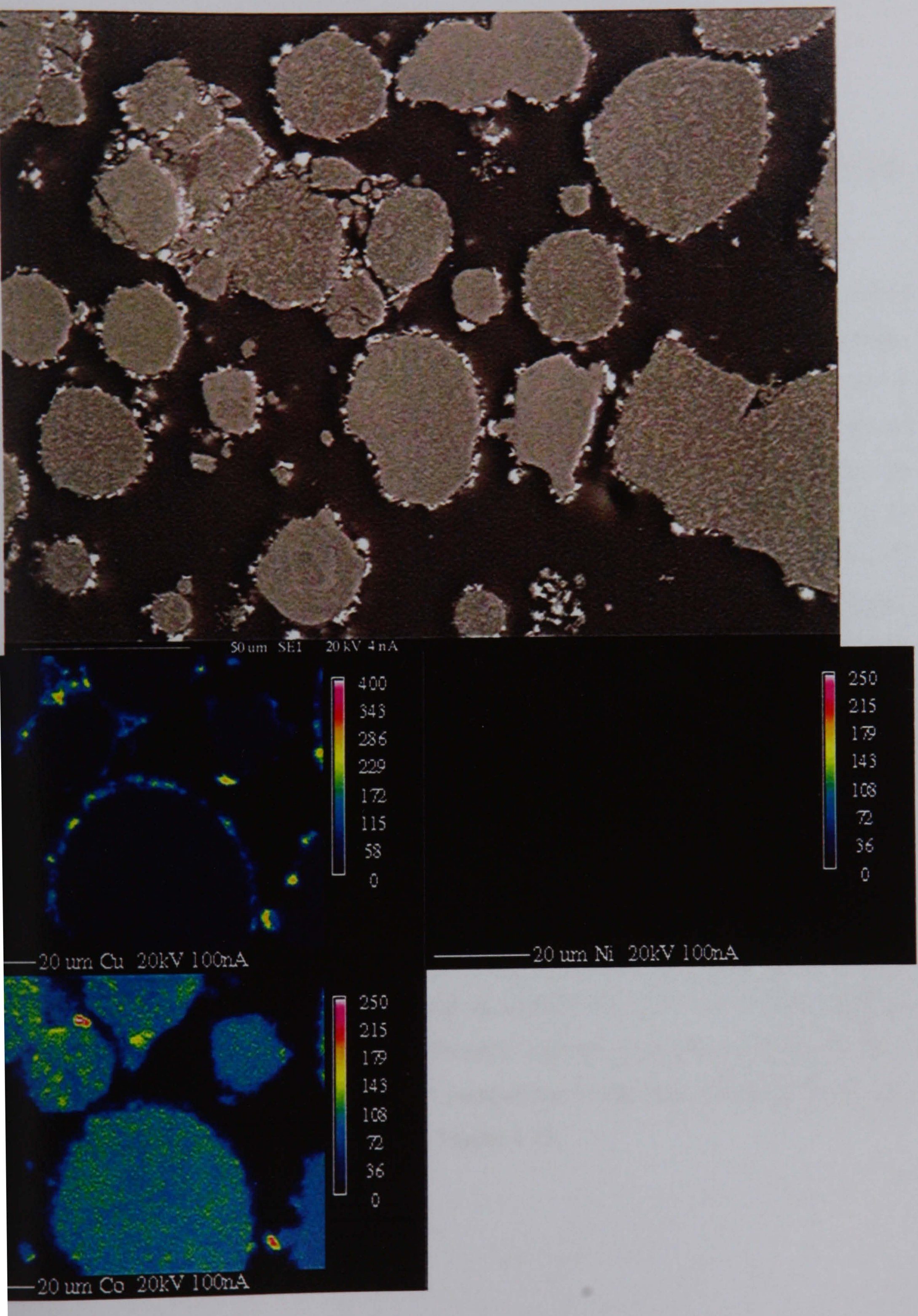

4.3 Catalyst Testing

4.3.1 Liquid Phase Hydrogenation

4.3.1.1 Nitrobenzene Hydrogenation at 0.5 bar g with Catalysts Pd/CN1, Pd/CA1 and Pd/CSXU

Catalysts Pd/CN1, Pd/CA1 and Pd/CSXU were used to perform the hydrogenation of nitrobenzene following the procedure outlined in Section 3.3.2.3 using both methanol and isopropanol (IPA) as reaction solvents. A pressure of 0.5 bar g and a temperature of 313 K were used. The rate of reaction was monitored using the hydrogen uptake from the gas flow controller and the data are displayed in Figures 4.19-4.21. All six reactions showed a linear uptake of hydrogen throughout the duration of the experiments, however different rates of reaction were observed in each case. The initial hydrogenation rate was easily determined from the hydrogen uptake curve by determining the gradient using the equation displayed below (Equation 4.3).

$$\text{Rate of reaction (mol min}^{-1}) = \frac{\text{difference in hydrogen consumption (mol)}}{\text{difference in time (min)}} \quad \text{(Equ. 4.3)}$$

The reaction rates have been expressed throughout this thesis with units of mmol $min^{-1}g^{-1}$ to allow direct comparisons between different catalysts and when different masses of catalysts have been used. A comparison of the rates of reactions obtained from these experiments is displayed in Figure 4.22.

Figure 4.19: Hydrogen consumption during the hydrogenation of nitrobenzene using catalyst Pd/CN1 in methanol and IPA.

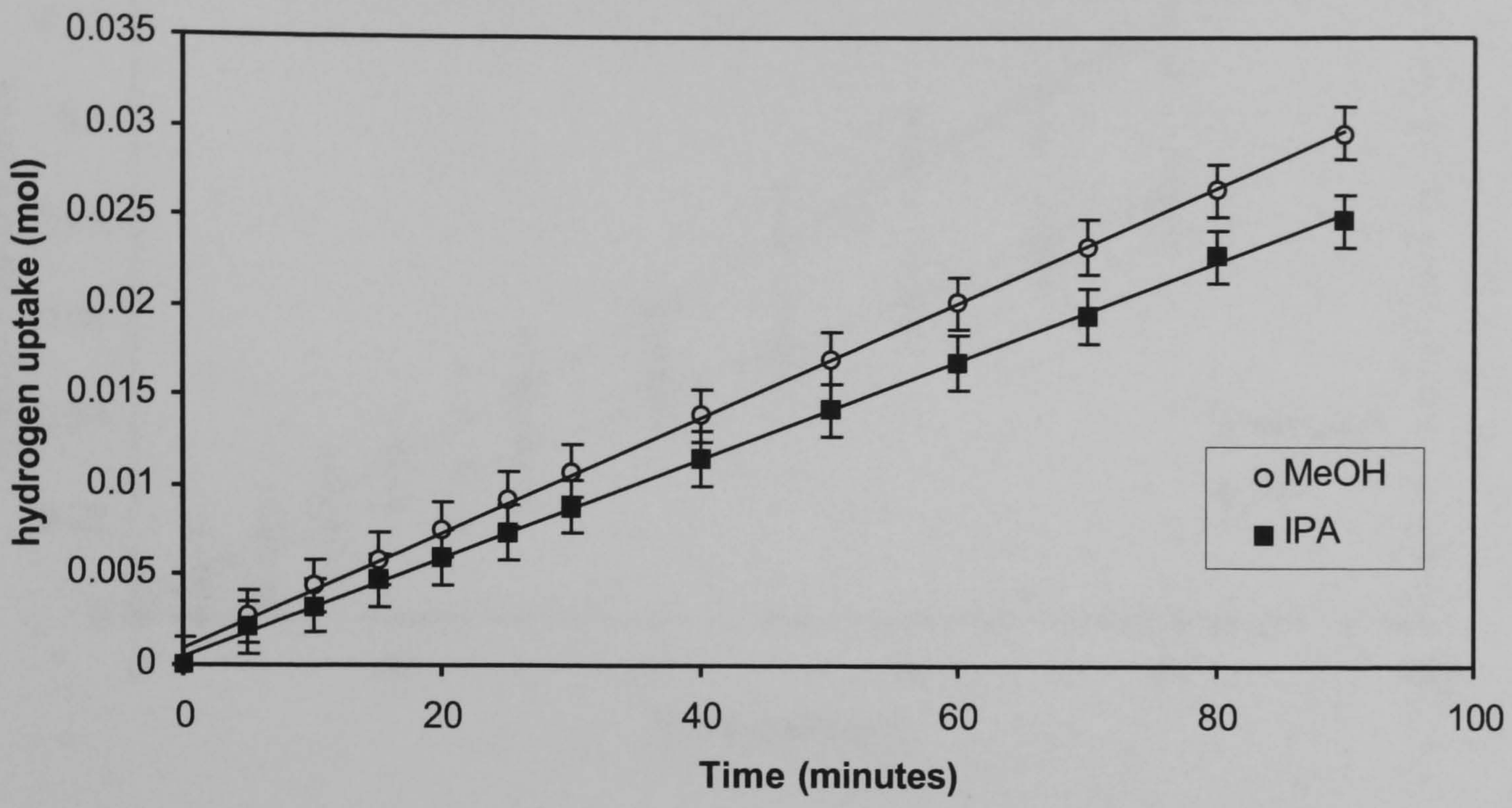

Figure 4.20: Hydrogen consumption during the hydrogenation of nitrobenzene using catalyst Pd/CA1 in methanol and IPA

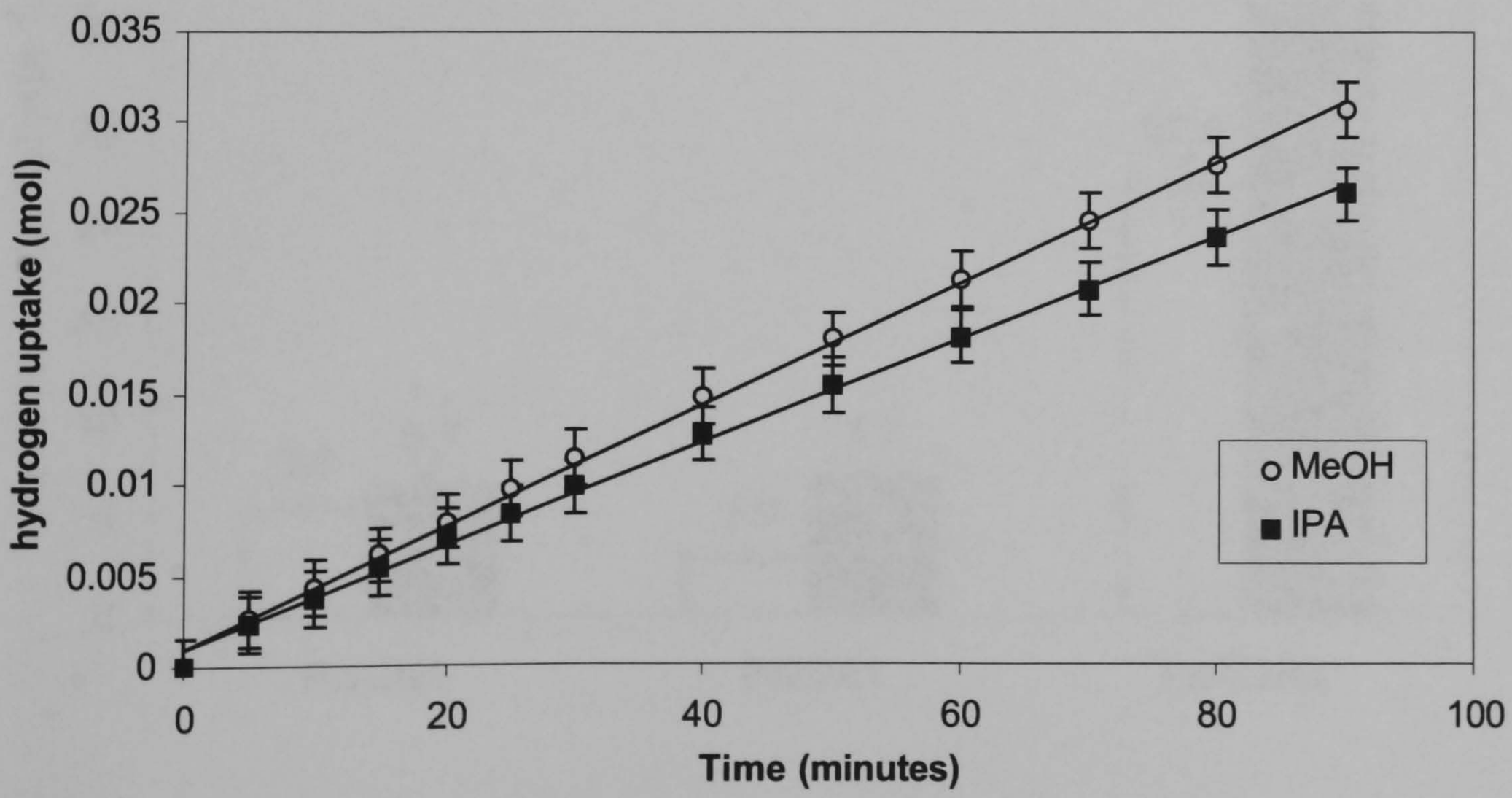

Figure 4.21: Hydrogen consumption during the hydrogenation of nitrobenzene using catalyst Pd/CSXU in methanol and IPA.

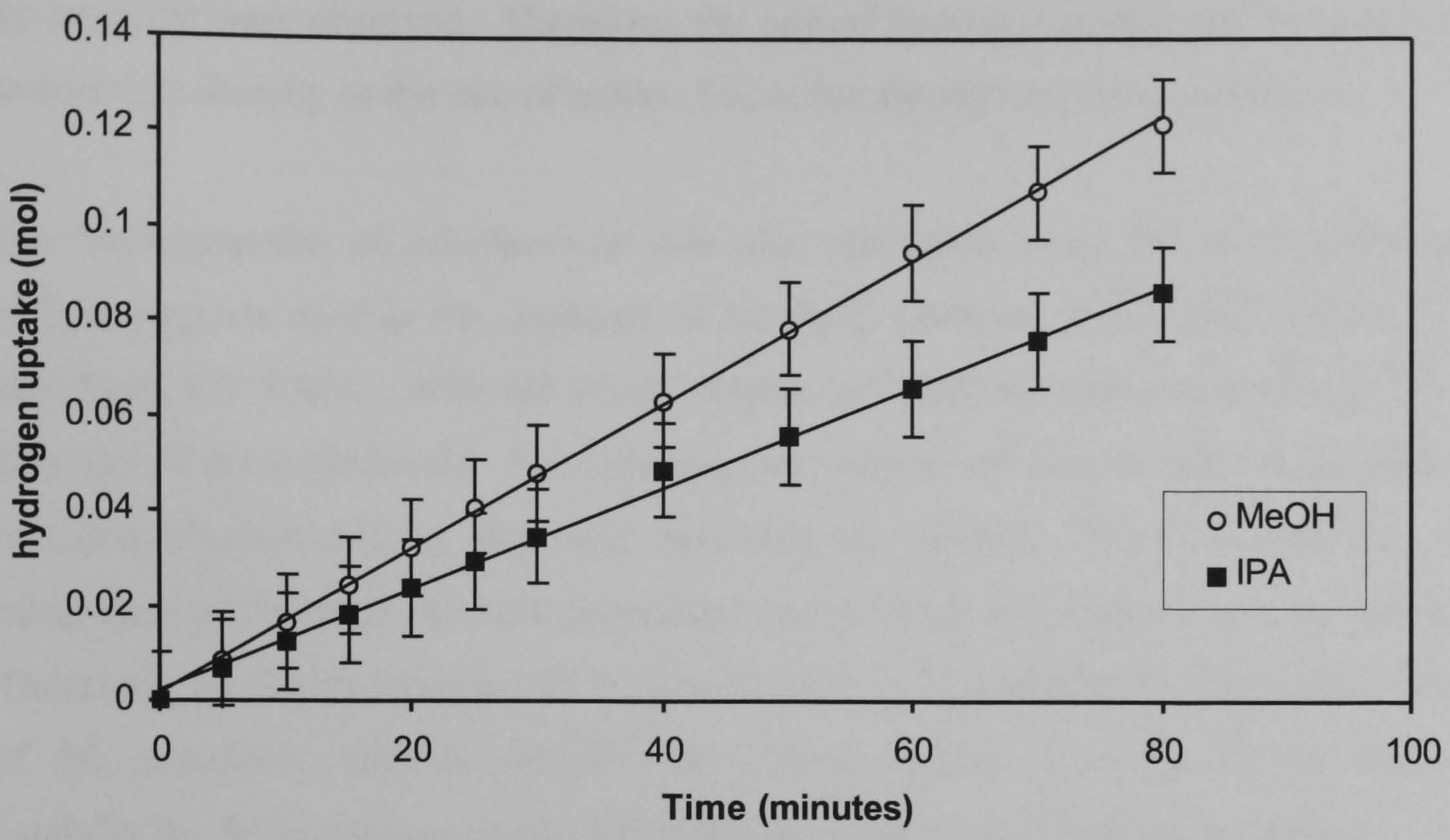

Figure 4.22: Comparison of the initial rates of reaction in methanol and IPA

A sample from each reaction mixture was removed post hydrogenation and analysed using GC to confirm that the production of aniline had taken place. Nitrobenzene and aniline were the only components visible on the GC chromatograms and no other by-products were observed. Therefore, the rate of hydrogen uptake can be assumed to correlate directly to the rate of aniline formation throughout these reactions.

The hydrogenation of nitrobenzene was also attempted using the three activated carbon supports used in the synthesis of the Pd/C catalysts: Norit CN1, Norit CA1 and Norit SX Ultra. With all three carbons no reaction was observed over the duration of the experiment. No hydrogen was consumed and the GC-MS analysis revealed nitrobenzene as the only molecule in solution. The concentration of nitrobenzene remained constant throughout and no other by-products were observed. Therefore, we can deduce that all the results previously reported are due to the effect of the palladium catalysis and that the carbon support materials are not active catalysts for the hydrogenation of nitrobenzene under these reaction conditions.

With each catalyst the hydrogenation reaction proceeded more rapidly in methanol than in isopropanol (IPA), which is consistent with previous studies by Kochetova et al, [123, 129] where they reported a faster rate of hydrogenation in ethanol than in IPA. The most rapid reaction was observed with catalyst Pd/CSXU that hydrogenated nitrobenzene at a rate of 31.6 mmol $min^{-1}g^{-1}$ in methanol and 22.0 mmol $min^{-1}g^{-1}$ in IPA. Similarly, a higher rate of hydrogenation in methanol was observed with the other two catalysts; Pd/CN1 with rates of 6.7 mmol $min^{-1}g^{-1}$ in methanol and 5.6 mmol $min^{-1}g^{-1}$ in IPA and Pd/CA1 with rates of 7.1 mmol $min^{-1}g^{-1}$ and 3.0 mmol $min^{-1}g^{-1}$ in methanol and IPA respectively. Although the reaction was consistently faster in methanol, the extent of the decrease in reaction rate observed when moving to IPA was variable among the catalysts. For instance, with Pd/CN1 the reaction rate reduced by 16.4 % when moving to IPA, whereas with catalyst Pd/CA1 the rate dropped by 57.7 % in IPA with catalyst Pd/CSXU the reduction in rate was 30.4 %. This indicated that the change in solvent was affecting each catalyst to a different degree and that the catalyst supports or palladium dispersion may have in some way influenced the catalytic process.

Consideration of hydrogen solubility data revealed that the slowing of rate in the more viscous solvent (IPA) was not caused by a decrease in hydrogen solubility as hydrogen dissolves to a greater extent in IPA than in methanol [174]. A graphical representation of the hydrogen solubility trend in methanol and IPA is shown in Figure 4.23. Therefore, the difference in hydrogenation rate could not be attributed to hydrogen solubility differences between the two solvents.

Figure 4.23: The solubility of hydrogen in methanol and IPA [173]

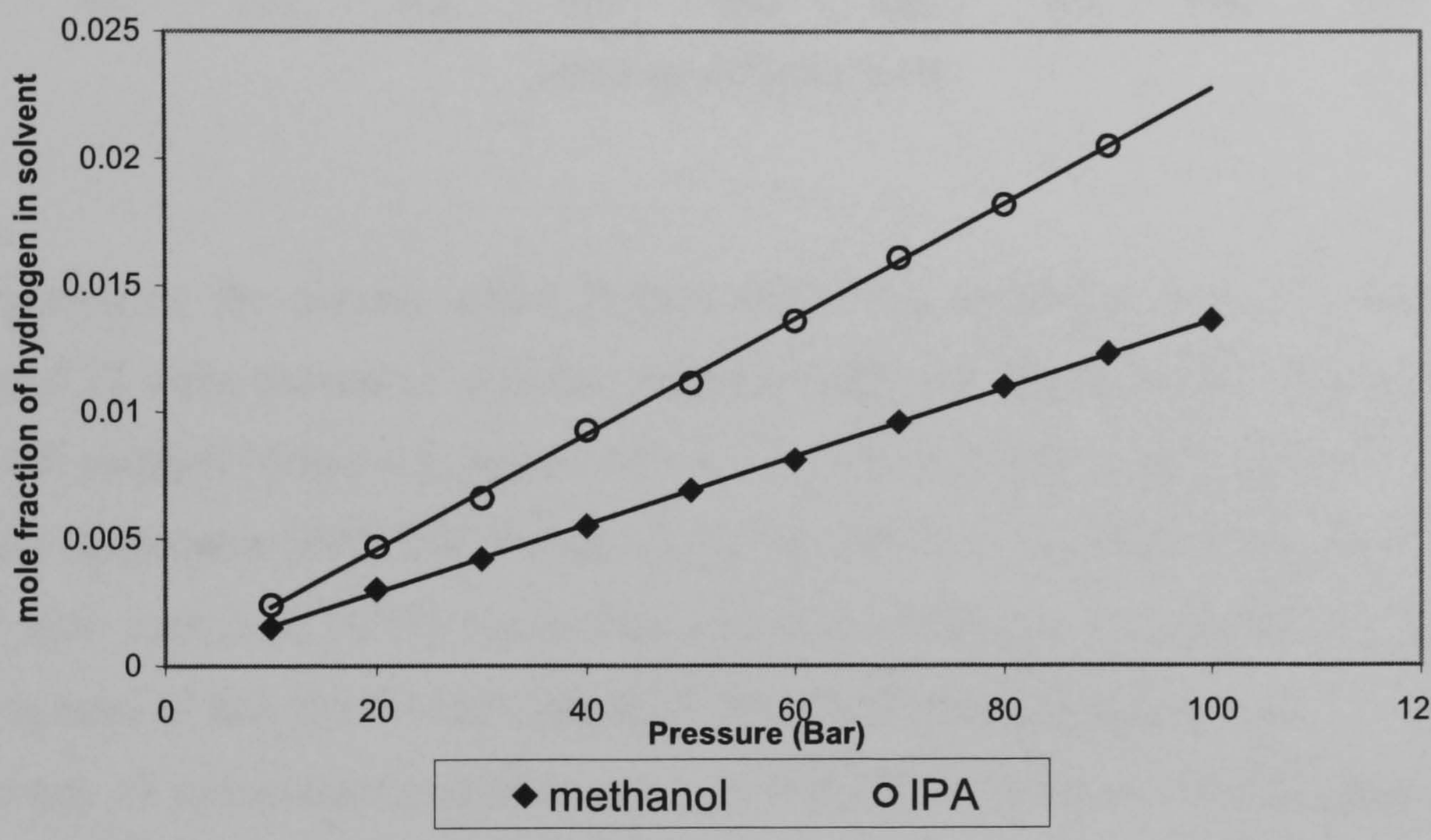

The reactions were checked further for external mass transport control by carrying out a series of nitrobenzene hydrogenation reactions in methanol with catalyst Pd/CSXU at varying stirrer speeds. This was the reaction with the most rapid rate of hydrogenation and therefore one that had potentially reached a limiting factor. The data from these reactions are presented in Figure 4.24 and show that the hydrogenation rate remained relatively constant across the range of stirrer speeds indicating the lack of an external mass transport control effect. Therefore, the diffusion of hydrogen through the solvent to the catalyst surface was not the rate-limiting step in these reactions.

Figure 4.24: The rate of nitrobenzene hydrogenation at a range of stirrer speeds

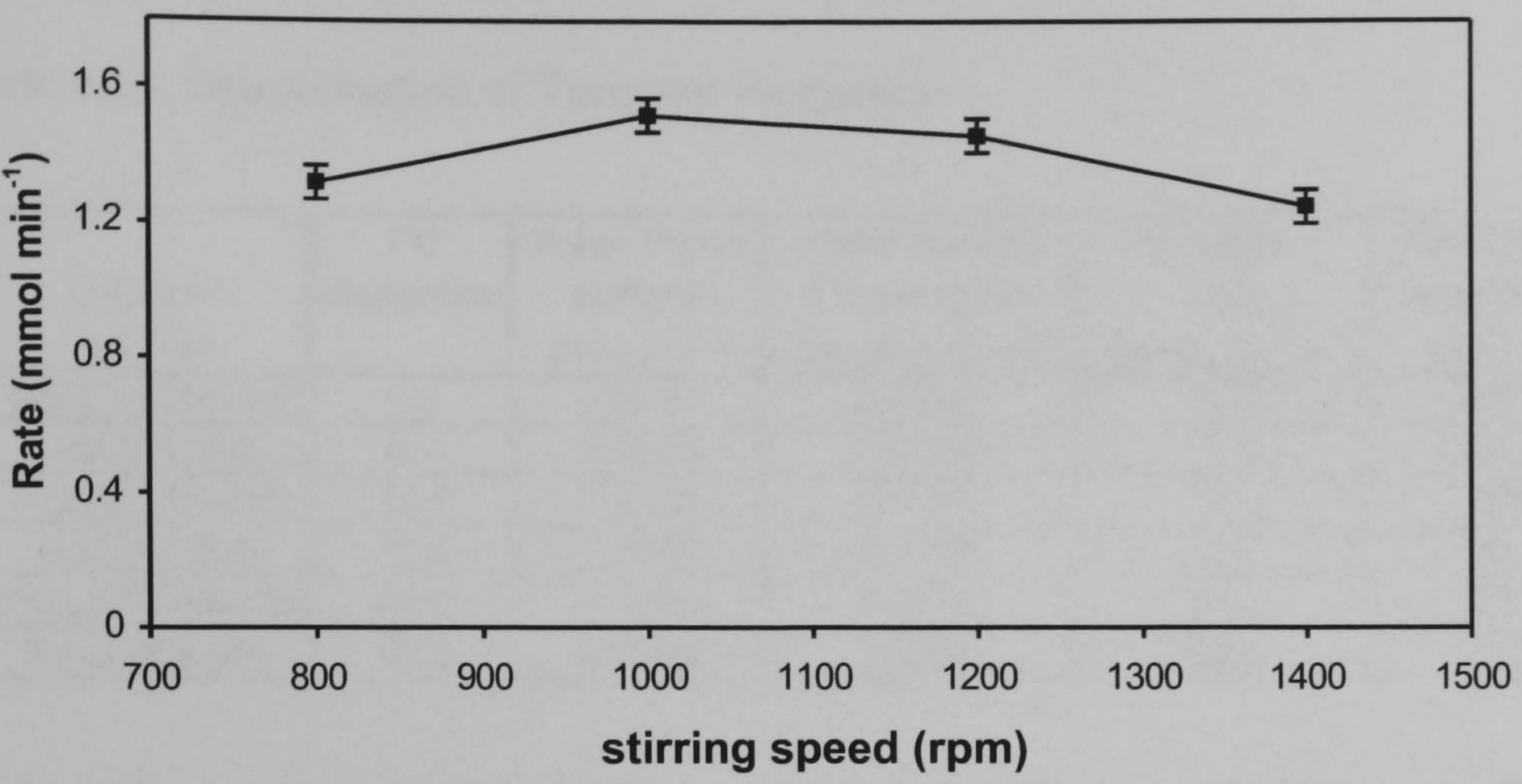

To investigate the solvent effect further, the initial hydrogenation rates shown in Figure 4.22 were compared with the experimentally calculated palladium dispersions for each catalyst (Table 4.1, Section 4.1.1). As expected, the metal catalyst with the highest dispersion (Pd/CSXU) showed by far the best hydrogenation rate and the other two catalysts, Pd/CA1 and Pd/CN1, with similar lower dispersion showed similar rates of reaction To take the difference in dispersions into account, a turnover frequency of nitrobenzene to aniline per available palladium site was calculated for each catalyst in the two solvents. Equation 4.4 shows the relationship used to generate the turnover frequencies [3].

$$\text{Turnover frequency} = \frac{\text{rate of reaction per gram}}{\text{surface sites per gram}} \qquad \text{Equation 4.4}$$

Where, the rate of reaction was taken from the hydrogen uptake graphs and the surface sites per gram taken from the CO chemisorption.

The steps involved in determining the turnover frequency from the palladium dispersion and reaction rate are shown in Table 4.15.

Table 4.15: Determination of Turnover Frequency

Catalyst/ solvent	Pd dispersion	moles Pd on surface (mmol g^{-1})	moles surface Pd per gram (mmol min^{-1} g^{-1})	reaction rate (mmol min^{-1} g^{-1})	**Turnover frequency (min^{-1})**
Pd/CN1 MeOH	8.9	0.0063	0.0252	6.7	**267**
Pd/CN1 IPA	8.9	0.0063	0.0252	5.6	**223**
Pd/CA1 MeOH	12.6	0.0089	0.0356	7.1	**199**
Pd/CA1 IPA	12.6	0.0089	0.0356	3.0	**85**
Pd/CSXU MeOH	42.0	0.0296	0.1184	31.6	**267**
Pd/CSXU IPA	42.0	0.0296	0.1184	22.0	**186**

Each catalyst had a palladium loading of 3 % by weight and a fixed mass of 0.25 g of catalyst was used to perform each chemisorption experiment.

The turnover frequencies are represented as a bar chart in Figure 4.25. A higher rate of reaction per palladium site in methanol was confirmed. In the methanol solvent, catalysts Pd/CN1 and Pd/CSXU showed identical turnover frequencies of 267 min^{-1} despite the large difference in the dispersion of the catalysts suggesting the hydrogenation reaction was not sensitive to palladium particle size. However catalyst Pd/CA1 showed a turnover frequency of 200 min^{-1}, substantially lower than the expected value of 267 min^{-1}. In this system the palladium was considerably less active than in the other two catalysts.

Furthermore, the catalysts showed different behaviour in terms of turnover frequency when the hydrogenations were performed in IPA. In this case all three catalysts displayed different behaviour. Catalyst Pd/CN1 was the most efficient catalyst with a turnover frequency of 224 min^{-1}, followed by catalyst Pd/CSXU with a frequency of 186 min^{-1} and catalyst Pd/CA1 with a turnover of 85 min^{-1}. In this solvent, as with methanol, catalyst Pd/CA1 showed the lowest turnover frequency and least active palladium. A difference in the turnover frequencies of Pd/CN1 and Pd/CSXU also emerged in IPA than was not observed in methanol. As the activity pattern is different going between the two solvents, this indicated that a definite solvent effect

was in operation where methanol and IPA were not merely acting as the reaction media but had an influence on the rate of reaction.

Figure 4.25: The Turnover frequencies of the Pd/C Catalysts

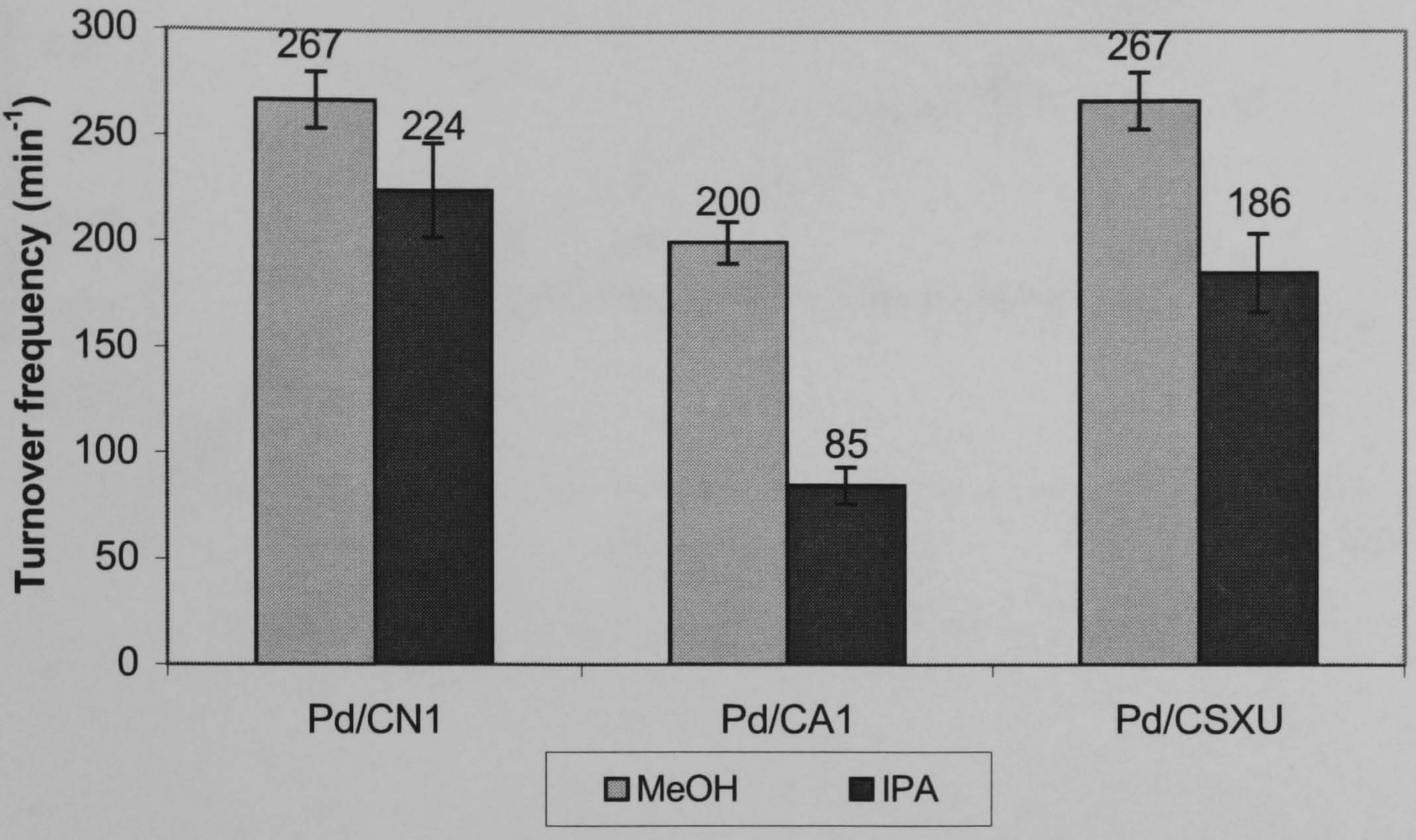

3.3.1.2 Nitrobenzene Reaction Order

To calculate the nitrobenzene reaction order a series of hydrogenations was carried out in methanol using a range of nitrobenzene concentrations. A pressure of 2 bar and a temperature of 323 K were used throughout. The reactions were monitored using hydrogen uptake and the collected data are shown in Figure 4.26. Samples were also removed at time intervals and analysed using GC-MS. Nitrobenzene and aniline were detected in each reaction with trace amounts of azobenzene. The levels of azobenzene did not reach more than 1 % of the reaction solution and no other by-products or intermediates were produced.

Figure 4.26: Hydrogen consumption during the hydrogenation of nitrobenzene in methanol using catalyst Pd/CSXU and varying concentrations of nitrobenzene.

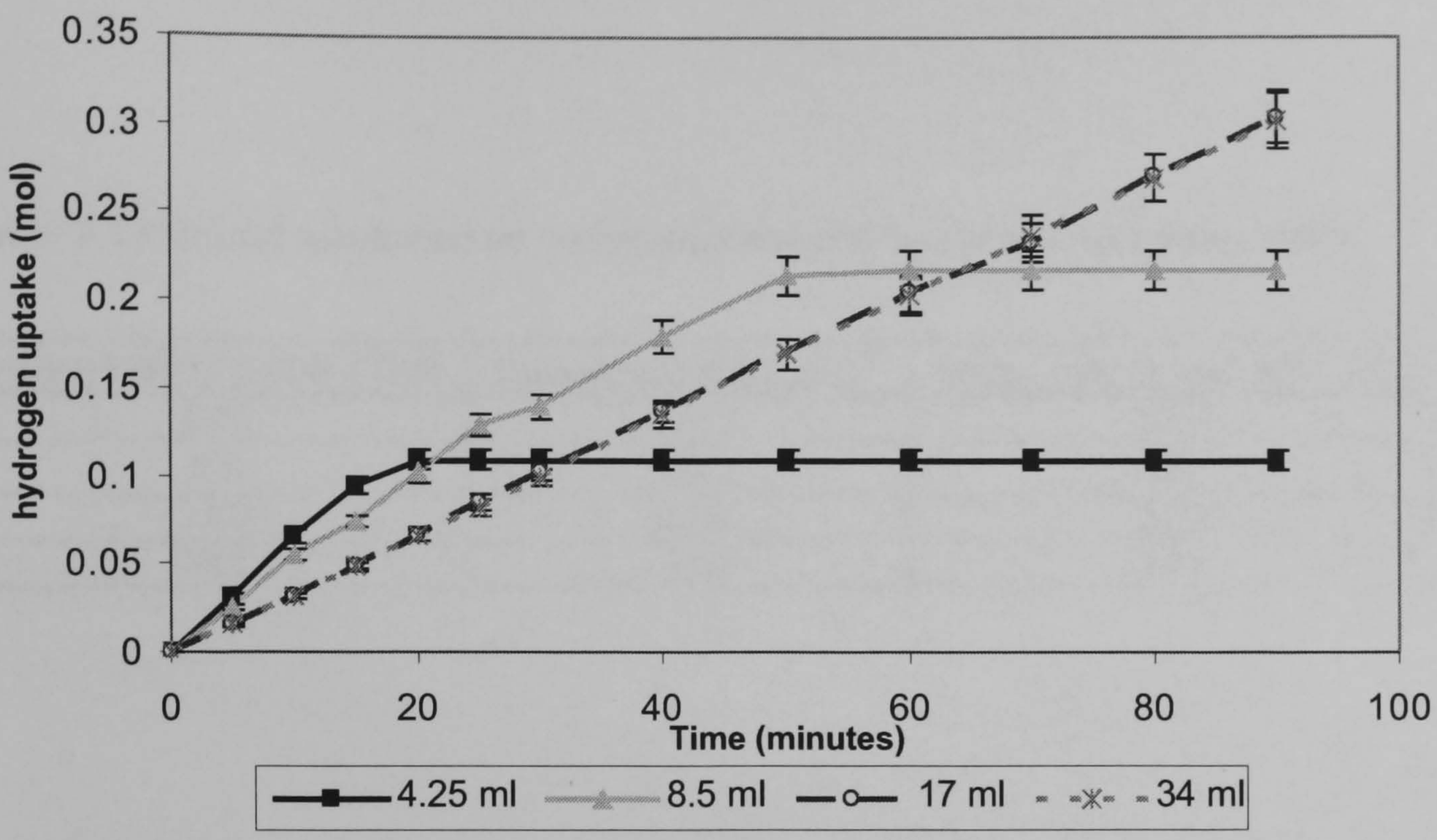

The initial rate of hydrogenation was calculated for each reaction from the hydrogen uptake data displayed in Figure 4.26. The initial concentrations of nitrobenzene and the corresponding rates of reaction are displayed in Table 4.16. From these data the order of the reaction with respect to nitrobenzene was determined. The concentration of dissolved H_2 (g) was assumed to be constant throughout all experiments and therefore the only variable was nitrobenzene concentration. Table 4.16 shows that with concentrations of 0.58 mol L^{-1} and above, the hydrogenation reaction was zero order with respect to nitrobenzene as the hydrogenation rate was unaffected by the change in concentration. Rates of 33 mmol $min^{-1}g^{-1}$ and 32 mmol $min^{-1}g^{-1}$ were obtained for nitrobenzene concentrations of 0.58 mol L^{-1} and 1.16 mol L^{-1} respectively. However, at concentrations below 0.58 mol L^{-1} the rate of hydrogenation was affected by the concentration of nitrobenzene. Halving the concentration to 0.29 mol L^{-1} resulted in the rate increasing by a factor of 1.5 to 49.5 mmol $min^{-1}g^{-1}$ and halving the concentration further to 0.145 mol L^{-1} caused the rate to increase again to 62.7 mmol $min^{-1}g^{-1}$, an increase by a factor of 1.3. To calculate the reaction order with respect to nitrobenzene a plot of the log of the initial rates versus the log of the initial nitrobenzene concentration was constructed and is

displayed in Figure 4.27 [175]. As the gradient of the line in this plot is equal to the reaction order, the hydrogenations were negative 2nd order with respect to the nitrobenzene concentration at concentrations lower than 0.58 mol L^{-1}.

Table 4.16: Initial nitrobenzene concentrations and initial hydrogenation rates

volume nitrobenzene (ml)	[nitrobenzene] mol L^{-1}	initial rate (mmol min^{-1} g^{-1})
4.25	0.145	62.7
8.5	0.29	49.5
17.0	0.58	33.0
34.0	1.16	32.1

Figure 4.27: Plot of the log of initial rate vs log of initial nitrobenzene concentration to calculate nitrobenzene reaction order.

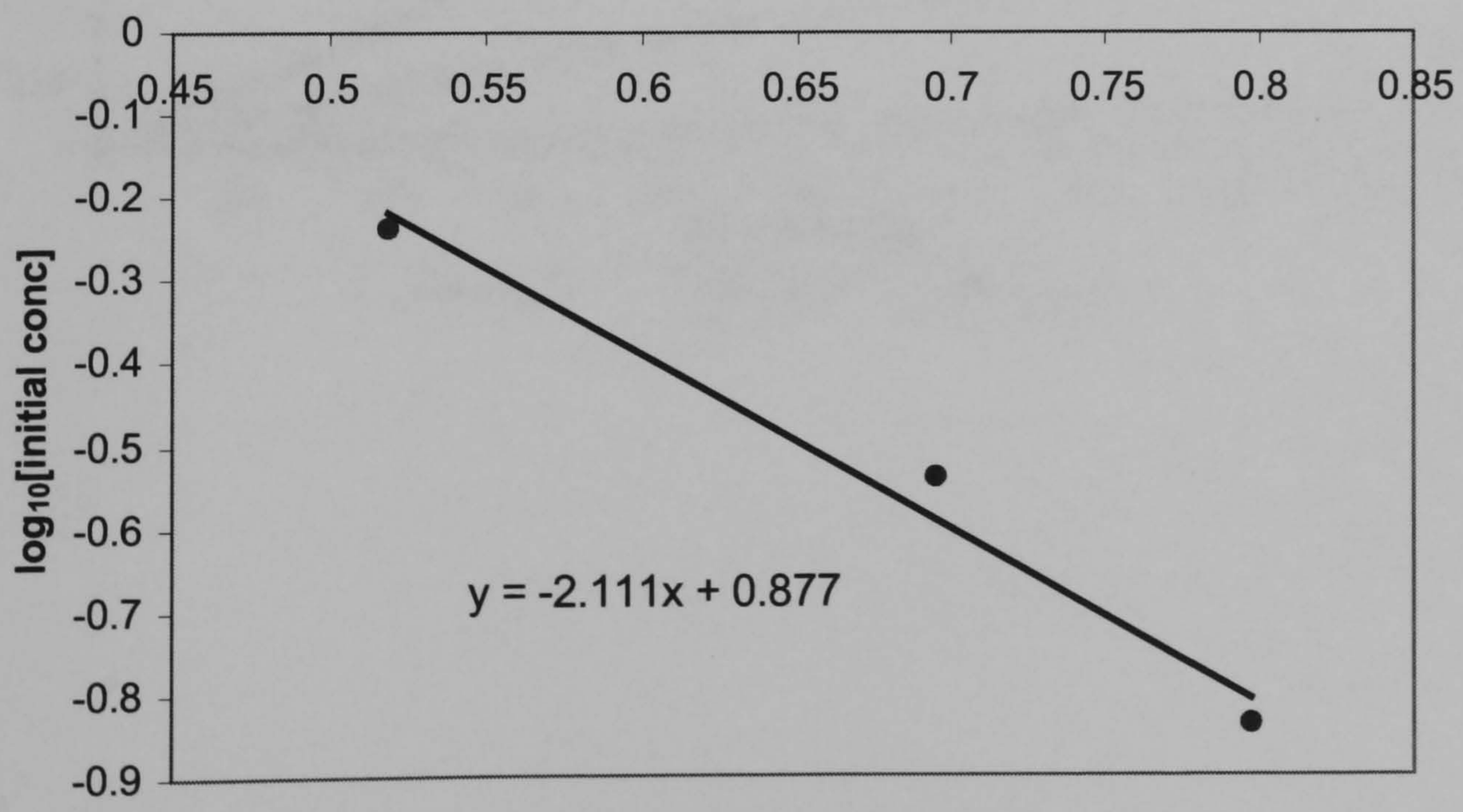

4.3.1.3 Deactivation Experiments with Recovered Pd/C Catalysts

A series of deactivation experiments was carried out in both methanol and IPA using catalysts Pd/CN1, Pd/CA1 and Pd/CSXU and following the procedure described in Section 3.3.2.4. Reactions were performed under 5 bar pressure and at 323 K. The hydrogen uptake data collected from the reactions using Pd/CN1 in methanol are displayed in Figure 4.28 and in IPA in Figure 4.29. The results from the GC analysis of each of the three hydrogenations in methanol and IPA are shown in Figures 4.30 and 4.31 respectively.

Figure 4.28: Hydrogen consumption during the hydrogenation of nitrobenzene using recovered and washed Pd/CN1 in methanol

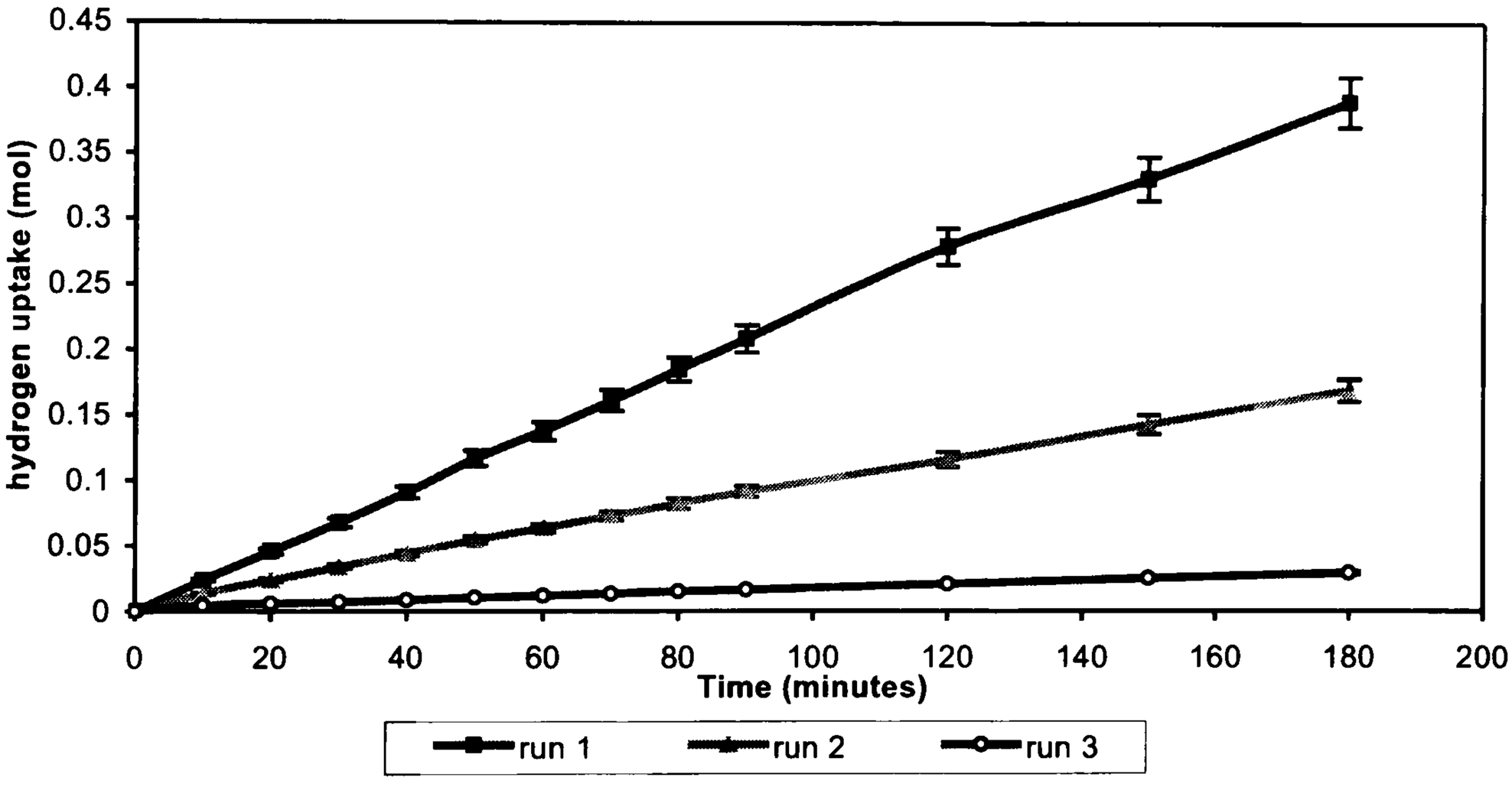

Figure 4.29: Hydrogen consumption during the hydrogenation of nitrobenzene using recovered and washed Pd/CN1 in IPA.

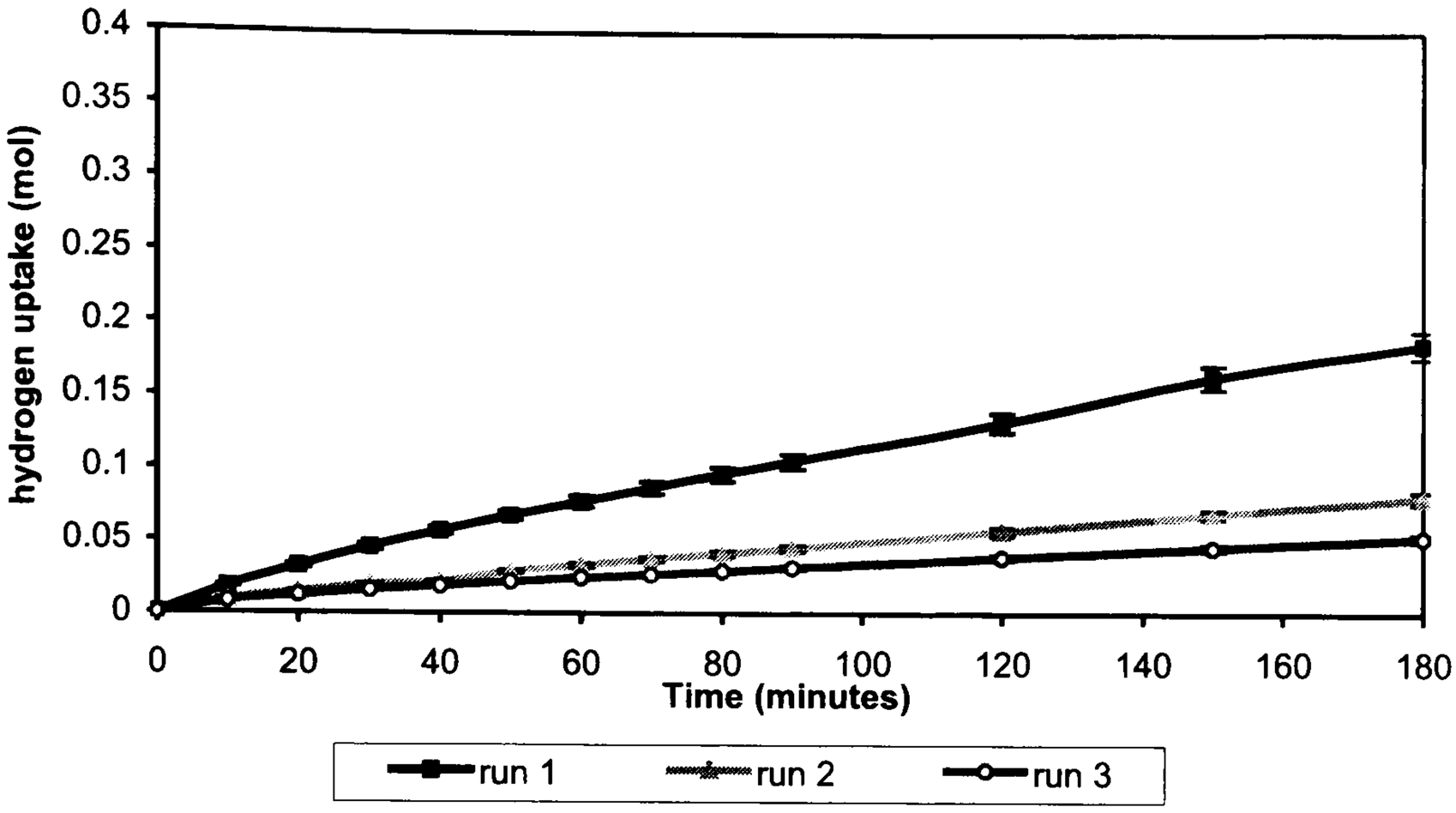

Figure 4.30a: Reaction profile for the hydrogenation of nitrobenzene with catalyst Pd/CN1 in methanol – run 1 of 3.

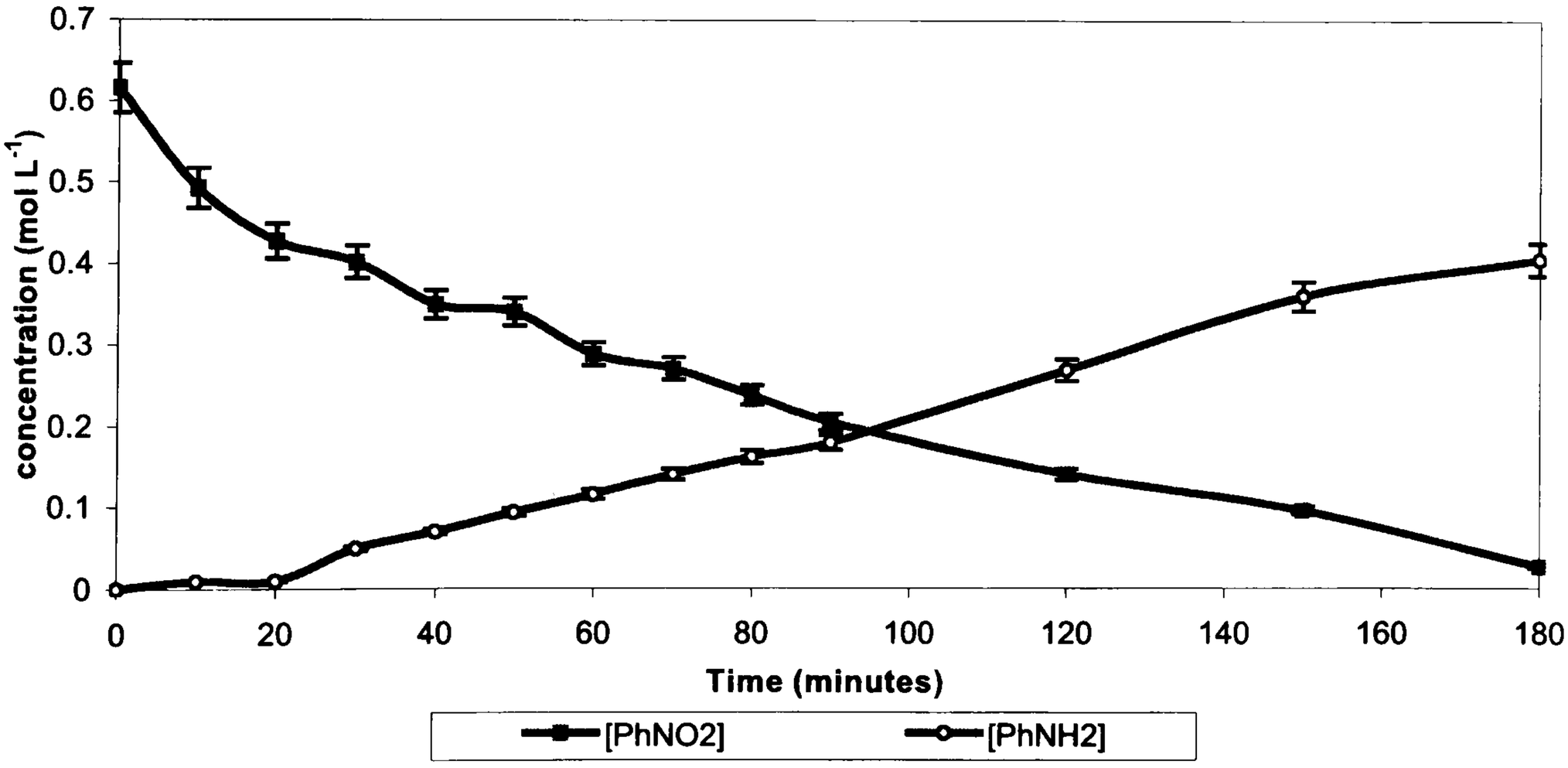

Figure 4.30b: Reaction profile for the hydrogenation of nitrobenzene using recovered catalyst Pd/CN1 in methanol – Run 2 of 3.

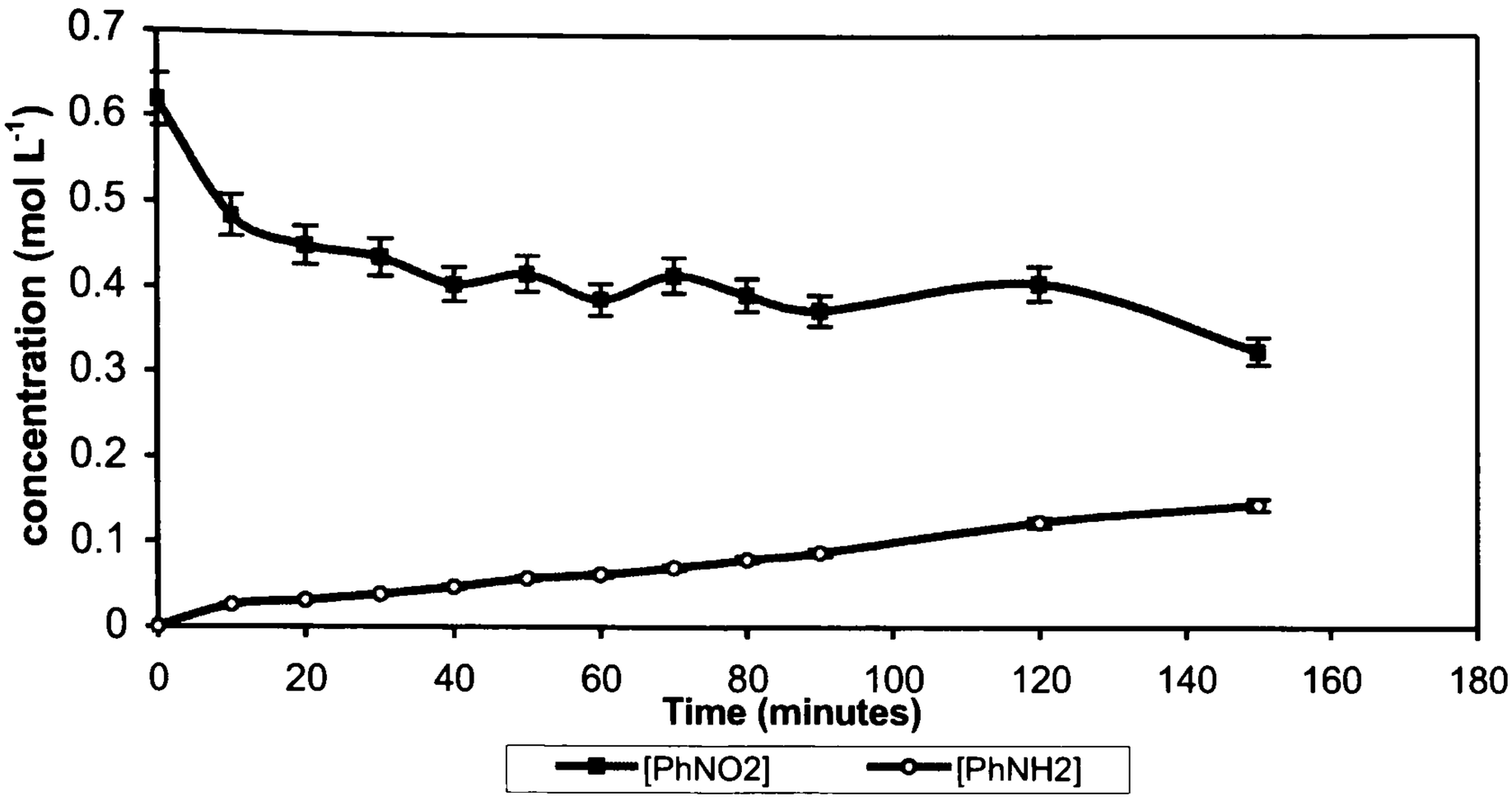

Figure 4.30c: Reaction profile for the hydrogenation of nitrobenzene using recovered catalyst Pd/CN1 – Run 3 of 3

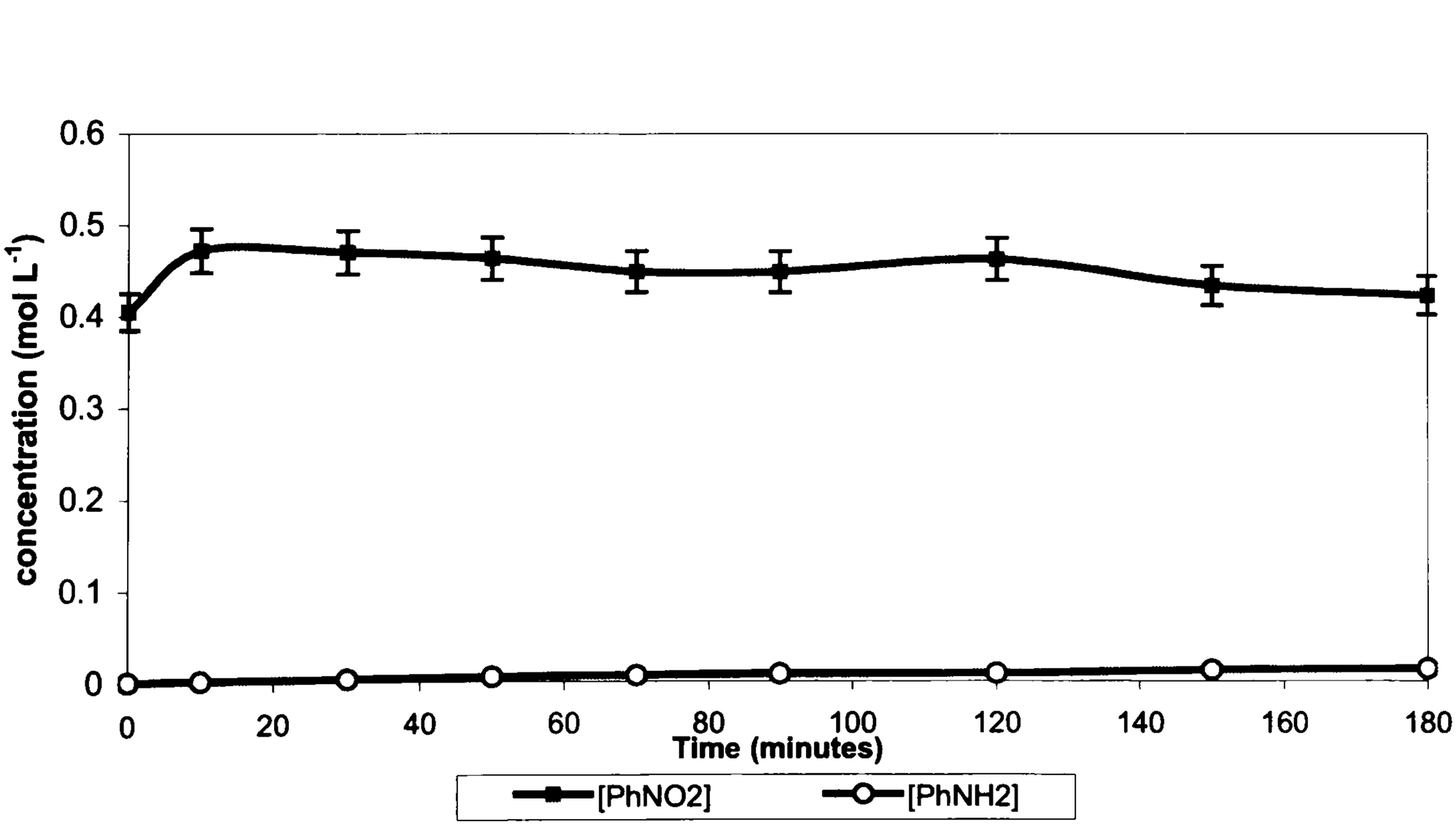

Figure 4.31a: Reaction Profile: the hydrogenation of nitrobenzene using catalyst Pd/CN1 in IPA – Run 1 of 3.

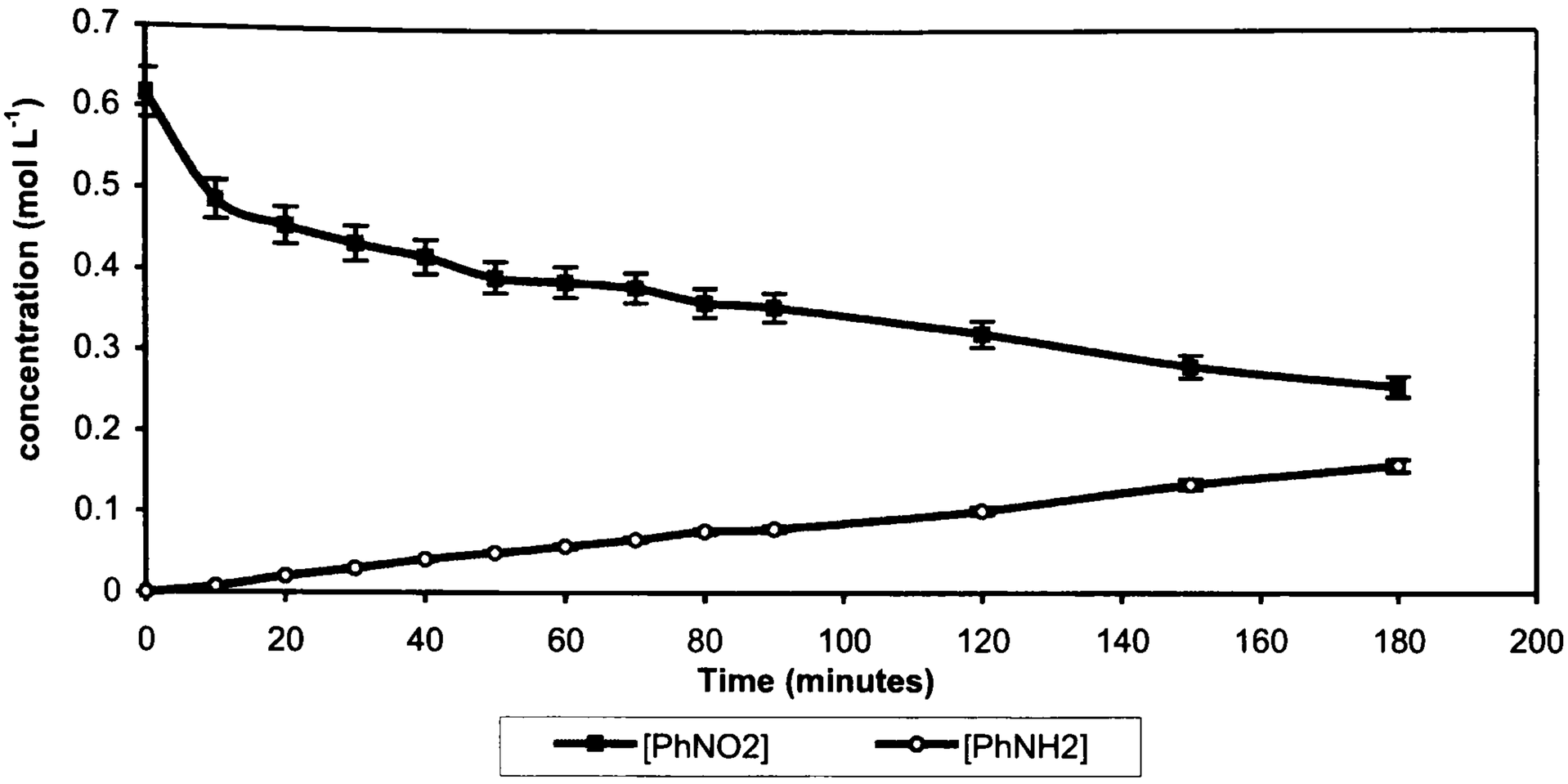

Figure 4.31b: Reaction Profile: the hydrogenation of nitrobenzene using recovered catalyst Pd/CN1 in IPA – Run 2 of 3

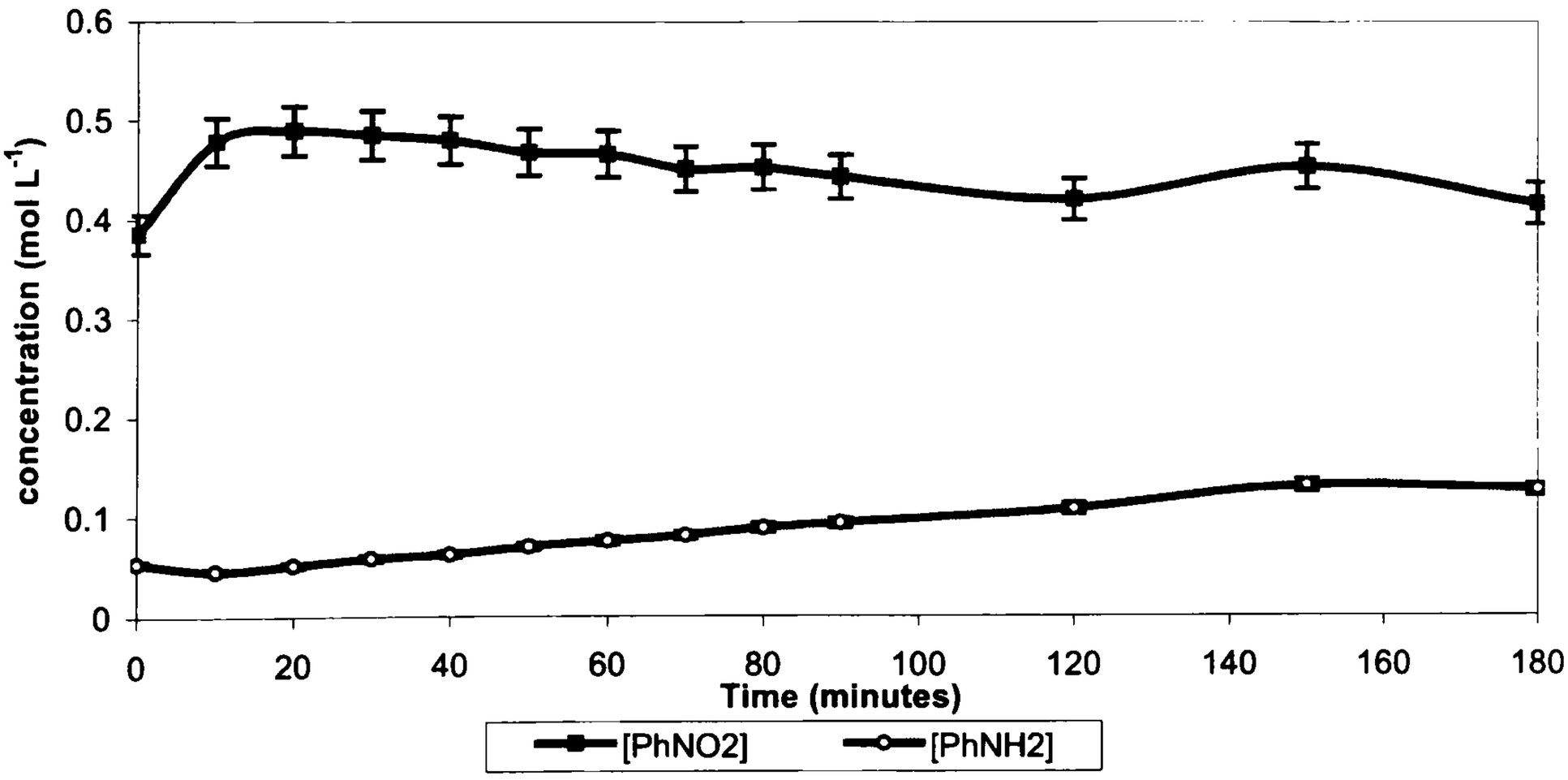

Figure 4.31c: Reaction profile: the hydrogenation of nitrobenzene using recovered catalyst Pd/CN1 in IPA – Run 3 of 3.

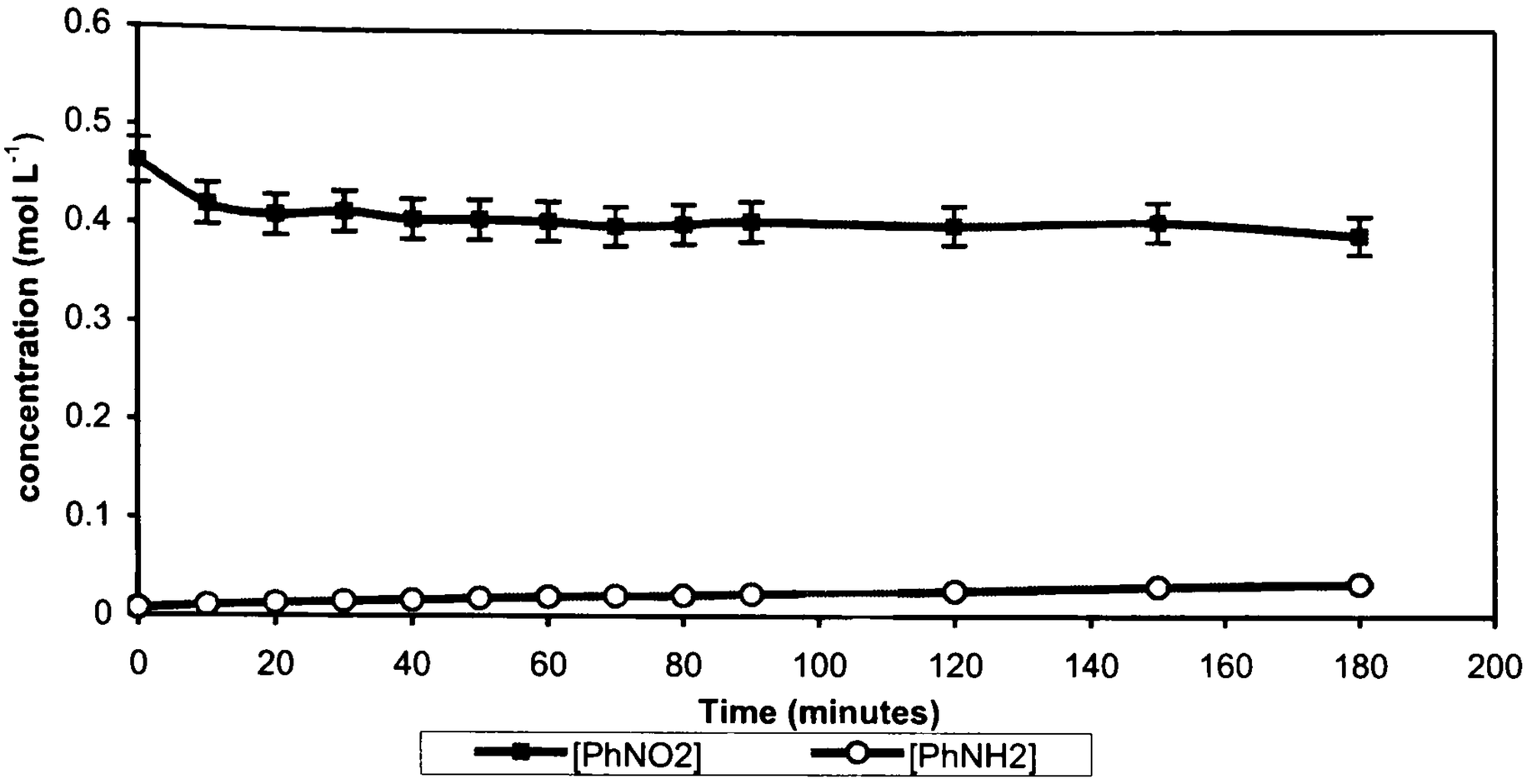

The hydrogen uptake results for the successive hydrogenation of nitrobenzene using recovered and washed catalyst Pd/CA1 in both methanol and IPA are shown in Figures 4.32 and 4.33 respectively. The GC analyses for all six reactions are displayed in Figures 4.34 and 4.35.

Figure 4.32: Hydrogen consumption during the successive hydrogenation of nitrobenzene using recovered and washed catalyst Pd/CA1 in methanol

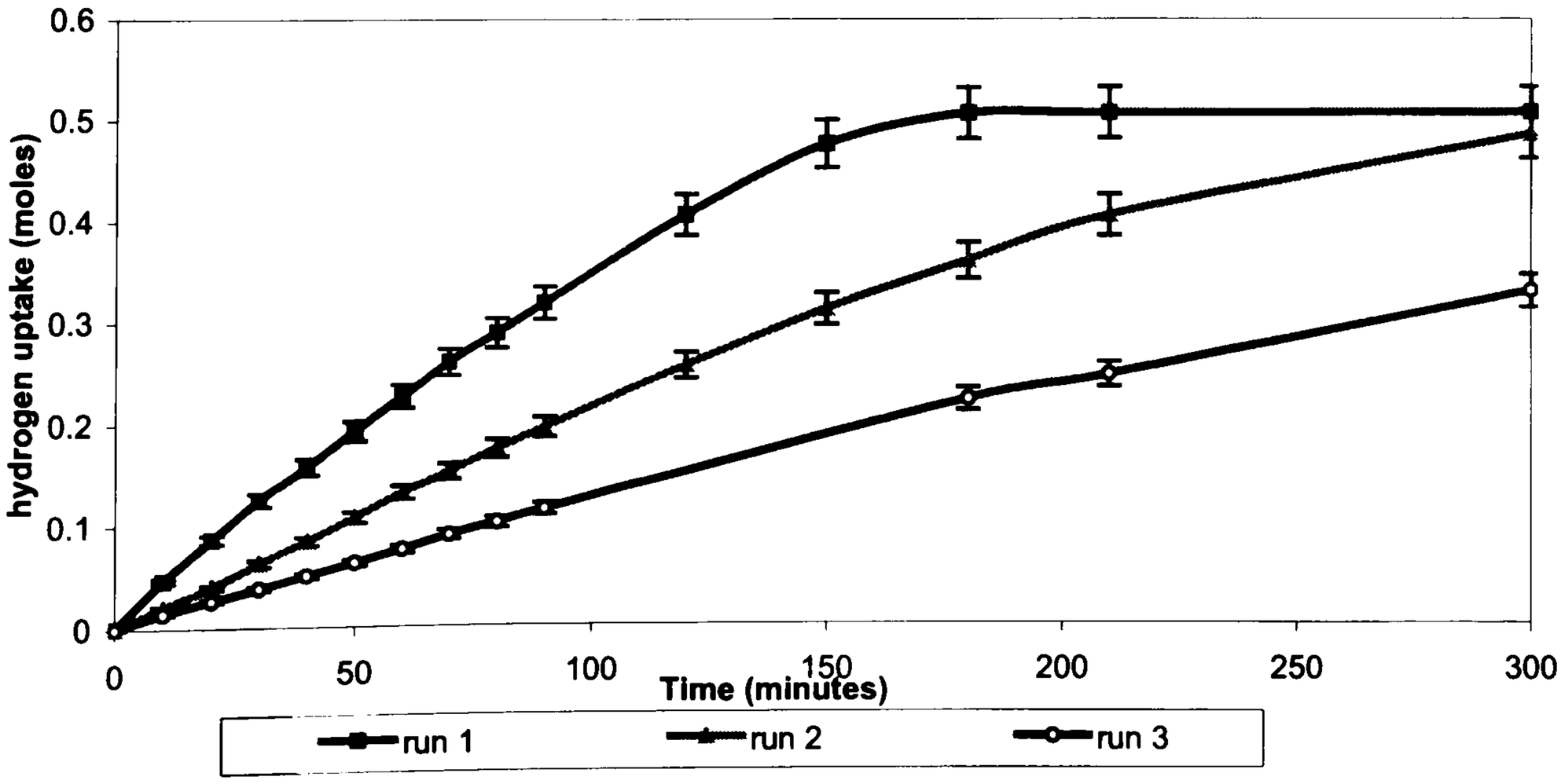

Figure 4.33: Hydrogen consumption during the successive hydrogenation of nitrobenzene using recovered and washed catalyst Pd/CA1 in IPA.

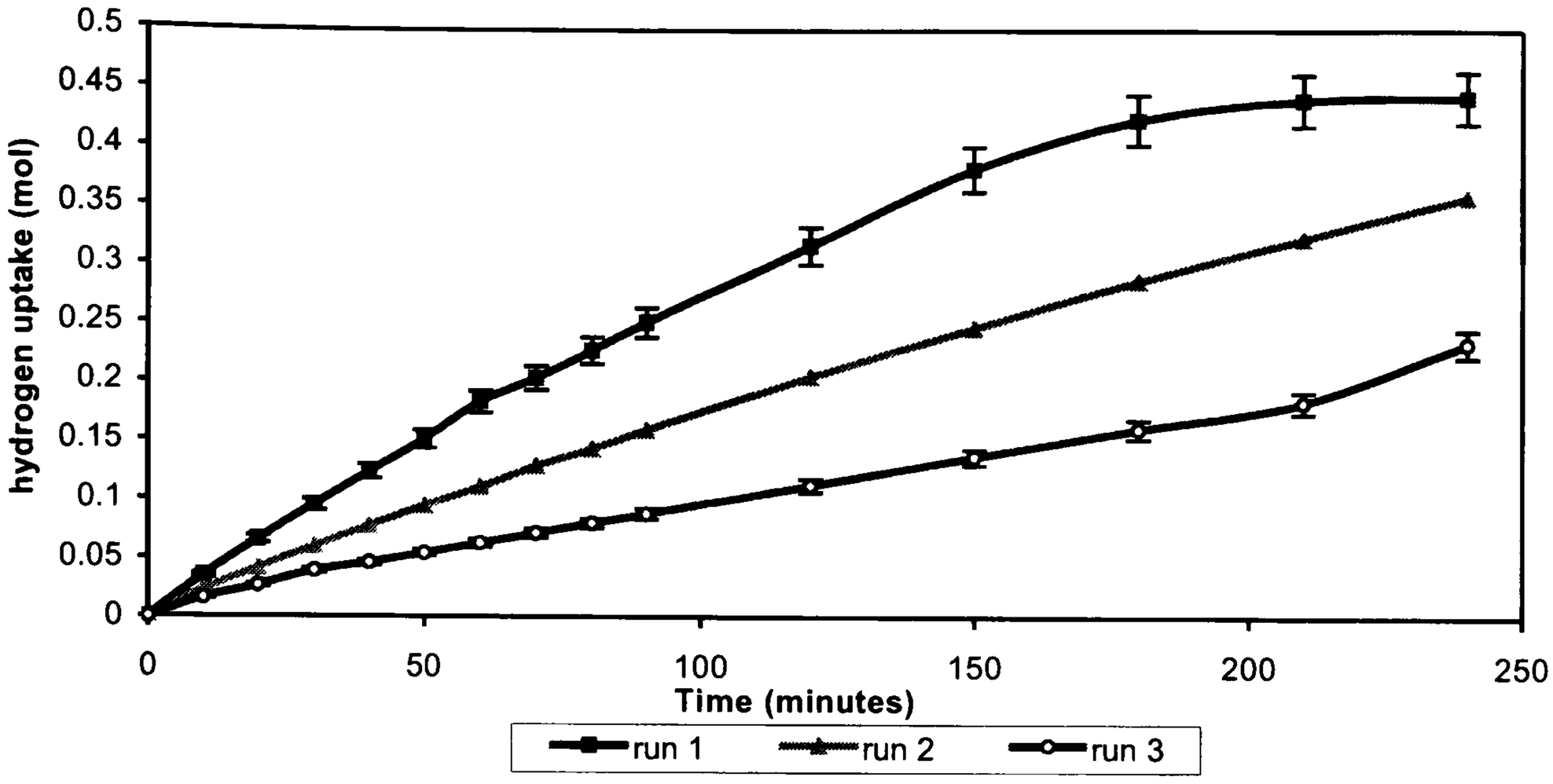

Figure 4.34a: Reaction profile: the hydrogenation of nitrobenzene using catalyst Pd/CA1 in methanol – Run 1of 3

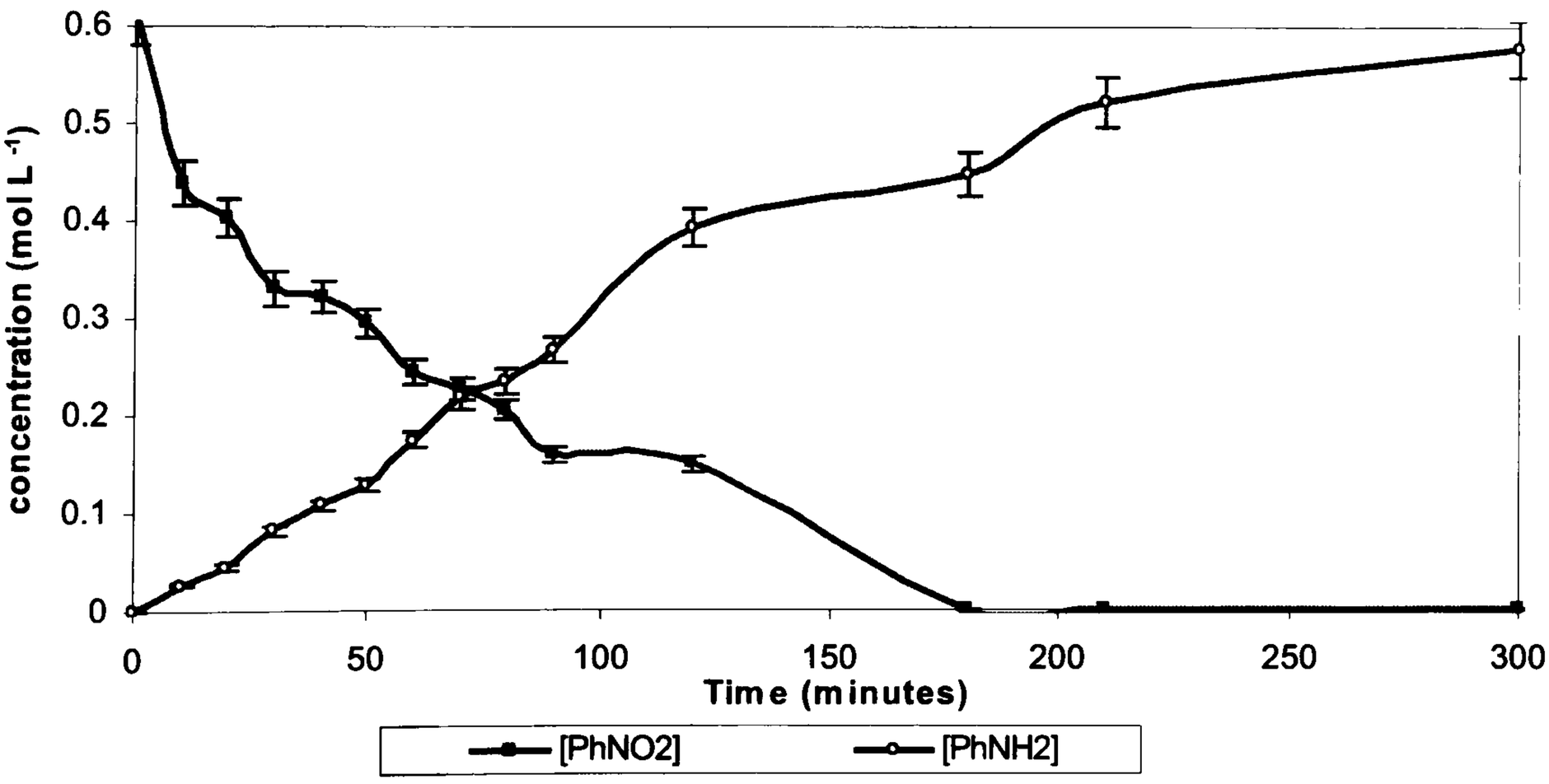

Figure 4.34b: Reaction Profile: the hydrogenation of nitrobenzene using recovered catalyst Pd/CA1 in methanol – Run 2 of 3.

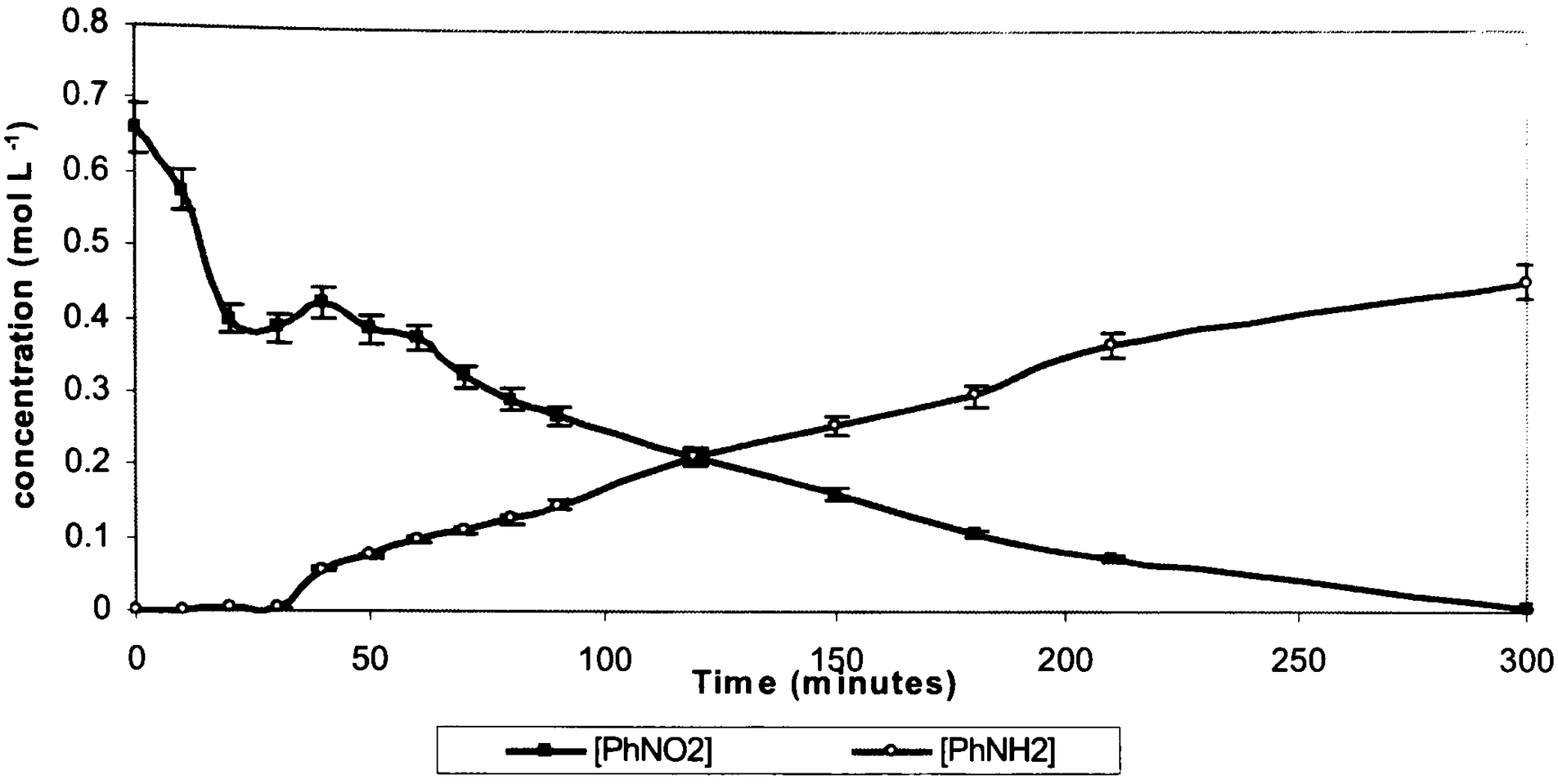

Figure 4.34c: Reaction profile: the hydrogenation of nitrobenzene using recovered catalyst Pd/CA1 in methanol – Run 3 of 3

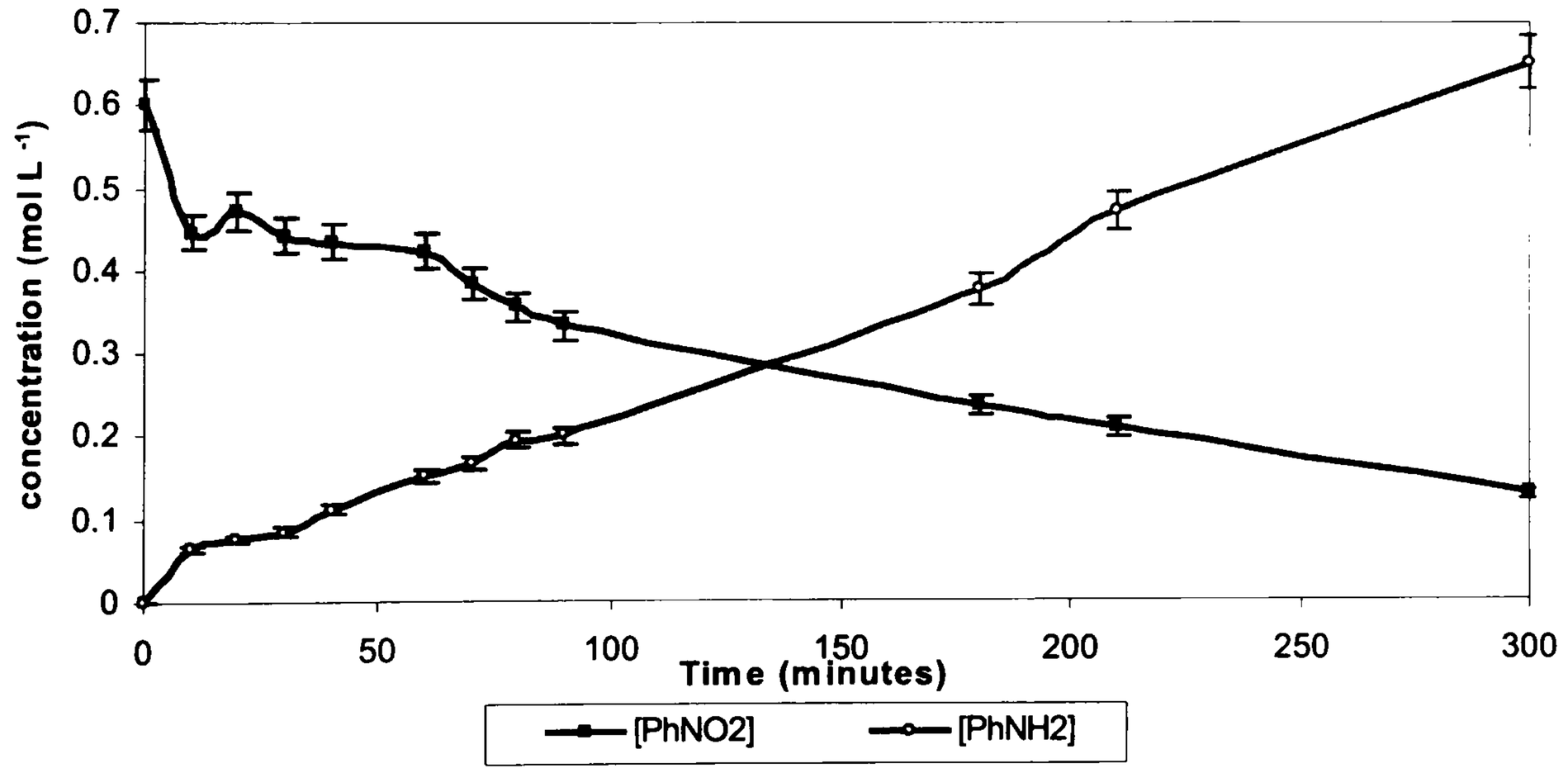

Figure 4.35a: Reaction Profile: the hydrogenation of nitrobenzene using catalyst Pd/CA1 in IPA – Run 1 of 3

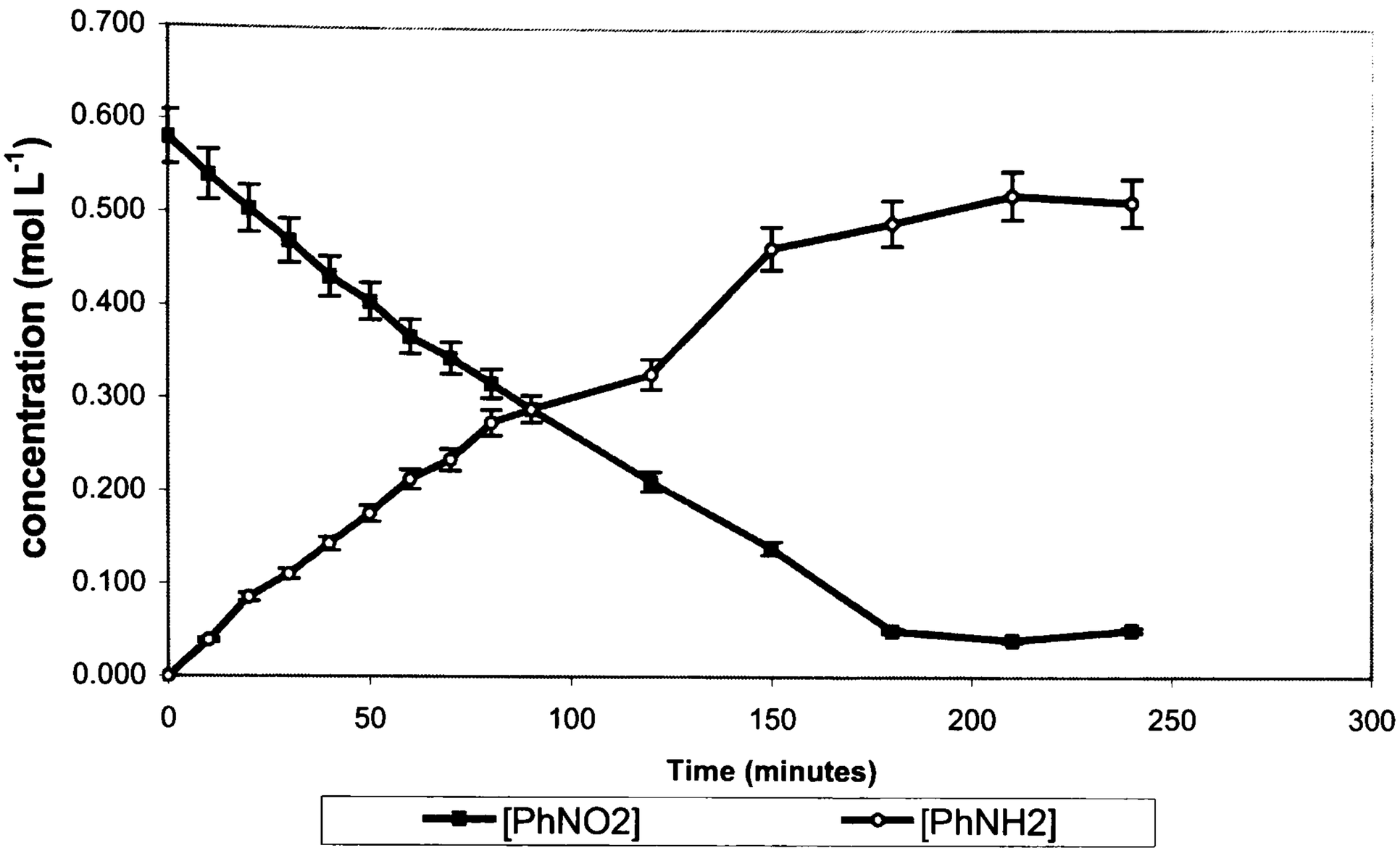

Figure 4.35b: Reaction Profile: the hydrogenation of nitrobenzene using recovered catalyst Pd/CA1 in IPA – Run 2 of 3

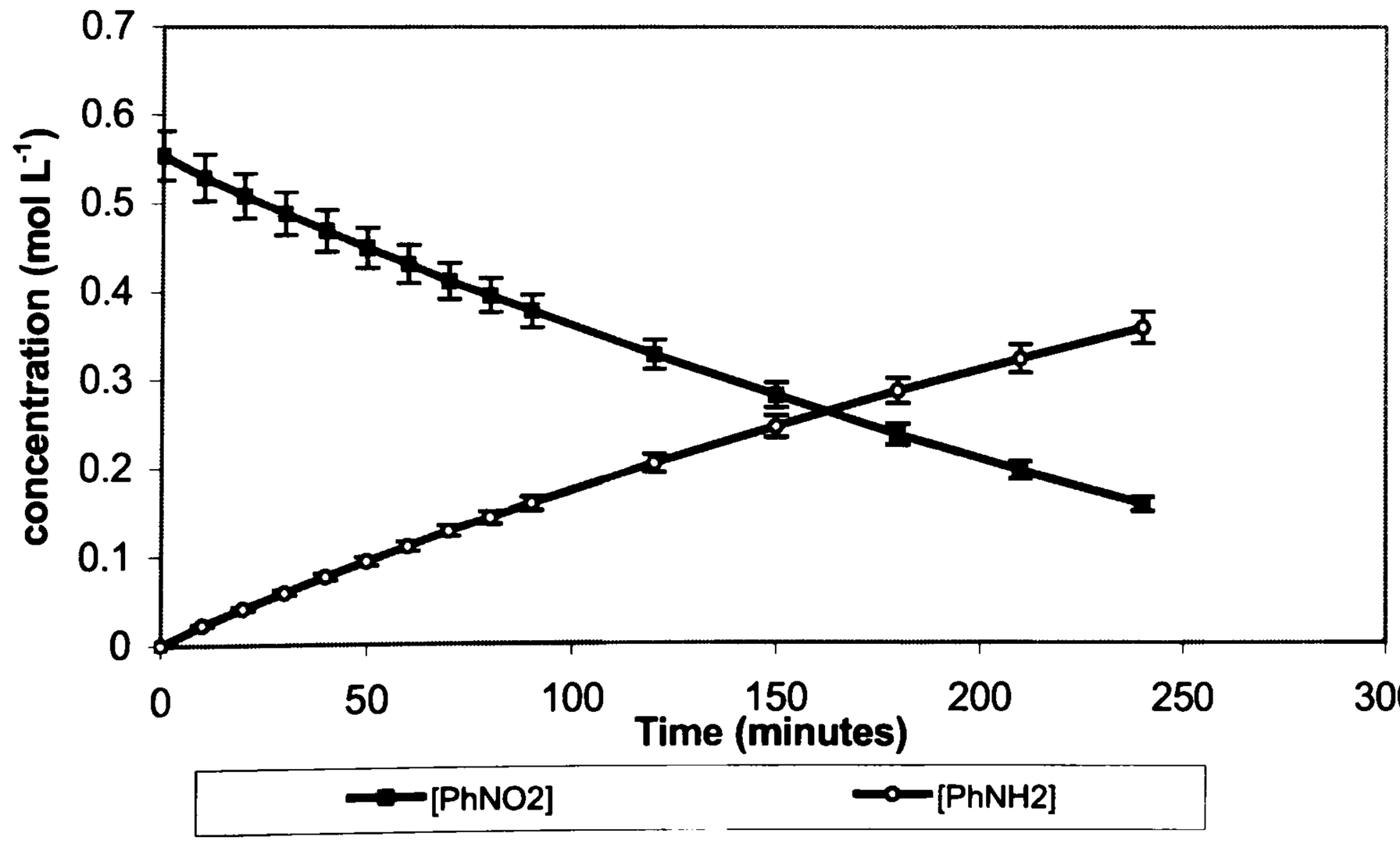

Figure 4.35c: Reaction Profile: the hydrogenation of nitrobenzene using recovered catalyst Pd/CA1 in methanol – Run 3 of 3

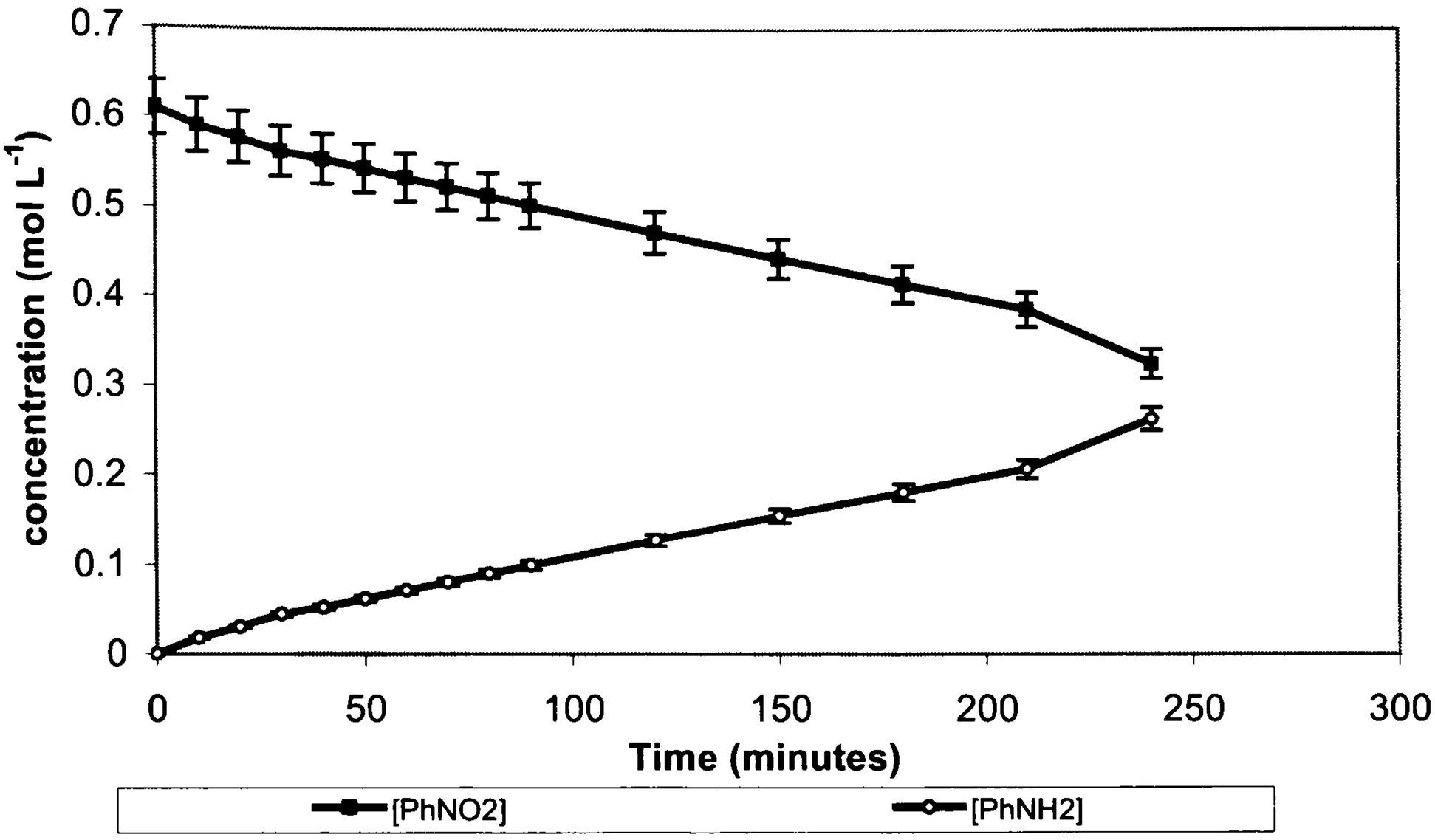

The hydrogen consumption data for the successive hydrogenation of nitrobenzene using recovered and washed catalyst Pd/CSXU in methanol and IPA are displayed in Figures 4.36 and 4.37. The GC reaction profiles are displayed in Figures 4.38 and 4.39.

Figure 4.36: Hydrogen consumption during the successive hydrogenation of nitrobenzene using recovered and washed catalyst Pd/CSXU in methanol

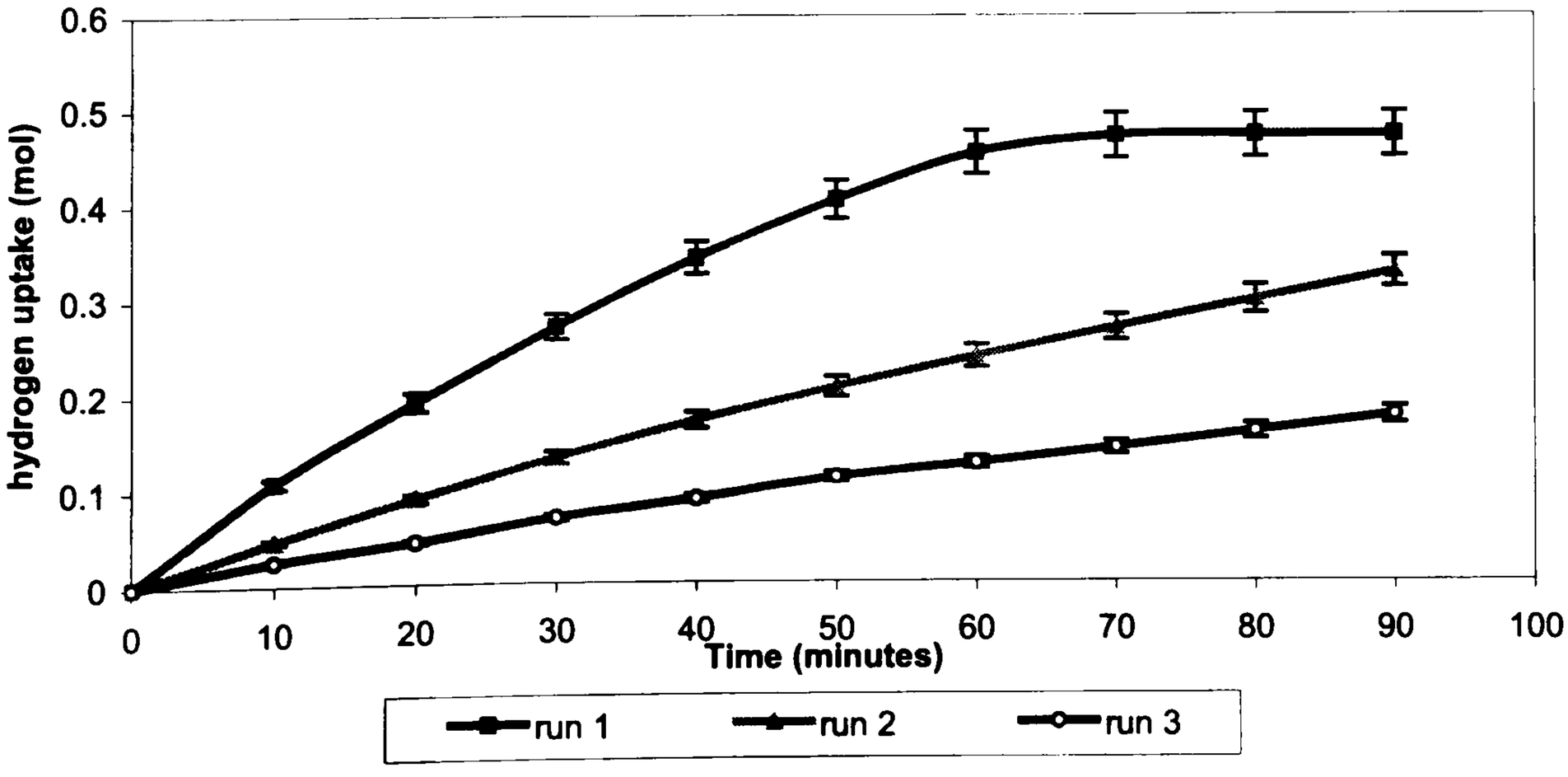

.

Figure 4.37: Hydrogen consumption during the successive hydrogenation of nitrobenzene using recovered and washed catalyst Pd/CSXU in IPA

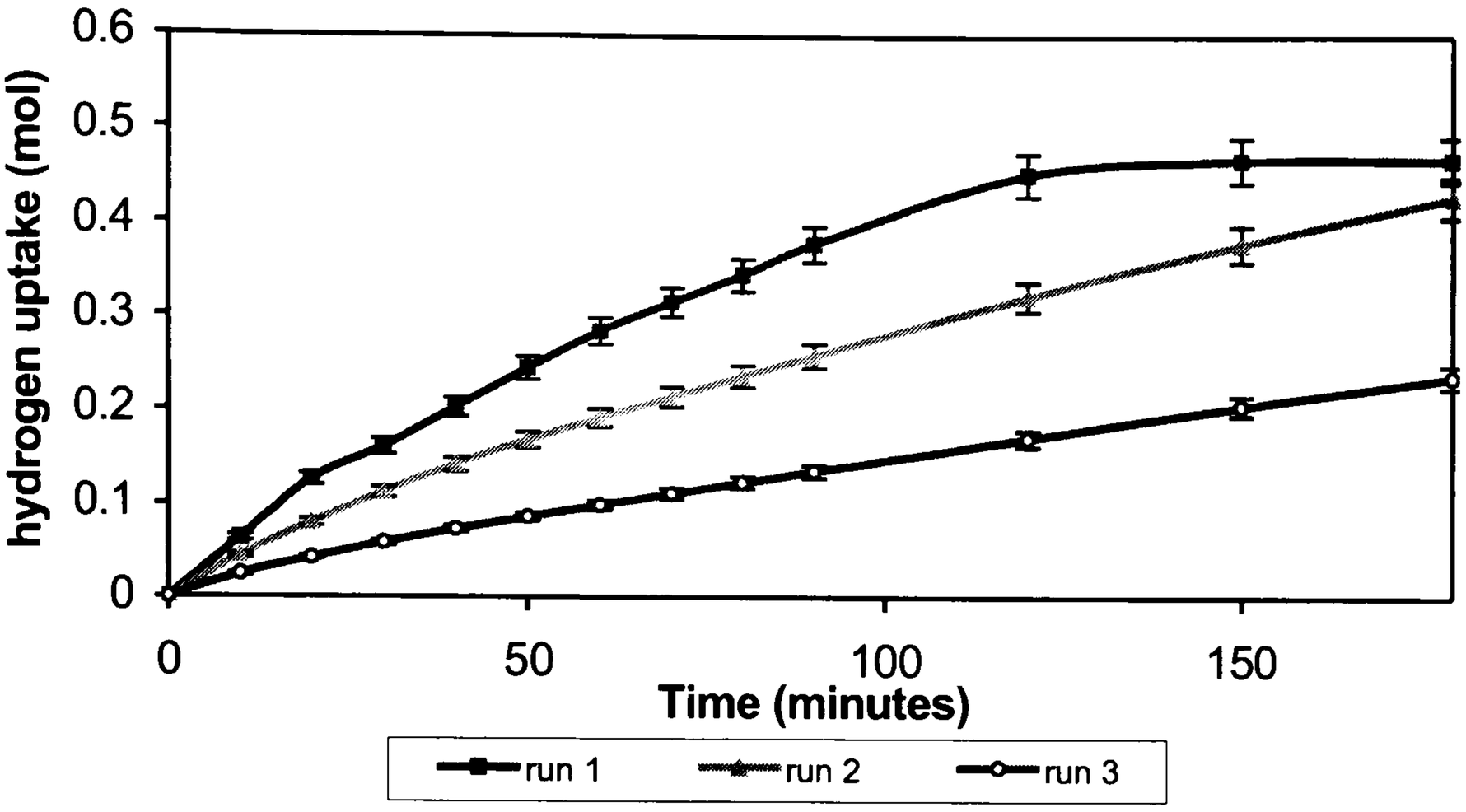

Figure 4.38a: Reaction profile: the hydrogenation of nitrobenzene using catalyst Pd/CSXU in methanol – Run 1 of 3

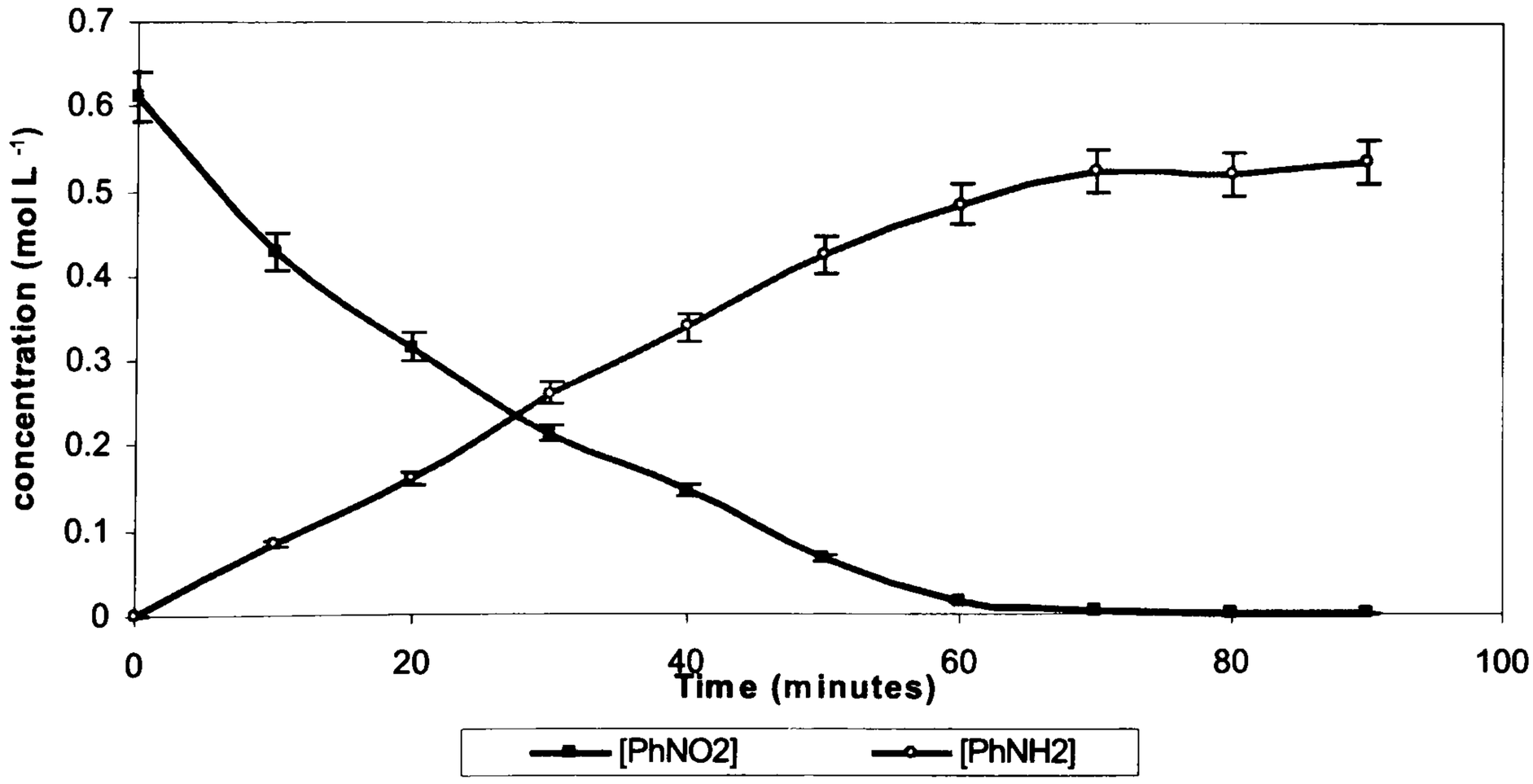

Figure 4.38b: Reaction Profile: the hydrogenation of nitrobenzene using recovered catalyst Pd/CSXU in methanol – Run 2 of 3.

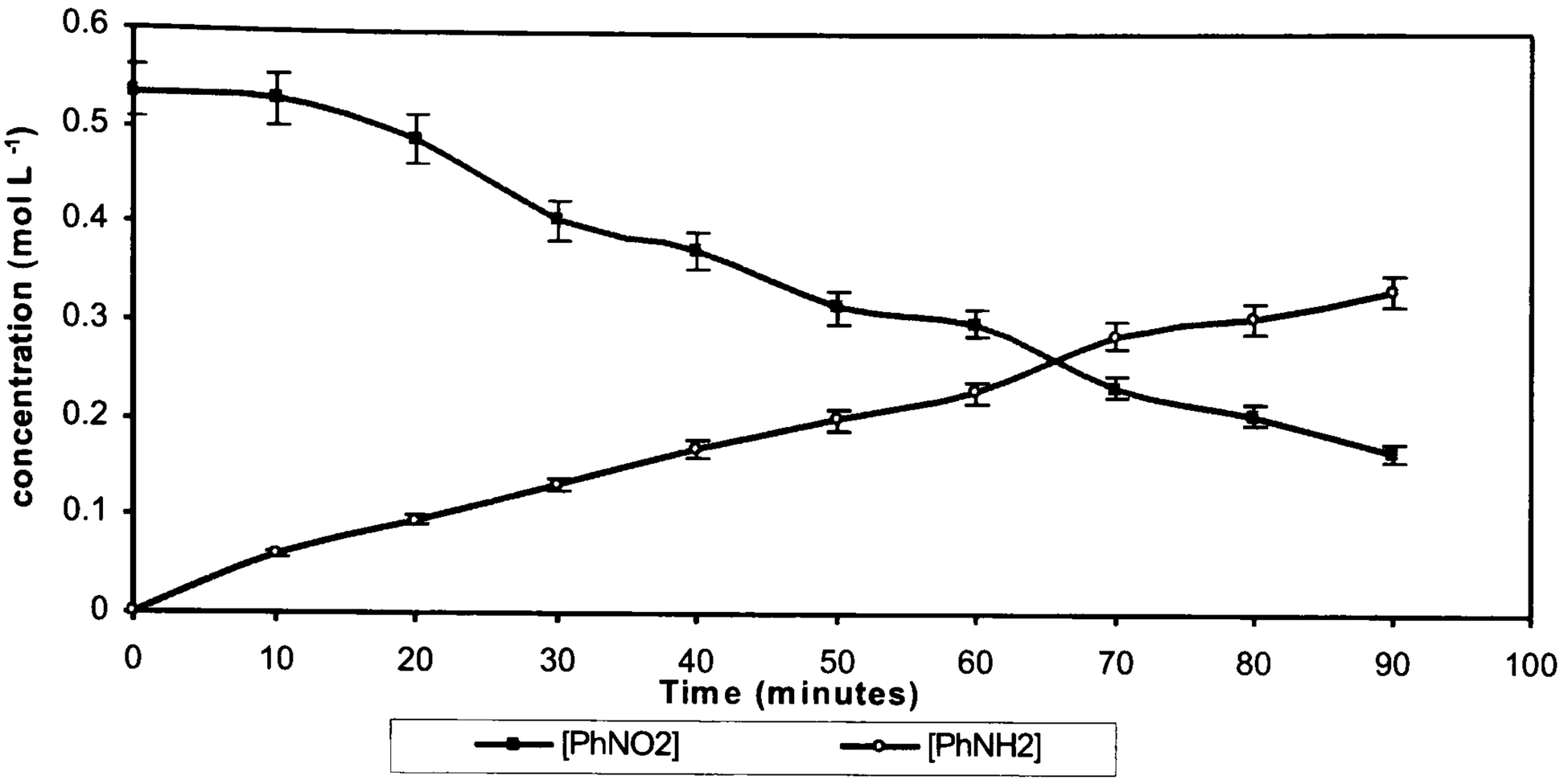

Figure 4.38c: Reaction profile: the hydrogenation of nitrobenzene using recovered catalyst Pd/CSXU in methanol – Run 3 of 3.

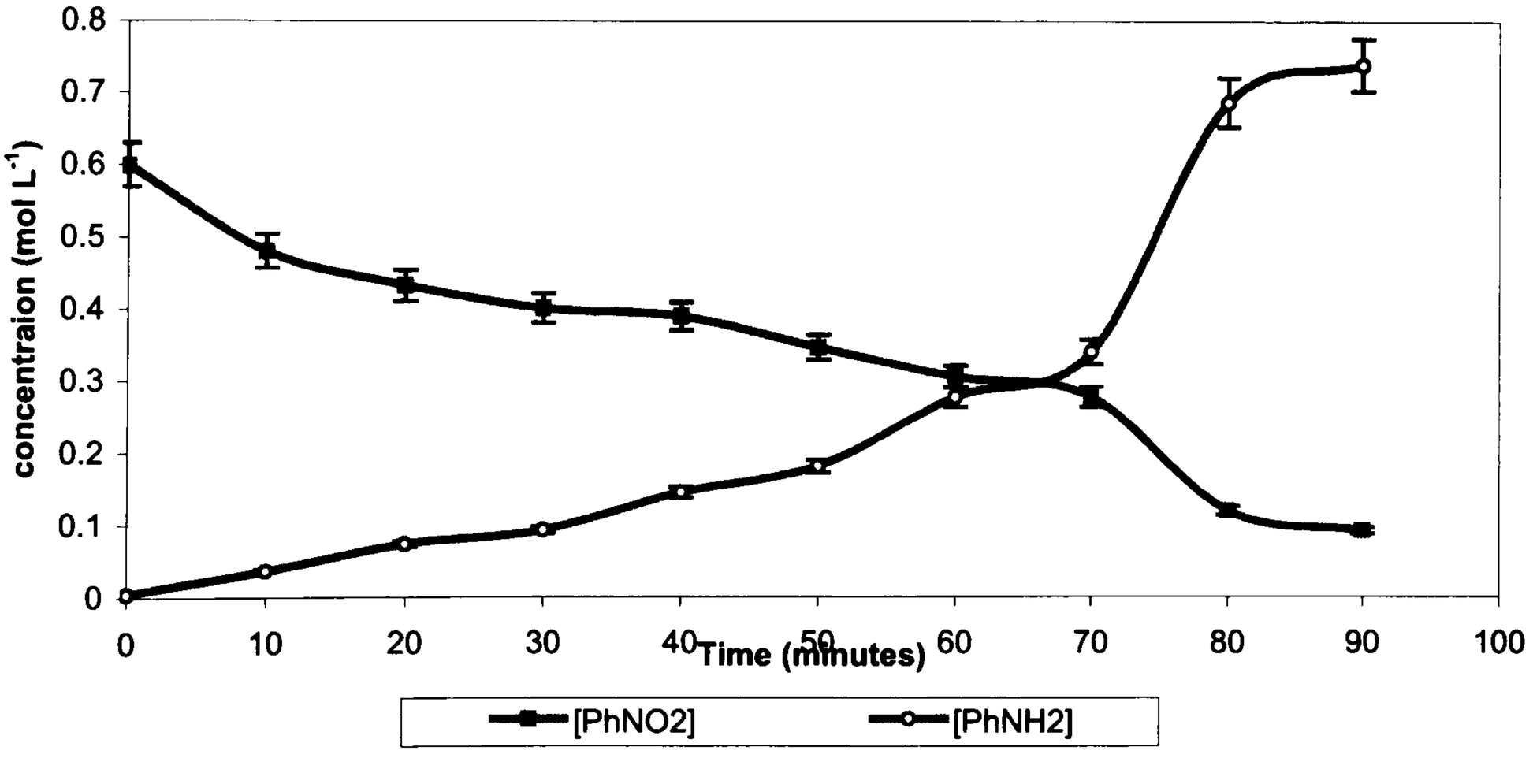

Figure 4.39a: Reaction Profile: the hydrogenation of nitrobenzene using catalyst Pd/CSXU in IPA – run 1 of 3

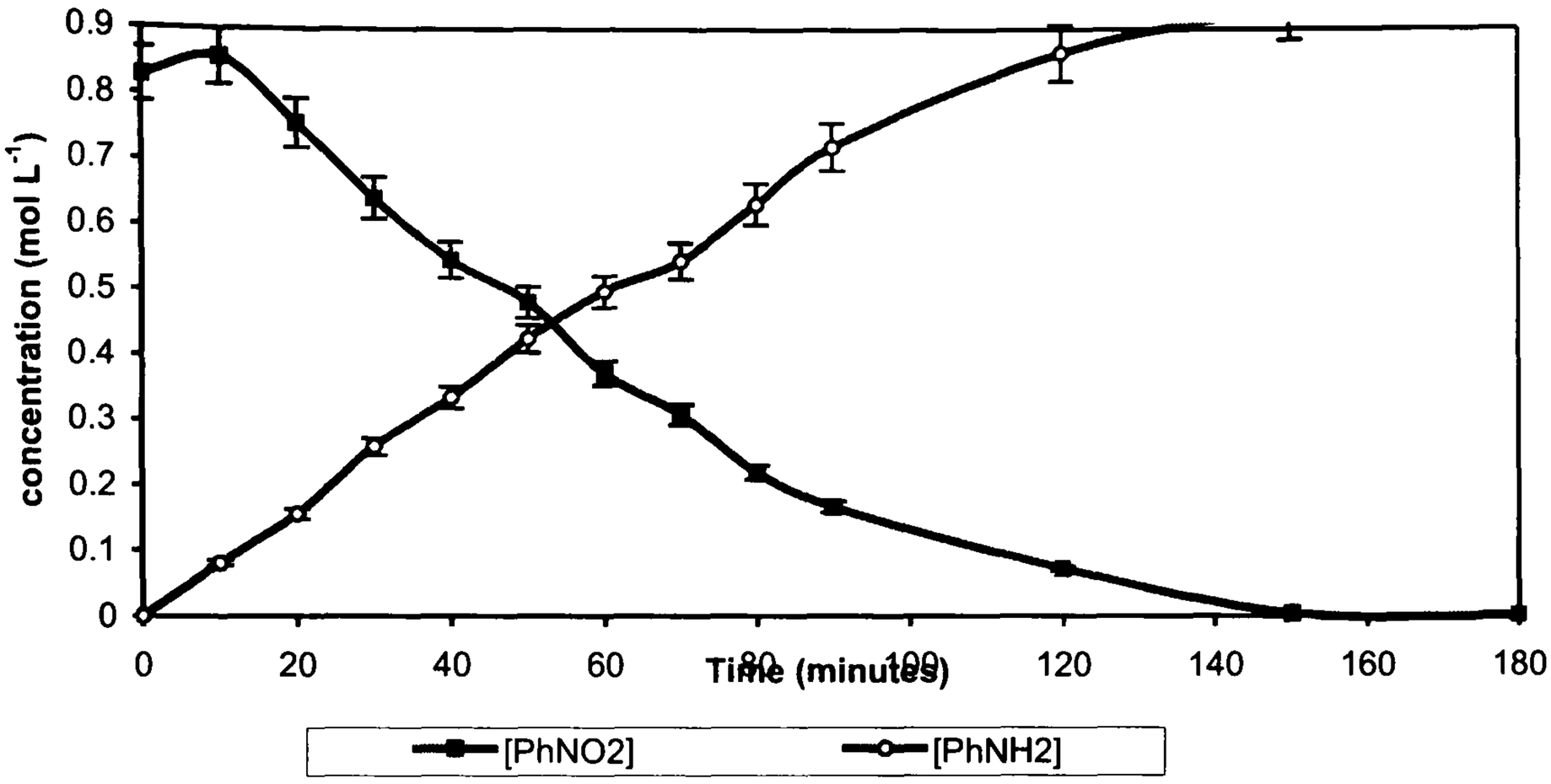

Figure 4.39b: Reaction Profile: the hydrogenation of nitrobenzene using recovered catalyst Pd/CSXU in IPA – run 2 of 3

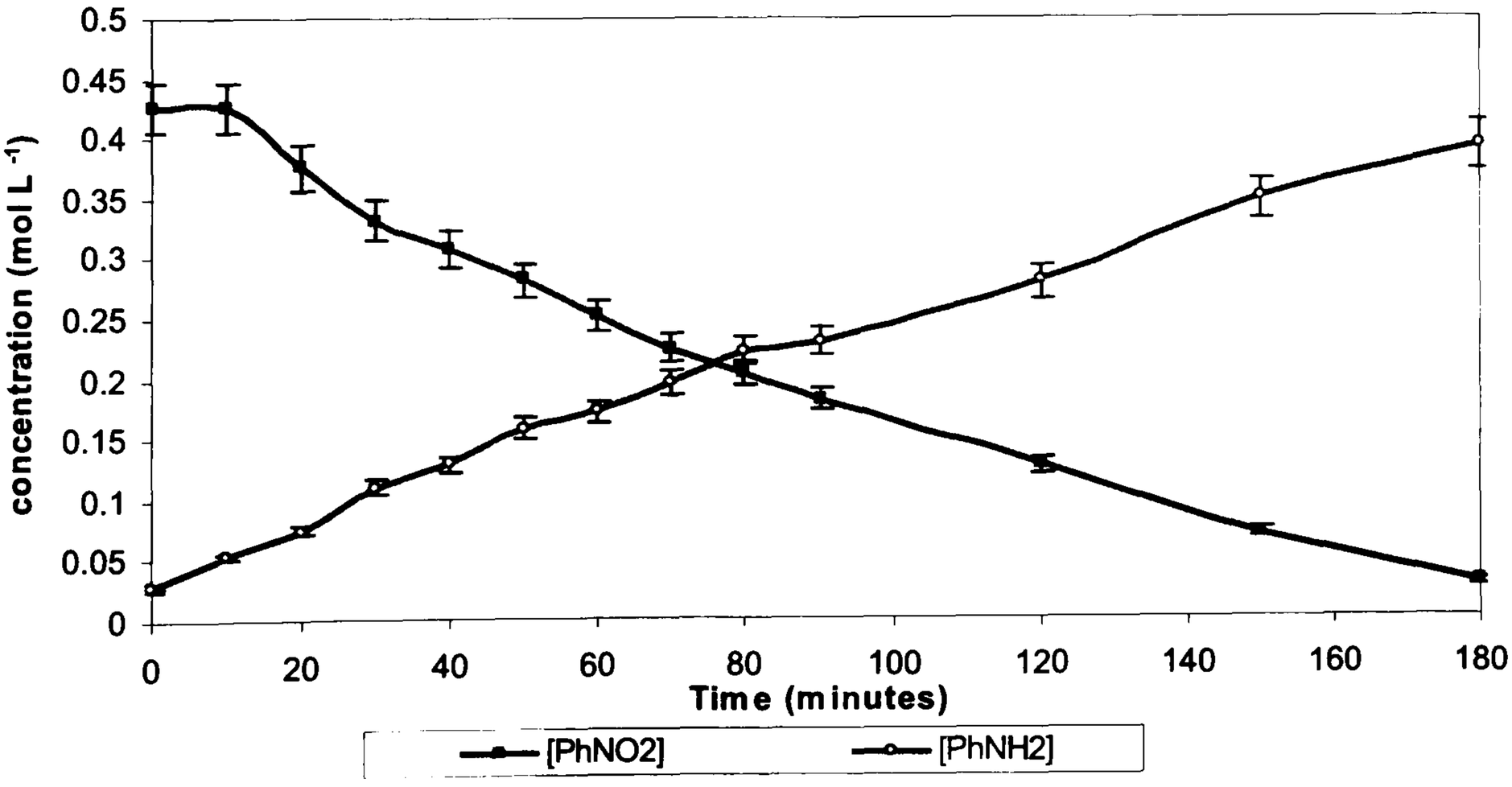

Figure 4.39c: Reaction Profile: the hydrogenation of nitrobenzene using recovered catalyst Pd/CSXU in IPA – run 3 of 3

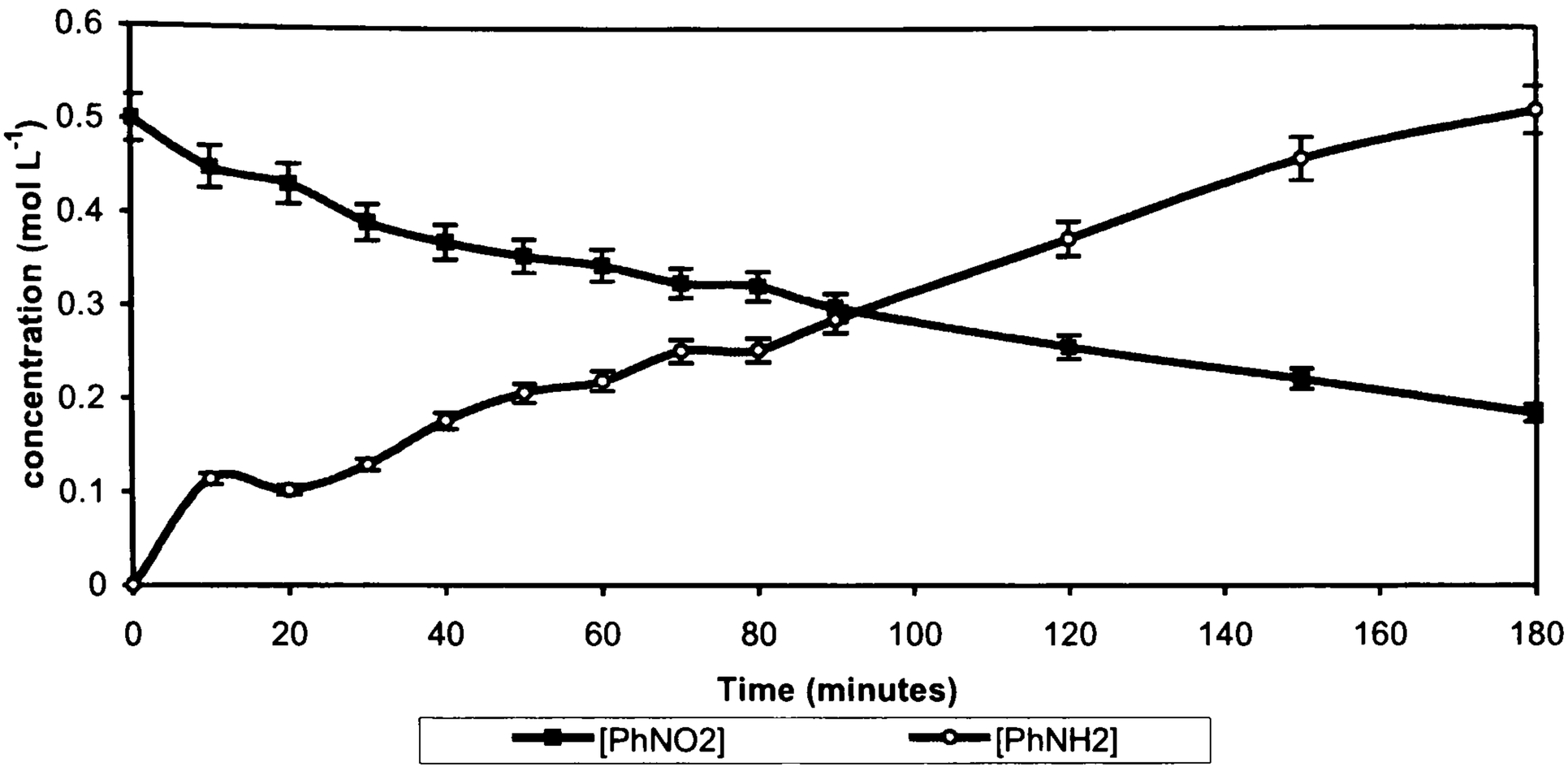

Significant deactivation was observed with repeated use of all three catalysts. A reduction in the number of moles of hydrogen gas consumed and a decrease in the reaction rate were observed with each successive run. In addition, the gas chromatographic analysis showed that the percentage of nitrobenzene converted to aniline decreased with each run. Figure 4.40 shows a comparison of the reaction rates for all three catalysts over the three runs in each of the solvents. Quantification of the amount of catalyst lost during the catalyst recovery and washing process indicated that less than 8 % of the catalyst was lost between each run. Assuming that the rate of reaction is proportional to the amount of catalyst, this small decrease in catalyst mass was insufficient to explain the relatively large drop in hydrogen consumption in each consecutive run.

Figure 4.40: Comparison of reaction rates using catalysts Pd/CN1, Pd/CA1 and Pd/CSXU during successive reactions in methanol and IPA

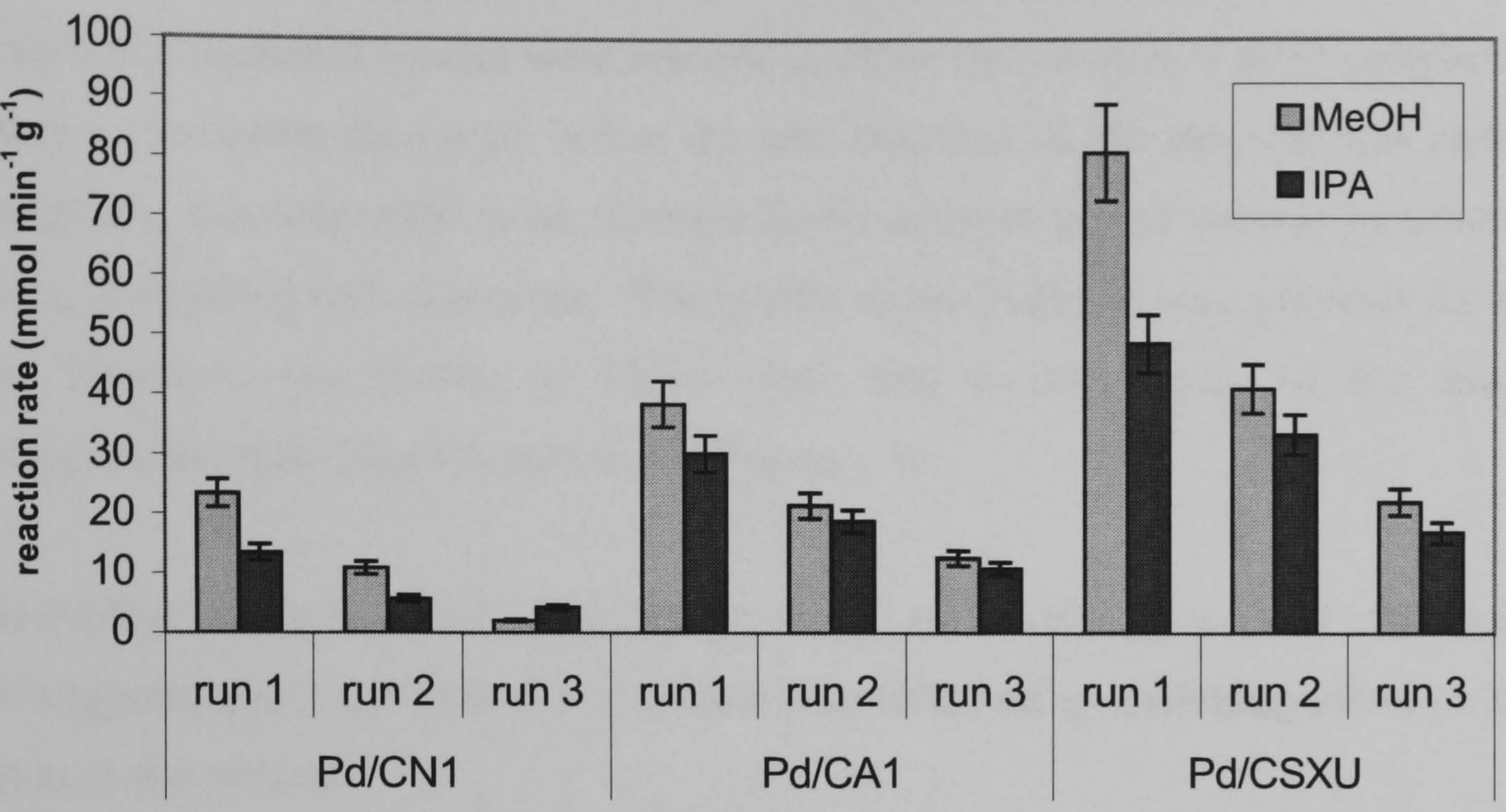

The percentage loss in catalytic activity between each successive run on the three catalysts was calculated and the values are displayed in Table 4.17. With the exception of the third runs with catalyst Pd/CN1 in methanol and IPA, all runs displayed a similar drop in activity, ranging from a loss of 31.4 % to 57.5 % in activity.

Table 4.17: Percentage loss in activity per successive catalytic run

	% of original activity					
	MeOH			**IPA**		
Catalyst	run 1	run 2	run 3	run 1	run 2	run 3
Pd/CN1	100	46.4	8.7	100	42.5	31.9
Pd/CA1	100	55.7	32.7	100	62.3	35.8
Pd/CSXU	100	50.9	27.4	100	68.6	34.9

4.3.1.4 Deactivation Experiments using Repeated Injections of Nitrobenzene.

Catalytic deactivation was also observed during the successive hydrogenations of nitrobenzene with catalyst Pd/CSXU left *in situ* in the reactor. The most active Pd/C catalyst and methanol solvent were selected to allow the reaction to go to completion within a reasonable time scale before the next injection of nitrobenzene was added. Effectively, this amounted to an increase in the level of aniline present in solution during the hydrogenation process. The results of the hydrogen consumption for the four injections are shown in Figure 4.41 and a comparison of the initial hydrogenation rates for each injection in Figure 4.42.

It is evident that as the levels of aniline increased, the reaction proceeded at a slower rate suggesting that the presence of aniline may have had an inhibiting effect on the action of the catalyst.

Figure 4.41: Hydrogen consumption during the successive injections of nitrobenzene using catalyst Pd/CSXU in methanol.

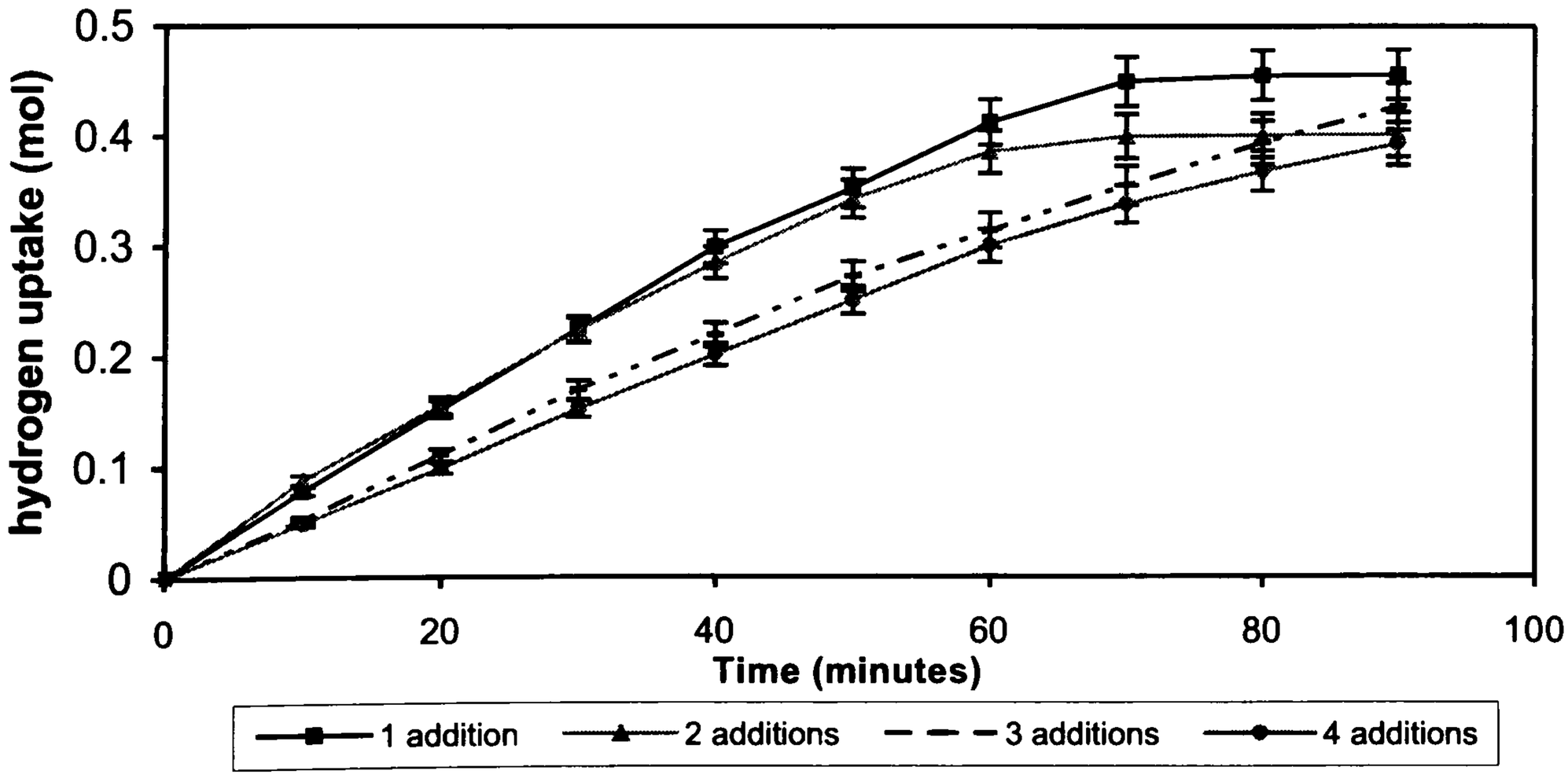

Figure 4.42: Comparison of initial reaction rates during the hydrogenation of nitrobenzene with Pd/CSXU in methanol over successive injections.

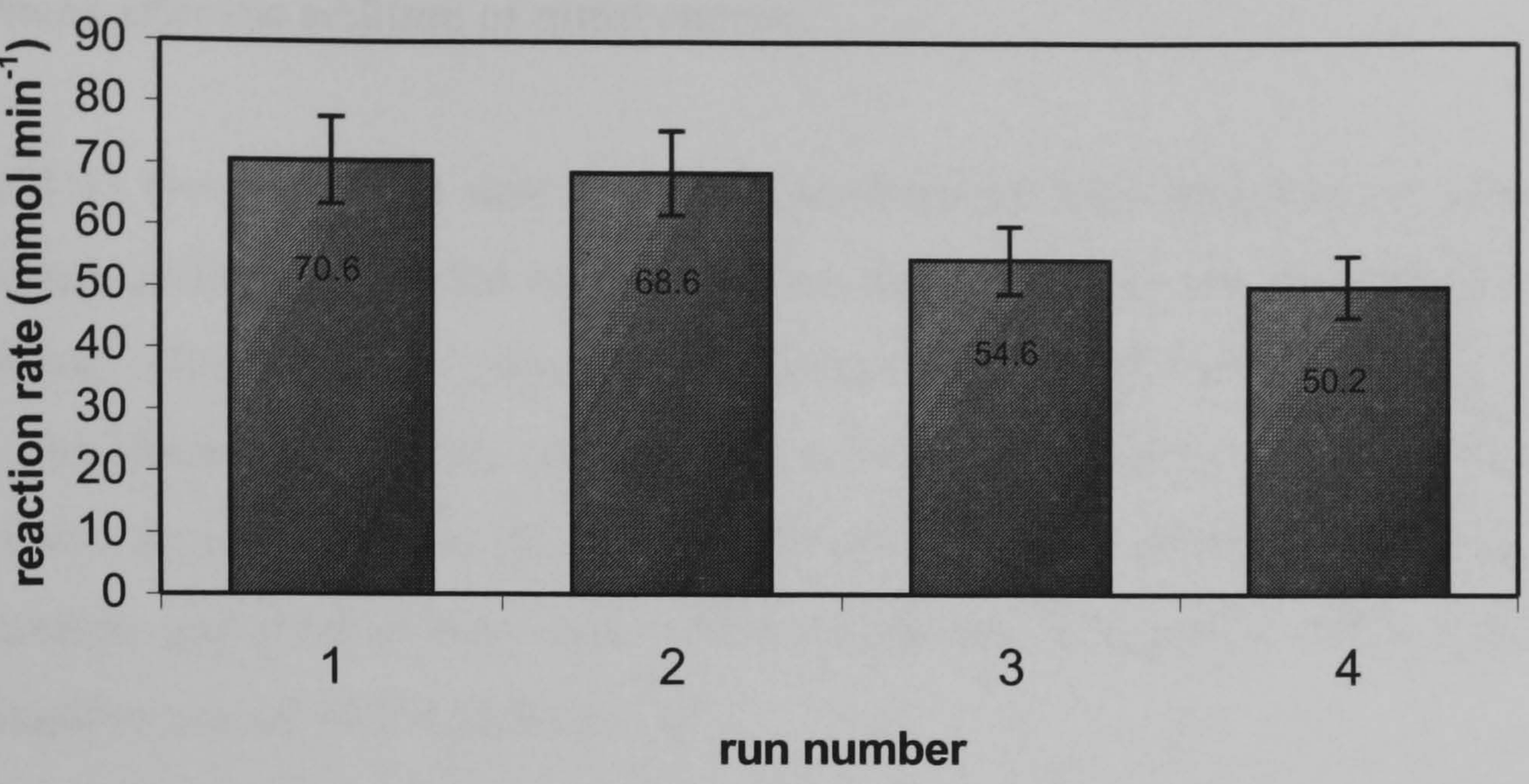

This system also appeared to undergo catalyst deactivation, although much more slowly than in the previous deactivation experiment. Smaller reductions in hydrogen consumption and reaction rate were visible with each run, which was possibly due to the removal of any error associated with catalyst loss during the isolation and washing procedures.

4.3.1.5 The Effect of the Reaction Products on the Hydrogenation of Nitrobenzene using Pd/CSXU Catalyst

Both products, aniline and water, were used to dope the nitrobenzene hydrogenation reaction mixture in a variety of experiments as described in the experimental (Section 3.3.2.6). The addition of either product to the reaction mixture resulted in a decrease in reaction rate. However, the effect was sensitive to the order the nitrobenzene and dopant were added.

4.3.1.5.1 The Effect of Aniline

The hydrogen uptake results for all reactions involving the addition of aniline are shown in Figure 4.43. The GC-traces for these reactions are shown in Figure 4.44

and 4.45. Figure 4.44 shows analyses from the experiment where aniline was added to the reaction vessel and mixed with the catalyst prior to the nitrobenzene being added whereas Figure 4.45 shows data from the experiment where the aniline was introduced after the addition of nitrobenzene.

Figure 4.43 revealed that a slowing of the nitrobenzene hydrogenation rate occurred only when aniline was added to the reaction mixture before the nitrobenzene was introduced. Hydrogen was consumed at a reduced rate of 60.9 mmol min^{-1} g^{-1} when aniline had been added first, compared to a rate of 70.6 mmol min^{-1} g^{-1} when no aniline was present. Adding the dopant after nitrobenzene addition and mixing with the catalysts appeared to have little effect on the rate of reaction with a hydrogen consumption rate of 67.9 mmol min^{-1} g^{-1}.

Figure 4.43: Hydrogen consumption during the hydrogenation of nitrobenzene with catalyst Pd/CSXU in methanol in the presence of aniline.

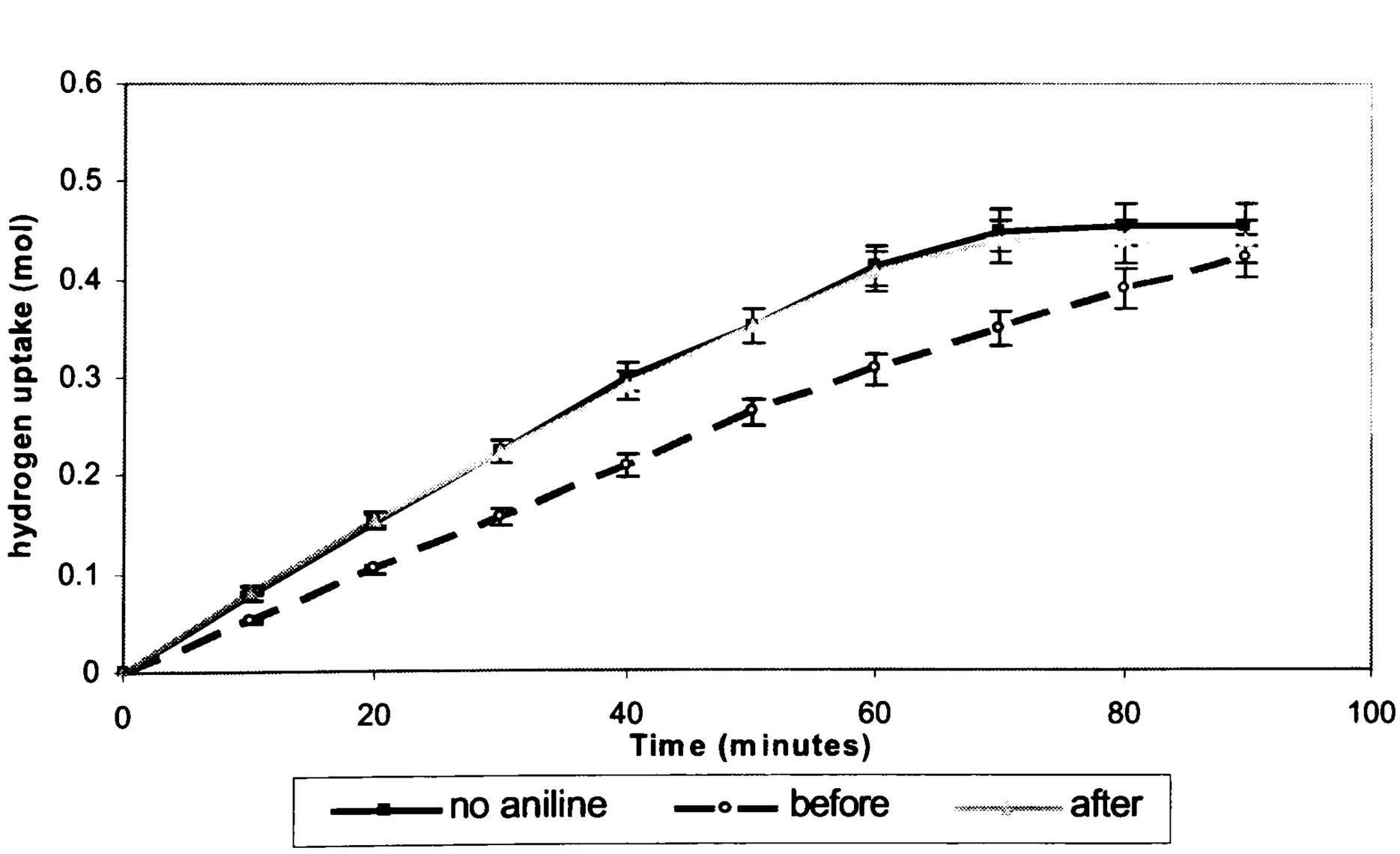

Figure 4.44: Reaction profile for the hydrogenation of nitrobenzene in methanol using catalyst Pd/CSXU with 1 mole equivalent of aniline added before nitrobenzene

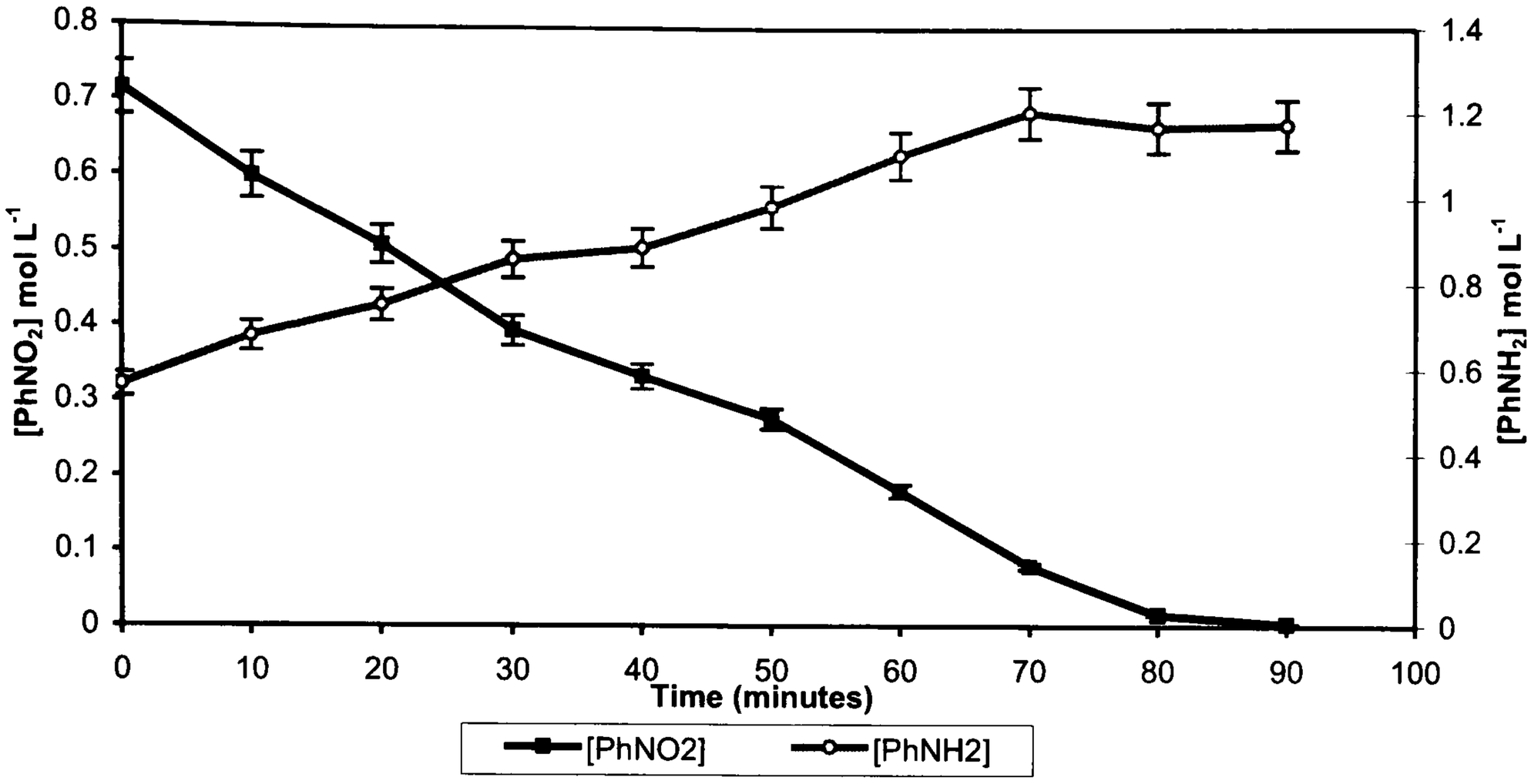

Figure 4.45: Reaction Profile for the hydrogenation of nitrobenzene in methanol using catalyst Pd/CSXU with 1 equivalent of aniline added after nitrobenzene.

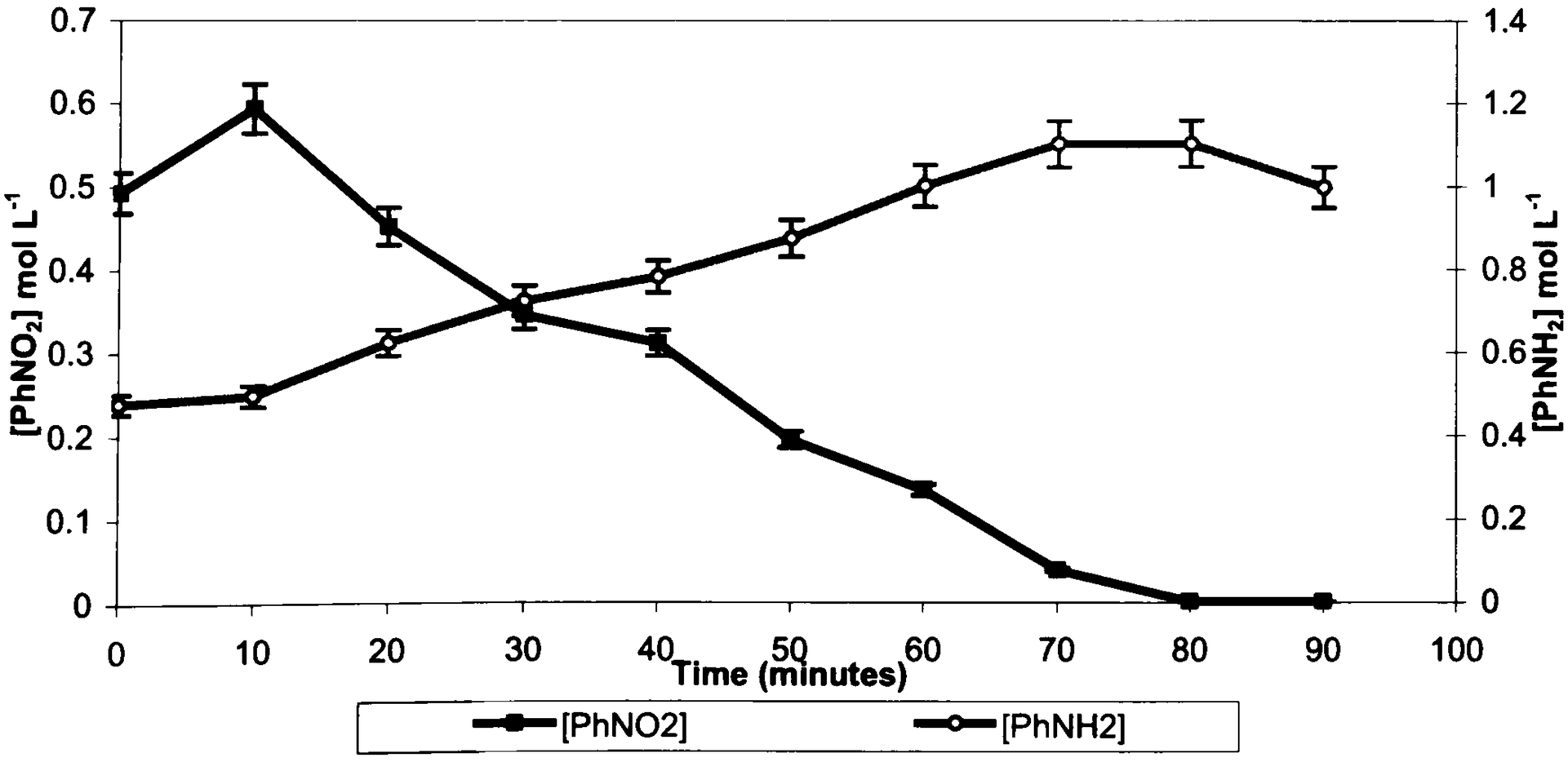

In both reactions only nitrobenzene and aniline and trace amounts of azobenzene were present in the reaction mixtures. No other species were detected by GC-MS indicating that the presence of aniline in the reaction mixture did not lead to the increased formation of dimeric by-products via reaction with transient intermediate species as suggested by Haber's mechanism. However, comparison of Figures 4.44 and 4.45 revealed a slightly slower rate of aniline production when aniline was added prior to the nitrobenzene that is consistent with the higher rate of hydrogenation observed during analysis of the hydrogen consumption data. Therefore, under these reaction conditions it can be concluded that pre-adsorption of aniline onto the catalyst surface leads to inhibition of the nitrobenzene reaction through a blocking of the catalytic sites required for the hydrogenation reaction.

4.3.1.5.2 The Effect of Water

The influence of the addition of water to the reaction mixture was investigated in an identical way to that used for aniline. The hydrogen uptake data for all experiments involving the addition of water are shown in Figure 4.46. The GC analysis for the reaction where water was added prior to nitrobenzene injection is shown in Figure 4.47 and the analysis for the reaction where the water was added after nitrobenzene had been injected in Figure 4.48.

Figure 4.46: Hydrogen consumption during the hydrogenation of nitrobenzene in methanol with catalyst Pd/CSXU and 2 mole equivalents of water.

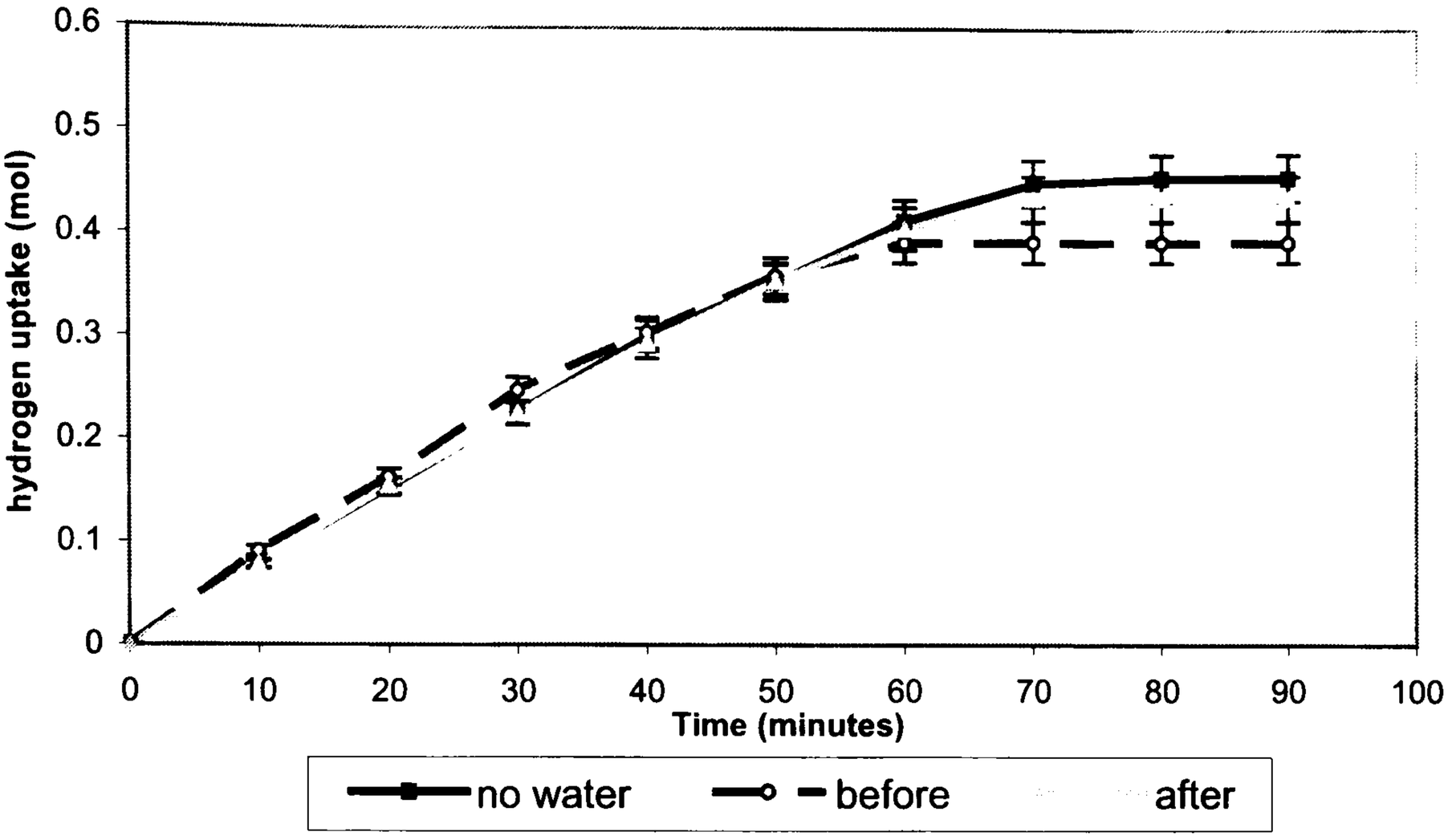

Figure 4.47: Reaction profile for the hydrogenation of nitrobenzene in methanol using catalyst Pd/CSXU and 2 equivalents of water added before nitrobenzene.

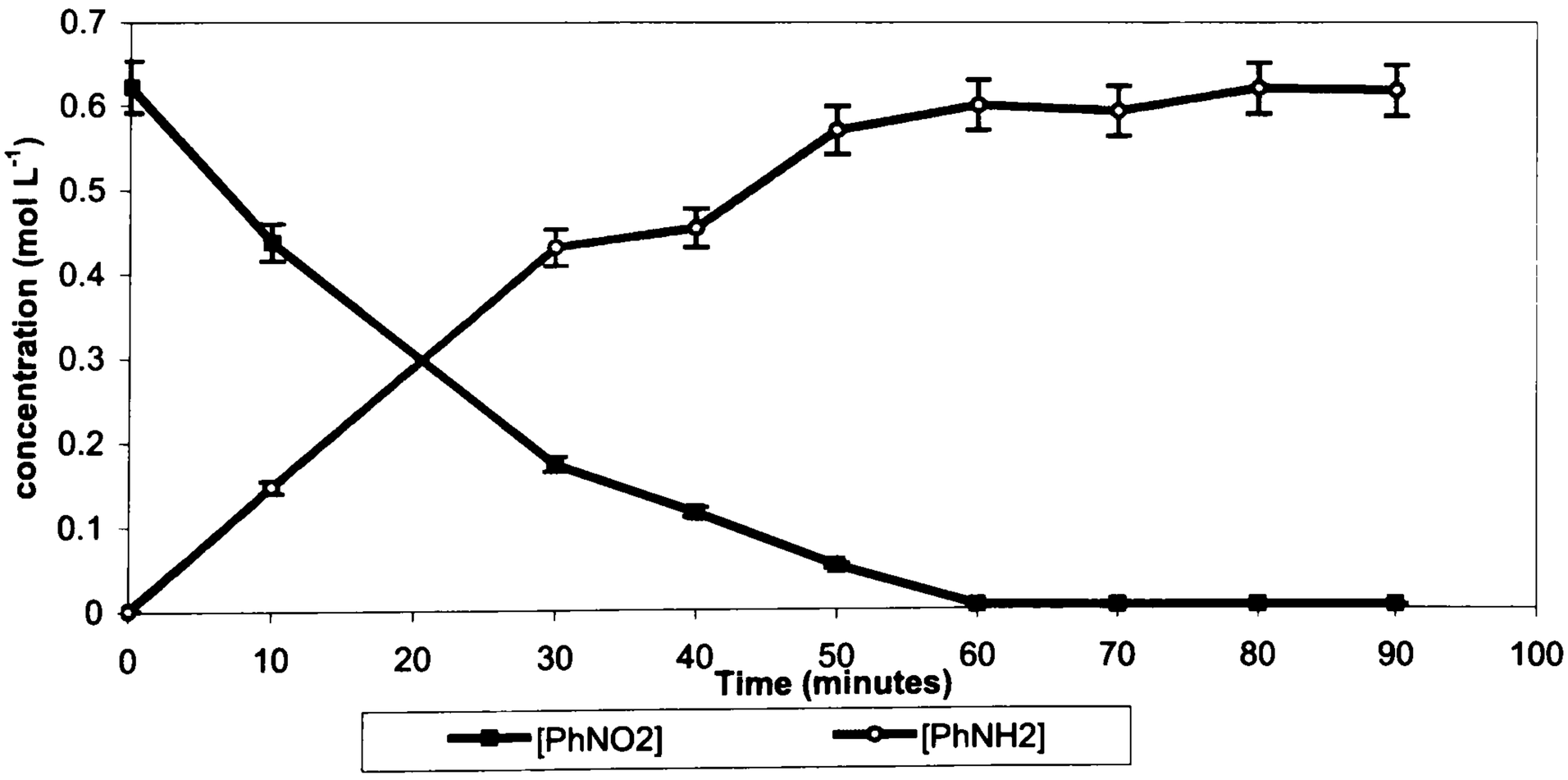

Figure 4.48: Reaction profile for the hydrogenation of nitrobenzene in methanol using catalyst Pd/CSXU with 2 equivalents of water added after nitrobenzene.

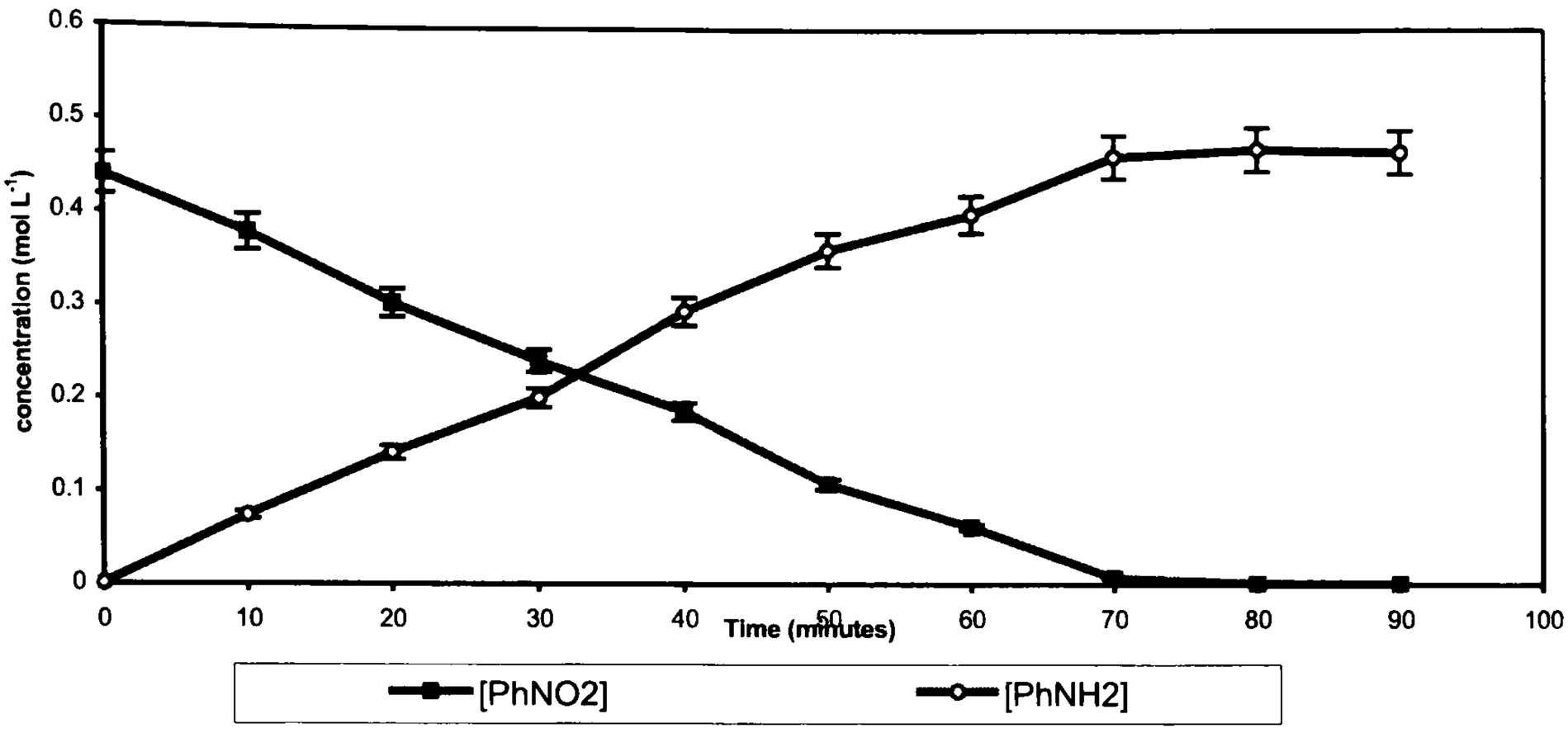

The addition of water to the nitrobenzene reaction mixture had no effect on the rate of hydrogenation. A rate of 70.6 mmol min^{-1} g^{-1} was obtained for a normal run and no significant effect was observed when water was added either before or after the nitrobenzene. The rate of hydrogen consumption was calculated to be 70.8 mmol min^{-1} g^{-1} when water was added first and to be 71.8 mmol min^{-1} g^{-1} when water was added second. Comparison of Figures 4.47 and 4.48 did not reveal any differences and no additional intermediates or by-products were observed throughout either experiment.

3.3.1.5.3 The Effect of the Co-addition of Aniline and Water

The effect of adding aniline and water simultaneously was investigated to determine whether any cumulative deactivation effect would be produced. One experiment was carried out where nitrobenzene, aniline and water were added at the same time. The hydrogen uptake data are displayed in Figure 4.49 and the GC reaction profile in Figure 4.50.

Figure 4.49: Hydrogen consumption for the hydrogenation of nitrobenzene in methanol with catalyst Pd/CSXU in the presence of 1 equivalent of aniline and 2 equivalents of water.

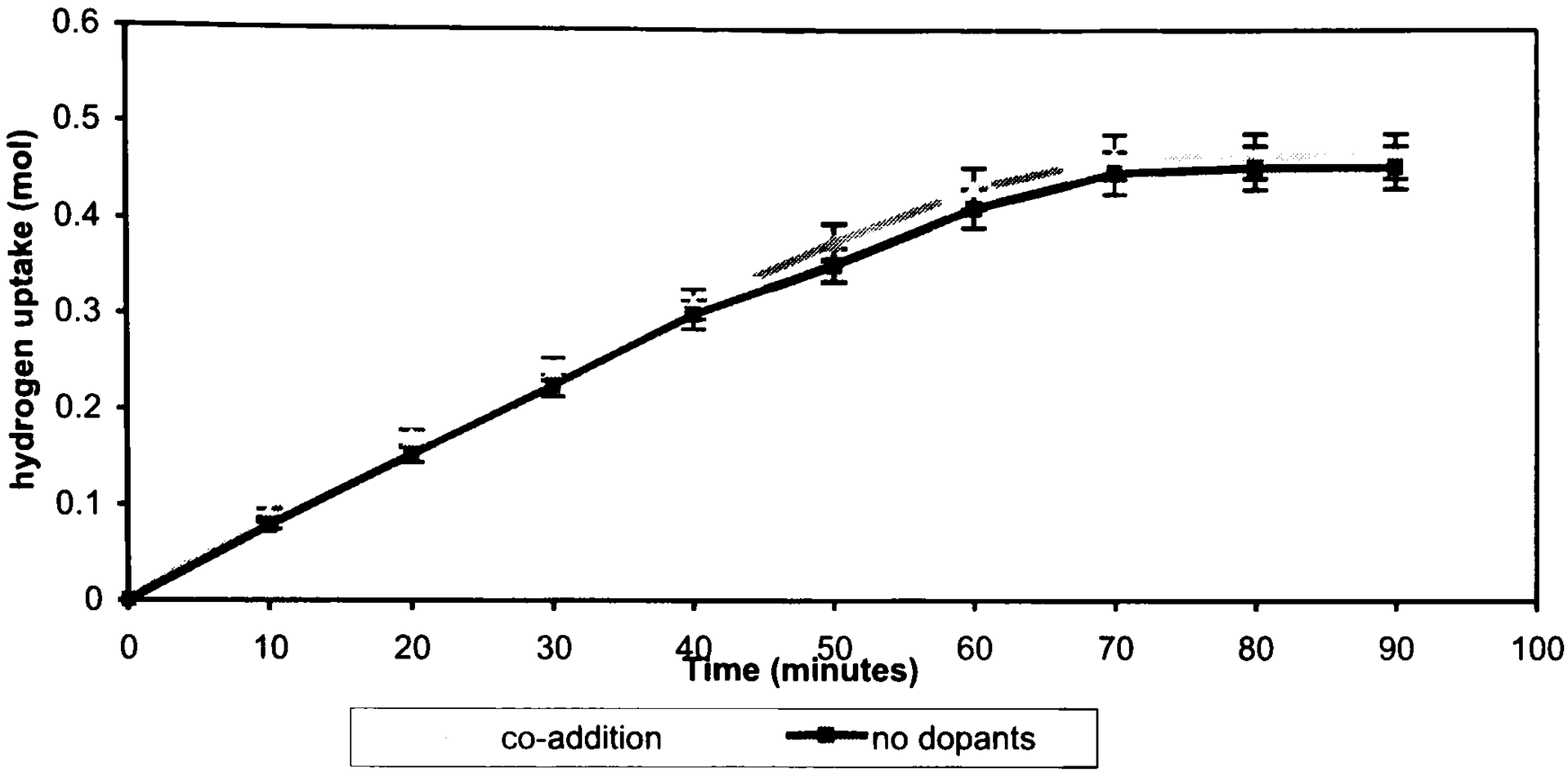

Figure 4.50: Reaction profile for the hydrogenation of nitrobenzene in methanol with catalyst Pd/CSXU in the presence of 1 equivalent of aniline and 2 equivalents of water.

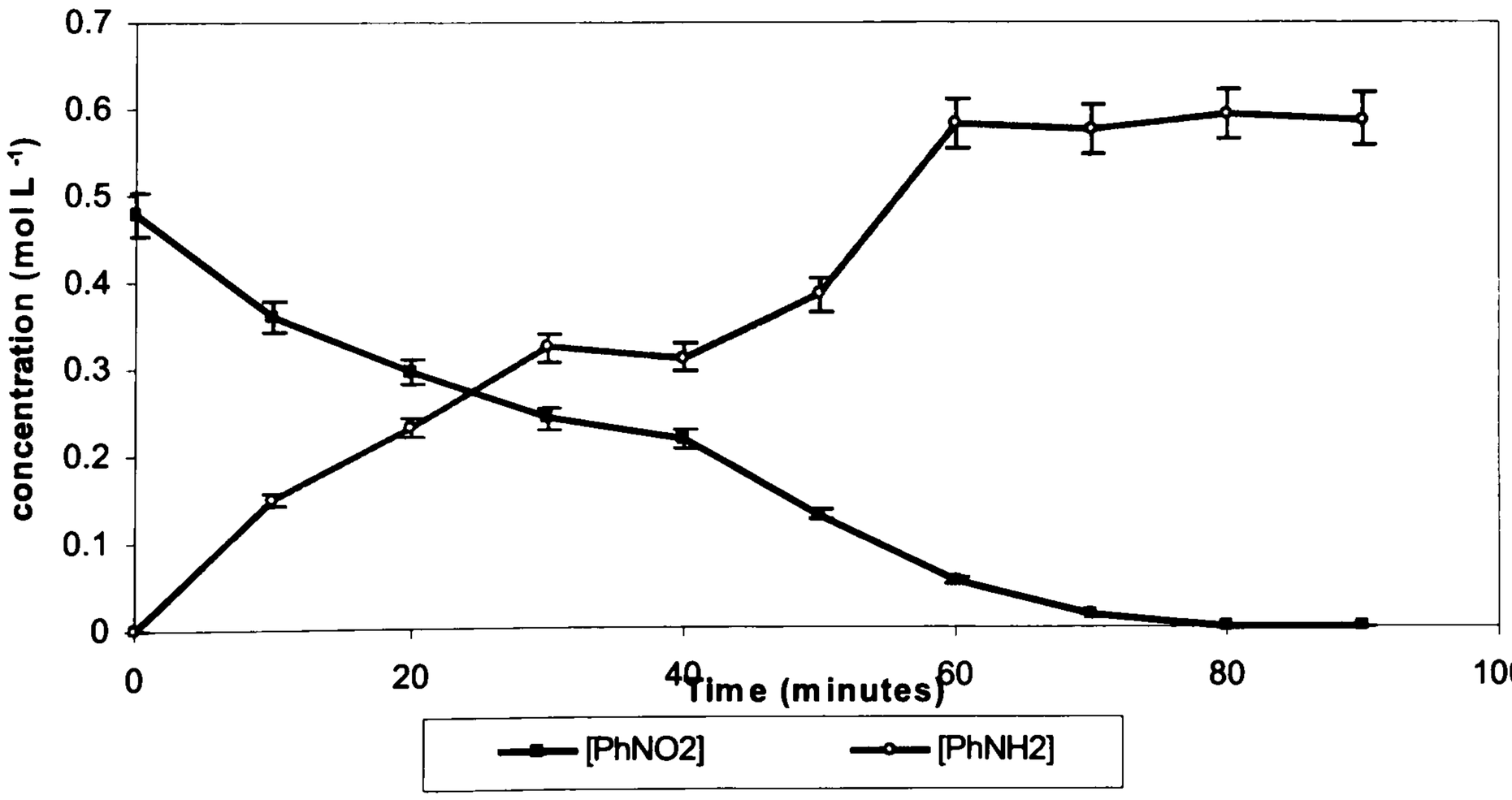

The co-addition of both aniline and water with nitrobenzene had no effect on the rate of hydrogenation as shown in Figure 4.49. Hydrogenation proceeded at a rate of 75.4 mmol min^{-1} g^{-1} compared with the reaction in the absence of any dopants at 70.6

mmol min^{-1} g^{-1}. Likewise no effect on the reaction profile (Figure 4.50) was observed with no additional intermediate species or by-products observed throughout the duration of the experiment. Under normal reaction conditions, simulated by this reaction, both aniline and water are produced simultaneously and compete with nitrobenzene for the adsorption sites on the catalyst. However, these products do not appear to have any detrimental effect on the hydrogenation reaction, so in effect we can deduce that the nitrobenzene reaction does not self-poison itself with the reaction products and that any deactivation observed must be due to an alternative source.

4.3.1.5.4 Summary of the Effect of the Products on the Hydrogenation of Nitrobenzene

The initial rate of hydrogenation was calculated from the hydrogen uptake data for each experiment involving the addition of aniline and water. These values are shown as a bar chart in Figure 4.51 and allow the effect of the products on the nitrobenzene hydrogenation reaction to be compared. With the addition of water no significant effect was observed, however when aniline was introduced before nitrobenzene was added a small inhibiting effect was observed. This may have been due to a competitive adsorption effect, where nitrobenzene was unable to displace all the aniline adsorbed on the required catalytic sites on the catalyst. With water, the small inhibiting effect was most likely due to competitive adsorption of water onto the catalyst surface sites required for hydrogen adsorption and dissociation or from partial re-oxidisation of the catalyst surface. No cumulative deactivation effect was observed when aniline and water were added together. In addition, adding the dopants at the same time to or after nitrobenzene addition had no effect on the catalysis, confirming that under reaction conditions the products of hydrogenation were not acting as inhibitors to the forward process and were not directly responsible for deactivation of the catalysts.

Figure 4.51: Comparison of initial reaction rates of the hydrogenation of nitrobenzene in methanol with catalyst Pd/CSXU in the presence of aniline and water dopants.

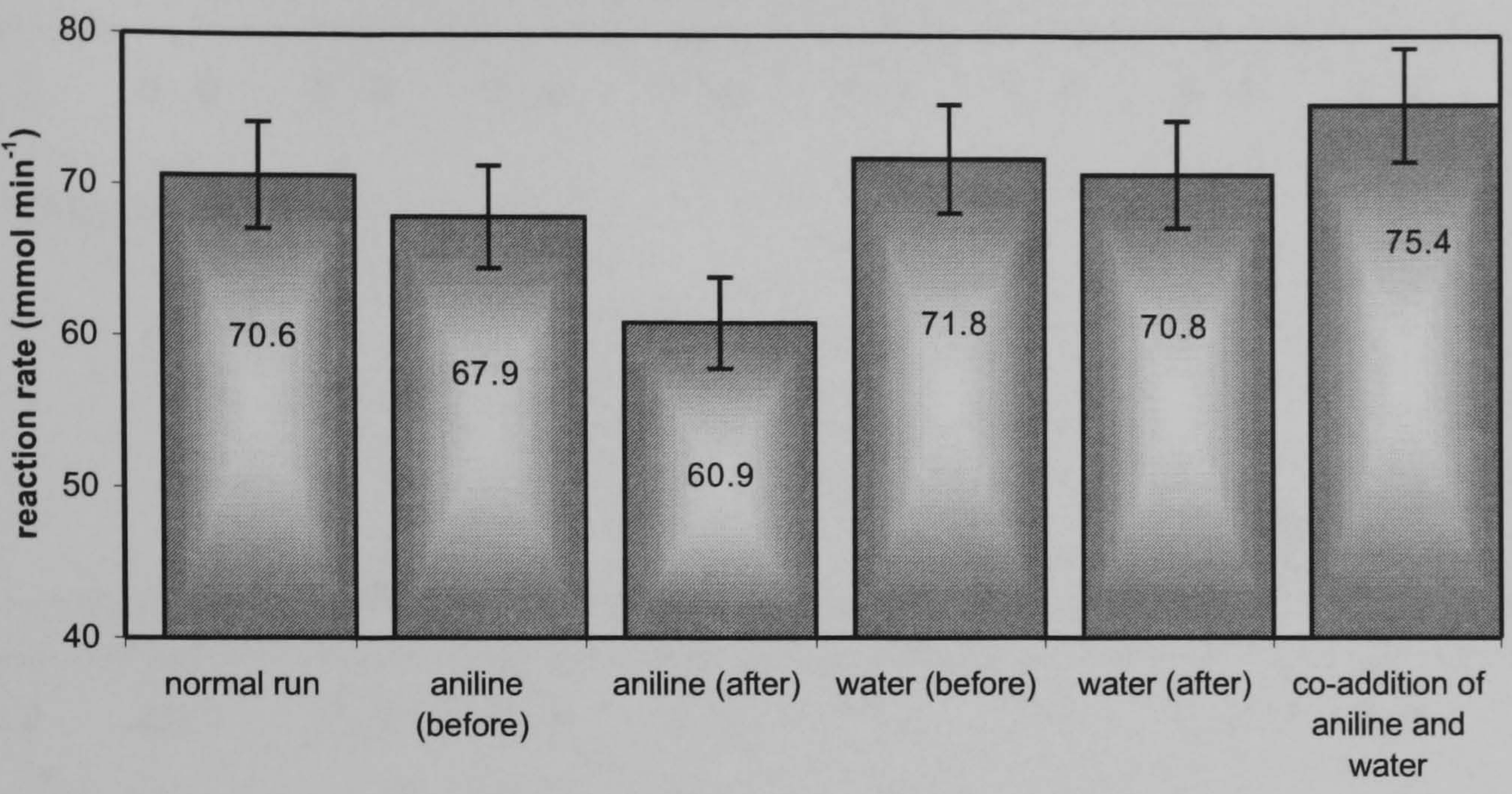

4.3.1.6 Hydrogenation of d_5-Nitrobenzene

The hydrogenation of d_5-nitrobenzene was carried out following exactly the same procedure as previous experiments. Details of the analysis are described in Section 3.3.2.7 of the experimental.

Samples were removed at time intervals for ^{1}H NMR analysis and the results compared with those obtained from reaction with fully protonated nitrobenzene. The NMR spectra obtained from the nitrobenzene hydrogenation reaction are displayed in Figure 4.52. During the hydrogenation of nitrobenzene, the initial signals visible in the ^{1}H NMR spectrum of the time zero sample corresponded to the five aromatic nitrobenzene protons. Three signals were present: a triplet around 7.6 ppm, another triplet around 7.8 ppm and a doublet at 8.2 ppm. These peaks have been assigned according to the estimated shifts calculated from a chemical shift data table [176] along with the splitting patterns and illustrated in Figure 4.53. These peaks gradually reduced in intensity over time until they disappeared from the spectrum completely.

Figure 4.52: ^{1}H NMR spectra from the hydrogenation of fully protonated nitrobenzene

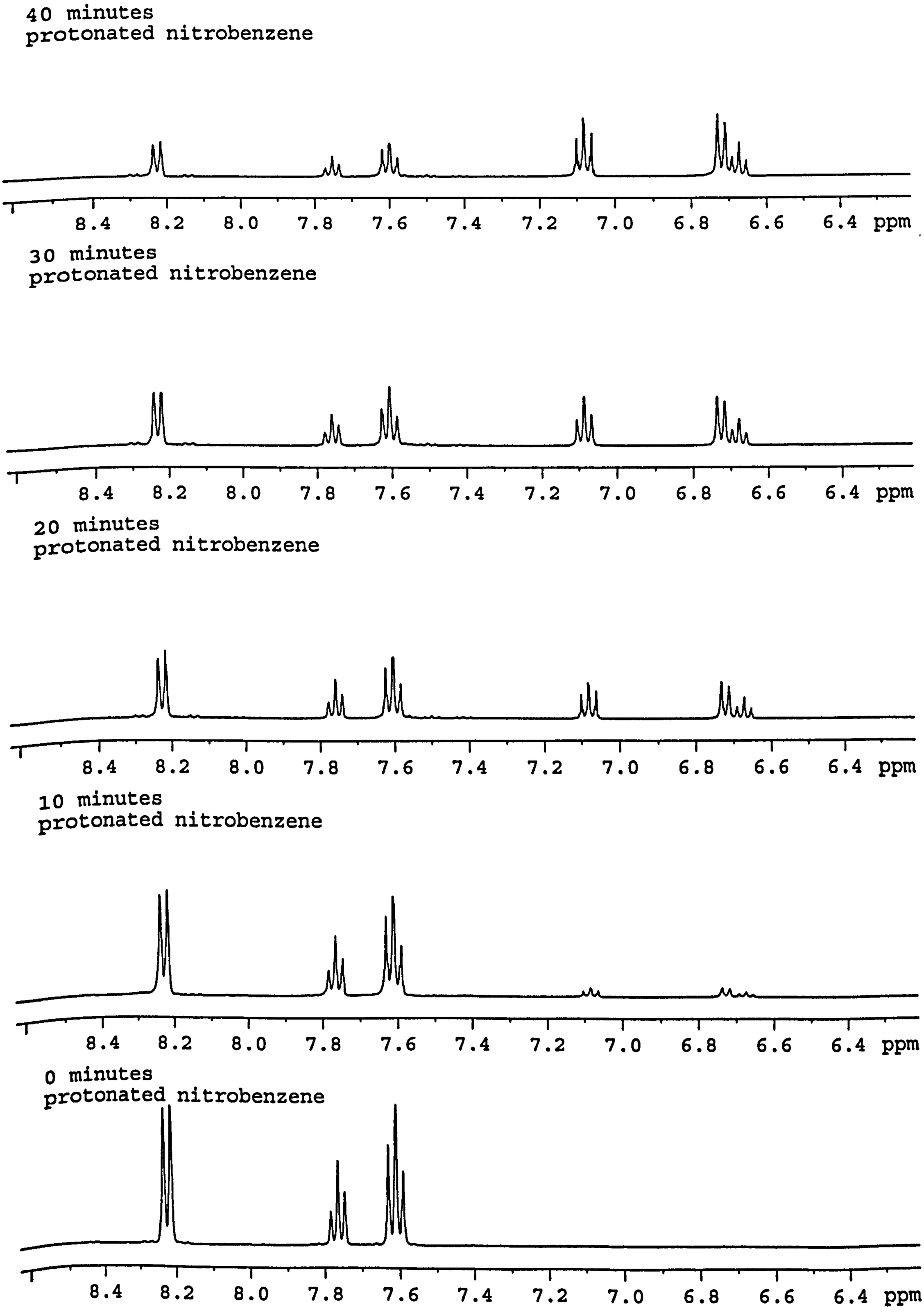

90 minutes
protonated nitrobenzene

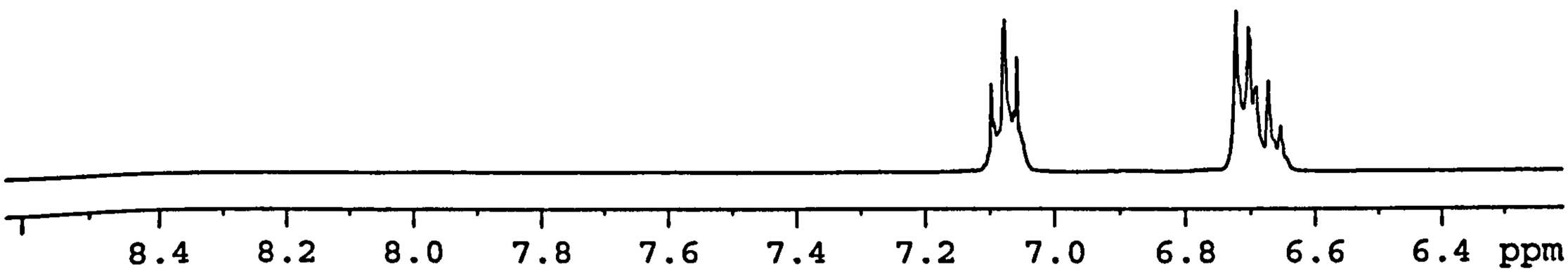

80 minutes
protonated nitrobenzene

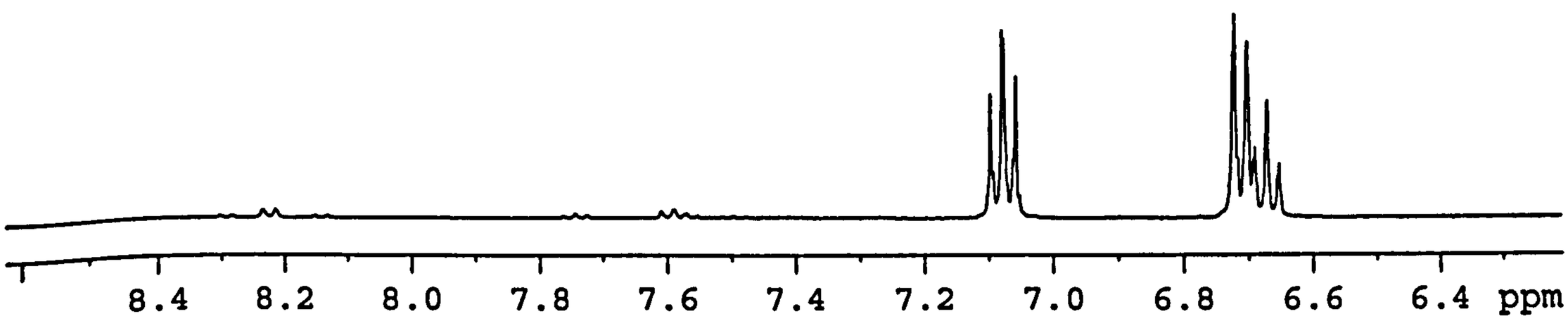

70 minutes
protonated nitrobenzene

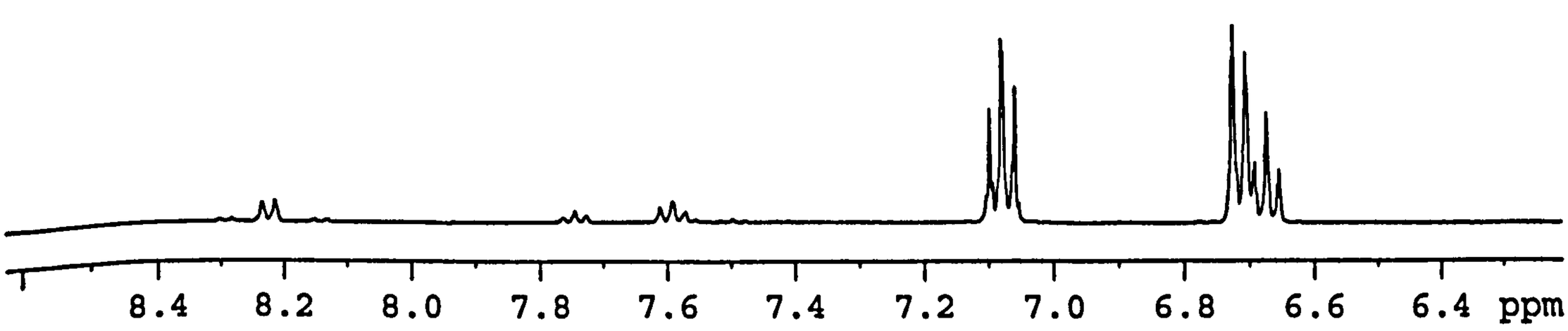

60 minutes
protonated nitrobenzene

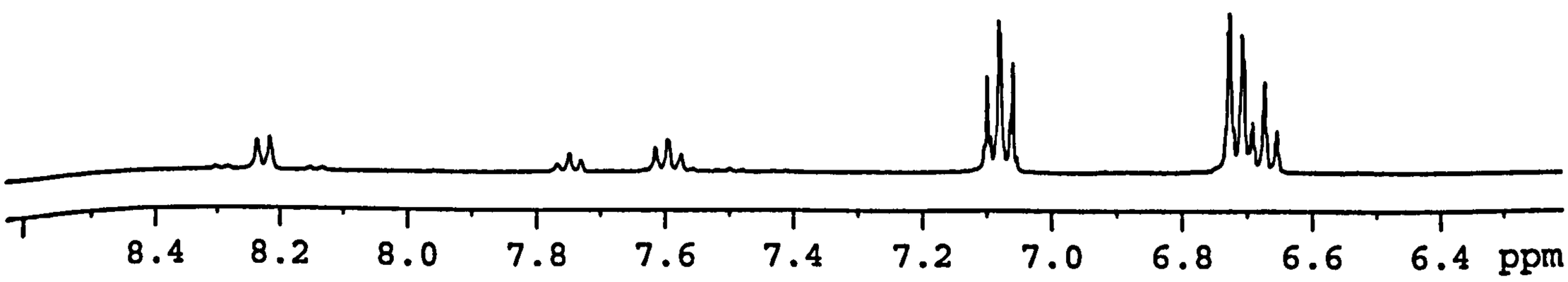

50 minutes
protonated nitrobenzene

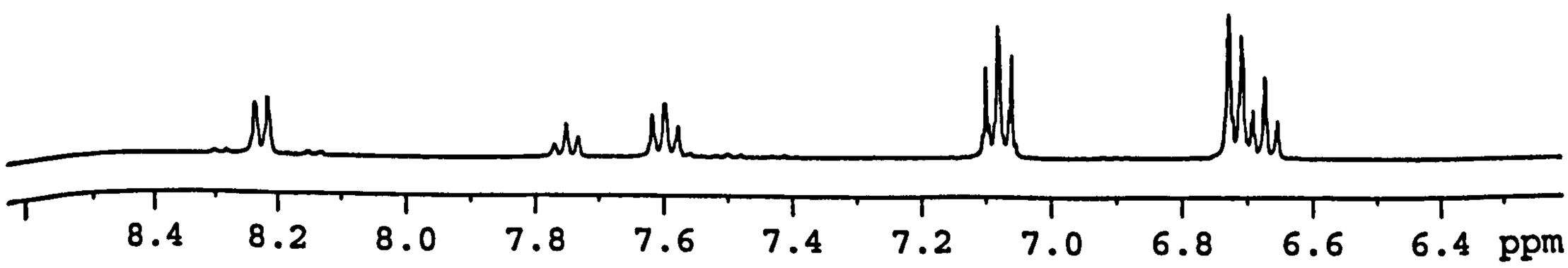

Simultaneously, the signals arising from the five aromatic protons on aniline; a muliplet at 6.7 ppm and a triplet at 7.1 ppm (also shown in Figure 4.53) gradually emerged from 10 minutes onwards and grew in size until the end of the reaction. No other signals are observed throughout the reaction confirming that detectable levels of other by-products were not forming.

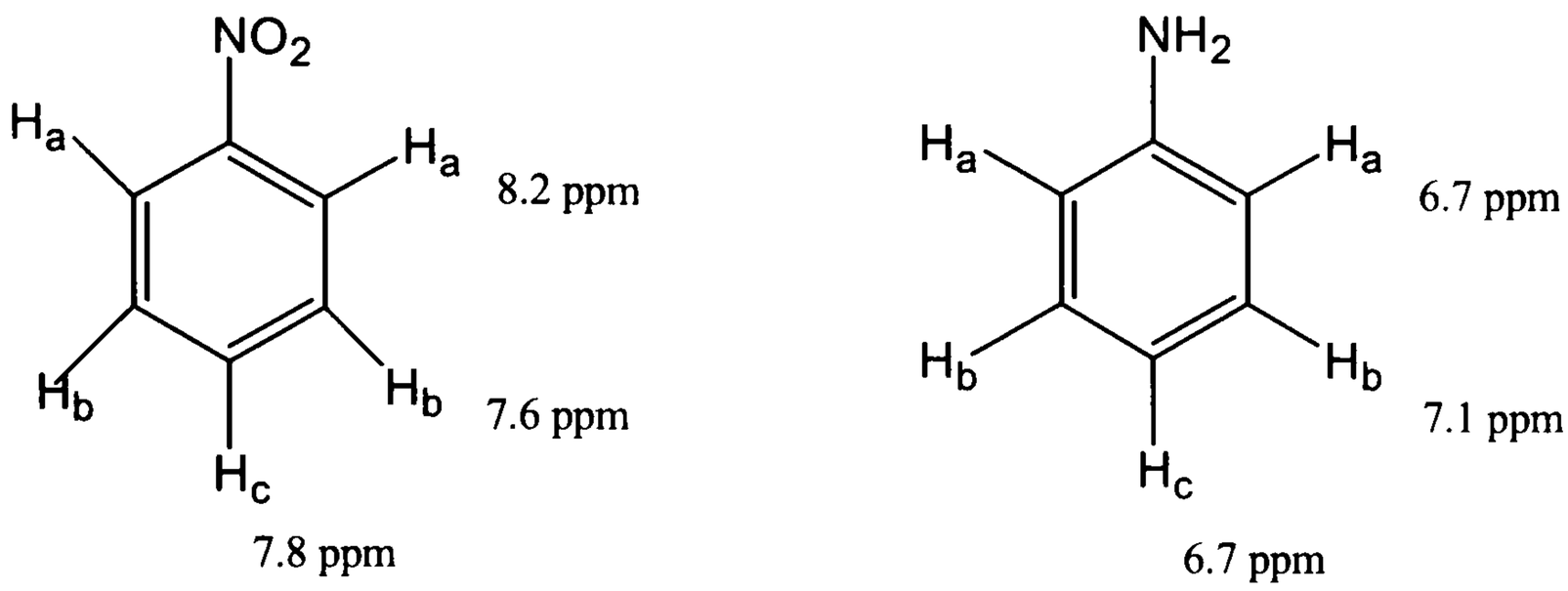

Figure 4.53: Chemical shifts of aromatic protons in nitrobenzene and aniline

Likewise, a similar situation is observed in the ^1H NMR spectra from the d_5-nitrobenzene hydrogenation reaction shown in Figure 4.54. In the initial time zero sample, signals corresponding to all five aromatic nitrobenzene protons are visible in the spectrum indicating that hydrogen-deuterium exchange has occurred in the reaction solution and fully protonated nitrobenzene is present in the NMR sample. The d_5 molecule would show no signals on the ^1H NMR spectrum and a sample of d_5-nitrobenzene in methanol also showed no response in the aromatic region of its NMR spectrum confirming that no hydrogen-deuterium exchange was occurring with the reaction solvent. Exchange had occurred equally at all five positions on the aromatic ring and was most likely a result of interaction with residual hydrogen from the reduction process remaining on the catalyst surface or from surface hydrogen dissociated during the adsorption of the solvent molecules to the catalyst. As the reaction proceeded over time the nitrobenzene signals diminished and the aniline signals appeared. From the original spectra it was clearly noted that the intensity of the signals arising from the deuterated reaction mixtures were very much smaller

than those visible in the NMR spectra from the fully protonated reaction. To quantify the difference in intensity, the integral of the C-H signal arising from the methanol solvent, present in huge excess, was set to 1 in each spectrum and assumed to be the same concentration in each. This allowed the relative intensities of the aromatic peaks and therefore the concentrations of the components to be compared. This revealed that at the beginning of the reaction, time zero, the sample from the d_5 reaction showed aromatic proton peaks arising from nitrobenzene that were 8 % of those observed during the straightforward hydrogenation of nitrobenzene. Analysis of the samples on completion of the reaction, at 90 minutes, showed a similar situation where the signals arising from protonated aniline from the deuterated reaction were 9 % of those from nitrobenzene hydrogenation. Therefore, it can be deduced that rapid hydrogen-deuterium exchange occurred with adsorbed hydrogen on the catalyst but that this only reached a level of around 10 % exchange and that this level was not increased throughout the reaction. This has also shown that the protons on the aromatic ring on nitrobenzene and any reaction intermediates do not undergo exchange with the hydrogen gas present throughout the reaction.

The hydrogen uptake curve for the reaction (Figure 4.55) was used to calculate a rate of hydrogenation and gave a value of 62.0 mmol min^{-1} g^{-1}. This is comparable with the rate of hydrogenation of nitrobenzene under identical conditions, with a hydrogenation rate of 69.0 mmol min^{-1} g^{-1}.

Figure 4.54: ^{1}H NMR spectra from the hydrogenation of fully deuterated nitrobenzene

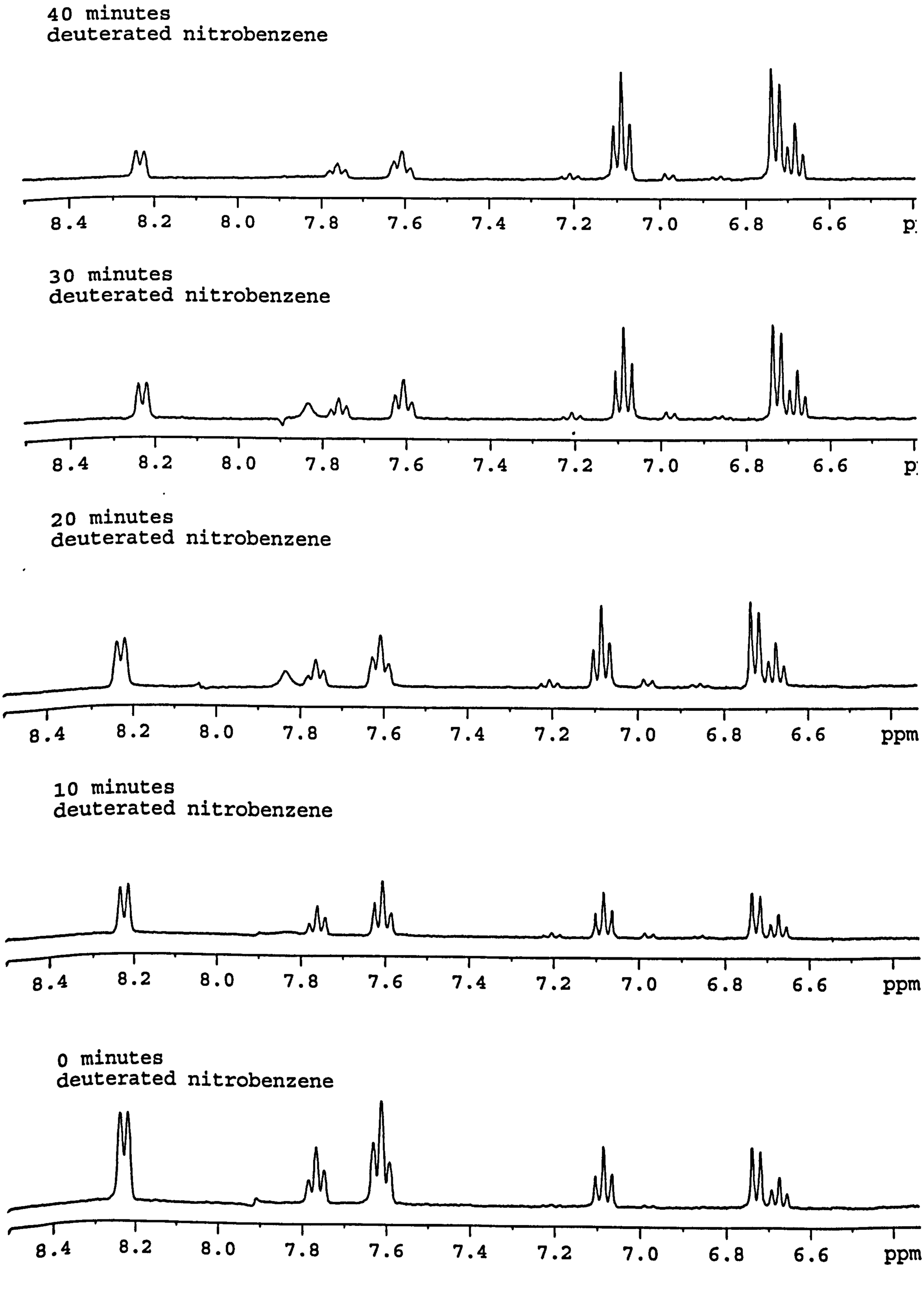

90 minutes
deuterated nitrobenzene

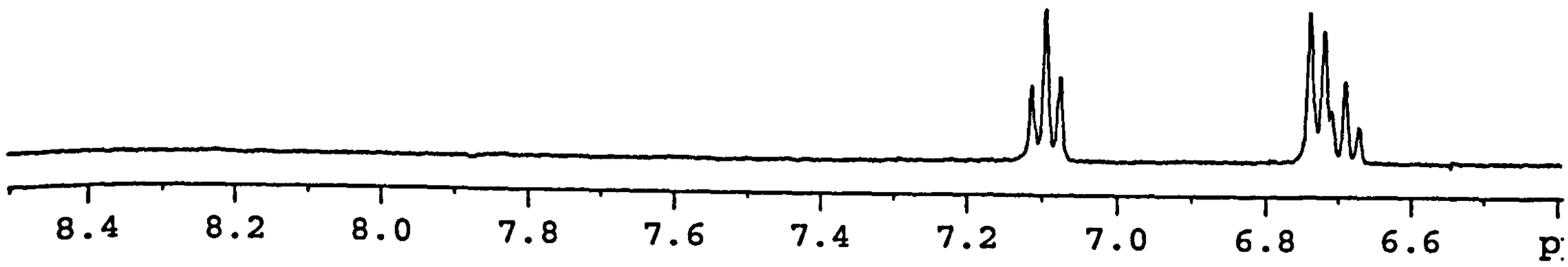

80 minutes
deuterated nitrobenzene

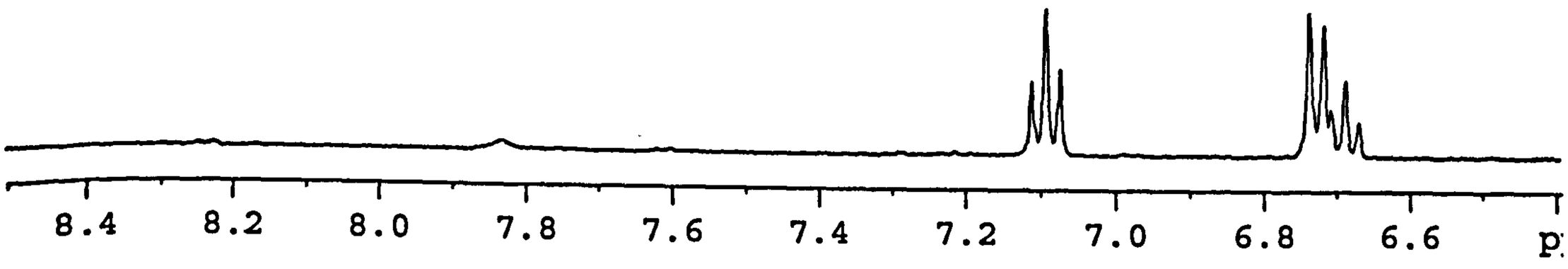

70 minutes
deuterated nitrobenzene

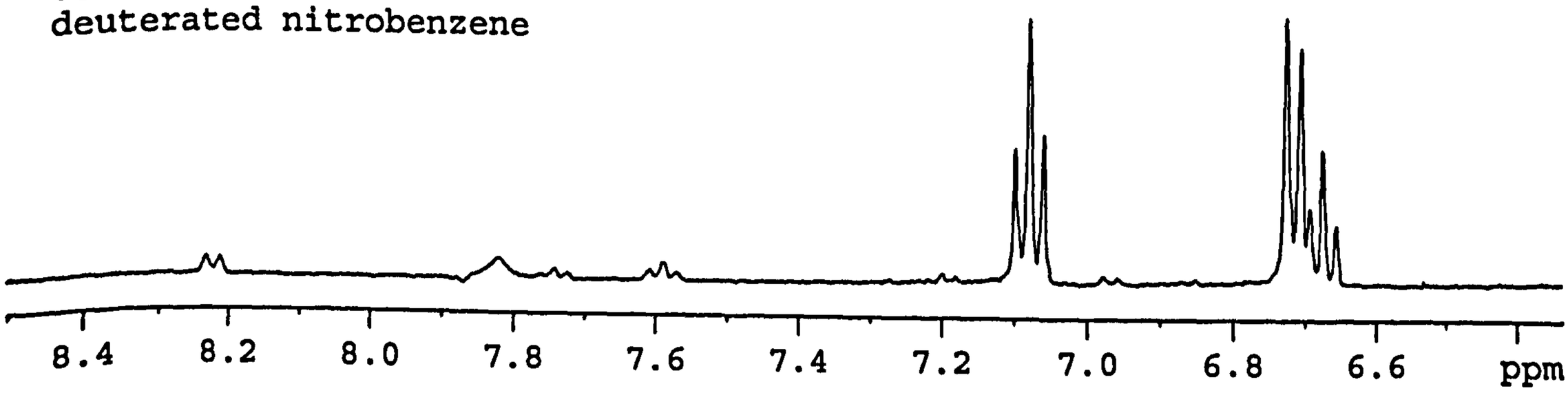

60 minutes
deuterated nitrobenzene

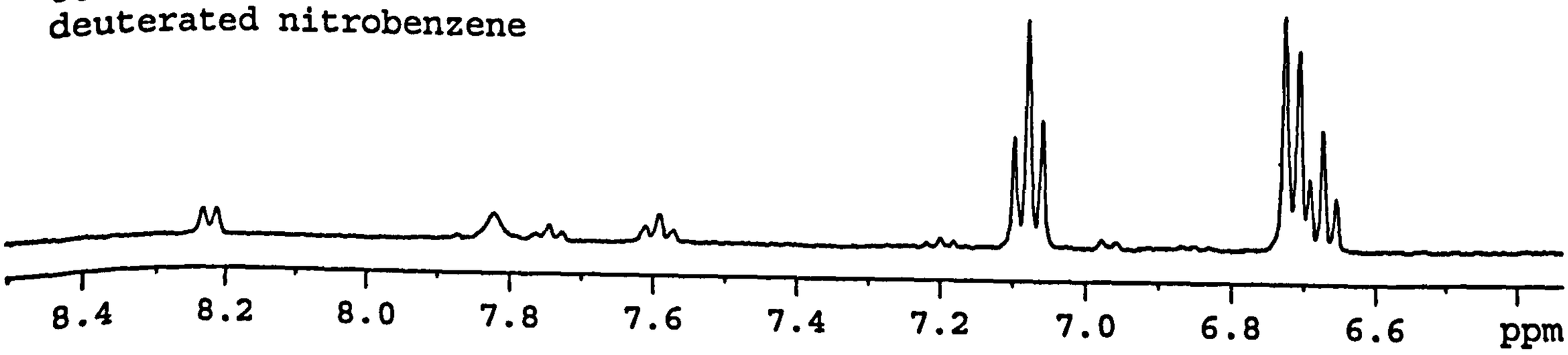

50 minutes
deuterated nitrobenzene

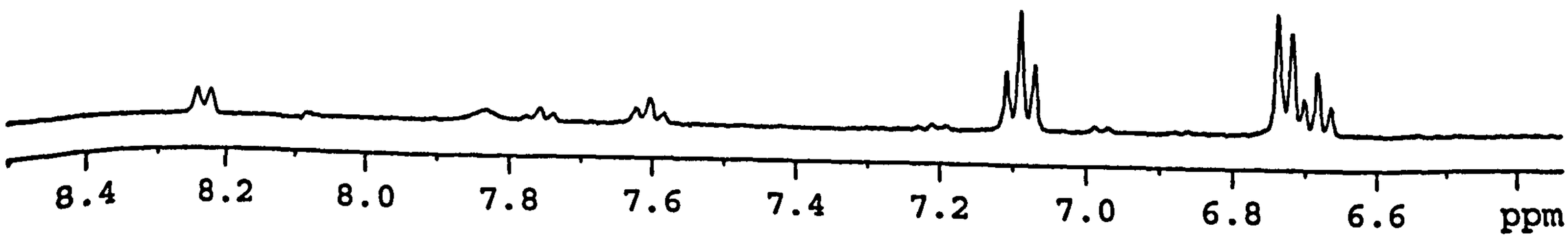

Figure 4.55: Hydrogen consumption during the hydrogenation of d_5-nitrobenzene in methanol using catalyst Pd/CSXU

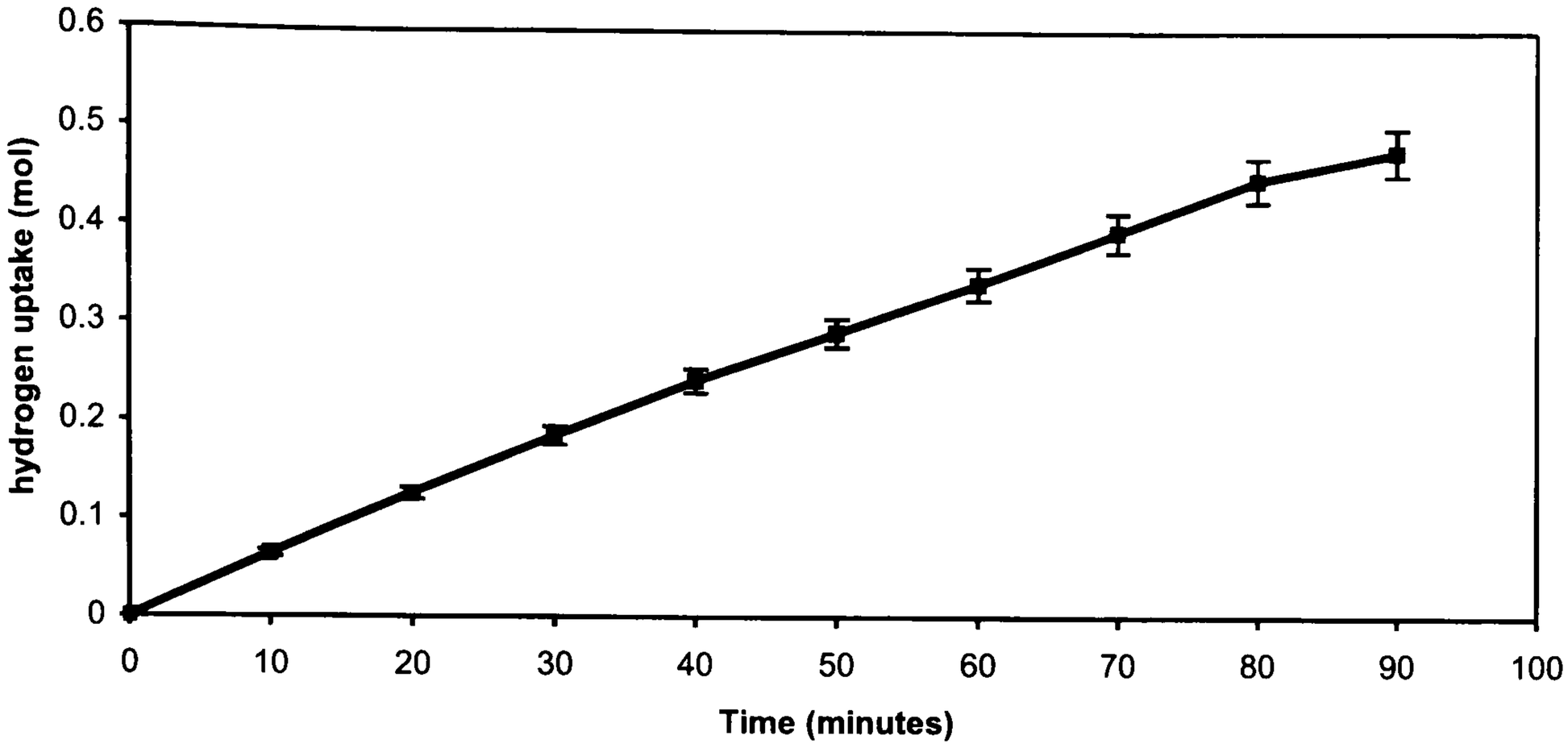

4.3.1.7 The Hydrogenation of Nitrobenzene using Deuterium Gas

The hydrogenation of nitrobenzene using deuterium gas in place of hydrogen was carried out to probe the reaction mechanism and kinetics further. The experiment was carried out as described in Section 3.3.2.8 of the experimental and ^{1}H NMR analysis collected as in the previous experiment. (Section 4.3.1.6)

The ^{1}H NMR spectra obtained were identical to those illustrated in Figure 4.52. The initial time zero sample displayed the three signals corresponding to aromatic nitrobenzene protons described in Figure 4.53. Over the course of the reaction these signals decreased in size until they were entirely absent from the spectrum. At the same time the signals corresponding to the aromatic aniline protons started to appear in the spectra and grew in size until the conclusion of the reaction. All signals were visible throughout the reaction indicating that no deuterium-hydrogen exchange was occurring with the aromatic protons on nitrobenzene, aniline or an intermediate species. This allows us to deduce that the fate of the deuterium was purely the amine group of aniline. Furthermore, it also suggested that the adsorption of nitrobenzene is occurring via the nitrogen or non-aromatic functionality on the molecules as any

adsorption via the aromatic ring would be expected to facilitate a degree of deuterium exchange with the aromatic protons.

The deuterium uptake data for this experiment is displayed in Figure 4.56 with the data collected from the straightforward hydrogenation of nitrobenzene with dihydrogen. As clearly shown on the graph, a kinetic isotope effect was in operation as the reaction with H_2 (g) occurred much more rapidly than the reaction with D_2 (g). Reaction with hydrogen proceeded at a rate of 58.7 mmol min^{-1} g^{-1} while reaction with deuterium proceeded at a rate of 30.3 mmol min^{-1} g^{-1}. The value of the kinetic isotope coefficient (η) was calculated as 1.9 using Equation 4.5. Therefore, it follows that the rate-determining step in the hydrogenation of nitrobenzene must involve a bond breaking or bond forming reaction with hydrogen.

$$\eta = \frac{\text{rate of reaction (H)}}{\text{rate of reaction (D)}} \qquad \text{Equation 4.5}$$

Figure 4.56: Deuterium/hydrogen consumption during the hydrogenation of nitrobenzene using deuterium (g) and hydrogen (g).

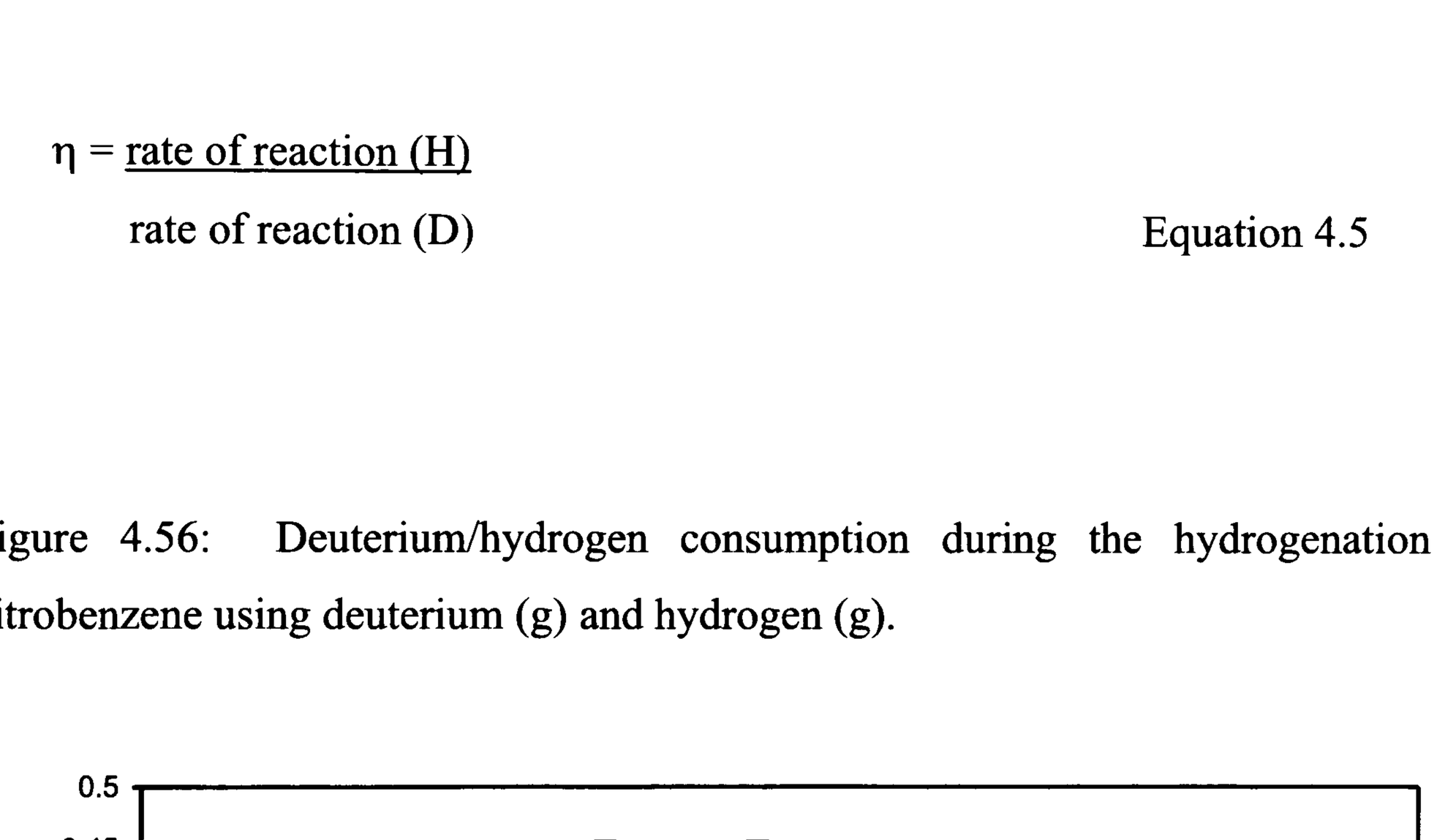

4.3.1.8 The Hydrogenation of Nitrosobenzene with Catalyst Pd/CSXU

The hydrogenation of nitrosobenzene was carried out exactly as described in section 3.3.2.9 under identical conditions to nitrobenzene hydrogenation. A reaction pressure of 2 bar and a temperature of 323 K were used. The hydrogen uptake data are shown in Figure 4.57 and the GC-MS analysis is displayed in Figure 4.58.

Figure 4.57: Hydrogen consumption during the hydrogenation of nitrosobenzene in methanol with catalyst Pd/CSXU.

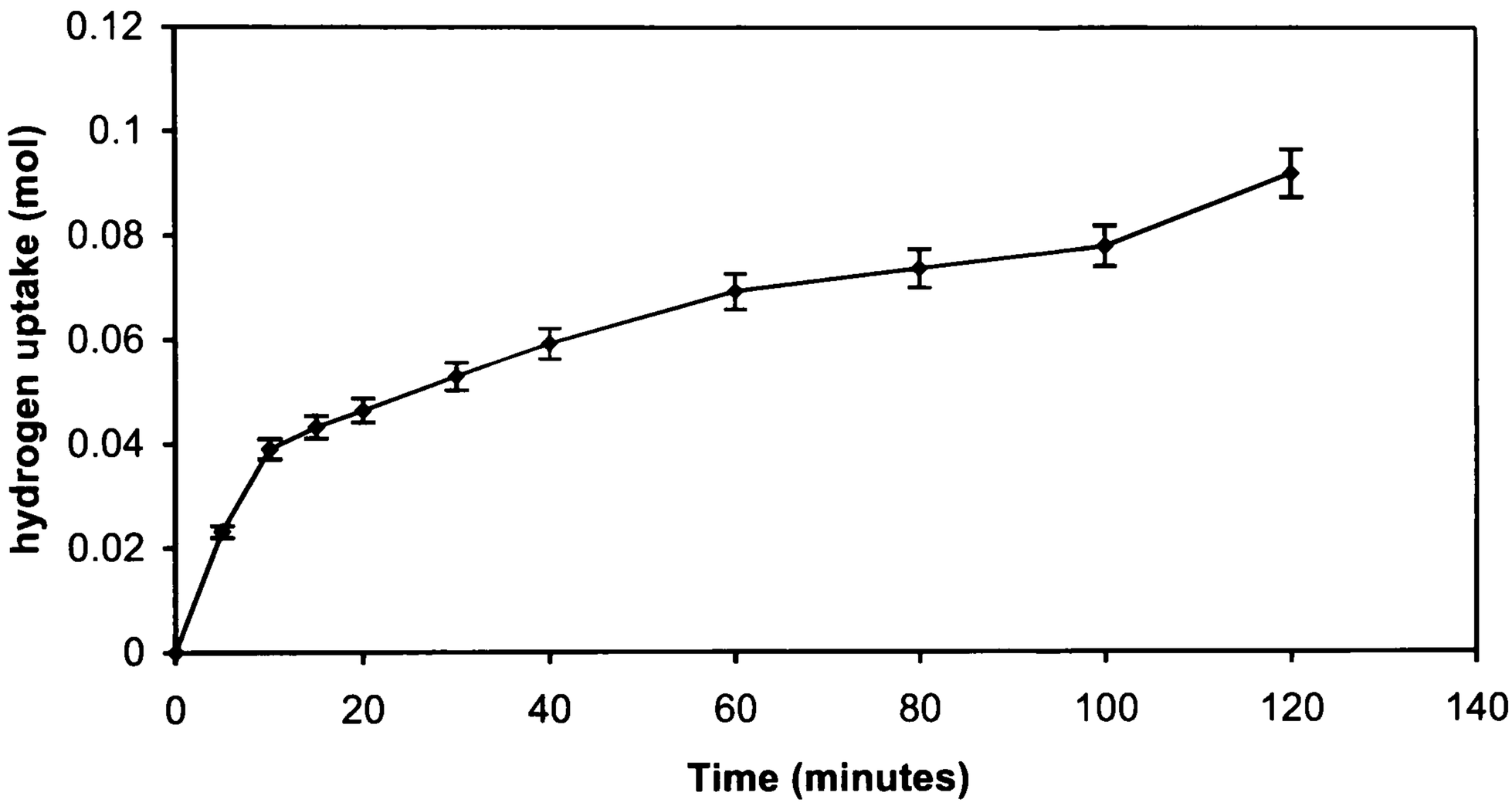

The graph of hydrogen uptake vs time for nitrosobenzene (Figure 4.57) showed two definite stages; an initial steeply rising portion between 0-15 minutes representing a rapid rate of hydrogenation (17.9 mmol min^{-1} g^{-1}) followed by a portion with a shallower gradient from 15 minutes onwards indicating a much slower rate of reaction (3.7 mmol min^{-1} g^{-1}) and the transition between the two gradients was visible at around 15 minutes reaction time. This relationship is very similar to that observed by Smith and co-workers [106] in their previous studies on the hydrogenation of nitrosobenzene.

Figure 4.58: Reaction profile – the hydrogenation of nitrosobenzene in methanol using catalyst Pd/CSXU.
(Starred reagents are plotted on the secondary axis)

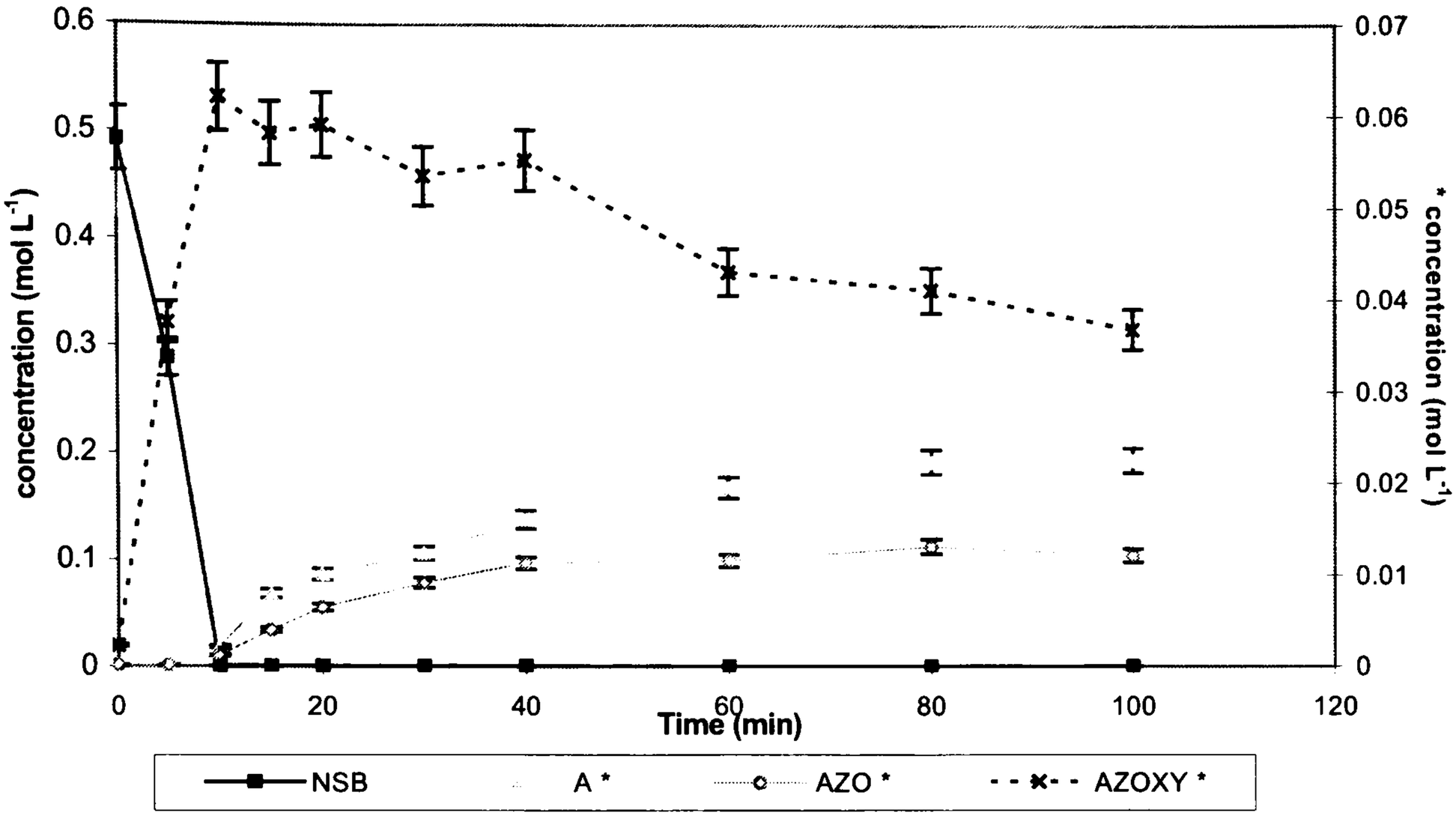

Furthermore, analysis of the reaction samples by GC-MS gave the reaction profile displayed in Figure 4.58 clearly showing a two-step hydrogenation process is occurring and is very different to those previously observed in this study. In contrast to the hydrogenation of nitrobenzene, where only the reagent and product and a very low level of by-product were observed, a number of compounds were identified in the reaction solution using GC-MS. In the initial stages of hydrogenation, a rapid disappearance of nitrosobenzene from solution was observed coupled with a concomitant rise in azoxybenzene. Nitrosobenzene had been fully removed and the maximum concentration of azoxybenzene formed at 15 minutes reaction time. This corresponded directly with the first steep part of the hydrogen uptake curve that now appeared to represent the rate of formation of azoxybenzene from nitrosobenzene. Above 15 minutes reaction time, a slower steady decrease in the azoxybenzene concentration occurred with the appearance and steady increase of aniline. The formation of aniline from azoxybenzene is represented by the second flatter portion of the hydrogen uptake curve. Therefore, it can be deduced that the production of aniline from nitrosobenzene proceeds through an azoxybenzene intermediate.

Another major difference in the nitrosobenzene hydrogenation profile when compared with that of nitrobenzene was the total number of moles in solution during the hydrogenation process. In the initial stages of the reaction, when the nitrosobenzene concentration dropped rapidly down to zero, only very low concentrations of the reaction products were observed. For instance at 10 minutes reaction time, all nitrosobenzene has been entirely removed from solution and the amount of azoxybenzene formed had reached its maximum with a concentration of 0.062 mol L^{-1} corresponding to 18.6 mmol of azoxybenzene and 37.2 mmol of reacted nitrosobenzene (as two aromatic rings are require to form azoxybenzene). As a result, 42.8 mmol of the original 80 mmol of nitrosobenzene, or 53.5 % of the original number of moles added, were unaccounted for. Analysis of the last sample taken during the reaction, after 100 minutes of reaction time, revealed that the equivalent of 36.1 mmol of nitrosobenzene were present in the reaction mixture and that a total of 43.9 mmol were unaccounted for. Therefore, it appears that over half the quantity of nitrosobenzene added has become irreversibly adsorbed on the palladium catalyst.

3.3.1.9 The Hydrogenation of Nitrosobenzene with Deuterium Gas

The reaction of nitrosobenzene with deuterium gas in place of hydrogen was performed as reported in Section 3.3.2.10. The reaction was followed using ^{1}H NMR however, due to the large number of aromatic molecules present in the reaction solution interpretation of the signals (positions, multiplicity, splitting patterns) proved extremely difficult. Therefore, the spectra are not displayed.

The deuterium uptake data were collected and compared with the data obtained from the hydrogenation of nitrosobenzene with H_2 (g). (Figure 4.59).

Figure 4.59: Hydrogen/Deuterium consumption during the hydrogenation of nitrosobenzene with catalysts Pd/CSXU in methanol

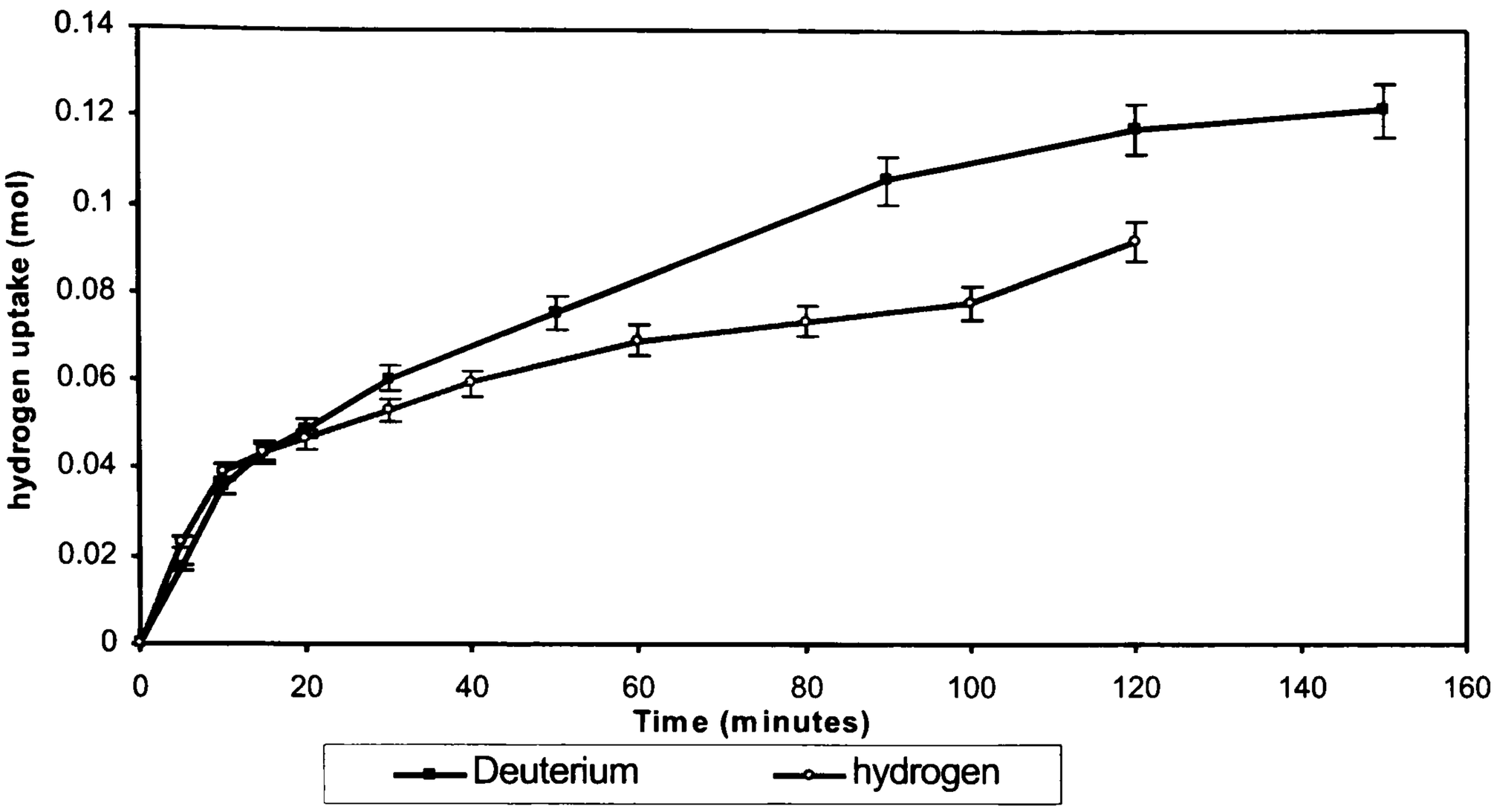

The rate of deuteration of nitrosobenzene was comparable with the rate of hydrogenation. During the first 15 minutes of reaction, the rates were almost identical at 29.1 mmol min^{-1} g^{-1} for D_2 (g) and 28.8 mmol min^{-1} g^{-1} for H_2 (g). After 15 minutes reaction time, when the rates had slowed, a difference in reaction rate was observed with deuterium being consumed at 8.1 mmol min^{-1} g^{-1} and hydrogen at a rate of 4.6 mmol min^{-1} g^{-1}. Surprisingly, an inverse kinetic isotope effect was evident as the reaction proceeded more rapidly with deuterium than with hydrogen. This was in direct contrast to the situation observed during nitrobenzene hydrogenation where a decrease in rate was observed on moving to deuterium gas. While the rate-determining step in the nitrobenzene hydrogenation mechanism involved reaction with hydrogen, with nitrosobenzene this can not be the case. Two distinct processes were in operation; one over the first 15 minutes of reaction that was not affected by the switch to deuterium gas and, therefore did not involve the hydrogenation gas, and a second occurring after 15 minutes of reaction that was increased on moving to deuterium gas. A value for η, the kinetic isotope coefficient, was calculated as 0.7 using the equation displayed previously in Equation 4.5 (Section 4.3.1.7). Therefore, it can be deduced that the rate-determining steps in the hydrogenation of nitrobenzene and nitrosobenzene are different.

4.3.1.10 The Hydrogenation of Azobenzene with Catalyst Pd/CSXU

The hydrogenation of azobenzene was performed in the same way as the hydrogenation of nitrosobenzene following the reaction procedure contained in Section 3.3.2.9.

The hydrogen uptake data obtained in this experiment are displayed in Figure 4.60 and the GC-reaction profile in Figure 4.61.

Figure 4.60: Hydrogen consumption during the hydrogenation of azobenzene in methanol using catalyst Pd/CSXU.

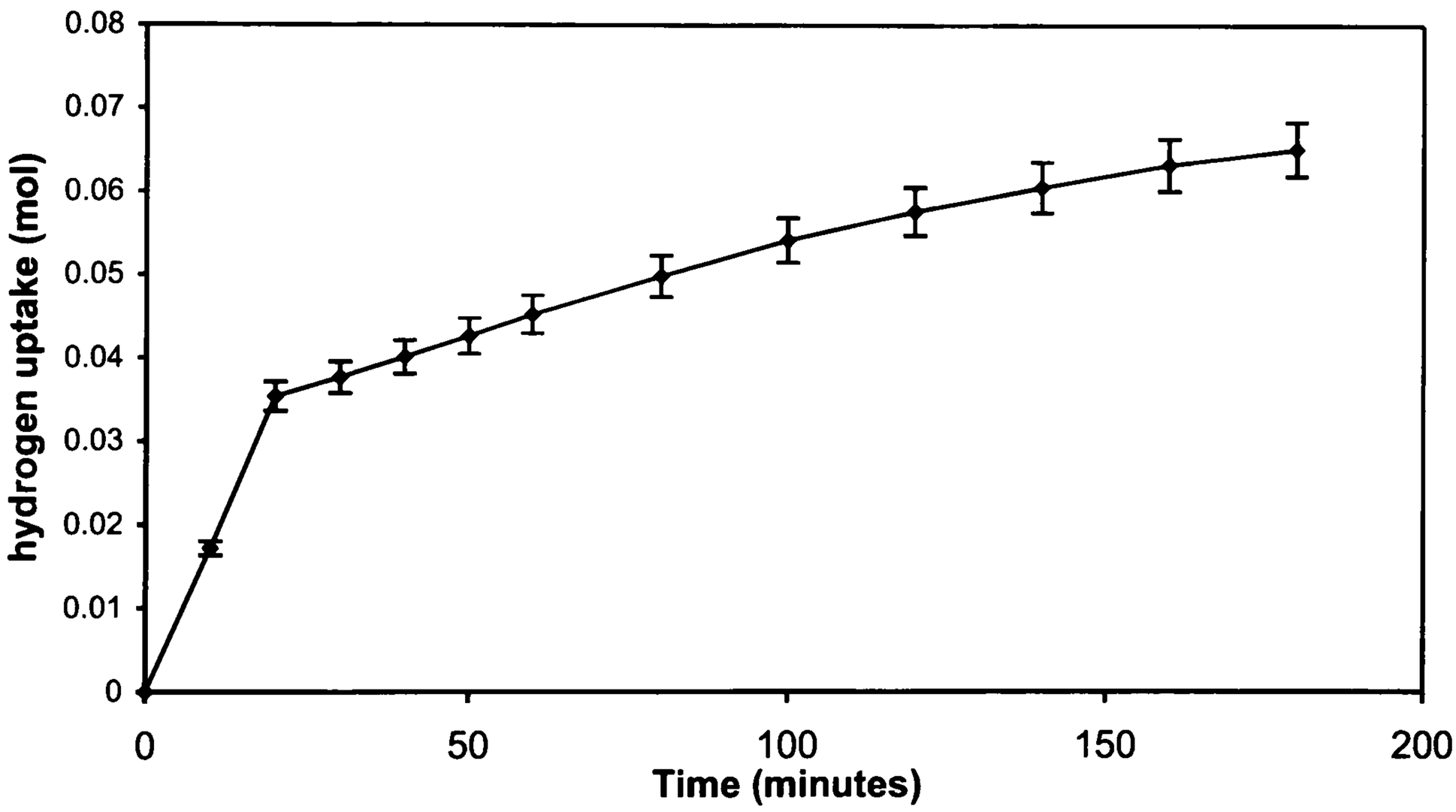

Figure 4.61: Reaction Profile – the hydrogenation of azobenzene in methanol using catalyst Pd/CSXU.

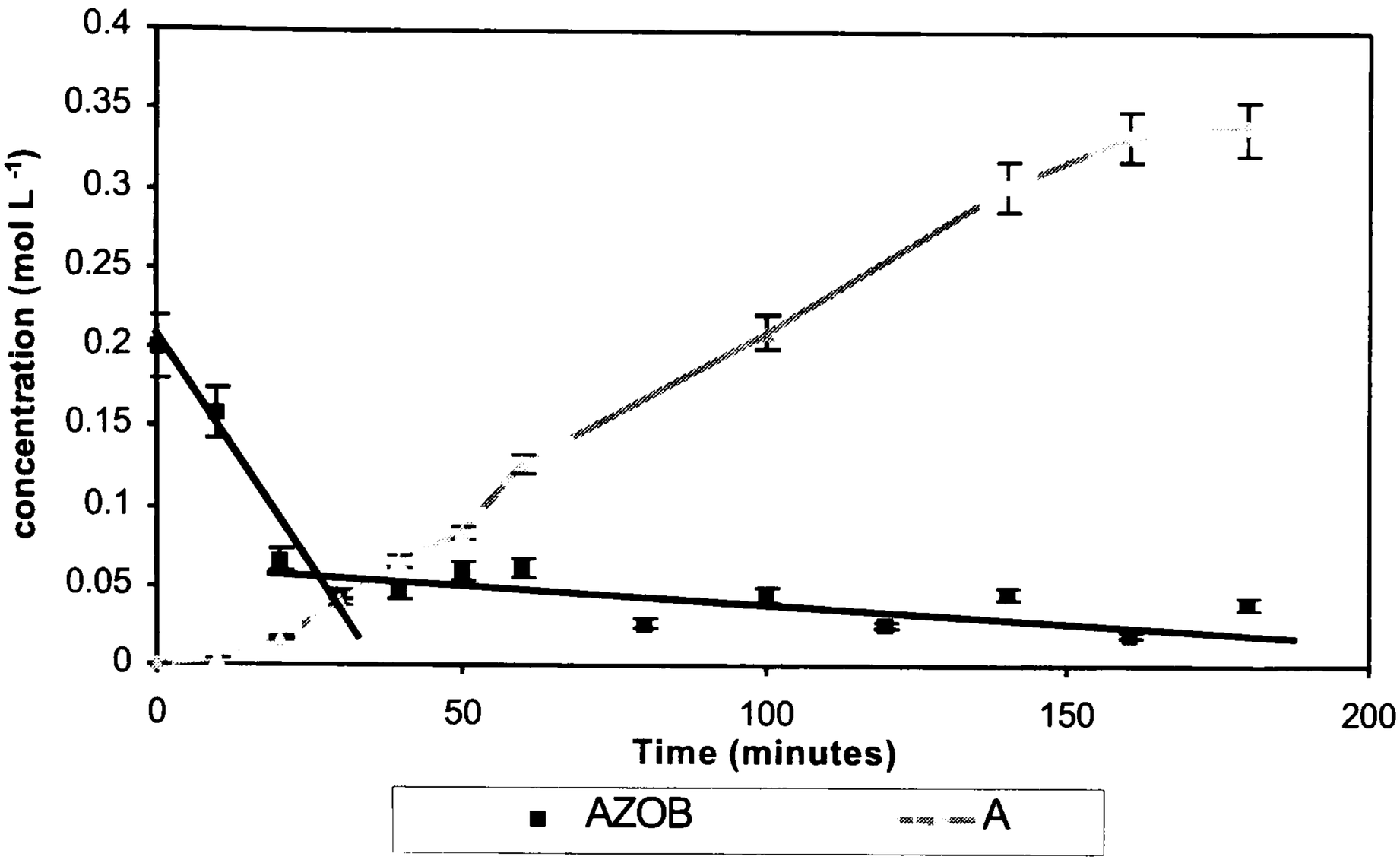

Like with nitrosobenzene, the hydrogen uptake graph for the hydrogenation of azobenzene (shown in Figure 4.60) showed a two-step curve. A relatively fast, linear rate of hydrogen consumption was observed between 0-20 minutes reaction time giving a hydrogen consumption rate of 17.7 mmol min^{-1} g^{-1}. After this point a much slower hydrogen uptake rate was evident with a rate of 2.5 mmol min^{-1} g^{-1}. This indicated that a two-step process might be occurring.

The reaction profile obtained from the GC analysis (Figure 4.61) also displayed two distinct regions. Over the first 20 minutes of reaction a relatively rapid decrease in azobenzene concentration was observed which corresponded to the initial part of the hydrogen uptake curve. After 20 minutes of reaction a much slower decrease in the azobenzene concentration was visible which corresponded to the second portion of the hydrogen uptake graph. The presence of only two reagents was observed: azobenzene and aniline and no other by-products were detected.

4.3.1.11 The Effect of Water on the Hydrogenation of Azobenzene

The influence of additional water on the hydrogenation of azobenzene was investigated following the procedure described in Section 3.3.2.11. This reaction was carried out at 2 bar pressure and 323 K.

The hydrogen uptake data for this reaction are displayed in Figure 4.62 and the GC reaction profile in Figure 4.63.

Figure 4.62: Hydrogen consumption during the hydrogenation of azobenzene in methanol with catalyst Pd/CSXU and 2 mole equivalents of water.

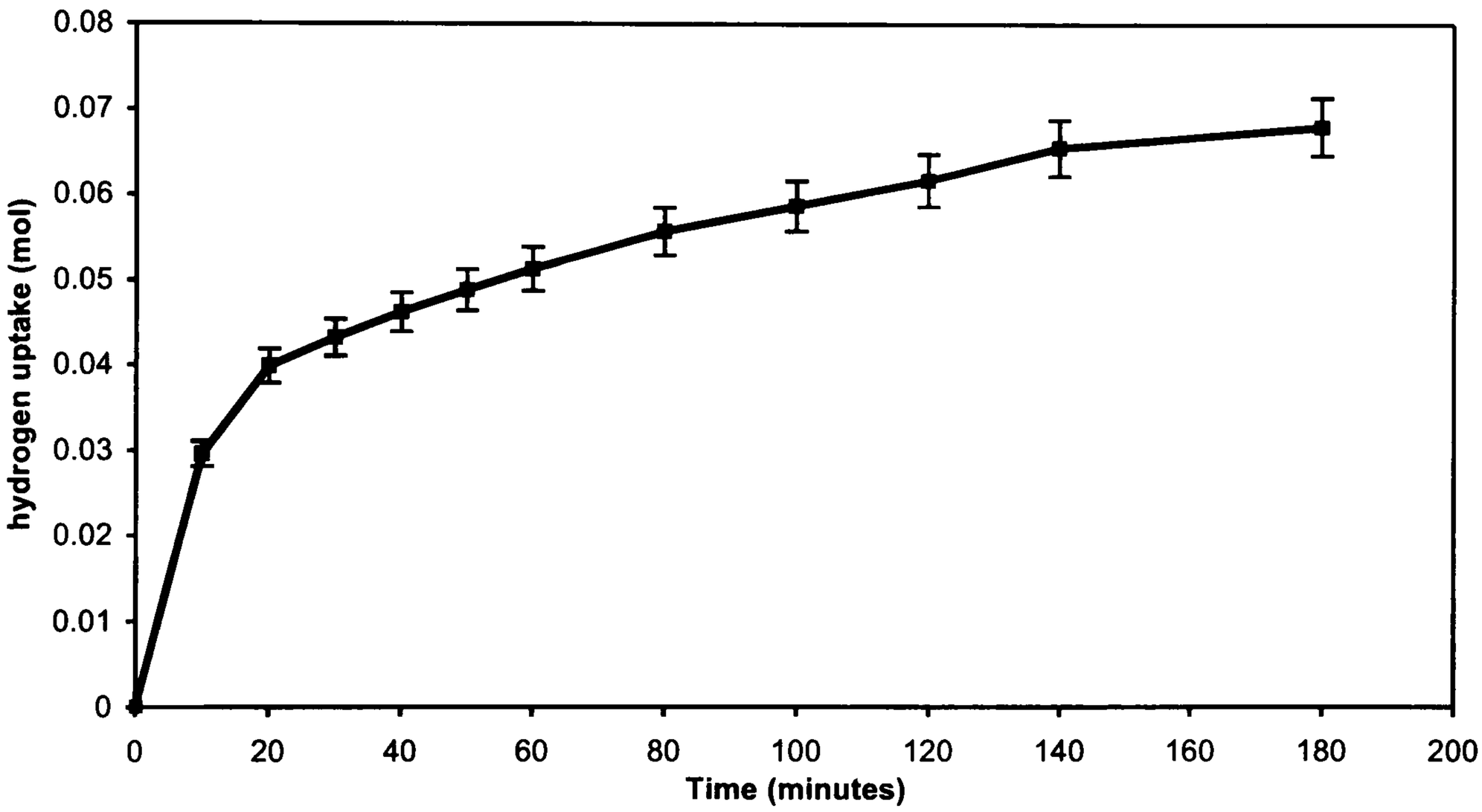

Figure 4.63: Reaction profile – the hydrogenation of azobenzene in methanol with catalyst Pd/CSXU and two mole equivalents of water.

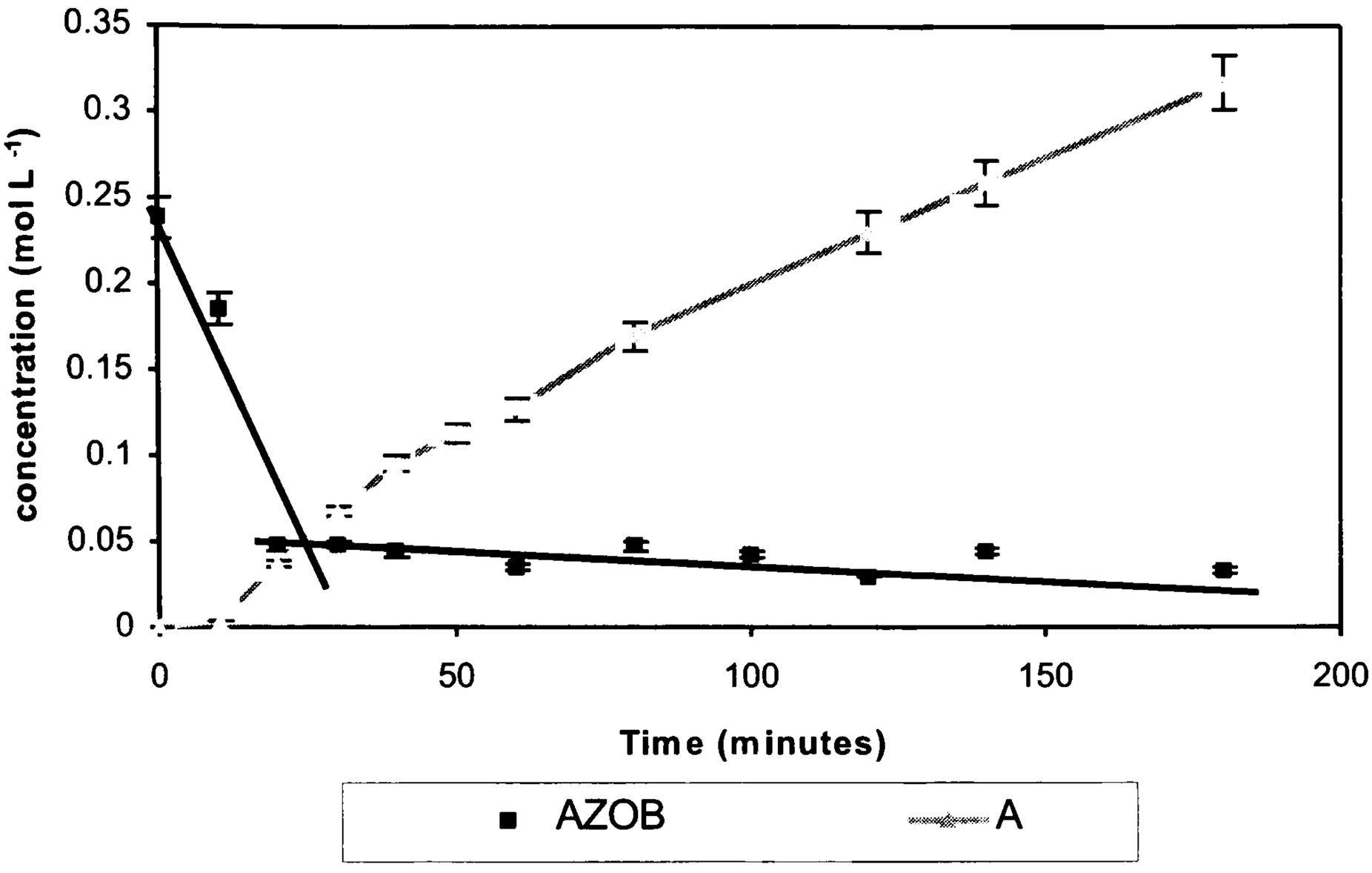

The hydrogen uptake curve displayed in Figure 4.62 shows an identical pattern to the curve observed during the hydrogenation of azobenzene in the absence of water and displayed in Figure 4.60. Over the first 20 minutes, the rate of hydrogen consumption was recorded as 3.0 mmol min^{-1} g^{-1} before it decreased to 0.3 mmol min^{-1} g^{-1} after 20 minutes.

In addition, the reaction profile shown in Figure 4.63 displayed two distinct regions equivalent to the two regions observed on the hydrogen uptake curve. Over the first 20 minutes of reaction, the azobenzene concentration decreased relatively rapidly and after 20 minutes the concentration decreased at a much slower rate. This profile is similar to the one obtained for the hydrogenation of azobenzene in the absence of added water (Figure 4.61, section 3.3.1.10).

Comparison between the GC analysis for the hydrogenation of azobenzene in the absence of added water (Figure 4.61) and for the hydrogenation of azobenzene in the presence of added water (Figure 4.63) revealed two very similar reaction profiles.

No additional by-products were observed when water was introduced, suggesting that water produced during the hydrogenation reaction was unlikely to react with azobenzene to form azoxybenzene or other by-products. A comparison of the rate of hydrogenation for both reactions is shown in Table 4.18 and revealed that the additional water acted as an inhibitor of the azobenzene hydrogenation reaction.

Table 4.18: The rate of hydrogenation of azobenzene in the presence and adsence of added water.

	rate of hydrogenation (mmol min^{-1} g^{-1})	
	0-20 minutes	20-60 minutes
normal run	17.7	2.4
added water	3	0.3

4.3.1.12 Comparison of Nitrobenzene, Nitrosobenzene and Azobenzene Hydrogenation

The data obtained from the hydrogenation on nitrobenzene, nitrosobenzene (Section 4.3.1.8) and azobenzene (Section 4.3.1.10) were considered more closely. An experiment was carried out to hydrogenate nitrobenzene under identical conditions and concentration to nitrosobenzene and azobenzene so a direct comparison of the rates of reaction could be made. The hydrogen uptake graph and reaction profile for the hydrogenation of nitrobenzene at this concentration are displayed in Figures 4.64 and 4.65 respectively.

Figure 4.64: Hydrogen consumption during the hydrogenation of nitrobenzene (40 mmol) in methanol with catalyst Pd/CSXU.

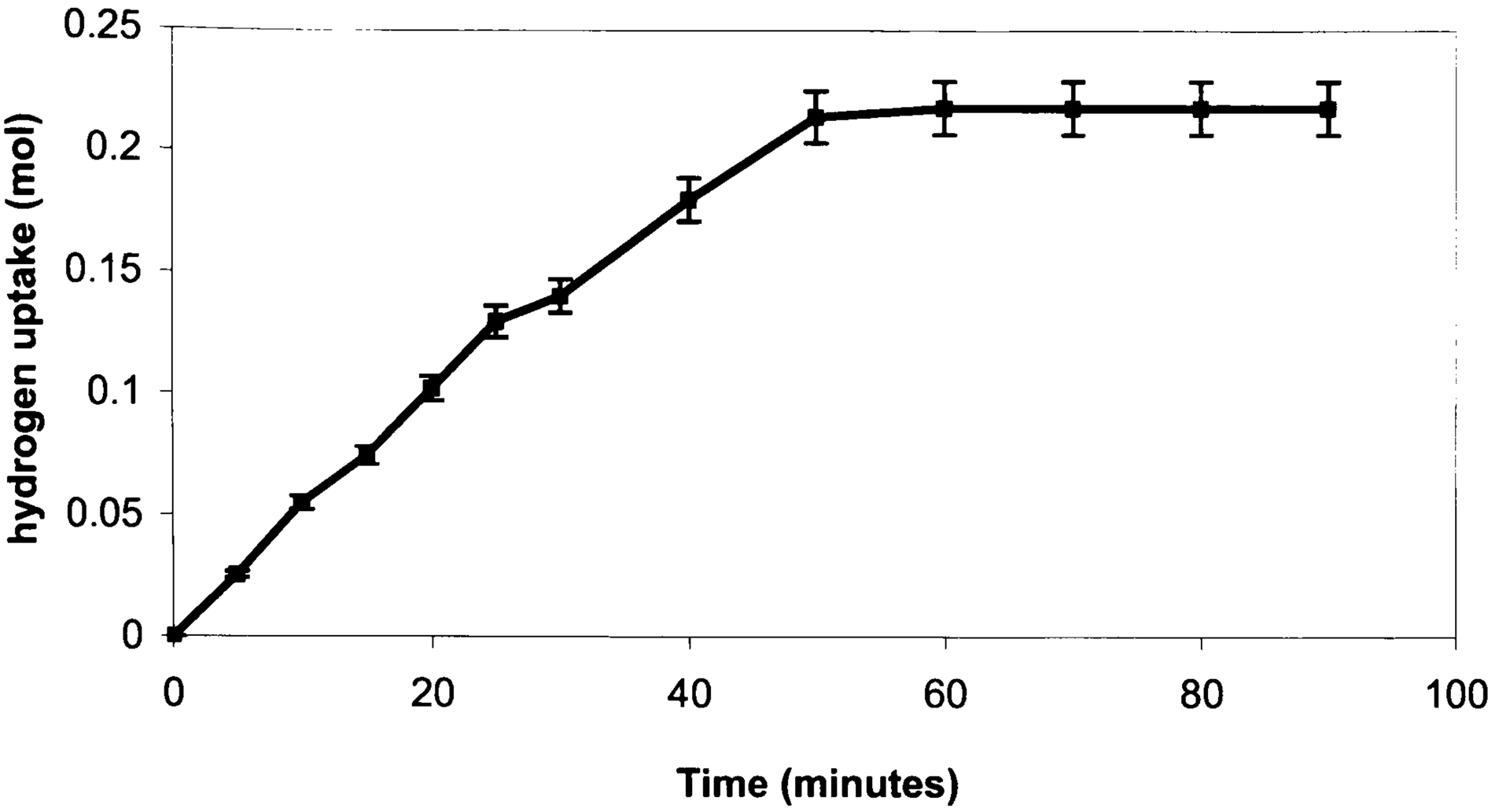

Figure 4.65: Reaction Profile- the hydrogenation of nitrobenzene (40 mmol) in methanol with catalyst Pd/CSXU.

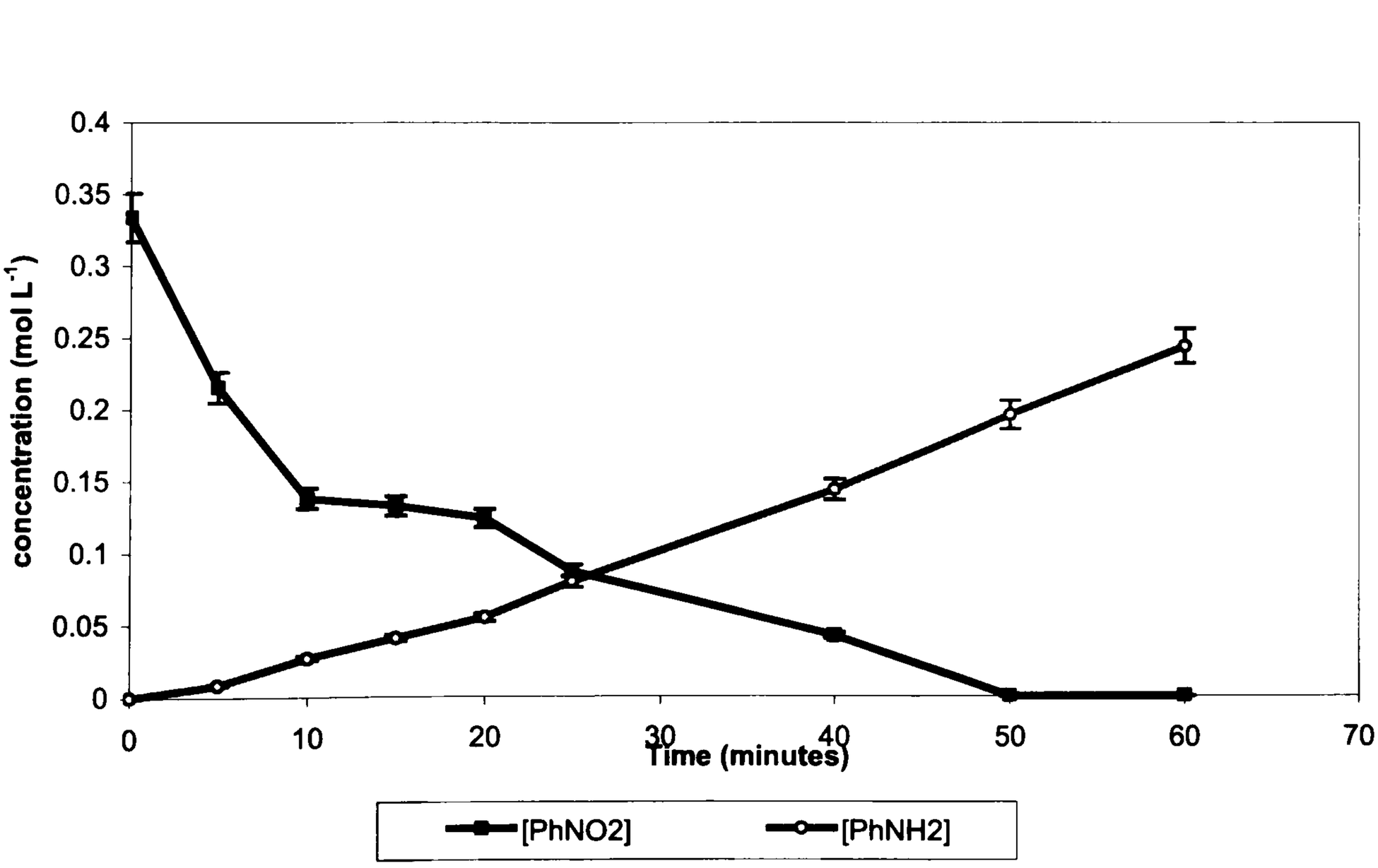

The initial rate of hydrogen uptake was calculated for the hydrogenation of nitrobenzene and compared with those already reported for nitrosobenzene and azobenzene in Sections 4.3.1.8 and 4.3.1.10 respectively. This data are displayed in

Table 4.19 and clearly shows that the hydrogenation of nitrobenzene proceeded at a very much faster rate of 49.5 mmol min^{-1} g^{-1} than nitrosobenzene and azobenzene. With nitrosobenzene, after an initial period of moderate hydrogen consumption (18.0 mmol min^{-1} g^{-1}), the rate slowed to just 3.7 mmol min^{-1} g^{-1}. Similarly, during azobenzene hydrogenation, an uptake of 17.7 mmo lmin^{-1} g^{-1} was observed in the initial stages of reaction, followed by a period of much slower hydrogen consumption (2.5 mmol min^{-1} g^{-1}). For nitrosobenzene to act as an intermediate species in the hydrogenation of nitrobenzene the rate of nitrosobenzene hydrogenation must be greater than or equal to that of the overall transformation. In this case, the reaction was slower indicating that nitrosobenzene was not involved as an intermediate species. In addition, the data shown in Table 4.19 also showed that the hydrogenation of azobenzene also proceeded much more slowly than the nitrobenzene reaction. This indicates that, although aniline may be produced following reaction of nitrobenzene or an intermediate to form azobenzene, the main route to aniline cannot involve azobenzene as an intermediate.

Table 4.19: Rate of hydrogen consumption during the hydrogenation of nitrobenzene, nitrosobenzene and azobenzene.

	hydrogenation rate (mmol min^{-1} g^{-1})	
	1st period	2nd period
nitrobenzne	49.5	
nitrosobenzene	18.0	3.7
azobenzene	17.7	2.5

To make a further comparison between the hydrogenation of nitrobenzene, nitrosobenzene and azobenzene, the rate of aniline production was calculated using the reaction profiles displayed in Figures 4.55, 4.58 and 4.62. This was done using Equation 4.6 displayed below. These data are shown as a bar chart in Figure 4.63.

$$\text{Rate of aniline production (mol L}^{-1}\text{ min}^{-1}\text{)} = \frac{\text{change in [PhNH}_2\text{] (mol L}^{-1}\text{)}}{\text{change in time (min)}} \quad \text{Equ 4.6.}$$

The rates were obtained from this equation with the units of mol L^{-1} min^{-1} but were converted to mmol min^{-1} g^{-1} for easy comparison with the other rates reported in this thesis.

Figure 4.66 shows that the rate of aniline production from nitrobenzene, at 15.5 mmol min^{-1} g^{-1}, is very much greater than the rate of aniline production from nitrosobenzene and azobenzene, with values of 0.4 mmol min^{-1} g^{-1} and 8.3 mmol min^{-1} g^{-1} respectively. For nitrosobenzene to act as an intermediate in the nitrobenzene hydrogenation mechanism, the rate of aniline production starting from nitrosobenzene would have to be greater than or equal to the rate of aniline production when starting from nitrobenzene. Therefore, like the hydrogen uptake results discussed earlier, the rates of aniline production obtained from these experiments clearly demonstrates that nitrosobenzene cannot act as an intermediate in the nitrobenzene hydrogenation pathway and, although it is possible to produce aniline from azobenzene, it also cannot act as a reaction intermediate.

Figure 4.66: Comparison of the aniline production from the hydrogenation of nitrobenzene, nitrosobenzene and azobenzene in methanol with catalyst Pd/CSXU.

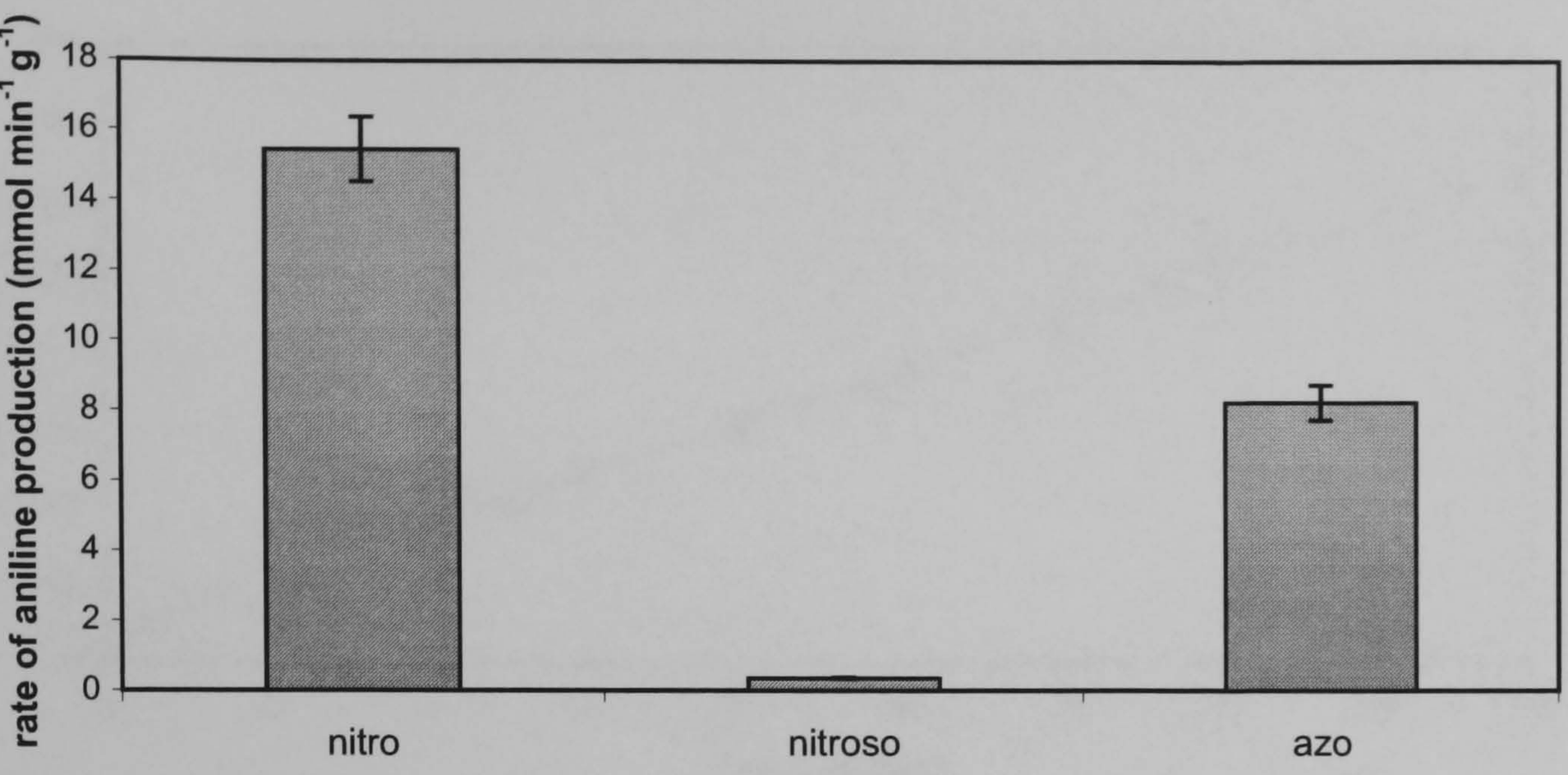

4.3.1.12 The Effect of Nitrosobenzene, Azobenzene and Cyclohexylamine on the Hydrogenation of Nitrobenzene.

To investigate the effect of adding an additional compound to the nitrobenzene hydrogenation reaction, nitrosobenzene, azobenzene and cyclohexylamine were used to spike the reaction mixture and hydrogenation performed according to the experimental procedure outlined in Section 3.3.2.12. All experiments were carried out at 2 bar pressure and 323 K.

4.3.1.12.1 The Effect of Nitrosobenzene on the Hydrogenation of Nitrobenzene

The hydrogen uptake data for the reaction involving nitrobenzene and nitrosobenzene are shown in Figure 4.67 and the GC-MS analysis in Figure 4.68.

Figure 4.67: Hydrogen consumption during the hydrogenation of nitrobenzene/nitrosobenzene in methanol using catalyst Pd/CSXU

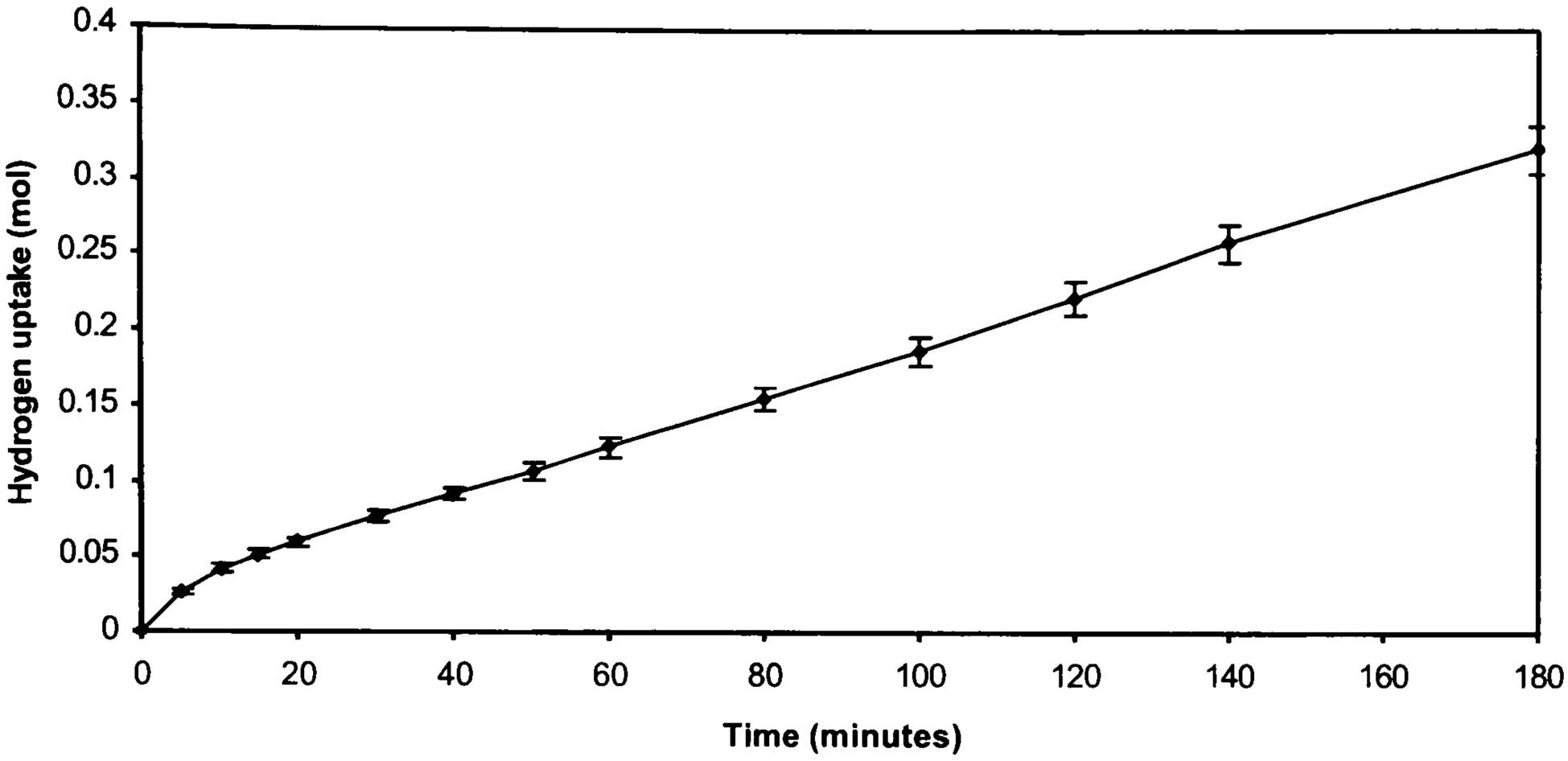

.

Figure 4.67 shows a smooth one-step curve for the consumption of hydrogen throughout the duration of the experiment similar to that observed for the hydrogenation of nitrobenzene and displayed in Figure 4.64. The distinctive hinge-shaped graph obtained in the hydrogenation of nitrosobenzene (Figure 4.57) is not observed in this experiment, although the first 10 minute period of the graph could be said to show a slightly faster rate of hydrogen uptake than the remainder of the curve. The rate of hydrogen consumption was calculated in two parts; once for the first 20 minutes of reaction, and second for the remainder of the experiment. The rates of hydrogen uptake were calculated at 29.8 mmol min^{-1} g^{-1} and 15.9 mmol min^{-1} g^{-1} respectively.

Figure 4.68: Reaction Profile – the hydrogenation of nitrobenzene/nitrosobenzene in methanol with catalyst Pd/CSXU.

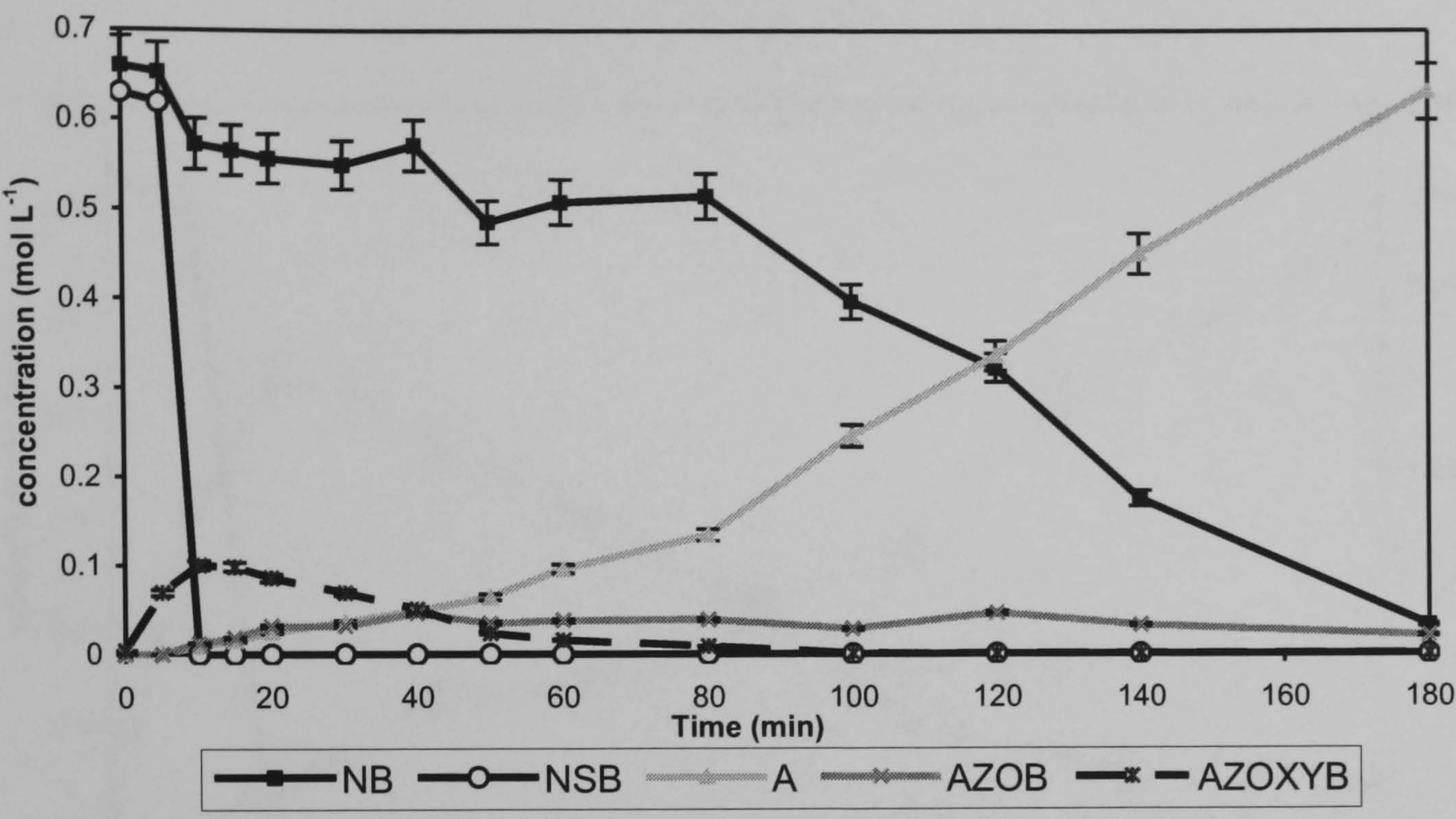

Examination of the reaction profile for the hydrogenation of nitrobenzene/nitrosobenzene (Figure 4.68) revealed a fairly complicated situation. In addition to the presence of the initial reagents, aniline, azobenzene and azoxybenzene were detected throughout the course of the reaction. However, Figure 4.68 can be split into two separate regions to illustrate the characteristics of the nitrobenzene/nitrosobenzene reaction more clearly. The region between 0-80 minutes reaction time is displayed in Figure 4.69a and the period from 80-180 minutes reaction time in Figure 4.69b.

Figure 4.69a: Reaction profile for 0-80 minutes of the hydrogenation of nitrobenzene/nitrosobenzene in methanol using catalyst Pd/CSXU.
(starred reagents are plotted on the secondary axis)

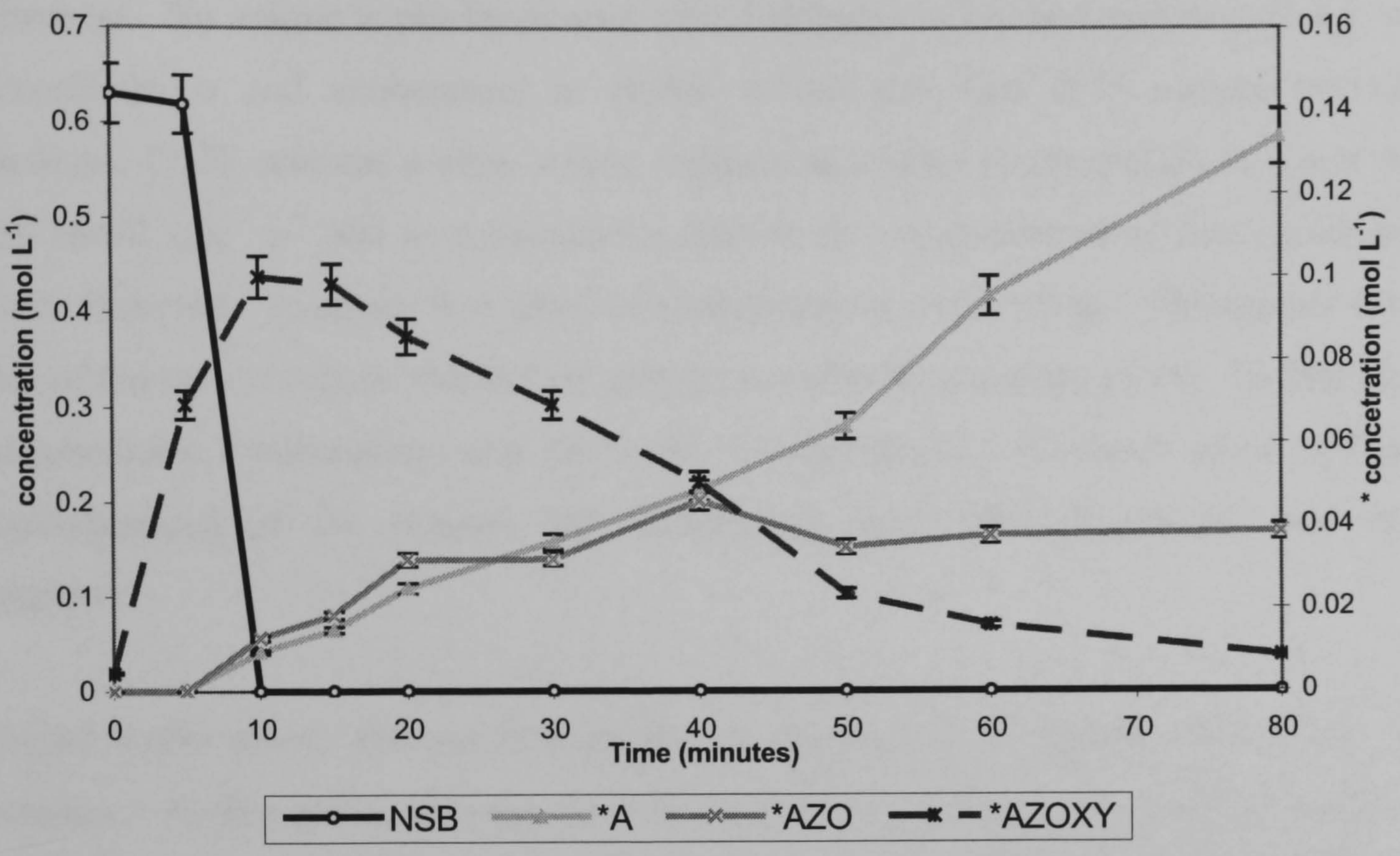

Figure 3.69b: Reaction profile for 80-180 minutes of the hydrogenation of nitrobenzene/nitrosobenzene in methanol with catalyst Pd/CSXU.

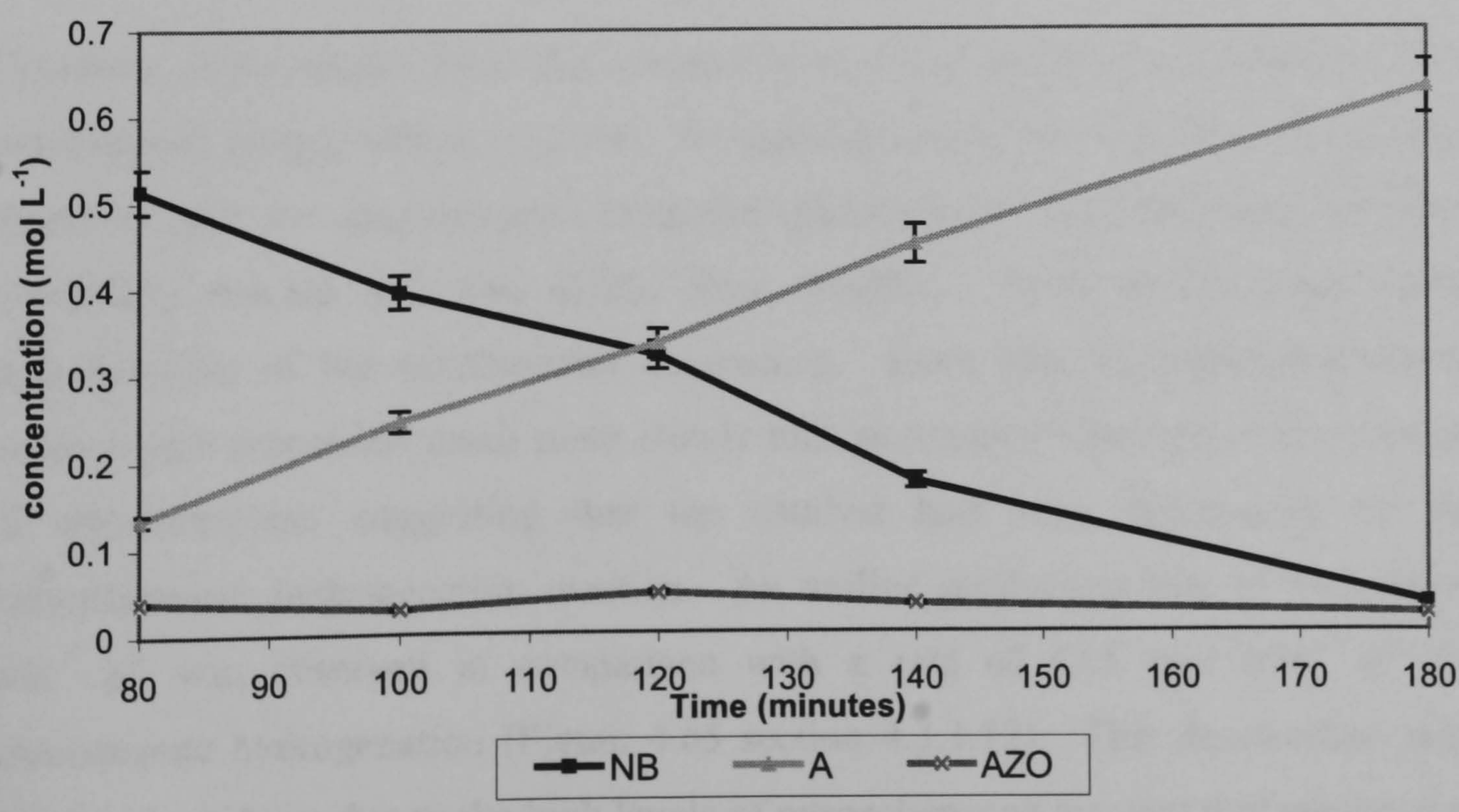

Examination of the reaction profile over the first 80 minutes of reaction (Figure 4.69a) revealed that the graph was remarkably similar to the profile obtained from the hydrogenation of nitrosobenzene displayed in Figure 4.58. Over the first 10-15 minute period of the reaction a rapid drop in nitrosobenzene concentration is observed. No aniline is produced until after 5 minutes of reaction and an increase in azoxybenzene and azobenzene is visible within this first 0-15 minute period. Between 15-80 minutes a slow steady increase in aniline concentration at a rate of 5.0 mmol min^{-1} g^{-1} and a simultaneous drop in the concentration of azoxybenzene were observed. A steady low level of azobenzene is also visible. Throughout this period the concentration of nitrobenzene did not alter to any great extent. In fact, the nitrobenzene concentration did not begin to significantly decrease, showing that hydrogenation of this reagent had commenced, until after 80 minutes into the reaction.

Figure 4.69b shows the reaction profile for the period of reaction following 80 minutes. At this point, all azoxybenzene had been removed from solution and the nitrobenzene present began to hydrogenate and produce aniline more rapidly than in the previous 80 minutes, at a rate of 14.93 mmol min^{-1} g^{-1}. The profile is remarkably similar to that obtained from the hydrogenation of nitrobenzene shown in Figure 4.65.

Therefore, these results show that nitrosobenzene was acting as an inhibitor to the nitrobenzene hydrogenation reaction. No significant reaction with nitrobenzene was observed until the azoxybenzene produced directly from nitrosobenzene had been completely reacted and was absent from solution. Only at this stage could hydrogenation of the nitrobenzene commence. Even then the hydrogenation of nitrobenzene proceeded much more slowly than previously observed in the absence of nitrosobenzene suggesting that the catalyst had been deactivated by the nitrosobenzene hydrogenation reaction. An aniline production rate of 14.9 mmol min^{-1} g^{-1} was observed in comparison with a rate of 49.5 mol min^{-1} g^{-1} for nitrobenzene hydrogenation (Figure 4.65 section 4.3.1.12). This deactivation may possibly have been due to the high levels of nitrosobenzene reactant that appeared to

be irreversibly adsorbed on the catalysts and removed from solution. This would cause either a blocking of the active sites required for the nitrobenzene hydrogenation reaction to occur, or by facilitating a range of carbon forming reactions on the surface of the catalysts leading to a decrease in catalytic activity.

4.3.1.12.2 The Effect of Azobenzene on the Hydrogenation of Nitrobenzene

The hydrogen uptake data and GC-MS analysis for the hydrogenation of the nitrobenzene/azobenzene are displayed in Figures 4.70 and 4.71 respectively.

The hydrogen consumption throughout the reaction followed a smooth curve similar to the one observed with the hydrogenation of nitrobenzene (Figure 4.64). The two-stage nature of the curve observed in the hydrogenation of azobenzene (Figure 4.60) was not visible in this graph. The rate of hydrogen uptake was calculated to be 11.0 mmol min^{-1} g^{-1}.

The reaction profile (Figure 4.71) revealed a concomitant drop in both nitrobenzene and azobenzene throughout the duration of the experiment. This was coupled to the appearance and subsequent rise in aniline concentration as the reaction proceeded. No other by-products or intermediate compounds were observed. The reaction profiles for the hydrogenation of nitrobenzene and azobenzene (Figure 4.65 and Figure 4.61) both resembled the reaction profile obtained in this case. Therefore, it can be proposed that the nitrobenzene and azobenzene were hydrogenating simultaneously in competitive reactions that both result in the formation of aniline. The rate of aniline production in the azobenzene hydrogenation reaction was calculated to be 3.4 mmol min^{-1} g^{-1}.

Figure 4.70: Hydrogen consumption during the hydrogenation of nitrobenzene/azobenzene in methanol using catalyst Pd/CSXU.

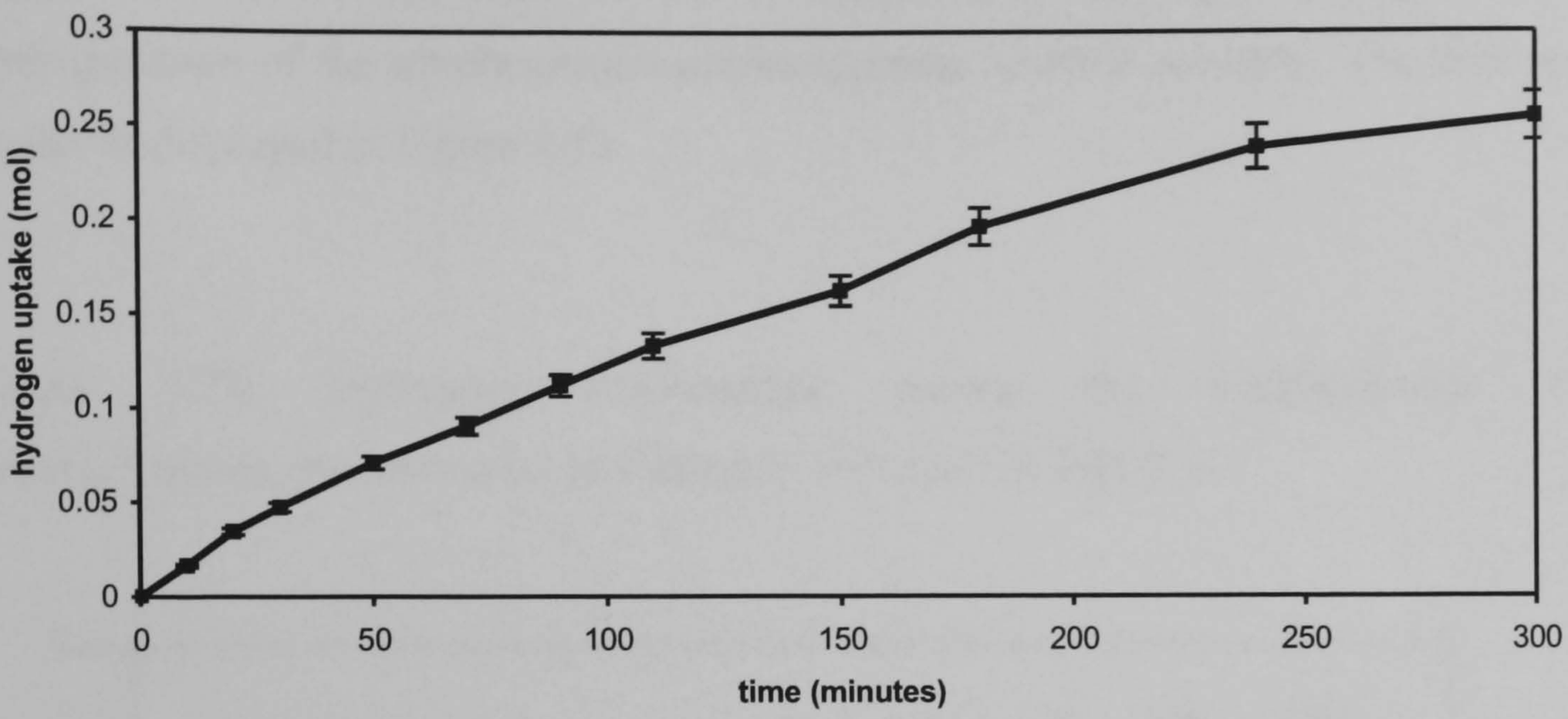

Figure 4.71: Reaction Profile – the hydrogenation of nitrobenzene/azobenzene in methanol with catalyst Pd/CSXU.

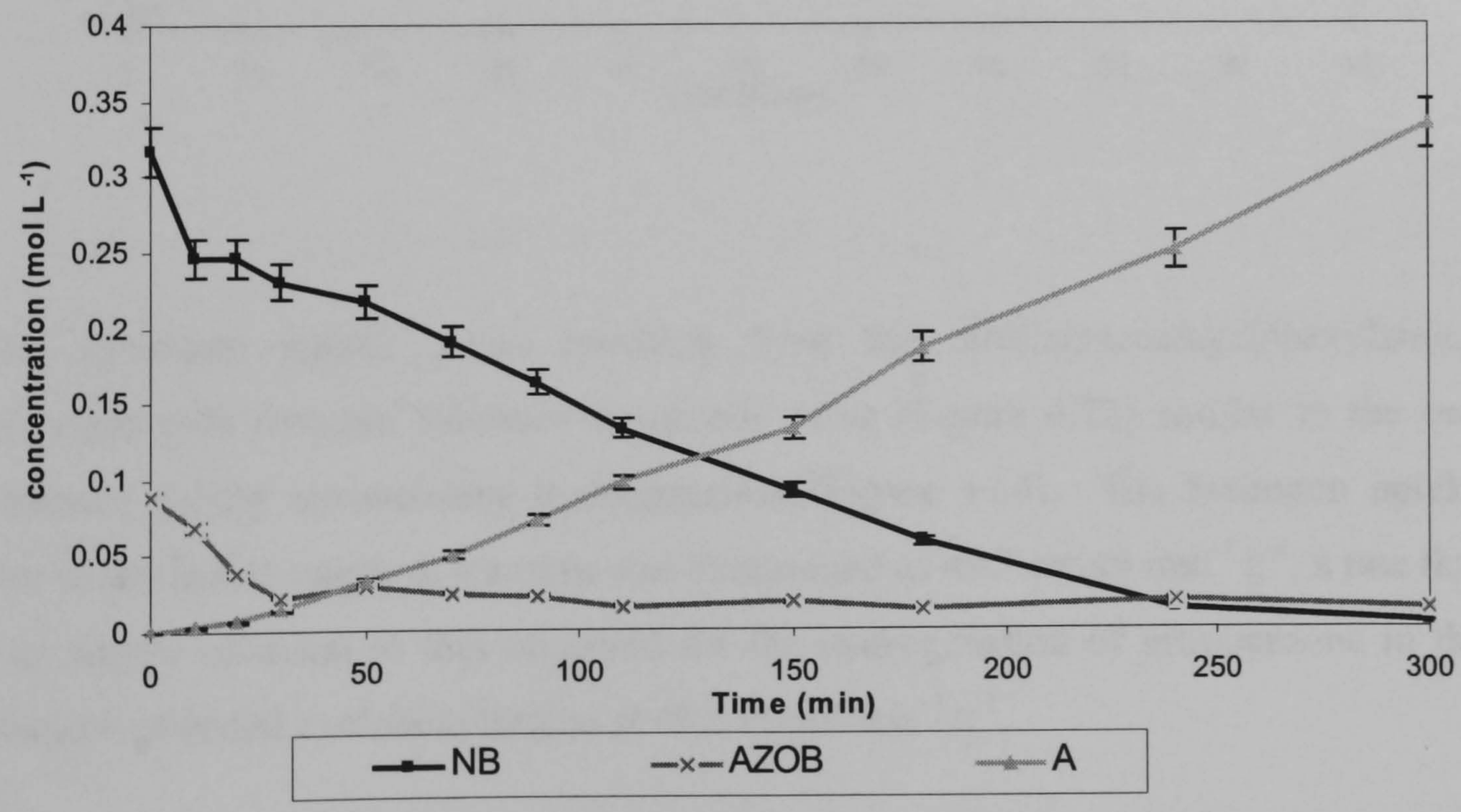

4.3.1.12.3 The Effect of Cyclohexylamine on the Hydrogenation of Nitrobenzene.

Figure 4.72 shows the data for the consumption of hydrogen throughout the hydrogenation of the nitrobenzene/cyclohexylamine reaction mixture. The reaction profile is displayed in Figure 4.73.

Figure 4.72: Hydrogen consumption during the hydrogenation of nitrobenzene/cyclohexylamine in methanol with catalyst Pd/CSXU.

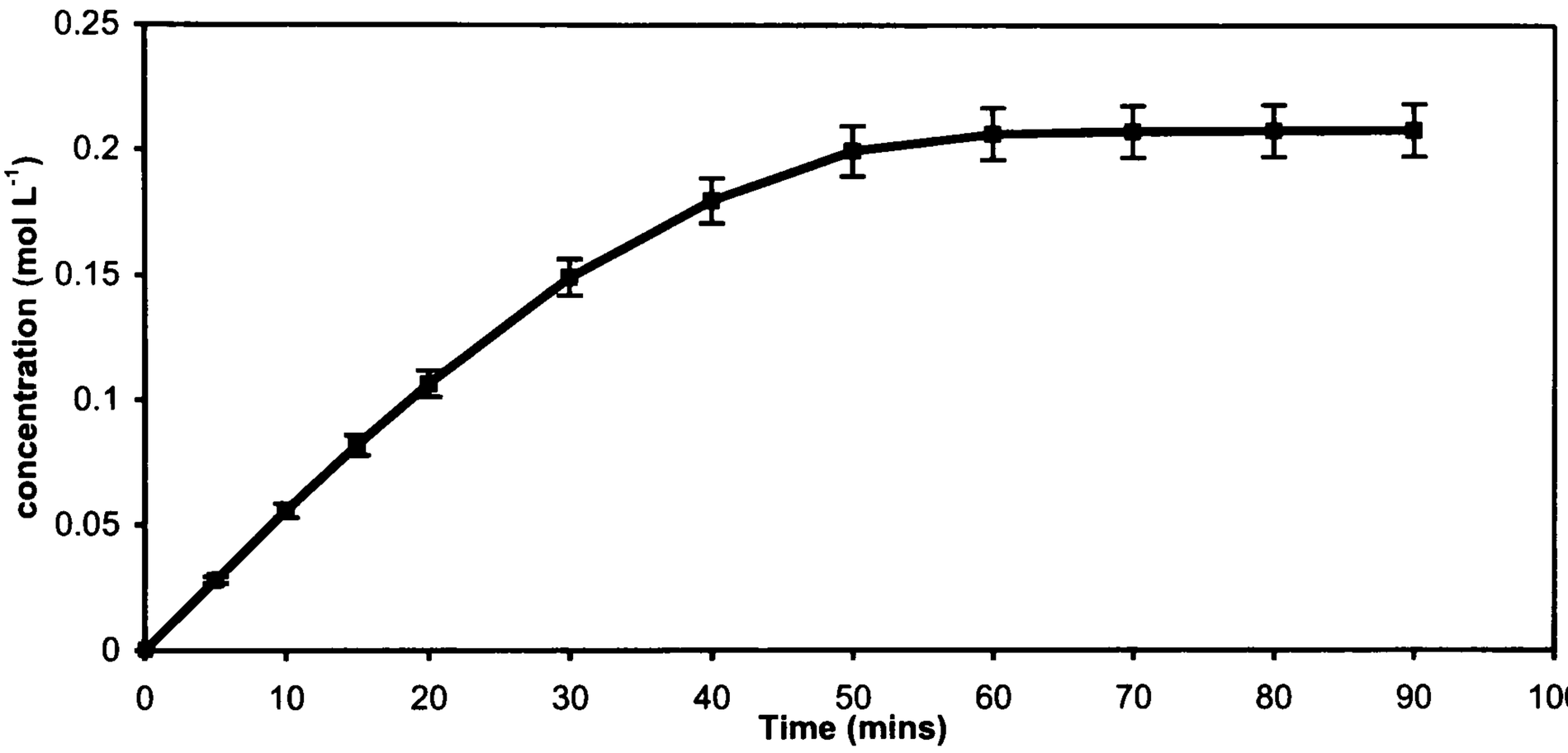

The hydrogen uptake graph resulting from the nitrobenzene/cyclohexylamine hydrogenation reaction followed a smooth curve (Figure 4.72) similar to the one obtained during nitrobenzene hydrogenation (Figure 4.64). The hydrogen uptake rate in the initial stages of reaction was determined as 49.7 mmol min^{-1} g^{-1}, a rate that was almost identical to that observed for the hydrogenation of nitrobenzene in the absence of added cyclohexylamine at 49.5 mmol min^{-1} g^{-1}.

Figure 4.73: Reaction Profile – the hydrogenation of nitrobenzene/cyclohexylamine in methanol using catalyst Pd/CSXU.

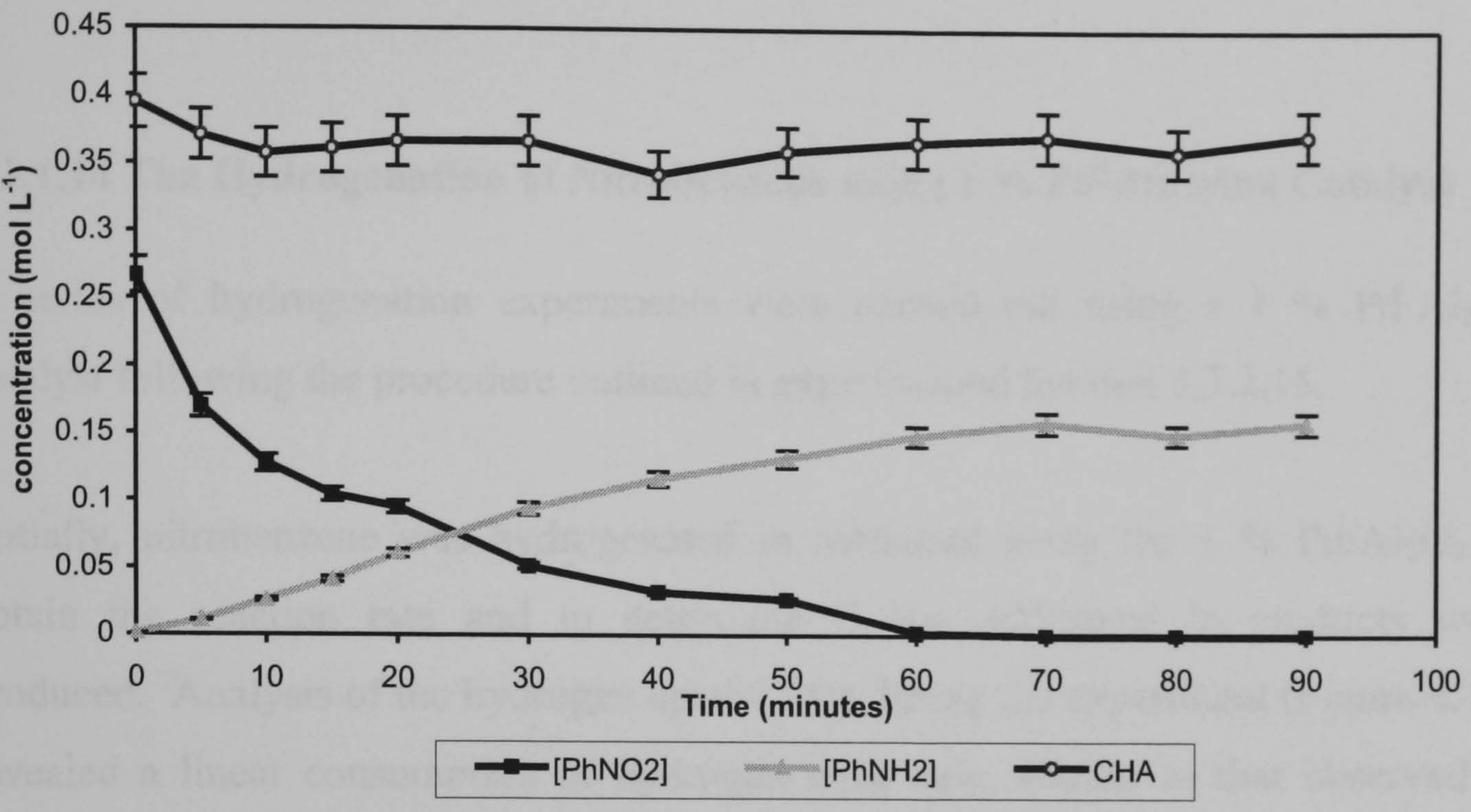

Figure 4.73 shows a reaction profile very similar to that for the hydrogenation of nitrobenzene. The concentration of nitrobenzene decreased as the aniline concentration increased, no other by-products were observed and the concentration of cyclohexylamine remained constant throughout the duration of the experiment.

Therefore, this experiment has shown that the presence of cyclohexylamine has no effect on the nitrobenzene hydrogenation reaction. It does not act as an inhibitor and appears to have no effect on the catalysis.

4.3.1.13 The Hydrogenation of Aniline

The hydrogenation of aniline was attempted using catalysts Pd/CN1, Pd/CA1 and Pd/CSXU under the conditions described in Section 3.3.2.13. In all three experiments no reaction was observed. The concentration of aniline remained unchanged throughout and no other species were observed in the reaction mixture showing that under our reaction conditions it was not favourable to begin

hydrogenation of the aromatic ring subsequent to the production of aniline and that the formation of cyclohexylamine was not occurring.

4.3.1.14 The Hydrogenation of Nitrobenzene using 1 % Pd/Alumina Catalyst

A series of hydrogenation experiments were carried out using a 1 % Pd/Al_2O_3 catalyst following the procedure outlined in experimental Section 3.3.2.15.

Initially, nitrobenzene was hydrogenated in methanol using the 1 % Pd/Al_2O_3 to obtain the reaction rate and to determine if any additional by-products were produced. Analysis of the hydrogen uptake data during the experiment (Figure 4.74) revealed a linear consumption of hydrogen with time, similar to that observed in previous nitrobenzene hydrogenations using Pd/C. The rate of hydrogenation was calculated at 13.7 mmol min^{-1} g^{-1}, decidedly slower than the rate of hydrogenation with catalyst Pd/CSXU under identical reaction conditions of 49.7 mmol min^{-1} g^{-1}. To take into account the differences in metal loading and palladium dispersions, a turnover frequency for each catalysts under these reaction conditions was calculated using Equation 4.5 (Section 4.3.1.1). The 1 % Pd/Al_2O_3 catalyst displayed a slightly higher frequency with a value of 469 min^{-1} compared to a value of 420 min^{-1} for the carbon supported catalyst, revealing the alumina supported catalyst was more efficient.

Figure 4.74: Hydrogen consumption during the hydrogenation of nitrobenzene in methanol using 1 % Pd/Al_2O_3 catalyst.

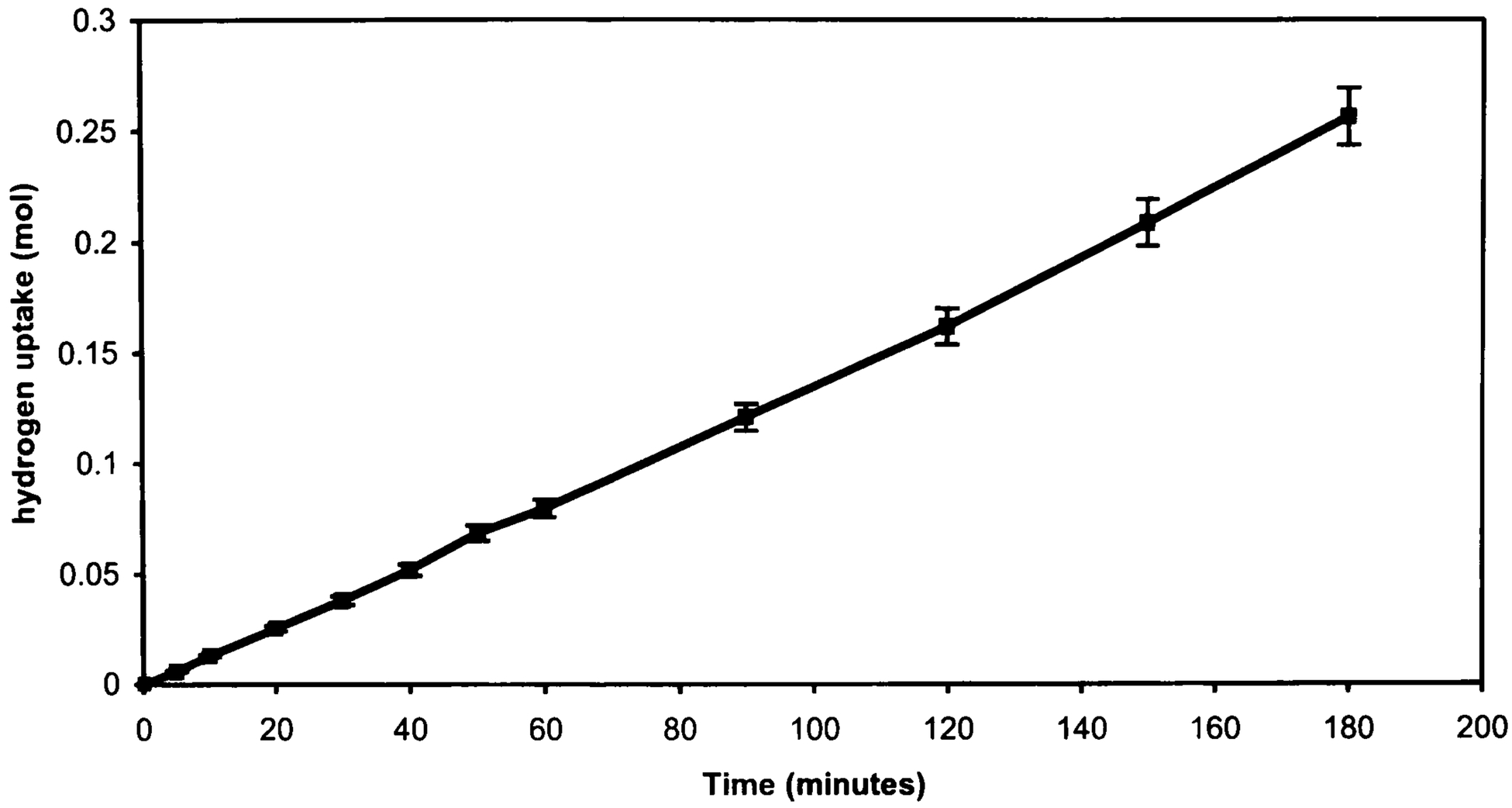

The reaction profile for this reaction is displayed in Figure 4.75. This is also similar to the reaction profiles obtained when using the Pd/C catalysts although there were low levels of two by-products, azobenzene and azoxybenzene, detected during the hydrogenation. This may have be a result of the slower rate of reaction allowing the formation of intermediates or by-products to be detected or due to an interaction arising from the change in support material.

Figure 4.75: Reaction Profile – the hydrogenation of nitrobenzene in methanol with 1 % Pd/Al_2O_3 catalyst

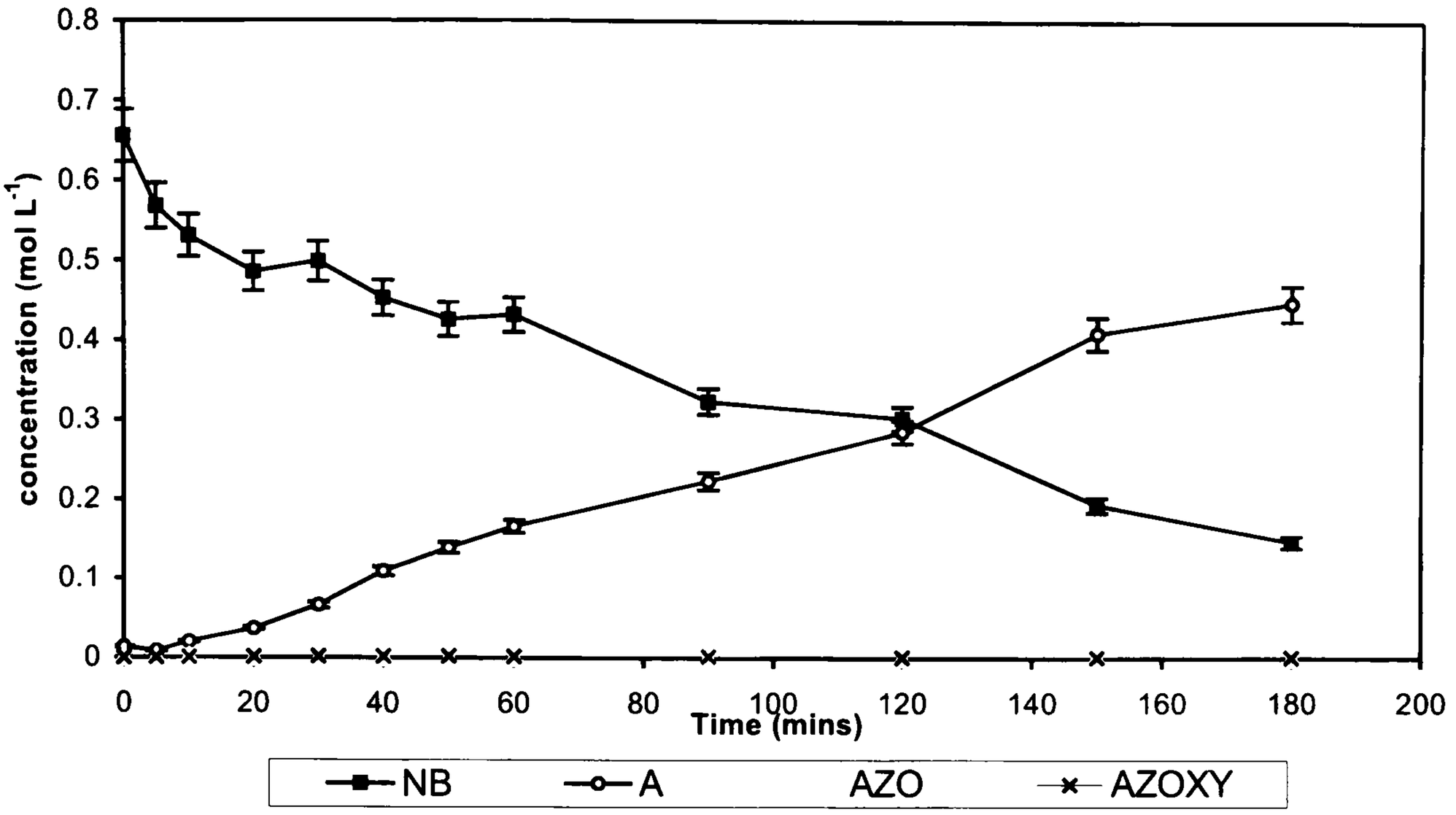

4.3.1.14.1 The Effect of Water on the Hydrogenation of Nitrobenzene using 1 % Pd/Al_2O_3.

The influence of additional water in the nitrobenzene reaction mixture was investigated in the same way as with catalyst Pd/CSXU, although this time only one experiment was carried out instead of two. The experimental results explained in Section 4.3.1.5.2 demonstrated that additional water in the reaction mixture had an inhibiting effect on the hydrogenation reaction only if it was introduced prior to the nitrobenzene. This same experiment was carried out using the Pd/Al_2O_3 catalyst to ascertain if water had a similar effect on this catalyst. The effect of increasing the water present was also investigated.

The hydrogen uptake curves for these experiments are shown in Figure 4.76. The reaction profiles for the two reactions are shown in Figures 4.77 and 4.78.

Figure 4.76: Hydrogen consumption during the hydrogenation of nitrobenzene in methanol with catalyst Pd/Al_2O_3 with added water.

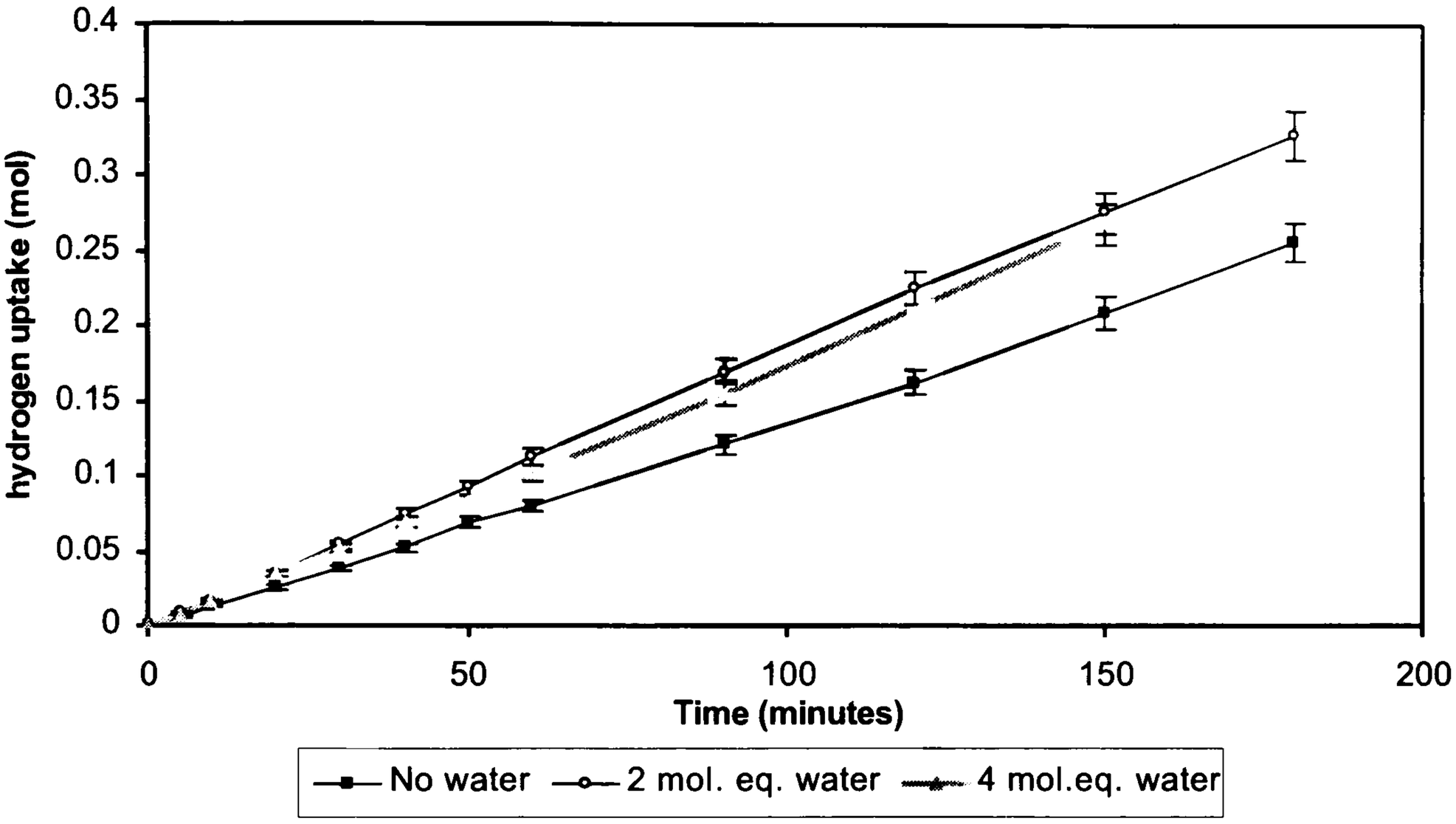

Figure 4.76 clearly shows that the addition of water to the nitrobenzene reaction mixture resulted in an increased rate of hydrogen consumption throughout the reaction. The rate increased from 13.7 mmol min^{-1} g^{-1} to 18.9 mmol min^{-1} g^{-1} when two mole equivalents of water were present and to 17.0 mmol min^{-1} g^{-1} when four mole equivalents of water were present. This promotional effect is the opposite to that expected considering the presence of water was found to have a negative effect on the reaction rate when a palladium carbon catalyst was used in the reaction. The promotional effect did not increase when the number of moles of water added was doubled to 4 mole equivalents.

Figure 4.77: Reaction profile – the hydrogenation of nitrobenzene in methanol with 1 % Pd/Al_2O_3 catalyst with 2 mole equivalents of water

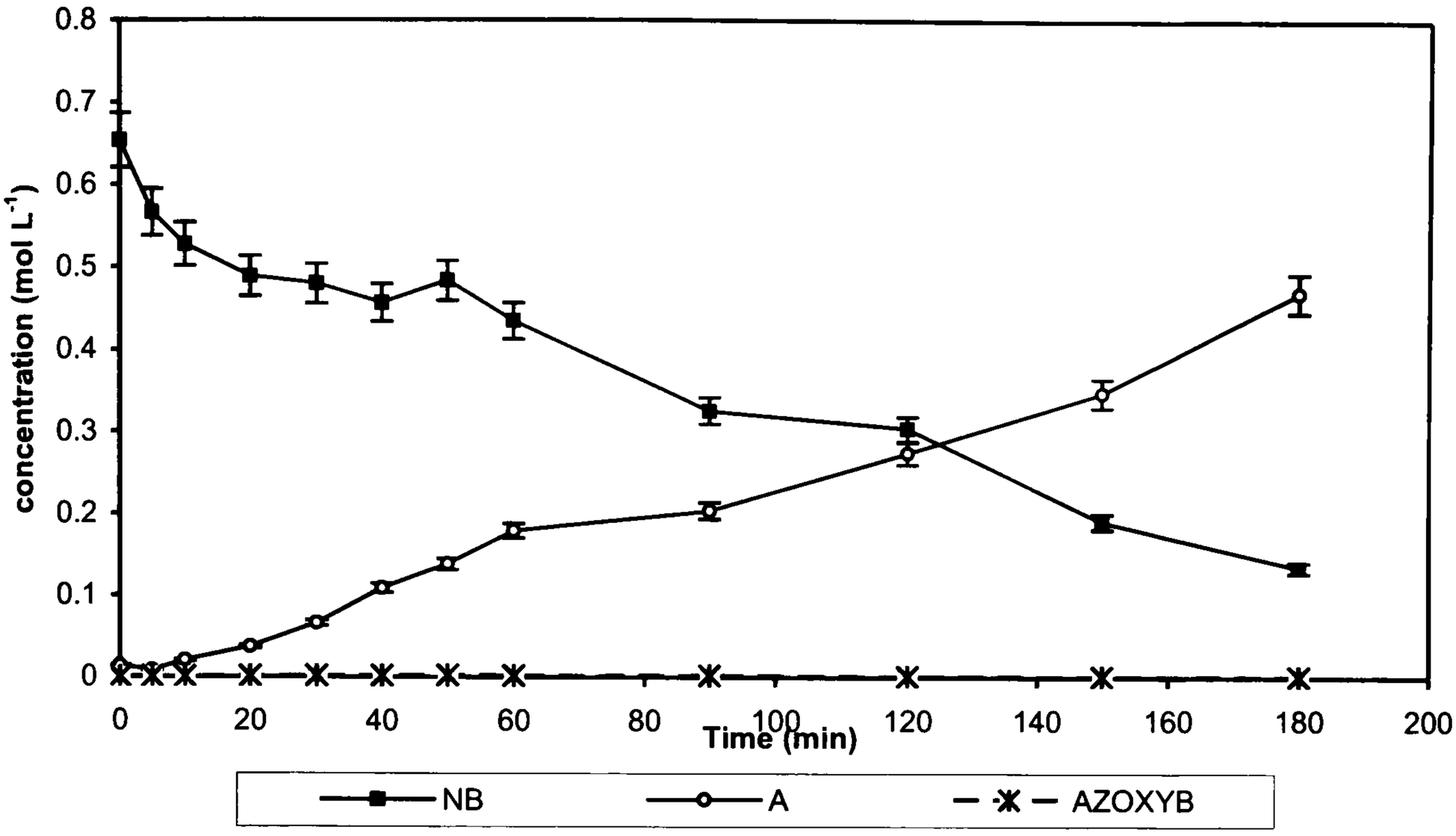

Figure 4.78: Reaction Profile – the hydrogenation of nitrobenzene in methanol with 1 % Pd/Al_2O_3 catalyst with 4 mole equivalents of water

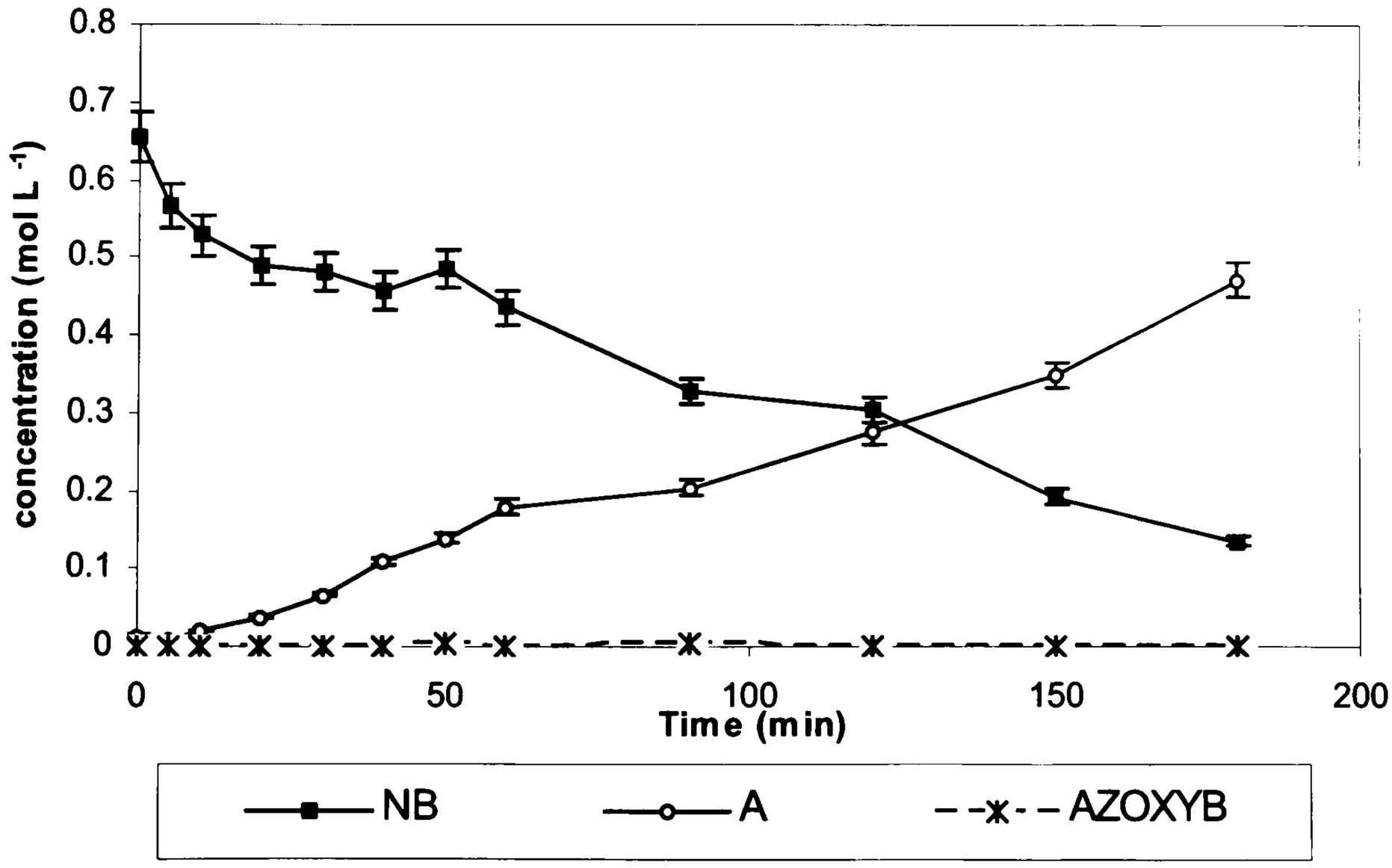

4.3.1.14.2 The Effect of Aniline on the Hydrogenation of Nitrobenzene using 1 % Pd/Al_2O_3.

The effect of aniline on the hydrogenation of nitrobenzene using the alumina supported palladium catalyst was determined by performing the hydrogenation reaction in the presence of 1 mole equivalent of aniline in the same way as reported in Section 4.3.1.5.1. The hydrogen uptake data are displayed in Figure 4.79 and the GC analysis in Figure 4.80.

Figure 4.79: Hydrogen consumption during the hydrogenation of nitrobenzene in methanol with 1 % Pd/C catalyst and one mole equivalent of aniline.

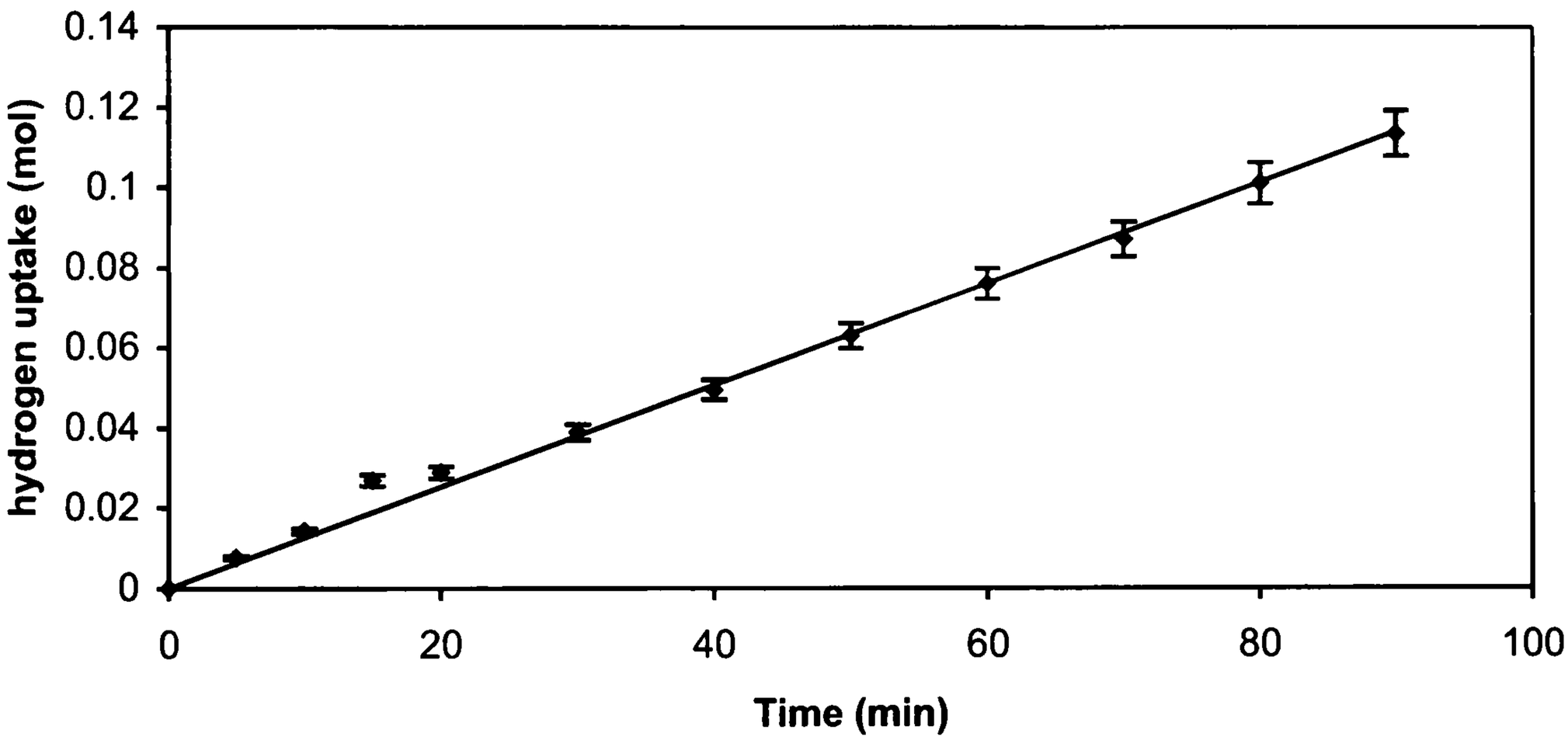

Figure 4.80: Reaction Profile – the hydrogenation of nitrobenzene in methanol with 1 % Pd/Al_2O_3 catalyst and one mole equivalent of aniline added.

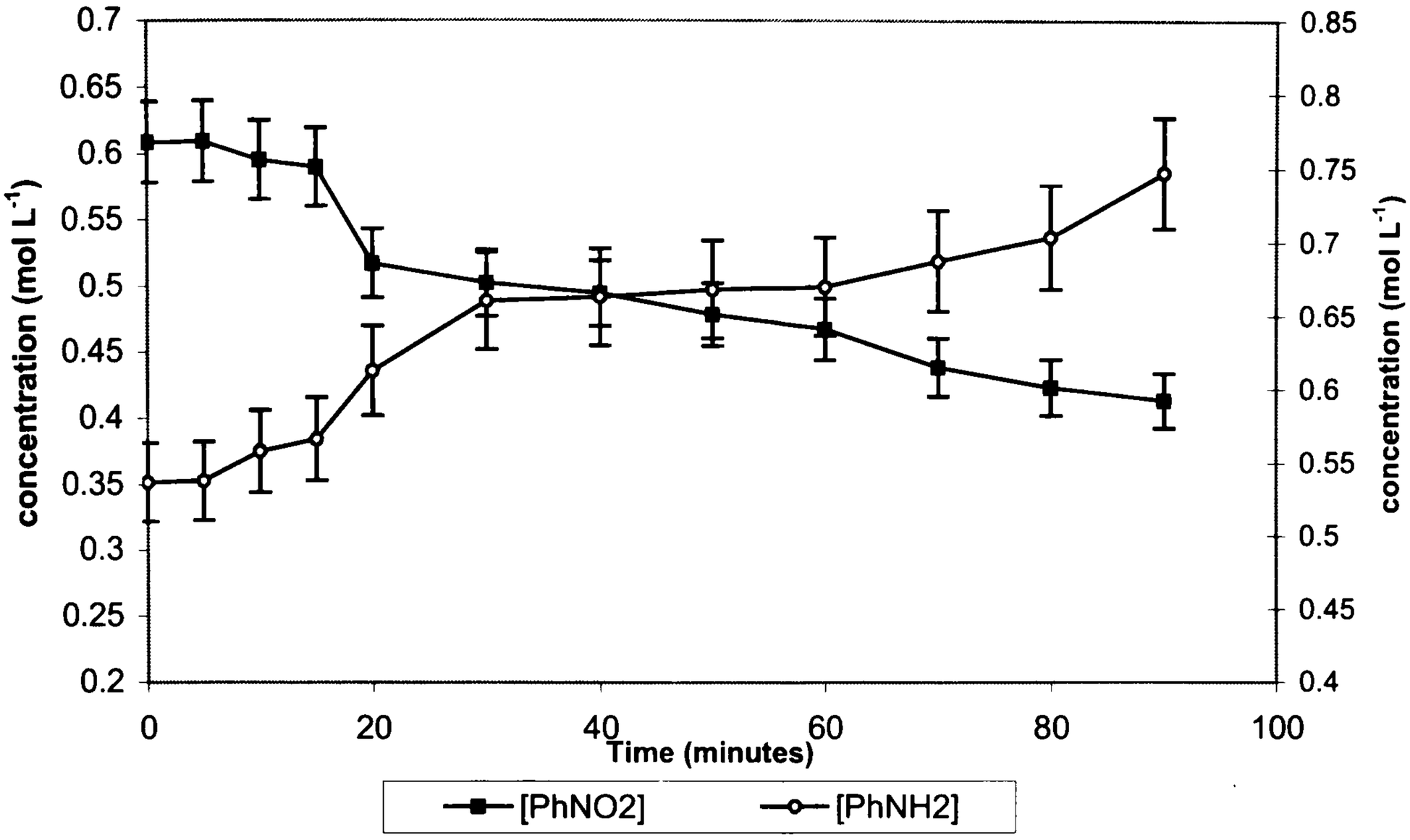

The hydrogen uptake curve shown in Figure 4.79 displays a linear uptake of hydrogen as expected from previous analyses. The rate of hydrogenation was calculated as 12.6 mmol min^{-1} g^{-1}, which was slightly slower than the rate of hydrogenation in the absence of aniline at 13.7 mmol min^{-1} g^{-1}. The reaction profile (Figure 4.80) was almost identical to those previously reported for this catalyst.

4.3.1.14.3 The Effect of Cyclohexylamine on the Hydrogenation of Nitrobenzene using 1 % Pd/Al_2O_3 Catalyst

The effect of adding 1 mole equivalent of cyclohexylamine to the nitrobenzene reaction mechanism was investigated following the procedure outlined in Section 3.3.2.12. The hydrogen uptake data are shown in Figure 4.81 and the GC reaction profile in Figure 4.82.

Figure 4.81: Hydrogen consumption during the hydrogenation of nitrobenzene in methanol with 1 % Pd/Al_2O_3 catalyst and one mole equivalent of cyclohexylamine.

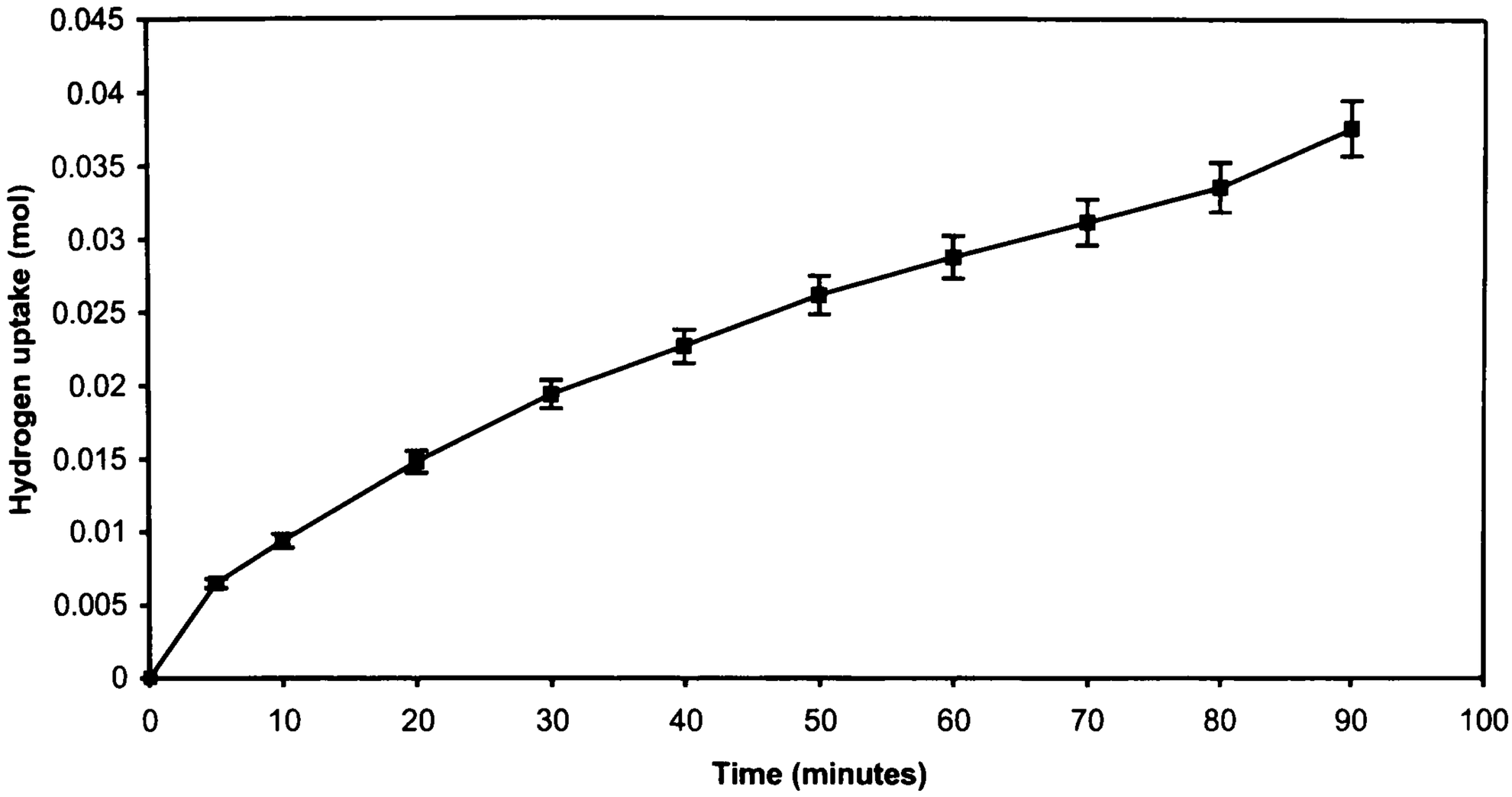

Figure 4.82: Reaction Profile – the hydrogenation of nitrobenzene in methanol with 1 % Pd/Al_2O_3 catalyst and one mole equivalent of cyclohexylamine.

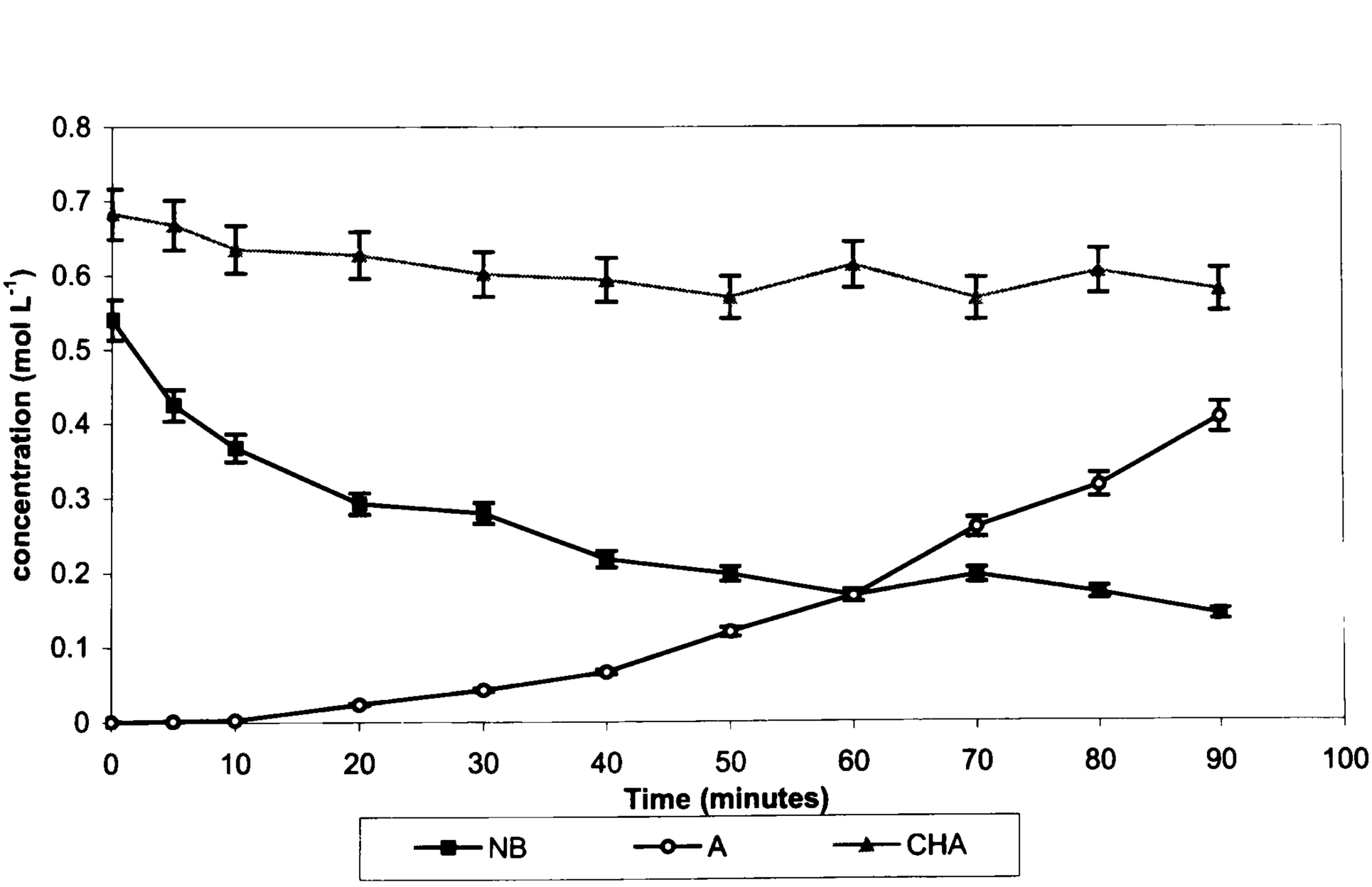

The rate of hydrogenation calculated from the hydrogen uptake curve displayed in Figure 4.81 was 6.5 mmol min^{-1} g^{-1}, which is considerably slower than that observed during the hydrogenation of nitrobenzene on its own at 13.7 mmol min^{-1} g^{-1}. The reaction profile, Figure 4.82, showed that the concentration of cyclohexylamine remained relatively constant throughout the experimental.

4.3.1.14.4 Summary of the Effect of Aniline and Cyclohexylamine on the Nitrobenzene Hydrogenation Reaction.

A summary of the effect on the hydrogen uptake of adding aniline and cyclohexylaime to the reaction mixture is shown in Figure 4.83.

Figure 4.83: Hydrogen consumption during the hydrogenation of nitrobenzene in methanol with 1 % Pd/Al_2O_3 catalyst in the presence of cyclohexylamine (CHA) and aniline.

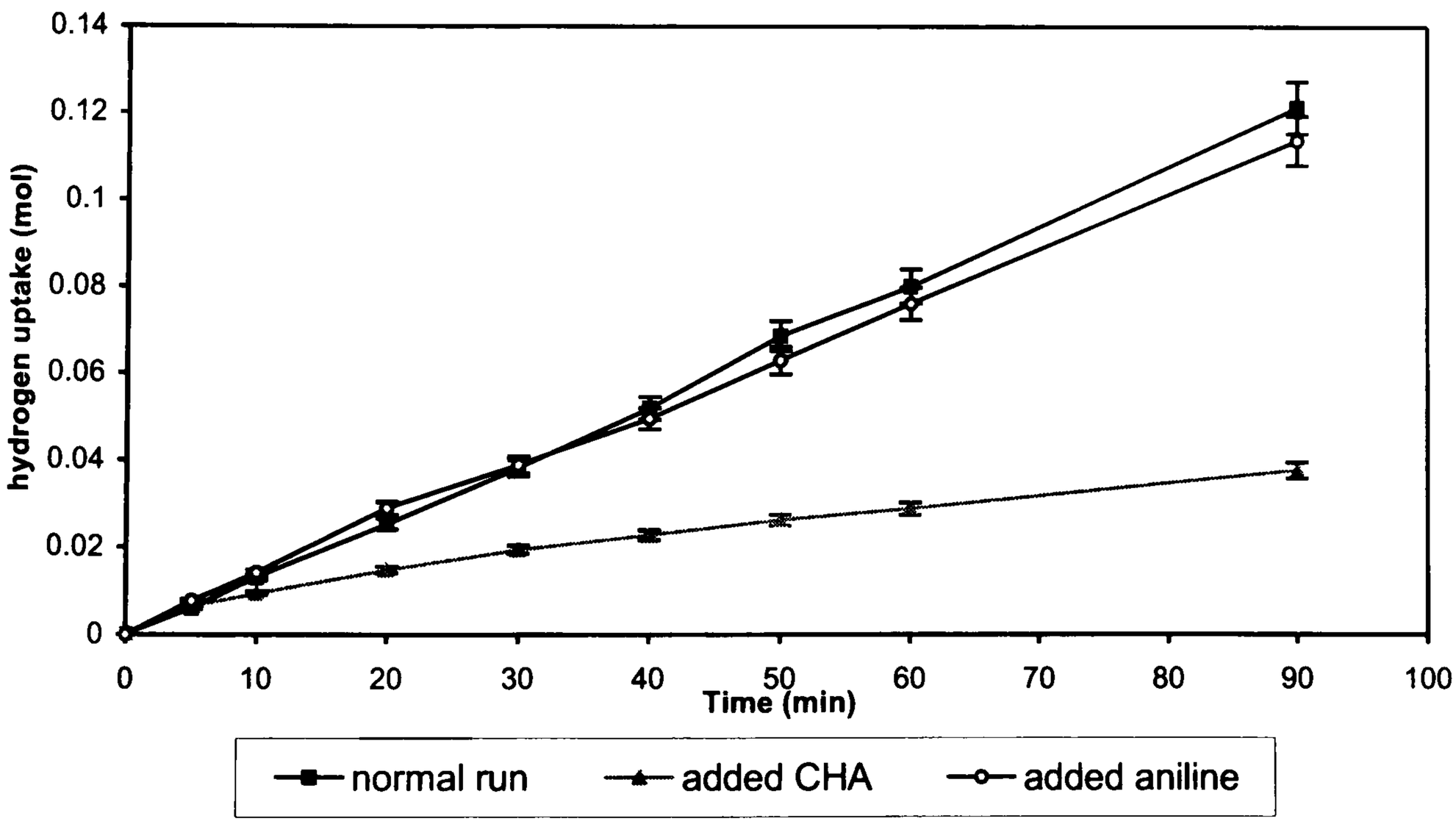

4.3.2 The Hydrogenation of Nitrobenzene, Nitrosobenzene and Azobenzene using Raney Catalysts

Raney nickel was utilised in the hydrogenation of nitrobenzene, nitrosobenzene and azobenzene following the procedure outlined in Experimental Section 3.3.3.2. The experiments were followed using GC-MS analysis.

4.3.2.1 The Hydrogenation of Nitrobenzene, Nitrosobenzene and Azobenzene using Raney Nickel

The reaction profiles for the hydrogenation of Nitrobenzene, Nitrosobenzene and Azobenzene are displayed in Figures 4.84, 4.85 and 4.86 respectively.

The rate of formation of the products from the reaction profiles have been calculated in the same way as previously described in Equation 4.7, section 4.3.1.12. However, in these experiments the rates have not been corrected per gram of catalyst. This is because the Raney catalysts were purchased as activated slurry catalysts and used in this wet form without further activation. As a result the precise mass of active metal used in each reaction could not be calculated accurately because of the unknown water content and mass of residual aluminium in the slurry aliquots. This is a common problem when working with Raney catalyst slurries [177]. Therefore, rates have been expressed as mmol min^{-1} throughout this section and can be compared with each other as an equal weight of slurry was used in each experiment, but not with the reaction rates in other sections of this thesis.

Figure 4.84: Reaction Profile – the Hydrogenation of Nitrobenzene with Raney Nickel.

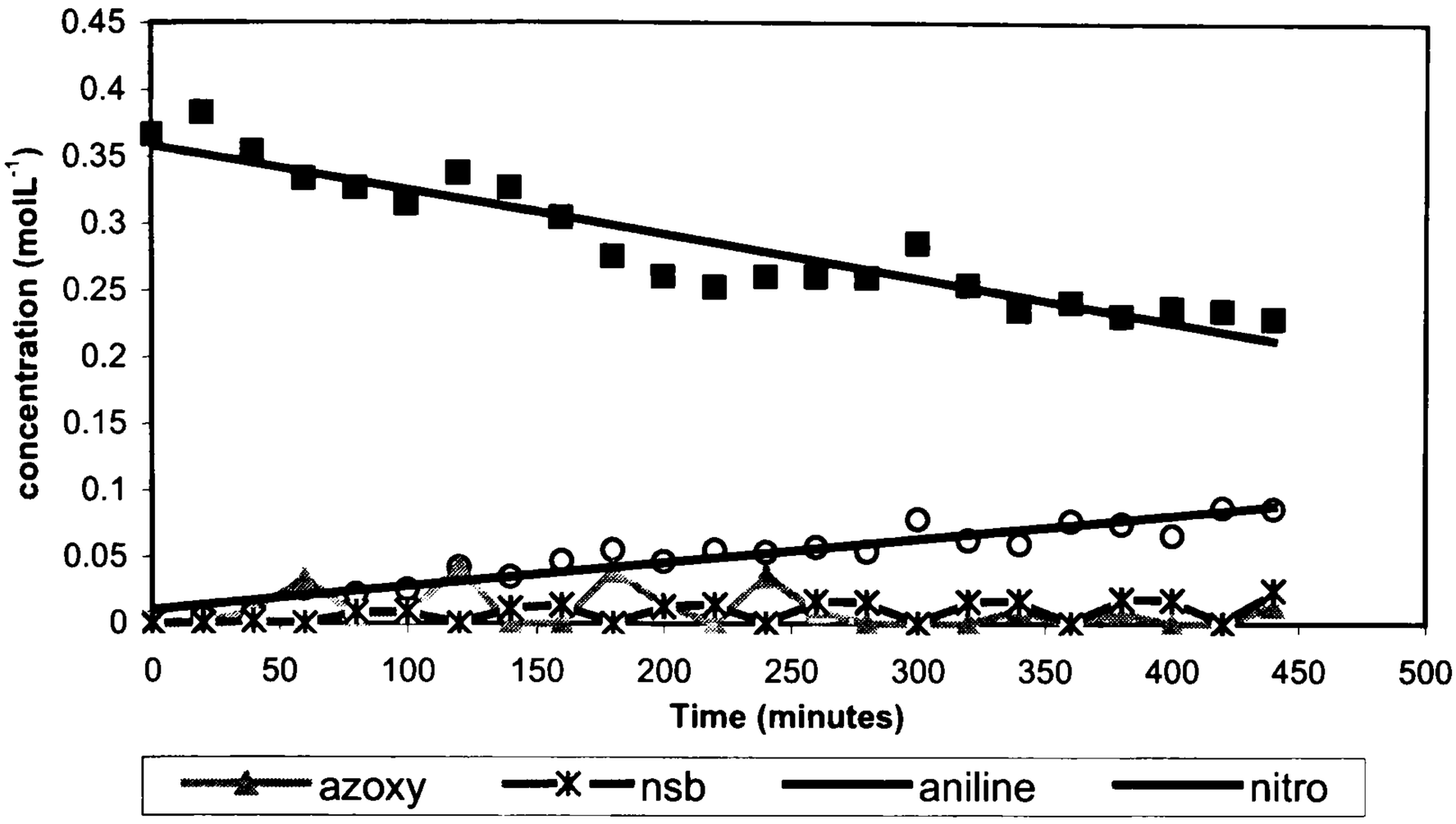

As shown in Figure 4.84, the reaction profile for the hydrogenation of nitrobenzene using Raney nickel displayed three products; aniline, azoxybenzene and nitrosobenzene. Azoxybenzene has been previously identified during catalysis with the palladium/carbon catalyst but this was the first experiment to show the presence of nitrosobenzene in the reaction mixture. The rate of reaction was very much slower than in previous hydrogenation experiments and was probably because reactions were performed under atmospheric pressure only. The rate of aniline production was calculated from the graph as 0.07 mmol min^{-1} and displayed a linear production throughout. The production of nitrosobenzene and azoxybenzene did not follow a linear relationship but levels fluctuated over time. Although only present in low concentrations, the quantity of azobenzene present was substantially greater than that observed during previous hydrogenation of nitrobenzene with palladium/carbon and palladium/alumina catalysts. At its maximum concentration after 440 minutes of reaction time the concentration reached 25.0 mol L^{-1}, which was 7 % of the reaction solution. At its maximum concentration at 180 minutes reaction time, the nitrosobenzene concentration was 40.0 mol L^{-1}, which was 10.7 % of the reaction solution.

Figure 4.85: Reaction Profile – the hydrogenation of nitrosobenzene with Raney nickel.

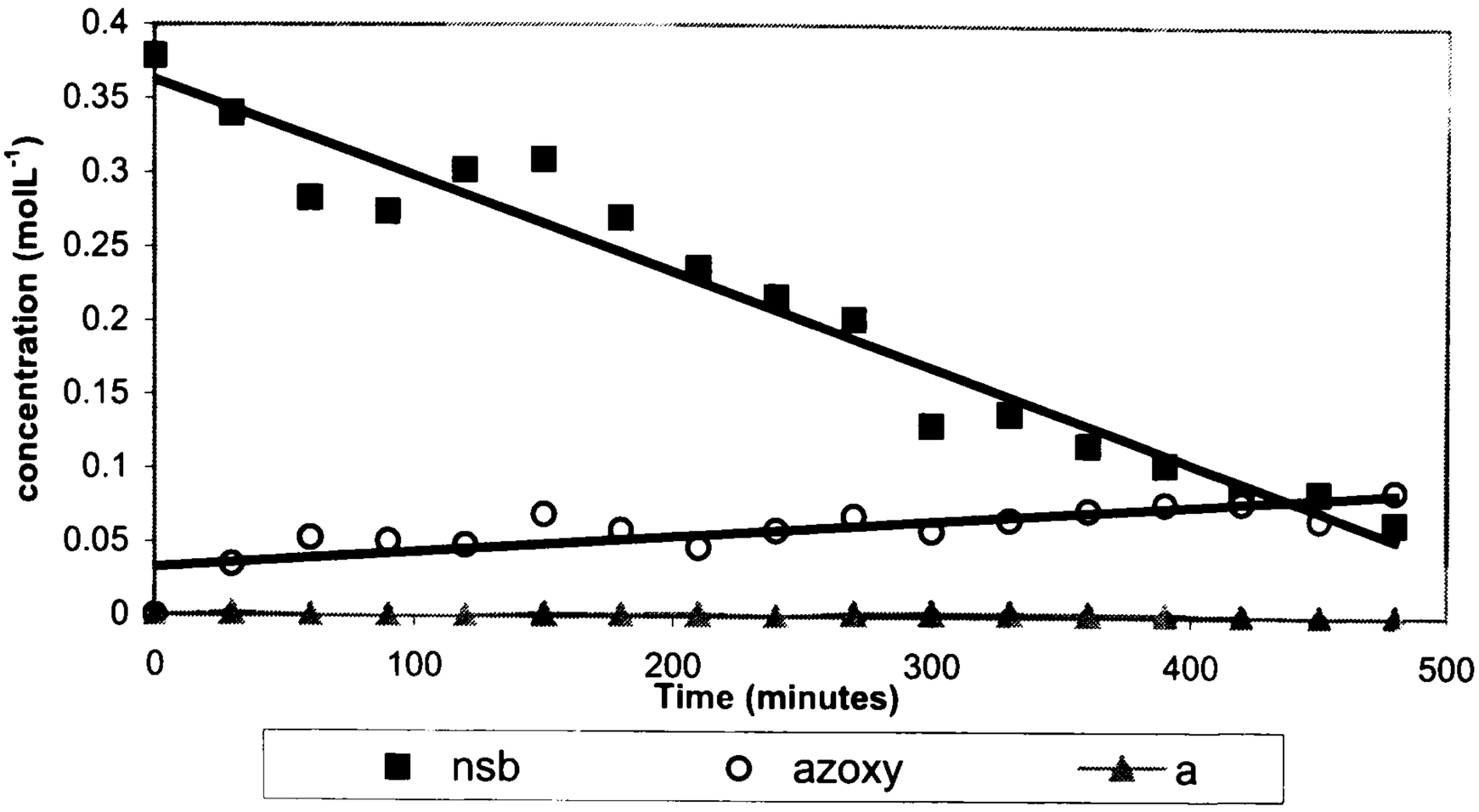

The hydrogenation of nitrosobenzene (Figure 4.85) shows a very different profile to that obtained for nitrobenzene. The nitrosobenzene reacted to produce azoxybenzene with aniline only produced at very low levels. The rate of azoxybenzene production was calculated as 0.07 mmol min^{-1}, similar to the production of aniline from nitrobenzene at 0.07 mmol min^{-1}. The concentration of the aniline reached its maximum of 2.4 mmol L^{-1} after 330 minutes of reaction time and accounted for only 1.2 % of the reagents in solution. Therefore, it can be deduced that the hydrogenation of nitrosobenzene with Raney nickel leads to the formation of azoxybenzene which accumulated in solution and was not hydrogenated further to aniline to any appreciable extent.

It is also clear from comparison of Figures 4.84 and 4.85 that nitrobenzene and nitrosobenzene show entirely different hydrogenation behaviour and it is not possible for nitrosobenzene to act as an intermediate in nitrobenzene hydrogenation with Raney nickel.

Figure 4.86: Reaction Profile – the Hydrogenation of Azobenzene with Raney nickel

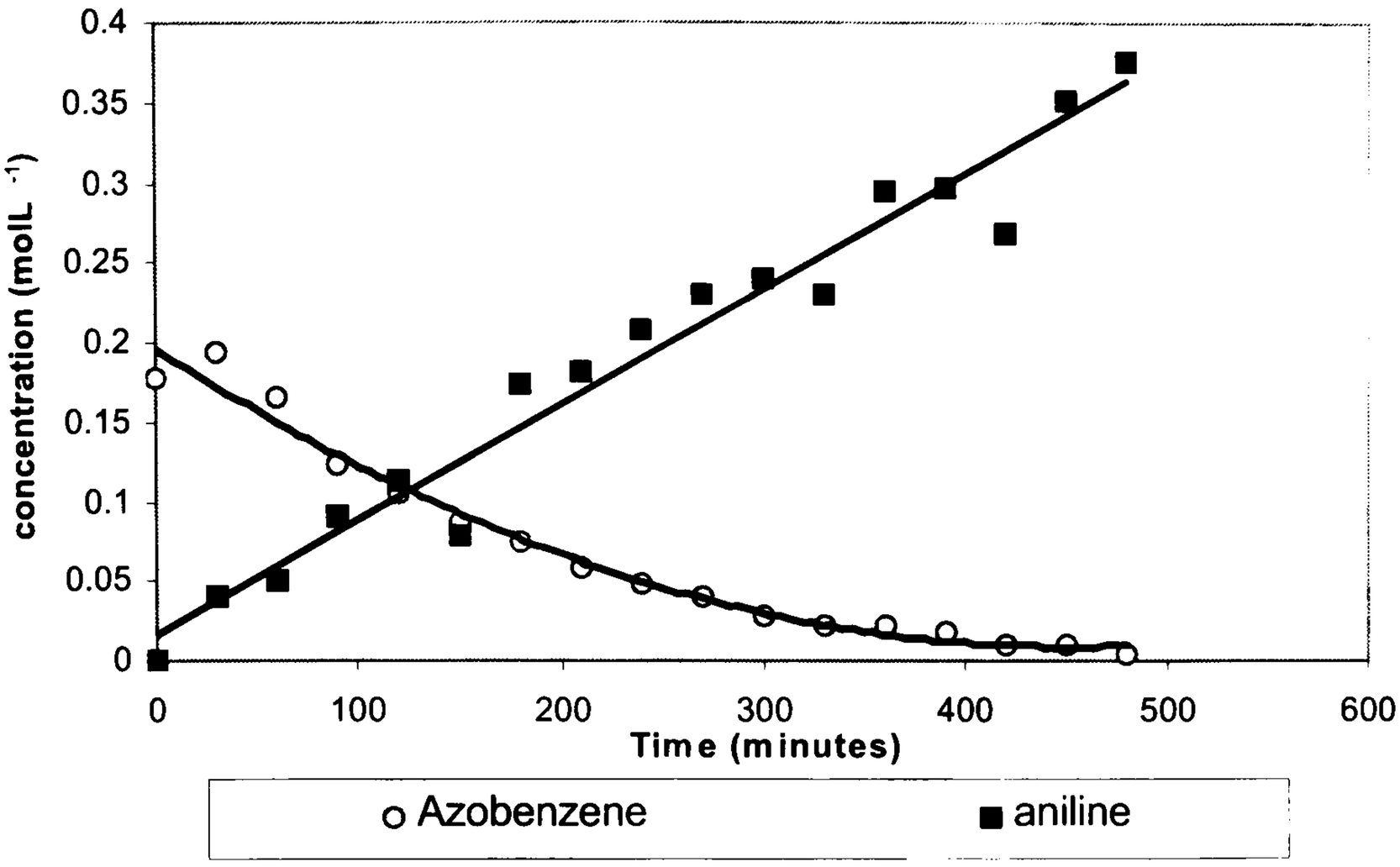

The hydrogenation of azobenzene with Raney nickel produced aniline with the generation of no other by-products or intermediate species. The reaction profile shown in Figure 4.86 is similar to the one obtained from the hydrogenation of azobenzene with catalyst Pd/CSXU and shown in Figure 4.61, Section 4.3.1.10. The rate of aniline production was calculated from Figure 4.86 as 0.7 mmol min^{-1}.

4.3.3 Nitrobenzene Hydrogenation over HDC Catalysts

4.3.3.1 Hydrogenation using Nitrobenzene Feed

A total of fifteen catalysts and the Puralox alumina support were used for the hydrogenation of nitrobenzene in the microreactor as described in Section 3.3.4.6 of the experimental section. Nitrobenzene was used as the inlet feed. Samples were removed from the reactor at 1 hour intervals and an exit analysis carried out. Each sample was analysed using GC-MS to identify and quantify each component. In the following sections the total number of moles present in each sample was normalised

to 100 %, and the contribution of each component in the feed stream expressed as a percentage of the total according to the relationship displayed in Equation 4.7. The data in the following sections have been presented graphically as the percentage composition of the samples at each point in time to give a representation of the product distribution in the feed stream as the reaction progressed. During the early stages of hydrogenation, delays in the time the feed took to pass over the catalyst bed were sometimes experienced; leading to varying volumes of sample collected each hour, often much lower than expected. Towards the end of each catalytic run, the volume of sample obtained began to increase towards that expected from inlet rate and become more stable suggesting a more consistent performance could have been achieved if the reactions were left for a longer period of time. However, all catalysts tested displayed a loss in catalytic activity throughout the duration of the experiment and sampling was required in the early stages to ensure the reaction was monitored when the catalysts were most active.

$$\text{Percentage composition of component I} = \frac{Pi}{\Sigma P_{(1\text{-}I)}} \times 100 \qquad \text{Equation 4.7}$$

4.3.3.1.1 HDC Catalysts and Nitrobenzene Feed

The exit analyses of the twelve HDC catalysts and the alumina support are shown in Figures 4.87-4.99.

Figure 4.87: The hydrogenation of nitrobenzene with 20 % Ni/Al_2O_3

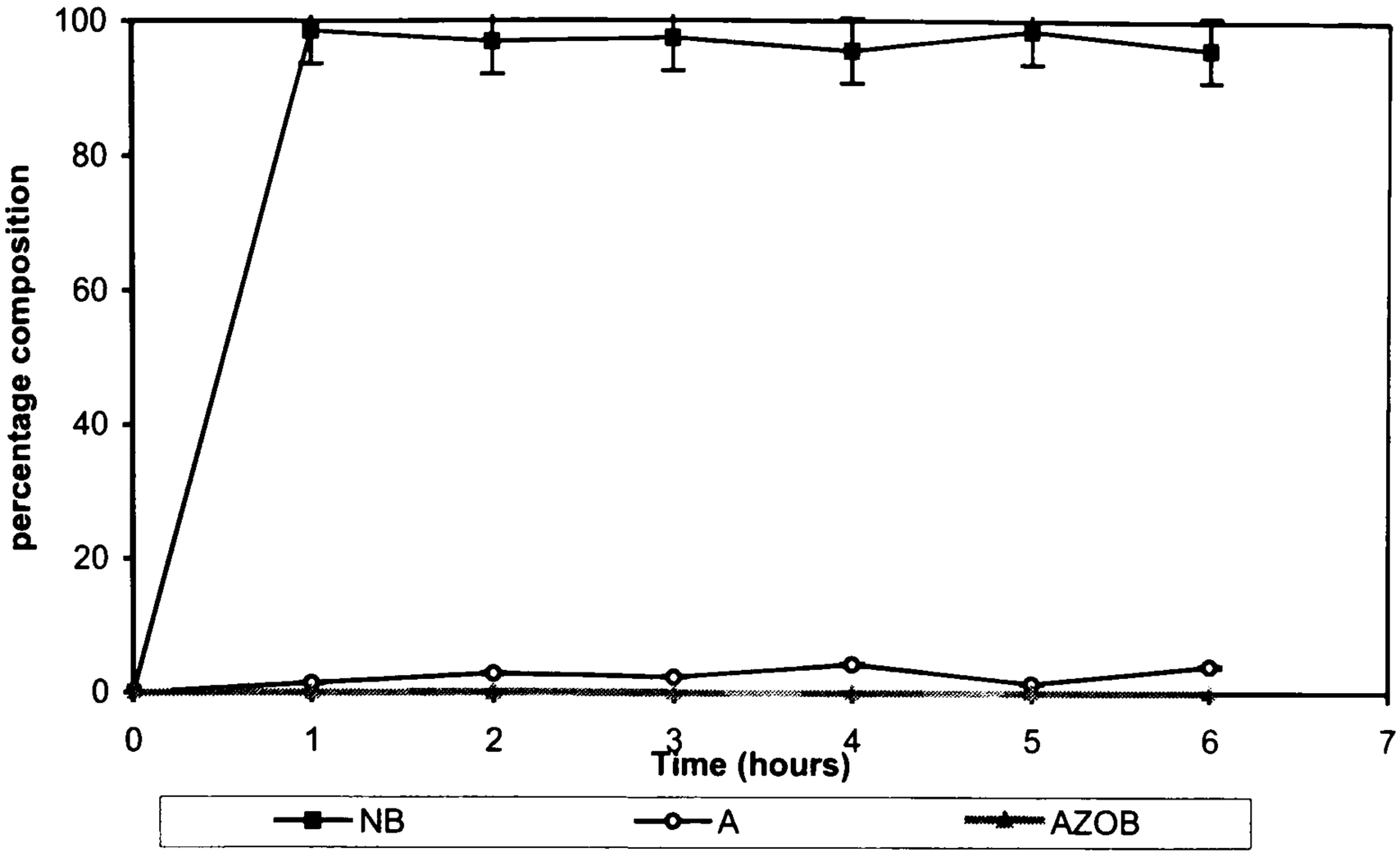

Figure 4.88: The hydrogenation of nitrobenzene with 20 % Cu/Al_2O_3

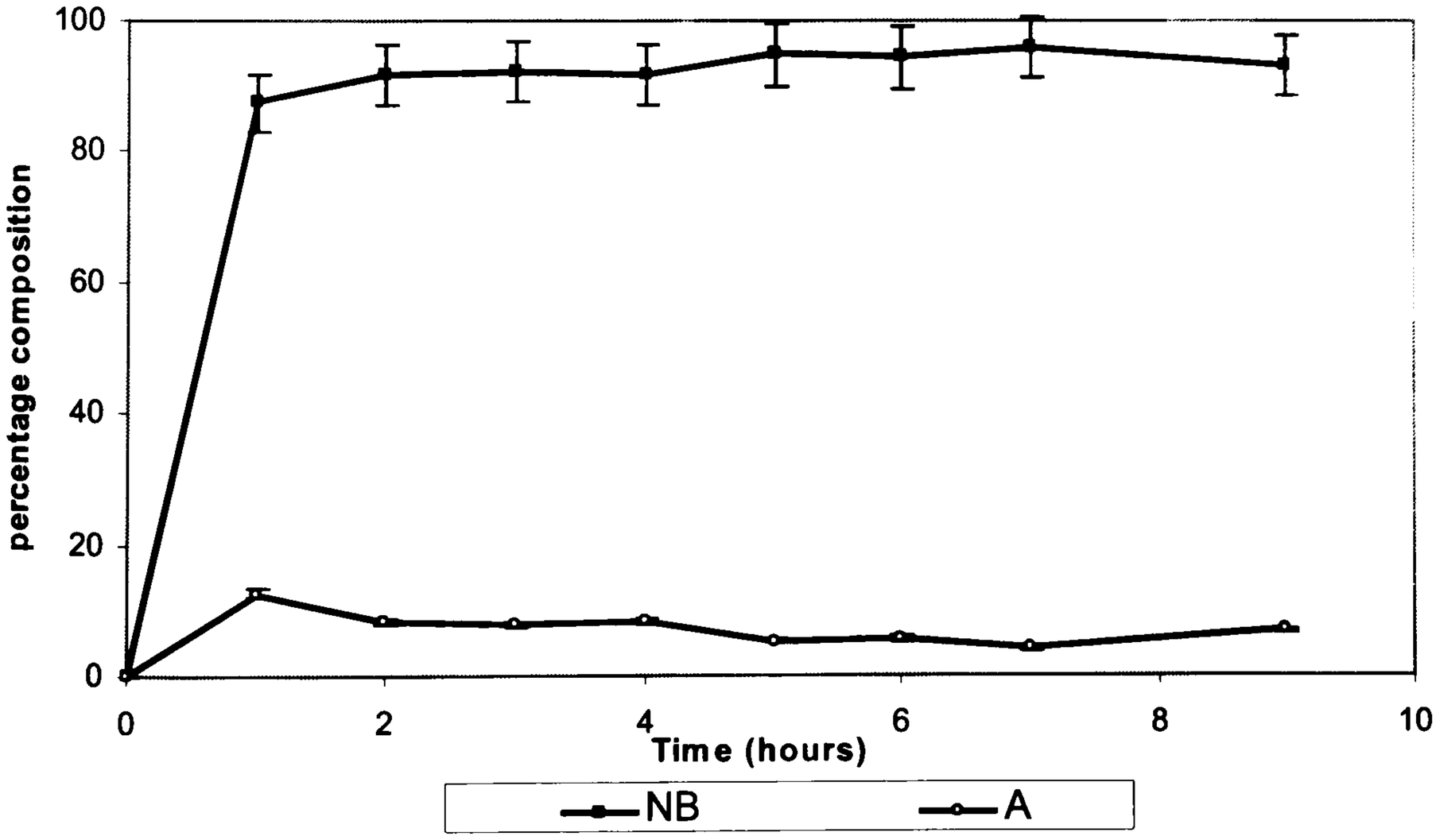

Figure 4.89: The hydrogenation of nitrobenzene with 20 % Co/Al_2O_3

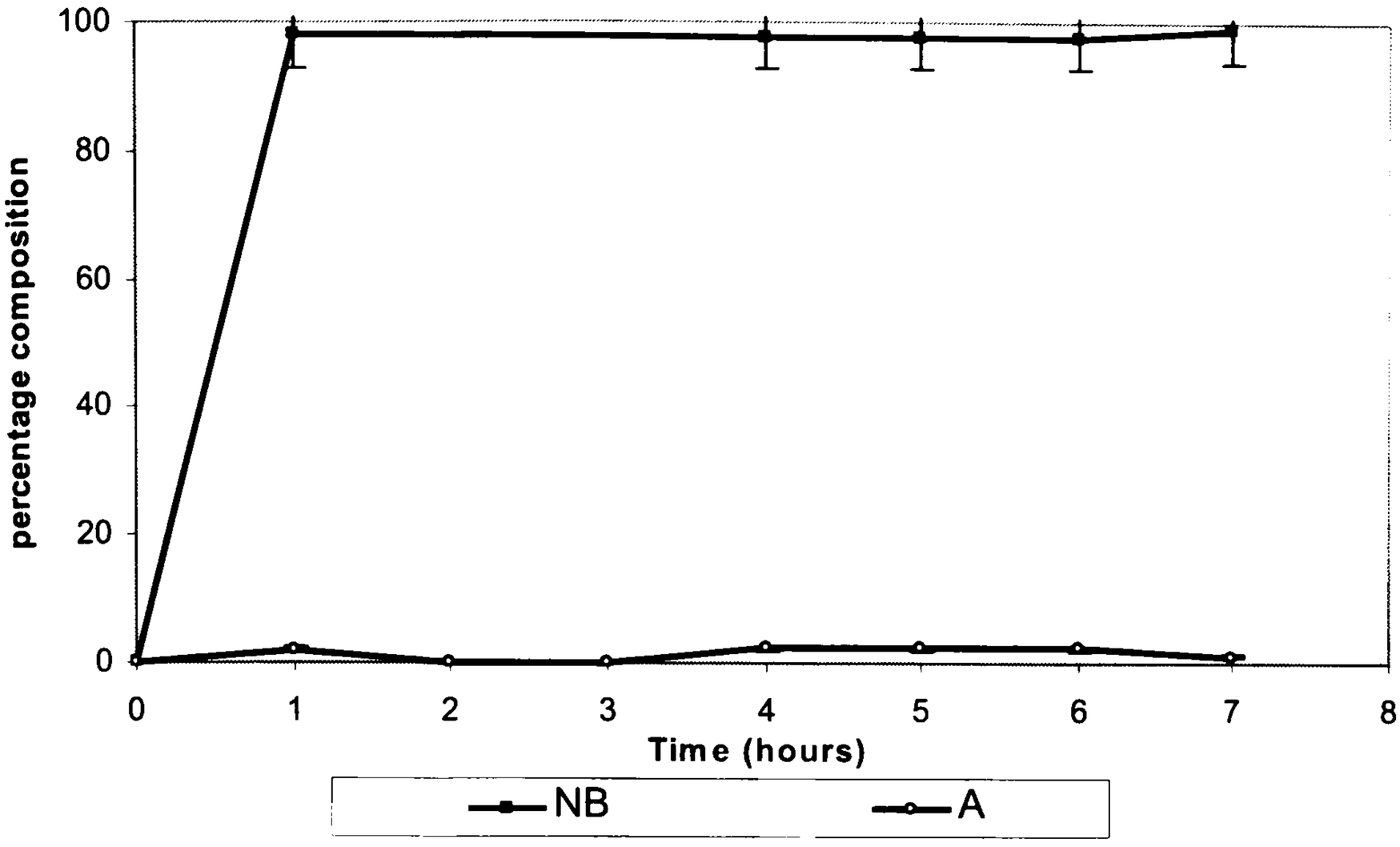

Figure 4.90: The hydrogenation of nitrobenzene with 15 % Ni/5 % Cu/Al_2O_3

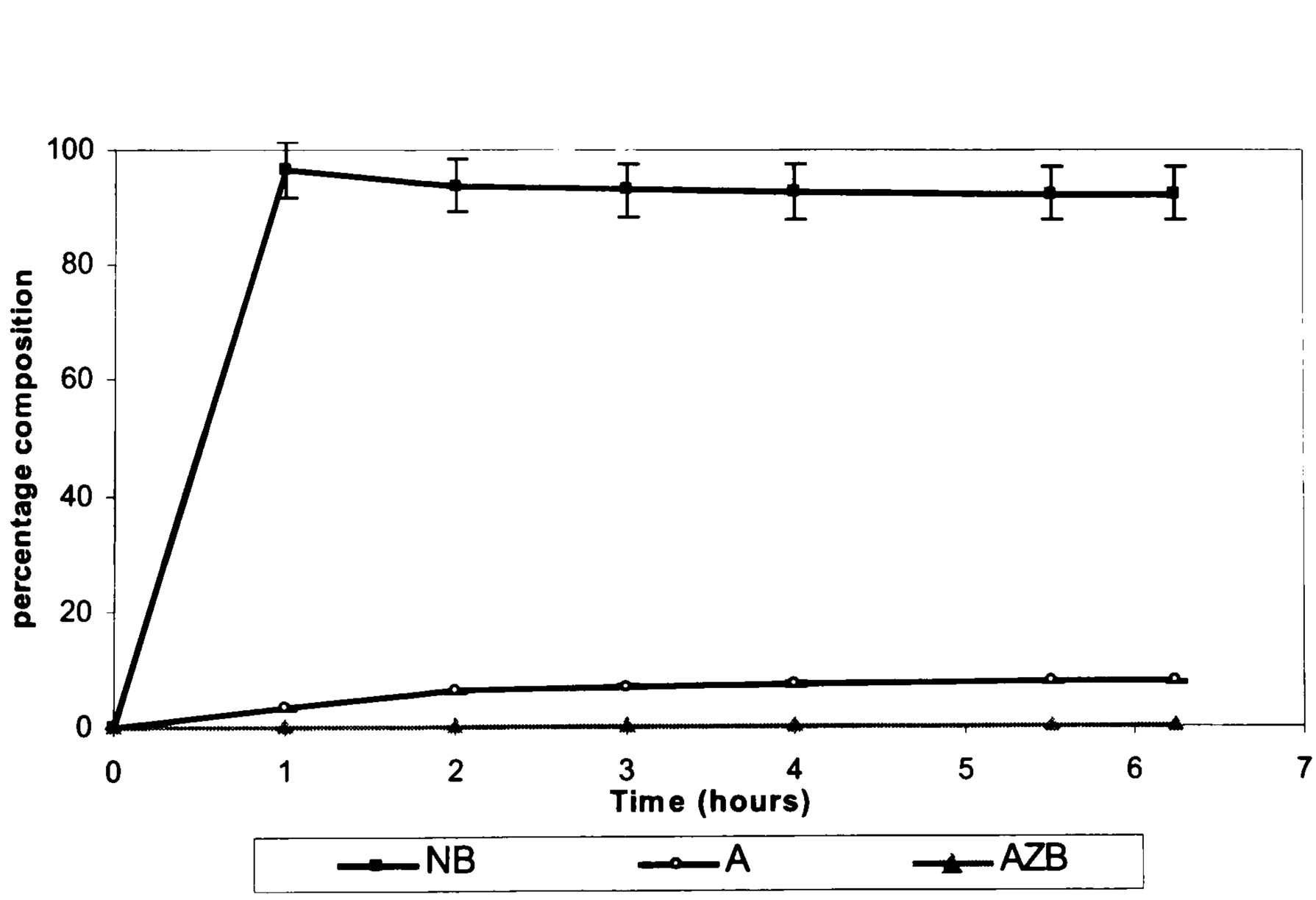

Figure 4.91: The hydrogenation of nitrobenzene using 10 % Ni/10 % Cu/Al_2O_3

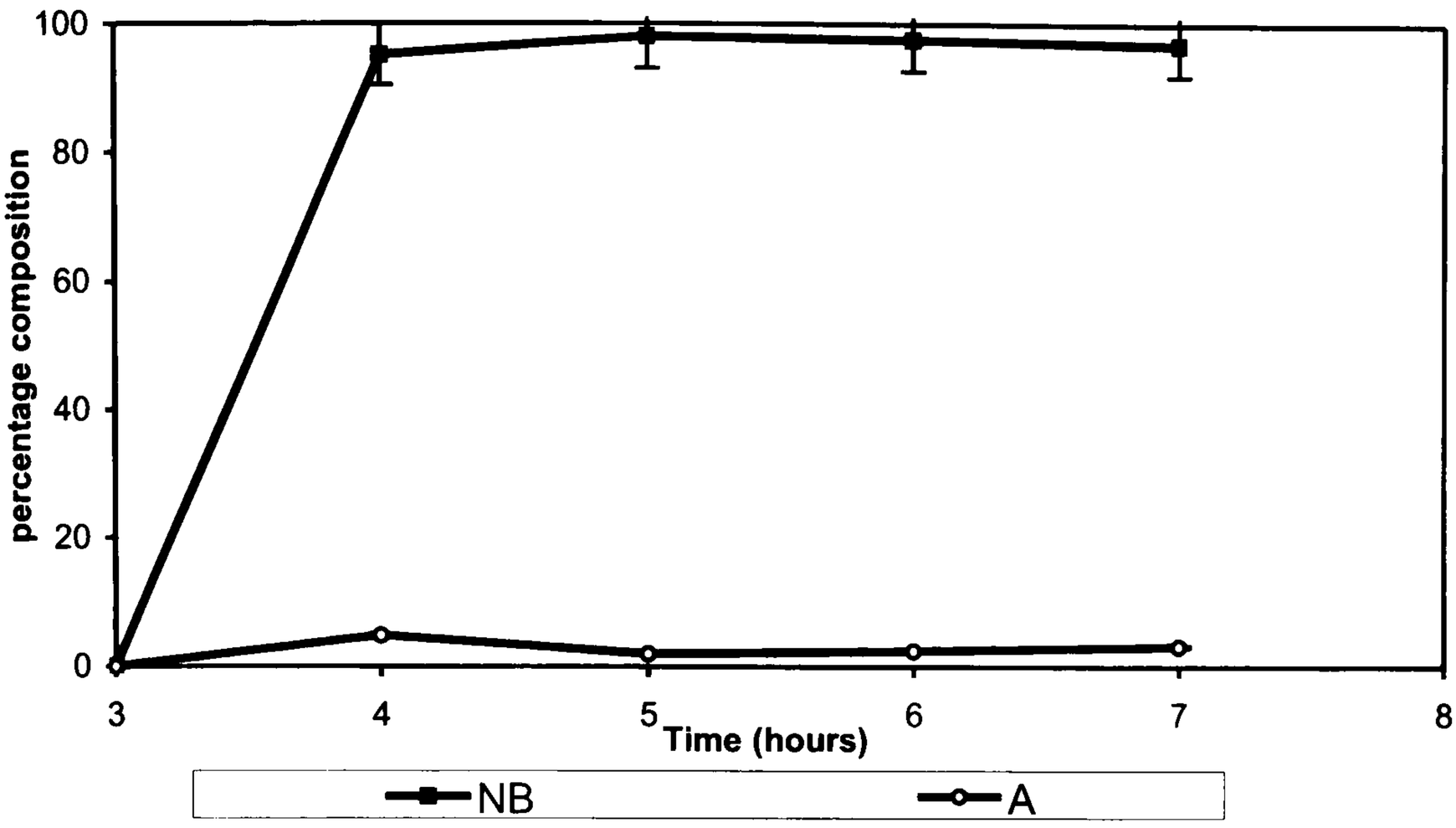

Figure 4.92: The hydrogenation of nitrobenzene using 5 % Ni/15 % Cu/Al_2O_3

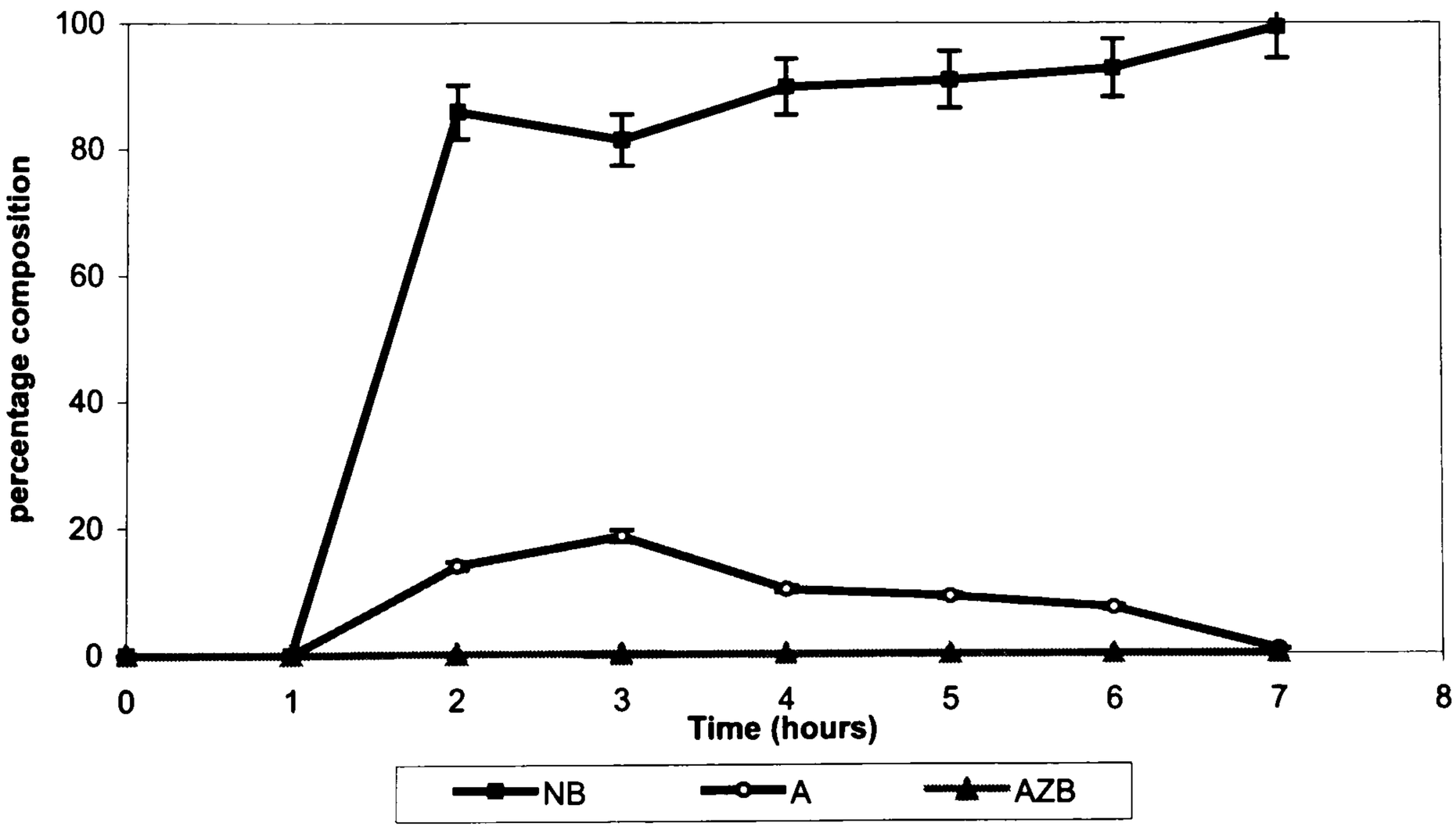

Figure 4.93: The hydrogenation of nitrobenzene with 15 % Ni/5 % Co/Al_2O_3

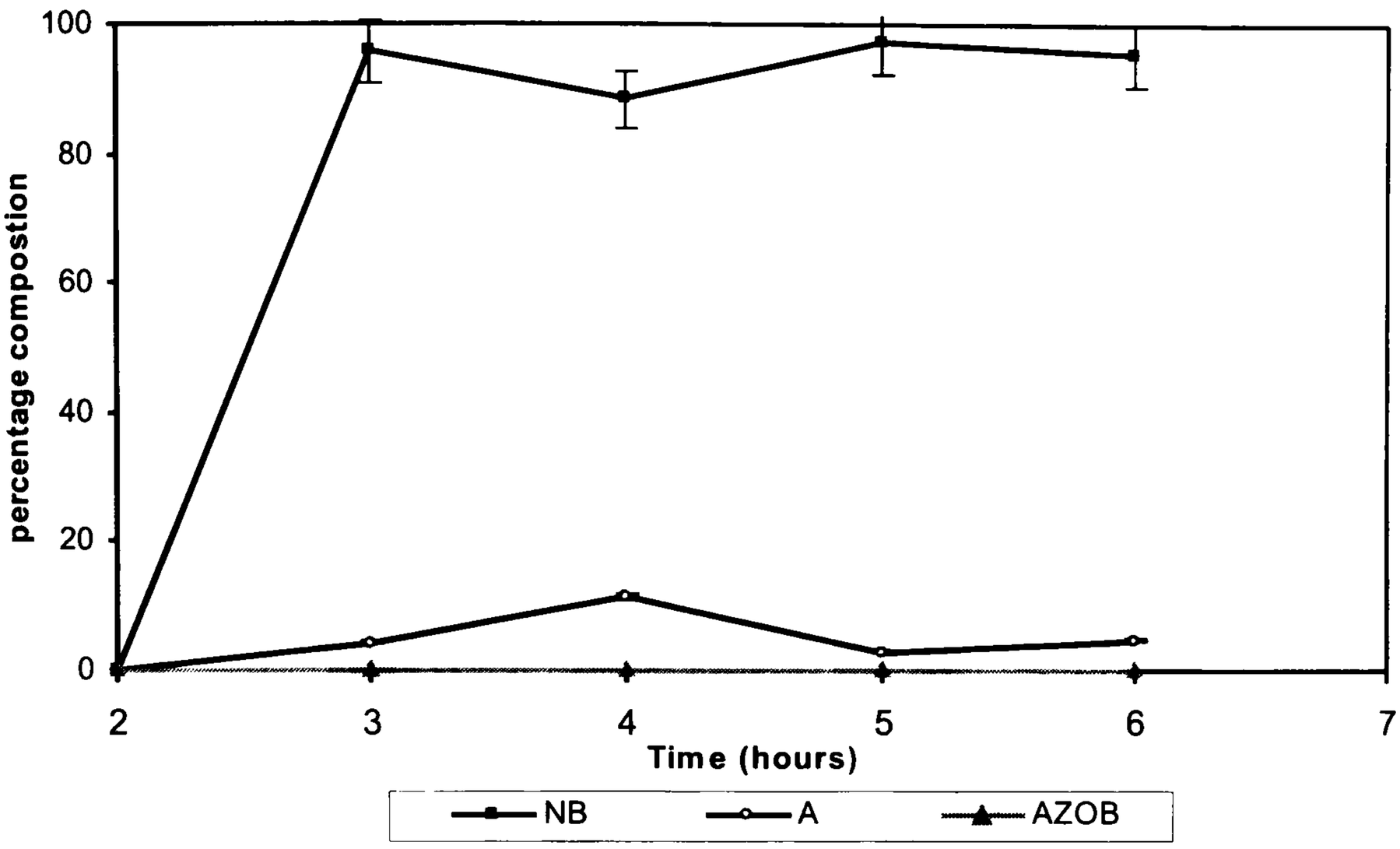

Figure 4.94: The hydrogenation of nitrobenzene with 10 % Ni/10 % Co/Al_2O_3

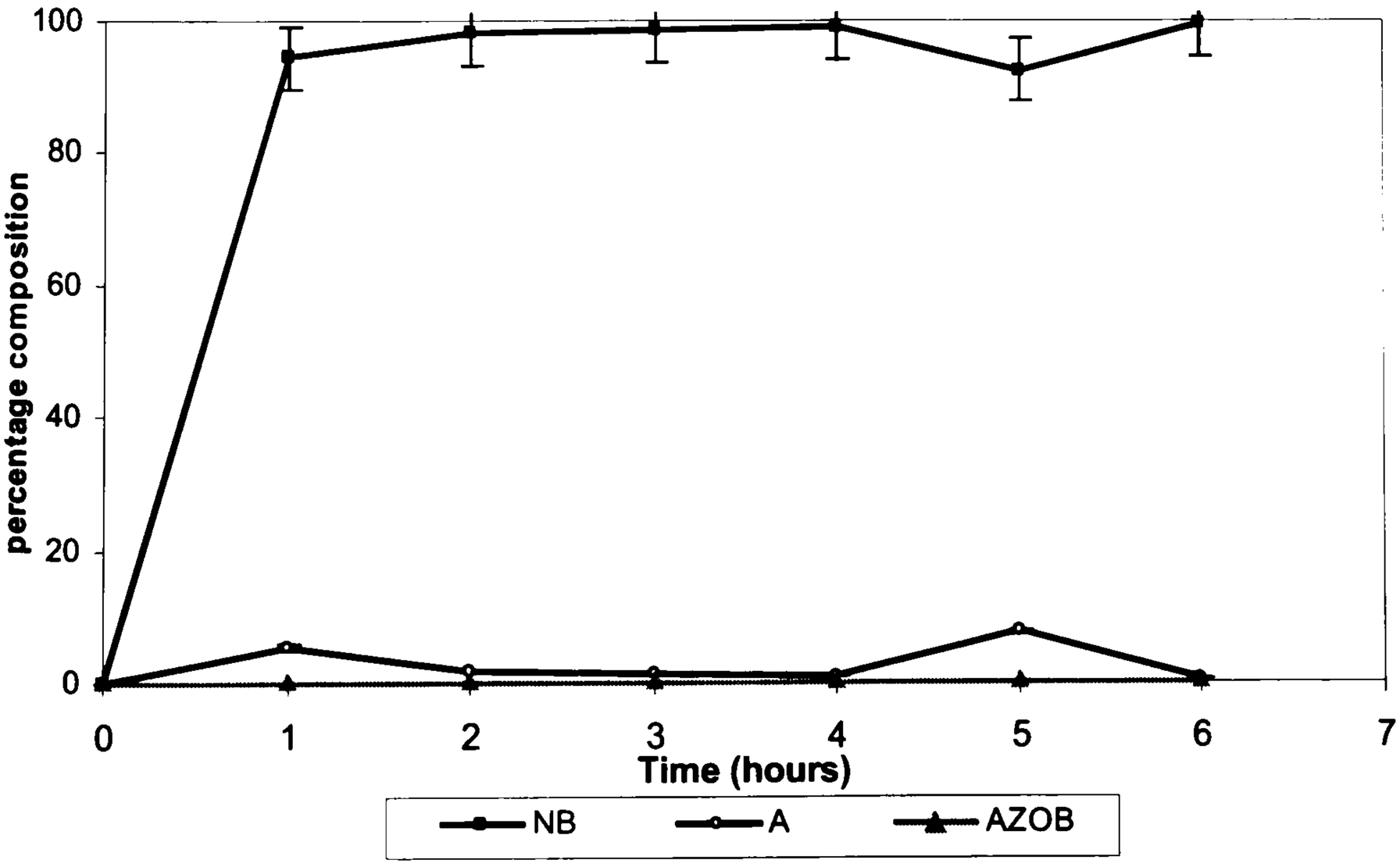

Figure 4.95: The hydrogenation of nitrobenzene using 15 % Co/5 % Ni/Al_2O_3

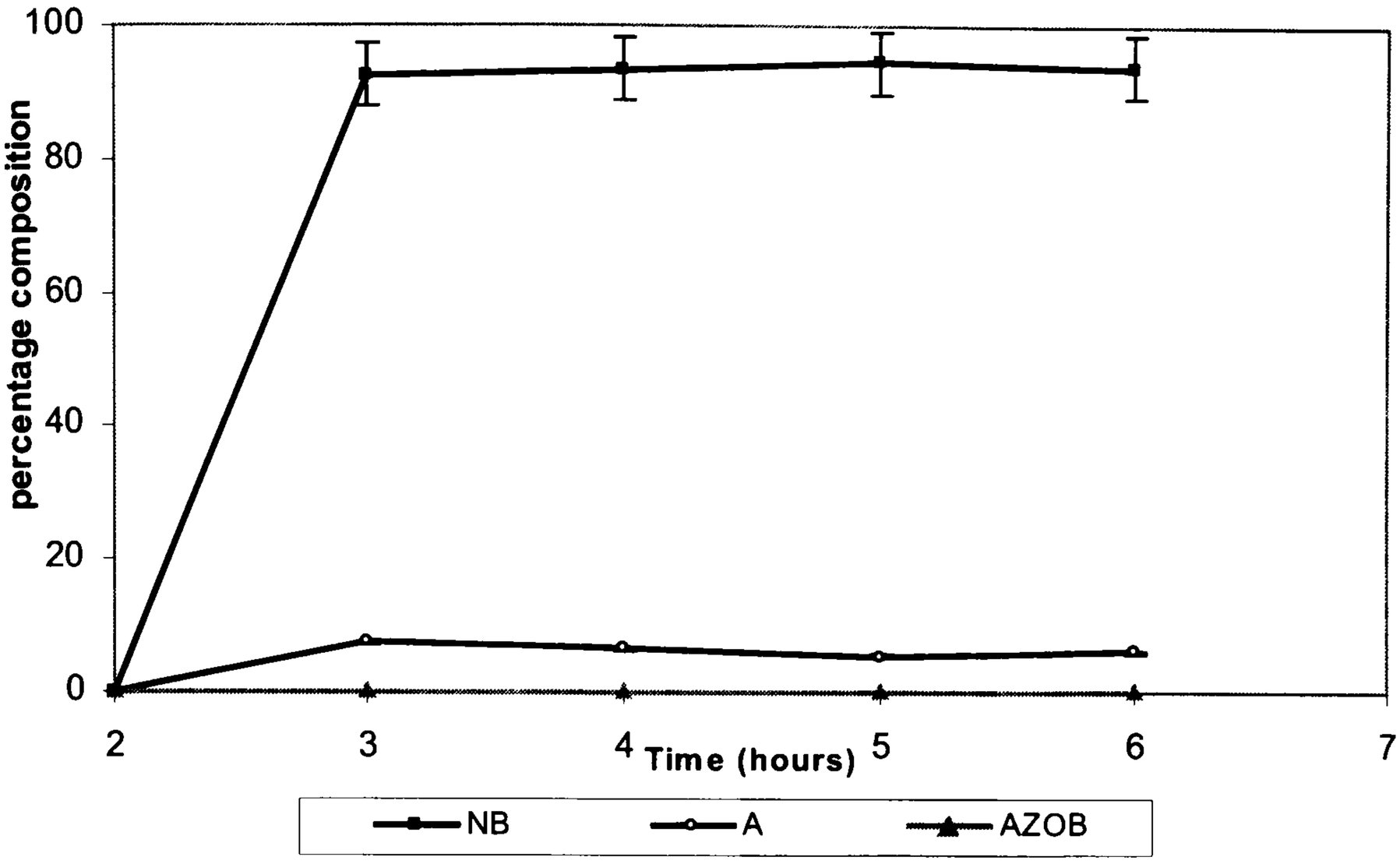

Figure 4.96: The hydrogenation of nitrobenzene using 15 % Cu/5 % Co/Al_2O_3

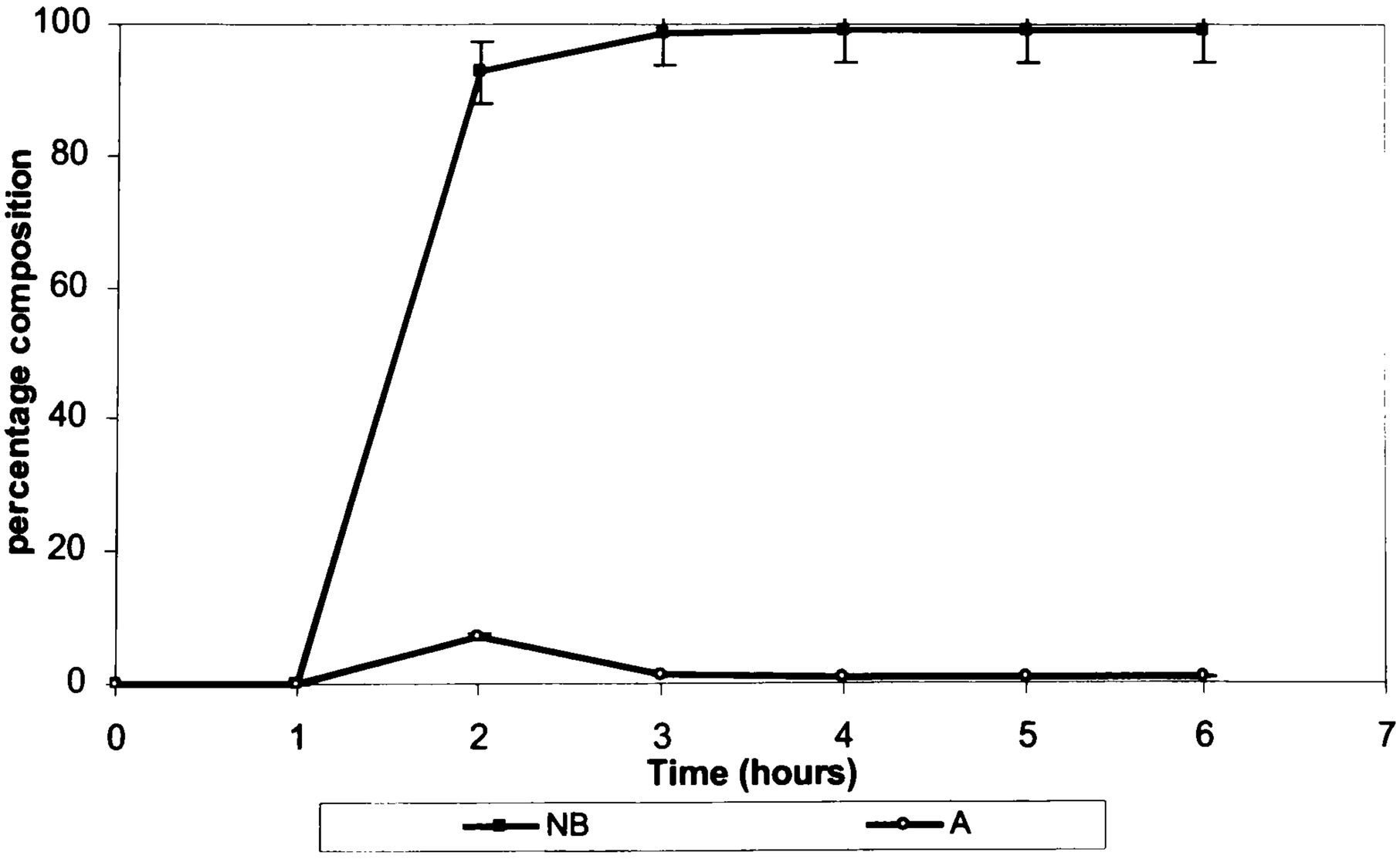

Figure 4.97: The hydrogenation of nitrobenzene with 10 % Cu/10 % Co/Al_2O_3

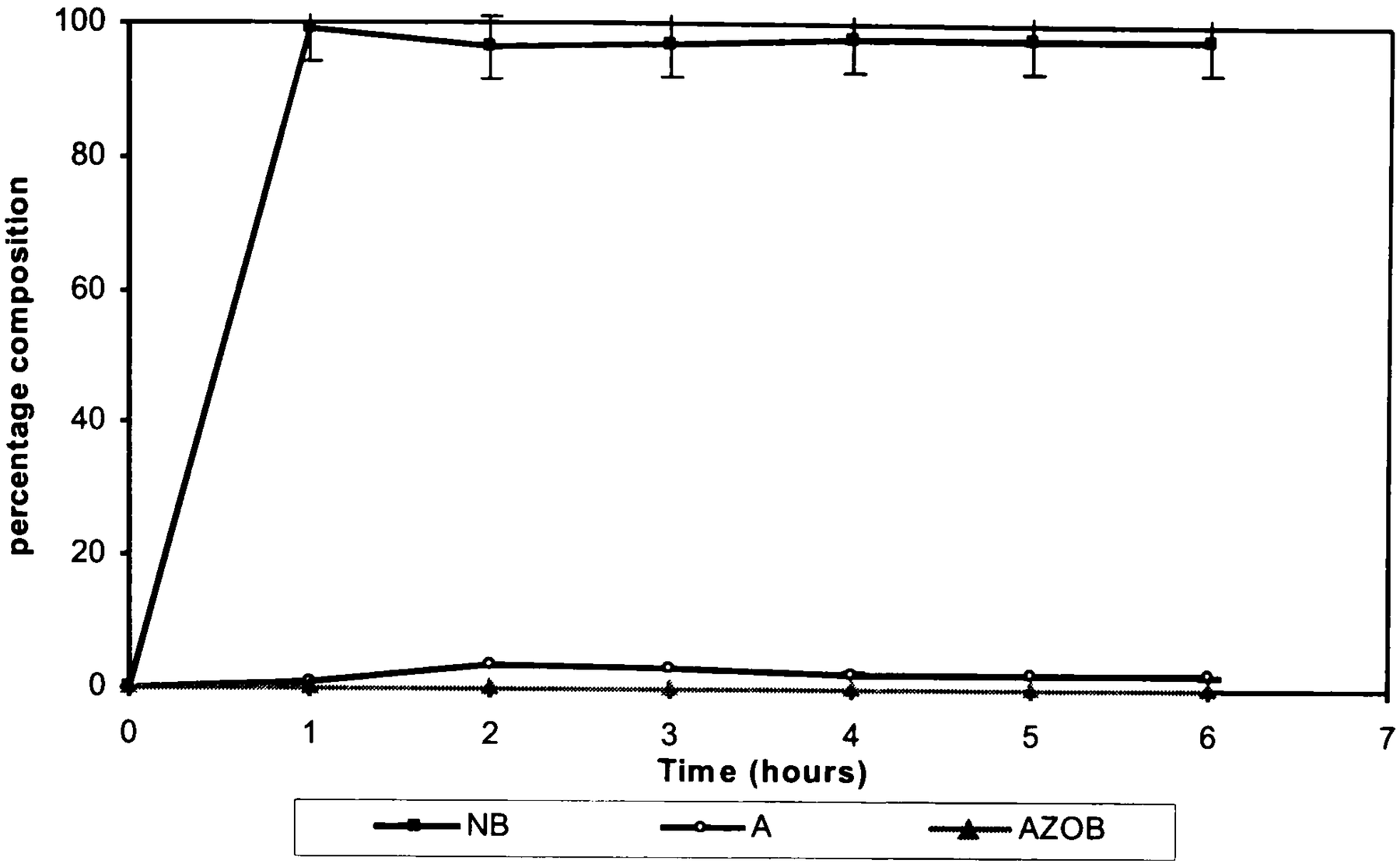

Figure 4.98: The hydrogenation of nitrobenzene using 15 % Co/5 % Cu/Al_2O_3

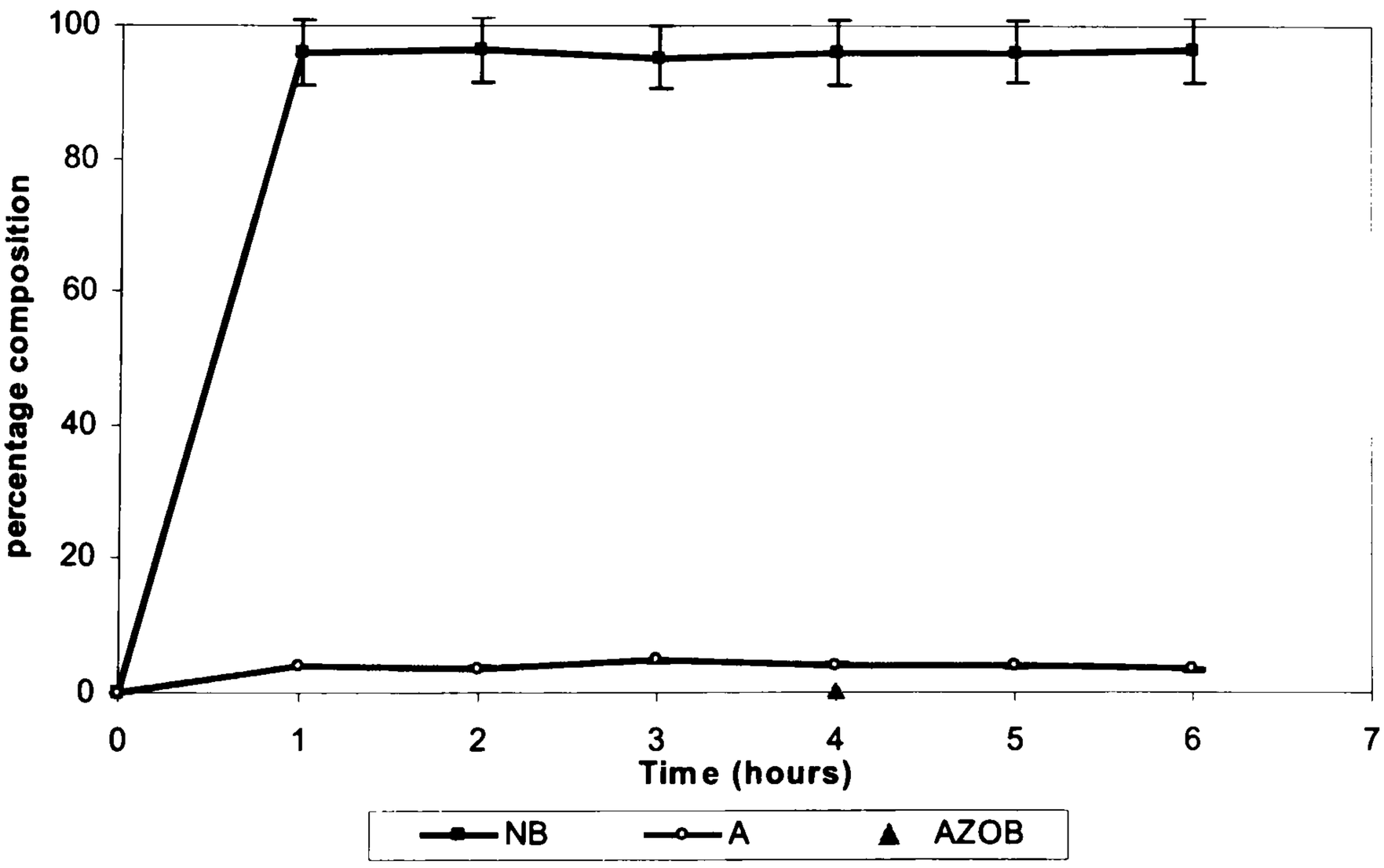

Figure 4.99: The hydrogenation of nitrobenzene with Puralox Al_2O_3 support.

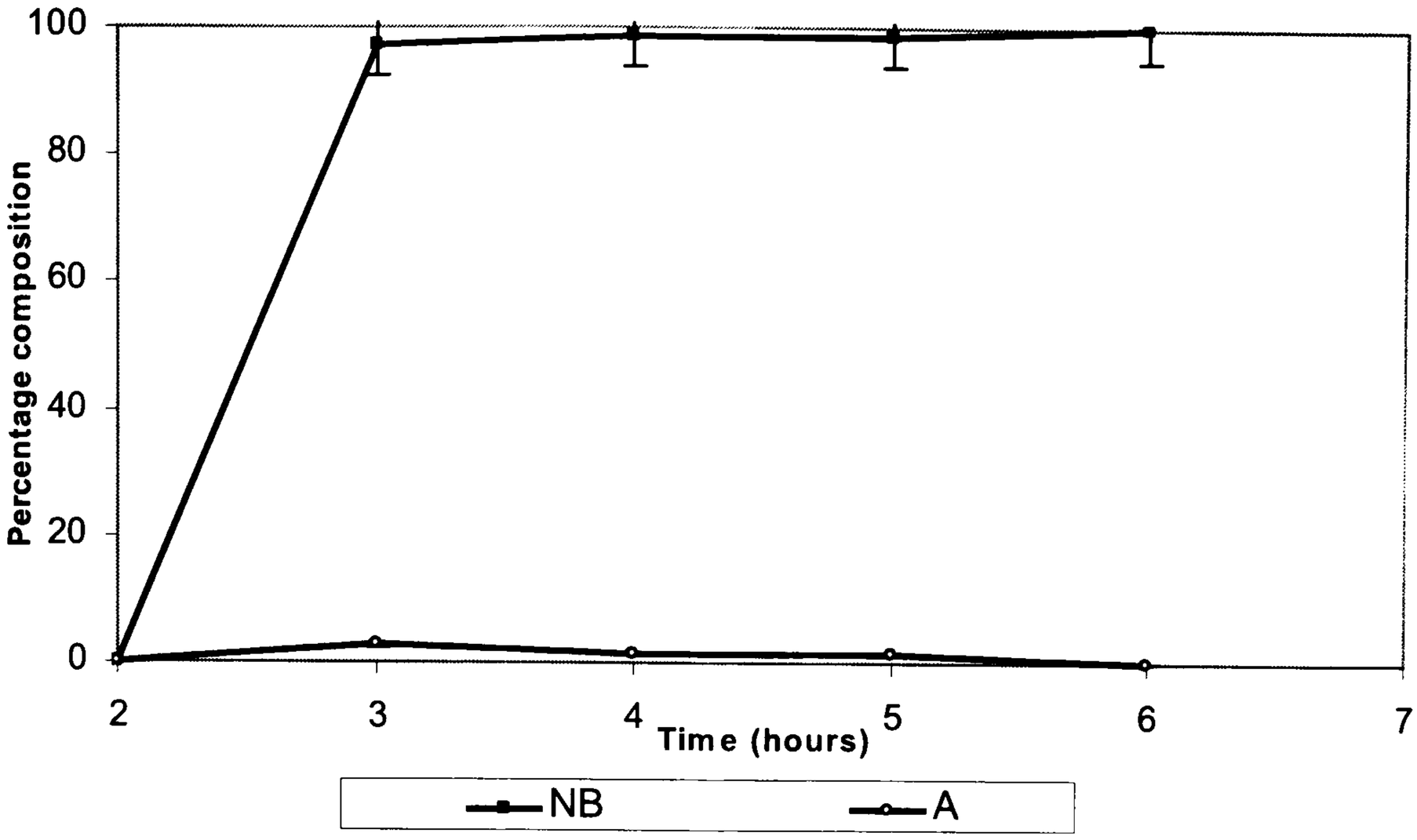

As Figures 4.87-4.99 show, the exit stream collected from the micro-reactor in each experiment contained very low percentages of aniline. The vast majority of each sample was unreacted nitrobenzene. Low levels of azobenzene and azoxybenzene (less than 1 % of the sample composition) were also detected in most of the reaction samples.

Of the three single metal catalysts: 20 % nickel (Figure 4.87), 20 % copper (Figure 4.88) and 20 % cobalt (Figure 4.89) the copper catalyst showed the highest levels of aniline in the feedstream with a maximum of 12.6 % aniline in the exit samples after 1 hour reaction time. The activity then dropped off as the reaction progressed until 4.0 % of the feed steam was composed of aniline after 7 hours. The nickel and cobalt catalyst showed similarly low productions with the aniline composition only reaching 4.3 % after 4 hours on stream with 20 % nickel and 2.3 % after 5 hours with 20 % cobalt.

The exit analyses of the reactions using the mixed metal nickel-copper catalysts are shown in Figures 4.90-4.92. The catalyst that showed the best activity was 5 % Ni/15 % Cu. At 3 hours reaction time, 18.6 % of the exit sample consisted of aniline,

although this activity did decrease as the reaction proceeded until after 7 hours where only 0.7 % of the exit feed was aniline. The 15 % Ni/5 % Cu catalysts also showed some measurable activity for the hydrogenation of nitrobenzene. From 2 hours of reaction onwards between 6-7.5 % of the exit samples consistently consisted of aniline and the activity of this catalyst did not appear to diminish throughout the course of the experiment. The 10 % Cu/10 % Ni only showed very limited activity for aniline production with just 4.8 % of aniline in the exit stream at maximum production after 4 hours hydrogenation.

Similarly low activities were observed with the mixed nickel-cobalt catalysts (Figures 4.93-4.95). The best of these catalysts was the 15 % Ni/5 % Co catalyst that produced a maximum of 11.5 % aniline in the exit feed at 4 hours reaction time. However, this activity dropped away over time as the hydrogenation proceeded. The 10 % Ni/10 % Co catalyst showed very low activity throughout the reaction, although increased levels of aniline were present in the exit feed at 1 hour (5.4 %) and 5 hours (7.5 %) reaction time. The graph of the exit analysis of the 5 % Ni/15 % Co catalyst displayed a steady production of aniline from 3 hours reaction time until the reaction was stopped at 6 hours. The percentage composition of aniline present in the exit feed ranged from between 5.4 % to 7.3 % over this period.

The exit analysis results for the set of mixed metal catalysts containing cobalt and copper are shown in Figures 4.96-4.98. All three catalysts displayed very low activity for the hydrogenation of nitrobenzene. Catalyst 5 % Cu/15 % Co showed a relatively constant percentage, between 3.5 %-4.8 %, of aniline in the exit feed throughout the reaction. Catalyst 10 % Cu/10 % Co also showed a fairly constant percentage of aniline in the exit stream although at a lower level of between 2.1 %-3.6 %. After an the initial sample of 2 hours with an aniline composition of 7.2 %, the activity of catalyst 15 % Cu/5 % Co dropped away to produce about 1 % of aniline after 3 hours of reaction and then maintained this level of activity until the reaction was stopped at 6 hours.

The analysis obtained from the hydrogenation of nitrobenzene using the alumina support is shown in Figure 4.99 and shows the support to have a very low activity for aniline production. The maximum amount of aniline detected in the exit stream was 2.6 % after 3 hours of reaction. However, this activity declined over the duration of the experiment until after 6 hours only 0.03 % of the exit stream consisted of aniline.

To compare how each catalyst was performing in relation to the rest, Equation 4.8 was used to generate a rate of reaction. At each point in time, this relationship was used to determine the rate using the actual number of moles of aniline produced by taking into account the volume of each sample. This gave a clear indication of the absolute quantity of aniline produced by each catalyst throughout hydrogenation. As the behaviour of each catalyst was slightly different, the maximum rate was selected as a comparison. These values are shown in Table 4.20.

$$\text{Rate of aniline production (mol min}^{-1}\text{ g}^{-1}) = \frac{f.x}{w} \qquad \text{Equation 4.8.}$$

Where,

f = nitrobenzene feed rate (mol min^{-1})

x = fractional conversion to aniline (%)

w = weight of catalyst (g)

Table 4.20: Maximum rate* of aniline production – HDC catalysts.

catalyst	maximum rate (μmol min^{-1} g^{-1})
20 % Ni	59
20 % Cu	5
20 % Co	16
15 % Ni/5 % Cu	112
10 % Ni/10 % Cu	57
5 % Ni/15 % Cu	122
15 % Ni/ 5 % Co	90
10 % Ni/10 % Co	56
5 % Ni/15 % Co	96
15 % Cu/5 % Co	13
10 % Cu/10 % Co	42
5 % Cu/15 % Co	60
Puralox alumina	1

(* The rates quoted in Table 3.20 were generally taken at around 4 hours into the reaction when the catalytic activity had been maximised.)

Table 4.20 revealed that all catalysts, except the 20 % copper catalyst, showed activity that was significantly greater than the alumina support material, which had a maximum aniline production rate of 1 μmol min^{-1} g^{-1}. The 20 % copper catalyst appears to be the least active catalyst for nitrobenzene hydrogenation, with a maximum activity of 5 μmol min^{-1} g^{-1}. Several other catalysts (20 % nickel, 20 % cobalt, 10 % Ni/10 % Cu, 10 % Cu/10 % Co and the copper-cobalt bimetallics) showed activity that was not substantially greater than 20 % copper. The catalyst displaying the greatest maximum rate of aniline production is 15 % Cu/5 % Ni at 122 μmol min^{-1} g^{-1}.

4.3.3.2 10 % Copper/SiO_2 Catalyst and Nitrobenzene Feed

The microreactor was also used to perform the hydrogenation of nitrobenzene was also carried out using a 10 % Cu/SiO_2 catalyst. This was a catalyst that had

previously proved to be active during a separate catalytic study and so was selected for use in the micro-reactor as a system check. The twelve HDC catalysts had displayed such surprisingly low activity for aniline production that it was necessary to check whether this was a problem with the experimental set up or an intrinsic feature of the catalysts.

The hydrogenation experiment was carried out in exactly the same way as the previous experiments with a nitrobenzene feed. The exit analysis of the feed stream is displayed in Figure 4.100.

Figure 4.100: The hydrogenation of nitrobenzene using 10 % Cu/SiO_2

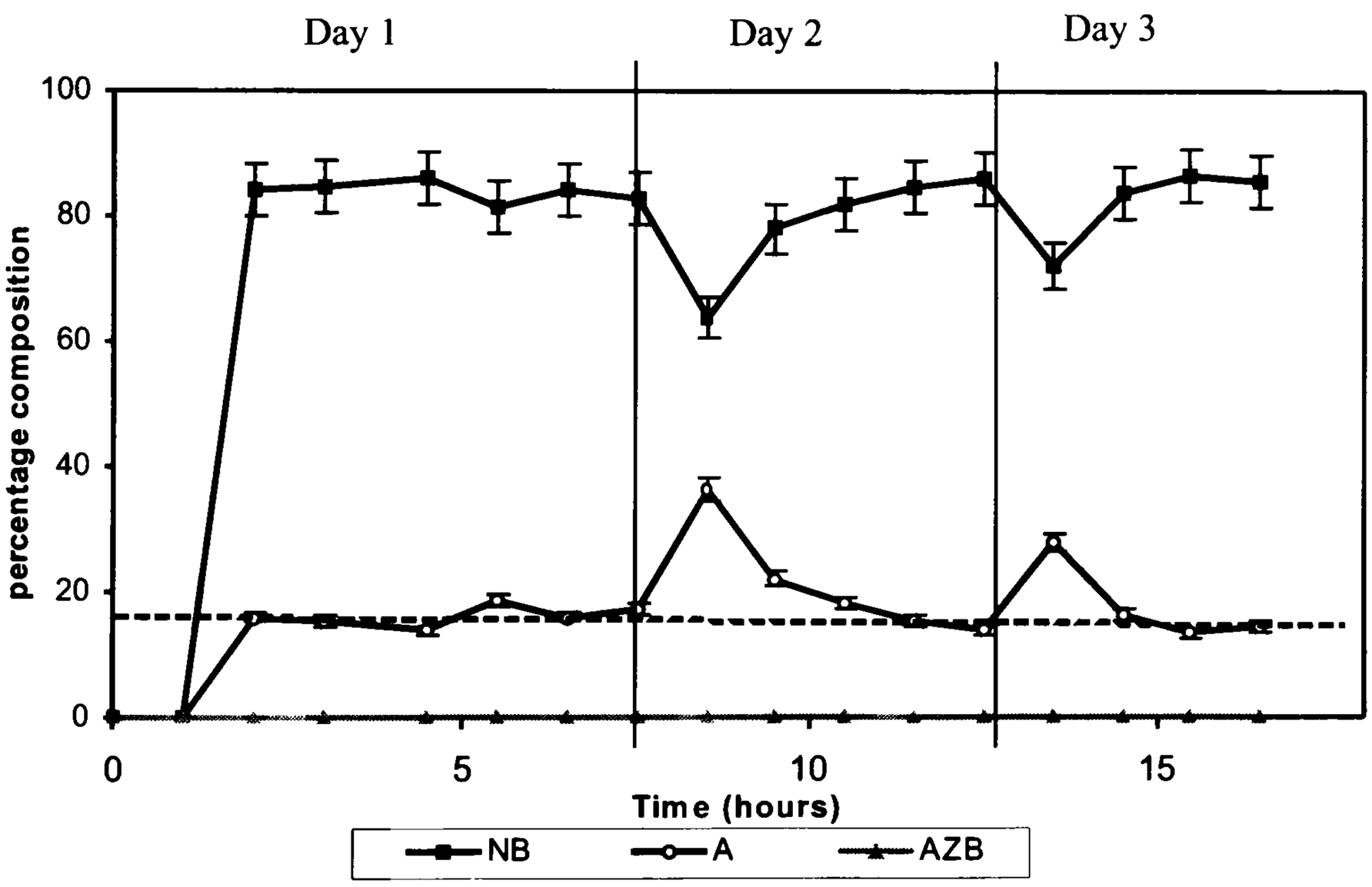

The 10 % copper/silica catalysts displayed much greater activity towards the nitrobenzene hydrogenation reaction when compared with the twelve HDC catalysts. The reaction was run over a three-day period with the start of each new day marked by a vertical line in Figure 4.100. Between each day the nitrobenzene feed was stopped and the catalyst bed left in a steady trickle flow of hydrogen overnight.

During the first six hours of hydrogenation, the maximum percentage of aniline in the exit stream reached 18.7 %, but remained relatively constant throughout this period of time. However, on the second day, immediately after the first night of hydrogen treatment, at 8.5 hours the maximum aniline composition was 36.4 %. Furthermore, the catalytic activity displayed an increase directly after the second night in hydrogen. With the exception of these samples, the activity of the catalyst remained relatively constant throughout indicating steady state behaviour. A dashed horizontal line in Figure 4.100 indicates the underlying activity, omitting the artificially high values for the samples at 8.5 hours and 13.5 hours. The catalyst percentage of aniline detected over time did not fluctuate significantly and the composition of the product stream did not drop below 13 % aniline.

The maximum rate of aniline production was calculated to be 559 μmol min^{-1} g^{-1}, a rate that was four and a half times faster than when using the most active HDC catalyst (15 % Cu/5 % Ni with a rate of 122 μmol min^{-1} g^{-1}) showing that the copper silica catalyst was very much more active for the nitrobenzene hydrogenation reaction and that the micro-reactor system was functioning efficiently.

4.3.3.3 Palladium Catalysts and Nitrobenzene Feed

Two of the palladium catalysts, Pd/CSXU and 1 % Pd/Al_2O_3 utilised in the liquid phase hydrogenation of nitrobenzene were also used to perform the hydrogenation of nitrobenzene in the microreactor. The exit analysis of the reaction with Pd/CSXU is shown in Figure 4.101.

Figure 4.101: The hydrogenation of nitrobenzene using Pd/CSXU

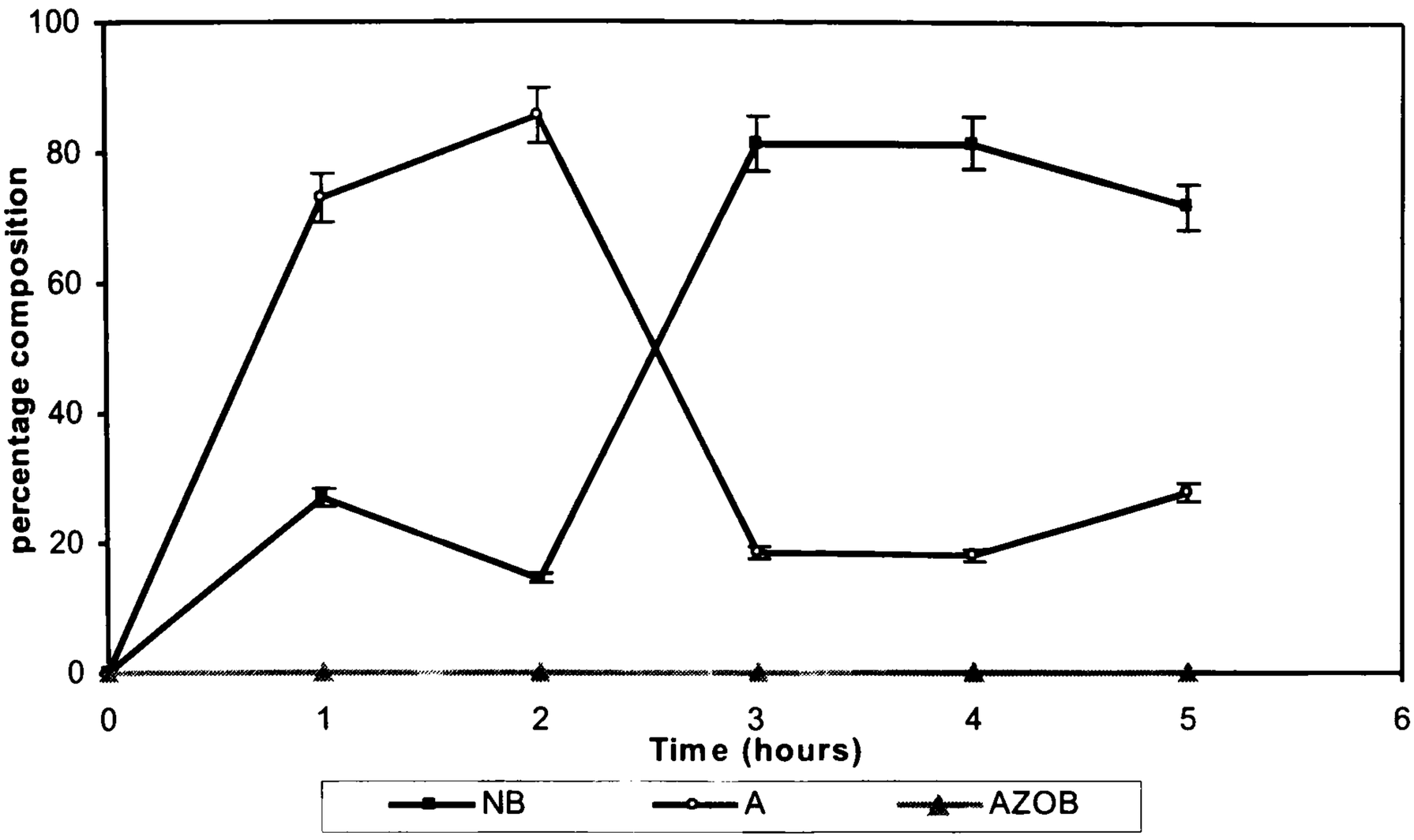

Catalyst Pd/CSXU displayed very high hydrogenation activity at the beginning of the catalytic run. (Figure 4.101) After 1 hour reaction time, 73.0 % of the exit stream consisted of aniline and after 2 hours reaction time this had increased to 85.5 %. Between 2 and 3 hours the system appeared to undergo rapid catalyst deactivation as after 3 hours the aniline content of the analysis sample had dropped to 18.6 %. This level of activity was maintained throughout the rest of the reaction. The maximum rate of aniline production, seen at the start of the reaction, was calculated at 170 $\mu mol\ min^{-1}\ g^{-1}$.

Analysis of the reaction with the 1 % Pd/Al_2O_3 catalyst is shown in Figure 4.102. This catalyst shows good activity for nitrobenzene hydrogenation with a maximum aniline composition of 28.6 % after 5 hours of reaction. A good level of activity is maintained throughout the experiment, with 23.1 % of the last analysis sample consisting of aniline.

The maximum rate of aniline production with this catalyst was calculated as 413 $\mu mol\ min^{-1}\ g^{-1}$, showing that the alumina supported catalyst was more active in the

vapour phase reactor than the carbon-supported catalyst, despite a lower metal loading and lower palladium dispersion.

Figure 4.102: The hydrogenation of nitrobenzene with 1 % Pd/Al_2O_3

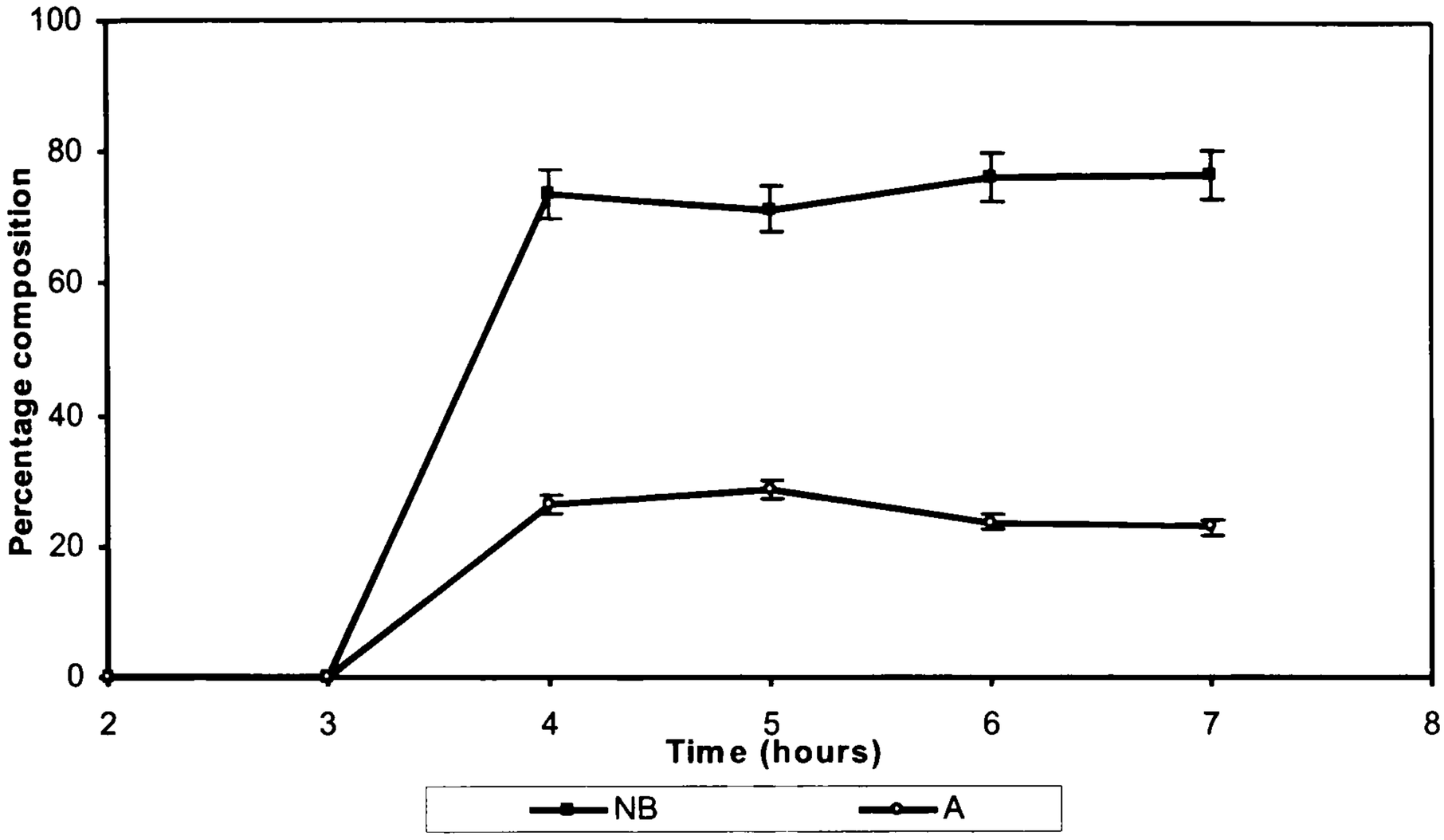

4.3.3.3.1 Hydrogenation using Pd/CSXU and Deuterium Gas

The hydrogenation of nitrobenzene in the microreactor was carried out using catalyst Pd/CSXU and deuterium gas in place of hydrogen. The reaction was sampled in the usual way however, each was also analysed using ^1H NMR in addition to GC-MS. The exit analysis of the reaction samples is shown in Figure 4.103.

Figure 4.103: The hydrogenation of nitrobenzene with Pd/CSXU and D_2 (g)

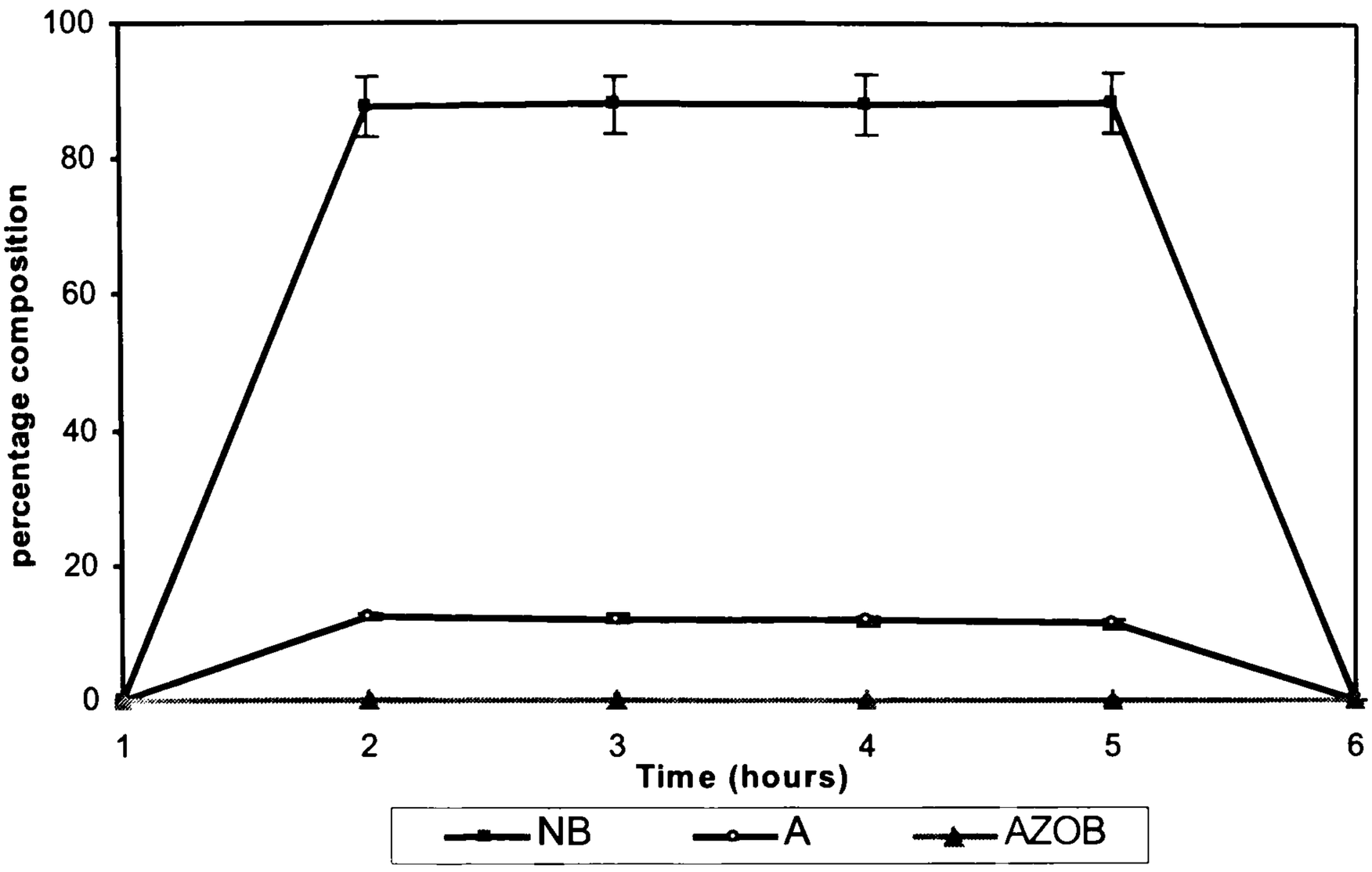

Analysis of the reaction of nitrobenzene and D_2 (g) using Pd/CSXU is shown in Figure 4.103. This catalyst showed good activity for the nitrobenzene hydrogenation reaction and a kinetic isotope effect was observed, as the activity was much reduced when compared to that obtained from the reaction using the same catalyst and H_2 (g) (Figure 4.101). After 2 hours of reaction, the percentage aniline in the exit stream was 12.3 % and the rate of aniline production was calculated to be 30 μmol min^{-1} g^{-1}. At the same point in time with the H_2 reaction the rate was 35 μmol min^{-1} g^{-1}. On moving to deuterium, a slightly slower rate or reaction was observed. The kinetic isotope effect coefficient was calculated, as described in Section 4.3.1.7, as $\eta = 1.2$. The magnitude of the kinetic isotope effect observed here is comparable to the value of η obtained in the liquid phase reactions in Section 4.3.1.7 of η=1.9.

4.3.3.4 Hydrogenation of Nitrobenzene where the Catalysts are Pre-Treated with Water

A selection of catalysts and the alumina support were used to perform the hydrogenation of nitrobenzene after each catalyst had been pre-treated with water vapour, under a flow of hydrogen for 1 hour prior to commencement of the nitrobenzene feed. Each experiment was run over the course of 15 hours. The water vapour treatment was repeated at several intervals throughout the duration of the experiment. Analysis of the exit stream was performed the same way as previously described in Section 4.3.3. The data from 20 % Ni/Al_2O_3, 20 % Cu/Al_2O_3, 20 % Co/Al_2O_3, 10 % Ni/10 % Cu/Al_2O_3, 10 % Ni/10 % Co/Al_2O_3 and 10 % Cu/10 % Co/Al_2O_3 are displayed in Figures 4.104-4.109. Data from hydrogenation with the alumina support are shown in Figure 4.110 and the results from catalysis with 1 % Pd/Al_2O_3 in Figure 4.111. The points in time where each water vapour treatment was performed in each reaction are marked on each graph with a dashed line at the corresponding place on the x-axis.

Figure 4.104: The hydrogenation of nitrobenzene using 20 % Ni/Al_2O_3 following water pre-treatment

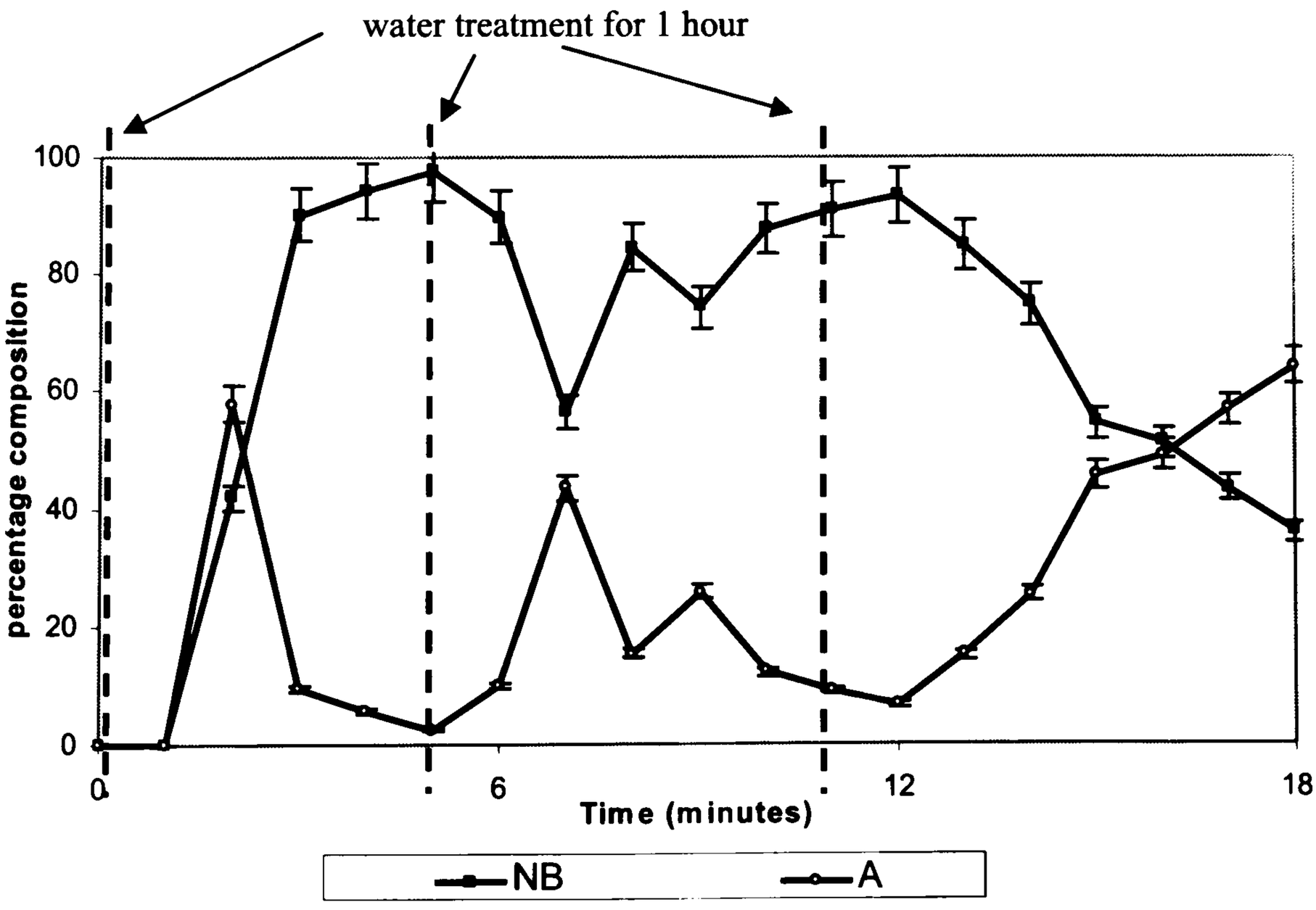

Figure 4.105: The hydrogenation of nitrobenzene using 20 % Cu/Al_2O_3 following water pre-treatment

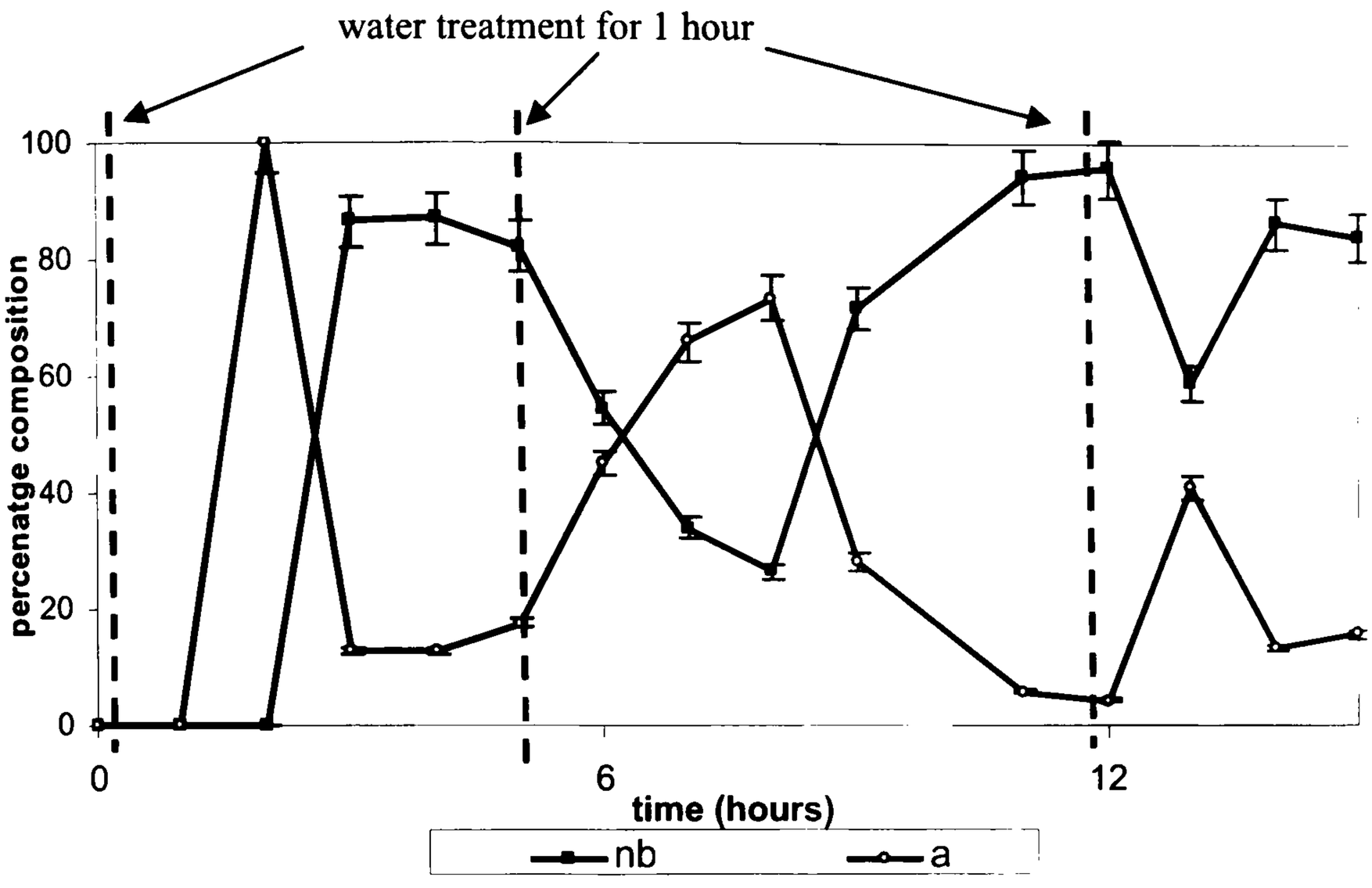

Figure 4.106: The hydrogenation of nitrobenzene with 20 % Co/Al_2O_3 following pre-treatment with water

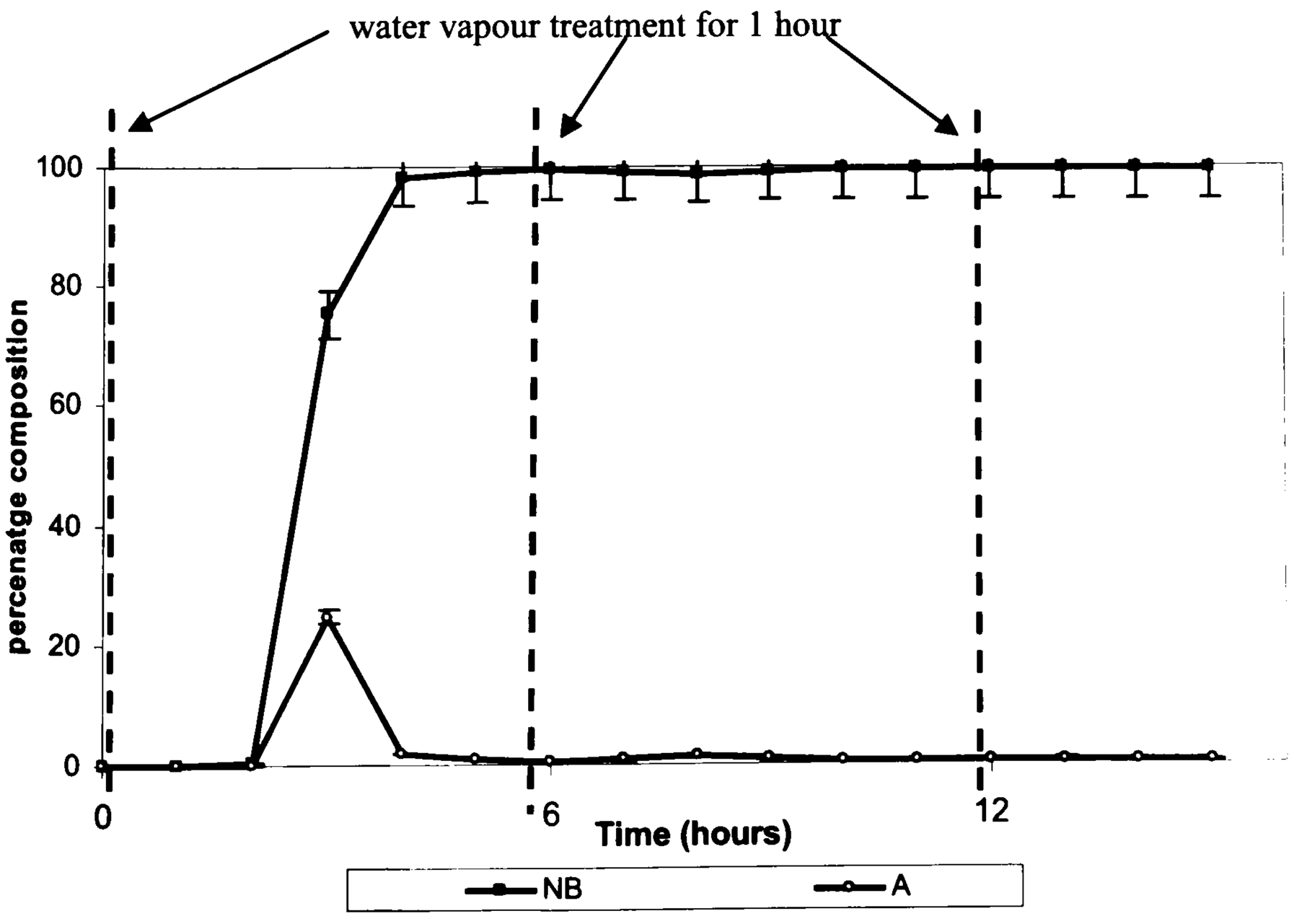

Figure 4.107: The hydrogenation of nitrobenzene with 10 % Ni/10 % Cu/Al_2O_3 following pre-treatment with water.

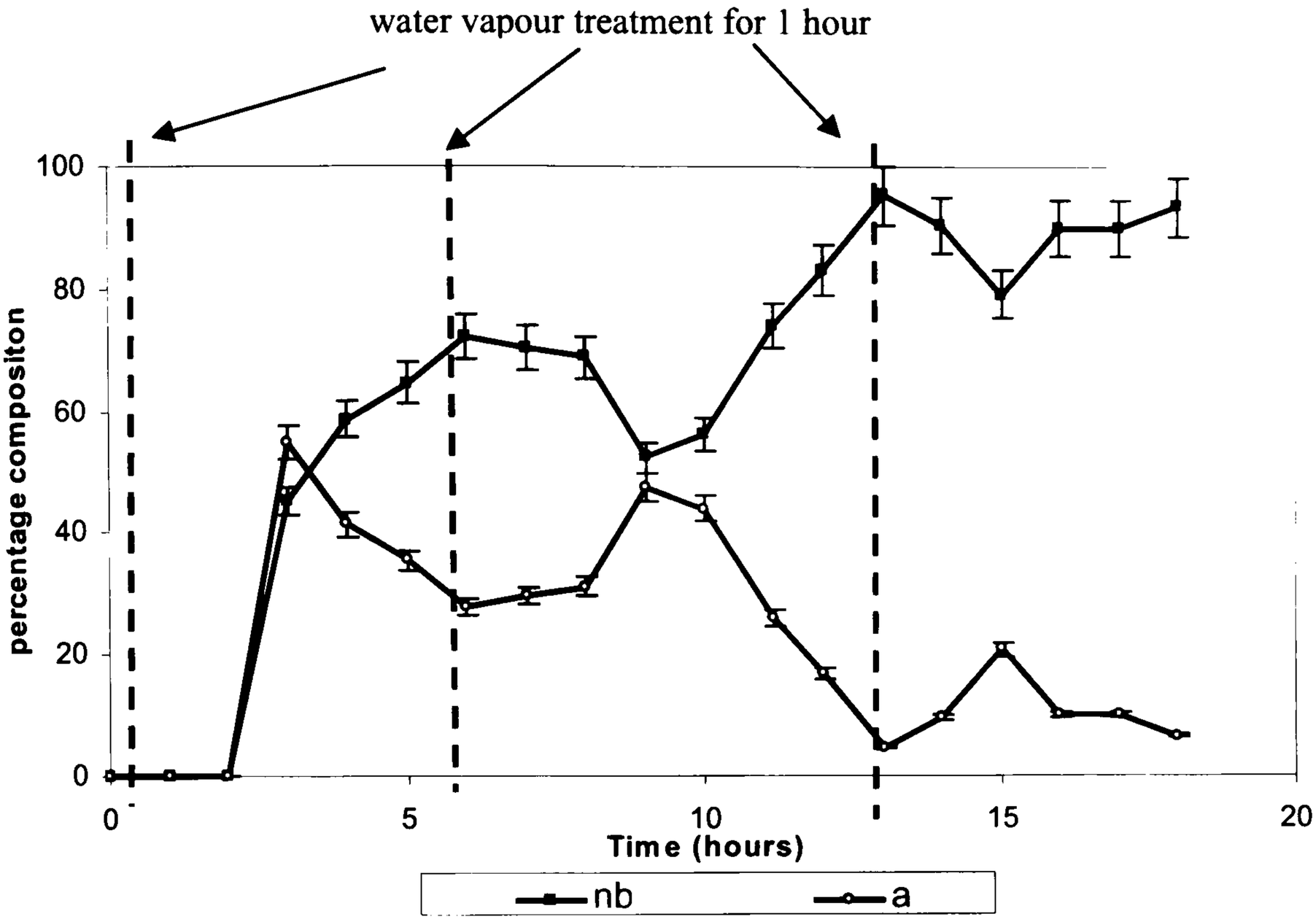

Figure 4.108: The hydrogenation of nitrobenzene with 10 % Ni/10 % Co following pre-treatment with water.

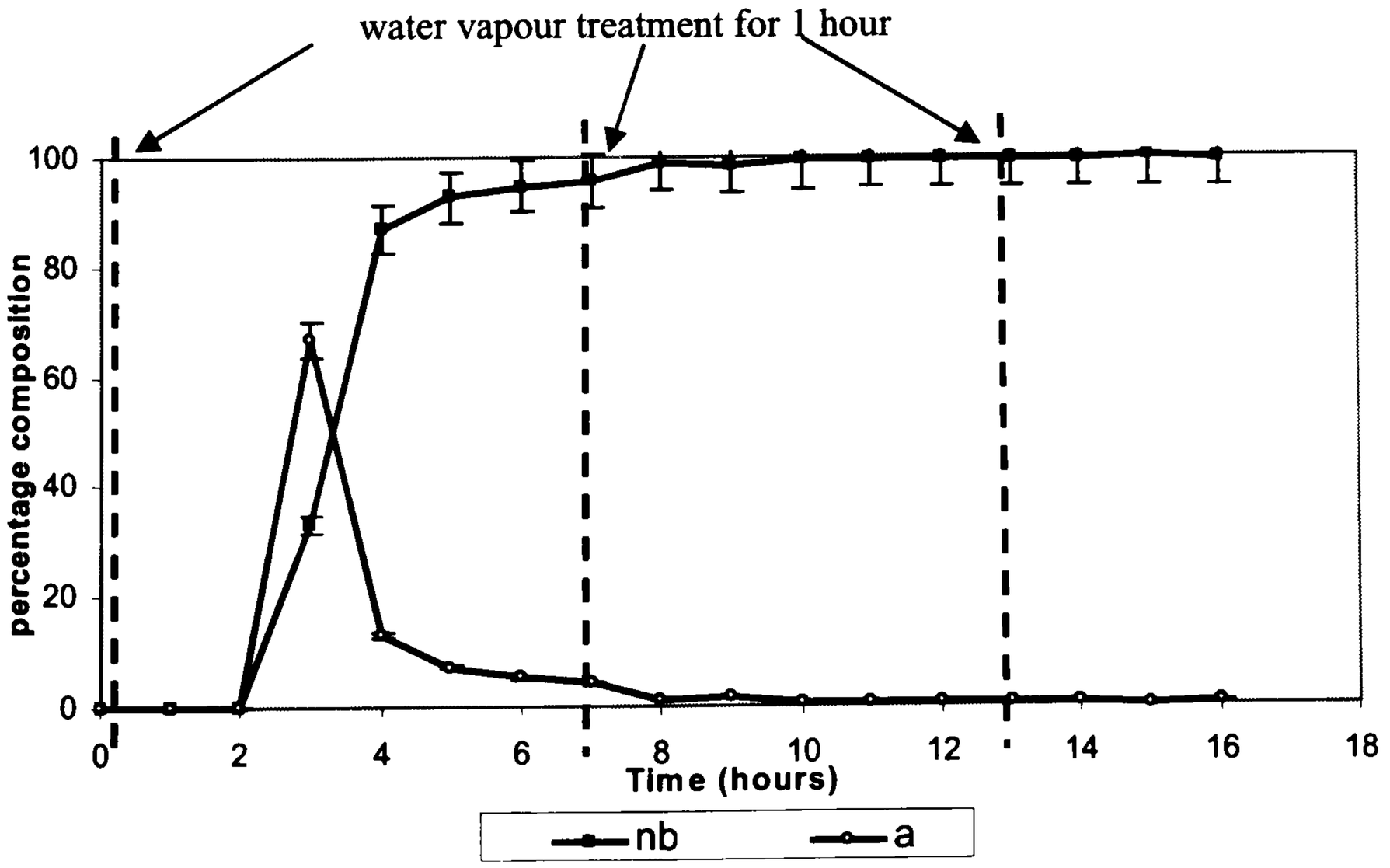

Figure 4.109: The hydrogenation of nitrobenzene using 10 % Cu/10 % Co following pre-treatment with water

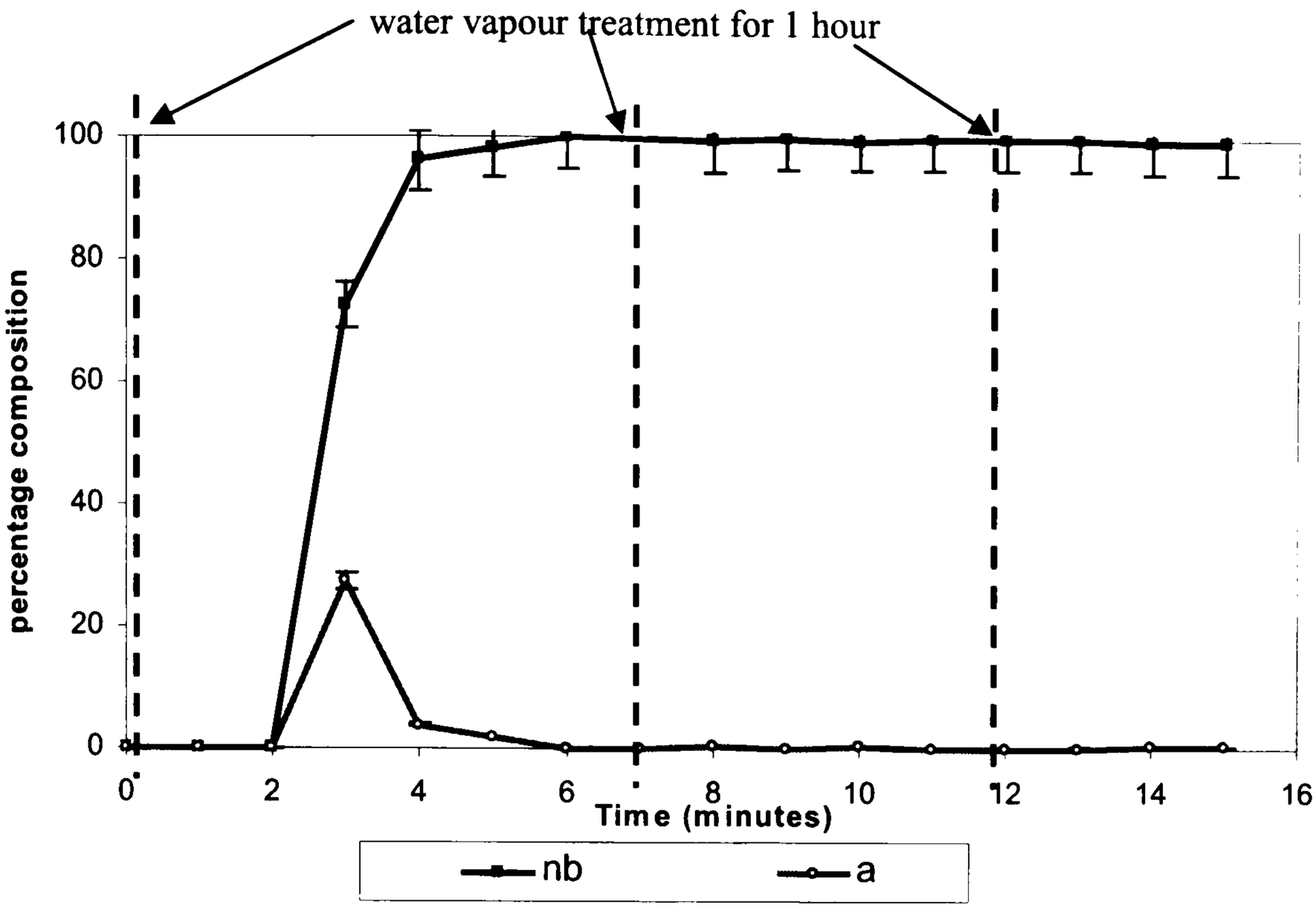

Figure 4.110: The hydrogenation of nitrobenzene with Puralox HP-14/150 Alumina after pre-treatment with water.

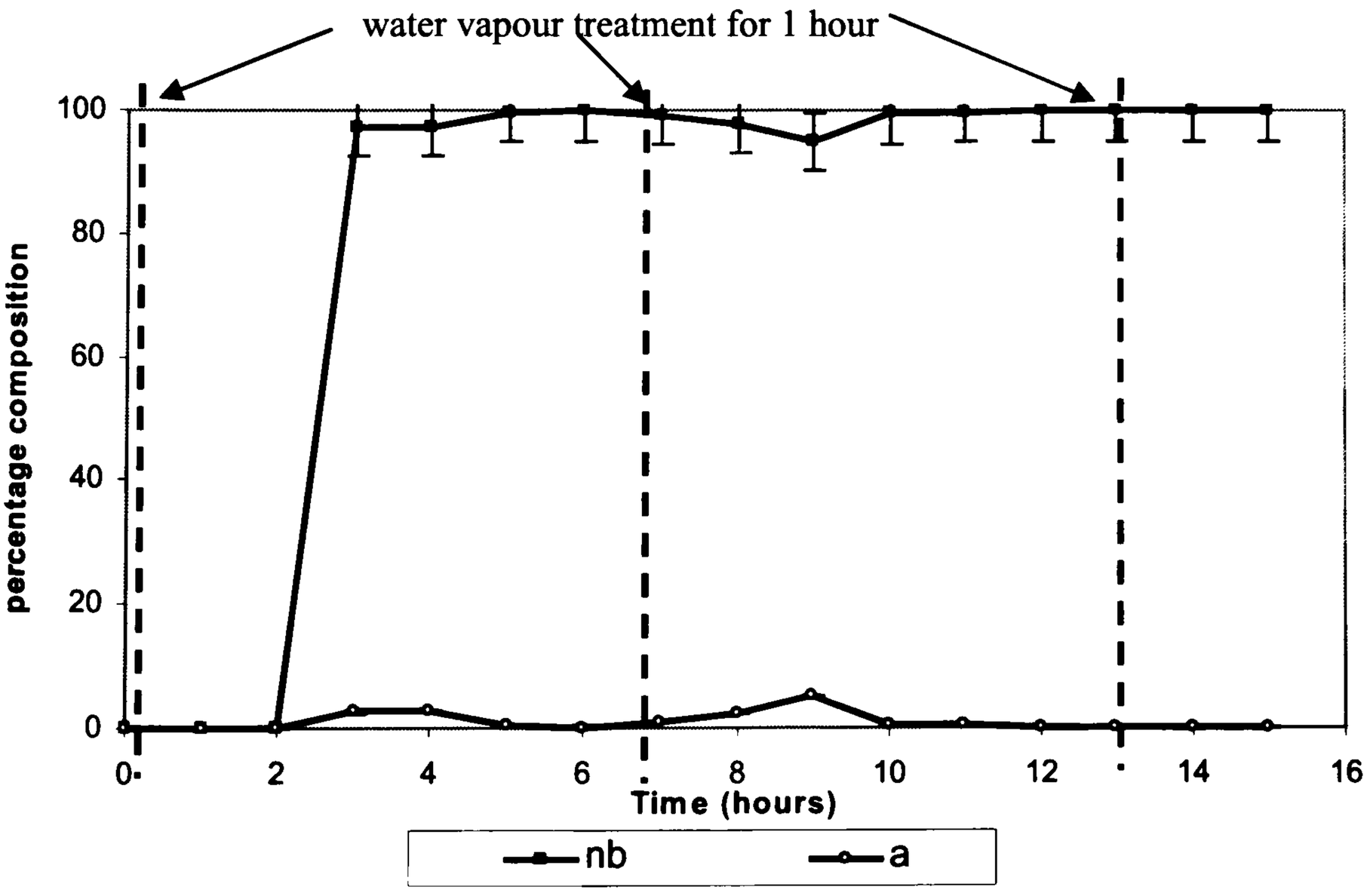

Figure 4.111: The hydrogenation of nitrobenzene with 1 % Pd/Al_2O_3 after pre-treatment with water

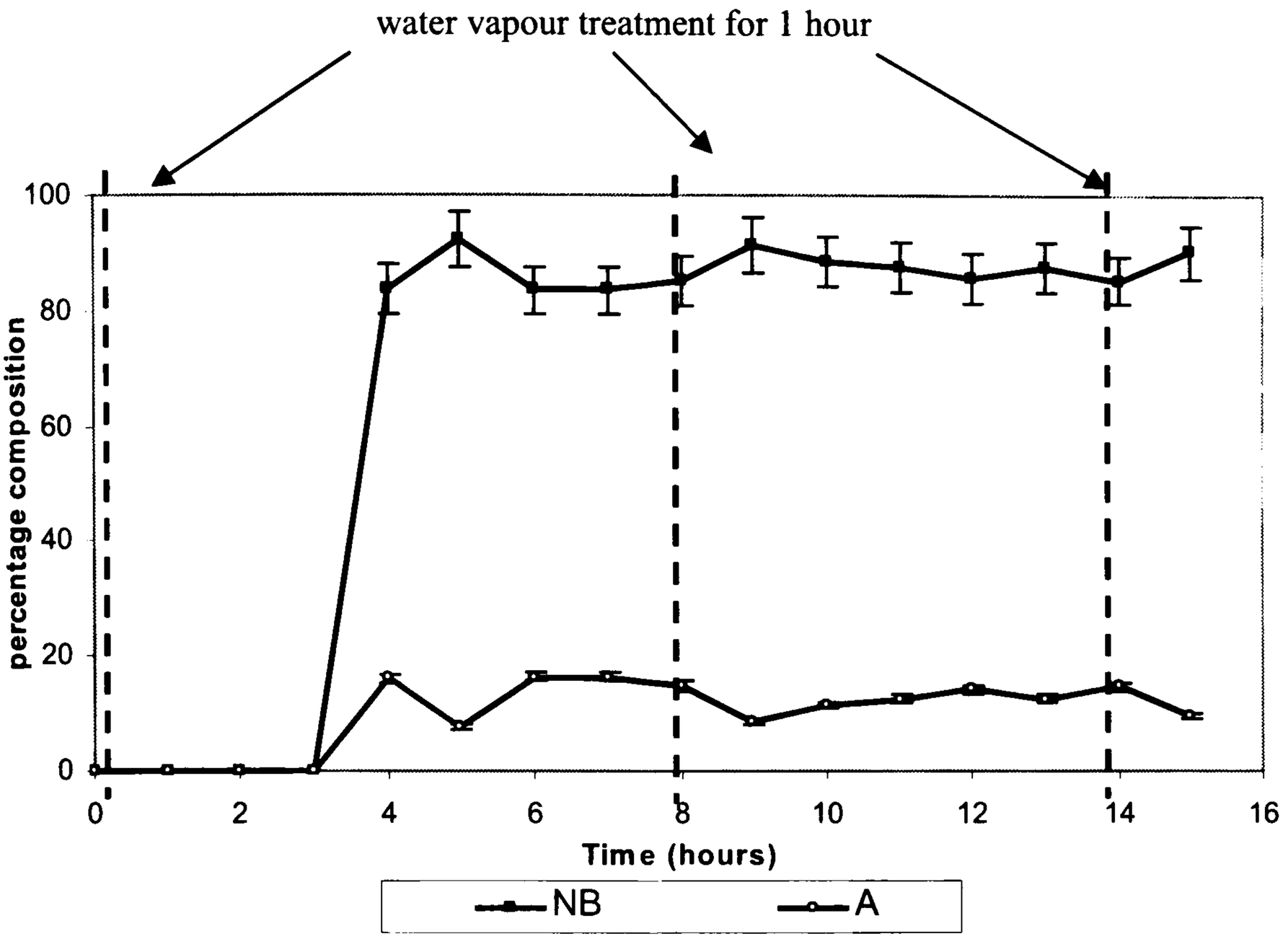

With the 20 % nickel catalyst (Figure 4.104) aniline production was greatly improved upon pre-treating the catalyst with water vapour before reaction. After 2 hours reaction time, 58 % of the exit stream consisted of aniline. The percentage aniline in the feed stream then dropped off fairly rapidly until after 5 hours only 2.6 % of the exit stream was aniline. At six hours the catalyst was again treated with a flow of water vapour for one hour. Immediately after this, at 7 hours, analysis revealed an aniline percentage of 43.5 %. Once again the percentage aniline began to decrease rapidly and after 12 hours the composition of the exit stream was down to 6.7 % aniline. At thirteen hours the catalyst was re-treated with water vapour for the second time and an increase in the percentage aniline obtained was again observed. The behaviour of the catalyst after this point was markedly different from that in the rest of the reaction. The aniline composition began to rise steadily over time and was still increasing when the reaction was stopped after 18 hours. The maximum aniline composition of 64.1 % was attained at this point.

A similar graph was obtained from analysis of the reaction using 20 % Cu/Al_2O_3 (Figure 4.105). The first treatment of the catalyst with water vapour facilitated a huge improvement in the percentage of aniline in the exit stream, as after 2 hours, 100 % of liquid leaving the reactor was aniline. No nitrobenzene remained in the exit feed. Like the reaction using 20 % nickel the aniline composition began to decrease fairly rapidly after this point and after 4 hours the aniline content of the exit stream had fallen to 12.9 %. At 5 hours the second water vapour treatment was performed and induced an increase in aniline composition over three hours until an exit feed aniline content of 73.5 % was reached after 8 hours. After this maximum the percentage aniline then sharply declined to 4.3 % after 12 hours. Also at 12 hours, the third water vapour treatment was performed and caused the aniline content to increase to 41.0 % after 13 hours. A decrease in the percentage of aniline present in the exit stream was observed after this point until the reaction was stopped after 15 hours of hydrogenation. Analysis of the last sample at 15 hours showed the presence of 15.8 % aniline.

Entirely different behaviour was observed with the 20 % cobalt catalyst (Figure 4.106). Pre-treatment of the catalyst with water prior to reaction did lead to an increase in the percentage of aniline present in the exit samples, like the other catalysts, and after 2 hours of reaction the level of aniline in the exit stream was 66.1 %. This rose again to reach maximum aniline content of 75.3 % after 3 hours. Also like the other two single metal catalysts, the percentage aniline dropped off sharply and after 6 hours only 0.9 % of the exit stream was product. After six hours the reaction using 20 % $CoAl_2O_3$ started to look strikingly different from when nickel or copper were employed. Following the second water treatment at 6 hours, no gain in aniline production was observed. Over the next six hours, the aniline composition fell below 1 %. The third water treatment at 12 hours also failed to trigger an increase in the aniline content of the exit feed. In fact, after 5 hours of reaction the cobalt catalyst appeared to have become totally deactivated and inactive for the nitrobenzene hydrogenation reaction.

Figure 4.107 shows analysis from the hydrogenation using the 10 % Ni/10 % Cu/Al_2O_3 catalyst. The behaviour of this catalyst closely resembled that of 20 %

Ni/Al_2O_3 and 20 % Cu/Al_2O_3. An initial large increase in the percentage of aniline obtained was observed following the first water vapour treatment and at 3 hours 55.0 % aniline was produced. This percentage then decreased until at 5 hours 28.0 % of the exit stream was aniline. The second water vapour treatment was performed at 6 hours and caused the production of aniline to increase to 47.6 % after 9 hours. The percentage composition then decreased again until after 13 hours only 4.7 % of the exit stream was aniline. The third water vapour treatment at 13 hours caused the aniline content of the exit stream to increase again to 20.8 % before it fell away until the reaction was stopped.

While the profile obtained from the 10 % Ni/10 % Cu/Al_2O_3 catalyst was similar to those obtained from copper and nickel, the profiles obtained from the 10 % Ni/20 % Co/Al_2O_3 (Figure 4.108) and 10 % Cu/10 % Co/Al_2O_3 (Figure 3.109) catalysts were extremely similar to the one obtained for 20 % Co/Al_2O_3. The 10 % Ni/10 % Co catalyst showed an initial rise in aniline composition to 66.7 % after 3 hours, while the 10 % Cu/10 % Co catalyst generated 27.3 % aniline in the feed stream, also after three hours reaction time. Sharp decreases in activity were observed after the initially high rate levels of aniline in the feed steam with both catalysts and further treatments with water vapour did not affect any recovery of the initial levels of aniline produced. Like 20 % Co/Al_2O_3 these catalysts had undergone complete catalyst deactivation.

The alumina support material was also tested for nitrobenzene hydrogenation activity in the same way and analysis of the reaction is shown in Figure 4.110. Only very low levels of aniline were produced throughout the duration of the experiment, with maximum percentage composition occurring directly after a treatment with water vapour. However, the maximum quantity of aniline present during analysis was only 5.1 % after 9 hours of reaction.

The final catalyst to be utilised in this way was the 1 % Pd/Al_2O_3 catalyst (Figure 4.111). Throughout the duration of hydrogenation a fairly constant level of aniline was produced. The percentage of aniline detected in the exit feed ranged between 7 %-16 %. The sample taken 1 hour after the water vapour catalyst treatments showed

the lowest percentage of aniline. At 9 hours, 1 hour after the second water vapour treatment the level of aniline produced was 8.6 % and after the third treatment at 14 hours was 9.6 %. So although the effect was small, the water vapour appears to have had the opposite effect on the catalysis with 1 % Pd/Al_2O_3 than on the HDC catalysts. The catalytic activity of the palladium catalyst was inhibited by the presence of water vapour, whereas with the HDC catalysts an initial increase in catalytic activity was observed following treatment with water.

The rate of aniline production throughout the hydrogenation experiments was calculated using Equation 4.9 (Section 4.3.3.1) for all catalysts tested with water vapour treatment. The variation in the rate over the duration of the experiment is displayed for each catalyst to illustrate the direct effect of the water vapour upon the rate of reaction. The data is displayed in Figures 4.112-4.119. To interpret the rate vs time graphs, they were compared with the sample composition graphs previously displayed in this section.

Figure 4.112: The rate of aniline production throughout the hydrogenation of nitrobenzene with water pre-treated 20 % Ni/Al_2O_3

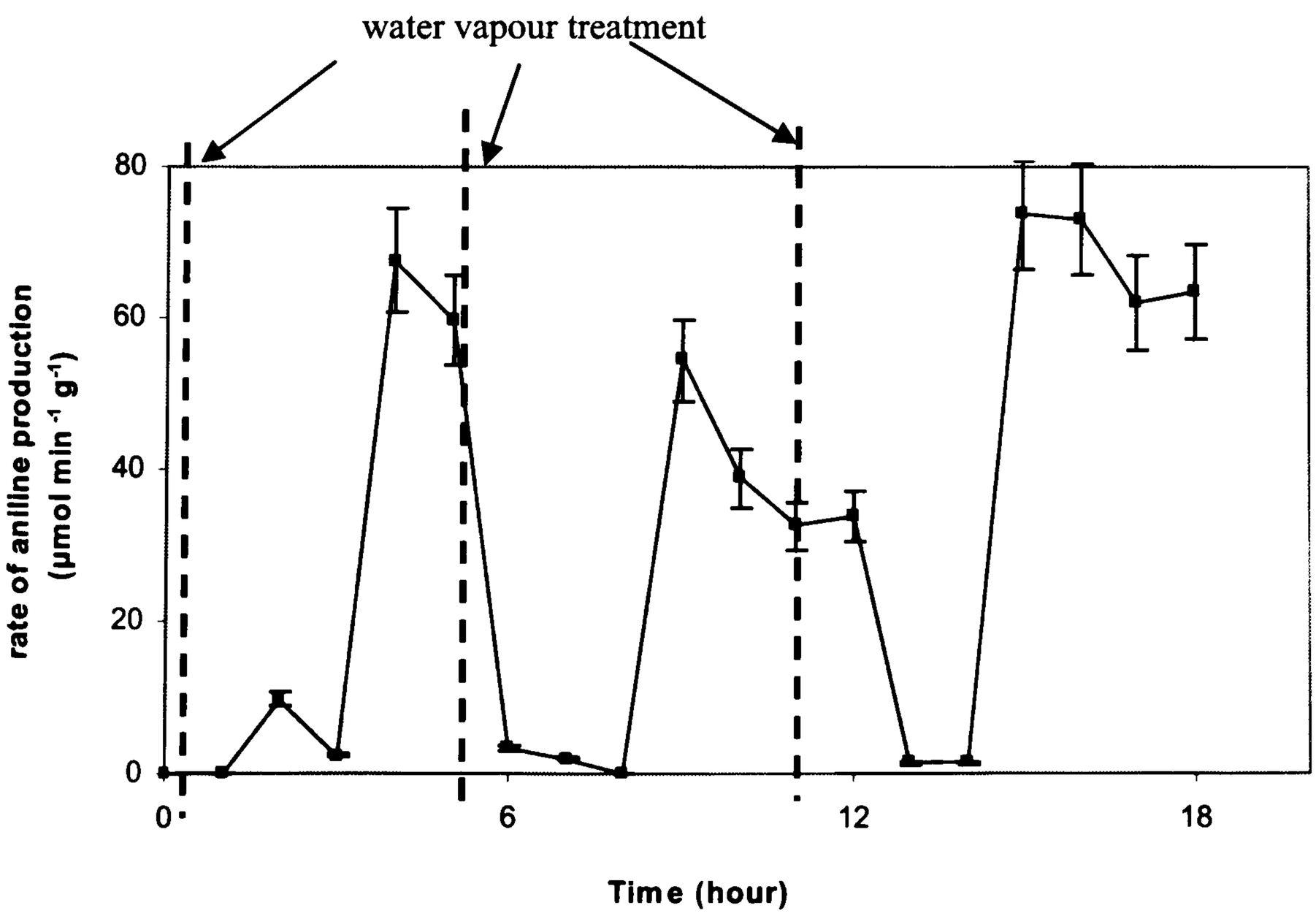

Figure 4.113: The rate of aniline production throughout the hydrogenation of nitrobenzene with water pre-treated 20 % Cu/Al_2O_3

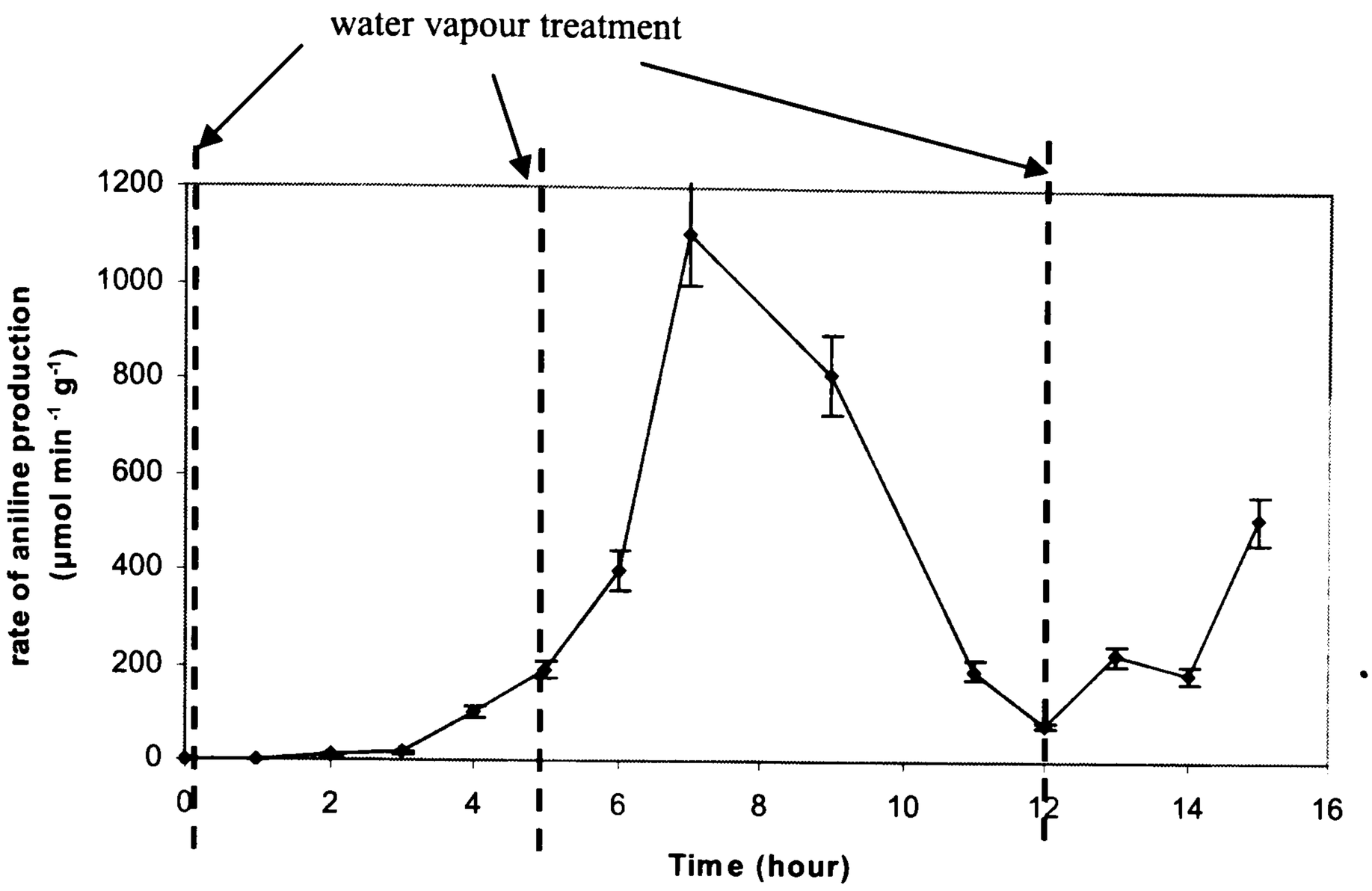

Figure 4.114: The rate of aniline production during the hydrogenation of nitrobenzene using water pre-treated 20 % Co/Al_2O_3

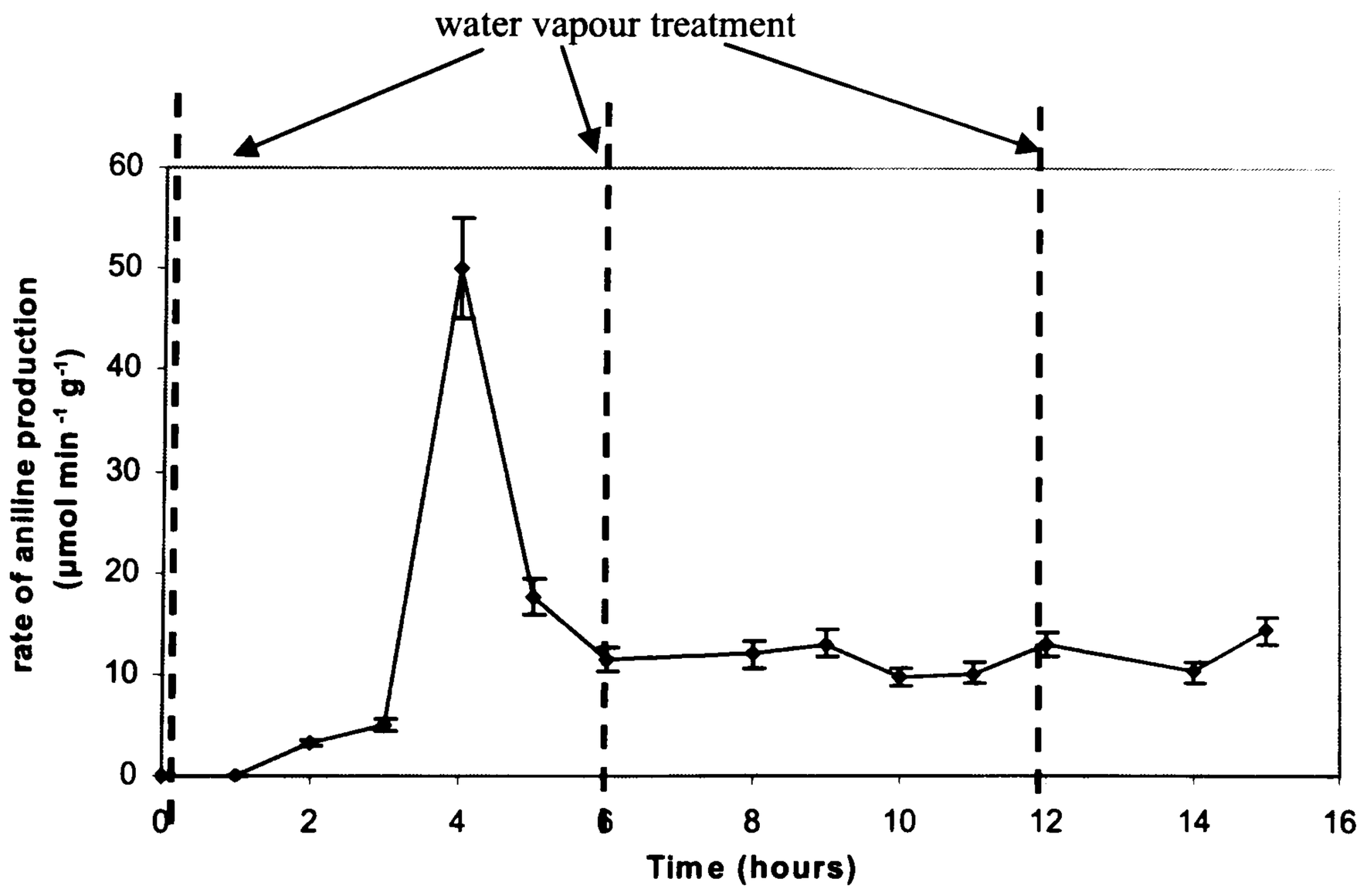

Figure 4.115: The rate of aniline production throughout the hydrogenation of nitrobenzene using water pre-treated 10 % Ni/10 % Cu/Al_2O_3

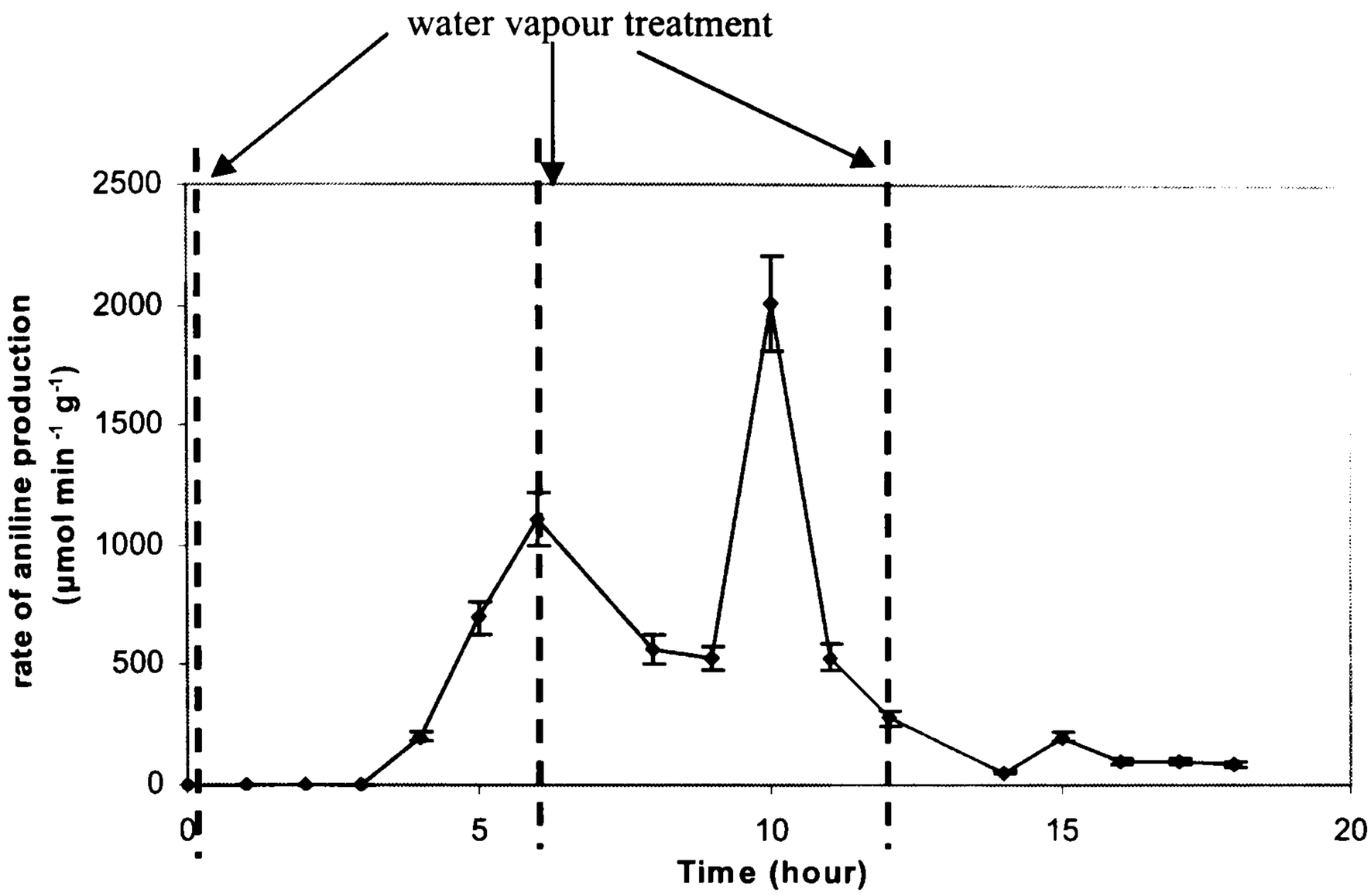

Figure 4.116: The rate of aniline production throughout the hydrogenation of nitrobenzene with water pre-treated 10 % Ni/10 % Co/Al_2O_3

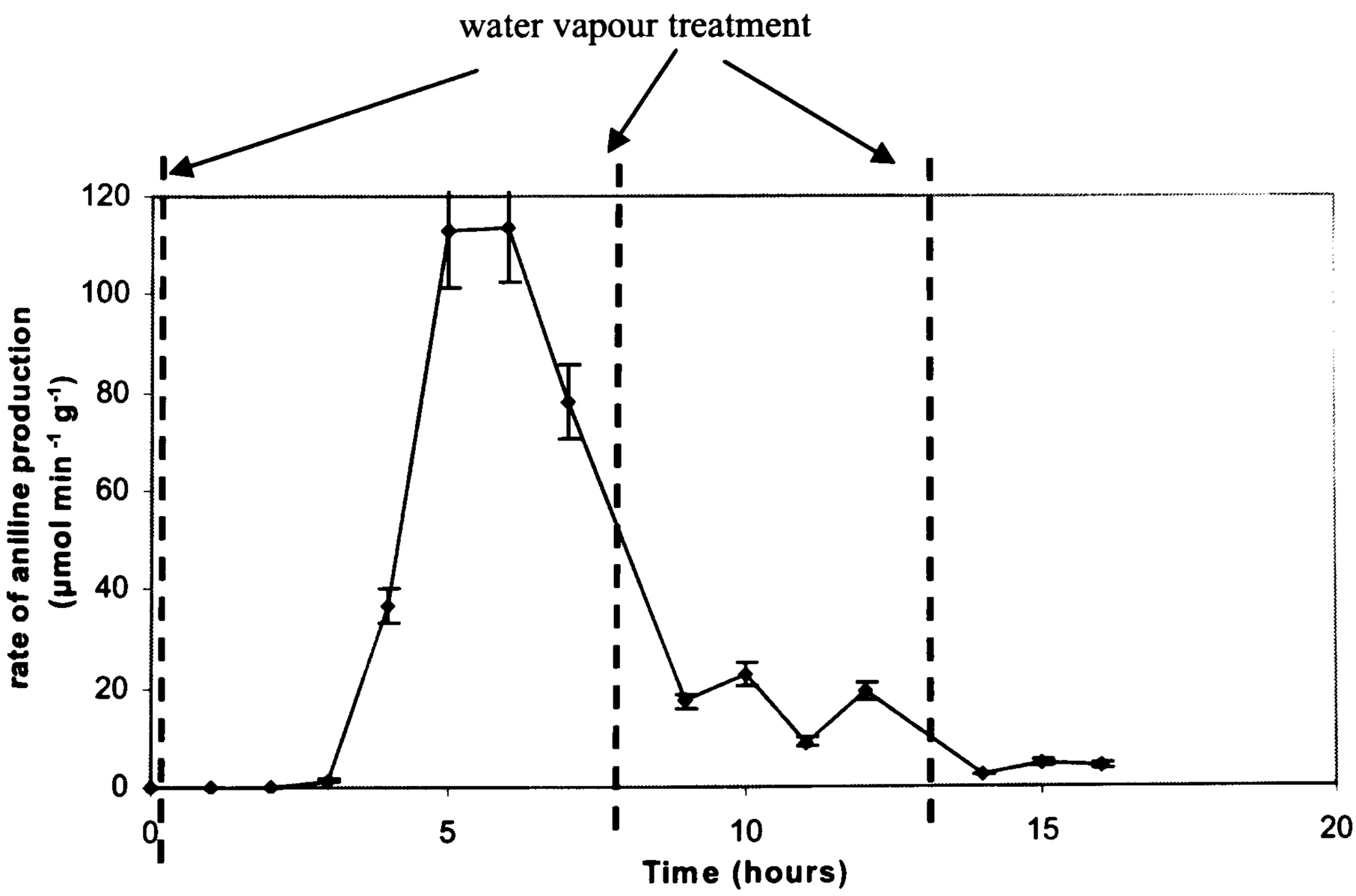

Figure 4.117: The rate of aniline production throughout the hydrogenation of nitrobenzene with water pre-treated 10 % Cu/10 % Co/Al_2O_3

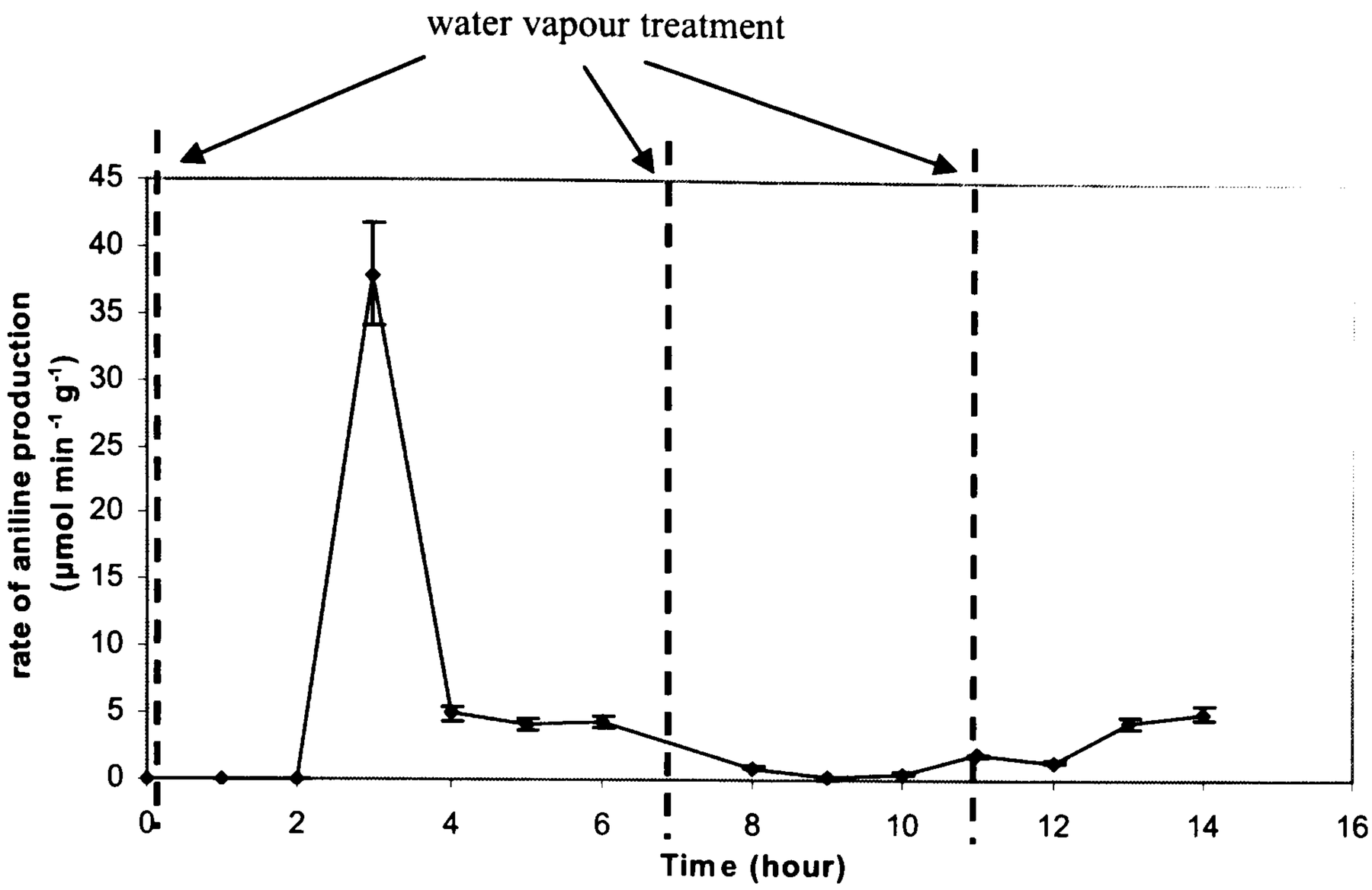

Figure 4.118: The rate of aniline production throughout the hydrogenation of nitrobenzene with water pre-treated Puralox Al_2O_3 support

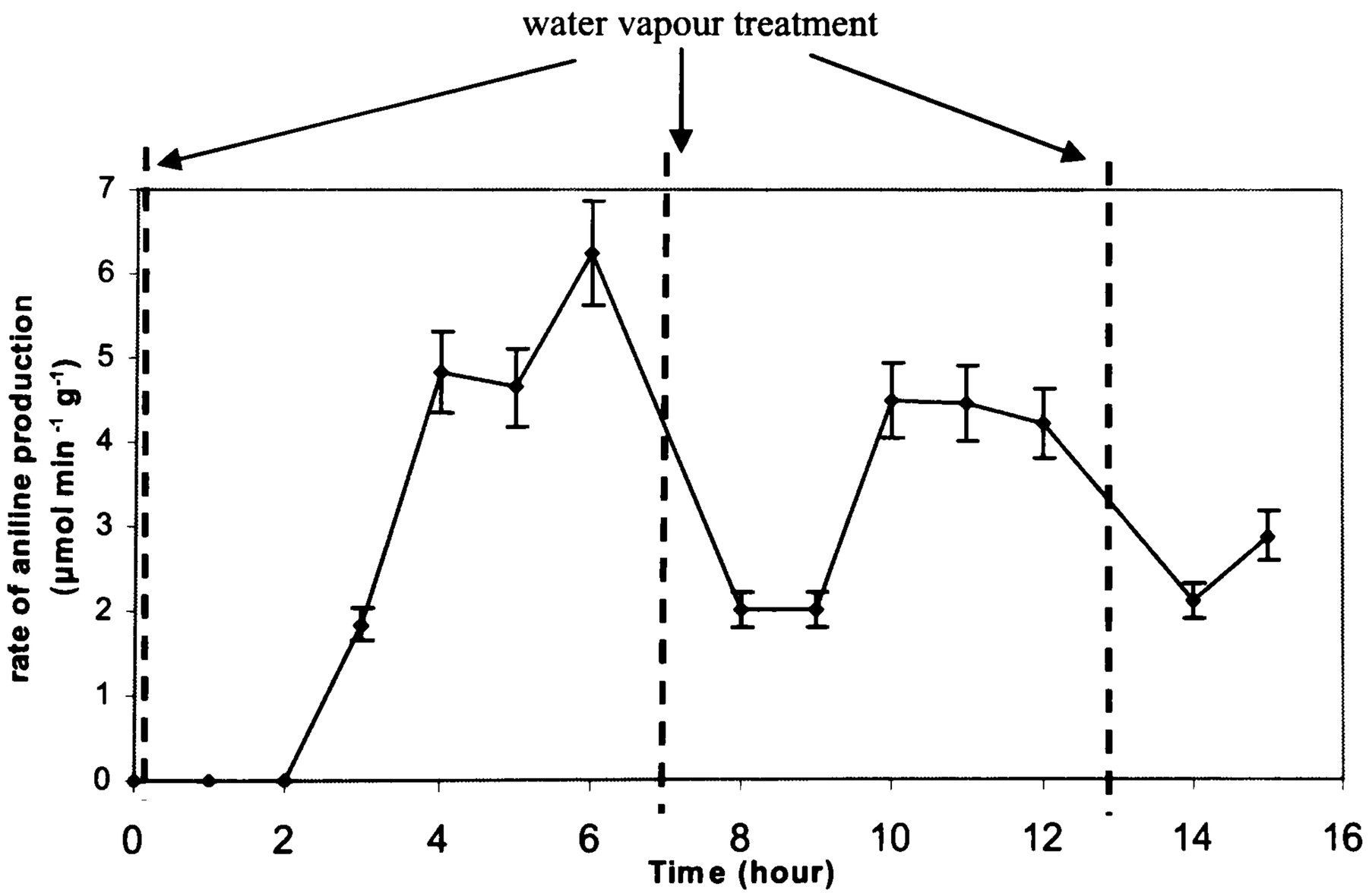

Figure 4.119: The rate of aniline production throughout the hydrogenation of nitrobenzene with water pre-treated 1 % Pd/Al_2O_3

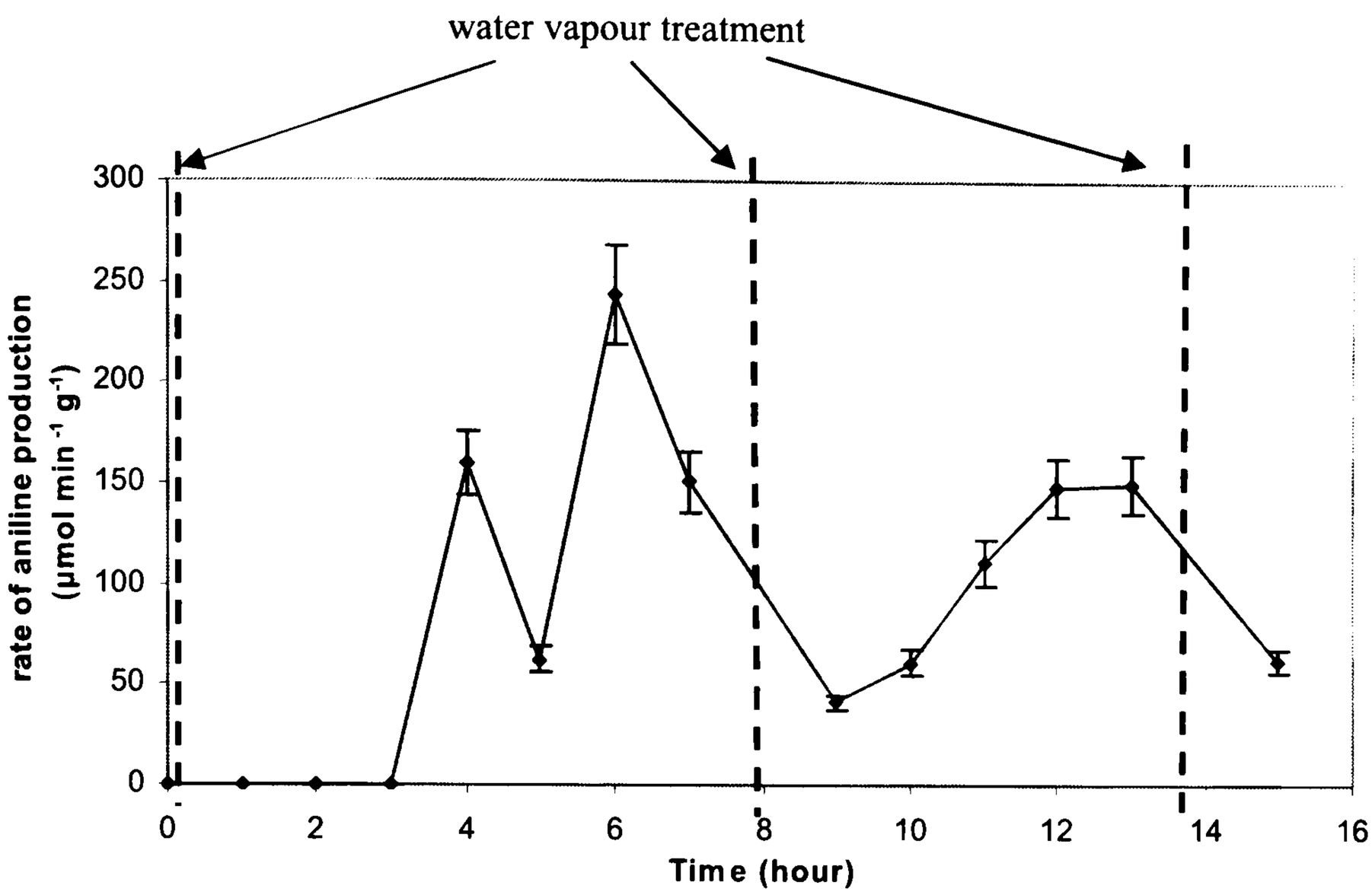

The graph of reaction rate over time for the 20 % Ni catalyst is displayed in Figure 4.112. Three rate maxima are clearly visible corresponding to 4 hours, 9 hours and 15 hours into the reaction with the aniline production rate at 4 hours equal to 64 µmol min^{-1} g^{-1}. The graph displaying composition of the exit stream from the same reaction is displayed in Figure 4.104 and shows a similar pattern, with the aniline composition maxima visible at 2 hours, 7 hours and 18 hours of reaction. So although the same activation/deactivation behaviour pattern is observed in both Figures, the effect of each water treatment on the reaction rate is delayed by approximately 2 hours when compared with the effect on the percentage aniline present in the reactor outlet. This may indicate that the water vapour present at the catalyst surface requires time to act and effect a change in catalytic behaviour.

The reaction rate graph for 20 % Cu/Al_2O_3 is displayed in Figure 4.113 and the graph of aniline composition has been previously shown in Figure 4.105. The rate graph displays a slowly increasing curve over the early stages after the initial water pre-

treatment. After the second feed of water at 5 hours the rate curve appeared to increase more rapidly, indicating a catalyst activation process was occurring. A maximum was reached at 7 hours when the rate of aniline production peaked at 1083 μmol min^{-1} g^{-1}. After this point the rate of reaction decreased to 57 μmol min^{-1} g^{-1} at 12 hours, where the second third water feed was commenced. A rise in the reaction rate was then observed until the reaction was stopped after 16 hours. With this catalyst, it appeared that the water vapour treatment was in some way aiding an activation process that allowed the catalyst to become more active towards the hydrogenation reaction that previously seen with the un-treated catalyst. Comparison of the rate graph with Figure 4.105 shows that the percentage aniline in the analysis samples followed a similar pattern. However, one striking difference was the shape of the graph over the first 3 hours of reaction. In Figure 4.105, the sample obtained at 2 hours was composed of 100 % aniline and no nitrobenzene, giving a sharp peak on the composition profile. In the rate graph, the rate at 2 hours is only 0.3 μmol min^{-1} g^{-1} and below that observed at 3 hours and 4 hours. As this sample was taken in the early stages of reaction, a very small volume of sample was collected, and although this was 100 % aniline the total number of moles of aniline obtained was much less than collected in subsequent samples. Therefore, the calculated rate of reaction is small. With the exception of this point the remainder of the graph in Figure 4.105 is comparable with the rate curve. The next maximum of aniline percentage was observed after 8 hours with clear activation and deactivation sections at either side of the peak. The promotional effect of the water vapour treatment is also observable on this graph.

Figure 4.114 shows the rate data for the 20 % cobalt catalyst. A maximum aniline production rate of 48 μmol min^{-1} g^{-1} was attained after 4 hours of reaction, whereas in the graph of sample composition in Figure 4.106, the maximum percentage of aniline was seen after 3 hours of reaction. After these maxima, both the aniline composition and the reaction rate decreased to a low level that was maintained throughout the rest of the reaction and unaffected by further water treatments. This behaviour indicated the catalyst had deactivated after the first wash with water and that, unlike the nickel and copper catalysts, the activity could not be even partially

regained with further water vapour treatment. After 6 hours the rate of reaction had decreased to 9 μmol min^{-1} g^{-1}.

The rate graph (Figure 4.115) and the aniline composition graph (Figure 4.107) for the 10 % Ni/10 % Cu/Al_2O_3 catalyst also proved to be comparable. The rate graph displayed three maxima at 6 hours (1106 μmol min^{-1} g^{-1}), 10 hours (2001 μmol min^{-1} g^{-1}) and 15 hours (212 μmol min^{-1} g^{-1}) of reaction. The graph of percentage aniline obtained from the reactor also displayed three maxima although at different points in time: at 3 hours, 9 hours and 15 hours. Thus like the 20 % Ni catalyst, there appeared to be a longer delay of the effect of a water vapour treatment on the rate of reaction, when compared to the percentage aniline collected from the reactor.

The behaviour of the 10 % Ni/10 % Co catalyst showed a very strong similarity to the behaviour of the 20 % Co catalyst. Figure 4.117 displays the data for the rate of reaction throughout the experiment. Little or no activity for aniline production was observed over the first 3 hours of reaction, however a rapid increase in rate to a value of 111 μmol min^{-1} g^{-1} was observed between 3 and 6 hours. After 6 hours the rate plummeted to just 12 μmol min^{-1} g^{-1} after 9 hours. Catalytic activity was not regained over the duration of the rest of the experiment, even following a water treatment. Comparison of this graph with Figure 4.108 shows a similar situation. Following the initial treatment with water vapour, the aniline composition was at its highest after 3 hours. After this point, very low percentages of aniline were collected in the remaining samples and the catalyst appeared to undergo a similar deactivation process to the 20 % cobalt catalyst.

Similarly, the 10 % Cu/10 % Co catalyst appeared to undergo irreversible catalyst deactivation after the first treatment with water. Figure 4.118 showed that the rate of aniline production reached a maximum of 38 μmol min^{-1} g^{-1} after 3 hours of reaction. After this catalytic activity was lost and a very slow rate, around 1 μmol min^{-1} g^{-1} was maintained throughout the remainder of the experiment. The behaviour displayed in Figure 4.109, the graph of sample composition, was very similar the variation in reaction rate. A maximum aniline content was obtained at 3 hours, after which only extremely low percentages of aniline were detected in the reaction

samples. Therefore, like the other cobalt containing catalysts, 10 % Cu/10 % Co appeared to have undergone an irreversible deactivation process.

Figure 4.119 displays the rate data collected for the hydrogenation experiment using the Al_2O_3 support. A low level of activity towards nitrobenzene hydrogenation was observed throughout the experiment with the aniline production rate ranging between 0-6 μmol min^{-1} g^{-1}.

The rate data from hydrogenation using 1 % Pd/Al_2O_3 is shown in Figure 4.120. The rate of aniline production was hugely variable throughout the experiment, with a maximum rate of 233 μmol min^{-1} g^{-1} observed after six hours. The minimum points in the graph are visible at 5 hours (67 μmol min^{-1} g^{-1}), 9 hours (33 μmol min^{-1} g^{-1}) and 15 hours (68 μmmol min^{-1} g^{-1}), with the latter to occurring directly after a water treatment. The graph of aniline composition over time shown in Figure 4.111 shows a relatively consistent level of aniline collected in the exit stream throughout the reaction.

4.3.3.5 Comparison of Reactions With and Without Water Vapour Pre-treatment.

The maximum rates of reaction for catalysts 20 % Ni/Al_2O_3, 20 % Cu/Al_2O_3, 20 % Co/Al_2O_3, 10 % Ni/10 % Cu/Al_2O_3, 10 % Ni/10 % Co/Al_2O_3, 10 % Cu/10 % Co/Al_2O_3, the Al_2O_3 support and 1 % Pd/Al_2O_3 using a nitrobenzene feed with and without water treatment were compared. Figure 4.120 shows this comparison as a bar chart.

Pre-treatment of the six HDC catalysts with water led to a dramatic increase in the rate of aniline production. The data displayed in Figure 4.120 revealed that the rate of reaction using the 20 % copper catalyst was increased by a factor of 204 on treatment with water. A smaller effect was observed with the 20 % cobalt catalysts where the rate rose from 16 μmol min^{-1} g^{-1} to 48 μmol min^{-1} g^{-1} an increase by a

factor of 3. However, the reaction rate of aniline production with the 20 % nickel catalyst was unaffected by the water pre-treatment.

Similar behaviour was observed with the mixed metal catalysts. Treatment of the 10 % Ni/10 % Cu/Al_2O_3 catalyst with water caused a huge increase in reaction rate to reach 2001 μmol min^{-1} g^{-1} compared with 57 μmol min^{-1} g^{-1} with the un-treated catalyst. With the 10 % Ni/10 % Co catalyst the rate increased to 112 μmol min^{-1} g^{-1} from 18 μmol min^{-1} g^{-1} upon treatment with water. The 10 % Cu/10 % Co catalyst was the only mixed metal catalyst to remain relatively unaffected by the water pre-treatment process giving reaction rates of 42 μmol min^{-1} g^{-1} and 38 μmol min^{-1} g^{-1} for before and after treatment respectively. The alumina support material also displayed a slight increase in catalytic activity upon water vapour treatment with the rate of aniline production rising from 1 μmol min^{-1} g^{-1} to 6 μmol min^{-1} g^{-1}.

Conversely, the 1 % Pd/Al_2O_3 catalysts exhibited a decrease in rate upon pre-treatment of the catalyst with water. The original rate with the untreated catalyst was 413 μmol min^{-1} g^{-1} whereas after water vapour treatment the rate dropped to 233 μmol min^{-1} g^{-1}.

Of the six HDC catalysts, the 20 % copper catalysts was the most efficient in both the un-treated and water treated state. However, the order of activity of the other catalyst altered depending upon the condition of the catalyst. For instance, the 20 % cobalt catalyst was the poorest of the six in the untreated state but after pre-treatment with water it became the second most efficient aniline producer.

Figure 4.120: Rates of reaction with un-treated and water pre-treated catalysts.

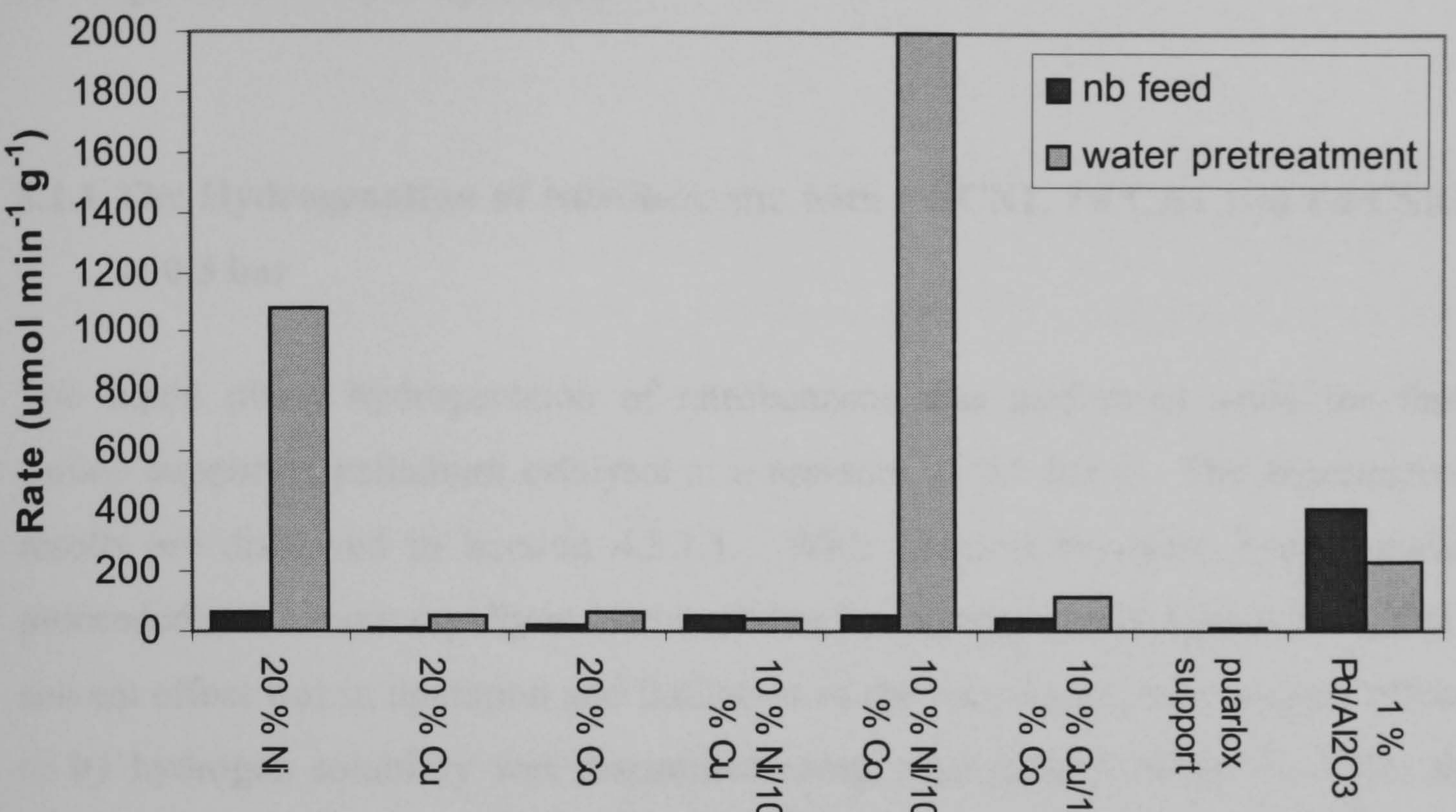

5.0 DISCUSSION

5.1 Liquid Phase Hydrogenation

5.1.1 The Hydrogenation of Nitrobenzene with Pd/CN1, Pd/CA1 and Pd/CSXU at 0.5 bar

The liquid phase hydrogenation of nitrobenzene was performed using the three carbon supported palladium catalysts at a pressure of 0.5 bar g. The experimental results are displayed in Section 4.3.1.1. With all three catalysts, hydrogenation proceeded much more rapidly in methanol than in isopropanol (IPA) indicating that a solvent effect was in operation and limitation of the reaction by mass transfer effects or by hydrogen solubility was discounted using experimental methods. From the initial rates of hydrogenation for each catalyst (Section 4.3.1.1, Figure 4.22) it is evident that the most disperse palladium catalyst with the smallest metal particles, Pd/CSXU, gave the highest activity, whereas the other two less highly dispersed catalysts display much slower rates.

5.1.1.1 Effect of Metal Particle Size on Specific Activity

A higher rate of reaction in methanol than in IPA was confirmed upon calculation of the specific activity, or turnover frequency, for each catalyst, although, a more complex situation was revealed (Section 4.3.1.1, Figure 4.22). In methanol, it was demonstrated that catalyst Pd/CN1, with the lowest dispersion, and catalyst Pd/CSXU, with the highest dispersion, were equally efficient catalysts and Pd/CA1 had the lowest activity. However, when IPA was used as the reaction solvent, a different pattern in turnover frequency is observed. Catalyst Pd/CN1, with the largest average particle size was the most efficient catalyst in terms of turnover frequency, followed by catalyst Pd/CSXU and Pd/CA1. This suggested that the reaction is structure sensitive as defined by Boudart in 1969 [178]. It is surprising that a particle size effect should be seen, as from the work by Hardeveld and Hartog

[179], the surface should be changing very little between 9 mm and 12 mm. However subsequent work by Bond in the early 1990s [180, 181], suggested that it was possible for metal crystallites to show some degree of structure sensitivity over a small diameter range, as the models proposed by Hardeveld and Hartog assumed the existence of perfectly regular and symmetrical metal particles across the support surface, which is not feasible under normal reaction conditions. Therefore, a much wider variation in the coordination number and number of neighbouring atoms to a surface metal atom was possible in imperfect crystallites, the factors considered ultimately responsible for changes in specific activity. Despite this, with particle sizes greater than 7 nm, the surface properties would still not be expected to change dramatically; meaning catalysts Pd/CN1 and Pd/CA1 would be expected to show near identical behaviour.

Earlier studies into the structure sensitivity of the nitrobenzene hydrogenation reaction have provided mixed results. Caturan and coworkers [182] studied the reaction in an *n*-octane solvent over palladium catalysts with a metal crystallite ranging between 1.3 – 10.6 nm and found the specific activity to decrease as the metal dispersion increased. This is contradictory to our experimental results where in both solvents: methanol and IPA, catalyst Pd/CSXU with an average crystallite diameter of 2.6 nm, displayed greater activity than Pd/CA1 with an average crystallite diameter of 8.7 nm. However Neri et al [183], examined the hydrogenation of 2,4-dinitrotoluene over Pd/C catalyst in ethanol. The palladium particles ranged between 2.6 – 8.4 nm and it was found that the specific activity increased as the palladium dispersion increased which is exactly as observed in our results over this particle size range.

The effect of particle size on the nitrobenzene hydrogenation reaction has also been studied over a variety of supported platinum catalyst, and like with palladium, a range of conflicting observations has been reported. The group of Macías Pérez [54] reported the hydrogenation in ethanol using Pt/C to be structure insensitive over an average platinum particle diameter of 1-7 nm. While Zhao, Ikushima and Arai [184], also using Pt/C and ethanol as the solvent, found the specific activity to decrease as

the Pt dispersion increased and the average platinum crystallite size decreased from 19.6 nm to 7.2 nm.

The dependence of the nitrobenzene reaction on the metal particle size appears to be a highly complicated area that can be strongly influenced by the specific reaction conditions including the choice of solvent, active metal and support. Therefore it is difficult to draw a conclusion from our experimental results. Hydrogenation reactions in general, are classed as structure sensitive reactions [185] and this does appear to be the case in our observations. However, why the catalytic activity of catalysts Pd/CN1 and Pd/CA1 is notably different and the activity of Pd/CA1 markedly lower than the other two are hard to explain. Therefore, it must also be considered that the support could be influencing the reactivity.

5.1.1.2 The Effect of Carbon Support on Specific Activity

Consultation of the manufacturers data sheets [186-188] for the three carbon support materials revealed that the surface pH of each carbon was different depending upon the chemical activation process. The surface pH of CN1 was reported as between 5.5 and 8.0, the surface pH of CA1 as between 2.0 and 3.5 and the surface pH of SX Ultra as neutral. A measurement of the pH of a methanol solution directly above the catalyst surfaces gave values of pH 6, pH 5.5 and pH 4.6 for catalysts Pd/CSXU, Pd/CN1 and Pd/CA1 respectively [189]. Comparison of the pH values with the turnover frequency graph displayed in Figure 4.22, revealed that in both methanol and IPA the catalyst displaying the lowest activity was the catalyst with the lowest surface pH; catalyst Pd/CA1. The surface pH of the other two catalysts, Pd/CN1 and Pd/CSXU, was of a similar value and close to neutral and, in methanol the specific activity of these catalysts was identical. There have been numerous studies into the effect of the surface properties of carbonaceous materials upon the catalysis by the supported metal and pH has been shown to be of importance [190]. It has been postulated that a lower pH is linked to higher oxygen functionality in the carbon support, which can affect the overall catalytic properties [191-194]. Recent studies [195] have revealed that carbons with a more acidic character have increased

interactions with cationic species in basic aqueous solutions and should lead to an increase in catalytic activity. A similar situation is described by Mikami et al with the adsorption of nitrogen containing species to a Pd-Cu/C catalyst in aqueous solution [196]. However, with our own hydrogenations, the reaction was carried out in methanol and IPA at neutral pH and so any surface oxygen moieties present on the support surface, such as –CO and $–CO_2$ will exist in a largely unprotonated form. An increase in these groups would lead to a build up of electronegative oxygen across the support material and would be likely to repel the nitro group of nitrobenzene as it approaches the surface to adsorb. Therefore, an acidic support material (Norit CA1) could be expected to reduce the specific activity of the nitrobenzene hydrogenation reaction by making the adsorption of nitrobenzene less favorable. The other two supports, with a near neutral surface pH would allow adsorption of nitrobenzene onto the support more readily and may increase the hydrogenation reaction by facilitating the adsorption of the reactant onto the metal active sites via a spillover mechanism.

5.1.1.3 The Effect of Reaction Solvent

The surface acidity of the carbon support may explain why the reactivity of catalyst Pd/CA1 is lower than the other two catalysts, however it does not explain why hydrogenation proceeds more slowly in IPA than methanol and why the relative activity of catalyst Pd/CSXU alters between the two solvents. These results are consistent with previous studies by Kochetova et al [123, 129] where reaction proceeded more rapidly in ethanol than in IPA. It was postulated in the later of these two papers that the slower rate may be due to a greater charge stabilisation of the intermediates in the reaction mechanism and a change of the rate-determining step in the reaction mechanism from the hydrogenation of nitrobenzene to the hydrogenation of nitrosobenzene. However, this thesis will go on to discuss our experimental results and their implications for the reaction mechanism in a subsequent part of this discussion.

A reduction in the reaction rate on moving from methanol to IPA was also observed by Takagi and co-workers during their studies on the hydrogenation of a number of

aromatic compounds [124] and by Clayton in her work on the hydrogenation of tertiary-butyl phenol [197]. The inhibiting effect of the solvents employed in their reactions was directly related to the donor number, δ, of the solvents, with negative delta values indicating an ability to accept electrons and facilitate the hydrogenation reaction. Solvents with positive values of δ which were incapable of accepting electrons were found to inhibit the hydrogenation. However, despite methanol, ethanol and IPA possessing very similar negative donor numbers, a much slower rate of hydrogenation in IPA was evident. The authors offered no explanation as to the existence of this difference. However, alcohol solvents are known to interact with the catalyst surface via the oxygen atom, frequently leading to dissociation of the solvent molecules onto the surface. However, analysis of the surface during the adsorption of IPA to activated carbon detected two adsorbed forms of the molecule: one in a non-dissociated state and the other dissociated to the alcohol anion and hydrogen [130]. Whereas, all adsorbed methanol was found to be present in the dissociated form [131] which would lead to a greater surface coverage of hydrogen across the carbon support. A more rapid rate of hydrogenation in methanol could then be achieved through an increased hydrogen spillover effect. This is summarised in Figure 5.1.

Figure 5.1: The adsorption of IPA and methanol onto the surface of activated carbon

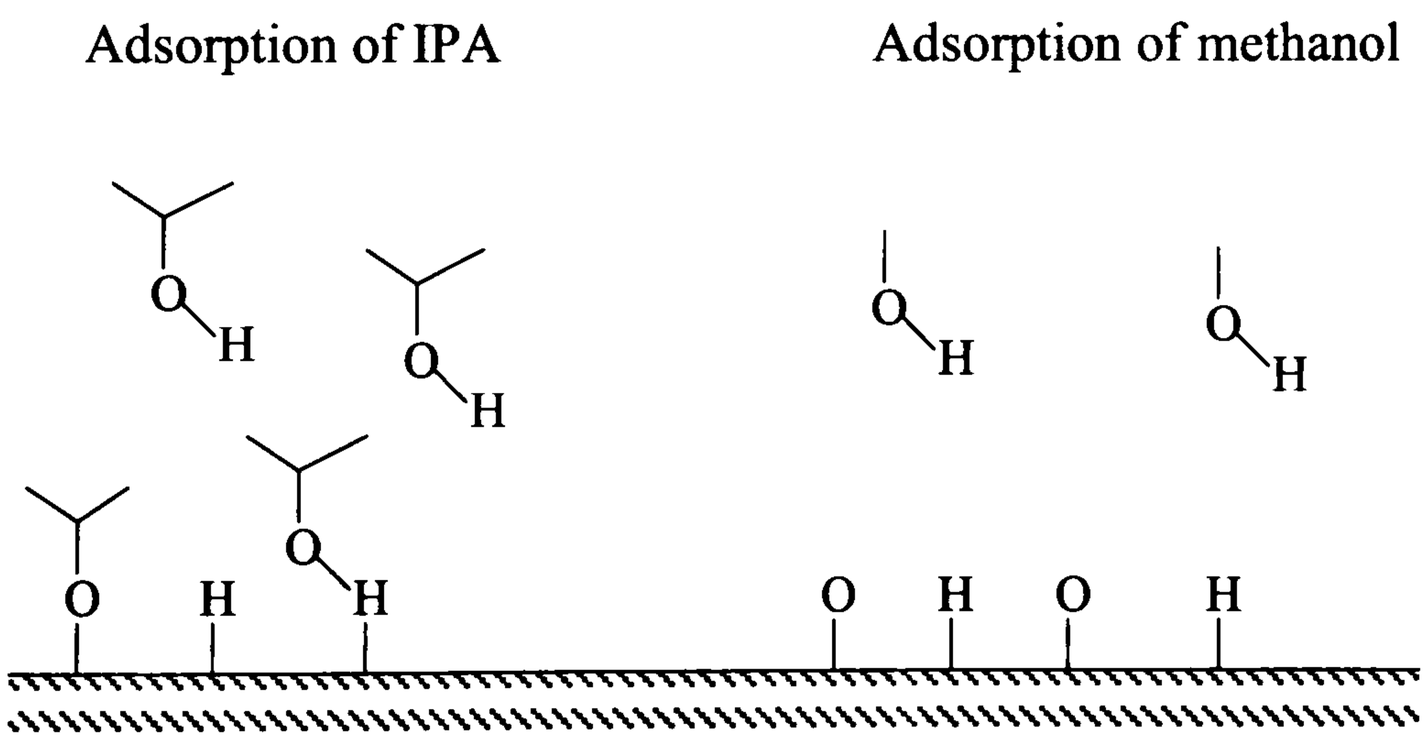

5.1.2 The Nitrobenzene Reaction Order

Experimental determination of the reaction order with respect to nitrobenzene, as described in Section 4.3.1.2, has revealed that below a nitrobenzene concentration of 0.58 mol L^{-1}, the order was –2, which was an unexpected result. Above this concentration, the reaction appeared to be zero order with respect to nitrobenzene. Previous studies by Acres [96, 97] and Metcalfe and Rowden [89] have also reported negative reaction orders with respect to the nitrobenzene concentration but did not provide any explanation for this phenomenon. However, studies by Han and co-workers [198] into the catalytic combustion of ethene over a palladium catalyst discovered a negative reaction order with respect to the alkene component and attributed this to the adsorbed ethylene blocking the rate-determining step of dissociation of diatomic oxygen onto the catalyst surface. A first order reaction dependence for the concentration of oxygen was calculated and confirmed this elementary reaction was the rate-determining part of the reaction mechanism. Dahl et al [199] also reported a similar situation in their study on the ruthenium-catalysed synthesis of ammonia. A negative reaction order with respect to ammonia was reported when its concentration was high and attributed a surface blocking effect. In this case, the rate-determining step of the transformation was attributed to the dissociation of nitrogen onto the catalytic surface and could be blocked by increasing the concentration of ammonia present in the reaction vessel.

If the dissociation of hydrogen is assumed to be the rate determining step in the nitrobenzene hydrogenation reaction, a similar argument to those detailed above can be applied. When the concentration of nitrobenzene is greater than 0.58 mol L^{-1}, the reaction appears to be zero order with respect to the nitro compound. At high concentrations, nitrobenzene would be expected to saturate the surface of the metal and carbon support thereby inhibiting the hydrogen dissociation reaction. However, when the nitrobenzene concentration is lowered, adsorption sites across the carbon support become available for both gaseous dihydrogen and dissociated hydrogen originating from adsorption of the solvent molecules. This hydrogen could then affect an increase in the reaction rate by spilling over to the active sites on the palladium holding the adsorbed nitrobenzene molecules. As the nitrobenzene molecule and the solvent molecules and diatomic hydrogen differ so much in their

chemical properties inhibition of the hydrogen dissociation reaction is unlikely to be due to competition for the same adsorption sites but more likely due to a physical blocking of sites by the large and bulky nitrobenzene structures.

5.1.3 Pd/C Catalyst Deactivation

The deactivation of the palladium/carbon catalysts was investigated using two separate methods. The first method, described in Section 4.3.1.3, involved the recovery and washing of the catalyst between a number of successive hydrogenations. A higher rate of reaction in methanol that in IPA was confirmed and steady deactivation of each catalyst was observed in both solvent systems. Deactivation by sintering can be completely ruled out as reactions were performed at low temperature, only 50 °C. Treatment of the catalyst after each reaction involved washing the recovered granules several times with cold methanol. As this procedure did not appear to prevent the deactivation process it can be deduced that any material retained by the catalyst was not soluble in methanol or was strongly adsorbed to the surface. Soxhlet extraction of the used catalyst with methanol was attempted at the conclusion of the experiment but analysis of the solution by GC-MS only revealed the presence of low levels of nitrobenzene and aniline. This is consistent with previous work by Dvorak [132], Petrov [133] on the deactivation of commercial nitrobenzene hydrogenation catalysts where the formation of a nitrogen containing carbonaceous over-layer was confirmed but the coke precursors could not be identified. Both authors were unable to remove any of the components of the deactivating coke from the catalyst surface, indicating these species must be very strongly adsorbed. Increasing the nitrobenzene feed flow rate appeared to increase the rate of coking and it was postulated that the carbon forming precursors were adsorbed surface species, possibly the reaction intermediates. A separate study by Amon et al. [136] reported similar behavior for alumina supported palladium catalysts and postulated that nitrobenzene itself acted as the coke precursor. This is a feasible explanation for our experimental results where the catalysts were in contact with a concentrated nitrobenzene solution and the reactant was successfully detected on the spent catalysts. In agreement with Yeong and co-workers [58], the activity of

our reused catalysts was not completely regained following reduction indicating that a permanent change to the catalytic surface had occurred.

Deactivation of the catalysts was also investigated in an experiment outlined in Section 4.3.1.4, where repeated injections of nitrobenzene were added to the reactor and hydrogenated with the catalyst left *in situ* throughout. This effectively measured the catalyst's response to increasing levels of aniline as each hydrogenation was run to completion before the following addition of nitrobenzene was made. Deactivation was observed using this methodology, although not to such a large extent as with the previous method detailed above. Aniline can therefore be ruled out as a coke-forming precursor, as an increase in the rate of deactivation would be expected under these conditions. Conversely, the presence of aniline in the reaction mixture appeared to have slowed down the deactivation process. The lack of effect of aniline on the deactivation process has previously been noted by a group of authors including Amon and Klemm, [90, 136] however no beneficial effects of adding aniline were noted.

Therefore, it seems likely that nitrobenzene or an adsorbed intermediate are responsible for the coke forming reactions as any competition with aniline for adsorption sites would hamper the coke formation reactions and lead to a slowed rate of deactivation. The migration of adsorbed neighbouring nitrobenzene molecules and reaction to form polymeric carbon species would also be prevented by the presence of adsorbed aniline. The rate of reaction would also be unaffected as the rate-determining step in the hydrogenation is unlikely to involve the surface coverage of nitrobenzene, as discussed above in Section 5.1.2. Due to the lack of data collected from the analysis of the used catalysts no further deductions concerning the nature of the coke precursors can be made.

5.1.3.1 The Effect of Aniline and Water

Further investigations into the effect of aniline, and the other reaction product, water, on the nitrobenzene hydrogenation reaction were carried out and the results are reported in Section 4.3.1.5.

The addition of aniline to the reaction mixture resulted in a slowing of the rate of nitrobenzene hydrogenation, however this effect was sensitive to the order in which the reagents were added. No inhibiting effect was observed when aniline was added after the introduction of nitrobenzene. However, pre-adsorption of aniline onto the catalyst surface caused a slight decrease in reaction rate. Competition between aniline and nitrobenzene for the active sites of the catalyst would be expected to lead to a decrease in reaction rate if the rate-determining step of the reaction involved adsorbed nitrobenzene, but as the nitrobenzene reaction order shows, the opposite situation is in fact true. Decreasing the nitrobenzene surface concentration appears to accelerate the overall reaction; the presence of high levels of nitrobenzene across the surface leads to the inhibition of the hydrogen dissociation reaction. Adsorption of aniline across the surface would also be expected to have the same effect by physically blocking the surface and preventing access of diatomic hydrogen to the surface. This may explain the deactivating effect of aniline but does not indicate why changing the order of addition of the two species has an effect. Pre-adsorption of aniline onto the surface may lead to a small number of active sites becoming unavailable for nitrobenzene adsorption and a decrease in activity. However, if nitrobenzene is added first and allowed to pre-adsorb to the catalyst, the low level of adsorption necessary for hydrogenation to occur can be achieved and the additional adsorption of aniline will have no effect, as was observed.

It should also be noted that analysis of the reaction mixtures revealed no additional species present when aniline was added. In particular, cyclohexylamine was completely absent showing that hydrogenation of aniline was not occurring in a competing reaction and again providing more evidence that aniline is unlikely to act as a precursor for the coke formation reactions thought to be responsible for the deactivation of nitrobenzene hydrogenation catalysts. This was confirmed experimentally when it was shown that all three palladium/carbon catalysts were

completely inactive for aniline hydrogenation. During these experiments the concentration of aniline in solution remained constant throughout and it did not appear that any surface reactions were occurring between adsorbed aniline molecules. As a result, the suggestion in previous studies that the formation of the by-products during the nitrobenzene hydrogenation reaction originates from the reaction of aniline and another reaction intermediate [85] can be discounted under these reaction conditions.

The small inhibiting effect of water was also sensitive to the order of addition of the reagents. A slowing of the nitrobenzene hydrogenation rate was observed when water was added prior to the introduction of nitrobenzene but not if water was added after the introduction of nitrobenzene. A similar effect has been reported by Chadwick, Oen and Siewe [200], where water was found to act as a mild kinetic inhibitor to the hydrogenation of tetralin over a sulfided metal catalyst and the magnitude of the inhibiting effect was found to be sensitive to the levels of the sulfide. At high levels of adsorbed hydrogen sulfide the inhibition effect caused by the addition of water was lessened. This was explained by invoking competition between the water and H_2S for adsorption sites on the catalyst. As the catalyst was always pre-sulfided before the water was added, the sites would be filled with the sulfur containing compound first and water appears unable to displace the H_2S from its positions on the surface. A similar effect could be in operation with our nitrobenzene hydrogenation catalysts, where pre-adsorption of nitrobenzene onto the surface prevents water adhering to the metal particles, most likely by blocking access, and causing a small level of deactivation. However, if the water is allowed to come into contact with the palladium crystallites before nitrobenzene is added, it can deactivate the catalyst in some way before the reagent is added. A possible negative effect could be caused by the oxidation of metallic palladium by the adsorption of water molecules. The oxidation of supported palladium by adsorbed water has previously been reported by Luo and co-workers [201] and Schmal and co-workers [202] both in 2000. It is postulated that the dissociative adsorption of water molecules can lead to the formation of Pd-OH across the catalyst surface and hence lead to a decrease in the number of catalytically active sites. In our reactor system,

any oxidation effect would be expected to be very small, as the hydrogen atmosphere would be expected to regenerate the reduced form of palladium very rapidly.

5.1.4 The Nitrobenzene Reaction Mechanism

Our experimental results have clearly shown that Haber's original mechanism for the hydrogenation of nitrobenzene is not adequate to explain our data and that some alterations to the scheme are necessary. The experiment results significant to the delineation of the mechanism and any anomalies with Haber's proposal are outlined below.

5.1.4.1 Implications of Deuterium Labelling Studies

Several experiments using deteruim gas or deuterium labelled materials were carried out with the aim of elucidating their involvement in the hydrogenation mechanism. Reactions were monitored using both ^1H NMR and by the hydrogen/deuterium uptake during reaction. However, the most valuable information was obtained from the gas consumptions as this method allowed a comparison of the relative rates of reaction and the determination of any kinetic isotope effects. The information gained from this was treated as described in several reviews [203, 204] on the use of deuterium and the analysis used to evaluate Haber's mechanism.

5.1.4.1.1 The Hydrogenation of d_5-Nitrobenzene

The data from hydrogenation of d_5-nitrobenzene are displayed in Section 4.3.1.6. The hydrogenation of h_5-nitrobenzene and d_5-nitrobenzene were shown to proceed with similar rates of hydrogen consumption. Therefore, the rate of hydrogenation was apparently unaffected by the substitution of the aromatic protons for deuterium atoms. The lack of any isotope effect indicates that the rate-determining step of the reaction does not involve interaction with the ring protons. This is expected as the

reaction order has already indicated that nitrobenzene is unlikely to be involved in the rate-determining step of the reaction. Furthermore, the low level of hydrogen-deuterium exchange, that occurred before the reaction commenced, suggests that although there is some degree of interaction between the catalyst surface and the aromatic ring required to allow this exchange to occur, the majority of interaction must be via the nitro group. This is consistent with the literature studies into the modes of adsorption of nitrobenzene onto a metal surface [73-77]. This low level exchange occurred almost immediately and was visible in the first reaction sample taken before the pressurised hydrogen atmosphere was introduced and did not increase as the reaction progressed. Initially, exchange was thought to occur with hydrogen on the palladium sites generated during reduction of the catalysts, however, calculation of the number of moles of hydrogen available from the source ($1.18 * 10^{-5}$ mol) shows that this would not sufficient to cause this level of exchange, where approximately $8.70 * 10^{-2}$ mol of hydrogen atoms were introduced into the nitrobenzene molecules. Therefore, the additional hydrogen must have been supplied either from the support surface via hydrogen spillover or originate from the dissociative adsorption of the methanol molecules with the carbon material. Both are likely and could occur simultaneously.

After exchange had occurred, the hydrogen atmosphere was introduced, which may have been expected to cause further exchange with the deuterium atoms. However, the limited interaction between the aromatic ring and the support surface appeared to have been lost completely after the introduction of the hydrogen atmosphere and the level of hydrogen-deuterium exchange remained constant.

5.1.4.1.2 The H_2/D_2 Kinetic Isotope Effect for Nitrobenzene Hydrogenation

When the nitrobenzene hydrogenation was preformed using deuterium gas in place of hydrogen, a kinetic isotope effect was observed, confirming that the rate-determining step in the nitrobenzene hydrogenation mechanism involved the making or breaking of a bond with a hydrogen atom. However, as no information on the surface concentration of reactant and intermediate species and the respective

contributions between any kinetic and thermodynamic isotope effects, or of the actual elementary steps involved in the hydrogenation of nitrobenzene, absolute interpretation of the observed effect is not possible. Despite this there are some useful conclusions to be drawn from these reactions. For instance, the absence of any isotopic substitution at the aromatic ring positions confirms our previous assumptions that the adsorption of the nitrobenzene molecule occurs via the nitro-group and the aromatic protons play no part in the catalytic process. As for the difference in reaction rate: a normal kinetic isotope effect was observed with a value greater than 1 [205]. This is consistent with what would be expected from a reaction involving the adsorption of H_2/D_2 to the catalyst surface or the surface reaction of a single H/D atom; the adsorption of H_2 on metals is considered to be thermodynamically more favourable than the adsorption of D_2 above room temperature and kinetically a surface bond to a deuterium atom will be stronger than that to a hydrogen atom through the zero point energy effect [206]. The magnitude of the observed effect at 1.9, is comparable to those found in other published hydrogenation studies. Ossipoff and Cant found a kinetic isoptope effect equal to 2.0 during the hydrogenation of propyne to propene using a copper silica catalyst [206], as did Meyer and Burwell with the hydrogenation of butynes to butanes over palladium [207]. The latter study went on to examine the reaction mechanism in detail and attributed the isotope effect to originate from the relative rates of adsorption of H_2 and D_2 from the reaction media onto the catalyst surface. Subsequent work by Inoue and Yasumori on the hydrogenation of acetylene over palladium, revealed a kinetic isotopic ratio of 1.6 in favour of hydrogen and also proposed the dissociative adsorption of H_2/D_2 to be the rate-determining step [208]. A similar scenario with the adsorption of hydrogen and deuterium onto our palladium catalysts could also exist, however, identification of a specific rate-determining step cannot be achieved with the available data.

5.1.4.1.3 The H_2/D_2 Kinetic Isotope Effect for Nitrosobenzene Hydrogenation

When the deuteration of nitrosobenzene, the first proposed intermediate in Haber's nitrobenzene hydrogenation scheme, was performed and compared with the

hydrogenation results some interesting observations were made. As for nitrobenzene a kinetic isotope effect was in evidence, however, an entirely different alteration in reactivity was observed. Over the first 15-20 minutes of reaction, the switch to deuterium gas had no effect on the rate of gas consumption indicating that the rate controlling part of the nitrosobenzene hydrogenation mechanism was unlikely to be the same as for nitrobenzene. The lack of an isotope effect strongly suggest that the rate-determining step in the reaction mechanism does not involve the substituted deuterium atom [209]. The situation changes again after 25 minutes of reaction when an inverse kinetic isotope effect was observed with the reaction proceeding more rapidly with D_2 (g) than with H_2 (g). A number of articles reporting the discovery of an inverse kinetic isotope effect can be found in the chemical literature; including studies by Aika and Ozaki on the catalytic synthesis of ammonia [210, 211]; Davis, Gillespie and Somorjai for hydrocarbon reactions over platinum [212] and Kellner and Bell during ruthenium catalysed Fischer-Tropsch synthesis [213]. Inverse isotope effects are generally considered to be a result of the many complex kinetic and thermodynamic consequences of substituting an isotope. Thermodynamic effects can become more dominant when the surface concentration of a reaction intermediate is altered as a result. This theory was used as a basis by Aika and Ozaki to explain the inverse effect, with a value of $\eta \sim 1$, observed during their afore mentioned studies. Surface species such as the adsorbed intermediates to ammonia synthesis were thought to inhibit the dissociation of N_2, the rate-determining step, onto the metal surface and use of D_2 (g) gas was found to alter the surface concentration of these species and increase the reaction rate. However, as for the nitrobenzene reaction there is not enough available information to deduce an exact rate-determining step in the hydrogenation of nitrosobenzene.

In summary, the most important point to draw from these experiments is that due to the conflicting results from the reactions with D_2 (g), the hydrogenation of nitrobenzene and the hydrogenation of nitrosobenzene can not proceed via the same reaction mechanism and, hence, it is very unlikely that nitrosobenzene acts as an intermediate in the hydrogenation of nitrobenzene as described in Haber's scheme. The mechanism of both reactions in considered in depth in the following sections as further experimental results are discussed.

5.1.4.2 Is Nitrosobenzene an Intermediate in Nitrobenzene Hydrogenation?

The rates of hydrogen consumption, and the reaction profiles determined from GC-MS analysis of the reaction mixtures from the hydrogenations of nitrobenzene (Section 4.3.1.12) and nitrosobenzene (Section 4.3.1.8) under identical reaction conditions, were examined and compared closely with the aim of collating information on the nitrobenzene hydrogenation mechanism. These results and their implications for the nitrobenzene hydrogenation mechanism have been explained in the relevant sections of the results section and have shown that the involvement of nitrosobenzene as a nitrobenzene reaction intermediate is unlikely. The evidence leading to this conclusion is summarized below.

The shape of the hydrogenation uptake curve for nitrobenzene was a smooth one-step curve, whereas the hydrogenation uptake curve for nitrosobenzene was distinctly different. The hydrogen uptake curve for nitrosobenzene displayed two distinct regions with a definite visible point of inflection, indicating that the hydrogenation reaction could be separated into two separate parts. The difference in the pattern of hydrogen consumption for nitrobenzene and nitrosobenzene immediately indicated that these compounds were not following an identical hydrogenation pathway.

The rates of hydrogen consumption during the reactions of nitrobenzene and nitrosobenzene revealed that nitrobenzene hydrogenation proceeded with the highest rate. The lower rate of hydrogenation of nitrosobenzene shed doubt on its involvement of this compound as an intermediate to the hydrogenation of nitrobenzene as, following normal kinetic theory, the rate of hydrogenation of the slowest elementary step in a reaction mechanism can not be slower than the rate of the over all transformation. The necessary omission of nitrosobenzene in the direct nitrobenzene hydrogenation pathway was confirmed when the rate of aniline production during the reaction was considered. A higher rate of production from nitrobenzene was observed and a much slower rate of production from nitrosobenzene.

Furthermore, examination of the GC reaction profiles revealed further evidence that nitrobenzene and nitrosobenzene hydrogenated via distinctly different reaction

mechanisms. Throughout the hydrogenation of nitrobenzene only very low levels of azoxybenzene were detected, amounting to less that 1 % of the molecules in solution at its maximum concentration. This reaction intermediate has been widely reported as present in the hydrogenation mixture during numerous published studies [86, 87, 91, 101, 102, 184] and confirms that the formation of dimeric ring species, as side products, is possible during the production of aniline from nitrobenzene, although these compounds do not act as direct intermediates. On the other hand, the hydrogenation of nitrosobenzene produced a range of species that were detectable during analysis of the reaction mixture. The reaction profile obtained during our experiments was remarkably similar to the one appearing in Smith's previous publication [106] and to work by another experimenter in our laboratory [214], the only two studies currently available for comparison with our results. Nitrosobenzene was initially converted to azoxybenzene during the first part of the reaction, which then reacted to produce the product aniline, however azobenzene could also be detected. This striking difference in reactivity provided further evidence that the nitrosobenzene was not following the same hydrogenation pathway as nitrobenzene.

5.1.4.2.1 Mass Balance of Nitrobenzene and Nitrosobenzene Hydrogenation Reactions

Throughout the hydrogenation of nitrosobenzene, a considerable quantity of material appeared to become adsorbed to the surface of the Pd/C catalyst and removed from solution. The rapid disappearance of nitrosobenzene without a concurrent rise in an equal number of moles of intermediates suggests that it is the nitrosobenzene species that is accumulating on the catalyst and not an intermediate further down the line. It is not possible to tell whether Smith and his group experienced the same dramatic loss of mass during their own nitrosobenzene hydrogenation reactions as the concentration of each component in the reaction data has been presented as a percentage of the total number of moles in solution and not as absolute concentrations [106]. Normalising our reaction profiles in this way produces a graph identical to the one presented by Smith et al.

However, a large mass balance loss, like the one experienced with nitrosobenzene, is not observed during nitrobenzene hydrogenation indicating that the interaction between nitrobenzene and the catalyst surface also differs from that of nitrobenzene. As part of a separate research project in the same laboratory [215], numerous attempts were made to measure the adsorption behaviour of nitrobenzene over a range of metal catalysts including the palladium/carbon used in this study. Despite the use of a wide range of techniques, reaction temperatures and concentrations, nitrobenzene adsorption could not measured leading to the conclusion that the interaction with the surface was weak and small below the levels of detection. Substantial adsorption to the carbon support material was observed, however, use of the supported palladium catalysts did not lead to any further measurable metal adsorption.

The adsorption behaviour, of both nitrobenzene and nitrosobenzene, has been studied in detail by Koutstaal et al. over a selection of metal oxides and has been shown to be very weak [216]. The interactions of both nitrobenzene and nitrosobenzene with the surfaces were followed using IR spectroscopy. Nitrobenzene was found to associate with the surfaces through a very weak interaction as the characterictic IR signals originating from nitrobenzene appeared at very similar frequencies upon adsorption. However, more significant signal shifting was visible in the IR spectra of adsorbed nitrosobenzene when compared with the spectrum of the free molecule. As a result it is concluded that the adsorption behaviour of nitrobenzene and nitrosobenzne is considerably different. Although the adsorption behaviour over an oxide surface would be expected to be quite different from that of the reduced state, the study confirms the earlier observations that the adsorption is very weak and difficult to observe.

The electrostatic potentials and reactivities of both nitrobenzene [217] and nitrosobenzene [218] have been extensively discussed by Politzer and co-workers and from this work it can be deduced how both molecules would be expected to interact with a reduced metal surface. The nitrobenzene molecule is though to exist in one dominant resonance due to the large electronic inductive effect whereas

nitrosobenzene can exist in three resonance forms, with retention of the nitrogen lone pair in each (Figure 5.2).

Figure 5.2: The charge centres in nitrobenzene and nitrosobenzene

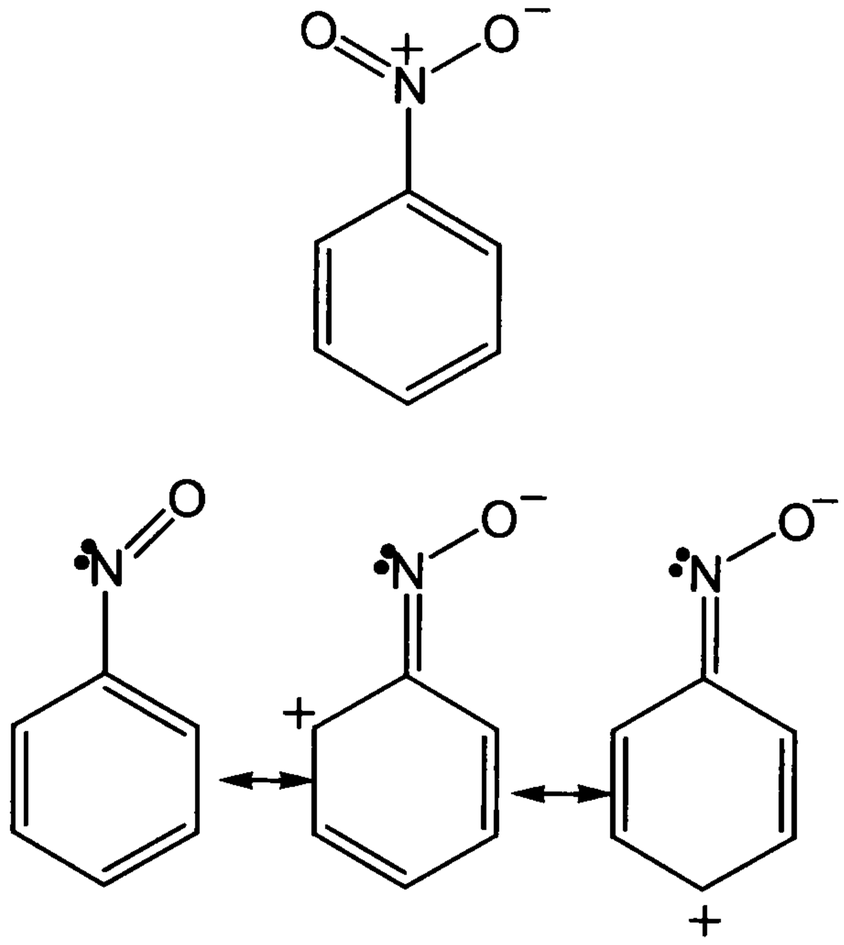

The nitrogen atom in nitrobenzene holds a strong electropositive charge, whereas in nitrososbenzene the nitrogen atom is strongly electronegative due to the localized lone pair. As a result, nitrobenzene and nitrosobenzene will display completely different adsorption behaviour. Due to the magnitude of the nitrosobenzene adsorption, which we observed it seems likely that the majority of interaction was occurring with the support material. The surface of the carbon would be expected to involve a large number of oxygen-containing functionalities [190, 192] providing an array of lewis acid sites available for interaction with the lone pairs on both the nitrogen and oxygen in the nitrosobenzene molecule, as well as a high surface concentration of hydrogen from the reduction process, available for hydrogen bonding. Nitrobenzene has no nitrogen lone pair available for bonding and only one oxygen atom likely to be reactive enough to form a surface bond. Due to its more favourable electronegative properties, nitrosobenzene would be expected to adsorb more strongly to the catalyst surface than nitrobenzene. This stronger interaction could have feasibly led to the large adsorption of nitrosobenzene, possibly as multilayers, onto the carbon support material during our reactions.

5.1.4.3 Inhibition of Nitrobenzene Hydrogenation by Nitrosobenzene and Azobenzene and Cyclohexlyamine

The addition of nitrosobenzene, azobenzene and cyclohexylamine to the nitrobenzene hydrogenation mixture all led to the inhibition of the nitrobenzene reaction. However, the degree and method of retardation was different for each compound and analysis of these effects has led to a greater understanding of the surface interactions.

The addition of nitrosobenzene completely inhibited the nitrobenzene hydrogenation reaction for occurring until the nitrosobenzene hydrogenation process was over. Nitrosobenzene was hydrogenated through to aniline before any reaction with the nitrobenzene could take place confirming that the adsorption of nitrosobenzene is much stronger than the adsorption of nitrobenzene. As described above (Section 5.1.4.3.1), it was suspected that nitrosobenzene was strongly adsorbing to the catalyst surface possibly via a series interactions to form a multilayer, hence completely blocking the active sites and preventing access of the competing nitrobenzene molecules to the metal surface. Therefore, pre-adsorption of nitrosobenzene onto the catalyst can stop the nitrobenzene hydrogenation reaction from occurring. Furthermore, adsorbed material, retained on the surface after nitrosobenzene had reacted also appeared to inhibit nitrobenzene hydrogenation when it finally began to proceed. There are two possible explanations for this effect. Firstly, the adsorbed material, consisting of bulky aromatic rings, can slow the rate of hydrogenation by hampering hydrogen adsorption: either by retarding its dissociation or by interfering with the surface diffusion of the adsorbed species. This in effect is similar to the situation observed during calculation of the nitrobenzene reaction order, discussed in Section 5.1.3, where increasing the nitrobenzene concentration decreased the over all rate of hydrogenation. Secondly, retention of adsorbed material could have led to a restructuring of the surface and an alteration in the active sites making them less effective for the nitrobenzene hydrogenation reaction. This can occur by blocking the active sites through irreversible adsorption, or poisoning, or through the generation of a carbonaceous deposit consisting of polyaromatic species and deactivation through coking.

A different inhibition effect was noted when azobenzene was added to the nitrobenzene hydrogenation mixture. In this case the hydrogenation of nitrobenzene and azobenzene appeared to occur simultaneously, however, at a much slower rate than observed with the hydrogenation of nitrobenzene on its own. The rate of hydrogenation, which was comparable to that observed for the hydrogenation of azobenzene however, was maintained over the later part of the graph, where the azobenzene experiments have shown a visible reduction in reaction rate, indicating that the nitrobenzene hydrogenation reaction was occurring very slowly. As the nitrobenzene reaction is not inhibited completely, azobenzene must not be as strongly bound to the surface as nitrosobenzene. However, the same causes of catalyst deactivation still apply. Inhibition of the dissociative adsorption or surface reactivity of adsorbed hydrogen by blocking the surface is likely due the large stereochemistry of the azobenzene molecules. It is unlikely, although still possible, that the catalyst has become deactivated through coke deposition, as there is no evidence that the catalyst has retained a significant amount of material.

The addition of cyclohexylamine to the nitrobenzene hydrogenation reaction mixture did not appear to have any detrimental effect on the catalytic activity. Similar rates of reaction were observed in the presence and absence of cyclohexylamine, and no additional by-products were visible during sample analysis. This was a slightly surprising result considering previous data collected by Hindle in a recent study into the hydrogenation of *para*-toluidine [219] in which found cyclohexylamine to poison the rhodium catalysts. The inhibiting effect was attributed to the loss of acidic sites across the surface due to irreversible adsorption of cyclohexylamine via the highly basic nitrogen lone pair as described in earlier studies into the toxicity of amines [116, 117, 220]. Therefore, it can be concluded that the adsorption of nitrobenzene does not occur on acidic sites across the catalyst. This is consistent with our previous results using palladium supported over three different carbons where the most acidic support displayed the lowest catalytic activity (Section 5.1.1.2) and with the only slight deactivating effect observed with the addition of aniline (Section 5.1.3.1). A recent study into the hydrogenation of cinnamaldehyde by Toebes and co-authors has described a similar situation where hydrogenation activity decreases as the number of acidic surface sites across the carbon supported platinum catalyst

increases [221]. Therefore, adsorption of cyclohexylamine on acidic surface sites does not interfere with the nitrobenzene hydrogenation reaction, as the two molecules are not in direct competition for the catalytically active sites. It would be of interest to determine the effect of adding cyclohexylamine to the nitrosobenzene reaction mixture, as this research has implied that the adsorption sites for nitrobenzene and nitrosobenzene are different. Nitrosobenzene, with possession of a lone pair on the nitrogen would be expected to bind to acidic sites across the surface and may be in direct competition with cyclohexylamine, which may lead to a poisoning of the reaction. Furthermore, the electrochemical and steric properties for the nitrogen containing aromatics and cyclohexylamine are very different, which may explain why adsorption of aniline, nitrosobenzene and azobenzene appear to inhibit the adsorption and/or surface diffusion of hydrogen whereas adsorption of non-aromatic cyclohexylamine has no effect on the reaction rate.

5.1.4.4 A New Mechanistic Proposal

Following our study into the hydrogenation of nitrobenzene, nitrosobenzene and azobenzene, it was concluded that our experimental results could not be adequately explained using Haber's original mechanistic proposal. This led us to look at the reaction scheme more closely. The initial pioneering work by Haber was carried out using electrochemical reduction methods and details the possible solvated intermediates in the reaction mixture. However, this scheme has been widely applied to the heterogeneously catalysed hydrogenation reaction, without taking into account the interaction of the reactants with the catalyst surface or consideration of probable surface reactions; a shortcoming that was recognized by Wisniak and Klein during their unsuccessful attempts to elucidate the reaction mechanism in 1984 [86].

As part of this study, detailed analysis of the surface reaction mechanisms for both nitrobenzene and nitrosobenzene was carried out and ultimately led us to propose a new mechanism for the hydrogenation of nitrobenzene and nitrosobenzene to aniline. The first step any catalytic reaction involves the adsorption of the reactants to the

surface of the catalyst. In this particular reaction, both nitrobenzene/nitrosobenzene and hydrogen are required to be adsorbed on the active site and in the correct orientation for reaction to occur. It is generally accepted that H_2 (g) dissociatively adsorbs into the surface of supported metal crystallites, especially on noble metals such as palladium [103]. As a result the hydrogenation of both reactions must proceed via a series of one-hydrogen addition steps. This was not accounted for in Haber's proposal, which shows the addition of two hydrogen atoms in each step along the pathway. The full analysis of the probable surface reactions of nitrobenzene is shown in Figure 5.3 and of nitrosobenzene in Figure 5.4.

Figure 5.3: Surface analysis of nitrobenzene hydrogenation

1. Adsorption of nitrobenzene and hydrogen

$$Ph\text{-}NO_2 \longrightarrow Ph\text{-}NO_2^* \qquad H_2\,(g) \longrightarrow 2H^*$$

2. Surface reactions

$$Ph\text{-}NO_2^* + H^* \longrightarrow Ph\text{-}NO(OH)^*$$

$$Ph\text{-}NO(OH)^* + H^* \longrightarrow Ph\text{-}NOH(OH)^*$$

$$Ph\text{-}NOH(OH)^* + H^* \longrightarrow \boxed{Ph\text{-}NOH^*} + H_2O$$

$$Ph\text{-}NOH^* + H^* \longrightarrow Ph\text{-}NH(OH)^* \quad \text{phenylhydroxylamine}$$

$$Ph\text{-}NH(OH)^* + H^* \longrightarrow Ph\text{-}NH^* + H_2O$$

$$Ph\text{-}NH^* + H^* \longrightarrow Ph\text{-}NH_2^* \quad \text{ANILINE}$$

3. Desorption of Product

$$Ph\text{-}NH_2^* \longrightarrow Ph\text{-}NH_2$$

During the analysis of the surface reactions, several considerations had to be taken into account. It was decided to avoid the use of nitrosobenzene as an intermediate species in the nitrobenzene pathway and also to include the formation of

azoxybenzene from nitrosobenzene during the early stages of that pathway to reflect the physical observations made during the actual reactions. The addition was more than one hydrogen atom at a time was discounted as was reactions requiring the interaction of more than two species simultaneously. In addition, the involvement of species, such as Ph-N^{-}, where the nitrogen has lost all bonds except to the phenyl ring were also avoided as the likelihood of forming very rare and unstable molecules when numerous more favourable reactions were available was thought to be low. As a result, it was decided that the most feasible reaction mechanisms for the hydrogenation of nitrobenzene and nitrosobenzene were the ones displayed in Figures 5.3 and 5.4 respectively.

Figure 5.4: Surface analysis of nitrosobenzene hydrogenation

1. Adsorption of nitrosobenzene and hydrogen

2. Surface reactions

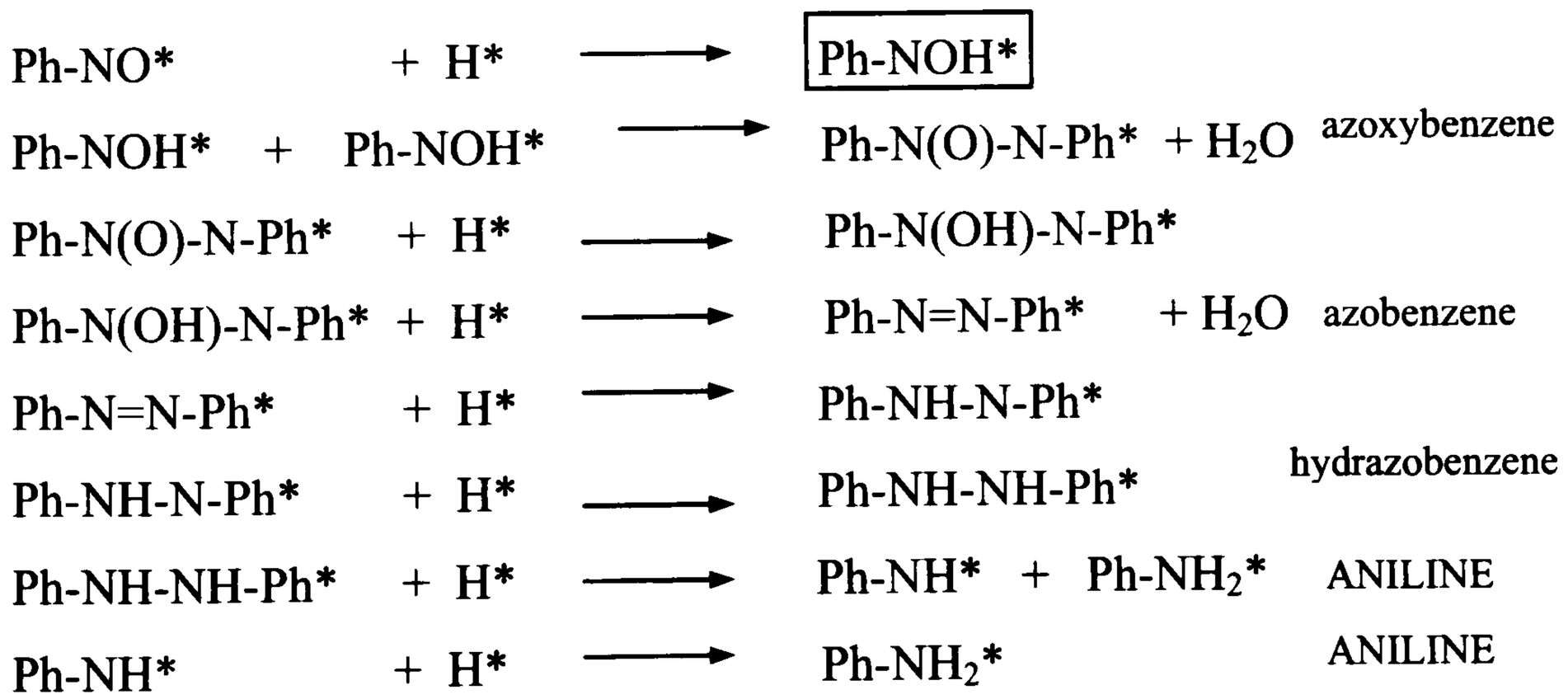

3. Desorption of products

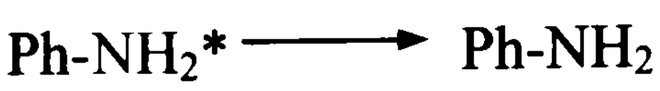

Examination of Figure 5.3, reveals the involvement of phenylhydroxylamine as an intermediate species, which was also invoked by Haber in his initial proposal. This intermediate has also been positively identified in previous published studies on the hydrogenation of nitrobenzene [91, 102]. None of the other compounds detailed in Figure 5.3 have been reported in the chemical literature but it is proposed that they are involved as adsorbed species and it is entirely feasible that intermediates that exist only as surface species can be involved in a catalysed reaction.

Figure 5.4, detailing the surface analysis of nitrosobenzene described the formation of dimeric species, including azoxybenzene, azobenzene and hydrazobenzene. These three species were included in Haber's original mechanism as by-products to nitrobenzene hydrogenation through the reaction of nitrosobenzene and phenylhydroxylamine. Our proposal suggests that azoxybenzene can be formed through the self-reaction of the first adsorbed intermediate in the nitrosobenzene hydrogenation pathway.

Comparison of the two separate mechanisms for the hydrogenation of nitrobenzene and nitrosobenzene reveal the involvement of a common adsorbed intermediate species, the boxed compound, Ph-NOH. Initially, the use of a common intermediate in the two pathways was an unattractive proposition, however, it became evident that is necessary to involve this surface species in both pathways. After the adsorption of nitrosobenzene to the surface, this must formulate the first step in the reaction mechanism, as it was required to react nitrosobenzene with one adsorbed hydrogen. If this species were to be avoided during the nitrobenzene hydrogenation pathway, addition of a dihydrogen molecule or use of an unfavourable species would have to be invoked. Furthermore, the observation of dimeric by-products, such as azoxybenzene and azobenzene in our reaction mixtures stipulated that the pathway towards these biphenyl compounds had to be accessible from the nitrobenzene hydrogenation mechanism without the involvement of nitrosobenzene. This was possible via the condensation reaction of two of these adsorbed molecules. Therefore, it transpired that the nitrobenzene and nitrosobenzene hydrogenation mechanisms were intricately linked through this common surface species.

This revelation led to the construction of a novel nitrobenzene hydrogenation mechanism incorporating hydrogenation of nitrosobenzene. This new proposal is presented in Figure 5.5. In this diagram, the solid arrows represent a single step whereas the dashed arrow indicates several steps have occurred to generate the illustrated species. After the adsorption of nitrobenzene there are three surface reactions involved to reach the adsorbed Ph-NOH intermediate; the addition of one hydrogen atom to give Ph-NO(OH), the addition of another hydrogen atom to this species to give Ph-NOH(OH) and the addition of a third hydrogen atom to give Ph-NOH with the simultaneous elimination of one molecule of water.

Figure 5.5: A new mechanism for the hydrogenation of nitrobenzene and nitrosobenzene

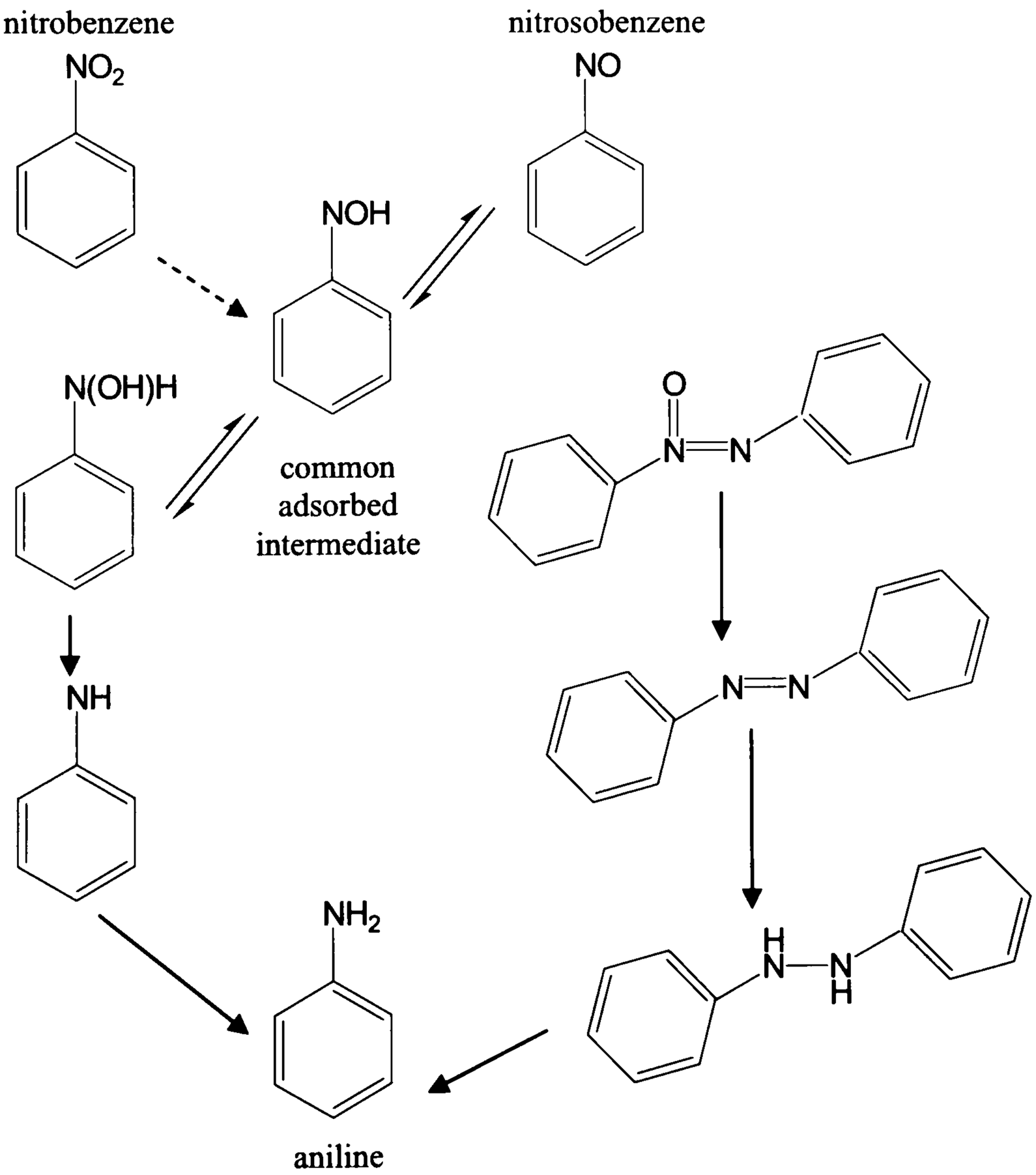

During the hydrogenation of nitrobenzene, the common adsorbed species is generated through a series of surface reactions. The rate-determining step in this pathway is likely to be one of these early reactions, possibly the dissociation of hydrogen onto the surface however; it may also involve the addition of an adsorbed hydrogen onto an adsorbed species and it is not possible to ascertain the exact identity of the rate-determining step with the available data. As the adsorption of the nitrobenzene molecule has been shown to be very weak, the surface concentration of the common intermediate, Ph-NOH, will be very low. In contrast the catalytic surface will be saturated with adsorbed hydrogen, therefore, reaction between the aromatic molecule and hydrogen to form phenylhydroxylamine is more favourable and statistically more likely. This reaction appears to occur very rapidly, as do the rest of the following elementary steps in the formation of aniline. This can be confirmed by the GC-MS analysis of the reaction mixtures, as none of these intermediate species were identified, suggesting that these hydrogenations were occurring quickly and one slow step was not causing the build-up of a particular reagent in solution. The formation of the dimeric by-products during the nitrobenzene hydrogenation reaction can also be explained by this mechanism. As shown in Figure 5.5, the common adsorbed intermediate can also react with itself to form azoxybenzene. As the surface concentration of this intermediate is assumed to be very low, the formation of only a low level of azoxybenzene would be expected during reaction and is consistent with our experimental observations.

The mechanism displayed in Figure 5.5 also describes the nitrosobenzene hydrogenation process. The nitrosobenzene molecule is strongly adsorbed to the catalyst surface and may even form a series of multiple layers across the metal surface and carbon support. Therefore, the surface concentration of the common adsorbed species will be extremely high and reaction between two neighbouring species highly probable. Azoxybenzene is generated in this manner and is hydrogenated through to aniline following the same pathway as previously described by Haber in his initial publication. The rate-determining step in this pathway must occur after the common intermediate has been formed, as during the initial stages of the reaction no kinetic isotope effect is observed when moving to deuterium gas, indicating the rate of hydrogen adsorption is not controlling the overall rate of

reaction. The coupling of two Ph-NOH molecules to make azoxybenzene must occur more rapidly than its disappearance to form azobenzene as an accumulation of azoxybenzene is observed during hydrogenation. Therefore, the most likely candidate for the rate-determining step is the second in the transformation of azoxybenzene to azobenzene (see Figure 5.4) involving the elimination of water from Ph-N(OH)-N(H)-Ph to give azobenzene. It is proposed that the reaction of azobenzene to give hydrazobenzene and the hydrogenation of hydrazobenzene to aniline both occur rapidly as hydrazobenzene was not visible in our reaction mixtures. Furthermore, the later step, decoupling the hydrazobenzene may be responsible for the inverse kinetic isotope effect observed during the second part of the nitrosobenzene hydrogenation reaction.

Figure 5.5 can also be used to explain the appearance of nitrosobenzene during the hydrogenation of nitrobenzene under some reaction conditions. The detection of this species has been reported during some previous reaction studies. However, consideration of the hydrogenation conditions, more specifically the hydrogen pressure and method of introduction, show that when the pressure is low or reactions performed under flowing hydrogen, the generation of nitrosobenzene in the reaction mixture is more likely, whereas when a large hydrogen pressure is used, the formation of nitrosobenzene is prevented. Our mechanistic proposal shows that phenylhydroxylamine, the common intermediate and nitrosobenzene are linked via two equilibrium steps. A pressure of hydrogen over the surface will drive the formation of phenylhydroxylamine via reaction of the common intermediate with adsorbed hydrogen, however, under low pressure or flowing hydrogen, a small number of Ph-NOH species can equilibrate back to nitrosobenzene through loss of a hydrogen atom. This is the less favoured reaction and only low levels of nitrosobenzene will be expected to form. Therefore, it is suggested that managing the hydrogen pressure can be used to control the by-products observed during the nitrobenzene hydrogenation reaction.

5.1.4.4.1 The Nitrobenzene Hydrogenation Mechanism Over Raney Nickel

The experimental results originating from the use of Raney nickel have proven to be extremely useful and have allowed us to formulate two important conclusions.

These reactions were performed at atmospheric pressure under a flow of hydrogen gas as opposed to the rest of the liquid phase hydrogenations performed under a pressure of hydrogen in the autoclave. Consequently these reactions were used to test our previous postulations in Section 5.1.4.5 that reducing the hydrogen pressure can lead to the formation of nitrosobenzene in the nitrobenzene hydrogenation reaction solution. This proposal was confirmed when a low level of nitrosobenzene was found to be present throughout nitrobenzene hydrogenation. It was not possible to utilise Raney nickel in the autoclave due to safety considerations and hence prove beyond doubt that the mechanism not altered upon use of an un-supported metal catalysts however, with the exception of the appearance of nitrosobenzene the reaction profiles obtained for nitrobenzene, nitrosobenzene and azobenzene were identical to those observed during the pressurised reactions. The formation of azoxybenzene from nitrosobenzene followed by decay to azobenzene and aniline was confirmed and was in agreement with our new mechanism.

Therefore, it was decided that the formation of nitrosobenzene during the hydrogenation of nitrobenzene could be adequately explained using our new mechanism displayed in Figure 5.5. In addition, we are also confident that this mechanism is consistent over metal catalysts and is not specific to palladium. This hypothesis will require testing over a variety of other metals and supports before this can be proven completely and forms a basis for future work into this area.

5.1.5 Hydrogenation using Alumina Supported Palladium

To ascertain the effect of the support on the palladium catalysis, a series of reactions using an alumina-supported catalyst was carried out as a comparison with the reactions using carbon-supported palladium. Initial investigations determined that the 1 % Pd/Al_2O_3 catalyst was slightly more efficient than the 3 % Pd/C catalyst in

terms of turnover frequency, indicating that the support was having an effect on the nitrobenzene hydrogenation reaction. Despite a much smaller surface area, of 110 $m^2 g^{-1}$ compared with 1200 $m^2 g^{-1}$ for the carbon, the alumina support was a more efficient catalysis promoter. This effect is probably due to the ability of alumina to dissociate hydrogen efficiently [222], increasing the availability of adsorbed hydrogen required in the rate-determining step in the hydrogenation of nitrobenzene. Whereas, although carbon is widely known to act as a hydrogen storage material [223-225], it can hold dihydrogen molecules ready for dissociation on a metal crystallite or accept dissociated hydrogen via spillover from the metal surface, hydrogen molecules are not widely reported to dissociate on carbon supports.

5.1.5.1 The Effect of Water on the Alumina-supported Catalysts

In contrast to the Pd/C catalyst, adding water to the nitrobenzene hydrogenation reaction mixture over the alumina supported palladium catalyst, produced an increase in the rate of reaction. This was an unexpected result, as water would be expected to have a negative effect on palladium catalysis, through partial oxidation of the metal particles (see Section 5.1.3.1), irrespective of the choice of support material. However, in this case it is evident that treatment of the alumina with a small quantity of water has resulted in promotion of the catalytic process. The adsorption of water onto alumina is known to occur at the acid sites on the support surface and even at room temperature, the dissociation of the molecule into H(ad) and OH(ad) is thermodynamically and kinetically favourable [226, 227]. Therefore, under our reaction conditions the added water would be expected to dissociate over the alumina support. As previously discussed in Section 5.1.4.3, active sites for the adsorption of nitrobenzene are unlikely to be of an acidic nature, and loss of Lewis acid sites across the alumina support would be unlikely to have a detrimental effect on catalytic activity. The dissociation of water ultimately leads to an increase in the surface concentration of adsorbed hydrogen, which may increase the rate of reaction if it is involved in the rate-determining step of the nitrobenzene hydrogenation mechanism. Moreover, if the interaction between the water and the alumina support is more favourable or more facile than the palladium oxidation reaction, the support may

protect the metal crystallites from partial and transient oxidation by removing the inhibiting effect of the water molecules. As any oxidation of the palladium would be expected to be reversed rapidly, due to the over pressure of reducing hydrogen, this small effect may be removed completely through support mediated water dissociation.

5.1.5.2 The Effect of Aniline and Cyclohexylamine on Nitrobenzene Hydrogenation

The addition of the nitrogen containing bases, aniline and cyclohexylamine to the nitrobenzene hydrogenation solution caused a reduction in the rate of reaction. This was in contrast to the effect observed during hydrogenation when the Pd/C catalyst was utilised; aniline caused a small reduction in rate and cyclohexylamine appeared to have no effect (see Section 5.1.4.3). The behaviour of these compounds over the alumina catalyst was more like that expected from previous literature where the strong adsorption of these compounds, via the nitrogen lone pair, led to a reduction in the acid sites and a reduction in catalytic activity [116-118, 122, 219, 220]. In this case a bigger deactivation effect would be expected from the more basic, non-aromatic molecule of cyclohexylamine. However, it has already been postulated that the acid sites are not involved in the catalysis of the nitrobenzene hydrogenation reaction. The small deactivating effect upon addition of aniline can be explained using the same arguments, given in Section 5.1.3.1, for the influence of aniline on catalysis using the Pd/C catalysts. Here it was postulated that the pre-adsorption of aniline onto the catalyst surface led to the physical blocking of the surface, preventing access of molecular hydrogen to begin the adsorption process, and reducing the mobility of the adsorbed hydrogen species. The difference in the effect of cyclohexylamine on the Pd/C and Pd/Al_2O_3 catalyst is harder to explain but shows that a definite support effect is in existence.

5.2 Nitrobenzene Hydrogenation using HDC Catalysts

5.2.1 The HDC Catalyst Preparation Method: Mechanism of Catalyst Synthesis

Although the HDC method of catalyst preparation has been used extensively in industry to prepare a range of commercial products, the majority of research into the technique and resultant catalysts has focused upon the precipitation of one metal ion from solution. In this project, a range of catalysts was synthesised involving the deposition of two metals onto the support surface. Therefore, it was of interest to investigate how the process was affected by the addition of the second metal.

Comparison of the pH profiles collected during synthesis of the twelve catalysts (Section 4.2.1) revealed that a similar pattern of pH reduction is observed for both the single metal and mixed metal catalysts. The decrease in pH was monitored throughout reaction for all catalysts and was found to stabilise between 7.5 and 8.5 in a similar time period, indicating that ammonia was being totally removed from solution by the distillation process and was not retained by any of the metals used. Therefore, it can be concluded that both metals were completely deposited during synthesis of the mixed metal catalysts and the addition of a second complex was not hindering the lay down of the other metal. This was confirmed by the elemental analysis shown in Section 4.2.3, and the elemental ratios obtained from the XPS data in Section 4.2.10, which both identified the intended ratio of metals present in the collected catalysts.

In addition to the pH, the colours of the preparative solutions were carefully monitored during catalyst synthesis. An analysis of the colour changes observed during synthesis of the catalysts is given in Section 4.2.2 and from these data it was deduced that a two-step deposition process was occurring during preparation of the mixed metal systems. Consultation of stability constant data [228-230] for the three metal amine complexes confirmed that expected order of reactivity. Cobalt (II), with the lowest over all stability constant (Log K = 5.14), would be expected to release the ammonia ligands during distillation most easily and precipitate more rapidly than the

copper (II) or nickel (II) ions. Nickel has the next lowest overall stability constant of Log K = 9.08, which is smaller than copper's value of Log K = 13.1. Therefore, nickel would be expected to deposit before copper, the most stable ammonia complex. This generally is in agreement with the colour change observations, although there are some discrepancies, detailed in Section 4.2.2. However, the precipitation of one metal onto the alumina support did on occasions lead to the formation of a dark coloured catalyst, which may have distorted the colour of the remaining metal ion solution and made it difficult to identify visually the remaining metal ion by colour. It addition, although the precipitation process was occurring largely in two distinct stages there may also have been periods in the reaction where both metals were depositing simultaneously; the deposition of the second metal may commence before the ammonia complexes with the first metal have been degraded completely. Simultaneous deposition would be expected to give a random distribution of both metal ions across the support surface, where both metal phases were thoroughly mixed. However, the more likely scenario involves the precipitation of one metal, which can then have a directing influence upon the other metal ion. Further characterisation was carried out in order to ascertain the nature of this influence. More specifically, to determine if the second metal precipitated into the spaces on the alumina left vacant by the initial precipitation of the other metal ion, or if the second metal deposited on top on the already existing metal crystallites forming mixed metal particles across the surface.

5.2.2 Evaluation of Catalyst Characterisation Results

Characterisation of the twelve catalysts prepared for this project, using the highly dispersed catalyst (HDC) method described in section 3.1.4.4, was carried out with the main aim of ascertaining how the two metals in the bimetallic systems were interacting, and more specifically were they forming bimetallic particles? The classification of the interactions in mixed-metal catalysts can be a controversial subject. To qualify as a true alloy, two metals must be capable of forming a continuous series of homogeneous solid solutions, with the atoms of one metal distributed randomly through the atoms of the other. This can be achieved if a second

metal can infiltrate the crystal lattice of another by replacing some of the lattice atoms to form a substitutional alloy or by occupying the interstices between the lattice atoms to form an interstitial solid solution. A substitutional alloy can only form if the two metals have similar enough physical properties and crystal structures to prevent compound for formation and favour the creation of the alloy. Copper and nickel are known to form a range of alloys under a range of conditions [231].

An alloy catalyst is defined as a system that contains an alloy as the active catalytic component or as the catalytic precursor [232]. The problem of deciding whether the supported metal crystallites can be rightly classified as an alloy is both complicated and difficult to investigate. If the metals are used in a low loading and a highly dispersed state then the likelihood of alloy formation is greatly reduced. However, with metal loadings reaching significant levels, like the ones used during this study, the situation is still unclear. To avoid confusion, catalysts consisting of two or more metals, which exhibit an enhancing or inhibiting effect on catalytic activity, are referred to as bimetallic catalysts. A number of theoretical situations arise, for instance the two metals may not be fully alloyed and particles containing one metal only may be present, or all metal particles may not have the same metal composition, or be homogeneously distributed throughout the catalyst support. Furthermore, segregation may occur if one metal preferentially occupies one type of site and gas induced segregation, where adsorption of a gas molecule causes one metal to preferentially move to the surface [233, 234], is commonly reported in alloy catalysts. Unfortunately, these queries cannot be resolved using normal catalyst characterisation techniques and the situation remains unclear. However, a variety of different surface probing analyses can be used in combination to give an idea of the over all picture and allow educated hypotheses to be drawn. In this research a range of characterisation methods was utilised some providing positive evidence for the formation of alloys and some suggesting the metals were maintaining their individual identities. This work was performed on the freshly synthesised catalysts prior to use in the reactor, therefore, these techniques give information about the metal interactions in the precursor state but do not indicate how these metal interactions are likely to change, if at all, in their reduced states and under reaction conditions. However, the activities, and reaction behaviour, of all the catalysts were compared

and contrasted with each other to try and draw some conclusions about the effects of adding a second metal. Significant beneficial differences in reactivity can indicate that an alloy has formed.

The evidence most in favour of the formation of mixed-metal particles was found during characterisation of the catalysts using UV-Vis spectroscopy. Significant effects were visible in the UV-Vis spectra of the single metal upon the addition of a second component. Band shifting and band splitting were observed in the spectra of the copper-nickel, copper-cobalt and nickel-cobalt catalysts indicating that the second metal had perturbed the immediate coordination sphere of the original metal. For this effect to have been visible the two metal ions must have existed in very close proximity, perhaps sharing common bridging ligands. A situation such as this has been observed recently by Salerno, Mendioroz and Lopez Agurdo [235] during characterisation of newly synthesised Ni-Mo bimetallic catalysts, where UV-Vis spectroscopy was used to confirm the formation of an $NiMoO_4$ compound on the surface of their catalysts. Therefore, the results from this technique strongly indicate that bimetallic particles consisting of copper-nickel, copper-cobalt and nickel-cobalt were present in the catalysts. Although copper and nickel would be expected to form an alloy under the correct specific conditions, an interaction between copper and cobalt, and cobalt and nickel is less well known. Due to the lack of literature available on the UV-Vis characterisation of mixed metal catalysts consisting of copper-cobalt and nickel-cobalt, no direct comparisons with similar catalysts can be made, however, it is generally accepted that species, which are unable to integrate in the bulk material can interact as small, supported crystallites [232].

Analysis of the catalytic surface by Raman spectroscopy also suggested that the mixed metal catalysts were significantly different from that expected from a combination of the two discrete metals on the catalyst. The disappearance of bands and the appearance of different bands, caused by band splitting or band mixing, were both observed in the spectra of the mixed metal systems. The spectra also indicated that the surface of the catalysts across a series of mixed metals became progressively more like that in the single metal system indicating that the addition of a second metal was altering the electronic properties of the initial metal. This could be

produced by an alloying effect or by the formation of a layer of the second metal across the original metal particles causing a screening effect.

The TPR analysis was unable to clarify the situation further. Although definite reduction promotion effects were visible in the reduction profiles of the mixed metal catalysts it was not possible to ascertain the exact mechanism of enhancement from the available data. In the past, the merging of two TPR peaks in a bimetallic catalyst, as seen for the 10 % Ni/10 % Co catalyst has been considered an indicator of mixed-metal particle formation, however, it is now agreed that this is not a reliable detection method. Hydrogen spillover by either an interparticular or intraparticular mechanism can elicit the same response. Nevertheless, if the addition of a second metal can aid the reduction process and increase the active metal surface area, an improvement in catalytic performance may be observed. With these particular catalysts the activity for nitrobenzene hydrogenation did not appear to be greatly enhanced in the use of two metal phases, except with the 10 % Cu/10 % Ni catalyst where a vast improvement was visible.

Electron microscopic analysis of the 10 %/ 10 % catalysts in their unreduced precursor states provided further interesting information about the nature of the interaction between the two metal carbonate salts. The image obtained for the mixed nickel/cobalt catalyst clearly showed that both metals are dispersed evenly across the surface of the support particles, forming an almost homogenous layer. This evidence strongly suggests that mixed metal or "alloy" particles have been formed during the catalyst preparation method. As discussed earlier, this could be achieved in two ways; either by the metals depositing simultaneously during the precipitation process or by one metal depositing first and the second metal attaching to the sites left vacant by the first metal complex, which is more consistent with the colour changes observed during preparation of the bimetallic catalysts. However, the opposite effect is evident with the interaction of copper on the support. This was confirmed by the SEM images for the mixed copper/nickel and copper/cobalt catalysts showing that copper was not well dispersed across the alumina particles but localised in distinct crystallites. A poor copper dispersion was confirmed by the reactive

chemisorption results, which revealed a very low total metal surface area contribution from copper in all relevant HDC catalysts.

In contrast to the rest of the characterisation data, the XPS results appeared to describe an entirely different situation. Analysis of the XPS spectra indicated that the cobalt metal was the poorly dispersed phase, producing a metal: support ratio much lower than nickel and copper and hence suggesting that the cobalt crystallites were much larger and poorly dispersed. Conversely, copper appeared to be the most efficiently dispersed metal. However, it should be considered that the XPS technique might have given results biased towards copper. The technique is used to detect the metal ions present in the few layers of the surface and for well-dispersed metals, like cobalt, where the ions are well distributed across the alumina surface, variation in the surface coverage is possible. This can affect the signal intensity as the cobalt atoms lying beneath the top layer may not be detected. However, if the copper is concentrated in discrete particles of a small enough size and high percentage of the ions present will be detected and a falsely high signal obtained.

5.2.3 Discussion of Catalyst Reactivities

It is evident from the experimental results displayed in Section 4.3.3.1 that none of the HDC catalysts displayed activity comparable to both of the palladium catalysts tested nor the Cu/SiO_2 wet impregnated catalyst. All twelve HDC catalysts tested appeared to be extremely unsuitable for use as hydrogenation catalysts, with very low percentages of aniline present in the exit streams. However, it should be noted that as undiluted reagent was used in the feed stream, the large quantities of unreacted nitrobenzene exiting the reactor made detection of the products more difficult and exaggerated the poor activity of the catalysts. Examination of the reaction rates determined from these data shows that the levels of activity, although not approaching the precious metal catalysts, are not of an unreasonable level. Of the three single metal catalysts, the 20 % nickel catalysts demonstrated the most rapid rate, which is expected from the general reactivities of the three metals. However, the most active catalysts were shown to be the catalysts containing both

copper and nickel metal. The observed activities here were of a magnitude greater than the combined activities of the single metal indicating that a positive influence had been exerted upon the addition of a second metal to the surface of the catalyst. Similarly, the mixing of any of the two metals appeared to promote catalytic activity and strongly suggested that mixed metal particles had been formed.

Future work with these catalysts on this apparatus would benefit from using a solvent, to feed a less concentrated solution of nitrobenzene across the catalyst bed and allow the reaction to be observed more easily. Unfortunately, selection of a suitable reaction solvent proved to be extremely difficult. Previous work by Anderson [126] covered the use of various solvents for the nitrobenzene hydrogenation reactions. Most of the common solvents such as the alcohols can react with the product aniline to produce N-methylated compounds, an unwanted side product. This has also been observed during our research where methanol used to rinse the reactor post reaction was found to react with the products in the next reaction and contaminate the reaction samples if the residues were not removed properly after cleaning. A similar situation was also observed when acetone was used to clean out the reactor vessel and feed tubes. In addition, choice of reaction solvent is further complicated by the immiscibility of nitrobenzene with hydrocarbons and the expense of more obscure options.

5.2.3.1 Effect of Adding Water

Pre-treating each HDC catalyst with water undoubtedly led to an increase in catalytic activity. The water treatment was attempted following a suggestion from a personal industrial contact where this method of catalyst promotion is well known. From a practical consideration this method was known to be effective but the mechanisms behind this phenomenon were not known. To investigate this further the deactivation behaviour of the catalysts was examined closely and provided some interesting information. The water pre-treatment was observed to have significantly different influence on cobalt than on copper and nickel.

5.2.3.1.1 Cobalt Containing Catalysts

The 20 % Co catalyst displayed identical irreversible deactivation behaviour to the 10 % Ni/10 % Co and the 10 % Cu/10 % Co catalyst following pre-treatment with water vapour. The addition of water to the hydrogen stream appeared to initially promote catalytic activity but then led to complete deactivation of the catalysts. Unlike the copper and nickel catalysts, no partial activity could be regained by re-treating the catalyst bed for a further hour with water vapour. A thorough study of the available literature was then carried out, particularly into the use of cobalt catalysts for Fischer-Tropsch synthesis. Supported cobalt catalysts are widely used in the synthesis of higher hydrocarbons from synthesis gas as they can offer both high activity and selectivity at a low cost and HDC prepared catalysts have been widely used for this application. During the reaction, oxygen is removed and expelled as water meaning that high levels of water can be generated in the reaction mixtures. A significant amount of research has been carried out into the effect of altering the hydrogen/water ratios in contact with the catalyst and on its effect on the activity of the cobalt. This has been investigated in a variety of ways including the introduction of additional water to the feed stream during reaction [236-238], during catalyst reduction [170, 239], post reduction but prior to reaction similar to our experimental approach [238, 240] and by increasing conversion to the water product [241, 242]. It has been generally found that Co/Al_2O_3 catalysts deactivate more rapidly when additional water is added, although there are several complexities to this generalisation.

The type of support material has proved to be crucial to the behaviour of the catalysts. The introduction of water vapour has proved to have little effect on unsupported cobalt catalysts [237, 239], with activity largely unaltered from that in the absence of additional water. The deactivating effect of water on supported cobalt is most evident where alumina is employed as the catalyst support. The use of silica, as in studies by Huffman and co-workers [243] and of both silica and titania by Schulz and co-workers [244, 245], did not result in significant deactivation, with only a slight deactivation effect observed with the Co/SiO_2 catalysts. In contrast, the titiania catalysts were found to have their hydrogenation activity enhanced upon treatment with water vapour. This is not the only reported instance of water

promotion; studies by Li and co-workers [241] detail an increase in catalytic activity of a silica supported cobalt catalyst and Exxon Research have patented work by Kim [246] claiming the use of water to promote the Fischer Tropsch hydrocarbon synthesis activity using an alumina supported cobalt catalyst. However, the majority of available articles on the use of alumina supported cobalt Fischer Tropsch catalysts describe situations where the catalysts underwent irreversible deactivation post water treatment.

In gaseous reactions, the effect of water has been found to be variable depending upon the partial pressure of the water vapour with respect to the hydrogen partial pressure [170, 236-238, 247-249]. There appears to be two distinguishable systems in operation: when the water partial pressure is relatively low and totals under 30 % of the total gas composition, the deactivating effect of water is small or negligible and can be reversed by withdrawing the water vapour from the gas feed, however, when the water partial pressure is high and the percentage of the total gas composition exceeds 30 %, a more dramatic irreversible deactivating influence is exerted.

The cause of the water-induced catalyst deactivation is universally agreed to be surface oxidation of the cobalt crystallites by the water vapour. This phenomenon is already described for supported iron catalysts in a 1990 paper by Dry [250]. As already discussed, unsupported cobalt is unaffected by the addition of water and thermodynamically the oxidation of bulk cobalt to CoO or to Co_3O_4 is unfeasible especially under normal Fischer Tropsch reaction conditions [251-253]. However, the introduction of a support material allows surface reactions, not possible in unsupported or in the bulk of large cobalt particles, to become more favourable. Well-dispersed small cobalt crystallites, like the ones generated during the HDC preparation route are considered to be more susceptible to oxidation than larger particles like the ones found on the surface when silica is used as a support. Jacobs et al, describe the greater re-oxidation of surface cobalt supported on alumina when compared to cobalt supported on silica in a recent paper [254]. It is the intense reaction between the alumina support and the cobalt particles that allows the HDC method to work so efficiently in the production of small cobalt catalysts, however the

strength of this interaction also leads to a decrease in the reducible metal that may be present on the support [255].

The exact mechanism of the water-induced re-oxidation of surface cobalt has been explored in various experimental studies. The formation of cobalt aluminate, the form of irreducible cobalt identified in the high temperature region of the TPR profiles of the cobalt catalysts during characterization and described in Section 4.2.5, has been widely detected. Jacobs et al examined the surface of their deactivated cobalt catalyst post water exposure and detected increased levels of cobalt aluminate using XAFS [236], an effect that was also reported by Jongsomjit, Pranpranot and Goodwin Jr. in a similar study [170]. Whereas, Hilmen, Schanke, Hanssen and Holmen [238] noted the appearance of the $CoAl_2O_4$ peak in the TPR profile of their used catalysts and used H_2 adsorption experiments to provide further evidence for the loss of active cobalt (0). In fact, an enhancement of the interaction between the alumina support and the small cobalt crystallites is generally accepted to occur on contact with sufficiently high concentrations of water vapour [256]. It has been postulated that the formation of catalytically inactive cobalt-support compounds proceeds via a CoO intermediate species. Sirijaruphan and co-workers [248] found their results to be in agreement with the conclusions reported by van Berge et al [251], where it was postulated that CoO formed at the surface and in the sub-surface regions on the metal particles and acted as a precursor to the formation of the ultimate $CoAl_2O_4$ state. Extensive Raman work carried out by Jongsomjit at al detected a number of signals in the spectra indicating a non-stoichiometric surface Co compound, intermediate between Co and Co aluminate, was forming on the surface of the catalysts and was possibly forming by cobalt atom migration into the alumina matrix. These suggestions are consistent with the findings of a group lead by Moen [257] who have performed an in-depth investigation into the mechanisms of Co reduction. During catalyst preparation, cobalt ions can migrate into the vacant tetrahedral and octahedral holes in the alumina support material and this can lead to a Co phase that is strongly bonded to the alumina support and resistant to reduction. It has been found that in most cobalt catalysts, about 78 % of the metal is present as crystallites on the surface, the rest being 'lost' in aluminate compound formation with the alumina support [237, 258]. Furthermore, evidence presented by Arnoldy

and Moulijn [157] and Hilmen and coworkers [238] suggests that water vapour may facilitate the migration of Co^{2+} ions throughout the support and allow the formation of cobalt aluminate compounds with the spinel structure through the exchange of Co^{2+} in Co_3O_4 with Al^{3+} ions.

Once the small cobalt particles have become oxidised in it very difficult for the reduced state to be regenerated when water vapour is still present in the atmosphere. Work by groups led by Chernavskii [259] and Castner [260] explain how the water vapour generated in the catalyst support pores as reduction of the small CoO particles (less than or equal to 20 nm), produces a localised high partial pressure of water vapour around the metal crystallites which forces the equilibrium back towards the Co^{2+} state. To regenerate Co metal an extremely high reaction temperature would be required.

Consequently, it appears that during our experimental procedure, the surface of the reduced cobalt crystallites are becoming re-oxidised during the water pre-treatment to form CoO. Initially, this appears to have a positive effect on hydrogenation activity before the catalysts begins to undergo catastrophic irreversible deactivation as irreducible $CoAl_2O_4$ spinel is formed on the surface layers of the catalyst.

5.2.3.1.2 Copper and Nickel Containing Catalysts

In contrast to the deactivation behaviour of the cobalt-containing catalysts, those containing copper, nickel or a mixture of the two metals, displayed a degree of reversible catalyst deactivation. Following pre-treatment of the catalyst beds with water vapour, an initial promotional effect was observed with nitrobenzene hydrogenation activity exceeding that in the absence of additional water. This activity was observed to diminish as the reaction proceeded but can be partially regained following another water vapour passivation. Although, ultimately, the catalysts did undergo irreversible deactivation, short-term recovery was affected.

To explain this phenomenon, the situation described above in Section 5.2.3.1.1 concerning the deactivation of the cobalt containing catalysts was applied to copper and nickel. Although cobalt is undoubtedly considered to be substantially more reactive towards alumina than either of the other two metals, the irreversible deactivation of a nickel Fischer-Tropsch catalyst through the formation of nickel aluminate has been reported in the chemical literature by Zielinski in 1997 [261]. The introduction of additional water vapour was found to result in the generation of NiO at temperatures very much lower than expected and ultimately lead to the formation of a variety of complex surface moieties involving particles of NiO decorated around the perimeter with nickel aluminate crystallites. The generation of a small quantity of NiO was identified during reduction of these catalysts using TPR analysis techniques, however it was indicated that these species were similar in chemical nature to bulk oxide material, unlike the nickel oxide species appearing upon interaction with the water treated catalysts. In our own characterisation experiments, the formation of nickel aluminate, equivalent to that visible in the TPR spectrum of the 20 % Co/Al_2O_3 catalyst during the catalyst reduction process, was not observed with either the pure Ni/Al_2O_3 catalyst, nor with any of the nickel-containing, mixed-metal catalysts. In addition, under reaction conditions, the nickel-containing catalysts were found to be more resistant to rapid lethal deactivation than the cobalt cases, making in unlikely that the formation of a nickel aluminate species was occurring. However, the involvement of surface nickel aluminate species in the ultimate irreversible deactivation of the catalysts cannot be discounted. The formation of NiO through the partial oxidation of the supported nickel crystallites is however highly likely. Despite the lack of published corroborating evidence, it can be fairly confidently concluded that the deactivation of the nickel catalyst must follow a similar path to that of the cobalt catalysts prepared using an identical preparation method. Unfortunately, it was not possible to locate any literature describing the formation of copper oxide species upon reduction. However considering the initial uniform reaction of the three metals upon catalyst treatment with water vapour, that is the initial increase in catalytic activity, it seems likely that all are undergoing a similar promotion process.

It is proposed that the water-effected oxidation of the surface metal atoms to CoO. NiO or CuO induced an increase in catalytic activity and that these partially oxidised systems were more active towards the nitrobenzene hydrogenation reaction than the zero valent metal systems. This hypothesis is represented diagrammatic form in Figure 5.6.

There has also been suggestion in the literature that hydroxylating the alumina surface at the interface between the metal crystallite and support can lead to an increase in catalytic activity. In studies conducted by Mărginean and Olariu [262], hydroxylation of the alumina was found to improve the performance of a supported nickel catalyst when the –OH group was added at the metal/support junction. This may or may not be a contributing factor to the promotion effect noted with the water treatment of the HDC catalysts. Although water would be expected to lead to a widespread hydroxylation of the alumina support, the dissociation of water has been shown to occur at on both the support and a range of metal crystallites by Jackson et al. [263, 264] but it is the interaction of the water molecules with the supported metals that it deemed the most important factor in this case.

Figure 5.6: Water promotion and deactivation of HDC catalysts

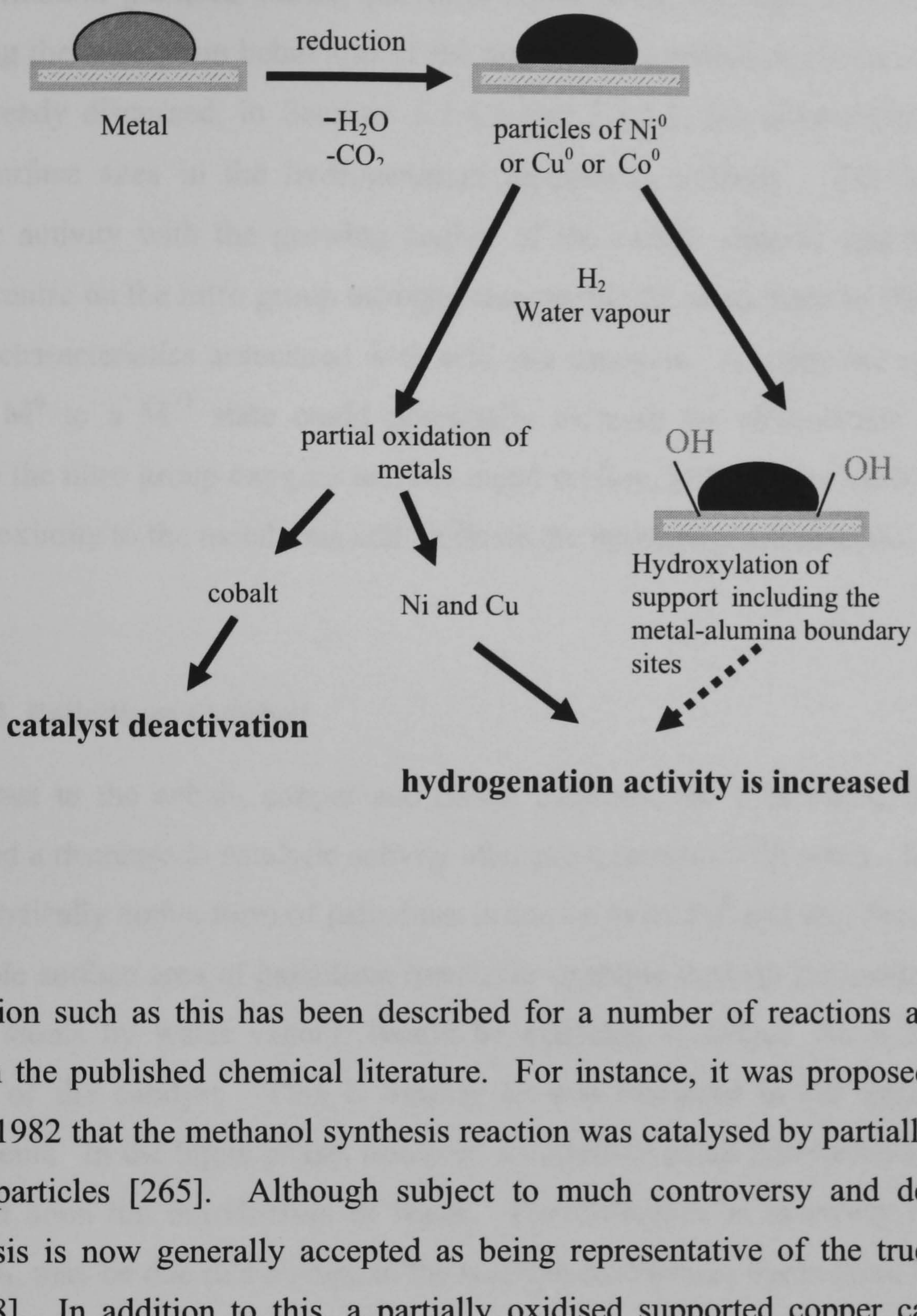

A situation such as this has been described for a number of reactions and can be found in the published chemical literature. For instance, it was proposed by Klier back in 1982 that the methanol synthesis reaction was catalysed by partially oxidised copper particles [265]. Although subject to much controversy and debate, this hypothesis is now generally accepted as being representative of the true situation [266-268]. In addition to this, a partially oxidised supported copper catalyst has proven to be more active in the hydrogenation of the alkene double bond in the furfural molecule [269, 270], where a combination of Cu^0 and Cu^1 sites was found to be necessary for hydrogenation. But perhaps most significantly, work published by Jebarathinam and coworkers in 1998 on the hydrogenation of nitrobenzene using a copper spinel catalyst [48] described the beneficial influence of increasing the levels of Cu^I in the spinel structure. Here the catalytically active species was identified as the partially oxidised copper metal.

Initially considered an unexpected outcome, this hypothesis can be explained using the information gathered during previous liquid phase hydrogenation experiments regarding the adsorption behaviour of the nitrobenzene molecule (Section 5.1.4.2.1). Also already discussed, in Sections 5.1.1.2 and 5.1.4.3, the involvement of acidic metal surface sites in the hydrogenation reaction is unlikely. The lowering of catalytic activity with the growing acidity of the carbon support and the positive charge centre on the nitro group nitrogen responsible for adsorption to the active site are not characteristics associated with acid site catalysis. Altering the metal atoms from a M^0 to a M^{+1} state could potentially increase the electrostatic interaction between the nitro group oxygens and the metal surface, bringing the nitro nitrogen in close proximity to the metal ions and facilitate the hydrogenation reaction.

5.2.3.1.3 Palladium Catalyst

In contrast to the cobalt, copper and nickel catalysts, the 1 % Pd/Al_2O_3 catalysts displayed a decrease in catalytic activity after pre-treatment with water. In this case, the catalytically active form of palladium is known to be Pd^0 and any decrease in the accessible surface area of palladium metal, for example through the oxidation of the surface atoms by water vapour, would be expected to reduce the hydrogenation activity of the catalyst. This is exactly as was observed in the gaseous phase experiments. In the liquid phase, however, an opposite small promotional effect was observed upon the introduction of water. The difference in reactivity of the 1 % Pd/Al_2O_3, may be due to a change in the reaction mechanism but is more likely to be a result of the relative amount of water interacting with the alumina surface. As described in Section 5.2.3.1.1 concerning the effect of water on the cobalt catalysts, the effect can be very different depending upon the water: hydrogen ratio. At high hydrogen and low water concentrations as observed in the liquid phase system, where the high partial pressure of hydrogen would be expected to largely out weigh the partial pressure generated by adding a small quantity of water, a small promotional effect may be possible. However, when the partial pressure of water vapour is permitted to rise to above that of the hydrogen, as made possible in the gaseous phase system, the water vapour can interact with the palladium metal to oxidise the surface metal atoms and cause a decline in the catalytic potential of the

catalyst. In both systems, the effect would be expected to be small as the hydrogen atmosphere and reaction temperature would be expected to re-reduce the palladium ions to palladium metal very rapidly.

5.2.4 Overview of the HDC Catalyst Preparation Technique and its Possible Application to Industry

The catalyst characterisation and reaction testing results described in this thesis shown that the HDC method can be used effectively to produce well dispersed catalysts containing a mixture of two metals. Of the metals utilised in this research, the method was most effect in the production of catalysts with small cobalt crystallites in a well-dispersed form, for which the method was originally designed. It has also proved effective for the formation of well-dispersed nickel catalysts. The use of this method for the production of copper catalysts was less successful, as low surface area copper catalysts were produced, where the copper crystallites were not well dispersed across the support surface. The use of the HDC method for the preparation of copper catalysts does not appear to hold many advantages over more traditional synthetic methods, such as impregnation, which produced a catalyst superior to the HDC catalyst used in this study. It may be possible to alter the reaction conditions in some way to make the process more favourable for copper deposition and improve the copper dispersion. However, the interaction between the solvated copper ions and the alumina surface may be insufficiently strong, or the stability of the copper tetraammine complex too high to make this method viable for copper, regardless of how the physical reactions conditions are manipulated. Such investigations are beyond the scope of this project and further experimental evaluation is required to resolve this problem, if at all. As a result, the conclusion regarding the unsuitability of this method for the production of high surface area copper catalysts can not be generalised but is definitive under these specific reaction conditions and experimental set-up.

However, the strength of the interaction between the supported cobalt and the alumina surface favoured during catalyst preparation has also proven to be very unfavourable during reaction conditions, where the formation of inactive cobalt

aluminate species is facilitated leading to irreversible deactivation of the catalyst. A lesser effect is noted with copper and nickel and these catalysts proved to have considerable potential for a future application in industry, particularly in the mixed "alloy" form. In fact, the increased activity observed with the use of the 10 % Cu/10 % Ni/Al_2O_3 catalyst provided the most conclusive evidence that true mixed-metal particles had been formed and a definite beneficial promotional effect on the hydrogenation activity was evident. Furthermore, the uniform deactivation behaviour of all the cobalt-containing catalysts also provided additional evidence for the formation of mixed metal particles across the metal surface, as a complete loss in activity was observed in all systems meaning the activity of the second metal has also been irreversibly lost with the oxidation of the surface cobalt.

The addition of water vapour to the reaction feed stream may initially seem an abstract concept, however, consideration of actual industrial practice allows the results to be applied directly to commercial nitrobenzene production. When the industrial process uses a stirred tank reactor to perform the hydrogenation reaction, the reagents and catalyst precursor are added to the vessel and the hydrogen feed commenced. In this situation, catalyst reduction is commenced in the presence of the nitrobenzene reagent and aniline solvent and the reaction allowed to occur as the catalyst is ready. As a consequence, the water produced during reduction, will be able to oxidise the localised metal crystallites on the catalyst surface as it is generated. So perhaps the reaction conditions stipulated by our experimental set-up are close to the actual environment experienced by the catalyst in an industrial setting.

Therefore, the use of cobalt containing catalysts in an industrial setting does not appear to be a feasible option as it would shorten further the already limited active life of the hydrogenation catalysts and lead to problems regenerating the catalyst. However, the use of copper and nickel bimetallic catalysts in an industrial context provides a basis for further research into the nitrobenzene hydrogenation reaction.

6.0 CONCLUSIONS

Throughout this research project, the experimental work was carried out with the aim of compiling information regarding the nitrobenzene reaction mechanism and the causes of catalyst deactivation. Valuable insights into both concerns were obtained and are summarised in this section.

6.1 Reaction Particulars

Extensive work was carried out in the liquid phase using three carbon-supported and one alumina-supported palladium catalysts. It was discovered that the nitrobenzene hydrogenation was a structure sensitive reaction with a variation in catalytic activity over a remarkably small particle size range. The acidity of the support material appeared to have an effect on the rate of hydrogenation; the involvement of acidic surface sites in the catalytic reaction was largely discounted following experiments showing that the addition of similar basic compounds, such as cyclohexylamine and aniline, did not lead to significant inhibition of the hydrogenation reaction.

A solvent effect was also observed with hydrogenation proceeding more rapidly in methanol than in IPA. The reasons for this effect were not understood completely but given the available evidence, the cause was attributed to the more favourable dissociation of hydrogen from the primary than the secondary alcohol.

The adsorption behaviour of nitrobenzene and nitrosobenzene was found to be very different, as expected from analysis of the electron distributions in both molecules. In particular, the adsorption behaviour of nitrobenzene was found to be weak and difficult to measure whereas that of nitrosobenzene much stronger, which allowed this molecule to bind to the catalyst, possibly in a number of multilayers, and remove itself from solution during hydrogenation.

6.2 The Reaction Mechanism

A new nitrobenzene hydrogenation mechanism was proposed, as it became apparent that Haber's original proposal could not be utilised to adequately explain our

experimental observations. The novel scheme was constructed on the basis that nitrosobenzene was unable to act as an intermediate in the nitrobenzene reaction pathway, due to its distinctively different reaction profile and isotopic substitution effects, along with its much slower rate of aniline production. Furthermore, the addition of two hydrogen atoms simultaneously in any one elementary step, as seen in Haber's scheme, was avoided completely and a more realistic approach involving the addition of a single hydrogen atom at a time in a series of bimolecular reactions was adopted. The new mechanistic proposal describes how aniline can be generated from either nitrobenzene or nitrosobenzene in a duel pathway, passing through a common adsorbed intermediate species. Intricately linking both hydrogenation routes in this way allows the appearance of species previously reported in published hydrogenation studies to be rationalised.

This mechanism was confirmed over palladium and also over Raney nickel, so initial investigations suggest this mechanism is likely to be consistent over a range of metals and is not specific to palladium. However, additional research over a more extensive range of metals is required to confirm this hypothesis beyond doubt.

6.3 Catalyst Deactivation

The deactivation behaviour of the catalysts used in the liquid phase experiments was studied extensively and although no specific species could be identified on the spent catalysts, it was deduced that contrary to previous opinion, aniline was not involved in the deactivation process either as a poison or a coke-precursor. The most likely candidate for a coke-precursor is an adsorbed surface species originating from nitrobenzene itself.

6.4 Use of the HDC Catalyst Preparation Method

As part of this project, a novel set of bimetallic catalysts bases on mixtures of cobalt, copper and nickel, were prepared and characterised. The HDC method was successful in producing catalysts with a homogeneously distributed, well-dispersed monolayer of metals. The method worked well for both cobalt and nickel but was

not deemed to hold any advantages over alternative catalyst preparation routes for the synthesis of supported copper catalysts.

Characterisation of these catalysts produced mixed evidence for and against the formation of mixed metal particles across the surface of the bimetallic catalysts and as all characterisation was performed in the catalyst pre-cursor state, a definitive conclusion about the nature of the interaction between the two surface species cannot be drawn. However, evidence from the behaviour of the catalysts under hydrogenation conditions strongly suggests that mixed metal particles have indeed been formed. The most convincing evidence is the substantially enhanced activity of the 10 % Cu/10 % Ni catalyst and the identical deactivation behaviour of all cobalt containing catalysts.

The HDC catalysts were found to have moderate activity for the nitrobenzene hydrogenation reaction, although not of a level approaching that of the precious metal catalysts. Catalytic activity was found to be greatly enhanced by pre-treating the catalyst bed with water vapour under a hydrogen atmosphere prior to commencing the nitrobenzene feed. It was postulated that the water vapour was causing oxidation of the surface layer of metal atoms to produce CoO, CuO or NiO which were considerably more active towards the nitrobenzene hydrogenation reaction than the metals in their zero valent states.

All the water treated catalysts were found to deactivate over the course of the reaction, although by far the most dramatic effect was observed with the cobalt containing catalysts, which underwent rapid catastrophic permanent catalyst deactivation, most likely through the formation of inactive cobalt alumina spinel. Water vapour has been postulated to increase the cobalt-alumina interaction and to facilitate the migration of CoO into the support matrix. This deactivation was not observed to any great extent with copper or nickel.

The potential for the future application of cobalt containing catalysts in the industrial production of nitrobenzene was evaluated to be low due to the serious deactivation

problem. Use of alloyed copper and nickel looks promising due to the impressive activity enhancement noted during catalyst testing.

7.0 REFERENCES

1. J.J. Berzelius, Edinburgh new philosophical journal, 1836. **21**: p. 223.
2. J.H. Clark, *Catalysis of organic reagents by supported inorganic reagents*. 1994, New York: VCH.
3. M. Bowker, *The Basis and Applications of Heterogeneous Catalysis*. Oxford Chemistry Primers. 1998, Oxford: Oxford Science. 42-43.
4. R.J. Wijngaarden, A. Kronberg and K.R. Westerterp, *Industrial Catalysis*. 1998, Weinheim: Wiley-VCH.
5. J.M. Thomas and W.J. Thomas, *Principles and Practice of Heterogeneous Catalysis*. 1997, Weinheim: VCH Verlagsgesellschaft.
6. M. Twigg, ed. *The Catalyst Handbook*. 2nd ed. 1996
7. C.H. Bartholomew, *Appl. Catal. A*, 2001. **212**: p. 17-60.
8. C.R. Bemrose and J. Bridgewater, *Powder Technol.*, 1987. **49**: p. 97-126.
9. H.N. Pham, J. Reardon and A.K. Dayte, *Powder Technol.*, 1999. **103**: p. 95-102.
10. G. Emig and F.G. Martin,. *Ind. Eng. Chem. Res.*, 1991. **30**: p. 1110-1116.
11. M.J. Adams, M.A. Mullier and J.P.K. Seville, *Powder Technol.*, 1994. **78**: p. 5-13.
12. P. Wynblatt and N.A. Gjostein, *Prog. Solid-state. Chem.*, 1975. **9**: p. 21-58.
13. P. Albers, J. Pietsch and S.F. Parker,. *J. Mol. Catal. A*, 2001. **173**: p. 275-286.
14. D.B. Dadyburjor, in *Catalyst deactivation*, B. Delmon and G.F. Froment, Editors. 1987, Elsevier: Amsterdam. p. 21-38.
15. C.H. Bartholomew, *Appl. Catal. A*, 1993. **107**: p. 1-57.
16. C.H. Bartholomew, in *Catalyst Deactivation*, B. Delmon and G.F. Froment, Editors. 1987, Elsevier: Amsterdam. p. 81-104.
17. W. Erley and H. Wagner,. *J. Catal.*, 1987. **53**: p. 287-294.
18. D.W. Goodman and M. Kiskinova,. *Surf. Sci.*, 1981. **105**(2-3): p. L265-L270.
19. M. Kiskinova and D.W. Goodman,. *Surf.Sci.*, 1981. **108**: p. 64-76.
20. E.L. Hardegree, P. Ho and L.M. White, *Surf. Sci.*, 1986. **165**: p. 488-506.
21. E. Formisky and F.E. massoth, *Catal. Today*, 1999. **52**: p. 381-389.
22. D. Dong, S. Jeong and F.E. Massoth, *Catal. Today*, 1997. **37**: p. 267-275.
23. M.J. Grigis and B.C. Gates, *Ind. Eng. Chem. Res.*, 1991. **30**: p. 2010-2030.
24. V.L. Vopa and C.N. Satterfield, *J. Catal.*, 1988. **110**: p. 375-381.
25. M.V. Twigg and M.S. Spencer, *Topics in Catalysis*, 2003. **22**: p. 191-203.
26. V.R. Choudhary and M.G. Sane, *J. Chem. Technol. Biotechnol.*, 1998. **73**: p. 336-340.
27. P.C. Largentiere, D.A. Liprandi and N.S. Figoli,. *Ind. Eng. Chem. Res.*, 1995. **34**: p. 3713-3717.
28. P.G. Menon, *J. Mol. Catal.*, 1990. **59**: p. 207-220.
29. D.L. Trimm, *Appl. Catal.*, 1983. **5**: p. 263.
30. M. Absi-Halabi, A. Stanislaus and D.L. Trimm, *Appl. Catal.*, 1991. **72**: p. 193-215.
31. D. Espinat, E. Freund, H. Dexpert and G. Martino, *J. Catal.*, 1990. **126**: p. 496-518.
32. R.A. Cabrol and A. Oberlin, *J. Catal.*, 1984. **89**: p. 256-166.
33. C.A. Querini and S.C. Fung, *Catal. Today*, 1997. **37**: p. 277-283.
34. R.P.D. Pauw and G.F. Froment, *Chem. Eng. Sci.*, 1975. **30**: p. 789-801.
35. F. Besenbacher, I. Chorkendorff, B.S. Clausen, B. Hammer, A.M. Molenbroek, J.K. Norskov and I. Stensgaard, *Science*, 1998. **279**: p. 1913-1915.
36. T. Nemes, A. Chambers and R.T.K. Baker, *J. Phys. Chem. B*, 1998. **102**: p. 6323-6330.
37. W.G. Appleby, J.W. Gibson and G.M. Good, *Ind. Eng. Chem. Process. Des. Dev.*, 1962. **1**: p. 102-110.
38. P. Zeuthen, P. Blom, B. Muegge and F.E. Massoth, *Appl. Catal.*, 1991. **68**: p. 117-130.
39. P. Zeuthen, B.H. Cooper, F.T. Clark and D. Arters, *Ind. Eng. Chem. Res.*, 1995. **34**: p. 755.
40. E. Furimsky, *Ind. Eng. Chem. Prod. Des. Dev.*, 1978. **17**: p. 329.
41. J.R. Rostrup-Nielsen, *Catal. Today*, 1997. **37**: p. 225-232.
42. G.A. Cook, *Survey of Modern Industrial Chemistry*. 1975, Michigan: Ann Arbor Science. 231-241.
43. C.A. Heaton, ed. *An Introduction to Industrial Chemistry*. 1991, Blackie: Glasgow. 392-393.
44. B.G. Reuben and M.L. Burstall, *The Chemical Economy*. 1973, London: Longman. 267-269.
45. R.S. Downing, P.J. Kunkeler and H.v. Bekkum, *Catal. Today*, 1997. **37**: p. 121-136.

46. K. Weissermel and H.-J. Arpe, *Industrial Organic Chemistry (3rd Ed.)*. 1997. Weinheim: VCH,. 375-377.
47. C. Haas, in *European Chemical News*. 2004. p. 16-18.
48. N.J. Jebarathinam, M. Eswaramoorthy and V. Krishnasamy, in *Recent Advances in Basic and Applied Aspects of Industrial Catalysis*, T.S.R.P. Rao and G.M. Dhar, Editors. 1998. Elsevier Science. p. 1039 - 1043.
49. G.S. Samuelson, V.L. Garik and G.B.L. Smith, *J. Am. Chem. Soc.*, 1950. **72**: p. 3872-3874.
50. G.C. Torres, E.L. Jablonski, G.T. Baronetti, A.A. Castro, S.R.d. Miguel, O.A. Scelza, M.D. Blanco, M.A.P. Jimenez, and J.L.G. Fierro, *Appl. Catal. A*, 1997. **161**: p. 213-226.
51. X. Fang, S. Yao, Z. Qing and F. Li, *Appl. Catal. A*, 1997. **161**: p. 129-135.
52. X. Yu, M. Wang and H. Li, *Appl. Catal. A*, 2000. **202**: p. 17-22.
53. S.R.d. Miguel, J.I. Vilella, E.L. Jablonski, O.A. Scelza, C.S.-M.d. Lecca and A. Linares-Solano, *Appl. Catal. A*, 2002. **232**: p. 237-246.
54. M.C.M. Perez, C.S.M.d. Lecca and A.L. Solano, *Appl. Catal. A*, 1997. **151**: p. 461-475.
55. J. Peureux, M. Torres, H. Mozzanega, A. Giroir-Fendler and J.-A. Dalmon, *Catal. Today*, 1995. **25**: p. 409-415.
56. M. Torres, J. Sanchez, J.A. Dalmon, B. Bernauer and J. Lieto, *Ind. Eng. Chem. Res.*, 1994. **33**: p. 2421.
57. M.M. Danilova, N.A. Kuzin, V.A. Kirillov, E.A. Panchenko, V.D. Meshcheryakov, E.M. Moroz and N.A. Rudina, *Kinet. Catal.*, 2002. **43**(6): p. 830-837.
58. K.K. Yeong, A. Gravrilidis, R. Zapf and V. Hessel, *Catal. Today*, 2003. **81**: p. 641-651.
59. V. Hatziantoniou, B. Andersson and N.-H. Schoon, *Ind. Eng. Chem. Process. Des. Dev.*, 1986. **25**: p. 964-970.
60. B. Macdonald, in *ECN Chemscope*. 1997. p. 38-39.
61. E. Camara, A.E. Leder and Y. Ishikawa, *Aniline*. 1997, CEH.
62. H. Chinn, G. Humphries and A. Kishi, *Aniline*. 2001, CEH.
63. S.B.S.Y. Xiaofei, *Xiandia Huagong*, 1998. **18**(6): p. 34-36.
64. S. Axon. personal communication, 2004.
65. CelaneseChemicals, *Nickel catalyst CelActiv Ni 55/5 TS*. 1999.
66. *Encyclopedia of Chemical Technology*. 4th ed. (1997): Kirk-Othmer. 695-726.
67. D. Randall and S. Lee, *The Polyurethanes book*. 2002, UK: J. Wiley and sons Ltd.
68. *www.halliburton.com/petro_poly*.
69. *http://www.psrc.usm.edu/macrog/urethane.htm*. 2001.
70. *http://www.polyurethane.org/polyurethane_material/made_used.htlm*.
71. *www.dow.com/polyurethane*.
72. *www.huntsman.com*.
73. Q. Chen, S. Haq, B.G. Fredrick and N.V. Richardson, *Surf. Sci.*, 1996. **368**: p. 310-317.
74. L. Gorb, J. Gu, D. Leszczynska and J. Leszczynski, *Phys. Chem. Chem. Phys.*, 2000. **2**: p. 5007-5012.
75. L. Gorb, M. Ilchenko, J. Leszczynski and D. Leszczynski, *Modeling of the molecular mechanisms of ecologically important chemical reactions*, in *molmech*. 2004.
76. I. Zilberberg, M. Ilchenko, O. Isayev, L. Gorb and J. Leszczynski, *J. Phys. Chem. A*, 2004. **108**: p. 4878-4886.
77. S. Meijers and V. Ponec, *J. Catal.*, 1994. **149**(2): p. 307-316.
78. A.J. Tench and R.L. Nelson, *Trans. Faraday Soc.*, 1967. **63**: p. 2254.
79. S.X. Huang, D.A. Fischer and J.L. Gland, *J. Vac. Sci. Technol., A*, 1994. **12**(4): p. 2164-2169.
80. S.X. Huang, D.A. Fischer and J.L. Gland, *Catal. Lett.*,1995. **34**: p. 365-375.
81. S.X. Huang, D.A. Fischer and J.L. Gland, *J. Phys. Chem.*, 1996. **100**: p. 10223-10234.
82. R.L. Augustine, *Organic Functional Group Hydrogenation*, in *Catalysis Reviews: Science and Engineering*. 1976. p. 285-313.
83. R.L. Augustine, Catal. Today, 1997. **37**: p. 419-440.
84. D.N. Rihani, T.K. Narayanan and L.K. Doraiswamy, *Ind. Eng. Chem. Process. Des. Dev.*, 1965. **4**: p. 1403.
85. H. Debus and J.C. Jungers, *No 148 - Memoires pre:entes a la societe chimique*, 1958: p. 785-784.
86. J. Wisniak and M. Klein, *Ind. Eng. Chem. Prod. Res. Dev.*, 1984. **23**(1): p. 44-50.
87. H.-C. Yao and P.H. Emmett, *J. Am. Chem. Soc.*, 1961. **84**: p. 1086-1091.
88. M.A. Aramendia, V. Borau, J. Gomez, C. Jimenez and J.M. Marinas, *Appl. Catal.*, 1984. **10**: p. 347-359.

89. A. Metcalfe and M.W. Rowden, *J. Catal.*, 1971. **22**: p. 30-34.
90. E. Klemm, B. Amon, H. Redlingshofer, E. Dieterich and G. Emig, *Chem. Eng. Sci.*, 2001. **56**: p. 1347-1353.
91. V. Holler, D. Wegricht, I. Yuranov, L. Kiwi-Minsker and A. Renken, *Chem. Eng. Technol.*, 2000. **23**(3): p. 251-255.
92. H.-C. Yao and P.H. Emmett, *J. Am. Chem. Soc,* 1961. **83**: p. 796-799.
93. C. Li, Y.-W. Chen and W.-J. Wang, *Appl. Catal. A,* 1994. **119**: p. 185-194.
94. D.J. Collins, A.D. Smith and B.H. Davis, *Ind. Eng. Chem. Prod. Res. Dev.*, 1982. **21**: p. 279-281.
95. P.B. Kalantri and S.B. Chandalla, *Ind. Eng. Chem. Process. Des. Dev.*, 1982. **21**: p. 186-188.
96. G.J.K. Acres and G.C. Bond, *Platinum Metals. Rev.*, 1966. **10**: p. 122.
97. G.J.K. Acres and B.J. Cooper, *J. Appl. Chem. Biotechnol.*, 1972. **22**: p. 796.
98. F. Haber, *Zeit. Electrochem.*, 1898. **4**: p. 506.
99. O.W. Brown and C.O. Henke, *J. Phys. Chem.*, 1922. **16**: p. 161-190.
100. K.H. Gharda and C.M. Sliepcevich, *Ind. Eng. Chem.*, 1960. **52**(5): p. 417-418.
101. H.D. Burge, D.J. Collins and B.H. Davis, *Ind. Eng. Chem. Process. Des. Dev.*, 1980. **19**: p. 389-391.
102. J. Maestro, J. Aracil and M. Martinez, *Afinidad*, 1986. **43**(401): p. 60-62.
103. K.R. Christmann, *Hydrogen Sorption on pure metal surfaces*, in *Hydrogen Effects in Catalysis*, Z. Paal and P.G. Menon, Editors. 1988, Marcel Dekker: New York.
104. F. Figueras and B. Coq,. *J. Mol. Catal. A*, 2001. **173**: p. 223-230.
105. S.S. Scholnik, J.R. Reasenberg, E. Lieber and G.B.L. Smith, *J. Am. Chem. Soc.*, 1941. **63**: p. 1192-1193.
106. G.V. Smith, R. Song, M. Gasior and J. R. A. Malz, *Hydrogenation of nitrosobenzene over palladium catalysts*, in *Catalysis Organic Reactions*, J.R. Kosak, Editor. 1994, Marcel Dekker: New York. p. 137-149.
107. D. Groskova, M. Stolcova and M. Hronec, *Catal. Lett.,* 2000. **69**: p. 113-116.
108. P. Zuman and B. Shah, *Chem. Rev.,* 1994. **94**: p. 1621-1641.
109. G.A. Russell, E.J. Geels, F.J. Smentowski, K.-Y. Chang, J. Reynolds and G. Kaupp, *J. Am. Chem. Soc.*, 1967. **89**(15): p. 3821-3828.
110. A. Furst and R.E. Moore, *J. Am. Chem. Soc.*, 1957. **79**(20): p. 5492-5493.
111. H.S. Prasad, S. Gowda and D.C. Gowda, *Syn. Comm.*, 2004. **34**(1): p. 1-10.
112. S.L. Karwa and R.A. Rajadhyaksha, *Ind. Eng. Chem. Res.*, 1987. **26**: p. 1746-1750.
113. S.L. Karwa and R.A. Rajadhyaksha, *Ind. Eng. Chem. Res.*, 1988. **27**: p. 21-24.
114. A. Furst and R.E. Moore, *J. Am. Chem. Soc.*, 1957. **79**: p. 5492-5493.
115. D. Balcom and A. Furst, *J. Am. Chem. Soc.*, 1953. **75**(4334-4336).
116. J.M. Devereux, K.R. Payne and E.R.A. Peeling, *J. Chem. Soc.,* 1957: p. 2845-2851.
117. H. Greenfield, *J. Org. Chem.*, 1964. **29**: p. 3082-3083.
118. E.L. Pitara, B. N'Zemba, J. Barbier, F. Barbot and Miginiac, *J. Mol. Catal. A*, 1996. **106**: p. 235-240.
119. V. Vishwanathan, S.M. Sajjad and S. Narayanan, *Indian. J. Chem. A*, 1991. **30**(8): p. 679-681.
120. S. Narayanan and R.P. Unnikrishnan, *J. Chem. Soc. Faraday Trans.*, 1997. **93**(10): p. 2009-2013.
121. S. Narayanan, R. Unnikrishnan and V. Vishwanathan, *Appl. Catal. A*, 1995. **129**(1): p. 9-19.
122. G. Mink and L. Horvath, *React. Kinet. Catal. Lett.*, 1998. **65**(1): p. 59-65.
123. L.B. Kochetova and M.V. Klyuyev, *Petrol. Chem.*, 1997. **37**(5): p. 414-421.
124. H. Takagi, T. Isoda, K. Kusakabe and S. Morooka, *Energy and Fuels*, 1999. **13**: p. 1191-1196.
125. E.A. Gelder, S.D. Jackson and C.M. Lok, *Catal. Lett.,* 2002. **84**(3-4): p. 205-208.
126. D. Anderson, PhD Thesis (1999) , Department of Chemistry, University of Glasgow Glasgow.
127. R.P. Rice and E.J. Kohn, *J. Am. Chem. Soc.*, 1955. **77**: p. 4052-4054.
128. E.A. Gelder and S.D. Jackson, *Unpublished observations*. 2004.
129. L.B. Kochetova, T.G. Volkova and M.V. Klyuev, *Petroleum Chemistry*, 2000. **40**: p. 371-376.
130. J. Zawadzki, M. Wisniewski, J. Weber, O. Heintz and B. Azambre, *Carbon*, 2001. **39**: p. 187-192.
131. J. Zawadzki, B. Azambre, O. Heintz, A. Krzton and J. Weber, *Carbon*, 2000. **38**: p. 509-515.

132. B. Dvorak, J. Pasek, P. Pavlas and Z. Hejda, *Deactivation of a supported copper catalyst in the industrial aniline plant.*, in *Catalyst Deactivation*, B. Delmon and G.F. Froment, Editors. 1987, Elsevier: Amsterdam. p. 535-544.
133. L. Petrov, K. Kumbilieva and N. Kirkov, *Appl. Catal.*, 1990. **59**: p. 31-43.
134. M.V. Twigg and M.S. Spencer, *Appl. Catal. A*, 2001. **212**: p. 161-174.
135. P.B. Babkova, *Khimiya Promyshlennost*, 1990. **22**: p. 142-143.
136. B. Amon, H. Redlingshofer, E. Klemm, E. Dieterich and G. Emig, *Chem. Eng. Process.*, 1999. **38**: p. 395-404.
137. C.M. Lok, G. Gray and G.J. Kelly, *Catalysts with high cobalt surface area - Patent number WO 01/87480 A1*, in *World Intellectual property Organization*. 2000, Imperial Chemical Industries PLC: International.
138. C.M. Lok, D. Verzijl and J.van Dijk, *Nickel upon transition alumina catalysts Application number 83200575.5*, in *European Patent Office*. 1983, Unilever PLC: European.
139. R.L. Bonne and C.M. Lok, *Cobalt on alumina catalysts Patent No 5, 874, 381*, in *US Patent Office*. 1999, Crosfield Limited: United States.
140. R.C. Reuel and C.H. Bartholomew, *J. Catal.*, 1984. **85**(1): p. 63-77.
141. McArthur, *US Patent A4 191 664*, in *US Patent Office*: US.
142. T. Shido, C.M. Lok and R. Prins, *Topics in Catalysis,* 1999. **8**: p. 223-236.
143. B.W. Hoffer, A.D.van Langeveld, J.-P. Janssens, R.L.C. Bonne, C.M. Lok and J.A. Moulijn, *J. Catal.*, 2000. **192**: p. 432-440.
144. C.M. Lok, *Prepr. Pap.-Am. Chem. Soc., Div. Pet. Chem.*, 2004. **49**(2): p. 169-171.
145. M. Nele, A. Vidal, D.L. Bhering, J.C. Pinto and V.M.M. Salim, *Appl. Catal. A*, 1999. **178**: p. 177-189.
146. J.H. Bitter, M.K.van de Lee, A.G.T. Slotboom, A.J.van Dillen and K.P.d. Jong, *Catal. Lett.*, 2003. **89**: p. 139-142.
147. H.G.J.L. Rotgerink, J.G.v. Ommen and J.R.H. Ross, *The preparation and characterisation of sequentially precipitated and co-precipitated Ni-alumina catalysts and comparison of their properties*, in *Preparation of Catalysts IV: Scientific basis for the preparation of heterogeneous catalysts*, B. Delmon, P. Grange, P.A. Jacobs, and G. Poncelet, Editors. 1987, Elsevier: Amsterdam. p. 795-807.
148. K. Sohlberg, S.J. Pennycook and S.T. Pantelides, *J. Am. Chem. Soc.*, 1999. **121**: p. 7493-7499.
149. B.W. Hoffer, R.L.C. Bonne, A.D.van Langeveld, C. Griffiths, C.M. Lok and J.A. Moulijn, *Fuel,* 2004. **83**: p. 1-8.
150. CrossfieldCatalysts, *HTC Nickel Catalysts - product brochure.* 1989.
151. Synetix, *High performance catalysts and absorbants for base chemicals - product brochure.* 2001.
152. Synetix, *Catalysts, Process Technologies and Services for edible oils, oleochemicals, chemical and chemical intermediate, refinery products and fine chemicals*. 2001.
153. N. Young, PhD thesis (1995) in *Department of Chemistry*, University of Glasgow: Glasgow.
154. Johnson Matthey, *internal report*. 2004.
155. J.P. Janssens, A.D.van Langeveld, R.L.C. Bonné, C.M. Lok and J.A. Moulijn, *Hydrotreating technology for pollution control*. 1996, New York: Marcel Dekker. 159-167.
156. B. Scheffer, P. Molhoek and J.A. Moulijn, *Appl. Catal.*, 1989. **46**: p. 11-30.
157. P. Arnoldy and J.A. Moulijn, *J. Catal.*, 1985. **93**: p. 38-54.
158. E.E. Khadiri and M.P. Astier, *Appl. Catal. A*, 1997. **163**: p. 177-186.
159. J. Zielinski, *Appl. Catal.*, 1987. **35**: p. 1-12.
160. J.A. Ryder, A.K. Chakraborty and A.T. Bell, *J. Phys. Chem. B*, 2002. **106**: p. 7059-7064.
161. A.L. Yakovlev, G.M. Zhidomirov and R.A.v. Santen, *Catal. Lett.*, 2001. **75**: p. 45-48.
162. F.A. Cotton and G. Wilkinson, *Advanced Inorganic Chemistry (2nd Ed)*. 1966, London: John Wiley and Son.
163. M.C. Marion, E. Grabowski and M. Primet, *J. Chem. Soc. Faraday Trans.*, 1991. **87**(11): p. 1795-1800.
164. F. Boccuzzi, S. Coluccia, G. Martra and N. Ravasio, *J. Catal.*, 1999. **184**: p. 316-326.
165. B. Scheffer, J.J. Heijeinga and J.A. Moulijn, *J. Phys. Chem.*, 1987. **91**: p. 4752-4759.
166. H. Hadjiivanov, M. Mihaylov, D. Klissurski, P. Stefanov, N. Abadjieva, E. Vassileva and L. Mintchev, *J. Catal.*, 1999. **185**: p. 314-323.
167. P. Gajardo, P. Grange and B. Delmon, *J. Catal.*, 1980. **63**: p. 201-216.
168. J. Llorca, J.-A. Dalmon, P.R.de la Piscina and N. Homs, *Appl. Catal. A*, 2003. **243**: p. 261-269.

169. R. Hopkins and S. Feeney, *Gold Crest Award Study*. 1999, Synetix: Billingham.
170. B. Jongsomjit, J. Panpranot and J.G.Goodwin. Jr, *J. Catal.*, 2001. **204**: p. 98-109.
171. T. Toupance, M. Kermarec and C. Louis, *J. Phys. Chem. B*, 2000. **104**: p. 965-972.
172. J.W. Niemantsverdriet, *Spectroscopy in Catalysis*. 1995, Weinheim: VCH. 42-45.
173. S. Bailey and M. Kett, *Internal research minute*. 2003, Johnson Matthey.
174. C.L. Young, ed. *Solubility Data Series - Hydrogen and deuterium*. Vol. 5/6. 1981, Pergamon Press: Oxford.
175. R.A. Alberty and R.J. Sibley, *Physical chemistry*. 2 ed. 1997, New York: John Wiley and Sons. 631.
176. D.H. Williams and I. Fleming, *Spectroscopic Methods in Organic Chemistry*. 5 ed. 1995, Cambridge: McGraw-Hill.
177. R.L. Augustine, *Heterogenous Catalysis for the Synthetic Chemist*. 1996, New York: Marcel-Dekker. 245.
178. M. Boudart, *Adv. Catal.*, 1969. **20**: p. 153-166.
179. R.van. Hardveld and F. Hartog, *Adv. Catal.*, 1972. **202**(22): p. 75.
180. G. Bond, *J. Catal.*, 1992. **136**: p. 631-632.
181. G. Bond,. *Chem. Soc. Rev.*, 1991. **20**: p. 441-475.
182. G. Carturan, G. Facchin, G. Cocco, G. Navazio and G. Gubitosa, *J. Catal.*, 1983. **82**: p. 56-65.
183. G. Neri, M.G. Musolino, C. Milone, D. Pietropaolo and S. Galvagno, *Appl. Catal. A*, 2001. **208**: p. 307-316.
184. F. Zhao, Y. Ikushima and M. Arai, *J. Catal.*, 2004. **224**: p. 479-483.
185. U.K. Singh and M.A. Vannice, *Appl. Catal. A*, 2001. **213**: p. 1-24.
186. *Norit CN1 data sheet*, Norit: Amersfoort.
187. *Norit CA1 data sheet*, Norit: Amersfoort.
188. *Norit SX Ultra data sheet*, Norit: Amersfoort.
189. E. Gelder, *Unpublished observation*. 2002: University of Glasgow.
190. F. Rodriguez-Reinsos, *Carbon*, 1998. **36**: p. 159-175.
191. J.M. Solar, C.A.L.y. Leon, K. Osseo-Asore and L.R. Radovic, *Carbon*, 1990. **28**: p. 369-375.
192. D.J. Suh, T.-J. Park and S.-K. Ihm, *Ind. Eng. Chem. Res.*, 1992. **31**: p. 1849-1856.
193. G.S. Szymanski and G. Rychlicki, *Carbon*, 1991. **29**: p. 489-498.
194. A. Tomita and Y. Tamai, *J. Colloid. Interf. Sci.*, 1971. **36**: p. 153-154.
195. A. Sepulveda-Escribano, F. Coloma and F. Rodriguez-Reinoso, *Appl. Catal. A*, 1998. **173**: p. 247-257.
196. I. Mikami, Y. Sakamoto, Y. Yoshinaga and T. Okuhara, *Appl. Catal. B*, 2003. **44**: p. 79-86.
197. C. Clayton, PhD thesis (2004), Department of Chemical Engineering, University of Cambridge: Cambridge.
198. Y.-F. Han, D. Kumar, C. Sivadinarayana and D.W. Goodman, *J. Catal.*, 2004. **224**: p. 60-68.
199. S. Dahl, J. Sehested, C.J.H. Jacobsen, E. Tornqvist and I. Chorkendorff, *J. Catal.*, 2000. **192**: p. 391-399.
200. D. Chadwick, A. Oen and C. Siewe, *Catal. Today*, 1996. **29**: p. 229-233.
201. H. Luo, S. Park, H. Yeung, H. Chan and M.J. Weaver, *J. Phys. Chem. B*, 2000. **104**: p. 8250-8258.
202. M. Schmal, D.A.G. Aranda, F.B. Noronha, A.L. Guimaraes and R.S. Monteiro, *Catal. Lett.*, 2000. **64**: p. 163-169.
203. P.H. Emmett, *Catal. Rev.*, 1992. **7**: p. 1-24.
204. R.L.Burwell. Jr, *Catal. Rev.*, 1992. **7**: p. 25-49.
205. M.A. Brundage and S.S.C. Chuang, *J. Catal.*, 1996. **164**: p. 94-108.
206. N.J. Ossipoff and N.W. Cant, *J. Catal.*, 1994. **148**: p. 125-133.
207. E.F. Meyer and R.L.B. Jr, *J. Am. Chem. Soc.*, 1963. **85**: p. 2877-2880.
208. Y. Inoue and I. Yasumori, *J. Phys. Chem.*, 1971. **75**: p. 880-887.
209. L. Melander and W.H.S. Jr, *Reaction rates of isotopic molecules*. 2 ed. 1980, New York: John Wiley and Sons.
210. K.-I. Aika and A. Ozaki, *J. Catal.*, 1969. **13**: p. 232-237.
211. K.-I. Aika and A. Ozaki, *J. Catal.*, 1970. **19**: p. 350-352.
212. S.M. Davis, W.D. Gillespie and G.A. Somorjai, *J. Catal.*, 1983. **83**: p. 131-140.
213. C.S. Kellner and A.T. Bell, *J. Catal.*, 1981. **67**: p. 175-185.
214. D.M.J. Williams, final year report (2003), University of Glasgow: Glasgow.
215. G. Ormsby, final year report *(2004)*, in *Department of Chemistry*. 2004, University of Glasgow: Glasgow.

216. C.A. Koutstaal, P.A.J.M. Angevaare, E.J. Grootndorst and V. Ponec, *J. Catal.*, 1993. **141**: p. 82-93.
217. P. Politzer, L. Abrahmsen and P. Sjoberg, *J. Am. Chem. Soc.*, 1984. **106**: p. 855-860.
218. P. Politzer and R. Bar-Adon, *J. Phys. Chem.*, 1987. **91**: p. 2069-2073.
219. K.T. Hindle, *PhD thesis* (2004), Department of Chemistry, University of Glasgow
220. E.B. Maxted and M.S. Biggs, *J. Chem. Soc.*, 1957: p. 3844-3847.
221. M.L. Toebes, Y.H. Zhang, J. Hajek, T.A. Nijhuis, J.H. Bitter, A.J.v. Dillen, D.Y. Murzin, D.C. Koningsberger, and K.P.d. Jong, *J. Catal.*, 2004. **226**: p. 215-225.
222. P. Lukinskas and D. Farcasiu, *Appl. Catal. A*, 2001. **209**: p. 193-205.
223. A. Lueking and R.T. Yang, *J. Catal.*, 2002. **206**: p. 165-168.
224. A.C. Dillon and M.J. Heben, *Appl. Phys. A*, 2001. **72**: p. 133-142.
225. M.A. Callejas, A. Anson, A.M. Benito, W. Maser, J.L.G. Fierro, M.L. Sanjuan and M.T. Martinez, *Mat. Sci. Eng. B*, 2004. **108**: p. 120-123.
226. T.N. Rhobin, R.P. Merrill, P.J. O'Hagan, S.C. Woronick, N.D. Shinn, G.L. Woolery and A.W. Chester,. *J. Phys. Chem.*, 1994. **98**: p. 2433-2440.
227. K.C. Hass, W.F. Schneider, A. Curioni and W. Andreoni, *Science*, 1998. **282(5387)**: p. 265-268.
228. J. Clark, *http://www.chemguide.co.uk/inorganic/complexions/stabconst.html*. 2003.
229. C.K. Jorgensen, *Inorganic complexes*. 1963, London: Academic Press.
230. R.M. Smith and A.E. Martell, *Critical Stability Constants*. Vol. 4: Inorganic complexes, New York: Plenum Press.
231. M. Hansen, *constitution of binary alloys*. 2 ed. 1958, New York: McGraw-Hill.
232. V. Ponec, *Appl. Catal. A*, 2001. **222**: p. 31-45.
233. J.A. Rodriguez, *Hetero. Chem. Rev.*, 1996. **3**: p. 17-32.
234. O.S. Alexeev and B.C. Gates, *Ind. Eng. Chem. Res.*, 2003. **42**: p. 1571-1587.
235. P. Salerno, S. Mendioroz and A.L. Agudo,. *Appl. Catal. A*, 2004. **259**: p. 17-28.
236. G. Jacobs, T.K. Das, P.M. Patterson, L.S. J. Li and B.H. Davis. *Appl. Catal. A*, 2003. **247**: p. 335-343.
237. D. Schanke, A.M. Hilmen, E. Bergene, K. Kinnari, E. Rytter, E. Adnanes and A. Holmen, *Catal. Lett.*, 1995. **34**: p. 269-284.
238. A.M. Hilmen, D. Schanke, K.F. Hanssen and A. Holmen, *Appl. Catal. A*, 1999. **186**: p. 169-188.
239. Y. Zhang, D. Wei, S. Hammanche and J.G.Goodwin. Jr, *J. Catal.*, 1999. **188**: p. 281-290.
240. F.M. Gottschalk, R.G. Copperthwaite, M.van de Riet and G. J. Hutchings, *Appl. Catal.*, 1988. **38**: p. 103.
241. J. Li, G. Jacobs, T. Das, Y. Zhang and B. Davis, *Appl. Catal. A*, 2002. **236**: p. 67-76.
242. S. Krishnamoorthy, M. Tu, M.P. Ojeda, D. Pinna and E. Iglesia, *J. Catal.*, 2002. **211**: p. 422-433.
243. G.P. Huffman, N. Shah, J. Zhao, F.E. Huggins, T.E. Hoost, S. Halvorsen and J.G.G. Jr, *J. Catal.*, 1995. **151**: p. 17-25.
244. H. Schulz, M. Claeys and S. Harms, *Stud. Surf. Sci. Catal.*, 1997. **107**: p. 193.
245. H. Schulz, E.van Steen and M. Claeys, *Stud. Surf. Sci. Catal.*, 1994. **81**: p. 455.
246. C.J. Kim, *Patent 5, 277, 407*, in *US Patent Office*. 1993, Exxon Research: USA.
247. K.F. Hanssen, E.A. Blekkan, D. Schanke and A. Holmen, *Stud. Surf. Sci. Catal.*, 1997. **109**: p. 193.
248. A. Sirijaruphan, A. Horvath, J.G.Goodwin. Jr and R. Oukaci, *Catal. Lett.*, 2003. **91**: p. 89-94.
249. J. Li, X. Zhan, G. Jacobs, Y. Zhang, T.K. Das and B.H. Davis, *Appl. Catal. A*, 2002. **228**: p. 223.
250. M.E. Dry, *Catal. Lett.*, 1990. **7**: p. 204.
251. P.J.van Berge, J.van de Loosdrecht, S. Barradas and A.M.van de Kraan, *Catal. Today*, 2000. **58**: p. 321.
252. A. Lapidus, A. Krylova, V. Kazanskii, V. Borovkov and A. Zaitsev, *Appl. Catal.*, 1991. **73**: p. 65.
253. R.B. Anderson, *Catalysis*, ed. P.H. Emmett. Vol. IV. 1956, New York: Rheinhold.
254. G. Jacobs, T.K. Das, Y. Zhang, J. Li and B.H. Davis, *Catal. Deactivat.*, 2001. **139**: p. 415.
255. G. Jacobs, T.K. Das, Y. Zhang, J. Li, G. Racallet and B.H. Davis, *Appl. Catal. A*, 2002. **233**: p. 263.
256. A. Kogelbauer, J.C. Weber and J.G.G. Jr, *Catal. Lett.*, 1995. **34**: p. 259.
257. A. Moen, D.G. Nicholson, M. Ronning and H. Emerich, *J. Mat. Chem.*, 1998. **8**: p. 2533-2539.

258. S. Vada, A. Hoff, E. Adnanes, D. Schanke and A. Holmen, *Top. Catal.*, 1995. **12**: p. 155.
259. P.A. Chernavskii, G.V. Pankina, A.S. Lermontov and V.V. Lunin, *Kinet. Catal.*, 2003. **44**: p. 651-661.
260. D.G. Castner, R.P. Watson and I.Y. Chan, *J. Phys. Chem.*, 1990. **94**: p. 819.
261. J. Zielinski, *J. Chem. Soc. Faraday Trans.*, 1997. **93**: p. 3577-3580.
262. P. Marginean and A. Olariu, *Appl. Catal. A*, 1996. **140**: p. 59-72.
263. S.D. Jackson, A.W. Owens and M.W. Roberts, *React. Kinet. Catal. Lett.*, 1992. **46**: p. 245-248.
264. S.D. Jackson, A.W. Owens and M.W. Roberts, *Ind. J. Tech.*, 1992. **30**: p. 85-88.
265. K. Klier, *Adv. Catal.*, 1982. **31**: p. 243-313.
266. T.M. Yurieva, L.M. Plyasova, V.I. Zaikovskii, T.P. Minyukova, A. Bliek, J.C.v.d. Heuvel, L.P. Davydova, I.Y. Molina, M.P. Demeshkina, A.A. Khassin, and E.D. Batyrev, *Phys. Chem. Chem. Phys.*, 2004. **6**: p. 4522-4526.
267. S.A. French, A.A. Sokol, J. To, C.R.A. Catlow, N.S. Phala, G. Klatt and E.v. Steen, *Catal. Today,* 2004. **93-95**: p. 535-540.
268. H. Yum, H. Zhang, J.H. Chen and H.B. Chen, *Acta. Chimica. Sinica,* 2004. **62**: p. 1729-1732.
269. R.S. Rao, R.T.K. Baker and M.A. Vannice, *Catal. Lett.*, 1999. **60**: p. 51-57.
270. R. Rao, A. Dandekar, R.T.K. Baker and M.A. Vannice, *J. Catal.*, 1997. **171**: p. 406-419.

8.0 APPENDICES

1. E. A. Gelder, S. D. Jackson and C. M. Lok, A study of nitrobenzene hydrogenation over palladium/carbon catalysts, *Catal. Letts.*, **84** (2002) 205-208

2. E. A. Gelder, S. D. Jackson and C. M. Lok, The hydrogenation of nitrobenzene to aniline: a new mechanism, *Chem. Commun.*, **4** (2005) 522-524

Catalysis Letters Vol. 84, Nos. 3–4, December 2002 (©2002)

A study of nitrobenzene hydrogenation over palladium/carbon catalysts

Elaine A. Gelder [a], S. David Jackson [a,*], and C. Martin Lok [b]

[a] *Department of Chemistry, The University, Glasgow G12 8QQ, Scotland*
[b] *Synetix, P.O. Box 1, Belasis Avenue, Billingham, Cleveland TS23 1LB, UK*

Received 27 August 2002; accepted 29 August 2002

The hydrogenation of nitrobenzene has been studied over three palladium/carbon catalysts using methanol and isopropanol as solvents. A solvent and palladium particle size effect have both been observed, with the nature of the particle size effect dependent upon the solvent. This may be related to a change in the rate-determining step.

KEY WORDS: palladium; nitrobenzene; hydrogenation; carbon; aniline; particle size effect.

1. Introduction

The catalytic hydrogenation of nitrobenzene is commonly employed as a standard reference reaction for testing and comparing the activity of hydrogenation catalysts for a range of applications [1–5]. In addition, it is an important industrial reaction used in the commercial production of aniline for use in the polyurethane industry [6]. However, although there is extensive literature available citing the use of this reaction as a test of catalyst activity, there are relatively few publications investigating the hydrogenation reaction. A reaction mechanism for nitrobenzene hydrogenation was first proposed by Haber in 1898 and has been widely accepted since [7]. Unfortunately, this mechanism is still not well understood and has never been thoroughly investigated. For example, in the industrial process the catalysts are prone to deactivation, yet no deactivation mechanism has been delineated. This study forms part of a wider investigation into the mechanistic scheme for the hydrogenation of nitrobenzene and into the deactivation of the catalysts. Initial studies have focused upon palladium metal, which has been employed extensively for the hydrogenation of nitrobenzene [8–10]. Three activated carbon supports were used to examine any support effect. In addition, two different solvents were employed to ascertain the influence of reaction solvent on the reaction mechanism.

2. Experimental

All catalysts were prepared by impregnation. Three different powdered activated carbon supports were used: Norit CN1 (surface area 1400 $m^2 g^{-1}$), Norit CA1 (surface area 1400 $m^2 g^{-1}$) and Norit SX Ultra (surface area 1200 $m^2 g^{-1}$). Sufficient palladium nitrate solution (PGP, assay 10.123% Pd), to produce a palladium loading of 3%, was added to each support. The resulting suspensions were dried and calcined at 423 K for 3 h.

The dispersion of each catalyst was measured by CO chemisorption. Taking a CO:Pd ratio of 1:2 the dispersions shown in table 1 were calculated and from these an approximate metal particle size determined assuming a spherical model.

Nitrobenzene hydrogenation was carried out in a Buchi stirred autoclave. The reactor design allowed regulation of reaction temperature, hydrogen gas pressure, and stirring speed. In addition, it also allowed *in situ* reduction of the catalyst prior to the reactant being added. The catalyst (0.10 g) was added to the reactor along with the reaction solvent (280 ml methanol or isopropanol (IPA)). The autoclave was then purged with nitrogen. The catalyst was reduced in a flow of hydrogen (30 $cm^3 min^{-1}$). With hydrogen being sparged through the solvent the mechanical stirrer was set to 300 rpm and the temperature increased to 323 K. The temperature was held for 30 min. The hydrogen flow and stirring were then stopped and nitrobenzene (17 ml, 0.166 moles) added *via* an injection port. Following purging with nitrogen, the system was pressurized with hydrogen (5 barg). The reaction commenced when the

Table 1.

Catalyst	Dispersion (%)	Average particle size (nm)
Pd/CN1	9	12
Pd/CA1	13	9
Pd/CSXU	42	3

*To whom correspondence should be addressed.

1011-372X/02/1200-0205/0

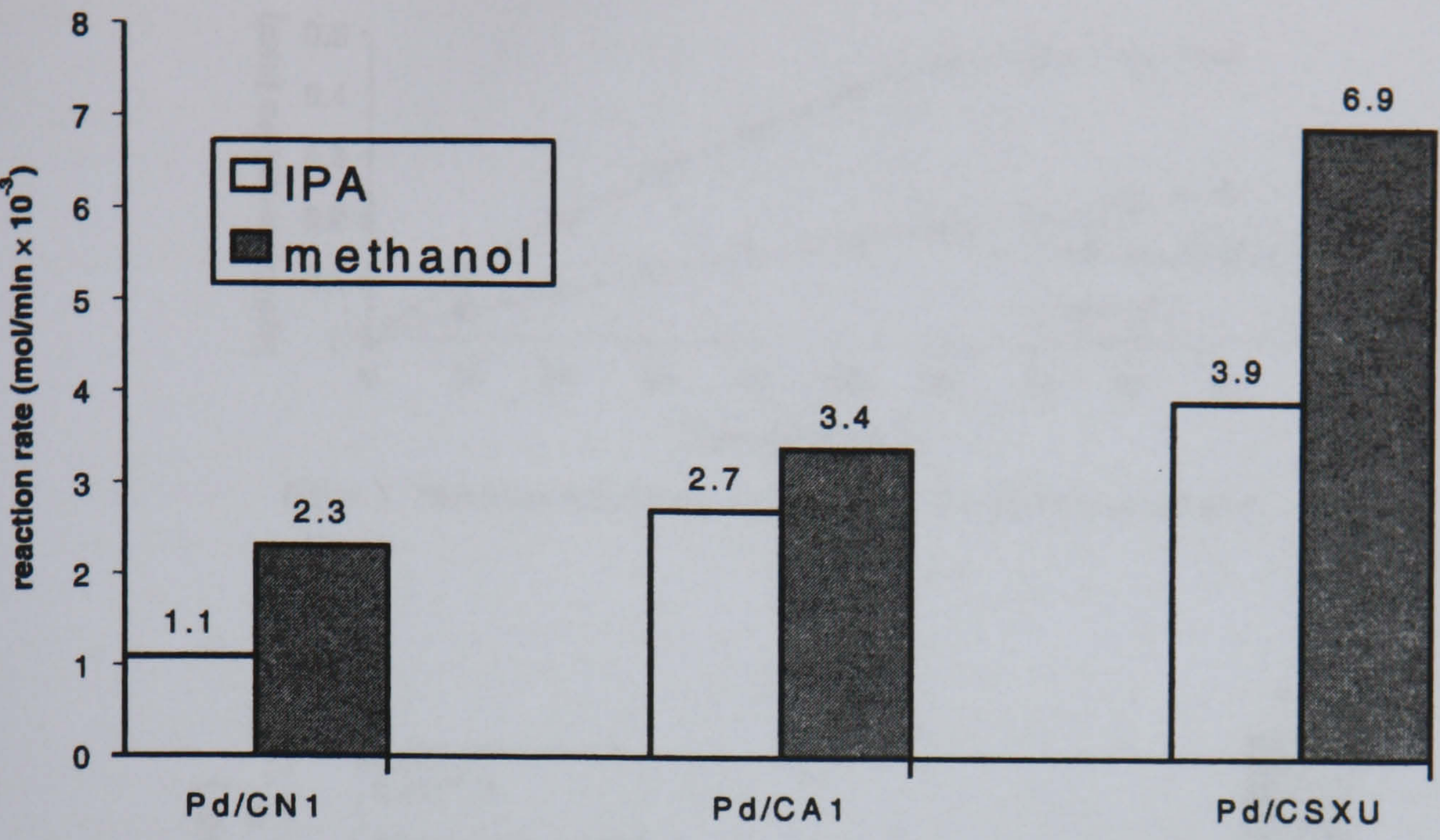

Figure 1. Nitrobenzene hydrogenation over Pd/CN1 in IPA and methanol.

stirrer was switched on. A temperature of 323 K was used for all reactions. The stirrer speed was set at 1000 rpm. No variation in hydrogenation rate was observed over a range of stirrer speeds (800–1500 rpm) indicating the absence of mass-transfer control. Analysis of the reaction mixture was performed by GC using a Chrompack CP 9000, with an FID detector fitted with a 30 m FFAP column.

3. Results

The three catalysts Pd/CN1, Pd/CA1, and Pd/CSXU were used to hydrogenate nitrobenzene under the conditions described in the experimental section using both methanol and IPA as the reaction solvent. The reaction rates were obtained by monitoring the hydrogen uptake. Liquid phase analysis confirmed the presence of only nitrobenzene and aniline as reactant and product: no other species were detected. All three catalysts, in both reaction media, show a linear uptake of hydrogen over the duration of the experiment. However, with each catalyst the reaction proceeds more rapidly in methanol than in IPA. The results are displayed in figures 1–3 and a comparison of the initial rates in figure 4.

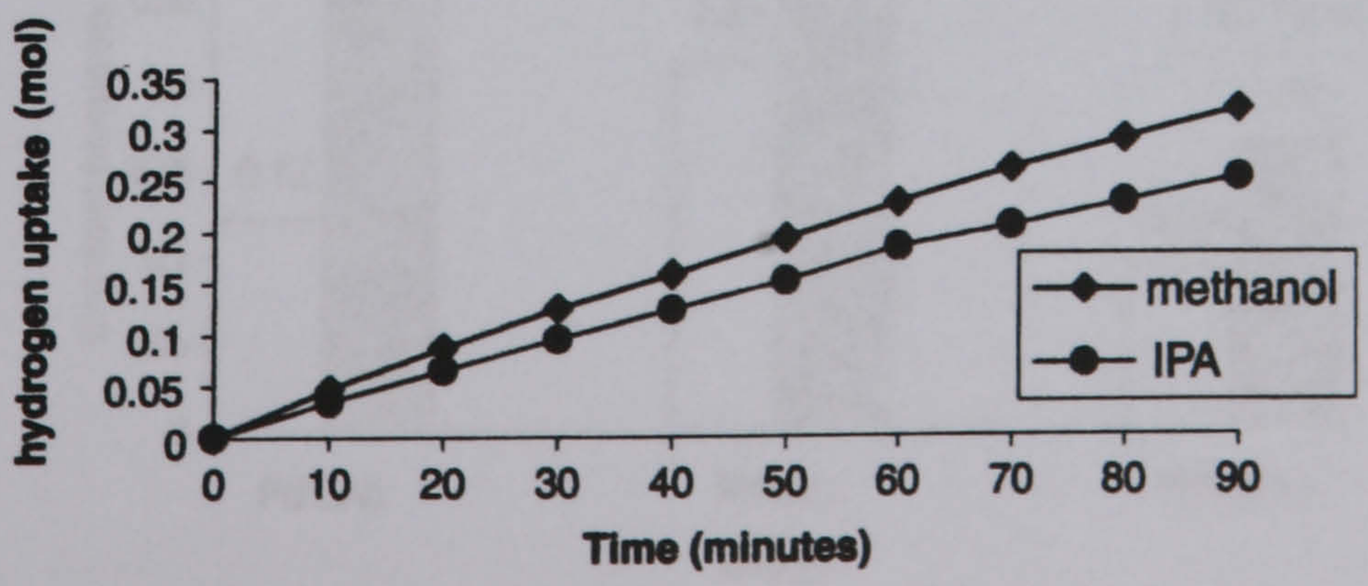

Figure 2. Nitrobenzene hydrogenation over Pd/CA1 in IPA and methanol.

4. Discussion

The difference in reaction rate when hydrogenation is performed in methanol or IPA indicates that a solvent effect is in operation (figures 1–3). From the initial rates of hydrogenation for each catalyst (figure 4) it is evident that the most disperse palladium catalyst with the smallest metal particles (Pd/CSXU) gives the highest activity whereas the least disperse catalyst (Pd/CN1) displays the slowest rate. In addition, the difference in rate between the two solvents is of a comparable magnitude for each catalyst. However, when the turnover frequency of nitrobenzene to aniline was calculated for each catalyst a more complex picture was seen (figure 5). Although a higher rate of reaction in methanol compared to IPA was confirmed, the graph demonstrates that catalyst Pd/CA1 is the most efficient catalyst in terms of the turnover frequency. Therefore, despite demonstrating the highest reaction rate, catalyst Pd/CSXU is shown to be the least effective in terms of the number of nitrobenzene molecules hydrogenated per metal atom. This suggests that the reaction is structure-sensitive. Examination of the results observed using methanol as the solvent reveals that Pd/CN1 and

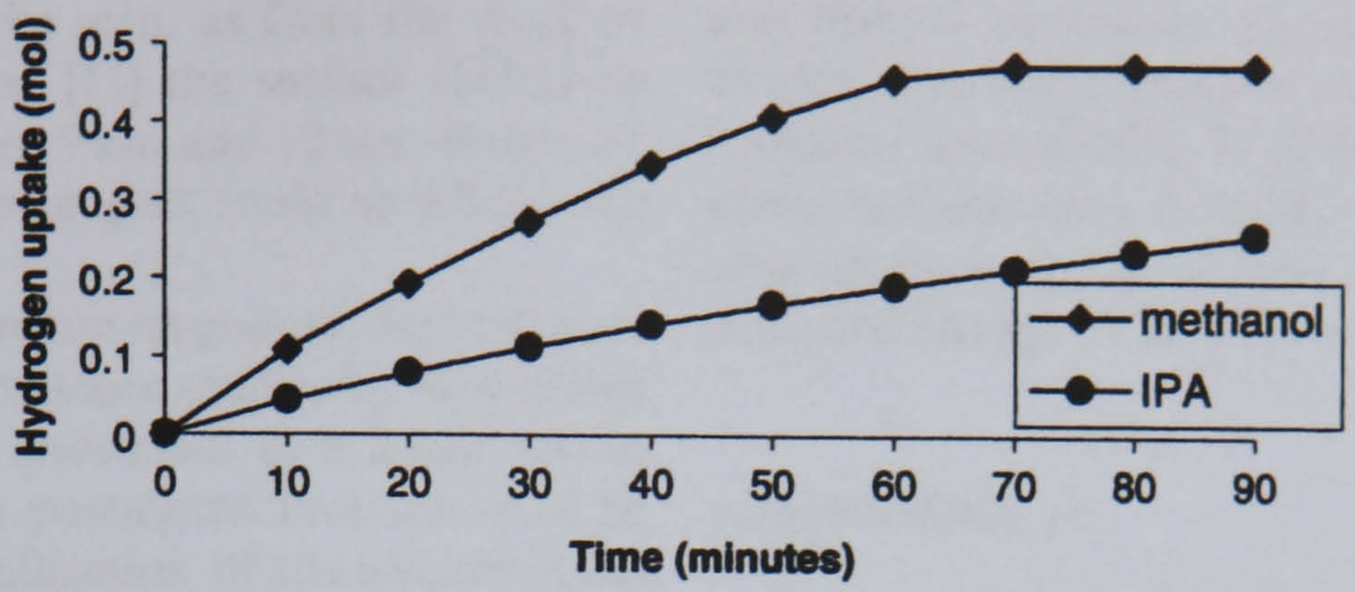

Figure 3. Nitrobenzene hydrogenation over Pd/CSXU in IPA and methanol.

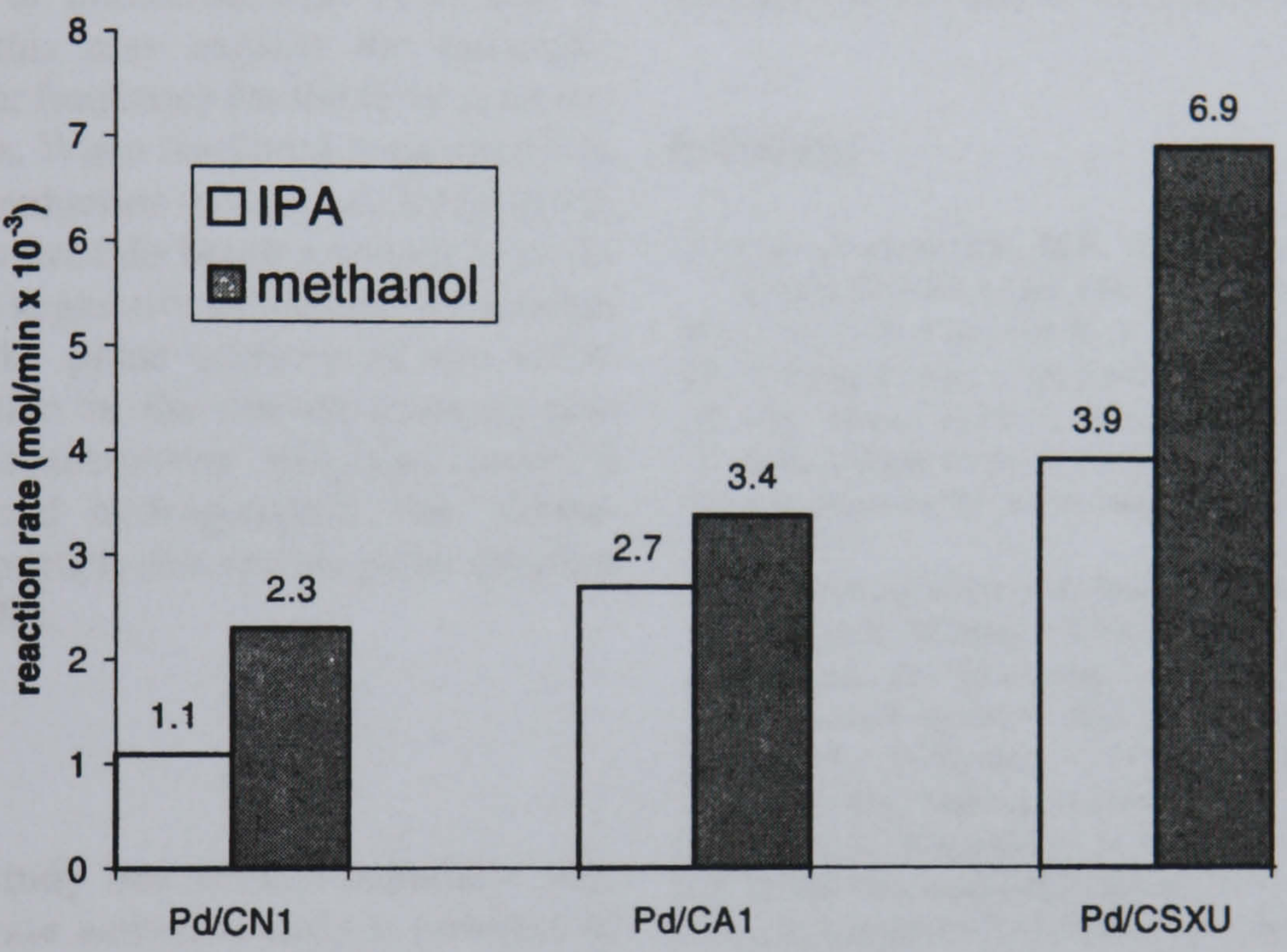

Figure 4. Comparison of rate of reaction in IPA and methanol.

Pd/CA1, the catalysts with the larger palladium particles, exhibit similar turnover frequencies, whereas Pd/CSXU, which has a smaller metal particle size, has a significantly reduced turnover frequency. Therefore, it can be postulated that, in a methanol solvent, the preferred sites for nitrobenzene hydrogenation are situated mainly on the plane surfaces of the catalysts as opposed to edges or corners.

When IPA is used as the solvent, however, a different pattern in turnover frequency is observed. Catalyst Pd/CA1 displays a significantly higher turnover frequency than Pd/CN1 or Pd/CSXU, showing that in IPA an optimal palladium crystallite size exists. Obviously with only three systems it is impossible to tell whether the size of ~9 nm is actually the maximum, but clearly a maximum is present. It is slightly surprising that a

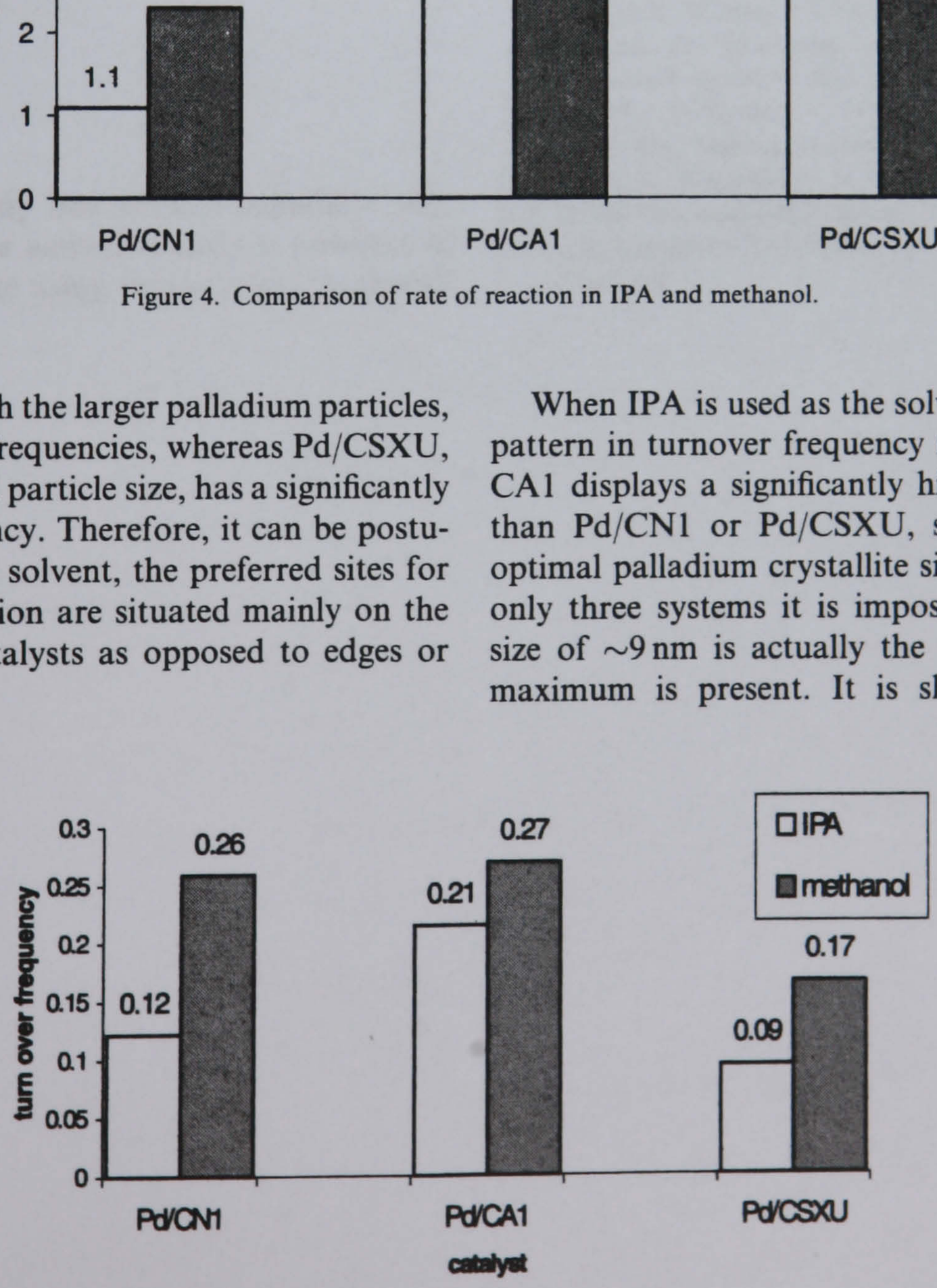

Figure 5. Comparison of turnover frequencies.

particle size effect should be seen, as from the work of van Hardeveld and Hartog [11] the surface should be changing very little between 9 nm and 12 nm. Hence we must also consider that the support could be influencing the reactivity.

This decrease in reaction rate on going from methanol to IPA is consistent with previous studies by Kochetova *et al.* [12], where reaction proceeded at a faster rate in ethanol than IPA. It was postulated that this may be due to greater charge stabilization of the intermediates in the reaction mechanism and a change of the rate-limiting step from the hydrogenation of nitrobenzene to the hydrogenation of nitrosobenzene. A change in mechanism such as this may explain the difference observed in the turnover frequency for the three catalysts in the different solvents. When methanol is employed as the reaction solvent, a reduction in turnover frequency is observed as the particle size falls below a certain level. As discussed above, this is suggestive of selective adsorption of nitrobenzene on the plane surfaces of the metal crystallites. An alteration in the rate-determining step to one involving nitrosobenzene will also mean a change in the preferred hydrogenation site. Consequently, the ability of particle size and shape to optimize these sites will also differ.

5. Conclusions

In summary, this study has utilized palladium supported on three separate activated carbon powders to hydrogenate nitrobenzene using two solvents, methanol and IPA. A significant solvent effect has been demonstrated with hydrogenation proceeding more rapidly in methanol than in IPA. In addition, a metal particle size effect has also been observed. The particle size effect is also sensitive to the solvent and may be related to a potential change in the rate-determining step.

Acknowledgments

The authors would like to thank L. Shaw for the preparation of the catalysts and the support of EPSRC and Synetix for one of us (E.A.G.).

References

[1] N.J. Jebarathinam, M.E. Eswaramoorthy and V. Krishnasamy, Studies Surf. Sci. Catal. 113 (1998) 1039.
[2] C. Li, Y.-W. Chen and W.-J. Wang, Appl. Catal. A 119 (1994) 185.
[3] X. Fang, S. Yao, Z. Qing and F. Li, Appl. Catal. A 161 (1997) 129.
[4] M.C. Macias Perez, C. Salinas Martinez de Lecca and A. Linares Solano, Appl. Catal. A 151 (1997) 461.
[5] J. Wisniak and M. Klein, Ind. Eng. Chem. Prod. Res. Dev. 23 (1984) 44.
[6] K. Weissermel and H.-J. Arpe, *Industrial Organic Chemistry*, 3rd edition (VCH, Weinheim, 1997) p. 375.
[7] F. Haber, Zeit. Electrochem. 4 (1898) 506.
[8] A. Metcalfe and M.W. Rowden, J. Catal. 22 (1971) 30.
[9] V. Holler, D. Wegricht, I. Yuranov, L. Kiwi-Minsker and A. Renken, Chem. Eng. Technol. 23 (2000) 251.
[10] X. Yu, M. Wang and H. Li, Appl. Catal. A. 202 (2000) 17.
[11] R. van Hardeveld and F. Hartog, Adv. Catal. 22 (1972) 75.
[12] L.B. Kochetova, T.G. Volkova and M.V. Klyuev, Petrol. Chem. 40 (2000) 371.

The hydrogenation of nitrobenzene to aniline: a new mechanism

Elaine A. Gelder,[a] S. David Jackson*[a] and C. Martin Lok[b]

Received (in Cambridge, UK) 29th July 2004, Accepted 8th October 2004
First published as an Advance Article on the web 2nd December 2004
DOI: 10.1039/b411603h

The Haber mechanism describing the process of hydrogenating nitrobenzene to aniline is shown to be incorrect and a new mechanism is proposed.

The catalytic hydrogenation of nitrobenzene is an industrially important reaction, utilised in the production of aniline for the plastics industry.[1] Commercially, the reaction is carried out in the gas phase over a nickel or copper based catalyst.[2] However, the transformation is extremely facile and is carried out under relatively mild conditions. For this reason, hydrogenation occurs rapidly over most metals and is commonly employed as a standard reference reaction for comparing the activities of other hydrogenation catalysts.[3–6] Despite the large volume of literature available citing the use of this reaction, very little has been published regarding actual mechanistic detail. Haber's initial scheme was published in 1898[7] and proposed that nitrobenzene was transformed to aniline in a three-step process involving nitrosobenzene and phenylhydroxylamine intermediates (Scheme 1). In addition, it was also proposed that azoxybenzene, azobenzene and hydrazobenzene by-products could be formed *via* reaction of the two intermediate species. This mechanism has been widely accepted since and a number of studies have reported the identification of the suggested reaction intermediates during hydrogenation.[8,9] In addition, Figueras and Coq[10] have reviewed the hydrogenation behaviour of these intermediates and by-products and found azobenzene to hydrogenate through to aniline. While these studies have appeared to provide further supporting evidence for Haber's reaction scheme, the mechanism is still not well understood and has never been fully delineated.

A palladium/carbon catalyst was used to study the hydrogenation of nitrobenzene and two of the proposed reaction intermediates, nitrosobenzene and azobenzene. The catalyst was prepared by impregnation of the powdered activated carbon support, Norit SX Ultra (surface area 1200 $m^2\ g^{-1}$), with sufficient palladium nitrate to produce a metal loading of 3%. The resulting suspension was dried and calcined at 423 K for 3 hours. The dispersion of the catalyst was measured using CO chemisorption. Taking a CO : Pd ratio of 1 : 2, the dispersion was calculated as 42.0%. Hydrogenation was carried out in a Buchi stirred autoclave. The catalyst (0.1 g) was added to the reactor with the reaction solvent (280 ml methanol) and reduced in a flow of hydrogen (30 $cm^3\ min^{-1}$) for 30 minutes with a stirring rate of 300 rpm. During reduction the reactor temperature was increased to 323 K. The reactant, nitrobenzene (0.08 mol), or nitrosobenzene (0.08 mol) was added and the hydrogen/deuterium pressure set at 3 bara and the stirrer speed at 1000 rpm. In reactions involving the addition of one of the intermediates along with nitrobenzene, the intermediate was added first and mixed with the solvent under nitrogen before nitrobenzene was added and reaction commenced. No variation in hydrogenation rate was observed over a range of stirrer speeds (800–1500 rpm) indicating the absence of mass transfer control. Analysis of the reaction mixture was performed by GC-MS using a Varian CP-3800 GC with a Varian Saturn 2000 Trace MS detector fitted with a 25 m DB-5 column. The rate of hydrogen uptake was measured independently, while the rate of aniline production was calculated using the GC-MS data.

The hydrogenation of nitrobenzene by hydrogen and deuterium is shown in Fig. 1 following the hydrogen uptake. The hydrogenation of nitrobenzene progressed to aniline without any significant by-product formation (<1% azobenzene) as the reaction went to completion. From Fig. 1 it can be seen that there is a kinetic isotope effect.

The hydrogenation of nitrosobenzene by hydrogen and deuterium was also studied and the hydrogen uptake is shown in Fig. 2. There is no kinetic isotope effect over the first 15–20 min and thereafter there is an inverse kinetic isotope effect. The reaction profile is shown in Fig. 3 and is dramatically different from that observed with nitrobenzene.

Comparison of the reaction profiles of nitrobenzene hydrogenation and nitrosobenzene hydrogenation show distinct differences as do the hydrogen uptake curves. The two stage hydrogen uptake curve observed with nitrosobenzene (Fig. 2) has been described

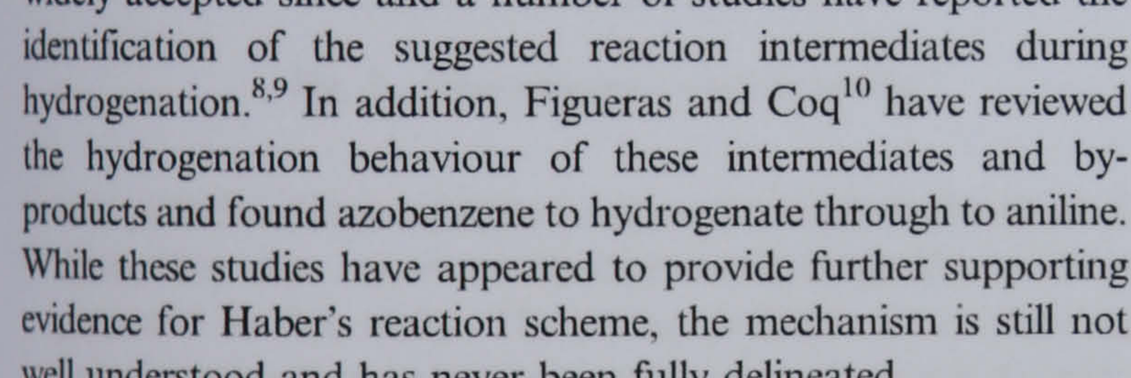

Scheme 1 The Haber mechanism.

*sdj@chem.gla.ac.uk

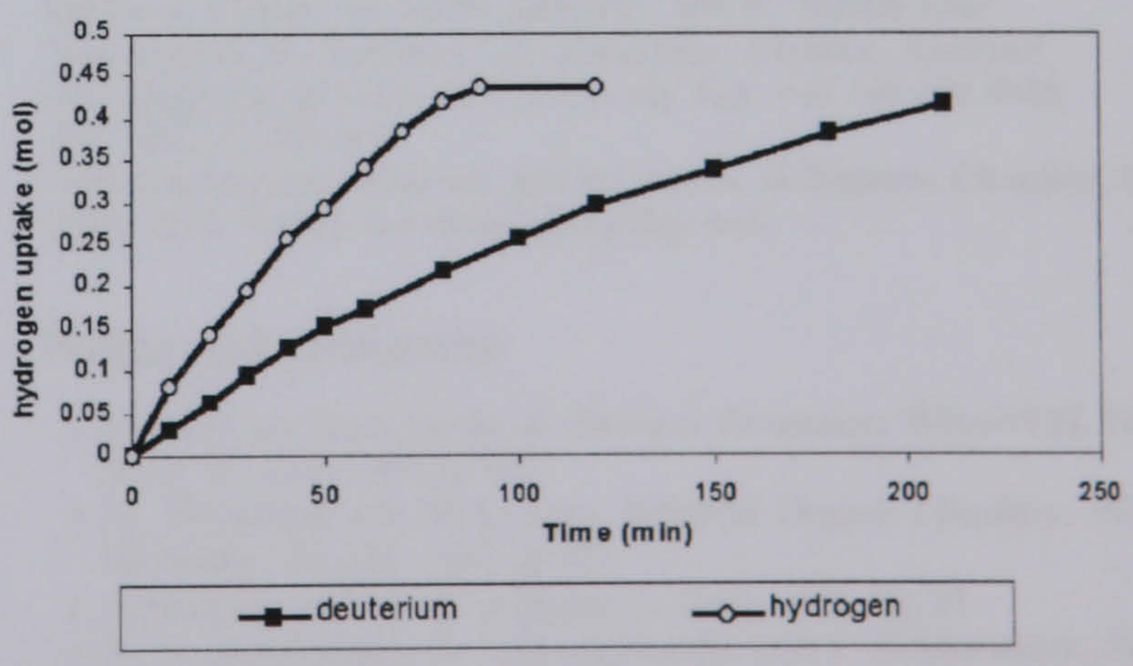

Fig. 1 Hydrogen/deuterium uptake during nitrobenzene hydrogenation.

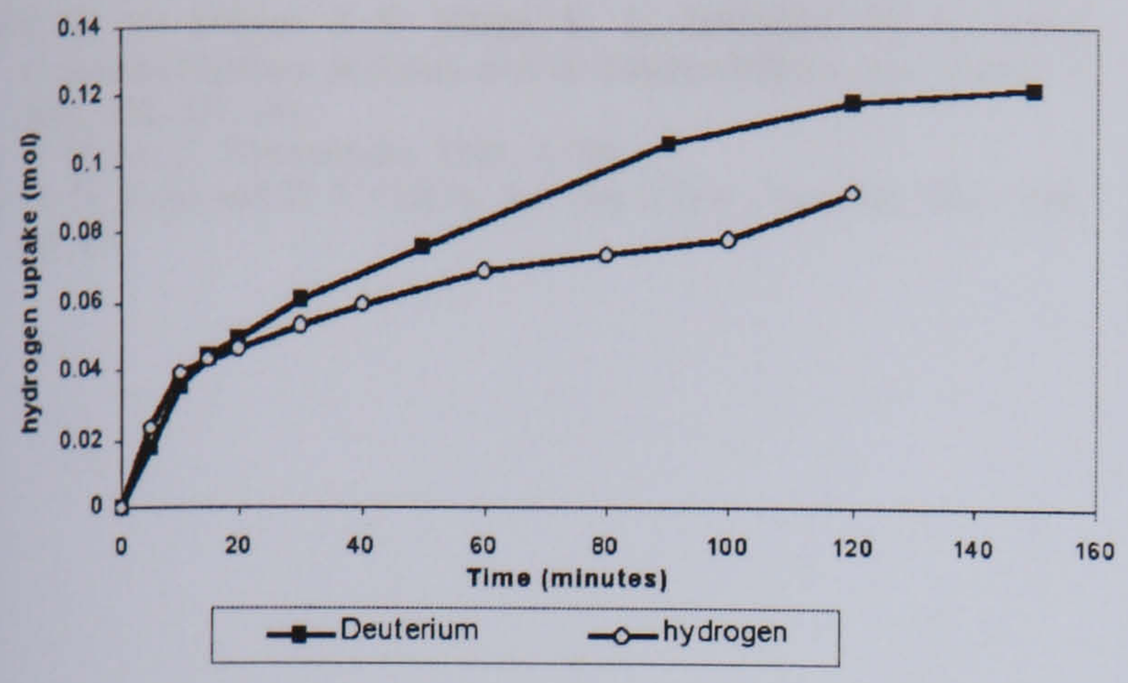

Fig. 2 Hydrogen/deuterium uptake during nitrosobenzene hydrogenation.

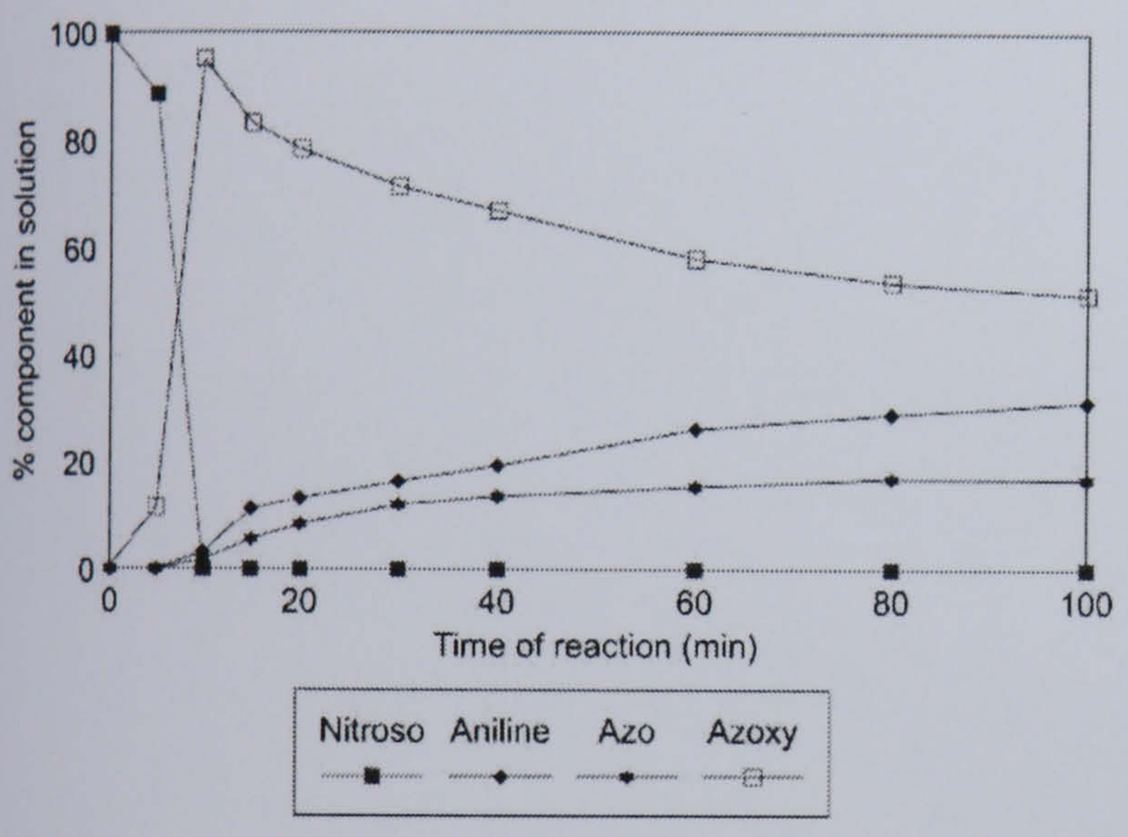

Fig. 3 Nitrosobenzene reaction profile.

over palladium/silica catalysts in a previous study by Smith *et al.*,[11] where they also report an identical reaction profile to the one presented in this study. The initial product of nitrosobenzene hydrogenation is azoxybenzene; aniline is not formed until after all the nitrosobenzene has been converted to azoxybenzene. The rate of aniline production was calculated at 15.5 mmol min^{-1} g^{-1} for nitrobenzene hydrogenation and 0.35 mmol min^{-1} g^{-1} for nitrosobenzene hydrogenation.

The lower rate of hydrogenation to aniline from nitrosobenzene and the different kinetic isotope effects make it clear that nitrosobenzene cannot be an intermediate in the hydrogenation of nitrobenzene. Therefore the Haber mechanism must be updated.

A detailed analysis of the surface reaction mechanisms for nitrobenzene and nitrosobenzene has led us to propose a new mechanism (Scheme 2). We are unable, due to the space limitations, to lay out the full detailed mechanism for both compounds, hence dotted arrows indicate multiple steps.

The analysis suggests that there is a common surface intermediate, namely Ph–N(OH)(a). In the nitrobenzene mechanism, Ph–N(OH)(a) reacts with adsorbed hydrogen whereas in the nitrosobenzene mechanism, Ph–N(OH)(a) reacts with itself to eliminate water and produce azoxybenzene. In nitrobenzene hydrogenation each step involves the addition of hydrogen hence

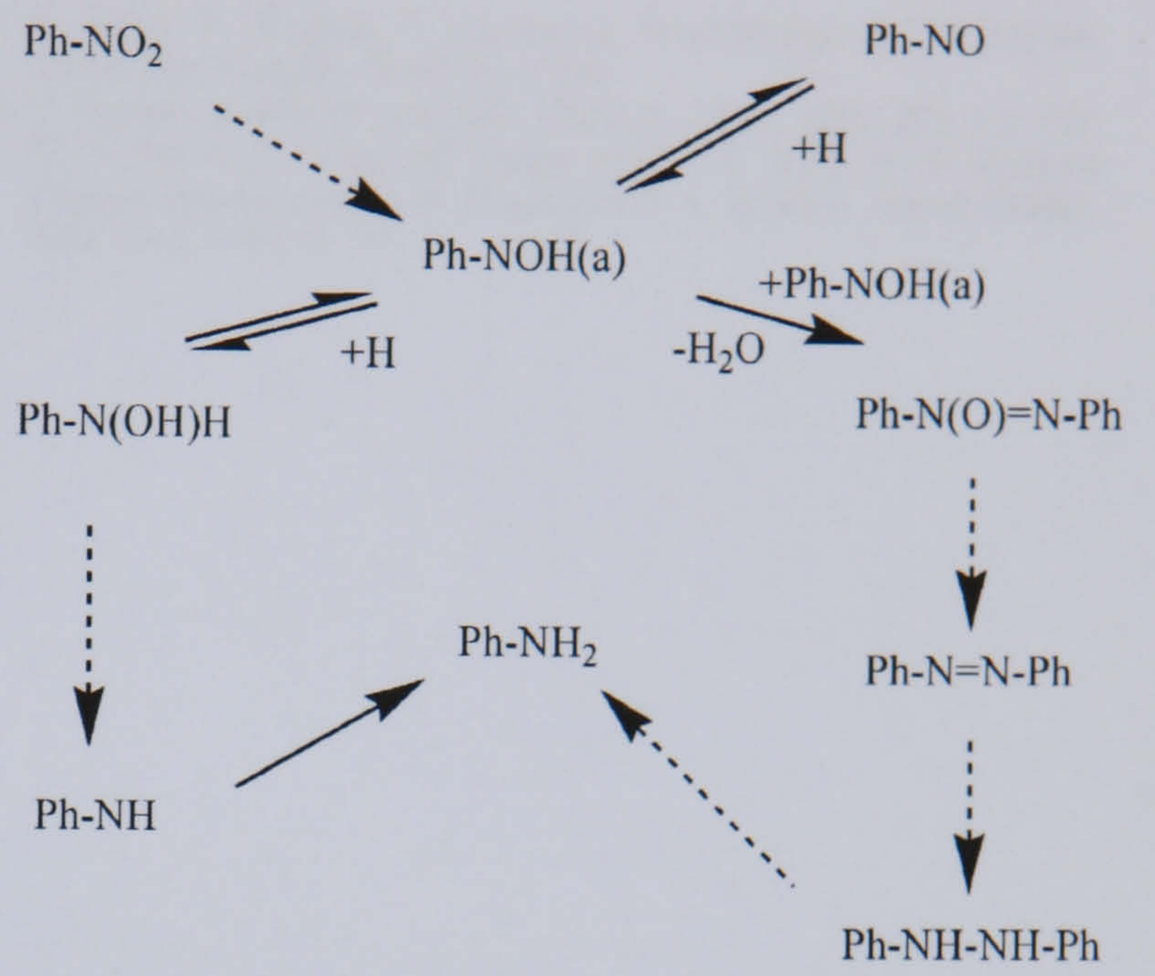

Scheme 2

the kinetic isotope effect. However in the nitrosobenzene mechanism there is a coupling reaction and a hydrogenolysis reaction either of which could lead to an inverse kinetic isotope effect. The different processes occurring in the two mechanisms would be consistent with the different rates observed and the fact that nitrosobenzene has a slower rate of aniline formation.

The nitrobenzene and nitrosobenzene hydrogenation reactions were repeated with a pre-activated Raney Nickel catalyst (Aldrich) and similar reaction profiles were obtained. When the hydrogen pressure was reduced to 1 bara, trace levels of nitrosobenzene were detected in the reaction mix. This is predictable from Scheme 2, as under reaction conditions where hydrogen is limited it is possible for Ph–N(OH)(a) to dehydrogenate to give nitrosobenzene as a by-product of nitrobenzene hydrogenation.

This new understanding of the mechanism has implications for both catalyst and reactor design. To obtain a high activity and selectivity it is essential that the hydrogen flux at the surface is maintained, with good access to the reaction site and no diffusion limitations. Indeed the presence of typical by-products such as azobenzene and azoxybenzene may indicate that there are local regions on the catalyst surface where the hydrogen flux is insufficient to inhibit Ph–N(OH)(a) coupling, even though the system overall may not be in a diffusion controlled regime.

Elaine A. Gelder,[a] S. David Jackson*[a] and C. Martin Lok[b]
[a]*Department of Chemistry, The University, Glasgow, Scotland, G12 8QQ. E-mail: sdj@chem.gla.ac.uk; Fax: +44 141 330 4888; Tel: +44 141 330 4443*
[b]*Johnson Matthey Catalysts, Belasis Avenue, Billingham, Cleveland, UK TS23 1LB. E-mail: martin.lok@matthey.com*

Notes and references

1 *Kirk-Othmer Encyclopedia of Chemical Technology*, Wiley-VCH, New York, 4th edn., 1997, p. 695.
2 K. Weissermel and H.-J. Arpe, *Industrial Organic Chemistry*, VCH, Weinheim, 3rd edn., 1997, p. 377.
3 A. Metcalfe and M. W. Rowden, *J. Catal.*, 1971, **22**, 30.
4 N. J. Jebarathinam, M. Eswaramoorthy and V. Krishnasamy, *Stud. Surf. Sci. Catal.*, 1998, **113**, 1039.
5 X. Yu, M. Wang and H. Li, *Appl. Catal., A*, 2000, **202**, 17.

6 S. R. de Miguel, J. I. Vilella, E. L. Jablonski, O. A. Scelza, C. Salinas-Martinez de Lecea and A. Linares-Solano, *Appl. Catal., A*, 2002, **232**, 237–246.
7 F. Haber, *Z. Elektrochem.*, 1898, **4**, 506.
8 H. D. Burge and D. J. Collins, *Ind. Eng. Chem. Prod. Res. Dev.*, 1980, **19**, 389.
9 V. Höller, D. Wegricht, I. Yuranov, L. Kiwi-Minsker and A. Renken, *Chem. Eng. Technol.*, 2000, **23**, 3, 251.
10 F. Figueras and B. Coq, *J. Mol. Catal. A: Chem.*, 2001, **173**, 1–2, 223.
11 G. V. Smith, R. Song, M. Gasior and R. E. Malz, Jr. in *Catalysis Organic Reactions*, eds. J. R. Kosak and T. A. Johnson, Marcel Dekker, New York, 1994, p. 137.